IN-37
070571

NASA
Contractor Report 195461

Army Research Laboratory
Contractor Report ARL–CR–224

571 P.

Advanced Rotorcraft Transmission Program (ART)

Joseph W. Lenski, Jr.
Boeing Defense & Space Group
Philadelphia, Pennsylvania

April 1995

Prepared for
Lewis Research Center
Under Contract NAS3–25421

National Aeronautics and
Space Administration

U.S. ARMY
RESEARCH LABORATORY

Advanced Rotorcraft Transmission Program (A.R.T.)

Final Report

Joseph W. Lenski, Jr., et al.

Boeing Defense & Space Group
Helicopters Division
Philadelphia, Pennsylvania

April 1995

Prepared under Contract
NAS3-25421
from
Vehicle Propulsion Directorate
U.S. Army Research Laboratory
Cleveland, Ohio 44135-3191
and
NASA Lewis Research Center
Cleveland, Ohio 44135-3191

ARL-CR-224
NASA CR-195461
Boeing D210-12966-1

SUMMARY

On May 20, 1988, Boeing Defense & Space Group, Helicopters Division, was awarded a contract by the U.S. Army Aviation Systems Command (AVSCOM) and the NASA Lewis Research Center to conduct the Advanced Rotorcraft Transmission (A.R.T.) program. The A.R.T. program is structured to incorporate key emerging technologies in materials and components into an advanced rotorcraft transmission with the intention of making significant improvements in the state of the art (SOA). The objectives of the A.R.T. program are to:

1. Reduce transmission weight by 25 percent relative to SOA trends (currently in the range of 0.40 lb/hp).
2. Reduce transmission noise by 10 db relative to SOA.
3. Improve transmission life and reliability while extending mean time between removals (MTBR) to 5,000 hours.

The A.R.T. contract required Boeing to select a baseline transmission design that was representative of SOA drive train production technology and then to compare this design with an advanced configuration developed during the program. Boeing selected a transmission sized for the tactical tiltrotor (TTR) aircraft which meets the future air attack vehicle (FAAV) requirements.

Component developmental testing was conducted to evaluate the high-risk concepts before finalizing the advanced-transmission configuration. Eight advanced-technology component tests were conducted:

- Noise reduction by active cancellation
- Hybrid bidirectional tapered-roller bearings
- Improved bearing-life theory and friction tests
- Transmission lubrication study with hybrid bearings
- Precision near-net-shape forged spur gears

- High-profile contact ratio noninvolute tooth form spur gears
- Surface-modified titanium accessory spur gears
- Parallel-axis gear noise study.

The work performed in the Advanced Rotorcraft Transmission program demonstrated significant reductions in weight and noise and an increase in the mean time between removals (MTBR). Intensive tests were conducted on key, advanced-technology components. Significant advances were demonstrated in the following areas:

- Noise reduction by active noise cancellation
- Bidirectional tapered-roller bearings
- Hybrid bearings
- Improved bearing technology
- Near-net-shape forged spur gears
- HCRNIV gears
- Noise reduction by tooth form and contact ratio.

This report summarizes the results of the studies and the eight component tests conducted under the A.R.T. contract.

FOREWORD

This report summarizes the work completed under contract NAS3-25421 from the U.S. Army Aviation Systems Command (AVSCOM) and NASA Lewis Research Center titled Advanced Rotorcraft Transmission (A.R.T.) program. The program was conducted under the technical cognizance of Dr. Mark J. Valco of the U.S. Army Aviation Systems Command, Lewis Research Center, Cleveland, Ohio, during the period from May 1988 to September 1993.

The work performed at Boeing Defense & Space Group, Helicopters Division, was under the technical direction of Joseph W. Lenski, Jr., program manager of the Advanced Power Train Technology organization. Other investigators at Boeing for this program were Ray Drago (Gear Technology), Robert Spencer and Harry Sternfeld (Noise Technology), Al Canonica, Steve Mainart, Ken Donahue, B. J. Johnston (Test), Mark Robuck, Kevin Zoghby, and Tim Beck (Design Support).

During this program five major subcontractors provided technical and manufacturing assistance. Acknowledgment is made to the following individuals:

- M. J. Burke and G. W. Tye of Noise Cancellation Technologies, Inc, for their technical assistance in developing active noise cancellation.

- Gary Kreider of The Timken Company, Canton, Ohio, for his work in the design, fabrication, and test of the hybrid bidirectional tapered-roller bearing.

- Mark Ragen of MRC Bearings, Engineering and Research, Jamestown, New York, for work on the SKF new life theory and ball-on-disk traction testing.

- Dick Douglas and Dale McCartney of Eaton Corporation, Manufacturing Technologies Center, Willoughby Hills, Ohio, for providing design and manufacture of precision near-net-shape forged spur gears.

- Barry Noonan, The Purdy Corporation, Manchester, Connecticut, for the fabrication of test gears.

Finally, acknowledgment is made to Fred B. Oswald and Mark J. Valco of the NASA Lewis Research Center for their technical assistance in running and evaluating test gears in the NASA gear noise test rig.

TABLE OF CONTENTS

Page

SUMMARY iii

FOREWORD v

LIST OF ILLUSTRATIONS xiii

LIST OF TABLES xxiv

LIST OF ABBREVIATIONS, ACRONYMS, AND SYMBOLS xxvi

INTRODUCTION 1

BACKGROUND 3

AIRCRAFT SELECTION 5

WEIGHT 5

Gear Set Weight Trend 8

NOISE 8

RELIABILITY 9

Reliability Analysis 9

SUMMARY 9

TRADE STUDIES 11

SELF-ALIGNING BEARINGLESS PLANETARY (SABP) CONFIGURATION 11

SPLIT-TORQUE CONFIGURATION 14

CONVENTIONAL SINGLE-STAGE PLANETARY CONFIGURATION 14

SELECTION PROCESS 14

Self-Aligning Bearingless Planetary Configuration 22

Split-Torque Configuration 22

Conventional Single-Stage Planetary Configuration 23

EFFECT OF TRANSMISSION IMPROVEMENTS ON TRANSMISSION AND AIRCRAFT PERFORMANCE 25

DESIGN AND ANALYSIS OF ADVANCED ROTORCRAFT TRANSMISSION 33

FINAL CONFIGURATION 33

Page

TECHNOLOGICAL FEATURES 38
DESIGN FEATURES 40
Description and Analysis of Gear Design 42
Description and Analysis of Bearing Design 47
Transmission Shafts 54
Spline Analysis 66
Gearbox Housings 67
Lubrication System Description 69
Interconnecting Drive Shaft 74
Accessory Installations 74
Structural Interface 76
Diagnostic Equipment 76
Assembly Procedures 78
Producibility 79
Maintainability 81
WEIGHT SUMMARY 82
SUMMARY 82
Design Activity 84
COMPONENT DEVELOPMENT TESTING 89
TRANSMISSION NOISE REDUCTION 89
Background 89
Introduction 89
Approach 94
Small-Scale Test 107
Full-Scale Test 109
Results 123
Conclusions 138

Page

HYBRID BIDIRECTIONAL TAPERED-ROLLER BEARINGS 145
Bearing Design 146
Design Code for Performance 154
Bearing Fabrication 154
Test Rig 154
Testing 155
Materials Tested 158
Results and Discussion 161
Conclusions 215
IMPROVED BEARING TECHNOLOGY 217
Implementation of Theory of Improved Bearing Life 218
Friction Testing 244
TRANSMISSION LUBRICATION STUDY WITH HYBRID BEARINGS 263
Density 263
Hardness 265
Elastic Modulus 265
Tensile Strength 265
Hertz Compressive Strength 265
Fracture Toughness 266
Temperature Capability 266
Thermal Expansion 266
Corrosion Resistance 266
Fatigue Life 266
Fabrication and Testing 267
PRECISION NEAR-NET-FORGED SPUR GEARS 283
Process Development 285
Design of Forging Tooling 288

Page

Manufacture of Forging Tooling 289
Forging of Near-Net-Shape Test Gear 289
Forging of Conventional Baseline Gear Blank 294
Finishing of Test Gears 294
Inspection of Test Gears 294
Testing and Evaluation 294
SPUR GEARS WITH HIGH PROFILE CONTACT RATIO, NONINVOLUTE TOOTH FORM 311
Introduction 311
Objective 311
Program 312
Design 315
Fabrication 320
Test Definition 326
Gear Loading 328
Test Procedures 330
Test Results 335
Conclusions 360
ACCESSORY SPUR GEARS OF SURFACE-MODIFIED TITANIUM 363
Introduction 363
Objective 364
Program 364
Design 364
Fabrication 366
Test Definition 366
Gear Loading 368
Test Procedures 369

Page

Failure Criteria 375

Results 375

Conclusions 382

PARALLEL-AXIS GEAR NOISE STUDY 385

Test Gear Design 386

Test Facility 388

Instrumentation 391

Noise Measurements 391

Processing Sound Power Data 394

Data Sampling 396

Test Gear Loading 397

Results 401

Conclusions 415

CONCLUSIONS 417

RECOMMENDATIONS 421

LITERATURE CITED 423

APPENDIXES

A. ENGINEERING DRAWINGS OF THE BOEING ADVANCED ROTORCRAFT TRANSMISSION A-1

B. DETAILS OF BEARING TESTS B-1

C. SOURCE CODE LISTING FOR BEARING-LIFE CALCULATION USING NEW SKF LIFE THEORY AS IMPLEMENTED IN PC-SHABERTH C-1

D. PC-CYBEAN2 OUTPUT LISTINGS FOR 114DS665 AND MR315C2 BEARINGS D-1

Page

E. PLOTS OF TRACTION COEFFICIENT VERSUS PERCENT SLIP FOR FRICTION TESTS OF MATERIALS AND LUBRICANTS E-1

F. NEAR-NET TOOLING DRAWINGS F-1

G. CONVENTIONAL TOOLING DRAWINGS G-1

LIST OF ILLUSTRATIONS

Figure		Page
1	Definition of Baseline Aircraft Mission Requirements	6
2	Tactical Tiltrotor Demonstrator	6
3	Baseline Aircraft Mission Performance	7
4	Original Baseline TTR Transmission With Two-Stage Planetary	10
5	Self-Aligning Bearingless Planetary (SABP) Arrangements	12
6	Self-Aligning Bearingless Planetary (SABP) Configuration	13
7	Split-Torque Configuration	15
8	Single-Stage Planetary Configuration	16
9	Tactical Tiltrotor Transmission in Left Nacelle	21
10	Aircraft Mission Performance With Advanced Rotorcraft Transmission Selected	26
11	Effects of A.R.T. on Aircraft Design Parameters	27
12	Cost Comparison of Aircraft Major Components	30
13	Comparison of Aircraft Flyaway Costs	31
14	Installation of Advanced Rotorcraft Transmission in Right Nacelle	34
15	Major Internal Components of Advanced Rotorcraft Transmission	35
16	Study of Gear Cutter Clearances	55
17	Locations of Fatigue Analysis Sections	60
18	Locations of Limit and Ultimate Analysis Sections	63
19	A.R.T. Lubrication Schematic	70
20	Planned Component Testing of A.R.T. Tactical Tiltrotor Transmission	87
21	Transmission Noise Spectrum of CH-47 Helicopter	90
22	Arrangement of Drive System Components of CH-47 Helicopter	92
23	Major Components of CH-47 Forward Rotor Transmission	93
24	Normalized Weight, Life, and Noise-Reduction Trends for a Large Rotor Transmission	96
25	Potential Noise Reduction of Transmission Mount	97

Figure		Page

26 Block Diagram of a Single-Channel, Single-Harmonic Controller 100
27 Transmission Gear Mesh Frequency and Sidebands 101
28 Harmonic Series Representation of Disturbance Signal 102
29 Small-Scale Transmission Test Stand 108
30 Measured Acceleration Levels at Leg 4 on the Small-Scale Test Stand 110
31 Measured Acceleration Levels at 16 Locations on the Small-Scale Test Stand 111
32 Side View of A.R.T. Full-Scale Noise Test Stand 112
33 The A.R.T. Full-Scale Noise Test Stand 113
34 Comparison of Rotor Transmission Noise Data: Flight Test and Unloaded Test Stand 115
35 Microphone Locations for Full-Scale Noise Test 116
36 Comparison of Direct and Cross Accelerations Measured on the Full-Scale Test Stand 122
37 Location of Residual Accelerometers 124
38 Typical Effect of Active Control on Vertical Axis Acceleration 126
39 Averaged Residual Sensor Accelerations at Three Locations 127
40 Averaged Platform Accelerations for Three Residual Sensor Locations 127
41 Locations of Shakers on Lower Case of Transmission 130
42 Effect of Active Control on Accelerations of Lower Case 131
43 Added Transmission Damping 132
44 Ring Gear Modification 133
45 Comparison of Sound Levels of Baseline and Modified Ring Gears 135
46 Effect of Damping on Input Pinion Gear 137
47 Damping Areas of Mounting Legs 139
48 Comparison of Sound Levels of Baseline and Damped Configurations 140
49 Summary Comparison of Three Transmission Configurations Tested 141
50 Transmission Input Shaft 147

Figure		Page

51 Conventional Bidirectional Bearing JXC25729 149

52 Hybrid Bidirectional Bearing JXC25729 150

53 Components of Bidirectional Bearing 151

54 Concept of Bidirectional Bearing 152

55 Cross Section of Test Head 162

56 Cup O.D. Temperature Versus Oil Flow, All-Steel Bearing, Cup Slots Closed 164

57 Rib O.D. Temperature Versus Oil Flow, All-Steel Bearing, Cup Slots Closed 165

58 Oil-Out Temperature Versus Oil Flow, All-Steel Bearing, Cup Slots Closed 166

59 Temperature Versus Speed at 3 Pt/Min, All-Steel Bearing, Cup Slots Closed (Top) and Open (Bottom) 167

60 Temperature Versus Speed at 3 Pt/Min, Hybrid Bearing With Silicon Nitride Rollers and Steel Cup Rib, Cup Slots Closed (Top) and Open (Bottom) 168

61 Temperature Versus Speed at 3 Pt/Min, Cup Slots Closed, Hybrid Bearing With Silicon Nitride Rollers and Zirconia Rib, Steel Cage (Top) and P.E.E.K. Cage (Bottom) 169

62 Temperature at Overload and Overspeed at 3 Pt/Min, All-Steel Bearing, Cup Slots Closed 171

63 Temperature at Overload and Overspeed, Cup Slots Closed, Hybrid Bearing With Silicon Nitride Rollers and Zirconia Rib, Steel Cage (Top) and P.E.E.K. Cage (Bottom) 172

64 Temperature, Torque, and Load Versus Time, All-Steel Bearing, Major-Minor Thrust 173

65 Temperature, Torque, and Load Versus Time, Hybrid Bearing With Silicon Nitride Rollers and Steel Cup Rib, Major-Minor Thrust 174

Figure		Page

66 Temperature, Torque, and Load Versus Time, Hybrid Bearing With Silicon Nitride Rollers and Zirconia Cup Rib, Major-Minor Thrust 175

67 Temperature, Torque, and Load Versus Time, Hybrid Bearing With Silicon Nitride Rollers, Zirconia Cup Rib, and P.E.E.K. Cage, Major-Minor Thrust 176

68 Temperature and Torque Versus Time in Rapid-Sequence Major-Minor Thrust, All-Steel Bearing 177

69 Temperature and Torque Versus Time in Rapid-Sequence Major-Minor Thrust, Hybrid Bearing With Silicon Nitride Rollers and Steel Cup Rib, Cup Slots Closed 178

70 Temperature and Torque Versus Time in Rapid-Sequence Major-Minor Thrust, Hybrid Bearing With Silicon Nitride Rollers and Zirconia Cup Rib, Cup Slots Closed 179

71 Temperature and Torque Versus Time in Rapid-Sequence Major-Minor Thrust, Hybrid Bearing With Silicon Nitride Rollers, Zirconia Cup Rib, and P.E.E.K. Cage, Cup Slots Closed 180

72 Hybrid Bearing No. 14 Cone, Cone Rib, Rollers, and Cage 182

73 Hybrid Bearing No. 14 Cup and Zirconia Cup Rib 183

74 Zirconia Rib Face Surface Outside and Inside Roller End/Rib Contact Area 185

75 Chipped Area on Outside Diameter of Zirconia Rib Faces 186

76 Bearing Movement for Major-Minor Thrust at Operating Speed, Load, and Temperature 187

77 Endurance Temperature and Torque Versus Time for Hybrid Bearings No. 21 and 22 in the DC and BC Positions; 8.3 Times L-10 Life With BC Damage 189

78 Hybrid Bearing No. 22 Cone, Cone Rib, Rollers, and Cage 190

79 Hybrid Bearing No. 22 Cup and Zirconia Cup Rib 191

Figure		Page

80 Hybrid Bearing No. 22 Silicon Nitride Roller 192

81 Endurance Temperature and Torque Versus Time for Hybrid Bearings No. 15 and 17 in the DC and BC Positions; 7.1 Times L-10 Life with DC Damage 194

82 Endurance Temperature and Torque Versus Time for Hybrid Bearings No. 24 and 25 in the DE and BE Positions; 11.9 Times L-10 Life With Test Suspended 195

83 Hybrid Bearing No. 25 Cone, Cone Rib, Rollers, and Cage After 11.2 Times L-10 Life Endurance Test 196

84 Hybrid Bearing No. 25 Cup and Zirconia Rib After 11.2 Times L-10 Life Endurance Test 197

85 Posttest Cone Race Profiles of Conventional and Hybrid Bearings 198

86 Posttest Cup Race Profiles of Conventional and Hybrid Bearings 199

87 Posttest Roller Race Profiles of Conventional and Hybrid Bearings 200

88 Posttest Roller Large-End Spherical-Radius Profiles of Conventional and Hybrid Bearings 201

89 Posttest Cup Rib Face Profiles of Conventional and Hybrid Bearings 202

90 Temperature and Torque Versus Time in Oil-Off Test of Hybrid Bearing With Silicon Nitride Rollers and Steel Rib at 23,000 rpm. 204

91 Temperature and Torque Versus Time in Oil-Off Test of Hybrid Bearing With Silicon Nitride Rollers and Zirconia Rib at 12,000 rpm 205

92 Temperature and Torque Versus Time in Oil-Off Test of All-Steel Bearing at 5,400 rpm 206

93 Conventional Bearing No. 18 Cone, Cone Rib, Rollers, and Cage After 62 Minutes in Oil-Off Test at 5,400 rpm 207

94 Conventional Bearing No. 18 Cup and Cup Rib After 62 Minutes in Oil-Off Test at 5,400 rpm 208

Figure		Page

95 Temperature and Torque Versus Time in Oil-Off Test of Hybrid Bearing With Silicon Nitride Rollers and Steel Rib at 12,000 rpm 210

96 Hybrid Bearing No. 12 Cone, Cone Rib, Rollers, and Cage After 60 Minutes in Oil-Off Test at 12,000 rpm 211

97 Hybrid Bearing No. 12 Cup and Cup Rib After 60 Minutes in Oil-Off Test at 12,000 rpm 212

98 Temperature and Torque Versus Time in Oil-Off Test of Hybrid Bearing With Silicon Nitride Rollers and Steel Rib at 18,000 rpm 213

99 Speed, Temperature, and Torque Versus Time for 5.0- and 7.5-CentiStoke Oil 214

100 Point Contact Normal Stress Distribution 228

101 Line Contact Normal Stress Distribution 228

102 Diagram for Fit-Up of Two Concentric Rings 234

103 Friction Curve Fit for μMAX - 0.063 and SRR_c = 0.0046 241

104 Friction Curve Fit for μMAX = 0.033, μ_c = 0.020, SRR_c = 0.0064, and K=60 241

105 Skidding Analysis Results Using PC-CYBEAN2 243

106 MRC Test Bearing MR315C2 245

107 Schematic Representation of a Traction-Versus-Slip Curve (Creep) for Unlubricated Surfaces 248

108 The MRC High-Temperature Traction-Testing Machine and Ball-on-Disk Test Arrangement 251

109 Peak Traction Coefficient Versus Temperature for M50 Ball/TDC-Coated M50 Disk 258

110 Hybrid Cylindrical-Roller Bearing MR315C2 269

111 Hybrid Outboard Cylindrical-Roller Bearing 5RNH214-A28 Manufactured by Split Ballbearing 270

Figure		Page

112 Hybrid Ball Thrust Bearing AAV314-12 MSR X1028 Manufactured by CERBEC 272
113 Full-Complement Hybrid Ball Thrust Bearing AAV314-14 FT X1087 Manufactured by CERBEC 273
114 Input Pinion With Three Test Bearings 274
115 Test Transmission and Instrumentation 275
116 Comparison of Different Oils With Standard and Hybrid Ball Thrust Bearings 277
117 Comparison of Different Oils With Standard and Hybrid Roller Bearings 278
118 Oil-Off Test of Standard Ball and Roller Bearings 280
119 Failed Input Pinion Standard Ball Thrust Bearing From Oil-Off Test 280
120 Oil-Off Test of Hybrid Ball and Roller Bearings 281
121 Failed Input Pinion Hybrid Ball Thrust Bearing From Oil-Off Test 281
122 Tooth, Die, and Punch Profiles 286
123 Finished-Part Forge Drawing 287
124 Forging Station 291
125 Heated Billet Loaded Into Preform Station 291
126 Preform Transferred to Final Forge Station 292
127 Finished Forged Gear 292
128 Still-Hot Near-Net Gear Forgings 293
129 Process Sheet For Rough-Machining Near-Net Gear 295
130 Standard Forged Gears 298
131 Near-Net-Shape Forged Gears 300
132 Single-Tooth Bending-Fatigue Test Setup 301
133 Master Instrumented Gear 303
134 Single-Tooth Bending-Fatigue Test Data From Conventional X2M Gears 304

Figure		Page
135	Single-Tooth Bending-Fatigue Test Data From Near-Net-Forged X2M Gears	305
136	Single-Tooth Bending-Fatigue Test Data From Near-Net-Forged X2M Gears With Nickel	306
137	Single-Tooth Bending-Fatigue Test Data Summary	307
138	Effect of Edge Break on Fatigue Origin: Typical Edge Break	308
139	Effect of Edge Break on Fatigue Origin: Machined Edge Break	309
140	Boeing Gear Research Test Facility	313
141	Test Rig for Overhung Gears on 10-Inch Centers	313
142	Spur Gears With High Contact Ratio, Noninvolute Tooth Form	314
143	Spur Gears With Standard Involute Tooth Form	314
144	Comparison of Standard Involute and HCRNIF Gear Tooth Profiles	318
145	Coordinates of HCRNIF Tooth Form	319
146	Tooth Control Charts for Test Pinions	321
147	Tooth Control Charts for Test Gears	322
148	Typical Involute Chart for a Baseline Gear	323
149	Typical "Involute" Chart for an HCRNIF Gear	324
150	Separation of Case and Core as a Result of Carburizing and Quenching	327
151	Calculated Bending Stress of Standard Contact Ratio Test Gears	329
152	Calculated Contact Stress of Standard Contact Ratio Test Gears	329
153	Flash Temperature Rise of Standard Contact Ratio Test Gears	329
154	Configuration of Gear Test	331
155	Locations of Strain Gages in Tooth Roots and Fillets	334
156	Locations and Identification of Strain Gages Around the Gear	334
157	Results of Scoring-Load Testing	336
158	Plastic Flow Failure of Gear Teeth	336

Figure		Page

159 Comparison of Noise Levels of Baseline and HCRNIF Gears at 60-Percent Torque 338
160 Comparison of Noise Levels of Baseline and HCRNIF Gears at 80-Percent Torque 339
161 Comparison of Noise Levels of Baseline and HCRNIF Gears at 100-Percent Torque 340
162 Summary of Peak Noise Levels of Baseline and HCRNIF Gears 341
163 Regions of Contact of Baseline and HCRNIF Gear Teeth 344
164 Stress Results in Pinion Fillets of Baseline Gears 347
165 Stress Results in Pinion Roots of Baseline Gears 347
166 Stress Results in Gear Fillets of Baseline Gears 348
167 Stress Results in Gear Roots of Baseline Gears 348
168 Stress Results in Pinion Fillets of HCRNIF Gears 349
169 Stress Results in Pinion Roots of HCRNIF Gears 349
170 Stress Results in Gear Fillets of HCRNIF Gears 350
171 Stress Results in Gear Roots of HCRNIF Gears 350
172 Comparison of Tension Stress at Pinion Fillet of Baseline and HCRNIF Gears 352
173 Comparison of Alternating Stress at Pinion Fillet of Baseline and HCRNIF Gears 353
174 Comparison of Tension Stress at Pinion Root of Baseline and HCRNIF Gears 354
175 Comparison of Alternating Stress at Pinion Root of Baseline and HCRNIF Gears 355
176 Comparison of Tension Stress at Gear Fillet of Baseline and HCRNIF Gears 356
177 Comparison of Alternating Stress at Gear Fillet of Baseline and HCRNIF Gears 357

Figure		Page
178	Comparison of Tension Stress at Gear Root of Baseline and HCRNIF Gears	358
179	Comparison of Alternating Stress at Gear Root of Baseline and HCRNIF Gears	359
180	Six Sets of Gears for Scoring Tests	365
181	Six Sets of Gears for Surface Durability Tests	367
182	Boeing Gear Research Test Facility	367
183	Bending Stress of Titanium Gears in Surface Durability Tests	370
184	Contact Stress of Titanium Gears in Surface Durability Tests	370
185	Flash Temperature of Titanium Gears in Surface Durability Tests	370
186	Bending Stress of Titanium Gears in Scoring Tests	371
187	Contact Stress of Titanium Gears in Scoring Tests	371
188	Flash Temperature of Titanium Gears in Scoring Tests	371
189	Laboratory Setup for Scoring Tests	372
190	Control of Oil Inlet Temperature in Tests	372
191	Scoring of Gear Hard-Coated by E/M Corporation	376
192	Scoring of Gear Treated by Spire Corporation	378
193	Results of Scoring Tests of Surface-Modified Titanium Accessory Spur Gears	378
194	Type of Wear With Steel Pinion Running With Titanium Gear	381
195	Overall Performance Summary of Surface-Modified Titanium Gears	381
196	Test Gears	389
197	NASA Lewis Gear Test Rig	390
198	Cutaway Section of Test Gearbox	390
199	Robotic Noise Measurement System	392
200	Noise Spectrum of Baseline Spur Gear	395
201	Enlarged View of First Harmonic (at 2,083 Hz) of Preceding Figure	395

Figure		Page

202 Stresses on Gears During Noise Testing: Bending Stress Versus Torque 399
203 Stresses on Gears During Noise Testing: Contact Stress Versus Torque 399
204 Stresses on Gears During Noise Testing: Flash Temperature Versus Torque 400
205 Summary of Test Results 402
206 Effect of Tooth Form on Noise Level 402
207 Effect of Helix Angle on Noise Level 404
208 Effect of Build (Assembly and Disassembly) on Noise Level of Spur Gears 407
209 Effect of Build (Assembly and Disassembly) on Noise Level of Helical Gears 407
210 Effect of Torque on Noise Level of Gears 410
211 Combined Effects of Speed and Torque on Gear Noise 410
212 Effect of Face Contact Ratio on Noise at Low Torque 412
213 Effect of Face Contact Ratio on Noise at High Torque 412
214 Effect of Modified Contact Ratio on Gear Noise 413
215 Effect of Total Contact Ratio on Gear Noise 413
216 Effect of Tooth Form on Gear Noise 414
217 Summary of Gear Noise at 3,000 rpm 414
218 Summary of Gear Noise at 4,000 rpm 416
219 Summary of Gear Noise at 5,000 rpm 416

LIST OF TABLES

Table		Page
1	Baseline Aircraft Parameters	7
2	Gear Count Summary for TTR Main Rotor Transmissions	17
3	Bearing Count Summary for TTR Main Rotor Transmissions	18
4	Drive System Weight per Aircraft for TTR Configurations	19
5	Potential for Noise Reduction for TTR Main Rotor Transmissions	19
6	MTBR Rates for TTR Main Rotor Transmissions	20
7	Selection Process for TTR Rotor Transmissions	21
8	Initial Values for Establishment of Baseline Cost Comparisons	29
9	Comparative Cost Estimates	32
10	Design Requirements of the A.R.T. Drive System	39
11	Gear Analysis Summary	45
12	Bearing Analysis Summary	50
13	Fatigue Analysis Summary	57
14	Limit Analysis Summary	61
15	Ultimate Analysis Summary	64
16	Spline Analysis Summary	68
17	Heat Load Summary	72
18	Weight Summary of Advanced Rotorcraft Transmission	83
19	Instrumentation Used for A.R.T. Noise Tests	119
20	Vibration With One Mounting Bolt Removed	120
21	Summary of Active Noise Control Configurations Evaluated	125
22	Results of Bearing Fatigue Life Calculations	153
23	Test Outline for A.R.T. Bearings	156
24	Bearing Test Conditions	157
25	Major/Minor Load Operating Conditions	157
26	Performance Data for JEX25729 All-Steel Bearing	159
27	Performance Data for JEX25729 Hybrid Bearing	160

Table		Page

28 Boeing A.R.T. Traction Testing Summary 256
29 Maximum Friction Coefficients in Boeing A.R.T. Traction Testing 258
30 Properties of an Advanced Silicon Nitride Ceramic Bearing Material 264
31 Comparison of Ceramic and Steel Properties 268
32 Hybrid Cylindrical-Roller Bearing 268
33 Oils Tested 277
34 Dimensional Inspection of Boeing Gears (Phase I) by Eaton Corporation 296
35 Dimensional Inspection of Finished-Machined Near-Net Gears (Phase II) by Eaton Corporation for Boeing 297
36 Test Gear Configuration 317
37 Torque Application Procedure 331
38 Configuration of Test Gears 365
39 Planned and Modified Test Conditions 376
40 Gear Noise Test Matrix 386
41 Configuration of Basic Test Gear 389

LIST OF ABBREVIATIONS, ACRONYMS, AND SYMBOLS

ACA	advanced cargo aircraft
AEO	all engines operating
A.R.T.	advanced rotorcraft transmission
BMS	Boeing Material Specification
CAD	computer-aided design
CMT	cubic mean torque
CNC	computerized numerically controlled
EHD, EHL	elastohydrodynamic
FAAV	future air attack vehicle
H^3	high hot hardness
HCRINV	high profile contact ratio, involute tooth form
HCRNIF, HCRNIV	high profile contact ratio, noninvolute tooth form
HPDTCP	highest point of double-tooth contact at pitch line
HPSTC	highest point of single-tooth contact
ICDS	interconnecting drive shaft
LPSTC	lowest point of single-tooth contact
MDN	M = millions, D = diameter of bearing bore in millimeters, N = shaft speed in rpm
MTBR	mean time between removals
MTBUR	mean time between unscheduled removals
N-m	Newton-meters
OEI	one engine inoperative
P.E.E.K.	polyether-ether-ketone
PRGB	prop-rotor gearbox
psf	pounds per square foot
RAIMS	robotic acoustic-intensity measurement system

ser no.	serial number
SOA	state of the art
TAGB	tilt-axis gearbox
TDC	thin dense chrome
TIF	true involute form
TTR	tactical tiltrotor
TVDS	transmission vibration diagnostic system
VIMVAR	vacuum-induction melt, vacuum-arc remelt

INTRODUCTION

The A.R.T. program is viewed as a means of providing the rotorcraft industry with a unique opportunity to advance the technological base for rotorcraft drive systems via a path similar to that traditionally followed in engine development.

The program is structured in two phases. The first phase involved four contracts and was the preliminary design and component validation phase. This phase allowed each contractor to develop advanced design concepts that incorporate key advanced technologies required to meet the A.R.T. program objectives. Tradeoff studies and component tests and evaluations were conducted to support each design concept. The results of the component tests and evaluations have been completed and their test results are reported. The second phase of the A.R.T. program will involve the selection of one or two contractors to conduct a full-scale demonstrator program.

BACKGROUND

The Advanced Rotorcraft Transmission (A.R.T.) program is a U.S. Army-funded, joint Army/NASA program to develop and demonstrate lightweight, quiet, durable drive train systems for the next generation of rotorcraft. This program allows the participants, which include Bell Helicopter Textron, Inc, Boeing, McDonnell Douglas Helicopter, and Sikorsky, to evaluate key emerging material and component technologies and novel design concepts for advancing the technology of future rotorcraft transmissions. The specific objectives of A.R.T. include the reduction of drive train weight by 25 percent, a reduction of noise level at the transmission source by 10 db, and the attainment of at least a 5,000-hour MTBR drive system.

The A.R.T. program requires all participants to select a vehicle fitting into one of the two distinct next-generation aircraft classes and to demonstrate their proposed advanced-concept drive trains. The two classes of aircraft are:

1. Future air attack vehicle (FAAV): a 10,000- to 20,000-pound aircraft capable of undertaking tactical support and air-to-air missions

2. Advanced cargo aircraft (ACA): a 60,000- to 80,000-pound aircraft capable of heavy-lift field support operations

The work conducted by Boeing under the A.R.T. contract was to select a baseline transmission that is representative of a current state-of-the-art production design and then compare this design with an advanced configuration developed during this program. The A.R.T. program is designed to provide a high return on weight improvement, noise reduction, and improved MTBR by developing novel concepts involving relatively high risk factors.

AIRCRAFT SELECTION

The Boeing aircraft selected for this program was a tactical tiltrotor (TTR) aircraft which met the requirements outlined for the FAAV (nominal gross weight of 10,000 to 20,000 pounds) and the mission requirements as defined in Figure 1. The TTR is a small, lightweight attack tiltrotor aircraft designed to be highly maneuverable and survivable. It is also applicable to counter-air attack and air-to-air combat missions. Its primary mission gross weight is about 17,223 pounds.

In general, the TTR drive system arrangement is similar to that of the V-22 Osprey aircraft. It is a twin-engine configuration (see Figure 2) with one engine mounted in each wingtip nacelle that pivots with the rotors as on the V-22. The engine size is in the 2,400-shp class; a candidate engine of this size was a growth derivative of the T700-701C. Some additional characteristics pertinent to the A.R.T. effort are given in Table 1 and Figure 3. Interconnecting cross-shafting is also required between the rotors and engines so that one engine can drive both rotors in the event of an engine failure. Specifics of accessory drives, APU, and details of the lubrication system (and cooling) are still to be developed and the transmissions will be designed to provide for 30 minutes of operation after loss of oil or gear/shaft damage. All subsystems of the TTR will provide both crashworthy and damage-tolerant characteristics.

Significant baseline information was developed with the VASCOMP V/STOL aircraft-sizing program which was then used to establish the baseline parameters to be compared to an aircraft using the A.R.T. drive system. The main areas of comparison were weight, noise, and reliability. The approaches taken to evaluate these parameters are as follows.

WEIGHT

The method of estimating the weight of various aircraft transmissions was based upon a paper written by Arling Schmidt of Boeing (SAWE paper no. 1120)[1]. The procedure defines equations

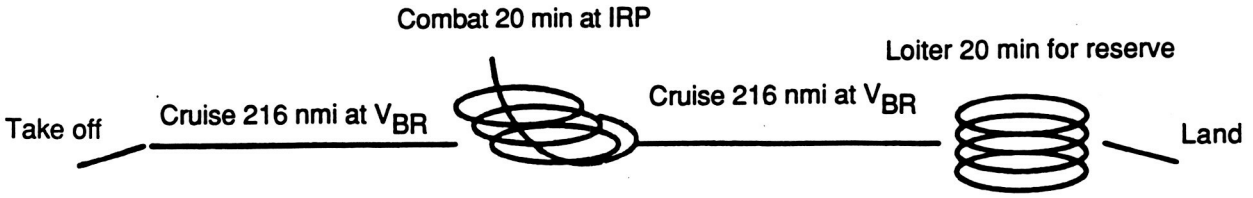

- Design based on tactical tiltrotor proposal
- Whole mission performed at 4,000 ft/95°F

Figure 1. Definition of Baseline Aircraft Mission Requirements

R0288

Figure 2. Tactical Tiltrotor Demonstrator

TABLE 1. BASELINE AIRCRAFT PARAMETERS

Primary mission gross weight (lb)	17,223	
Structural design gross weight (lb)	16,155	
Wingspan (ft)	36.2	
Wing area (sq ft)	224.0	
Wing loading at SDGW (psf)	72.0	
Rotor diameter (ft)	25.0	
No. blades per rotor	3	
Disk loading at PMGW (psf)	17.5	
Rotor solidity	0.117	
Engines	2 x GE 700 - 701C	
Max power installed (shp)	2 x 2,019	
	Hover	Cruise
Output power xmsn rating per shaft (shp)	2,444	1,955
Transmission input rating (AEO, installed, shp)	2,424	1,939
Mast output torque (ft-lb)	21,396	21,396
Main rotor rpm	600	480

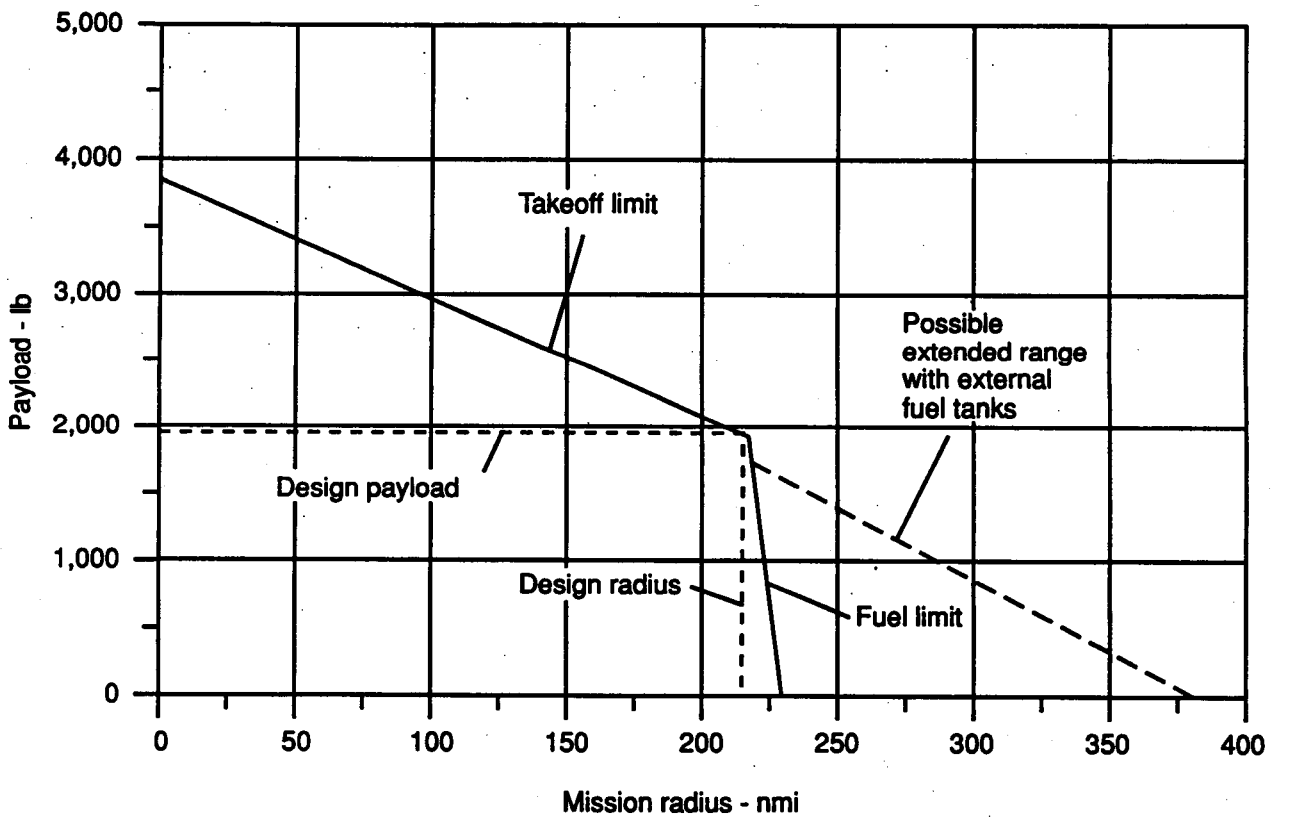

Figure 3. Baseline Aircraft Mission Performance

equations which estimate the weight of different components based upon various design parameters and configurations. A sample of a gear set weight trend is shown below. This procedure was used to establish weight trends based on a variety of design concepts.

Gear Set Weight Trend

$$Wt = 150 \left[\frac{QPUAB}{S_A N}\right]^{0.8} \tag{1}$$

where Q = a nondimensional effect of gear ratio on the weight of a simple gear set

P = design horsepower of a two-gear set

U = special features factor: overrunning clutches, extra pinion, dephasing mechanism

A = support factor: arrangement of gear stages in gearbox

B = gear shaft/bearing support factor: overhung, straddle-mounted

S_A = average compressive stress index based on gear tooth pressure angle and Hertz stress

N = gear or shaft input rpm

NOISE

Noise prediction was based upon the speech interference level (SIL_4), which is a simplified method of quantifying noise in four-octave band unit terms of its interfering effect on communication by speech. The approach for evaluating noise reduction is shown below.

1. SIL_4 = noise measurement unit to evaluate tradeoff studies of A.R.T. design.
2. Current state-of-the-art transmission baseline noise, SIL_4: main rotor transmission in load test cell and in test aircraft.
3. Source noise goal (10-db reduction) will be evaluated using SIL_4 as measure.

4. Major items to be evaluated are gear and shaft internal damping, isolation mounts of gear case, force cancellation at case mount points, and high-overlap gears.

NOTE: SIL_4 (speech interference level) is a simplified method of quantifying noise in four-octave band unit terms of its interfering effect on speech communication.

RELIABILITY

The reliability analysis conducted on the A.R.T. transmission concepts is defined below. Boeing used as its data base overhaul data for the CH-46/CH-47 transmissions and related this information to equivalent A.R.T. components by size and function.

Reliability Analysis

1. Identify components from baseline SOA transmission.
2. Relate components to equivalent CH-46/CH-47 parts by size and function.
3. Assess CH-46/CH-47 overhaul data for failure and replacement rates of generically equivalent parts to establish TTR baseline.
4. Apportion TTR baseline rates to meet MTBR requirements and goals.

SUMMARY

With these ground rules established, various trade studies were conducted and evaluated to determine the best configuration to be used for the A.R.T. transmission in the TTR aircraft. The results of these trade studies are presented in the following sections. These trade studies were compared against what was considered the original baseline configuration of a transmission for the TTR design with current state-of-the-art technology; this baseline transmission is shown in Figure 4. All new designs are compared against the weight, noise, and reliability of this transmission to determine if the goals of the A.R.T. program were achieved.

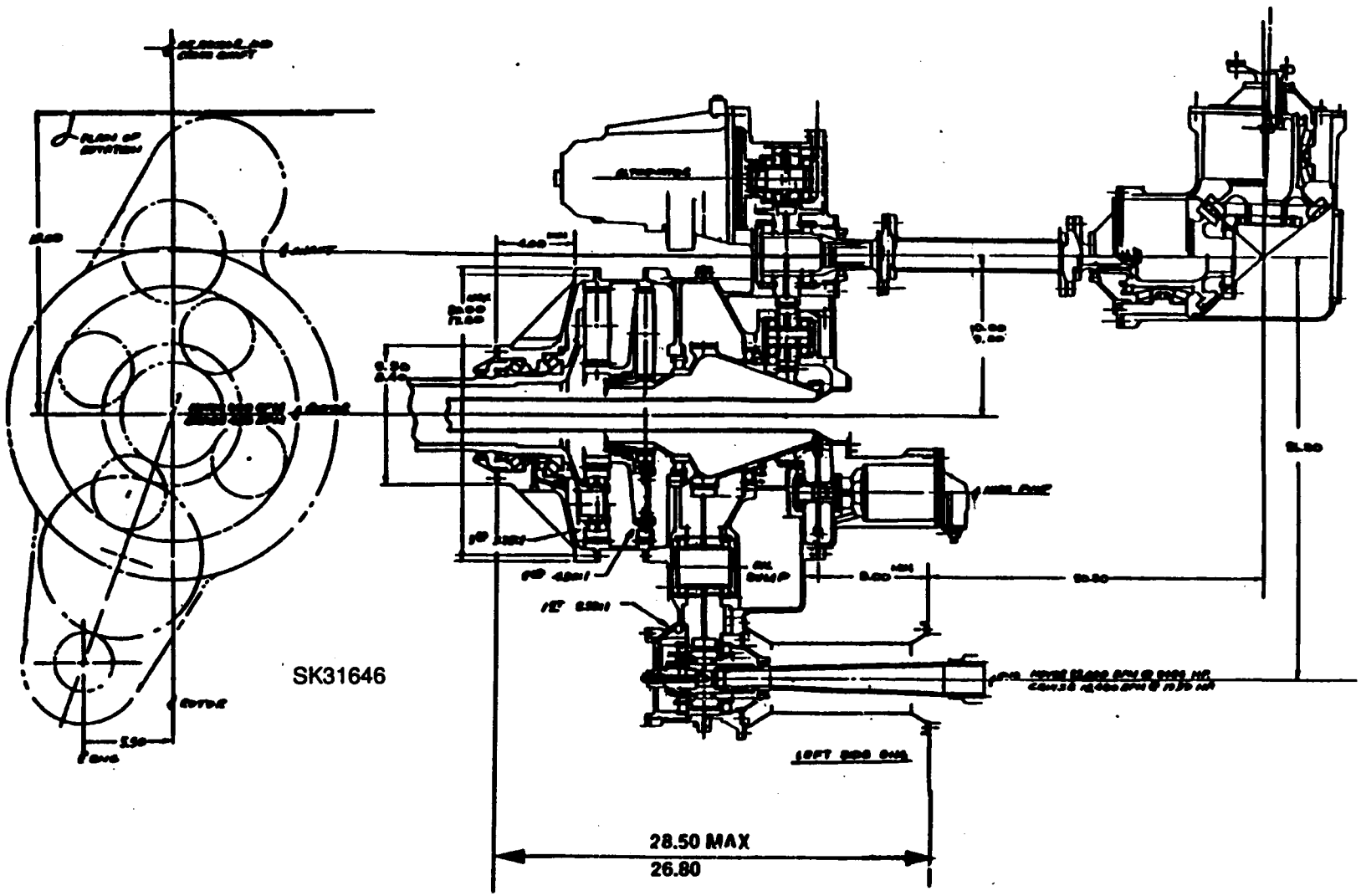

Figure 4. Original Baseline TTR Transmission With Two-Stage Planetary

TRADE STUDIES

In order to evaluate the effect of advanced-technology improvements on aircraft size and performance, computer programs were initially used to develop the reference aircraft design. In the early stage of this program a few key parameters were used to develop the drive system design. As the design progressed, detailed rotor and engine performance data were entered to improve the precision of the calculations. The program was used to discover broad trends early in the design process, and it was also used to determine the effect of relatively small modifications once the design was more developed.

During the early development of the A.R.T. drive system, comparisons and trade studies were conducted among novel transmission configurations with high payoff potential. In addition to the configuration, advanced features such as high-temperature materials, novel gear and bearing designs, composites, and lubrication methods were also evaluated in achieving the goals of the A.R.T. program. The Boeing approach included the study of the transmission configurations described in the following paragraphs.

SELF-ALIGNING BEARINGLESS PLANETARY (SABP) CONFIGURATION

The basic attributes of this configuration were the complete cancellation of static gear loads on the planet spindles which, in turn, because of the balanced forces allowed the elimination of planet spindle shaft bearings and planet carriers. Two basic arrangements of a self-aligning bearingless planetary system are shown in Figure 5. The line of action between the output, planet, and input mesh results in balanced loads on each spindle. These two arrangements were investigated to obtain the optimum arrangement as shown in Figure 6. The one noticeable feature of this configuration is the increase in the overall length of the transmission.

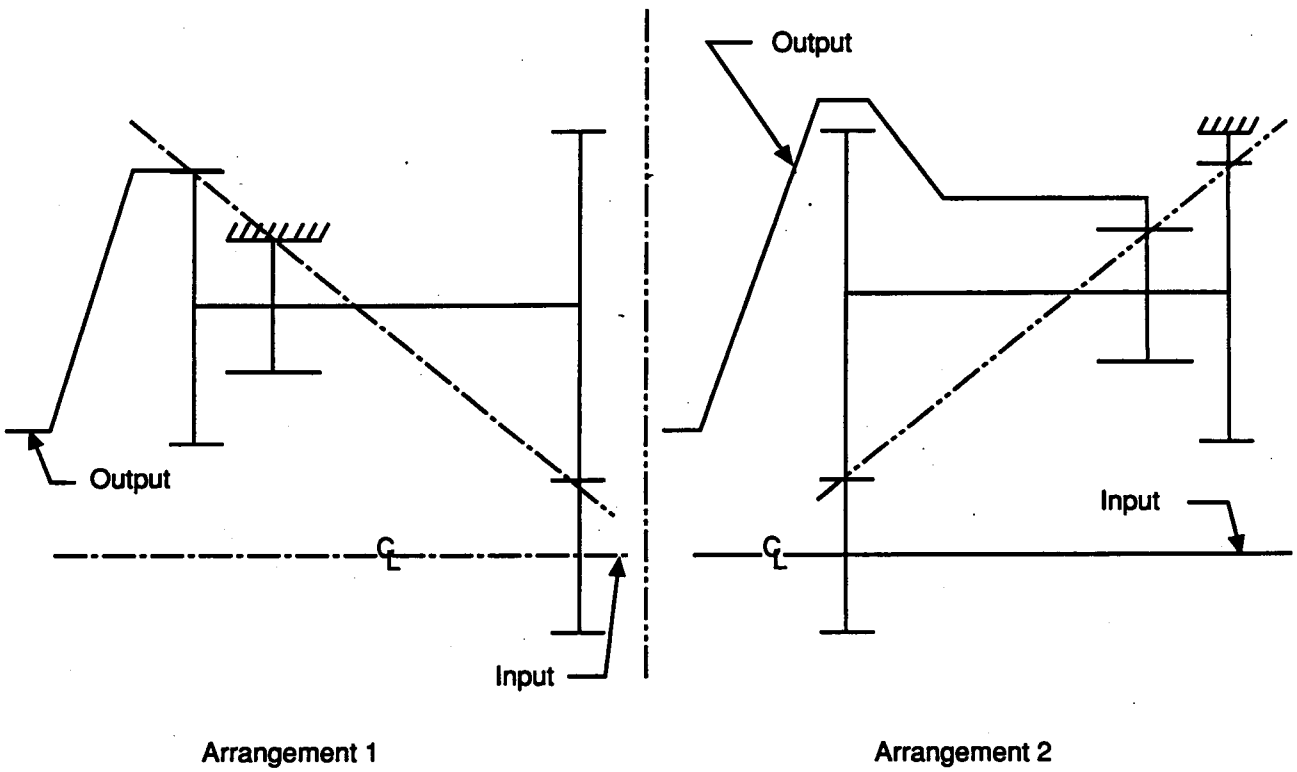

Figure 5. Self-Aligning Bearingless Planetary (SABP) Arrangements

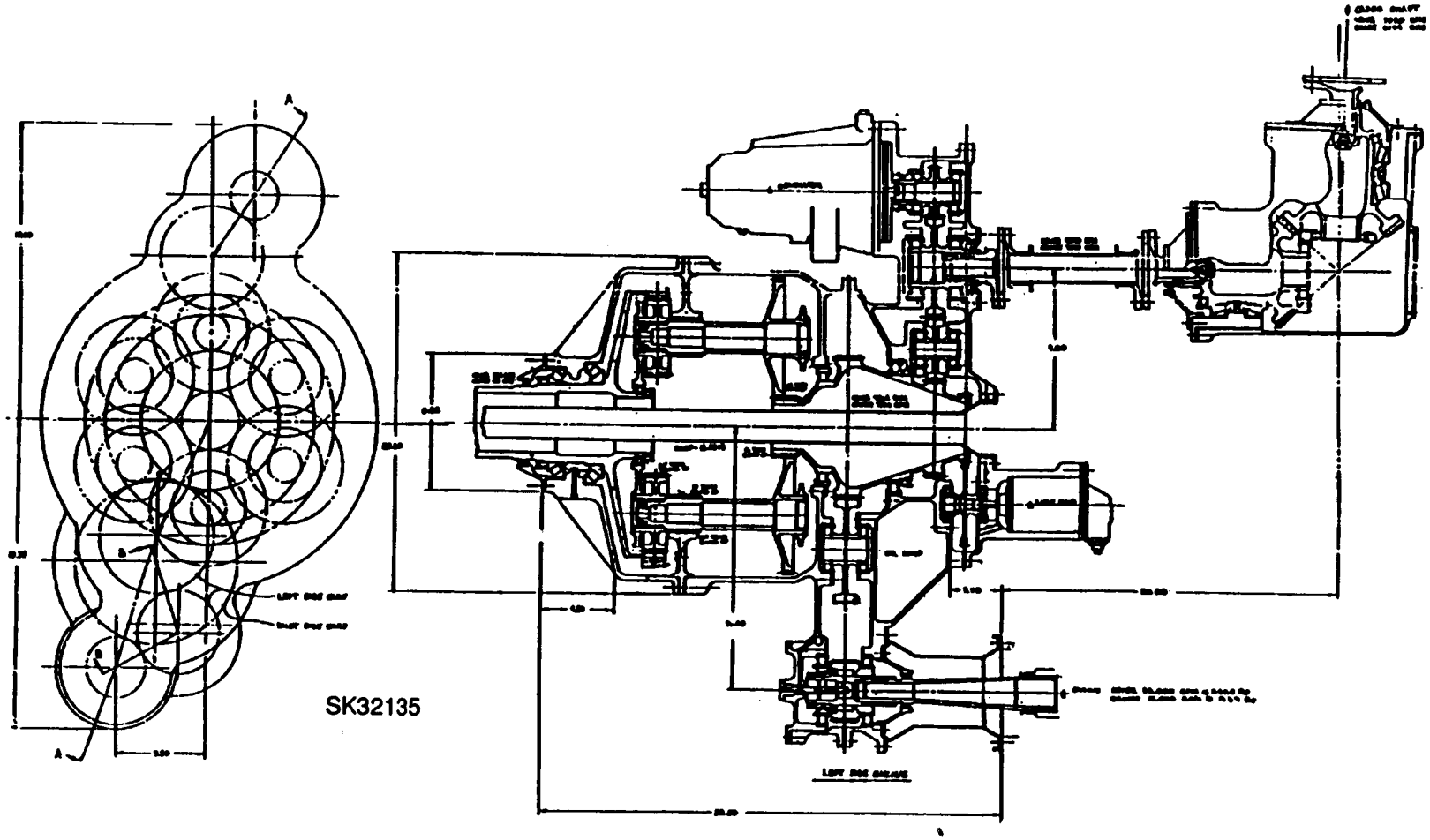

Figure 6. Self-Aligning Bearingless Planetary (SABP) Configuration

SPLIT-TORQUE CONFIGURATION

The basic attributes of this configuration are the multiple, parallel, torque load paths which allowed multiple pinion shafts to transfer the torque loads to the main bull gear and a high reduction ratio at the output stage. The configuration developed for the A.R.T. program is shown in Figure 7. A review of this configuration shows that large space is available in the output area with a large concentration of parts at the input area of this transmission. The design also shows a significant change in the location of the tilt-axis shaft.

CONVENTIONAL SINGLE-STAGE PLANETARY CONFIGURATION

The basic attributes of this configuration are its compact geometric arrangement and extensive experience with effective mesh load sharing. The configuration developed for the A.R.T. program is shown in Figure 8. The most significant difference with this transmission is the use of a high-ratio, single-stage planetary and helical gearing. This resulted in a very compact transmission.

SELECTION PROCESS

Extensive studies were conducted of each of these configurations to establish weight trends, reliability factors, and predicted noise characteristics. A summary of these various studies is presented in Tables 2 through 6. These data were compared with baseline data established for current state-of-the-art transmissions. For Boeing, these baseline data were the CH-47 and YUH-61 drive systems. Upon completion of the various comparisons and trade studies, a selection methodology was developed to rank the three configurations. This selection process is summarized in Table 7.

Based upon the selection methodology shown in Table 7, Boeing selected the single-stage planetary configuration as the TTR drive system concept most likely to achieve the A.R.T.

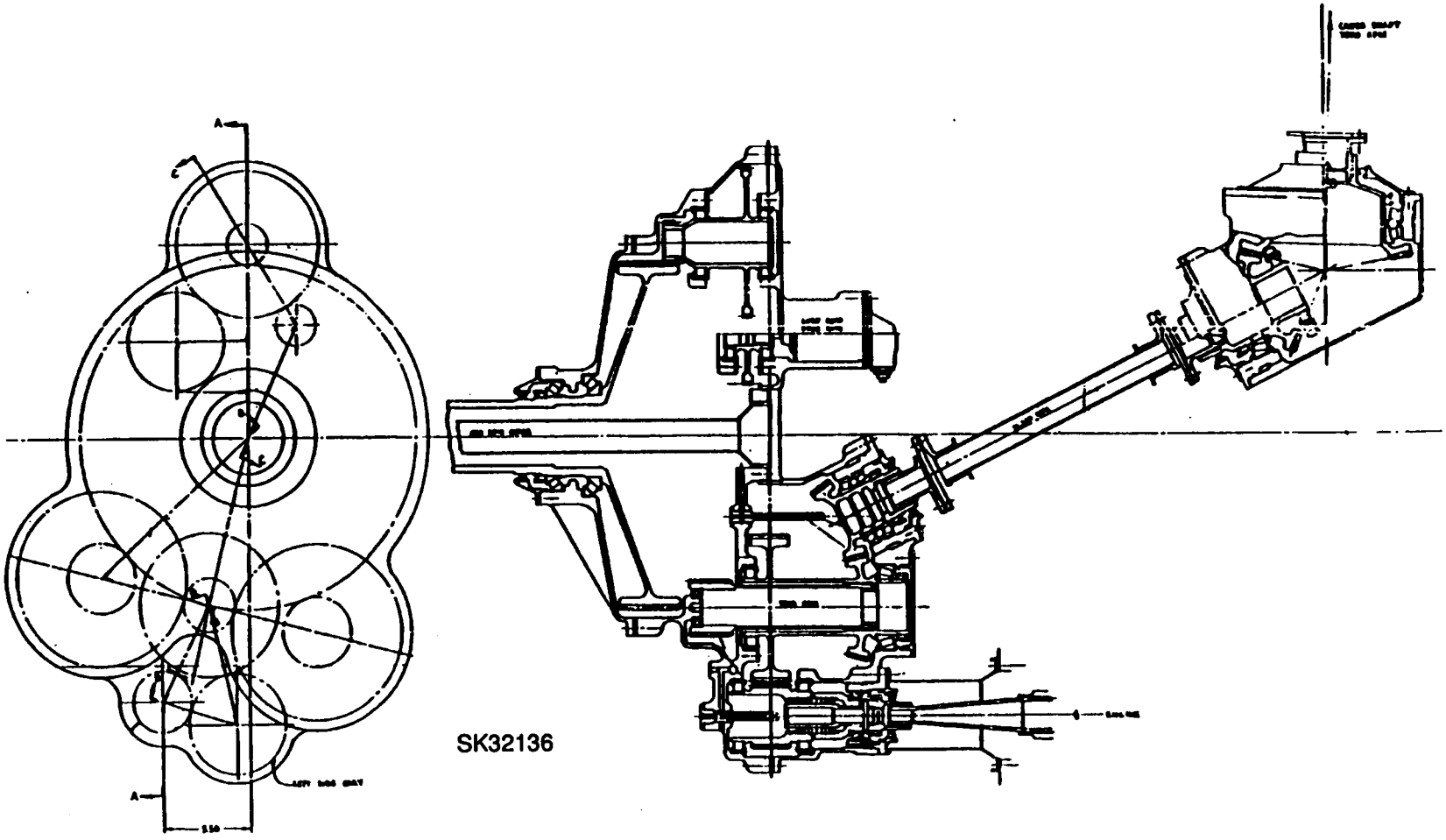

Figure 7. Split-Torque Configuration

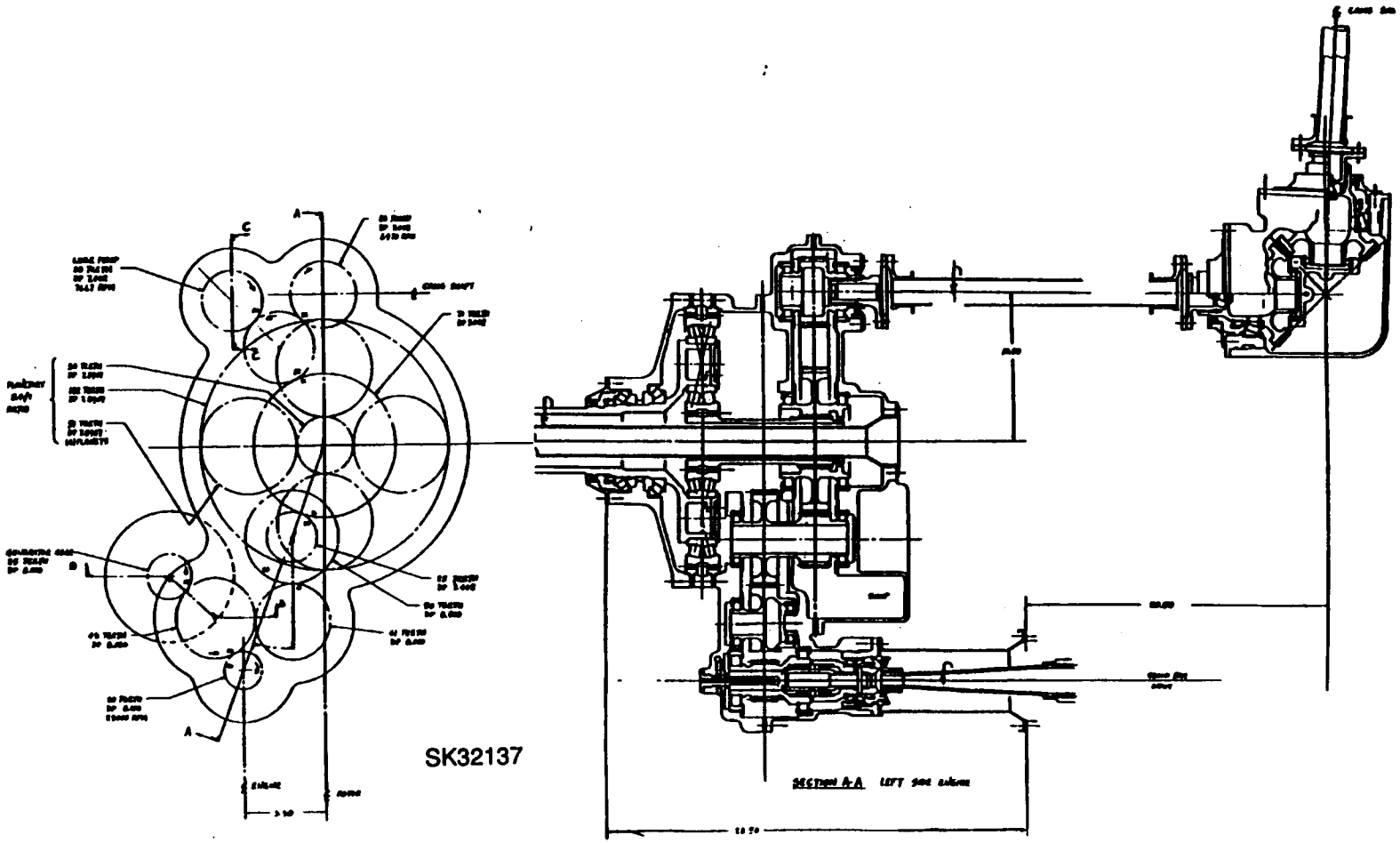

Figure 8. Single-Stage Planetary Configuration

TABLE 2. GEAR COUNT SUMMARY FOR TTR MAIN ROTOR TRANSMISSIONS

Drawing No.	Description		Number of Main Gears 1st rdcn	2nd rdcn	3rd rdcn	4th rdcn	Number of cross-shaft gears	Number of accessory gears*	Total number of gears
SK31646	Main rotor drive system - baseline two-stage planetary	Left	3	6	6	-	5	2	46
		Right	4	6	6	-	5	3	
SK32135	Main rotor drive system - self-aligning bearingless planetary design	Left	4	7	7	7	5	3	66
		Right	3	7	7	7	5	4	
SK32136	Main rotor drive system - split-torque design	Left	3	3	3	-	4	4	34
		Right	2	3	3	-	4	5	
SK32137	Main rotor drive system - one-stage planetary	Left	2	2	6	-	4	2	33
		Right	3	2	6	-	4	2	

*Lube pump may rotate in opposite directions on left and right gearboxes (requiring a -1 and -2 pump). Generator must rotate in same direction on left and right gearboxes.

TABLE 3. BEARING COUNT SUMMARY FOR TTR MAIN ROTOR TRANSMISSIONS

Drawing No.	Description		Number of bearings or rings*							
			Main rotor gearbox						Tilt-axis gearbox	Total number of bearings
			Gear mesh reduction				Cross-shaft	Access.		
			1st	2nd	3rd	4th				
SK31646	Main rotor drive system - baseline two-stage planetary	Left	6	5	6	-	4	4	6	66
		Right	8	5	6	-	4	6	6	
SK32135	Main rotor drive system - self-aligning bearingless planetary design	Left	8	4 rings	1	2	4	4	4	46
		Right	6	4 rings	1	2	4	6	4	
SK32136	Main rotor drive system - split-torque design	Left	6	5	2	-	2	6	4	50
		Right	4	5	2	-	2	8	4	
SK32137	Main rotor drive system - one-stage planetary	Left	4	2	6	-	4	4	4	50
		Right	6	2	6	-	4	4	4	

* All numbers are numbers of bearings unless otherwise noted.

TABLE 4. DRIVE SYSTEM WEIGHT PER AIRCRAFT FOR TTR CONFIGURATIONS

Component	2-stage planetary SK31646	Self-aligning bearingless planetary SK32135	Split-torque SK2136	Single-stage planetary SK32137
Gearbox	1,146.0	866.5	1,058.0	956.2
Rotor shaft	201.6	201.6	192.6	195.4
Lube system	259.0	259.0	239.8	240.0
Cross-shaft	145.8	145.4	138.2	138.2
Internal shaft	10.0	10.0	18.0	8.0
Total system weight (lb)	1,762.4	1,482.5	1,646.6	1,537.8
Lb/hp	0.364	0.306	0.340	0.317

TABLE 5. POTENTIAL FOR NOISE REDUCTION FOR TTR MAIN ROTOR TRANSMISSIONS

Transmission	Feature		Potential noise reduction
Self-aligning bearingless planetary SK32135	Very high gear stresses and deflections	++	
	Critical indexing of 3 gears per spindle	+++	
	Helical gears	-	
	Finer pitch	-	++
	Low pitch line velocity	-	
Split-torque SK32136	Lower power per load path	-	
	Gear stresses and deflections same	+	
	Low pitch line velocity	-	-
Single-stage planetary SK32137	Double helical planetary	--	
	Helical gears throughout	--	
	Finer pitch	-	--
	High pitch line velocity	+	

NOTE: + Potential for noise increase
- Potential for noise reduction

TABLE 6. MTBR RATES FOR TTR MAIN ROTOR TRANSMISSIONS

System subgroup	2-stage planetary SK31646		Self-aligning bearingless planetary SK32135		Split-torque SK32136		Single-stage planetary SK32137	
	Qty	Rate per 1,000 hr	Qty	Rate per 1,000 hr	Qty	Rate per 1,000 hr	Qty	Rate per 1,000 hr
Gear	19	0.119	22	0.138	12	0.075	14	0.088
Shafts/carriers	2	0.032	2	0.032	1	0.016	1	0.016
Bearings	29	0.145	19	0.095	21	0.105	21	0.105
Brg spacer/rtnr	13	0.097	16	0.120	12	0.090	8	0.060
Housing/supports	9	0.044	9	0.044	10	0.049	9	0.044
Lubricators	1	0.001	1	0.001	2	0.002	1	0.001
Dynamic seals	4	0.031	4	0.031	4	0.031	4	0.031
Packing/gaskets	2	0.001	2	0.001	2	0.001	2	0.001
Misc hardware	-	0.019	-	0.019	-	0.019	-	0.019
Clutch	1	0.011	1	0.011	1	0.011	1	0.011
Total rate		0.500		0.492		0.399		0.376
MTBR		2,000		2,033		2,506		2,660

NOTES:

1. Baseline review identified 104 component parts (excluding engine input shaft and housing, interconnecting shafts and shims, and right-angle gearbox).

2. Generically equivalent component failure/replacement rates from CH-46/CH-47 overhaul data provide TTR baseline of 15.9881 replacements per 1,000 hours.

3. Baseline components grouped in subsystems show need for significant improvement to meet 5,000-hr MTBR goal.

TABLE 7. SELECTION PROCESS FOR TTR ROTOR TRANSMISSIONS

Drawing no.	Description	Weight	Potential for noise reduction	Potential for MTBR increase	Producibility & fabrication complexity	Risk factor	Total rank
SK32135	Self-aligning bearingless planetary	1	4	3	4	4	12
SK32136	Split-torque design	4	2	2	2	2	10
SK32137	One-stage planetary	3	1	1	3	1	7
	Weighting factor	0.25	0.25	0.25	0.125	0.125	1.0

Ranking value: 1. Most likely to achieve objectives
4. High probability of not achieving objectives

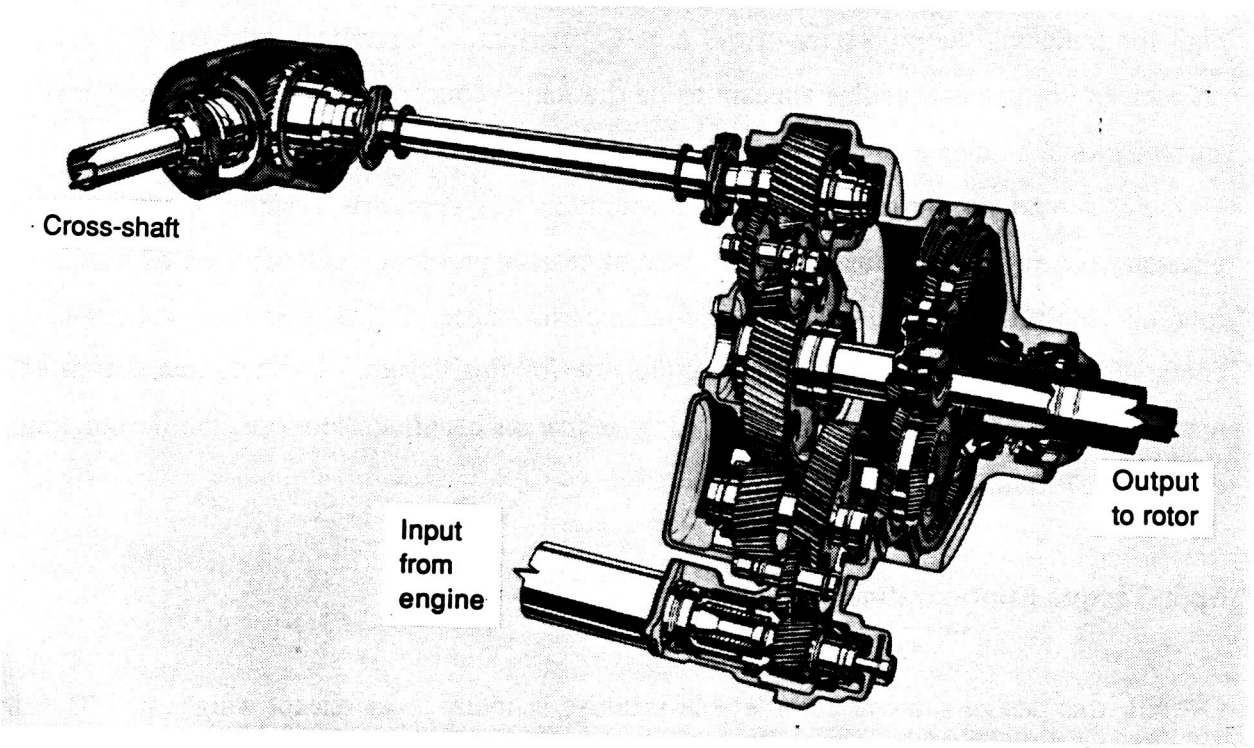

NASA C-89-06714
(CD-89-40562)

Figure 9. Tactical Tiltrotor Transmission in Left Nacelle

program objectives. The basis for selection was a combination of weight, noise, and reliability considerations. The basic configuration is illustrated in Figure 9. This configuration contained extensive application of hybrid (ceramic rolling-element) bearings, hybrid bidirectional tapered-roller bearings, advanced gear and bearing materials, a double helical planetary gear mesh, and helical gearing throughout the rest of the drive train, with the exception of a spiral bevel gear mesh at the nacelle conversion axis gearbox. The speed reduction taken in the planetary stage is roughly 5.28:1, which is a bit higher than typical rotorcraft planetary reductions which are usually in the range of 3 or 4:1. This configuration resulted in a lightweight, compact design, and high reliability gains are expected through a significant reduction in parts count. Highlights of the three transmissions studied are described briefly in the following paragraphs.

Self-Aligning Bearingless Planetary Configuration

The low weight (0.306 lb/hp) and reduced number of bearings of this configuration appear to be the most significant advantages of this design. All other ranking factors are considered very high for achieving the objectives of the A.R.T. program. The critical indexing of three gears on each of six planet spindles appears to be the major concern of this design; problems with current gear manufacturing would make this requirement hard to achieve. Also, any indexing problems would result in high noise and vibration and unknown dynamic loads. Although planetary bearings are eliminated, a new type of bearing problem will be created by each spindle rotating within two sets of rings. Long-term performance of this concept is unknown. The potential for improving MTBR is also quite low for this design. Overall, this design offers many potential problems for a relatively low return on benefits; therefore, the design was not considered further.

Split-Torque Configuration

Overall, this design showed considerable promise in many areas except weight (0.340 lb/hp); the weight of this design appears to be the highest of all four configurations. The biggest

unknown with this transmission is the ability to split the torque 50/50. To ensure an even split, additional features would be required which would further increase weight and reduce the other benefits. Therefore, this design was also rejected.

Conventional Single-Stage Planetary Configuration

Based upon the proposed ranking methodology, this design appears to have the greatest potential of achieving all objectives of the A.R.T. program. Although the transmission trend weight (0.317 lb/hp) is not the lowest, it appears that further work could reduce the weight and achieve the desired goal of 0.30 lb/hp or less. The use of single and double helical gears should significantly reduce noise. Also, this configuration achieves the best improvement in MTBR when compared to the baseline. Although the system still has many potential problem areas, it nevertheless appears to have the lowest risk for achieving the overall objectives of the A.R.T. program when compared to the other configurations. Therefore, Boeing has recommended that this transmission be selected for detailed analysis for Task 4 of this program.

EFFECT OF TRANSMISSION IMPROVEMENTS ON TRANSMISSION AND AIRCRAFT PERFORMANCE

After the selection of the A.R.T. transmission, studies were conducted to determine what effects improvements in transmission weight would have on aircraft size, performance, and operating cost. With the basic parameters of the baseline TTR aircraft established, it was possible to examine the effects on performance of the baseline vehicle by simply reducing the transmission weight without resizing the whole aircraft. Similar studies were also conducted to evaluate mission performance and expected aircraft flyaway cost based upon the expected improvement in the drive system only.

The aircraft performance was evaluated by retrofitting an existing baseline vehicle with the advanced-transmission design. In this case, the empty-weight reduction of the vehicle was used to increase the useful load capacity without increasing the gross takeoff weight. This useful-load increase can then be applied either to fuel or payload. If it is used to increase the fuel load, an extension of the radius of action can be achieved as shown in Figure 10. This figure illustrates a significant improvement in aircraft mission performance when compared with the original baseline data as shown in Figure 3.

The second application of the advanced-transmission technology is to apply the new design to a totally new aircraft design where the drive system benefits can be incorporated into the basic vehicle sizing. In this case, the reduced transmission weight has a spinoff effect with lower gross weight in performing the same mission. The effect on major aircraft design parameters is illustrated in Figure 11. The advanced drive system contributes greatly to a reduction in vehicle gross weight and empty weight. Also, engine power can be reduced from 4,038 to 3,724 hp. The reduction in vehicle gross weight and engine power rating will factor into the acquisition cost of such a vehicle.

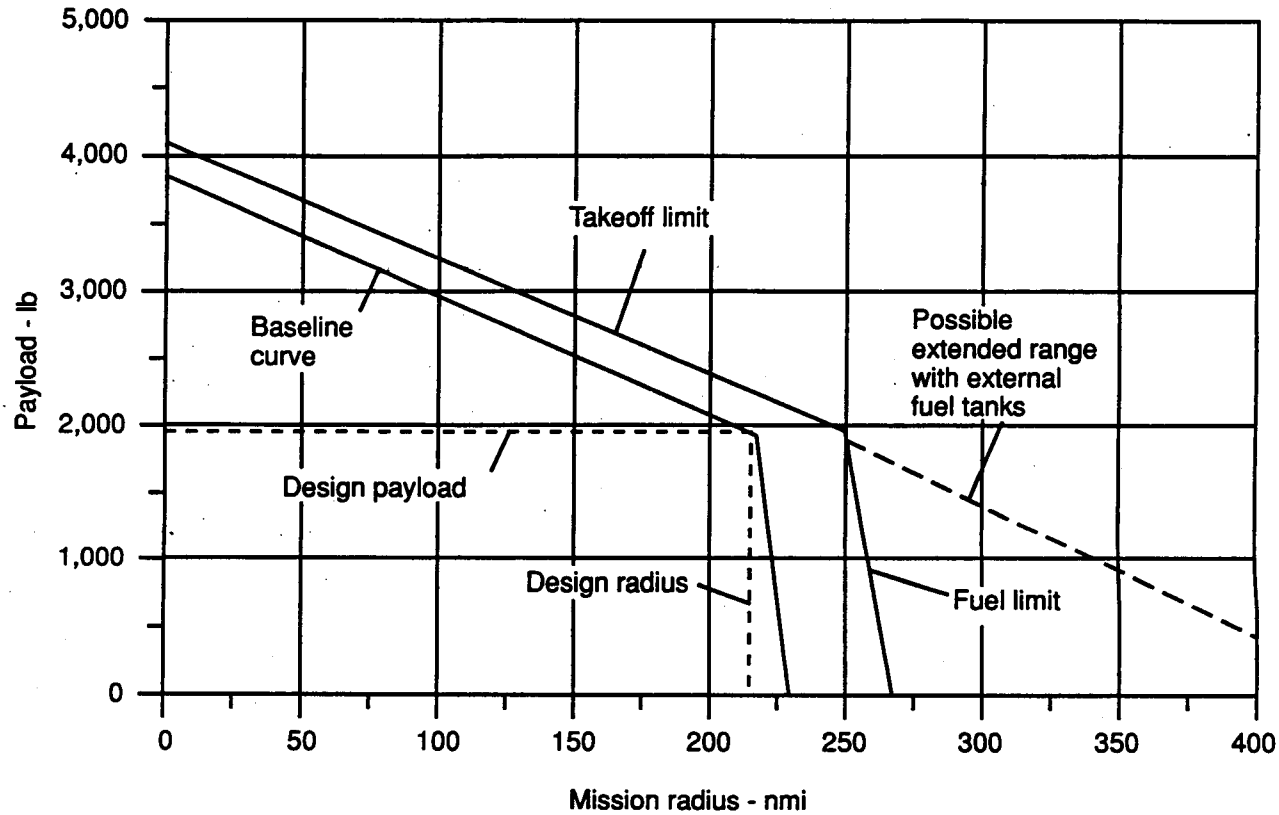

Figure 10. Aircraft Mission Performance With Advanced Rotorcraft Transmission Selected

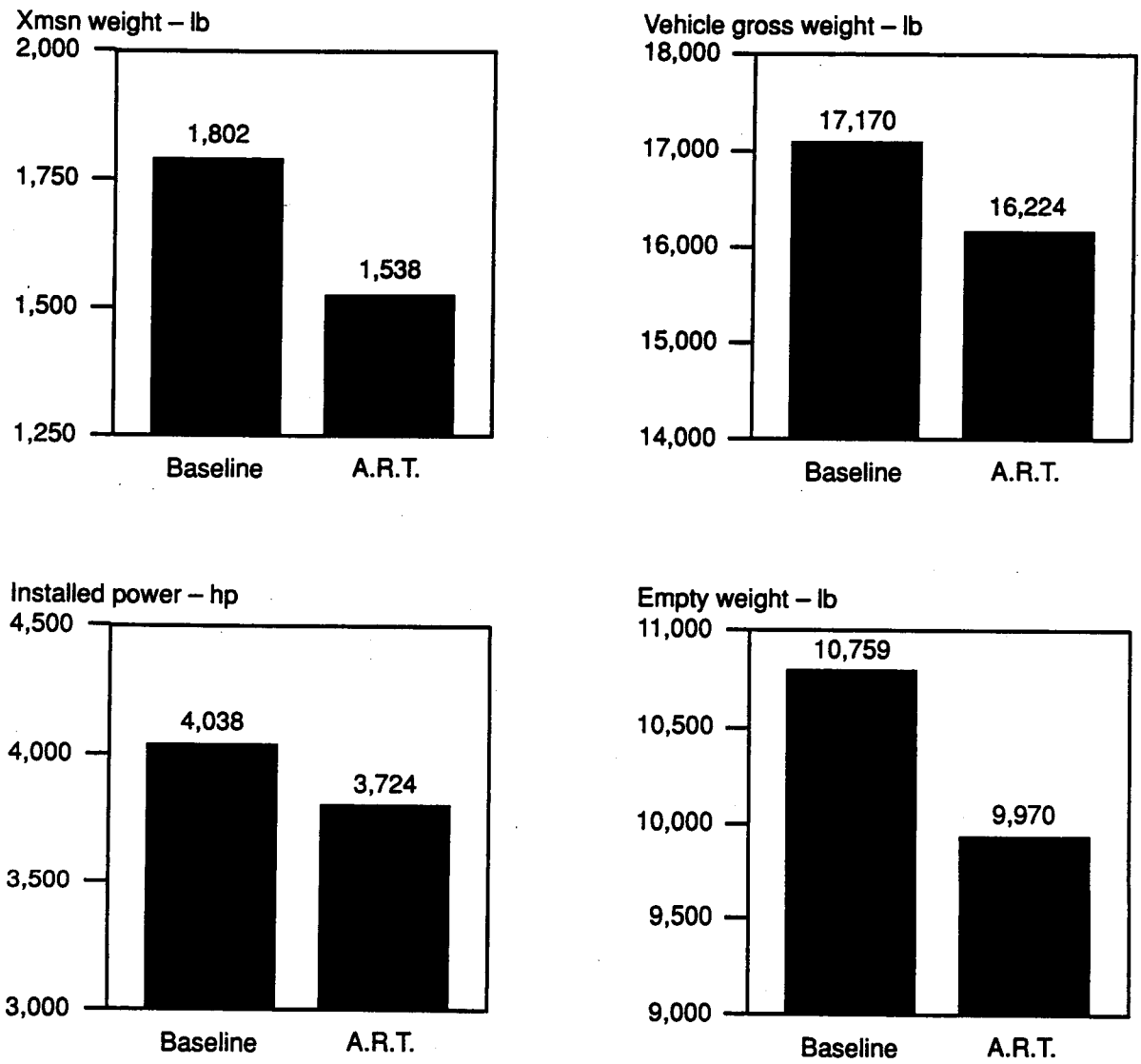

Figure 11. Effects of A.R.T. on Aircraft Design Parameters

In addition to improved aircraft performance, the A.R.T. technology will also impact the TTR aircraft flyaway cost. Cost studies were conducted comparing baseline and a modified A.R.T. aircraft. To evaluate the effect on flyaway cost, trend studies were conducted based upon the assumptions defined in Table 8 concerning the parameters that influence the economic aspects.

The results of these studies are summarized in Figures 12 and 13. In Figure 12, the greatest cost reduction occurs for the dynamic system, which is the result of the improvements identified in the A.R.T. drive system. This results in a 14-percent reduction in drive system cost based upon a 600-TTR-aircraft production run. The reduction in drive system cost also had some smaller effects on the engine (7 percent) and airframe (2 percent) costs. When the component cost breakdowns were incorporated into the flyaway cost, the cost reduction has been reduced to approximately 4 percent. Although the drive system cost reduction is quite significant, the drive system makes up only 10 percent of the total aircraft cost. The cost impact of A.R.T. will still result in a saving of approximately $250,000 per aircraft, or a total program saving of $150 million for a 600-aircraft production run. This cost saving represents a significant payback on the cost of the A.R.T. program. It is anticipated that additional cost savings will be achieved when improved MTBR's are included in the operating cost of the TTR aircraft. The results of this study (Table 9) indicate a 27-percent reduction in life-cycle cost when A.R.T. is incorporated. This is an additional saving of $152,552 for a 600-aircraft fleet.

These mission analyses have indicated that significant improvements in TTR aircraft sizing, performance, and cost can be achieved by incorporating the benefits of the A.R.T. program. These benefits can be achieved by retrofitting an existing aircraft with an A.R.T. drive system, which can result in either an increased mission radius of 17 percent or an increased aircraft payload of 18 percent. Even greater improvements can come from applying the A.R.T. drive system to a new aircraft design, which will have a greater impact on aircraft gross weight and engine power rating requirements. Additionally, the A.R.T. program will also have a significant impact on the acquisition and operating cost of the TTR aircraft. Conservative estimates indicate

TABLE 8. INITIAL VALUES FOR ESTABLISHMENT OF BASELINE COST COMPARISONS

Profit factor	10%
Number of prototypes in development program	3
Total number of production aircraft	600
Number of ground test articles	1
Number of flight test hours	2,000
Time between engine overhauls (hr)	5,000
Time between dynamic system overhauls (hr)	3,500
Transmission system used entire flight?	Yes
Annual interest rate on capital	10%
Depreciation period (yr)	25
Residual value	0
Annual utilization (hr)	420
Customer aircraft buy	60 per year

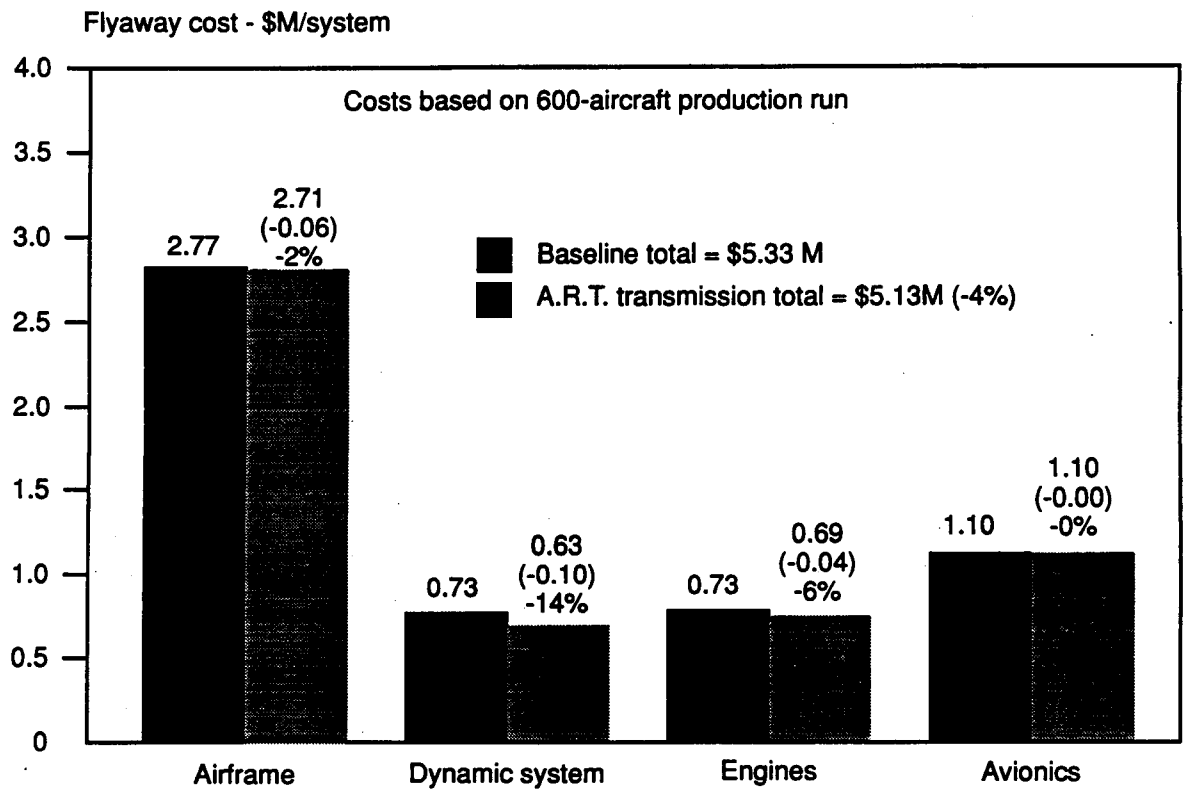

Figure 12. Cost Comparison of Aircraft Major Components

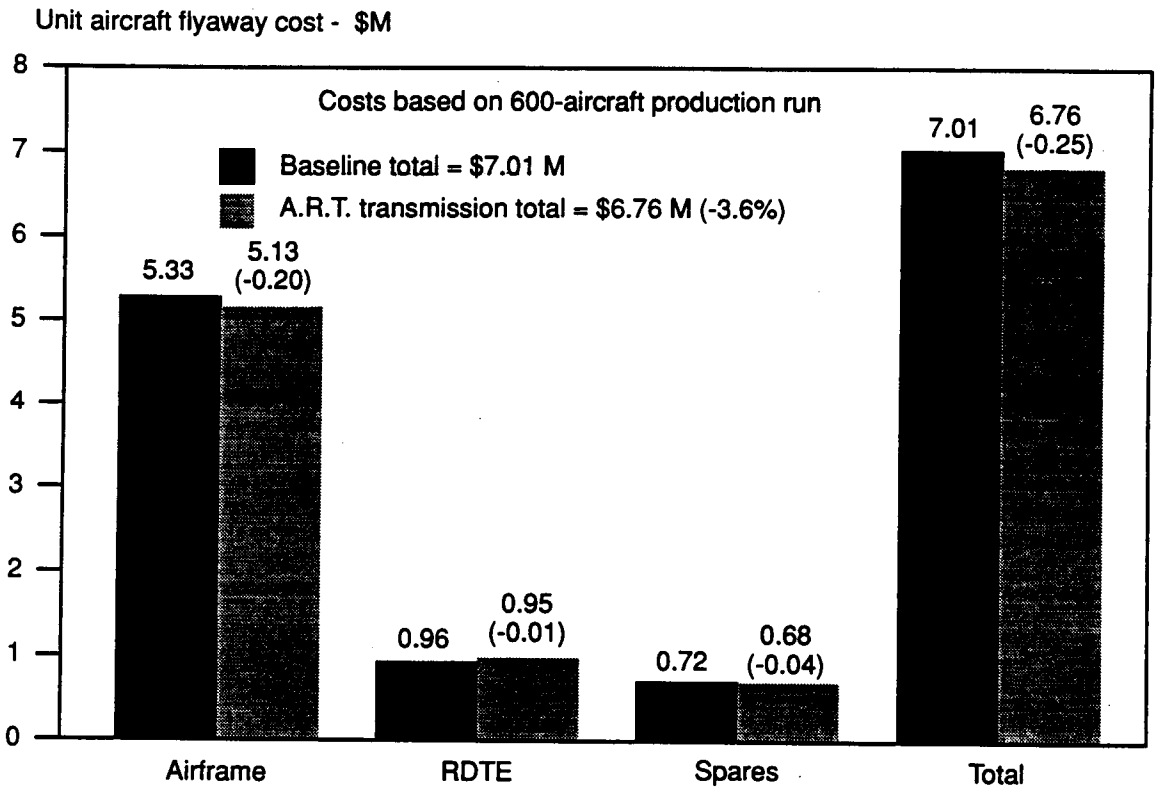

Figure 13. Comparison of Aircraft Flyaway Costs

a potential cost saving of more than $300 million on a production run of 600 TTR aircraft or an approximate cost reduction of $500,000 per aircraft.

TABLE 9. COMPARATIVE COST ESTIMATES[1]

Cost element	Baseline	A.R.T.
Line & base maintenance labor	$ 32,565	$ 24,486
Replenishment spares	245,079	184,275
Depot labor	11,753	8,837
Fuel & lubricants[2]	--	(73,340)
Initial spares	36,178	28,765
Total	$ 325,575	$ 173,023
Life-cycle cost savings of A.R.T.	$152,552 (26.9%)	

NOTES:
1. Costs are shown in 1988 dollars.
2. Cost savings resulting from A.R.T. improvements

DESIGN AND ANALYSIS OF ADVANCED ROTORCRAFT TRANSMISSION

Having selected the single-state planetary configuration as the best candidate for satisfying program objectives, Boeing focused its design efforts on incorporating material and component technologies, integrating airframe requirements, conducting trade studies and analyses, and further developing the design concepts. This section expands on design requirements, technology and design features, and system descriptions.

FINAL CONFIGURATION

The final configuration of the advanced rotorcraft transmission is provided on drawing SK32137, sheets 1 through 5, which is included as Appendix A of this report. Figures 14 and 15 show the TTR right nacelle with the single-stage planetary transmission. This drive train arrangement (Figure 14) consists of two gearboxes, prop-rotor (PRGB) and tilt-axis (TAGB), with interconnecting drive shaft (ICDS), engine outline, rotor controls, and accessory installations. The drive system must function in an upright vertical position (with rotor disk horizontal), then transition to a horizontal position, corresponding to hover and forward flight respectively. Because of the distributed arrangement and variety of positions the gearbox assumes, the lube system which services both PRGB and TAGB requires redundant scavenging from several areas. The PRGB is mounted to structure by the upper cover so that rotor aerodynamic forces and moments do not travel through the gearbox housings. Deflections in the structure between the PRGB and the TAGB are accommodated by the composite ICDS, which has integral flexible diaphragm couplings. The composite wing shafts with integral couplings, which are shown on SK32137, sheet 3, accommodate wing deflections. Rotor control actuators are mounted to the PRGB upper cover and trail back alongside the gearbox to achieve a compact overall design. The engine is shown mounted from the gearbox with struts and a torque tube in order to

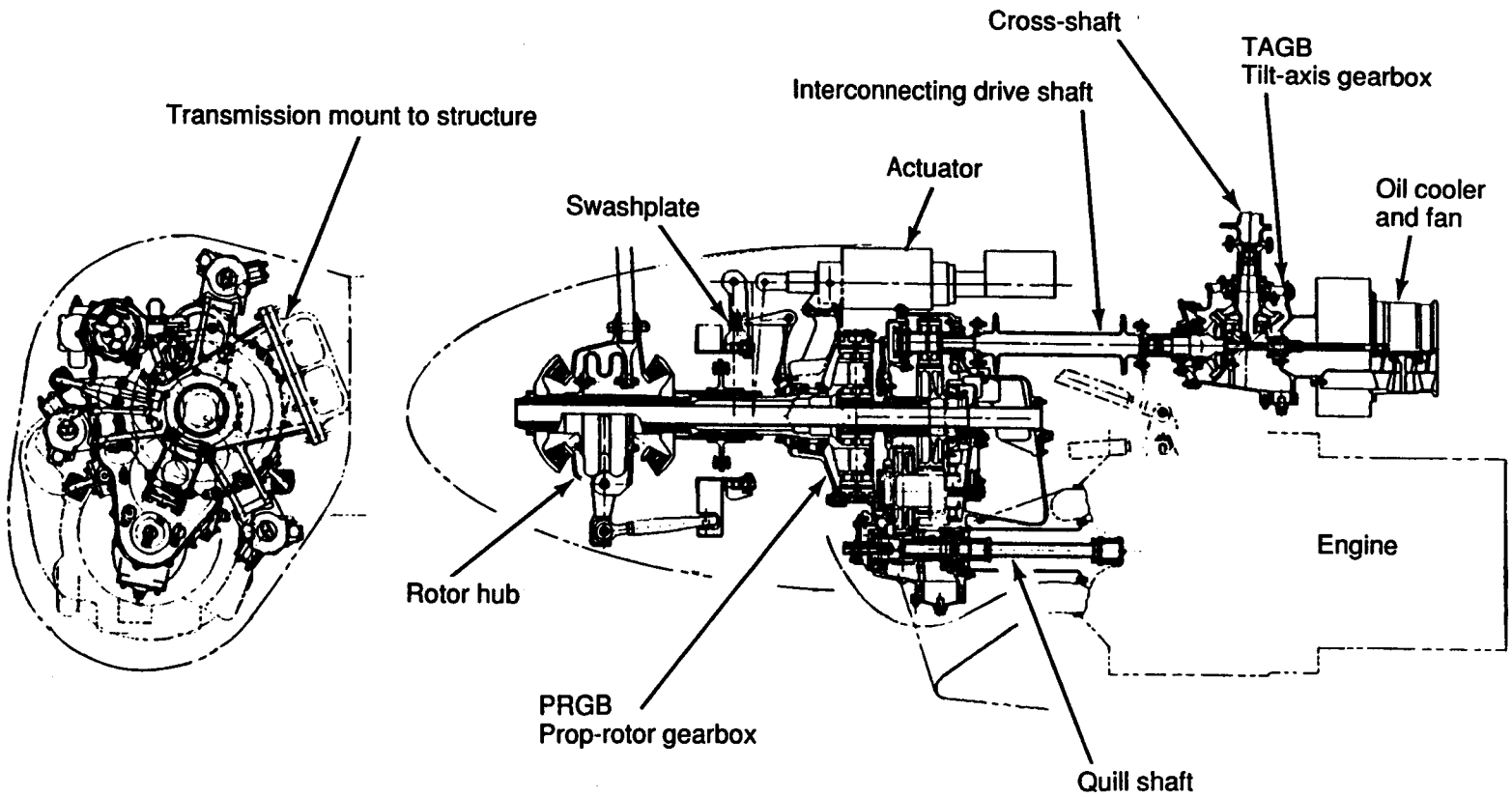

Figure 14. Installation of Advanced Rotorcraft Transmission in Right Nacelle

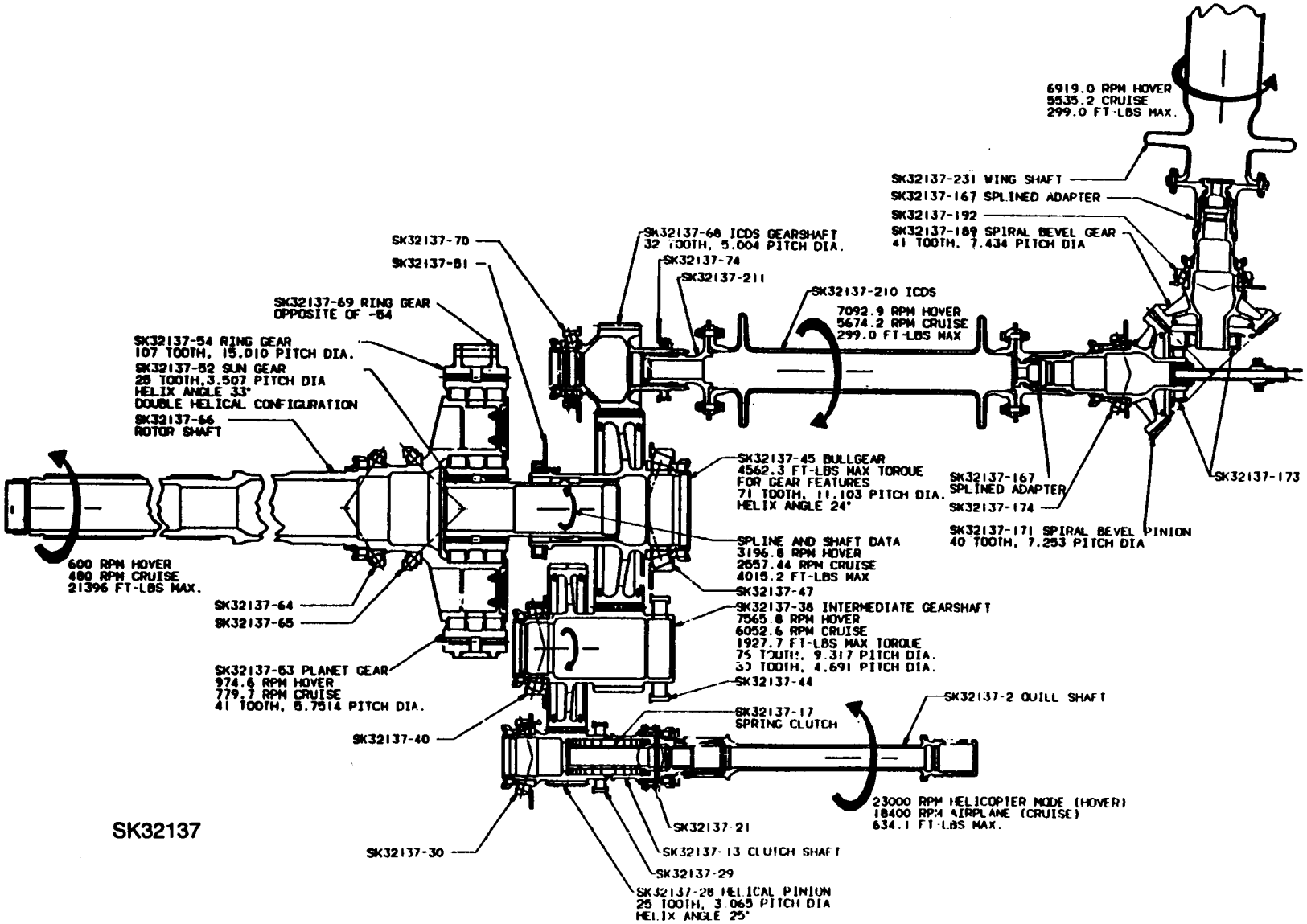

Figure 15. Major Internal Components of Advanced Rotorcraft Transmission

minimize misalignment at the high-speed input shaft. Accessory installations are kept as compact as possible, and sizes shown represent devices with current technology.

Figure 14 shows the major internal components of the A.R.T. gearbox. Power input to the PRGB drive train comes through the splined high-speed quill shaft which turns at 23,000 rpm in the hover mode. Power is then transmitted to the clutch input shaft, SK32137-13. This shaft is supported by a double-row, tapered-roller bearing which reacts moments and thrusts on the shaft. The clutch shaft spline is oil-lubricated and crowned as required to accommodate any misalignment or flexing in the engine mounting system. The -17 spring clutch unwraps and expands under torque to grip the -28 high-speed pinion shaft inner diameter. The pinion shaft and all other internal gear shafts will be fabricated from double-vacuum-melt, high-hot-hardness steel. As viewed from the front of the right PRGB, the input pinion shaft rotates counterclockwise. The -28 pinion is a helical gear with an overall contact ratio of 3.03 for reduced noise and improved load sharing. The 25-tooth pinion mates with a 76-tooth -38 intermediate gear shaft; their common diametral pitch is 8.157. The high pitchline velocity of these gears, 18,455 fpm, will require some lubrication system development to assure proper cooling and lube jet penetration into the mesh. The rotating speed of the intermediate gear shaft is 7,565.8 rpm and the gear ratio for the mesh is 3.04. Both shafts are supported in a straddle-mount configuration, with hybrid bidirectional tapered-roller bearings, SK32137-30 and -40, at the end of the shaft that receives the axial thrust, and -29 and -44 hybrid roller bearings at the other end. The term hybrid refers to the various materials used in the bearing construction, i.e., silicon nitride ceramic rollers, races of double-vacuum-melt, high-hot-hardness steels, and P.E.E.K. (polyether-ether-ketone) retainers. Similar bearing arrangements are used extensively throughout this A.R.T. gearbox and the benefits expected are improved oil-off operation, increased reliability, and lower bearing, housing, and shaft weight.

Within the intermediate shaft, axial thrusts from the two gear meshes are oriented opposing each other, with net thrust from the shaft acting in the forward direction. The generator accessory gear shaft takes power from the 76-tooth gear on the intermediate shaft and turns

counterclockwise at 20,000 rpm during hover. The intermediate gear shaft drives the 71-tooth -45 bull gear at 3,196.8 rpm with a 30-tooth pinion for a 2.37 gear ratio. The diametral pitch for this helical mesh is 6.395 and the overall contact ratio is 2.83. Axial thrust from the bull gear is reacted by the -47 bidirectional hybrid tapered-roller bearing into the housing, and the other end of the shaft is supported by the -51 hybrid roller bearing. The bull gear shaft rotates in the counterclockwise direction when viewed from the front of the right gearbox.

Also driven from the 71-tooth bull gear are the -68 ICDS and accessory gear shafts -128 and -144. The ~~internal spline at the forward end of the bull gear shaft~~ supports and drives the sun gear shaft. The -52 sun gear shaft is supported and retained axially at the opposite end by the double helical planetary gearset that it drives. In this final drive stage, the four planets are mounted with hybrid roller bearings on the planet posts, which are a part of the -66 rotor shaft. Two ring gears, -54 and -69, separated by a spacer, are attached directly to the housing and the -57 cover. Reduction through this stage is 5.28:1, bringing the overall drive reduction to approximately 38.3:1. The right rotor shaft turns counterclockwise, delivering a maximum torque of 21,369 ft-lb at 600 rpm. Each helical sun gear has 25 teeth with a diametral pitch of 7.129 and rotates at 3,196.8 rpm. The helical planet gear has 41 teeth and turns at 974.6 rpm on its post. The stationary ring gear has 107 teeth. The rotor shaft/planet carrier is supported by two high-contact-angle, tapered-roller bearings that react all rotor loads into the -57 cover, which carries the loads into the structure.

The left nacelle contains a similar drive system as described above and is linked to the right system with the ICDS, TAGB, and wing shaft. Power transfer normally may be quite low in the TAGB and shaft portion of the drive system, but transfer occurs when the rotors are loaded unequally or there is an engine out. With an engine out, the remaining engine will drive both rotors. The 32-tooth -68 ICDS gear shaft turns at 7,092.9 rpm and transmits power to the ICDS and then to the TAGB and wing shaft. When viewed from the front of the right gearbox, the ICDS is turning clockwise. The ICDS and the wing shafts are braided-composite shafts with integral flexible couplings. The splined shaft adapters at each end are grease-lubricated. The

spiral bevel TAGB gear shafts have 40 and 41 teeth for pinion and gear respectively for a nonhunting gear configuration. The shaft intersection angle is 92 degrees to allow for a forward-swept wing. As in the PRGB, the shaft bearings are thrust-carrying, bidirectional hybrid tapered-roller bearings and a hybrid roller bearing in a straddle-mount arrangement.

Drive train components from the engine to and including the -45 bull gear are designed for the one-engine-inoperative (OEI) condition or 2,777 hp at hover shaft speeds of 23,000 rpm. Components in the drive train between the left and right nacelles, from the bull gear through the ICDS, TA~~GB,~~ ~~and wing shafts~~, ~~are designed for 60 percent~~ of the OEI power, or 1,667 hp at hover shaft speeds. From the bull gear to the rotor, design loads were 60 percent of the installed engine power, or 2,424 hp AEO at hover shaft speeds and 1,939 hp AEO at cruise/forward flight shaft speeds. In Appendix A, sheet 1 of SK32137 contains a schematic diagram reflecting these design conditions.

Table 10 summarizes data extracted from our TTR proposal corrected to show the benefits of incorporating the A.R.T. drive system into the production aircraft.

TECHNOLOGICAL FEATURES

Several new-technology components are being investigated for incorporation into the A.R.T. drive system and are the subject of component testing as part of the A.R.T. program first phase:

- Noise reduction by active force cancellation: Noise waveforms are analyzed through a microprocessor and an antinoise waveform is generated 180 degrees out of phase with the original. Early tests show that noise reduction of 10 db or greater can be achieved.

- Hybrid bidirectional tapered-roller bearings: A high-load-capacity bearing with ceramic rolling elements and P.E.E.K. composite cages which react thrust in two directions. This bidirectional thrust capability eliminates the need for an additional bearing and shim

to preload the major thrust bearing. Weight savings stem from reduced number of bearings and lightweight materials.

- Improved bearing technologies through development of improved life-prediction theory, optimized hybrid bearings, and investigation of rolling-element surface interaction.

- Hybrid bearing minimum-lube study will yield information for lube system design and no-lube tolerance.

- Precision net-forged spur gears show potential for reducing machining of material and energy requirements, increasing fatigue life, and increasing endurance limit.

- High-profile contact ratio, noninvolute tooth form spur gears show potential for reducing noise and increasing load capacity through improved load sharing on gear teeth.

- Parallel-axis gear noise study investigates noise benefits of various gear tooth configurations and forms.

- Surface-modified titanium helical accessory gears with modified wearing surfaces at gear teeth and bearing journals show potential weight reduction for accessory drives, which are generally sized more by geometric requirements than load capacity.

DESIGN FEATURES

The A.R.T. transmission incorporates the following features in its design:

- Double helical gears at planetary output stage and helical gears throughout provide a high-contact-ratio, low-noise gear design. In addition, there are no net axial gear loads at the planetary output stage because of the double helical design.

- Resin-transfer-molded composite shafts with integral couplings use fewer parts and interfaces and lighter materials to yield significant weight reductions, corrosion resistance, and a reduction in maintenance.

- Double-vacuum-melt, high-hot-hardness carburizing steels will be used for gear shaft and bearing races.

- WE43 magnesium used for cast housings provides greater corrosion resistance and higher temperature capability.

- Spring clutch design uses fewer parts than ramp roller or sprag clutch designs.

- Accessory installations involve minimal gear meshes and related parts and employ titanium gear shaft designs. Polyimide adapters are used to reduce lube oil requirements. The generator shown is a high-speed, compact, dc machine compatible with current helicopter electrical systems. Fan installation is direct-driven from TAGB. Overall, accessories as configured will reduce weight and parts count.

- Lube system is compact, highly redundant, and ballistically tolerant. Five-micron filtration improves reliability and life while maintaining small filter package size. Aramid fiber composite sump design is lightweight and ballistic tolerant. The main sump has an internal auxiliary sump to support redundant lube systems.

- Rotor loads are not reacted through the gearbox magnesium casting but are taken out at the transmission forged-aluminum upper cover. This allows the gearbox casting to be designed for minimum weight.

- Segmented seal at rotor mast has Teflon field-replaceable elements. Pumping lip seals and carbon face seals are used at other locations.

- Vibration diagnostics provide health monitoring to attain real-time flight safety analysis.

- 3D computer design of hardware will work in a complementary way with weight and stress analysis, finite-element modeling requirements, computer-aided manufacturing, and inspection.

- Engine supported from transmission case for accurate input shaft alignment.

Description and Analysis of Gear Design

The anticipated successful performance of the gears used in the A.R.T. drive system is based on the incorporation of good design practice in combination with the proper analytical techniques and the selective application of new technology. This section presents the basic design practices employed in developing the gear designs, a synopsis of the analytical methodology used, potential new technology that may be applied, and the resulting load-rating factors for the gears in the A.R.T. drive system.

The gears used in this transmission are generally of integral design, thus eliminating the need for mechanical or welded connections between the gears and their supporting shafts. This technology was first developed by Boeing and is used on current production drives with great success. In addition, the contact ratio of the gears was optimized to provide maximum performance with minimum noise level. Helical gears are used throughout the design, with the exception of the spiral bevel set used at the TAGB. The planetary output-stage gears have been configured as double helicals to eliminate the net external thrust loads. Pending the outcome of noise and durability testing, the planetary stage may be reconfigured using high-contact-ratio, noninvolute tooth form spur gears (HCRNIV). The unconventional tooth form could reduce transmission weight by approximately 21 pounds and reduce assembly problems.

Methods of Analysis - The two gear computer programs that were used to assess the basic fatigue load capacity and other pertinent factors affecting the gear performance in the A.R.T. drive system are described briefly here.

SPURICAL - This program analyzes bending stress (strength), contact stress (durability), flash temperature (scoring hazard), elastohydrodynamic lubrication (EHL) film thickness (wear resistance), and tooth profile kinematics (wear, scoring, and durability) for parallel-axis gears. It will accommodate external or internal gears of either spur, single helical, or double helical type. It also provides the complete geometric definition required to prepare an engineering drawing for each gear analyzed. The tooth loads that must be reacted by the bearings are also generated for direct input to the bearing analyses described in a subsequent section.

R20 - This program analyzes bending stress (strength), contact stress (durability), and flash temperature (scoring hazard) for bevel gears. It will accommodate spiral, Zerol, and straight bevel gears with various tooth configurations, including the tilted root lines and small cutter configurations frequently required for integral bevel gears. Like its parallel-axis counterpart, it also provides the complete geometric definition required to prepare an engineering drawing for each gear analyzed. The tooth loads for any combination of hand of spiral and direction of rotation that must be reacted by the bearings are also generated for direct input to the bearing analyses described later.

The allowable stresses used in these analyses were 40,000 psi bending stress for spur, helical, and bevel gears and 165,000 and 245,000 psi contact stress for the parallel-axis and bevel gears, respectively. The allowable flash temperatures used were 350°F and 550°F, respectively, for parallel-axis and bevel gears. Obviously, each of these limits is not reached simultaneously in every gear set. In addition, since the gears and bearings are designed as a system rather than as components, allowable limits may not be reached on some gears due to optimization of the

gear and bearing system. This approach may result in a gear slightly larger than required but an overall gear and bearing system of minimum weight.

Gear Design Loads - The gear design loads are based on the expected maximum torque from the power spectrum for the TTR aircraft mission. Unlike the bearings which are designed to a finite life requirement, the gears are designed for infinite life at the maximum torque condition.

The results of this analysis and the selection of the gear sizes for the A.R.T. drive system are summarized in Table 11.

Basic Design Practices - The following design practices have been developed over many years of helicopter experience and are adhered to in order to achieve the maximum gear performance:

A. Wherever possible, gears are integral with their shafts; thus no joint problems can occur.

B. Slip ratio (specific sliding velocity) was maintained near or below unity for all low-contact-ratio designs, if any.

C. All gear teeth use modified profiles to accommodate expected tooth deflections under load.

D. Planetary tooth numbers are selected to have a completely nonfactorizing design (i.e., only a single tooth pair either starts or ends engagement anywhere in the system at any given moment).

E. Face contact ratios are maintained above 2.0 for all helical gears and 1.85 for all bevel gears.

TABLE 11. GEAR ANALYSIS SUMMARY

Component (see Fig. 15 & Appendix A)	Type	Pitch dia (in.)	No. teeth	Face width (in.)	Hel/ spir angle (deg)	Power[1] (hp)	Speed (rpm)	Gear loads: Tangential (lb)	Thrust (lb)	Separating (lb)	Moment (in.-lb)	Bending stress (psi)	Contact stress (psi)	Flash temperature (°F)
SK32137-28 input pinion	Helical	3.065	25	2.30	25	2,777	23,000.0	4,965.8	2,315.6	2,555.0	3,548.6	34,148.3	140,023.3	345.1
SK32137-38 intmd shaft 76T gear	Helical	9.317	76	2.30	25	2,777 60.3	7,565.8	4,965.8[2] 107.78[3]	2,315.6[2] 50.26[3]	2,555.0[2] 55.46[3]	10,787.7[2] 234.15[3]	30,243.0[2] 1,825.2[3]	140,023.3[2] 32,564.9[3]	348.2[2] 214.9[3]
SK32137-38 intmd shaft 30T gear	Helical	4.691	30	2.85	24	2,777	7,565.8	9,862.1	4,390.9	5,034.0	10,299.3	39,973.5	147,176.4	310.5
SK32137-45 bull gear shaft	Helical	11.103	71	2.80	24	2,777 1,667 72.4 1.0	3,196.8	8,608.3[4] 5,920.0[5] 257.12[6] 3.55[7]	3,832.7[4] 2,635.7[5] 114.48[6] 1.58[7]	4,394.0[4] 3,021.8[5] 131.24[6] 1.81[7]	21,277.2[4] -14,630.8[5] 250.63[6] 8.77[7]	36,621.8[4] 25,130.5[5] 1,855.3[6] 21.34[7]	146,519.7[4] 118,678.1[5] 41,235.3[6] 3,941.6[7]	309.8[4] 280.3[5] 217.0[6] 200.4[7]
SK32137-68 ICDS gear shaft	Helical	5.004	32	2.40	24	1,667	7,093.0	5,920.0	2,635.8	3,021.8	6,594.8	27,457.0	118,678.1	280.3
SK32137-52 planetary sun gear	Double helical[8]	3.507	25	1.50	33	2,424/4	3,196.8	3,405.4	2,211.5	1,681.9	3,879.2	32,725.1	135,047	246.1
SK32137-54 & 69 planetary ring gear	Double helical[8]	15.0097	107	1.50	33	2,424/4	0.0	3,405.4	2,211.5	1,681.9	6,361.8	26,936.3	62,179.8	204.5
SK32137-53 planet gear	Double helical[8]	5.7514	41	1.50	33	2,424/4 2,424/4	1,580.0	3,405.4	2,211.5	1,681.9	6,361.8	31,229.0[9] 28,354.6[10]	135,047[9] 62,179.8[10]	246.5[9] 204.5[10]
SK32137-171 tilt-axis spl bev pinion shaft	Spiral bevel	7.2529	40	1.52	30	1,667 1,667	7,093.0	4,798.9	114.4[11] 3,785.6[12]	3,786.9[11] 149.7[12]	352.9[11] 11,684.6[12]	28,817	204,548	278.7
SK32137-189 tilt-axis spl bev gear shaft	Spiral bevel	7.4343	41	1.52	30	1,667 1,667	6,920.0	4,798.9	3,780.6[11] 17.5[12]	246.4[11] 3,788.5[12]	11,960.7[11] 55.3[12]	28,860	204,548	278.7

TABLE 11. GEAR ANALYSIS SUMMARY (Continued)

Component (see Fig. 15 & Appendix A)	Type	Pitch dia (in.)	No. teeth	Face width (in.)	Hel/ spir angle (deg)	Power[1] (hp)	Speed (rpm)	Gear loads: Tangential (lb)	Thrust (lb)	Separating (lb)	Moment (in.-lb)	Bending stress (psi)	Contact stress (psi)	Flash temperature (°F)
SK32137-111 generator	Helical	3.555	29	0.80	25	60.3	19,828.5	107.78	50.26	55.46	89.34	1,360.0	32,564.9	214.9
SK32137-123 hydr pump, shaft, main	Helical	5.3168	34	1.20	24	72.4	6,675.7	257.12	114.48	131.24	304.33	2,415.8	42,409.3	219.7
SK32137-128 hydr pump, shaft, idler	Helical	4.3785	28	1.20	24	72.4	8,106.2	257.12	114.48	131.24	250.63	2,494.7[13] 2,449.0[6]	42,409.3[13] 36,743.8[6]	219.7[13] 214.3[6]
SK32137-144 aux pump shaft	Helical	5.6296	36	0.80	24	1	6,304.8	3.55	1.58	1.81	4.45	32.1	3,941.6	200.4

NOTES:
1. OEI power at input shaft, intermediate gear shaft, and bull gear, AEO power at planetary system, 60% OEI power at ICDS gear shaft, and TAGB
2. Gear data for jackshaft meshing with input pinion
3. Gear data for jackshaft meshing with generator gear
4. Gear data for bull gear meshing with jackshaft
5. Gear data for bull gear meshing with tilt-axis takeoff gear
6. Gear data from idler meshing with bull gear
7. Gear data for aux pump meshing with bull gear
8. Loads on one helical gear only
9. Gear data for planet meshing with sun gear
10. Gear data for planet gear meshing with ring gear
11. Loads when the crossbox pinion is the driving member
12. Loads when the crossbox gear is the driving member
13. Gear data from idler meshing with main pump gear

F. Gears and gear shafts are designed to avoid all damaging resonant conditions where practical. Damping for gear resonance will be provided when analysis and testing reveal a requirement.

G. All gears and shafts shall be serialized and manufactured to the requirements defined in Boeing document D210-11000-1[2].

Description and Analysis of Bearing Design

The anticipated successful performance of the bearings used in the A.R.T. drive system is based on the incorporation of good design practice in combination with the proper analytical techniques and application of new technologies. This section presents the basic design practices, a synopsis of the analytical programs and new technologies, and the resulting B-10 lives for the bearings in the A.R.T. drive system.

The design practice used in the A.R.T. drive system was to support all gear shafts with two hybrid roller-type bearings. These bearings would incorporate ceramic rolling elements in conjunction with rings that are produced from double-vacuum-melt, high-hot-hardness (H^3) carburizing steels. These steels could be either M50 NiL, CBS 600, VASCO X2M, or any combination of these. One bearing on each shaft will be a new-technology, hybrid, bidirectional tapered-roller bearing and the other end of the shaft will be supported by a hybrid, cylindrical-roller bearing which in most cases will operate directly on the integral shaft journal. This bearing configuration has resulted in a minimum of bearings, reduced assembly problems, fewer hardware components, and the highest capacity bearings for each shaft configuration.

Methods of Analysis - The following lists the bearing computer programs that were used to assess the bearing lives, internal load distribution, internal geometry, and other pertinent factors affecting bearing performance in the A.R.T. drive system.

S-73 Bearing Life Analysis Program - This program analyzes high-speed, tapered-roller and cylindrical-roller bearings and accounts for speed effects, EHL, and internal load distribution. The program was modified to analyze the new-technology, bidirectional, tapered-roller bearings used in the A.R.T. drive system.

Planetary Bearing Life Program - This program was used to analyze the planetary bearing of either spherical or cylindrical roller design. The program accounts for the effect of the outer race (gear member) flexibility and for its effect on the internal load distribution. The effect of internal radial clearance on bearing fatigue life was also determined.

The basic life calculation procedures used in these programs are based on the material life factor of unity. This factor is applicable to 52100 air-melt steel which will not be used in this application. The appropriate material factor for the bearing components used in the A.R.T. drive system has been established as 10. This factor includes the use of double-vacuum-melt, high-hot-hardness carburizing materials and ceramic rolling elements made from NBD-100 silicon nitride. The factor of 10 is considered realistic and relatively conservative for these materials which will be available for the FAAV aircraft production.

Bearing Design Loads and B-10 Life - The bearing fatigue loads are based on the expected cubic mean torque from the power spectrum for the TTR aircraft mission. For this aircraft, bearing fatigue loads were based upon the basic mission profile of 30 percent of the time in the helicopter mode and 70 percent of the time in the airplane mode.

An approximate mission profile was established for each flight mode. For this study, transient flight condition occurrences were not considered to have a significant impact on the effect of the cubic mean power for the bearing life calculations. Therefore, the derivation of the cubic mean torque (CMT) was developed by using the following relationship:

$$CMT = \left[\sum_{i=1}^{n} T_i^3 \; t_i\right]^{\frac{1}{3}} \tag{2}$$

where T_i = torque for any given flight condition and aircraft loading

t_i = decimal percentage occurrence for any given flight condition and aircraft loading

n = total number of combinations of flight condition and aircraft loading

For the TTR aircraft, a cubic mean power of 66 percent of the maximum power rating of the aircraft engines was established. At the cubic mean and at OEI power, the following bearing B-10 lives were used to select the bearing sizes as shown in the various sketches:

Load Condition	Minimum B-10 Life (includes material factor)
Maximum power rating (100-percent OEI)	500 hours
Cubic mean power (66-percent max)	5,000 hours

The bearings were selected to meet the above criteria. This means that both conditions must be met in bearing sizing. The results of this analysis and the selection of the bearing sizes for the A.R.T. drive system are summarized in Table 12.

Basic Design Practices - The following design practices have been developed over many years of helicopter experience and are adhered to in order to achieve the maximum bearing performance relative to the in-service bearing lives.

TABLE 12. BEARING ANALYSIS SUMMARY

Location (see Fig. 15 & Appendix A)	Vendor & similar part no.	Dwg dash no.	Inner dia (in.)	Outer dia (in.)	No. rlr	AEO[1] power (hp)	Rlr dia (in.)	Cont ang (deg)	Radial load at AEO max pwr (lb)	Thrust load at AEO max pwr (lb)	Speed (rpm)	Load cap.[2] (lb)	B-10 life at cubic mean power[3]	B-10 life at AEO max power[3]	B-10 life at OEI power[3]	Shaft slope at brg (in./in.)
-28 input	Timken 29500	-30	2.625	4.25	26	2,424	0.350	17.0	2,954.6	2,789.3	23,000.0	5,950	4,590	1,095	670	0.0000845
pinion	MRC MR-211	-29	2.500	3.937	14		0.551	0.0	2,128.2	0.0		17,510	16,744	4,279	2,700	0.0000776
-13 clutch	Timken LL510700	-21	2.50	3.625	31	2,424	0.240	15.1	0.0	0.0	23,000.0	2,090	>100,000	>100,000	>100,000	0.0
shaft	Timken LL510700	-21	2.50	3.625	31		0.240	15.1	0.0	0.0		2,090	>100,000	>100,000	>100,000	0.0
-38 intmd	Timken 497A	-40	3.375	5.375	23	2,424	0.460	16.5	8,354.7	2,075.3		8,330	11,337	2,299	1,358	0.0001513
gear shaft	MRC MR-217	-44	3.8386	5.9055	16		0.787	0.0	7,049.4	0.0	7,565.8	38,450	20,902	5,116	3,188	0.0001399
-45 bull	MRC MR-1920	-51	4.2126	5.5118	24	2,424	0.512	0.0	3,633.8[4]	0.0	3,196.9	21,780	54,008[4]	12,381[4]	7,549[4]	0.0001087
gear shaft	Timken 64400	-47	4.500	7.000	25		0.590	19.0	11,176.2[4]	6,468.6[4]		14,800	16,838[4]	3,440[4]	2,029[4]	0.0001196
-68 ICDS	Timken 390	-70	2.25	4.3307	22	201.9	0.410	15.0	4,293.1[4]	2,635.9[4]		5,340	-	-	652[4]	0.0003407
gear shaft	MRC MR-111K	-74	2.4606	3.5433	18		0.394	0.0	2,803.4[4]	0.0	7,093.9	11,260	-	-	1,054[4]	0.0002883
-53 planet	Special two-	-53														
gear	row roller	-53	1.42	2.08	16	2,424	0.660	-	13,621.0	0.0	1,580.2	44,621	-	-	-	-
-66 rotor	Timken (special)	-63	4.75	NA	38	2,424	0.375	35.0	4,866.4[5]	4,224.6[5]		NA	-	4,663[5]	-	0.0000558
shaft	Timken (special)	-65	5.00	NA	31		0.500	45.0	3,676.4[5]	-14,824.0[5]	605.5	NA	-	5,283[5]	-	0.000569
-171 TAGB	Timken 29600	-174	2.875	4.4375	27	201.9	0.350	18.0	4,686.6[4,7]	3,785.6[4,7]	7,093.9	5,960	-	-	531[4,7]	0.0001567
pinion shaft	MRC MR-208[6]	-173	1.8898	3.1496	12		0.472	0.0	5,403.8[4,7]	0.0	7,093.9	11,510	-	-	303[4,7]	0.0001527
-189 TAGB	Timken 29600	-192	2.875	4.4375	27	201.9	0.350	18.0	4,258.6[8]	3,780.6[8]	6,920.0	5,960	-	-	752[8]	0.0002301
gear shaft	MRC MR-208[6]	-173	1.8898	3.1496	12		0.472	0.0	5,132.6[8]	0.0	6,920.0	11,510	-	-	410[8]	0.0002255
-111 gen	Timken L44600	-113	1.000	1.98	19	60.3	0.210	14.0	85.17	50.3		1,620		>100,000	-	0.0001331
shaft	MRC MR-1907	-118	1.5217	2.1654	16		0.250	0.0	42.90	0.0	19,828.5	4,400		>100,000	-	0.0001075
-123 gear	MRC MR-108	-142	1.7717	2.6772	14	72.4	0.354	0.0	126.3	0.0		7,680	>100,000	>100,000	-	0.0000501
hyd & lube	Timken L68100	-138	1.3775	2.3612	23		0.210	15.5	193.5	114.5	6,675.9	2,070	>100,000	>100,000	-	0.0000797
pump shaft																

TABLE 12. BEARING ANALYSIS SUMMARY (Continued)

Location (see Fig. 15 & Appendix A)	Vendor & similar part no.	Dwg dash no.	Inner dia (in.)	Outer dia (in.)	No. rlr	AEO[1] power (hp)	Rlr dia (in.)	Cont ang (deg)	Radial load at AEO max pwr (lb)	Thrust load at AEO max pwr (lb)	Speed (rpm)	Load cap.[2] (lb)	B-10 life at cubic mean power[3]	B-10 life at AEO max power[3]	B-10 life at OEI power[3]	Shaft slope at brg (in./in.)
-128 idler gear, hyd & lube pumps	Timken L44600	-113	1.000	1.980	19	72.4	0.210	14.0	314.02	0.0		1,620	>100,000	>100,000	-	0.0003784
	MRC R-105K	-130	1.1417	1.8504	12		0.276	0.0	252.42	0.0	8,106.2	4,010	>100,000	>100,000	-	0.0003636
-144 aux pump shaft	MRC MR-206	-146	1.4173	2.4409	12	1.0	0.394	0.0	1.393	0.0		8,390	>100,000	>100,000	-	0.0000013
	Timken L68100	-138	1.3775	2.3612	23		0.210	15.5	3.127	1.58	6,304.8	2,070	>100,000	>100,000	-	0.0000016

NOTES:

1. AEO max power for reference only; cubic mean and OEI power ratings are considered where appropriate.
2. Timken tapered bearings are rated at 500 rpm for 3,000 hours; MRC roller bearings are rated at 33 rpm for 500 hours.
3. Life improvement factor of 10 included.
4. Bearing lives and loads are calculated assuming 60% of the power is transmitted to the cross-shaft.
5. Bearing reaction loads and lives are using the rotor loads to be the sum of the steady load + 1/3 alternating load.
6. The length of the roller being used is 0.625 inch instead of the standard 0.472 inch.
7. Bearing lives and reaction loads for the case where the gear shaft drives the pinion.
8. Bearing lives and reaction loads for the case where the pinion shaft drives the gear shaft.

A. Bearing-to-shaft interference fit will be 0.001 inch per inch of diameter with the following exceptions:

1. Rotor shaft bearings are designed for an interference fit which results in a pressure of 1,000 psi.

2. Bearing unmounted internal radial clearance is 0.0007 inch loose for cylindrical-roller bearings. Internal clearance for the bidirectional tapered-roller bearings will be established by various component test programs.

B. Bearing to housing fits will be:

1. Cylindrical-roller bearings will be line-to-line to loose for ease of assembly. The range of loose fit will be the combined tolerance on the bearing liner i.d. and the bearing outer race o.d.

2. Tapered-roller bearings will have an interference fit in the housing of 0.0005 in./in. tight.

C. Bearing mounting:

1. All tapered-roller bearings will be bidirectional and their internal clearances will be designed and manufactured into each bearing based upon requirements established by test for each application.

2. Fixed outer rings of the cylindrical and bidirectional tapered-roller bearings will be mechanically restrained from rotation in the housing by three tabs machined into the outer ring of each bearing.

3. Roller drop on the cylindrical-roller bearings shall be controlled and lead-in chamfer provided on the inner ring or shaft raceway to facilitate assembly and to prevent damage to the bearing.

4. Shafting and planet gears used as integral parts of a bearing will have a carburized case (58 Rc minimum) to a depth of five times the depth of the point of maximum subsurface shear at maximum design rated power.

5. Where possible, machined, inner land-riding cages will be used. The use of P.E.E.K. cages will be considered for all applications based upon results from various component tests being conducted under the A.R.T. program.

6. Steel liners shall be incorporated in all magnesium or aluminum housings designed to hold antifriction bearings. All bearing liners shall be finished machined after the liner is installed into the housing bore. Bearing liners supporting bearings in major load paths shall have a finished liner wall thickness of 0.060 inch minimum. The bearing liner finished inside diameter will have a maximum surface roughness of 62 AA.

7. Bearings shall be lubricated by supplying oil through the rotating shaft and holes machined into the bearing inner race and the shaft journal wherever possible. External oil jets shall be used when this condition cannot be met.

8. All bearings shall be serialized and manufactured to the requirements defined in Boeing document D210-10302-1[3].

Transmission Shafts

Gear Shaft Design - Rotating shaft components were designed with consideration for gear geometry and loads, bearing size and location, and torque loads. Special attention was given to eliminate stress concentrations, joints, and potential for fretting. Gearbox internal shafts were supported with two hybrid roller bearings. One roller operating directly on the integral shaft journal, and the other, a bidirectional tapered roller, taking all shaft axial loading as well as the radial component. Since all axial loads are reacted at one bearing, there is no danger of trapped thermal growth or need for ground shims, and the resulting system is light and efficient. Shaft materials will be H^3 carburizing steels such as VASCO X2M per Boeing Material Specification (BMS) 7-223[4].

Drive train components from the engine to and including the SK32137-45 bull gear are designed for the OEI condition or 2,777 hp at hover shaft speeds of 23,000 rpm. Components in the drive train between the left and right nacelles, from the bull gear through interconnecting drive shafts and tilt-axis gearboxes, are designed for 60 percent of the OEI power or 1,667 hp at hover shaft speeds. From the bull gear to the rotor, design loads were 60 percent of the installed engine power or 2,424 hp AEO at hover shaft speeds and 1,939 hp AEO at cruise/forward-flight shaft speeds.

Gear Shaft Analysis - A.R.T. program gear shafts were analyzed primarily with the Boeing WATFOR Shaft Analysis Program, with finite-element modeling used for the rotor shaft planet carrier posts and TAGB gear shaft webs. CATIA 3D solid modeling was also used at the PRGB SK32137-38 intermediate gear shaft to assure gear cutter clearances, as shown in Figure 16, and will be important to future transmission designs at Boeing. Stress analysis with the Shaft Analysis Program consisted of using the combined axial, bending, and shear stresses to calculate margins of safety at selected critical sections. The analysis also takes into account the slope of each shaft through their respective bearings. A critical requirement, the shaft slope cannot exceed 0.0005 in./in. Each gear shaft configuration is optimized by maintaining adequate

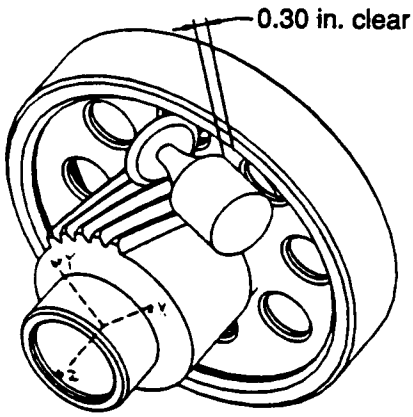

Grinding spindle clearance with large gear rim

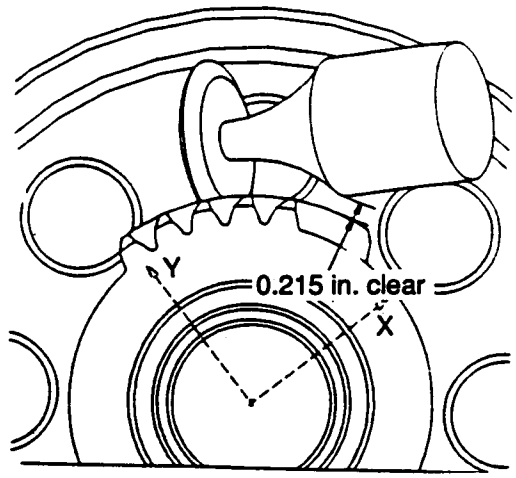

Grinding spindle clearance with small gear teeth

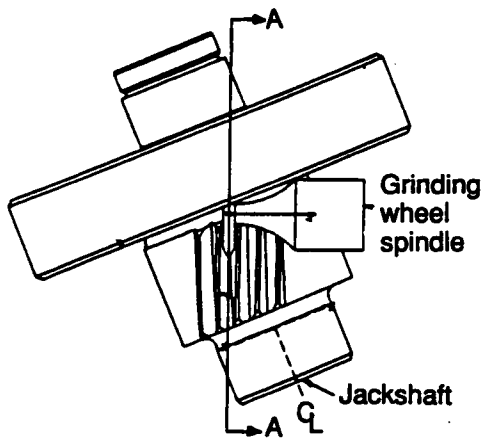

Grinding wheel path on jackshaft

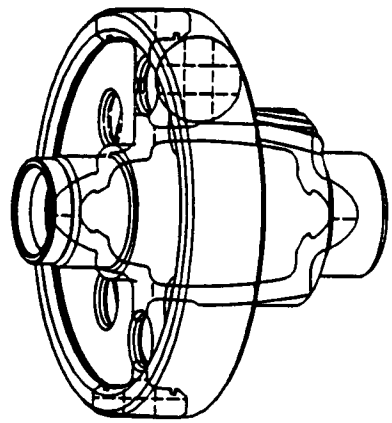

Solid model along section A-A

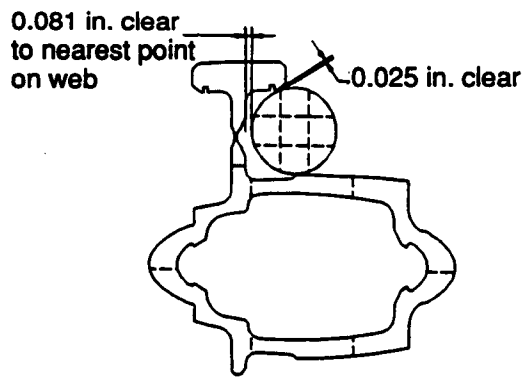

Wheel 0.100 in. past end of ground tooth

Grinding wheel clearance along section A-A

Figure 16. Study of Gear Cutter Clearances

stiffness while removing mass from low-stress areas. All stresses, shaft slopes, cross-sectional properties, etc, are computed and listed in the tables that follow. Tables 13, 14, and 15 correspond to the three criteria used for analysis: fatigue, yield, and ultimate analysis. In all cases the fatigue analysis proved to be the critical case. The computer program input loads are outlined in the paragraphs that follow. The strength allowables for VASCO X2M steel were used to calculate a margin of safety.

Fatigue Analysis - The Shaft Analysis Program calculated stresses based on loads seen by each shaft at maximum operating conditions and includes a vibratory torque component which is ± 10 percent of the steady torque. Margins of safety greater than zero in Table 13 indicate unlimited life. All stress concentrations, including concentration factors for radii, thickness changes, and lubrication orifices, were computed from Roark and Young's "Formulas of Stress and Strain."[5] The maximum shear strength, Fsu, is 96,000 psi. The endurance strength, Seb, is 32,000 psi. The stresses and margins of safety are summarized in Table 13 and Figure 17.

Limit Analysis - Loads used for the limit analysis are factored to 1.5 times fatigue loads. The margin of safety is the ratio of the material's yield strength to the Von Mises stress minus one at the critical section. The yield strength is 142,000 psi. The stresses and margins of safety are summarized in Table 14 and Figure 18.

Ultimate Analysis - The ultimate analysis compares shaft stress computed from factored loads to the material's rupture point. The load factor in this case was 1.5 times the limit loads. The ultimate tensile strength, Ftu, was 160,000 psi. The section factor K is dependent on the inner and outer diameters of the critical section. The K factor is also the ratio of the ultimate bending strength to the ultimate tensile strength. The torsional modulus of rupture, Fst, is a function of outer diameter, thickness, and length of the shaft. The margins of safety and stresses are summarized in Table 15 and Figure 18.

TABLE 13. FATIGUE ANALYSIS SUMMARY

Xmsn shaft	Section (Figure 17)	Section inner dia (in.)	Properties outer dia (in.)	KTB	KTS	FB (psi)	FS (psi)	F(steady) (psi)	Goodman corr factor	MS*
-28 input	A-A	2.126	2.625	2.260	1.710	99.3	0.0	0.0	1.000	141.591
pinion	B-B	2.000	2.620	1.814	1.445	1,034.0	0.0	0.0	1.000	16.061
	C-C	2.000	2.620	1.649	1.361	2,082.0	0.0	0.0	1.000	8.321
	D-D	1.800	2.440	1.825	1.449	1,872.0	378.5	3,785.0	0.961	7.668
	E-E	1.800	2.440	1.446	1.250	1,035.0	378.5	3,785.0	0.961	17.015
-13 clutch	A-A	1.980	2.500	1.000	1.931	0.0	408.9	4,089.0	0.957	21.403
shaft	B-B	1.485	2.370	1.000	2.052	0.0	344.2	3,442.0	0.964	24.221
	C-C	1.278	2.000	1.000	3.892	0.0	581.3	5,813.0	0.939	6.672
	D-D	1.278	1.666	1.000	1.752	0.0	1,282.0	12,820.0	0.866	6.127
	E-E	1.278	1.617	1.000	1.554	0.0	1,503.0	15,030.0	0.843	5.672
	F-F	1.278	1.617	1.000	3.874	0.0	1,503.0	15,030.0	0.843	1.676
-38 intmd	A-A	2.830	3.375	2.243	1.695	1,314.0	0.0	0.0	1.000	9.857
gear shaft	B-B	3.429	3.989	2.098	1.609	4,590.0	408.8	4,088.0	0.957	2.159
	C-C	3.338	3.779	1.706	1.377	3,366.0	0.0	0.0	1.000	4.573
	D-D	3.338	3.779	1.260	1.260	2,539.0	0.0	0.0	1.000	9.003
-45 bull gear	A-A	3.694	4.172	1.927	1.522	515.8	51.6	515.8	0.995	30.726
shaft	B-B	3.673	4.400	1.535	1.270	3,903.0	173.4	1,734.0	0.982	4.234
	C-C	3.673	4.852	1.990	1.559	650.0	0.0	0.0	1.000	23.739
-68 ICDS	A-A	1.800	2.438	2.359	1.770	130.4	0.0	0.0	1.000	103.00
gear shaft	B-B	2.100	2.750	1.440	1.230	1,057.0	0.0	0.0	1.000	20.02
	C-C	1.922	2.363	1.400	1.198	5,942.0	1,017.0	10,170.0	0.894	2.334
	D-D	1.862	2.363	1.560	1.311	1,164.0	0.0	0.0	1.000	16.62
-52 sun gear	A-A	2.460	3.080	1.000	1.260	0.0	796.8	7,968.0	0.917	15.875
shaft	B-B	2.460	3.080	1.000	1.260	0.0	1,594.0	15,940.0	0.834	6.672
	C-C	2.680	3.240	1.000	1.290	0.0	1,345.0	13,450.0	0.860	8.157
	D-D	2.680	3.080	1.000	1.230	0.0	1,952.0	19,520.0	0.797	5.130
-66 rotor	A-A	4.120	5.00	2.43	1.819	1,327.0	1,587.0	15,870.0	0.835	3.489
shaft	B-B	4.12	4.88	2.243	1.372	2,168.0	1,870.0	18,700.0	0.805	2.912
	C-C	3.62	4.75	2.262	1.726	2,399.0	1,506.0	15,060.0	0.843	2.826
	D-D	3.62	4.39	3.113	2.241	4,553.0	2,351.0	23,510.0	0.755	0.433
	E-E	3.19	4.24	2.93	2.006	4,519.0	2,064.0	20,640.0	0.785	0.668
	F-F	3.19	4.125	1.938	1.529	5,865.0	2,372.0	23,720.0	0.753	0.855
	G-G	3.19	4.065	1.460	1.212	6,091.0	2,565.0	25,650.0	0.733	1.256
	H-H	3.190	3.741	1.200	1.200	9,419.0	4,334.0	43,340.0	0.549	0.214
	I - I	2.300	3.250	1.774	1.411	6,084.0	4,158.0	41,580.0	0.567	0.224
-189 TAGB	A-A	1.363	1.769	1.788	1.443	0.0	2,157.0	21,570.0	0.775	3.602
spl bev gear	B-B	1.363	1.769	2.240	1.585	0.0	2,157.0	21,570.0	0.775	3.190
shaft	C-C	1.363	2.193	1.420	1.226	0.0	861.70	8,617.00	0.910	14.919
	D-D	1.884	2.243	1.750	1.398	0.0	1,369.0	13,690.0	0.857	7.277
	E-E	1.884	2.500	2.250	1.254	0.0	730.5	7,305.0	0.924	17.634
	F-F	2.326	2.875	2.188	1.664	0.0	569.3	5,693.0	0.941	17.347
	G-G	1.389	1.797	2.456	1.839	6,113.0	0.0	0.0	1.000	1.131
	H-H	2.326	2.875	2.937	3.924	0.0	569.3	5,693.0	0.941	6.780

TABLE 13. FATIGUE ANALYSIS SUMMARY (Continued)

Xmsn shaft	Section (Figure 17)	Section inner dia (in.)	Properties outer dia (in.)	KTB	KTS	FB (psi)	FS (psi)	F(steady) (psi)	Goodman corr factor	MS*
-171 TAGB	A-A	1.363	1.769	1.788	1.443	0.0	2,104.0	21,040.0	0.781	3.752
spl bev	B-B	1.363	1.769	2.048	1.585	0.0	2,104.0	21,040.0	0.781	3.326
pinion shaft	C-C	1.363	2.193	1.420	1.226	0.0	840.7	8,407.0	0.912	15.356
	D-D	1.884	2.242	1.750	1.398	0.0	1,331.0	13,310.0	0.861	7.553
	E-E	1.884	2.500	2.250	1.593	0.0	712.6	7,126.0	0.926	14.068
	F-F	2.338	2.715	1.451	1.254	0.0	837.5	8,375.0	0.913	0.606
	G-G	2.338	2.875	2.188	1.664	0.0	564.2	5,642.0	0.941	17.52
	H-H	1.389	1.798	1.456	1.839	6,491.0	0.0	0.0	1.000	1.007
-2 engine	A-A	1.330	2.552	1.808	1.441	0.0	749.6	7,496.0	0.922	14.769
quill shaft	B-B	1.490	1.890	2.051	1.589	0.0	935.3	9,353.0	0.903	0.000
	C-C	1.131	1.890	2.008	1.562	0.0	658.4	6,584.0	0.931	15.733
	D-D	1.590	1.850	2.046	1.581	0.0	1,347.0	13,470.0	0.860	6.458
	E-E	1.590	1.990	2.634	1.956	0.0	830.0	8,300.0	0.914	9.396
	F-F	1.590	1.850	2.889	2.048	0.0	1,347.0	13,470.0	0.860	4.758
	G-G	1.590	1.850	2.914	3.889	0.0	1,347.0	13,470.0	0.860	2.032
	H-H	1.590	1.850	2.914	3.889	0.0	1,347.0	13,470.0	0.860	2.032
-128 lube &	A-A	0.750	1.212	2.417	1.719	0.0	0.0	0.10	1.000	>1,000.0
hyd pump	B-B	0.997	1.377	2.100	1.603	104.1	12.7	127.0	0.999	143.3
gear shaft	C-C	1.353	1.651	1.577	1.313	174.1	131.2	1,312.0	0.986	76.8
	D-D	1.200	1.584	1.400	1.220	13.5	0.0	0.0	1.000	>1,000.0
-123 idler	A-A	0.694	1.000	1.962	1.516	541.3	0.0	0.0	1.000	29.13
gear shaft	B-B	0.807	1.109	1.391	1.176	6,303.0	0.0	0.0	1.000	2.650
	C-C	0.807	1.109	1.400	1.200	906.3	0.0	0.0	1.000	24.22
-144 aux lube	A-A	0.997	1.377	2.099	1.603	1.70	2.70	26.9	1.000	>1,000.0
gear shaft	B-B	0.997	1.297	1.460	1.218	5.20	3.60	35.8	1.000	>1,000.0
	C-C	0.997	1.297	1.460	1.218	22.4	3.40	33.8	1.000	954.2
	D-D	0.997	1.297	1.549	1.292	6.90	0.0	0.0	1.000	>1,000.0
-167 adapter,	A-A	1.643	2.375	1.000	1.224	0.0	730.4	7,304.0	0.924	18.09
TAGB	B-B	1.639	2.039	1.000	1.880	0.0	86.3	862.5	0.991	111.9
-211 adapter,	A-A	1.100	1.565	1.00	1.488	0.0	2,604.0	26,040.0	0.729	2.475
PRGB	B-B	1.100	1.709	1.000	1.800	0.0	1,824.0	18,240.0	0.810	3.558
	C-C	1.100	1.565	1.000	1.114	0.0	2,604.0	26,040.0	0.729	3.641
	D-D	1.539	5.500	1.000	1.710	0.0	59.1	590.8	0.994	180.7
-111 generator	A-A	0.638	1.000	1.780	1.403	135.1	0.0	0.0	1.000	132.068
shaft	B-B	0.760	1.000	1.385	1.174	379.6	146.4	1,464.0	0.985	51.157
	C-C	1.174	1.395	2.323	1.643	14.3	72.1	721.2	0.992	151.760
	D-D	1.000	1.333	1.535	1.286	13.5	60.3	602.9	0.994	233.045

TABLE 13. FATIGUE ANALYSIS SUMMARY (Continued)

Xmsn shaft	Section (Figure 17)	Section inner dia (in.)	Properties outer dia (in.)	KTB	KTS	FB (psi)	FS (psi)	F(steady) (psi)	Goodman corr factor	MS*
-196 quill shaft, TAGB	A-A	0.500	0.660	1.000	1.440	0.0	309.6	3,096.0	0.968	39.11
	B-B	0.500	0.984	1.000	1.603	0.0	67.1	671.2	0.993	169.5
	C-C	0.500	0.660	1.000	1.232	0.0	309.6	3,096.0	0.968	45.87
	D-D	0.500	0.712	1.000	1.255	0.0	218.5	2,185.0	0.977	64.84
	E-E	0.000	0.438	1.000	1.302	0.0	710.4	7,104.0	0.926	17.49
-203 quill shaft, fan	A-A	0.500	0.680	1.000	1.033	0.0	268.2	2,682.0	0.972	63.8
	B-B	0.500	0.680	1.000	1.371	0.0	268.2	2,682.0	0.972	47.8
	C-C	0.000	0.438	1.000	1.317	0.0	710.4	7,104.0	0.926	17.28

KTB: stress concentration factor for bending
KTS: stress concentration factor for torsion
FB: alternating bending stress in section
FS: alternating torsional shear stress in section (10% of steady shear stress)
F(steady): steady shear stress in section

$$* \; MS = \frac{S_{eb} \times GCF}{F_B \times K_{tB}} - 1 = \frac{S_{es} \times GCF}{F_s \times K_{tS}} - 1$$

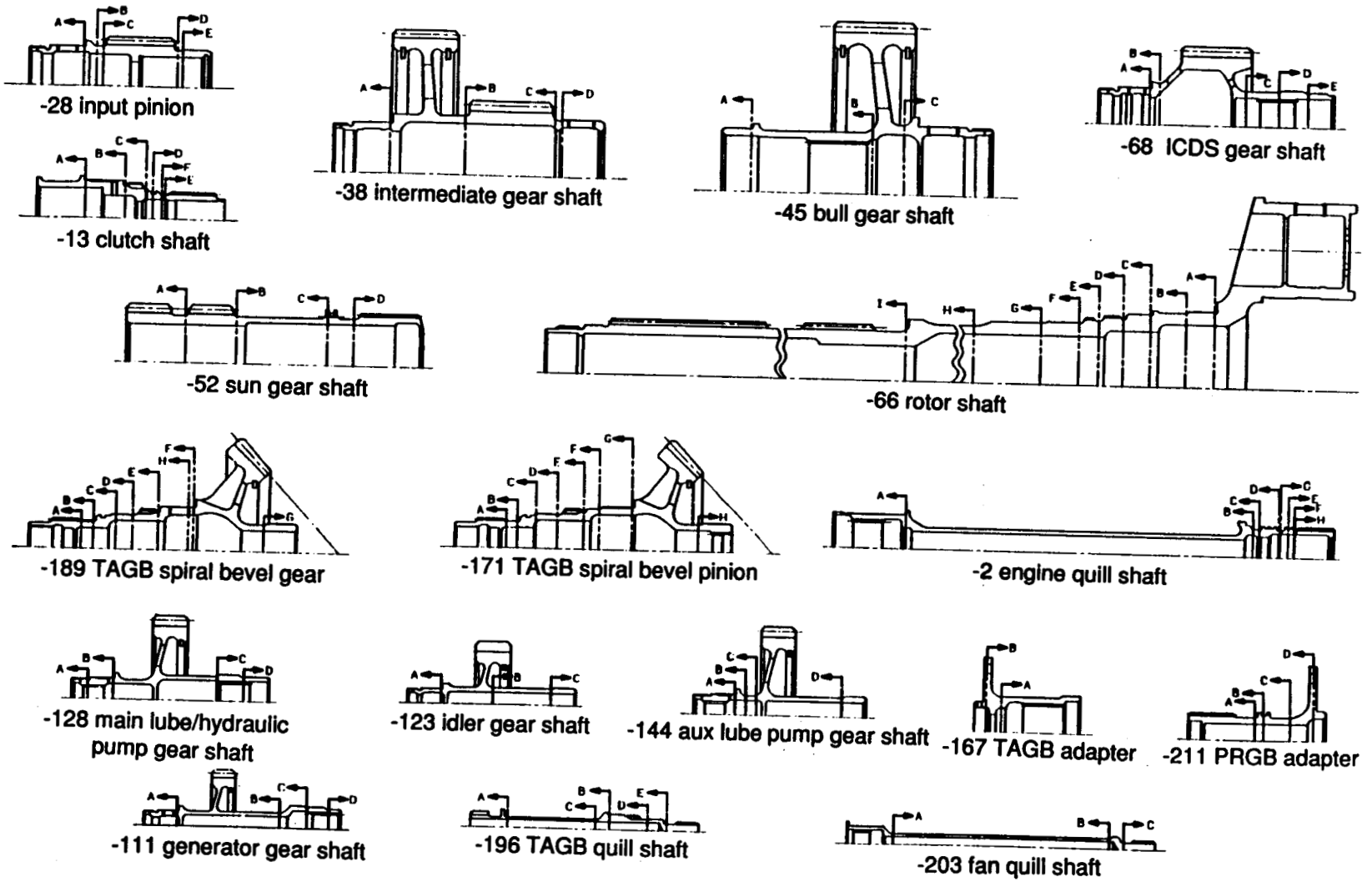

Figure 17. Locations of Fatigue Analysis Sections

TABLE 14. LIMIT ANALYSIS SUMMARY

Xmsn shaft	Section (Fig. 18)	Shaft inner dia (in.)	Properties outer dia (in.)	FA (psi)	FB (psi)	FS (psi)	Normal stress (psi)	Von Mises stress (psi)	MS
-28 input	A-A	2.000	2.620	-1,544.0	-3,122.0	0.0	-4,666.0	4,666.0	29.433
pinion	B-B	1.800	2.759	-1,012.0	-5,577.0	0.0	-6,589.0	6,589.0	20.551
	C-C	1.800	2.440	0.0	2,807.0	5,677.0	2,807.0	10,225.7	12.887
	D-D	1.940	2.300	0.0	0.0	9,660.0	0.0	16,731.6	7.487
-13 clutch	A-A	1.980	2.380	0.0	0.0	8,276.0	0.0	14,334.5	8.906
shaft	B-B	1.278	2.100	0.0	0.0	7,274.0	0.0	12,598.9	10.271
	C-C	1.278	1.666	0.0	0.0	19,230.0	0.0	33,307.3	3.263
	D-D	1.278	1.617	0.0	0.0	22,540.0	0.0	39,040.4	2.637
-38 intmd	A-A	2.830	3.375	-1,172.0	-197.2	0.0	-1,369.2	1,369.2	102.710
gear shaft	B-B	2.670	3.989	-451.3	-586.7	0.0	-1,038.0	1,038.0	135.802
	C-C	3.429	3.989	-2,019.0	-6,042.0	6,133.0	-8,061.0	13,334.9	9.649
	D-D	3.429	3.989	-2,019.0	-6,884.0	6,133.0	-8,903.0	13,860.2	9.245
-45 bull	A-A	3.488	4.133	0.0	5,500.0	0.0	5,500.0	5,500.0	24.818
gear shaft	B-B	3.673	4.133	0.0	9,293.0	4,292.0	9,293.0	11,900.6	10.932
	C-C	3.673	4.400	-2,105.0	-5,834.0	0.0	-7,939.0	7,939.0	16.886
	D-D	3.673	4.852	-1,229.0	-3,034.0	0.0	-4,263.0	4,263.0	32.310
-68 ICDS	A-A	1.504	2.800	0.0	-4,239.0	5,623.0	-4,239.0	10,621.8	12.37
gear shaft	B-B	1.922	2.390	0.0	-10,240.0	14,250.0	-10,240.0	26,721.6	4.314
	C-C	1.922	2.363	0.0	-6,271.0	15,250.0	-6,271.0	27,148.0	4.231
	D-D	1.862	2.363	0.0	-2,612.0	13,960.0	-2,612.0	24,320.1	4.839
-52 sun	A-A	2.460	3.200	0.0	0.0	17,120.0	0.0	29,652.7	3.789
gear shaft	B-B	2.460	3.080	0.0	0.0	29,280.0	0.0	50,714.4	1.800
	C-C	2.680	3.080	0.0	0.0	29,280.0	0.0	50,714.4	1.800
	D-D	2.680	3.376	0.0	0.0	19,780.0	0.0	34,260.0	3.145
-66 rotor	A-A	4.12	6.000	1,751.0	661.9	9,549.0	2,412.9	16,714.4	7.496
shaft	B-B	4.12	4.88	4,870.0	4,277.0	28,060.0	9,147.0	49,454.6	1.871
	C-C	3.62	4.75	3,522.0	4,303.0	22,590.0	7,825.0	39,901.8	2.559
	D-D	3.62	4.390	5,401.0	6,829.0	35,260.0	12,230.0	62,284.0	1.280
	E-E	3.190	4.240	4,270.0	7,096.0	30,970.0	11,366.0	54,832.5	1.590
	F-F	3.190	4.125	4,870.0	8,835.0	35,580.0	13,705.0	63,131.9	1.249
	G-G	3.190	3.741	6,628.0	14,130.0	65,010.0	20,758.00	114,498.0	0.240
	H-H	2.300	3.250	4,801.0	9,125.0	62,370.0	13,926.0	108,921.9	0.304
	I-I	2.600	3.250	6,657.0	9,529.0	79,150.0	15,715.0	137,989.1	0.029
-171 TAGB	A-A	1.363	1.769	0.0	0.0	24,170.0	0.000	41,863.7	2.392
spl bev	B-B	1.363	1.769	0.0	0.0	32,560.0	0.000	56,395.5	1.518
pinion	C-C	2.470	2.880	-3,296.0	-5,002.0	10,320.0	-8,298.000	19,706.90	6.206
shaft	D-D	1.389	1.798	-5,547.0	-29,800.0	30,240.0	-35,347.0	63,188.446	1.247
-189 TAGB	A-A	1.100	1.769	0.0	0.0	22,690.0	0.000	39,300.259	2.613
spl bev	B-B	1.363	1.769	0.0	0.0	32,350.0	0.001000	56,031.83	1.534
gear shaft	C-C	2.400	2.688	-4,928.0	-8,421.00	16,380.0	-13,349.000	31,354.509	3.529
	D-D	1.389	1.798	-5,540.0	-33,670.0	30,990.0	-39,210.00	66,472.200	1.136

TABLE 14. LIMIT ANALYSIS SUMMARY (Continued)

Xmsn shaft	Section (Fig. 18)	Shaft inner dia (in.)	Properties outer dia (in.)	FA (psi)	FB (psi)	FS (psi)	Normal stress (psi)	Von Mises stress (psi)	MS
-2 engine	A-A	1.151	1.451	0.0	0.0	31,500.0	0.000	54,559.600	1.603
quill shaft	B-B	1.490	1.890	0.0	0.0	14,030.0	0.000	24,300.673	4.843
	C-C	1.590	1.990	0.0	0.0	12,450.0	0.000	21,564.033	5.585
	D-D	1.590	1.850	0.0	0.0	20,210.0	0.000	35,004.747	3.057
-128 lube &	A-A	0.997	1.377	-242.5	-156.2	190.4	-398.7	517.4	273.4
hyd pump	B-B	0.997	1.297	-317.8	-2,913.0	253.9	-3,230.8	3,260.6	42.6
gear shaft	C-C	1.352	1.651	0.0	1,589.0	1,962.0	1,589.0	3,751.4	36.8
	D-D	1.200	1.772	0.0	20.4	1,106.0	20.4	1,915.8	73.12
-123 idler	A-A	0.694	1.000	0.0	812.3	0.0	812.3	812.3	173.8
gear shaft	B-B	0.807	1.343	0.0	849.8	0.0	849.8	849.8	166.1
	C-C	0.807	1.109	0.0	9,456.0	0.0	9,456.0	9,456.0	14.02
	D-D	0.807	1.109	0.0	1,364.0	0.0	1,364.0	1,364.0	103.1
-144 aux	A-A	0.997	1.377	0.0	0.0	40.3	0.000	69.8	>1,000
lube gear	B-B	0.997	1.377	-3.3	-2.6	40.3	-5.90	70.08	>1,000
shaft	C-C	0.997	1.297	-4.4	-33.7	53.7	-38.1	100.5	>1,000
	D-D	0.997	1.297	-4.4	-52.2	53.7	-56.6	108.9	>1,000
-167 adapter	A-A	1.750	2.375	0.0	0.0	11,980.0	0.000	20,749.9	5.843
TAGB	B-B	2.023	2.375	0.0	0.0	17,840.0	0.000	30,899.8	3.596
	C-C	1.643	2.375	0.0	0.0	10,960.0	0.000	18,983.2	6.48
	D-D	1.193	2.375	0.0	0.0	9,021.0	0.0	15,624.8	8.088
-211 adapter	A-A	1.100	1.565	0.0	0.0	39,050.0	0.0	67,636.5	1.099
PRGB	B-B	1.100	1.709	0.0	0.0	27,370.0	0.0	47,406.2	1.995
	C-C	1.100	1.920	0.0	0.0	17,920.0	0.0	31,038.35	3.575
	D-D	1.100	1.750	0.0	0.0	25,020.0	0.0	43,335.9	2.277
-111	A-A	0.760	1.000	-227.3	-1,044.0	0.0	-1,271.300	1,271.300	110.697
generator	B-B	0.760	1.000	0.0	-2,452.0	2,197.0	-2,452.0	4,526.900	30.369
shaft	C-C	0.760	1.000	0.0	-569.4	2,197.0	-569.4000	3,847.790	35.968
	D-D	1.174	1.395	0.0	-11.1	1,082.0	-11.100	1,874.021	74.7
-196 quill	A-A	0.500	0.750	0.0	0.0	2,645.0	0.0	4,581.0	29.99
shaft, TAGB	B-B	0.500	0.660	0.0	0.0	4,644.0	0.0	8,043.6	16.65
	C-C	0.500	0.712	0.0	0.08.0	3,278.0	0.07.6	5,677.6	24.01
	D-D	0.000	0.438	0.0	0.0	10,660.0	0.0	18,463.7	6.691
-203 quill	A-A	0.942	1.146	0.0	0.0	1,095.0	0.0	1,896.6	73.8
shaft, fan	B-B	0.500	0.680	0.0	0.0	4,024.0	0.0	6,969.8	19.374
	C-C	0.500	0.840	0.0	0.0	1,727.0	0.0	2,991.3	46.47
	D-D	0.000	0.438	0.0	0.0	10,660.0	0.0	18,463.7	6.691

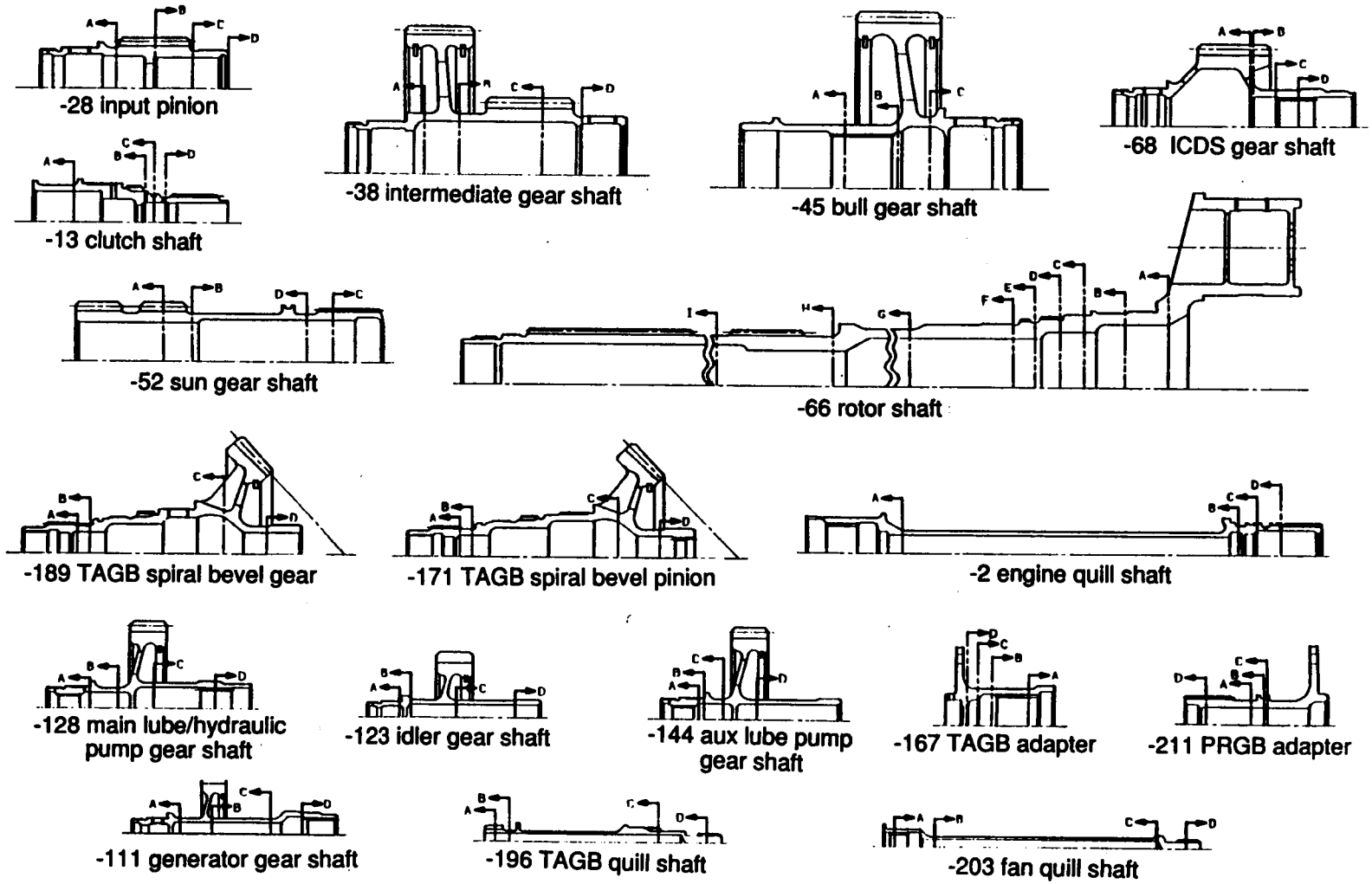

Figure 18. Locations of Limit and Ultimate Analysis Sections

TABLE 15. ULTIMATE ANALYSIS SUMMARY

Xmsn shaft	Section (Fig. 18)	Inner dia (in.)	Outer dia (in.)	FA (psi)	FB (psi)	FS (psi)	K factor	FBU (psi)	FST (psi)	RA	RB	RS	MS
-28 input	A-A	2.000	2.620	2,315.0	4,683.0	0.0	1.427	228,332.1	114,000.0	-0.0154	0.0205	0.0000	195.5
pinion	B-B	1.800	2.759	1,517.0	8,366.0	0.0	1.498	239,605.7	115,330.0	-0.0101	0.0349	0.0000	39.319
	C-C	1.800	2.440	0.0	4,210.0	8,516.0	1.444	230,986.2	113,300.0	0.0000	0.0182	0.0752	11.930
	D-D	1.940	2.300	0.0	121.4	14,490.0	1.375	219,960.6	103,700.0	0.0000	0.0006	0.1397	6.157
-13 clutch	A-A	1.980	2.380	0.0	0.0	12,410.0	1.382	221,170.5	105,600.0	0.0000	0.0000	0.1175	7.509
shaft	B-B	1.278	2.100	0.0	0.0	10,910.0	1.524	243,851.1	118,700.0	0.0000	0.0000	0.0919	9.880
	C-C	1.278	1.666	0.0	0.0	28,840.0	1.425	227,942.8	111,000.0	0.0000	0.0000	0.2598	2.849
	D-D	1.278	1.617	0.0	0.0	33,820.0	1.410	225,521.2	110,000.0	0.0000	0.0000	0.3075	2.253
-38 intmd	A-A	3.429	3.989	-1,431.0	1,549.0	0.0	1.364	218,269.7	102,300.0	0.0095	0.0071	0.0000	59.108
gear shaft	B-B	3.429	3.989	-3,028.0	9,062.0	9,199.0	1.364	218,269.7	102,300.0	0.0202	0.0415	0.0899	7.387
	C-C	3.429	4.289	-1,895.0	9,435.0	5,680.0	1.404	224,567.0	110,000.0	0.0126	0.0420	0.0516	11.626
	D-D	3.338	3.779	0.0	7,570.0	0.0	1.349	215,789.9	99,000.0	0.0000	0.0351	0.0000	27.506
-45 bull	A-A	3.488	4.133	0.0	8,249.0	4,916.0	1.374	219,912.3	103,700.0	0.0000	0.0375	0.0474	15.542
gear shaft	B-B	3.673	4.133	0.0	13,940.0	6,438.0	1.345	215,225.6	98,000.0	0.0000	0.0648	0.0657	9.840
	C-C	3.673	4.852	-1,841.0	1,463.0	0.0	1.431	228,991.0	110,000.0	0.01230	0.0646	0.0000	52.580
-68 ICDS	A-A	1.504	2.800	0.0	6,358.0	8,434.0	1.565	250,370.9	121,300.0	0.0004	0.0254	0.0695	12.51
gear shaft	B-B	1.922	2.390	0.0	15,350.0	21,370.0	1.400	224,075.9	107,000.0	0.000	0.0685	0.1997	3.736
	C-C	1.922	2.363	0.0	9,494.0	22,880.0	1.394	223,114.5	106,000.0	0.0000	0.0421	0.2158	3.547
	D-D	1.862	2.363	0.0	3,916.0	20,940.0	1.411	225,768.7	110,000.0	0.0000	0.0173	0.1904	4.231
-52 sun	A-A	2.460	3.200	0.0	0.0	25,680.0	1.424	227,772.0	110,000.0	0.0000	0.0000	0.2335	3.283
gear shaft	B-B	2.460	3.080	0.0	0.0	31,650.0	1.404	224,649.2	103,000.0	0.0000	0.0000	0.3073	2.254
	C-C	2.680	3.080	0.0	0.0	43,920.0	1.357	217,168.4	100,000.0	0.0000	0.0000	0.4392	1.277
	D-D	2.680	3.376	0.0	0.0	30,270.0	1.407	225,157.2	110,000.0	0.0000	0.0000	0.2752	2.634
-66 rotor	A-A	4.120	6.000	2,626.0	992.9	14,320.0	1.476	236,190.9	115,000.0	-0.0175	0.0042	0.1245	8.338
shaft	B-B	4.120	4.880	7,305.0	6,415.0	42,090.0	1.374	219,878.4	98,300.0	-0.0487	0.0292	0.4282	1.628
	C-C	3.620	4.750	5,283.0	6,454.0	33,880.0	1.428	228,462.2	110,700.0	-0.0352	0.0282	0.3061	2.675
	D-D	3.620	4.390	8,101.0	10,240.0	52,900.0	1.387	221,938.7	99,700.0	-0.0540	0.0461	0.5306	1.089
	E-E	3.190	4.240	6,404.0	10,640.0	46,450.0	1.434	229,472.6	110,700.0	-0.0427	0.0464	0.4196	1.635
	F-F	3.190	4.125	7,305.0	13,250.0	53,370.0	1.421	227,295.2	110,000.0	-0.0487	0.0583	0.4852	1.273
	G-G	3.190	3.740	9,942.0	21,190.0	97,510.0	1.369	218,968.9	96,000.0	-0.0663	0.0968	1.0157	0.048
	H-H	2.300	3.250	7,201.0	13,680.0	93,560.0	1.463	234,061.3	115,000.0	-0.0480	0.0584	0.8136	0.303
	I-I	2.600	3.250	9,985.0	14,290.0	118,700.0	1.403	224,513.0	112,000.0	-0.0666	0.0636	1.0598	0.005
-189 TAGB	A-A	1.100	1.769	0.0	0.0	34,040.0	1.524	243,898.6	118,300.0	0.0000	0.0000	0.2877	2.475
spl bev	B-B	1.363	1.769	0.0	0.0	48,530.0	1.422	227,590.0	110,000.0	0.000	0.0000	0.4412	1.267
gear shaft	C-C	2.400	2.688	-7,393.0	12,630.0	24,580.0	1.342	214,791.3	96,300.0	0.0493	0.0588	0.2552	2.213
	D-D	1.389	1.798	-8,311.0	50,500.0	46,490.0	1.421	227,379.4	110,000.0	0.0554	0.2221	0.4226	0.877
-171 TAGB	A-A	1.363	1.769	0.0	0.0	36,250.0	1.449	231,854.4	113,000.0	0.0000	0.0000	0.3208	2.117
pinion	B-B	1.363	1.769	0.0	0.0	47,350.0	1.422	227,590.9	110,000.0	0.0000	0.0000	0.4305	1.323
shaft	C-C	2.470	2.880	-4,945.0	7,504.0	154,800.0	1.365	218,476.6	101,700.0	0.0330	0.0343	0.1522	4.291
	D-D	1.389	1.798	-8,321.0	44,700.0	43,500.0	1.421	227,379.4	110,000.0	0.0555	0.1966	0.4123	0.952

TABLE 15. ULTIMATE ANALYSIS SUMMARY (Continued)

Xmsn shaft	Section (Fig. 18)	Inner dia (in.)	Outer dia (in.)	FA (psi)	FB (psi)	FS (psi)	K factor	FBU (psi)	FST (psi)	RA	RB	RS	MS
-2 engine	A-A	1.151	1.451	0.0	0.0	47,250.0	1.408	225,219.1	110,000.0	0.0000	0.0000	0.4295	1.328
quill	B-B	1.490	1.890	0.0	0.0	21,040.0	1.411	225,729.2	110,000.0	0.0000	0.0000	0.1913	4.228
shaft	C-C	1.131	1.890	0.0	0.0	14,820.0	1.530	244,811.1	119,300.0	0.0000	0.0000	0.1242	7.050
	D-D	1.59	1.85	0.0	0.0	30,310.0	1.364	218,285.9	108,000.0	0.0000	0.0000	0.2806	2.563
1-128 lube	A-A	0.997	1.377	-363.7	234.2	285.7	1.452	232,391.1	113,300.0	0.0024	0.0010	0.0025	193.5
& hyd	B-B	0.997	1.297	-476.8	4,369.0	380.9	1.424	227,777.5	111,000.0	0.0032	0.0192	0.0034	43.1
gear shaft	C-C	1.352	1.651	0.0	2,383.0	2,942.0	1.391	222,536.0	105,300.0	0.0000	0.0107	0.0279	32.42
	D-D	1.200	1.772	0.0	31.3	1,658.0	1.482	237,141.7	117,300.0	0.0000	0.0001	0.0141	69.7
-123 idler	A-A	0.694	1.000	0.0	1,218.0	0.0	1.472	235,450.0	113,700.0	0.0000	0.0052	0.0000	192.31
gear shaft	B-B	0.807	1.343	0.0	1,274.0	0.0	1.529	244,577.0	118,700.0	0.0000	0.0052	0.0000	190.9
	C-C	0.807	1.109	0.0	14,180.0	0.0	1.450	232,017.1	113,000.0	0.0000	0.0611	0.0000	15.362
	D-D	0.807	1.109	0.0	2,037.0	0.0	1.450	232,017.1	113,000.0	0.0000	0.0088	0.0000	112.9
-144 aux	A-A	0.997	1.377	0.0	0.0	60.5	1.452	232,391.1	113,000.0	0.0000	0.0000	0.0005	>1,000
lube gear	B-B	0.997	1.377	-5.0	3.8	60.5	1.452	232,391.1	113,000.0	0.0000	0.0000	0.0005	>1,000
shaft	C-C	0.997	1.297	-6.6	50.5	80.6	1.424	227,777.5	110,000.0	0.0000	0.0002	0.0007	>1,000
	D-D	0.997	1.297	-6.6	78.4	80.6	1.424	227,777.5	110,000.0	0.0000	0.0003	0.0007	>1,000
-167	A-A	1.750	2.375	0.0	0.0	17,970.0	1.444	231,075.1	113,000.0	0.0000	0.0000	0.1590	5.288
adapter,	B-B	2.023	2.375	0.0	0.0	26,750.0	1.369	219,089.0	105,300.0	0.0000	0.0000	0.2540	2.936
TAGB	C-C	1.643	2.375	0.0	0.0	16,430.0	1.473	235,674.2	114,000.0	0.0000	0.0000	0.1441	5.939
	D-D	1.193	2.375	0.0	0.0	13,530.0	1.583	253,325.6	122,000.0	0.0000	0.0000	0.1109	8.017
-211	A-A	1.100	1.565	0.0	0.0	58,580.0	1.466	234,551.2	113,000.0	0.0000	0.0000	0.5184	0.929
adapter,	B-B	1.100	1.709	0.0	0.0	41,050.0	1.503	240,466.2	117,000.0	0.0000	0.0000	0.3509	1.850
PRGB	C-C	1.100	1.920	0.0	0.0	26,880.0	1.545	247,175.3	119,700.0	0.0000	0.0000	0.2246	3.453
	D-D	1.100	1.750	0.0	0.0	37,530.0	1.512	241,933.8	116,700.0	0.0000	0.0000	0.3216	2.110
-111	A-A	0.760	1.000	-340.9	1,566.0	0.0	1.429	228,680.7	112,000.0	0.0023	0.0068	0.0000	108.641
generator	B-B	0.760	1.000	0.0	3,676.0	3,295.0	1.429	228,680.7	112,000.0	0.0000	0.0161	0.0294	28.829
shaft	C-C	0.760	1.000	0.0	849.9	3,295.0	1.429	228,680.7	112,000.0	0.0000	0.0037	0.0294	32.723
	D-D	1.174	1.395	0.0	49.19	1,623.0	1.376	220,159.8	101,000.0	0.0000	0.0002	0.0161	61.224
-196 quill	A-A	0.500	0.750	0.0	0.0	3,967.0	1.489	238,193.0	119,600.0	0.0000	0.0000	0.0332	29.149
shaft,	B-B	0.500	0.660	0.0	0.0	6,966.0	1.431	228,932.1	111,000.0	0.0000	0.0000	0.0628	14.94
TAGB	C-C	0.500	0.712	0.0	0.0	4,917.0	1.466	234,615.0	114,000.0	0.0000	0.0000	0.0431	22.185
	D-D	0.000	0.438	0.0	0.0	15,980.0	1.698	271,624.4	130,300.0	0.0000	0.0000	0.1226	7.154
-203 quill	A-A	0.942	1.146	0.0	0.0	1,642.0	1.389	222,212.2	99,600.0	0.0000	0.0000	0.0165	59.66
shaft,	B-B	0.500	0.680	0.0	0.0	6,035.0	1.445	231,234.5	113,000.0	0.0000	0.0000	0.0534	17.72
fan	C-C	0.500	0.840	0.0	0.0	2,591.0	1.532	245,109.1	126,600.0	0.0000	0.0000	0.0205	47.86
	D-D	0.000	0.438	0.0	0.0	15,980.0	1.698	271,624.4	130,300.0	0.0000	0.0000	0.1226	7.154

Spline Analysis

The load capacity of an involute spline is determined by its ability to resist failure by wear, tooth fracture, and tooth shear. These parameters are evaluated by calculating tooth bearing, bending, and shear stresses, respectively, for each spline joint. In evaluating all of the stresses, the load is assumed to be uniformly distributed among all of the teeth in contact and uniformly across the net face width in contact. The effects of misalignment and spline tooth inaccuracy are evaluated by applying suitable modifying factors or adjusting the allowable stresses for particular generic conditions (e.g., fixed or working splines, type of lubricant, etc). All spline data are computed with the Boeing SPLINE computer program, which provides stress, geometry, tolerance data, and complete design information.

The spline tooth-bending stresses are calculated by the same basic method as used for gear teeth except that the tooth load is assumed to be applied at the pitch diameter of each tooth. In calculating the spline tooth shear stresses, the same pitch line loading is assumed.

Unlike a gear in which each tooth is fully loaded and unloaded with each revolution of the gear, each tooth on a spline remains in contact and loaded at a more or less constant level during an entire rotation of the joint. For this reason, the spline tooth shear and bending stresses are seldom the limiting factors in the design of the spline. Almost universally, for A.R.T. and most other aerospace applications, tooth wear and surface degradation, as evaluated by the bearing stress, are generally the controlling factors in the design.

The bearing and shear stresses for each spline were calculated with equations 3 and 4, respectively.

$$S_{BEARING} = \frac{(K\ T)}{(D_P^2\ L)} \tag{3}$$

$$S_{SHEAR} = \frac{(2\ T)}{(N\ D_P\ L\ t)} \tag{4}$$

where T = design-rated torque, in.-lb

D_P = pitch diameter, inches

N = number of teeth

L = net engaged spline tooth length, inches

t = tooth thickness at pitch diameter, inches

K = unity (1) for whole-depth splines and 2 for half-depth splines

The maximum allowable bearing stress is dependent upon the amount of lubrication and the spline fixity. If the spline is working with marginal lubrication (typically grease), the maximum allowable bearing stress is 4,000 psi. If the spline is working and well lubricated (typically by an oil flow), the allowable bearing stress is 6,000 psi. If the spline is fixed (i.e., piloted and locked into relative position), the allowable is 15,000 psi. In order to minimize the effects of misalignment, the spline length-to-diameter ratio was maintained as low as possible and less than 1 in all cases; thus these allowable stresses are applicable.

The results of this analysis and spline sizes are summarized in Table 16.

Gearbox Housings

Gearbox housings react internal gear loads, support accessories, and provide lubrication through cored and machined passages to various areas of the transmission assembly. Since housings comprise a large portion of the transmission weight, attention has been given to assure a compact layout of drive train components and accessories. Rotor aerodynamic forces and moments are reacted to nacelle and airframe structure at the gearbox planetary upper cover, which is to be

TABLE 16. SPLINE ANALYSIS SUMMARY

Spline location	Type	Member	Pitch dia (in.)	Number of teeth	Spline length (in.)	Type of lubrication	Pitch	Speed (rpm)	Torque (lb-in.)	Tooth shear stress (psi)	Tooth bearing stress (psi)	Tooth bending stress (psi)
Quill shaft	Half-	Internal			1.0283					3,177.3		995.2
to	depth											
clutch shaft	(working)	External	1.75	28	1.0283	Oil	16/32	23,000	7,609.6	3,222.1	4,832.8	5,627.5
Bull gear shaft	Half-	Internal			2.00					2,767.5		-4,148.9
to	depth											
sun gear shaft	(working)	External	3.375	54	2.00	Oil	16/32	3,196.8	47,789.2	2,812.0	4,833.5	2,118.8
Tilt-axis t/o	Full-	Internal			1.20					5,289.8		11,215.8
gear to	depth											
coupling adapter	(working)	External	1.75	28	1.20	Grease	16/32	7,093.0	14,812.2	5,374.5	4,448.0	25,464.2
Coupling adapter	Full-	Internal			0.875					6,322.1		13,689.9
to	depth											
tilt-axis pinion shaft	(fixed)	External	1.875	30	0.875	Grease	16/32	7,093.0	14,812.2	6,672.5	5,142.7	31,930.4
Tilt-axis gear shaft	Full-	Internal			0.875					6,480.1		14,032.0
to	depth											
adapter	(fixed)	External	1.875	30	0.875	Grease	16/32	6,920.0	15,182.4	6,839.3	5,271.2	32,728.4
Engine	Half-	Internal			1.191					2,098.0		801.6
to	depth											
quill shaft	(working)	External	2.00	32	1.191	Oil	16/32	23,000	7,609.5	2,131.6	3,194.6	3,505.3
Access. hyd/lube pump	Half-	Internal			0.691					140.7		109.1
gear shaft to	depth										160.1	
main lube pump	(working)	External	0.800	16	0.691	Polyimide, oil	20/30	6,675.7	47.2	143.6		515.0
Access. hyd/lube pump	Half-	Internal			1.036					563.6		632.0
gear shaft to	depth											
hydraulic pump	(working)	External	1.20	24	1.036	Polyimide, oil	20/30	6,675.7	636.3	575.0	639.8	1,643.6
Aux pump gear	Half-	Internal			0.691					29.8		23.1
to	depth											
aux pump	(working)	External	0.80	16	0.691	Oil	20/30	6,304.8	9.99	30.4	33.9	109.0

made of forged aluminum alloy 7175 T736. All other housings except the sump housing are to be cast magnesium alloy WE43A, which offers excellent corrosion resistance and good strength properties up to 570°F (300°C). The sump housing is to be constructed of an aramid fiber and epoxy composite for reduced weight and ballistic tolerance. Additional anticorrosion coatings (i.e., HAE, resin, etc) will be employed to ensure maximum protection against harsh environmental conditions.

Three-dimensional computer design and analysis will be used extensively to model complex case geometries. The Boeing electronic mockup program has demonstrated the value and accuracy of CATIA solid modeling by eliminating hard mockups in a trial effort for the V-22. The finished 3D model provides a base for accurate computer weight calculations, finite-element modeling, clearance and assembly animations, and computerized numerically controlled (CNC) machining of foundry patterns, forging molds, and finished parts. Inspections and automated inspections also use the same data base.

Lubrication System Description

The lubrication system, shown schematically in Figure 19, provides main and auxiliary lubrication and cooling oil by directing high-load-capacity synthetic oil to gears, bearings, splines, and the overrunning clutch, at altitudes and maneuver conditions expected for a TTR aircraft. A weight saving was realized by combining both the TAGB and the PRGB portions of the drive train on one oil system but separate from the engine oil system. This philosophy will be reviewed again later in the program to see that all aircraft safety, redundancy, and ballistic-tolerance requirements are satisfied. Previous Boeing experience has provided several parameters to guide the A.R.T. lube system design, while new improvements are incorporated where beneficial.

Pressure-regulated, positive-displacement gerotor gear pumps deliver cooled and filtered oil to the gearboxes at 40 psig nominal pressure. Main and auxiliary lube pump units are driven by

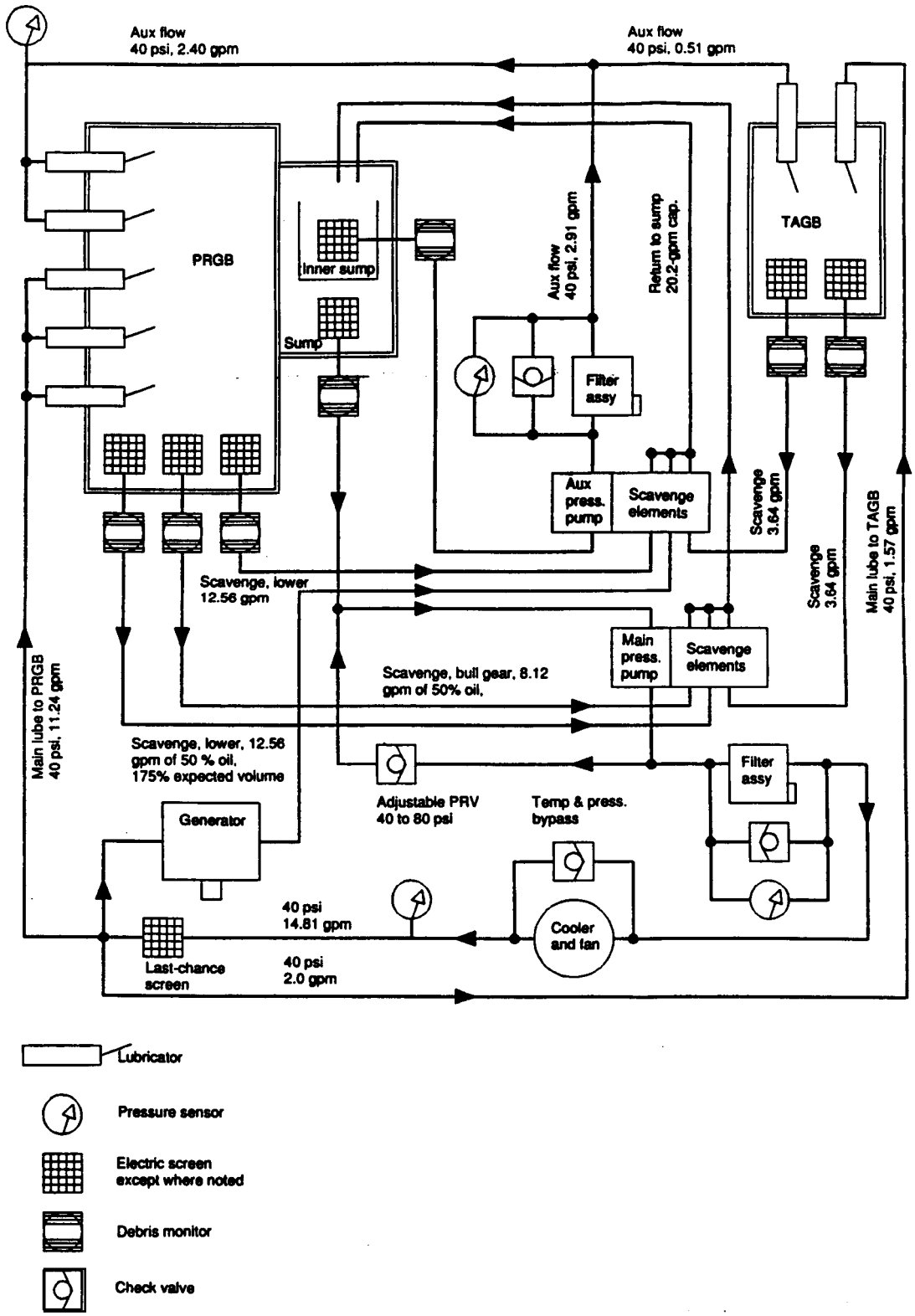

Figure 19. A.R.T. Lubrication Schematic

separate shafts taking power from the main bull gear. A redundant oil supply is provided to drive-system-critical bearings and gears via the auxiliary oil system. The pump installations are completed by insertion into the PRGB housing to engage splines and align oil ports to pump inlets and outlets. Each pump unit has a pressure control valve and four pump elements, one pressure and three scavenge. These gerotor-type pumps have proven to be reliable and debris-tolerant in many years of service.

A plate-and-fin annular cooler with an axial blower provides oil temperature control and is driven from the spiral bevel pinion at the TAGB. The cooler is equipped with temperature and pressure bypass valves to control temperature and to prevent loss of lubrication due to oil cooler blockage. Heat rejection is expected to be approximately 2,400 Btu/minute maximum as shown in Table 17.

Filtration is accomplished with a replaceable, pleated filter element rated at 5-micron nominal, 10-micron absolute. The filter rating was selected as an optimum tradeoff between component life and reliability, filter system weight, and maintenance. Differential-pressure (impending bypass) pop-out buttons, switches, and bypass valves are employed on the main and auxiliary filters. There is further debris protection in the form of screens. At or near each of the lubricators, there are small mesh jet-protecting screens, and further upstream there is a coarser screen at each gearbox inlet, accessible from outside of the gearbox assembly. A minimum jet orifice size of 0.032 inch is used to prevent clogging.

Lube oil per DOD-L-85734 with a flash temperature of approximately 350°F has been selected for the A.R.T. transmission. Oil is directed to the bearings generally through jet lubricators which deliver to shaft inner diameters and distribution grooves at the bearing inner diameters. Internal features have been incorporated in the shafts to inhibit bearing contamination from debris or sludge buildup. At the TAGB forward shaft, lube oil is fed into the bearing with a scoop spacer which forces oil under the bearing race. Gear mesh lubrication is provided by multiple-orifice lubricators which ensure adequate penetration of oil into gear teeth and across

TABLE 17. HEAT LOAD SUMMARY

	Mesh no.	Mesh type	Pitch Line vel (fpm)	Design hp	Mesh pwr loss (%)	Windage loss (hp)	Torque loss (hp)	Hp loss, max load	Hp loss at cubic mean loads	Heat loss (Btu/min)
Input shaft LS to jackshaft	1	Helical	18,455	2,424	0.5	6.06	6.06	12.12	10.06	514.0
Jackshaft to output shaft	2	Helical	9,292	2,424	0.5	6.06	6.06	12.12	10.06	514.0
Output shaft to cross-shaft	3	Helical	9,292	1,667	0.5	4.17	4.17	8.34	6.92	353.5
Sun gear to planet gear	4	Helical	2,935	2,424	0.5	6.06	6.06	12.12	10.06	514.0
Planet gear to ring gear	5	Helical	0	0	0.5	0.00	0.00	0.00	0.00	0.0
Generator	6	Helical	18,455	60.3	0.5	0.15	0.15	0.30	0.25	12.7
Lube pump shaft	7	Helical	9,292	1	0.5	0.0025	0.0025	0.005	0.004	0.2
Hyd pump shaft	8	Helical	9,292	72.4	0.5	0.18	0.18	0.36	0.30	15.4
Idler shaft	9	Helical	9,292	72.4	0.5	0.18	0.18	0.36	0.30	15.4
Tilt-axis gear shafts	10	Spiral bevel	13,468	121.2	0.5	0.303	0.303	0.606	-	25.7
Fan drive brg	-	-	-	-	-	-	-	-	-	0.1
Generator lube circuit	-	-	-	-	-	-	-	-	-	400.0
									Total heat loss =	2,365.0

the face of the tooth. In the case of the high-speed gear mesh, lube system development is recommended to determine type of orifice and proper placement, quantity, and velocity of lube oil for efficient operation. Oil-lubricated splines on both ends of the engine input shaft and the bull gear shaft are submerged in oil while in operation. Oil to the spring clutch assembly is fed by lubricator to the inside of the clutch mandrel and metered to the clutch and nearby tapered bearings; oil overflow from the clutch goes to the input spline.

Lube oil is collected at scavenge ports at several locations in order to return oil from low-lying areas during various flight attitudes and nacelle incidence angles. All suction ports are equipped with electric screen assemblies and debris monitors. Scavenge pumps are sized so that main or auxiliary scavenge can handle total return oil flow in the case of single-element pump failure. Some gravity drainback is used for PRGB during helicopter mode. Collected oil is conveyed to the aramid fiber composite sump assembly. Internal sump design includes an auxiliary system sump chamber to complete redundancy requirements, electric screens, debris monitors, and baffles or strainers as required.

The pressure-equalized gearbox is sealed from the environment except for filtered breather vents, with single lip seals, high-speed carbon seals, O-rings, and a segmented Teflon seal at the prop-rotor shaft. The single lip seals direct any leakage back into the interior of the gearbox with molded directional grooves. The segmented seal, located on the prop-rotor shaft between the rotor controls and the PRGB, will be field-repairable. Oil system self-sealing capabilities are being investigated for incorporation at a later phase in the program. Self-sealing would be accomplished through the use of a fabric applied in gearbox low-lying oil-collection areas. The fabric, when punctured, stretches and forms a small opening which tends to close upon itself. A similar fabric is employed in fuel tanks and bladders on fixed-wing aircraft to prevent hydraulic shock from damaging structure when penetrated by a projectile.

The splines at the ICDS are grease-lubricated to reduce demands on the oil system.

Interconnecting Drive Shaft

Power is transmitted between the rotors during flight maneuvers or OEI operation through an interconnecting drive shaft system. This system consists of a single shaft between the rotor and tilt-axis transmissions and multiple shaft sections between the tilt-axis transmissions at each nacelle. The shafts are of a braided-fiberglass construction and consist of a center shaft joined by a pair of diaphragm-type couplings with flanges at each end to provide bolt attachments to the transmissions. In addition to transmitting torque and accommodating misalignment, the shaft must weigh as little as possible and provide adequate stiffness in order to provide a 30-percent margin for critical frequency. Composites offer significant advantages over metals for this application because of their lower weight, higher stiffness-to-weight ratio, higher fatigue-strain capability, and corrosion resistance. Automated braiding-fabrication techniques are used to combine the shaft and coupling into a single unit and eliminate the problems associated with hardware and joints. This gives a lighter, simpler, more reliable and maintainable, and less costly system. A similar shaft has been successfully fabricated and tested under the Army Integral Shaft/Coupling Program, contract DAAJ02-87-C-0005, and reported in Boeing document D210-12871-1[6].

Accessory Installations

Accessory installations include a fan and cooler at each tilt-axis gearbox and the hydraulic pump, generator, and main and auxiliary oil pumps at each prop-rotor gearbox. The accessories have been designed with the same type of bearing and gear shaft arrangement as in the primary drive train. Throughout the accessory installations, care has been taken to reduce installation size and to use current-technology-driven hardware. Accessory drive shafts are made of titanium with "Ionguard" modified wearing surfaces at gear teeth and bearing journals. These shafts are generally sized more by geometric requirements than load capacity, and a weight saving will be realized by using the titanium material. The ion implanting procedure toughens the surface of the part where applied, while part dimensions are left unchanged. As in other areas of the

transmission, a hybrid tapered-roller bearing is used to react thrust loads in two directions, with a plain roller bearing at the opposite end of the shaft. Polyimide adapters are used in most spline interfaces to reduce wear and oil system requirements.

The fan assembly is driven directly by thin titanium shafting from the tilt-axis gearbox forward gear, which saves weight by eliminating a gear mesh and bearing. Polyimide adapters are used at spline interfaces. The cooler moves approximately 2,750 cfm of air to reject heat loads up to 2,400 Btu/minute (maximum heat load).

The hydraulic pump and main lube pump share a common titanium drive shaft which is driven from a titanium idler gear driven by the bull gear shaft. The hydraulic pump has an integral polyimide adapter. The lube pump, which is driven from the opposite end of the titanium drive shaft, has a splined quill shaft coated with thin, dense chrome (TDC) and lubricated with oil from within the pump. The hydraulic pump selected was a 3,000-psi, pressure-compensated, variable-flow, axial-piston pump, maximum flow 37 gpm in the hover mode at 6,675 rpm, 33 gpm airplane mode, 18 pounds wet. Developed by Vickers, the pump is scheduled to go into production in mid-1991. Maximum power drawn at the common shaft is approximately 70 hp.

The gerotor auxiliary lube pump gear shaft is driven from the bull gear shaft at 6,305 rpm in hover mode. The TDC-coated pump quill shaft engages the titanium gear shaft and is lubricated with oil from within the pump. Maximum power drawn is 0.5 hp.

The generator gear shaft is driven from the PRGB SK32137-38 intermediate gear shaft at 19,827 rpm in hover mode. The 270-volt dc, 20-kw Lucas machine uses an internal quill shaft with polyimide adapter to engage the titanium gear shaft. Dc generators are proposed for the RAH-66 program and promise weight and size advantages over more traditional ac devices for future helicopter applications. Cooling and lubrication are provided for the generator from the gearbox main lube circuit. Electric screens and debris monitors will detect generator-produced contamination.

Structural Interface

Rotor loads are reacted from the rotor shaft through to the prop-rotor gearbox upper cover and directly into structure. The structural concept shown uses a main box beam to react loads in all directions and carry them back to the wing interface and a tension strut to help react tension loads from PRGB to TAGB and wing structure. Use of the tension strut counteracts moments induced by the offset at the PRGB/structure interface. The combination of these elements provides a weight-effective support system that prevents rotor forces and moments from producing deflections in the gearbox housings. The overall resulting system is lighter as a result of these features. Structural parts are anticipated to be 60-percent graphite/epoxy composites, with the remainder aluminum, titanium, and steel.

Preliminary structural analysis of the support system primary load path was conducted to evaluate the design concept and to establish that the required strength and stiffness levels could be produced in later development as the full load spectrum with such items as landing loads, higher harmonic rotor loads, etc, becomes available. A driving requirement is that the aerodynamic forces and moments produce deflection at the ICDS no greater than 1.5 degrees at maximum steady-state conditions.

Diagnostic Equipment

The majority of the current state-of-the-art helicopter transmission health-monitoring diagnostics flying today rely on the theory that most types of transmission faults manifest themselves by initially producing small amounts of metallic debris. They also assume that as the defect grows, so does the debris-generation rate, and this is generally true for bearing failures. Even though the use of hybrid (ceramic) bearings in the A.R.T. transmission could produce nonmetallic debris from ceramic rolling elements, preliminary tests have shown that the predominant failure mode will be spalling of the metal races. However, experience has shown that fatigue failures of gears and shafts in most cases produce no metallic debris during failure. Most fatigue failures

in helicopter transmission load-carrying gears and shafting can be catastrophic and are presently not reliably detectable in flight with the production diagnostic equipment flying today. Results of research conducted by Boeing over the last five years strongly indicate the successful use of computer-based vibration diagnostics for in-flight detection of impending fatigue failures in helicopter transmission major dynamic components.

In addition to all the standard transmission diagnostic equipment, temperature and pressure indication, and debris detection, the A.R.T. transmission design specification shall include the use of a transmission vibration diagnostic system (TVDS). The TVDS will be based on existing diagnostic computer hardware now being installed on S-61 helicopters owned by British International Helicopters, Ltd, for use in the North Sea. The computer will have the minimum capability to analyze every major rotating component in the A.R.T. rotor and tilt-axis transmissions with as many as 12 different analytical techniques once every 150,000 (approximately) fatigue cycles of normal operation. The unit will be programmed to perform only the analytical techniques applicable to the type of component being analyzed. The TVDS will be able to store, for future download or data comparison, a minimum of the previous 15 hours of run-time analytical results for all techniques on all the major transmission components analyzed. The TVDS will be programmed to download all stored analytical results to an IBM-PC-compatible computer by use of a portable ground station display terminal for printed tabulation and/or plotting of trend data. The unit will also have two warning lights. An amber light will illuminate after any single analytical technique on an individual component exceeds five times the standard deviation (5 sigma) of the previous steady-state operating condition. A red light will illuminate after more than one analytical technique result exceeds the 5-sigma value at any given time.

This TVDS can be used during the A.R.T. program transmission bench testing to alert the test engineers to any impending fatigue failures during bench tests. This approach will have a twofold benefit, i.e., the first, to protect the limited A.R.T. transmission assets during

development testing from unforeseen catastrophic failures, and the second to be the further development of the technology of transmission vibration diagnostics.

Assembly Procedures

The assembly of the A.R.T. drive system requires some special considerations. The final assembly consists of four distinct subassemblies: upper and lower housing assemblies, clutch cartridge assembly, and cover/planetary system assembly. Based on the need to reduce transmission-generated noise, helical gearing, including a double helical planetary system, was selected. In addition, a high-speed spring clutch was selected for use in the input pinion section to reduce weight and complexity. The use of helical gearing and a spring clutch require some unique assembly fixtures, tools, and procedures.

The upper and lower housings, SK32137-97, -10, and their associated hardware, are similar in their method of assembly. The bidirectional tapered-roller bearings are pressed onto their respective gear shafts and the bearing locknuts installed. The bidirectional tapered-roller bearings and cylindrical-roller bearings are then installed and secured into their respective housings; then the upper and lower housings are mated together. The gear teeth of the -45 bull gear in the lower housing, the -38 intermediate gear shaft, and the interconnecting drive gear shaft in the upper housing must be fitted together and then rolled down the helix angle of the teeth to assemble the two housings. In addition, the shafts must also be guided into their cylindrical-roller bearing bores during this assembly.

The clutch cartridge is assembled with tapered-roller bearing, locknut, seal ring, seal, and clutch shaft with clutch guide. Next, the -17 spring clutch is installed into the -13 clutch shaft with a special installation tool. The -23 clutch cartridge is then installed into the assembled upper and lower housing. A special tool is used to keep the spring clutch wound (compressed) against the clutch guide to enable it to be installed into the pinion shaft bore in the upper housing.

The cover/planetary system subassembly requires two distinct procedures: one for the planetary assembly and one for the carrier/output shaft and cover assembly. Because the -52 double helical sun gear shaft is locked into position when in mesh with the -53 planets, it is necessary to preassemble the planetary system before assembly with the -66 carrier/output shaft. The preassembly requires a fixture that locates the four planets (90 degrees apart) on four spring-loaded guide posts while meshing with the sun gear. The four integral posts on the carrier/output shaft are then fed into the planets, depressing the spring-loaded guide posts of the fixture. The assembly is then turned over and the fixture removed so that the planet retainers can be installed onto each planet post. The upper and lower ring gears and spacers are then installed around the planets. The ring gear teeth must be fitted to the planet gear teeth and then the ring gear is rolled down the helix angle of the gear teeth to the installed position. A couple of detent pins installed through the bolt holes of the ring gears and spacer lock the whole planetary system together. The planetary system is then installed into the -57 cover. The lower planetary tapered-roller bearing cone assembly is pressed onto the carrier/output shaft. The upper and lower rotor shaft tapered-roller bearing cups are pressed into the cover. The cover is then lowered onto the carrier/output shaft using the detent pins in the planetary assembly to align the bolt holes of the cover and planetary system. A shim will be ground to size to achieve proper preload on the tapered bearings. The final ground-to-size shim will be installed and the upper rotor shaft tapered-roller bearing pressed onto the carrier/output shaft. The bearing locknut, seal, and seal cover are also installed. The cover/planetary system assembly is then installed onto the assembled upper and lower housings. Installing the remaining components (accessories, lubricators, transfer tubes, chip detectors, sump, etc) completes the rotor transmission assembly.

Producibility

Producibility has been optimized in the A.R.T. drive system by incorporating design concepts which achieve a major reduction in the number of components and also reduce manufacturing time. Parts reduction has been achieved through various design features including integral-race

bearings, bidirectional tapered-roller bearings, spring clutch, and ICDS with integral couplings and flanges. Manufacturing time has been reduced by the use of polyimide splined inserts, single-carburizing case depth, and oil-dip finish as a protective coating for steel.

Integral-race bearings use the gear shaft as the inner race for the bearing. This eliminates the need for bearing inner ring, locknut, retainer, and retaining ring. It also eliminates the need for a threaded shaft end with machined slots for the lockring and retainer, which reduces manufacturing cost and time during gear shaft fabrication.

The use of bidirectional tapered-roller bearings eliminates one bearing from each gear shaft. This bearing design can react thrust in two directions and also eliminates the problems of preloading a set of tapered-roller bearings.

The spring clutch, in addition to saving weight, will also reduce parts count. The spring clutch consists of seven or eight detail components, compared to 30 or more for a comparable ramp roller or sprag clutch design. In addition, the extended fabrication time required for camshaft or sprag is eliminated.

The ICDS with its integral flexible couplings and flange also eliminates numerous parts. The integral coupling eliminates the separate coupling components and bolts, washers, and nuts associated with a conventional shaft/coupling system. The integral flange eliminates the need to rivet or pin a flange connection to the shaft, further reducing components.

Polyimide splined inserts are used at various accessory locations for small-diameter splines. This eliminates the need for a hardened, ground spline and the carburizing and subsequent finishing operations of the spline to correct for heat-treat distortions.

Components that do require carburizing are designed so that only a single-carburizing case depth and hardness are required. This eliminates multiple-carburizing cycles and reduces fabricating

times associated with carburizing, quenching, and masking of components with multiple-carburizing areas.

Oil-dip finish is used on all internal oil-wetted steel components as a protective coating. This eliminates the need for phosphate or black oxide coatings normally applied to these parts. Many recent surveys of overhaul and repair facilities by both contractors and military sources have shown no indications that oil-dip-finished parts differed from phosphate or black oxide-treated components with regard to corrosion. In addition, many parts will have a thin, dense chrome (TDC) coating which further protects the surface from corrosion.

Maintainability

Many factors that contribute to the ease of maintenance were considered during this preliminary design phase of the A.R.T. program. The transmission system design uses lessons learned from fleet operations, the identification of major contributors to maintenance tasks, and the incorporation of new technologies to improve maintainability. Maintenance activities are primarily on an on-condition basis; preventive maintenance is limited to periodic transmission oil changes and ICDS spline regreasing. Components requiring regreasing are limited to drive shafting splines and bearings. There are no primary transmission drive splines or bearings requiring grease. Transmission diagnostic capabilities, including TVDS, self-closing debris monitors, accessible and removable electric screens, lube oil pressure and temperature monitoring, and filter and cooler bypass valves provide on-condition maintenance assessment. Easily accessible and removable components, such as splined plug-in accessories and segmented rotor shaft seal which allows field replacement of seal elements without removal of rotor controls and interconnecting drive shafts, further reduce maintenance time.

WEIGHT SUMMARY

The weight of the A.R.T. drive system, as shown on drawing SK32137, is 1,496 pounds, which corresponds to 0.309 lb/hp. This is an improvement of approximately 2.5 percent over the drive system as defined in the concept selection phase (Task 3) of the program. The drive system weight can be further reduced 21 pounds by changing the planetary output stage from a double helical to a spur gear configuration. That change would produce a drive train that weighs 0.304 lb/hp.

The current Task 4 drive system weight, as shown in Table 18, is based on calculations from stressed layouts. The items that were calculated include gears, bearings, rotor shaft, standpipe, and ICDS. The miscellaneous hardware associated with the assembly was estimated from SK32137 drawings. The gearbox housing and lubrication system weights were determined from parametric trends.

It is expected that additional weight can be removed from the various shafts and gears used in the A.R.T. transmission. The margins of safety shown in Tables 13, 14, and 15 appear to be very high in many cases. During detail design and final stress analysis of the A.R.T. transmission, shaft sections will be reduced to minimize weight and still maintain adequate margins of safety.

SUMMARY

Preliminary design of the Boeing advanced rotorcraft transmission, which advances and incorporates key emerging material and component technologies, has been completed. This report is issued to document design considerations and criteria. In addition, the preliminary design drawings, SK32137, sheets 1 through 5, are included in Appendix A. Specific program goals defined at the beginning of the A.R.T. program include:

TABLE 18. WEIGHT SUMMARY OF ADVANCED ROTORCRAFT TRANSMISSION

Component	Task 4	Task 3
PRGB + TAGB (includes rotor shaft)	1,192	1,159.6
Lubrication system	214	240
Cross-shafts	90	138.2
Total system weight (lb)	1,496	1,537.8
lb/hp	0.309	0.317
Planetary spur gears	-21	-
Revised system weight (lb)	1,475	-
lb/hp	0.304	

1. Reduce transmission weight by 25 percent relative to SOA trends (currently in the range of 0.40 lb/hp).

2. Reduce transmission weight by 10 pounds relative to SOA.

3. Improve transmission life and reliability while extending mean time between removals (MTBR) to 5,000 hours.

A.R.T. program participants selected aircraft from two categories, Future Air Attack Vehicle (FAAV) and Advanced Cargo Aircraft. The Boeing aircraft selection of the Tactical Tiltrotor (TTR) satisfied the requirements outlined for the FAAV category, a 10,000 to 20,000-pound aircraft. The TTR drive system is similar to that of the V-22, using two engine and transmission installations, one at the end of each wing, and interconnecting drive shafts. Aircraft primary mission gross weight, taking into account A.R.T. program implementation, is 17,223 pounds.

Three transmission and drive train concepts were evaluated for suitability with respect to program goals. They are the self-aligning bearingless planetary configuration (SABP), the split-torque configuration, and the conventional single-stage planetary configuration. Through a selection methodology that studies weight trends, reliability factors, and noise characteristics (shown in Table 7), the single-stage planetary configuration appeared to have the greatest potential of achieving all of the A.R.T. program objectives with the lowest risk.

Design Activity

Maximum power seen by certain sections of the gearbox was 2,777 hp (OEI). Output speed was 600 rpm hover, 480 airplane cruise. Gear shaft design employs an integral gear and shaft arrangement to eliminate joint problems. Highly loaded gear shafts will be made of VASCO X2M. Helical gears are used extensively and double helicals are used at the planetary output stage. Gear shafts are supported with roller bearings: at one end, a hybrid cylindrical-roller

bearing operating directly on an integral shaft journal; the other, a hybrid bidirectional tapered-roller bearing with ceramic rollers, H^3 steel races, and P.E.E.K. retainers. These bearings take thrust in both directions. Bearing lives were calculated and gear shafts were analyzed for stresses and deflections. In the case of engine failure, the transmission is protected with an overrunning spring clutch which uses fewer parts than a conventional sprag clutch design, and drive system shafting transfers power from the remaining engine to both rotors.

Gearbox housings were designed in WE43A magnesium. WE43A is a new alloy which offers excellent corrosion resistance and high-temperature strength. Cored lube passages in the housings channel oil per DOD-L-85734 for distribution to the bearings and gears through lubricators. Wherever practical, oil is delivered to shaft inner diameters, then to the various bearing inner races. Gear lubricant is provided by finger jets both into and out of mesh for primary drive components. Lubricant oil is filtered to 5-micron nominal, 10 absolute for longer component life. The lube system is highly redundant both in the delivery of oil and in scavenging.

The ICDS is a braided-composite design with integral couplings capable of large misalignments.

Titanium gear shafts with ion-implanted wear surfaces drive accessories using polyimide splined adapters where possible.

Vibration diagnostics will provide a real-time health-monitoring method in addition to standard debris-monitoring techniques.

Considerations for assembly, producibility, and maintainability have guided the design to assure that technical and weight advantages are not lost on impractical arrangements.

Weight studies have supported initial projections of approximately 0.30 lb/hp pending the incorporation of high-profile contact ratio, noninvolute tooth form (HCRNIF) gears.

Some further preliminary design work would be desirable but is beyond the scope of this portion of the design effort or contract. These efforts would be:

- Trade studies for splash lubrication of the tilt-axis gearbox
- Trade studies for integral nacelle/support structural arrangement
- Incorporation of selected technologies proven feasible from testing.

Principal technological studies in support of A.R.T. program objectives include (Figure 20):

- High-profile contact ratio, noninvolute tooth form spur gears
- Noise reduction by active force cancellation
- Hybrid bidirectional tapered-roller bearings
- Improved bearing technology
- Minimum-lube study of hybrid bearings
- Precision net-forged spur gears
- Parallel-axis gear noise study
- Surface-modified titanium gears.

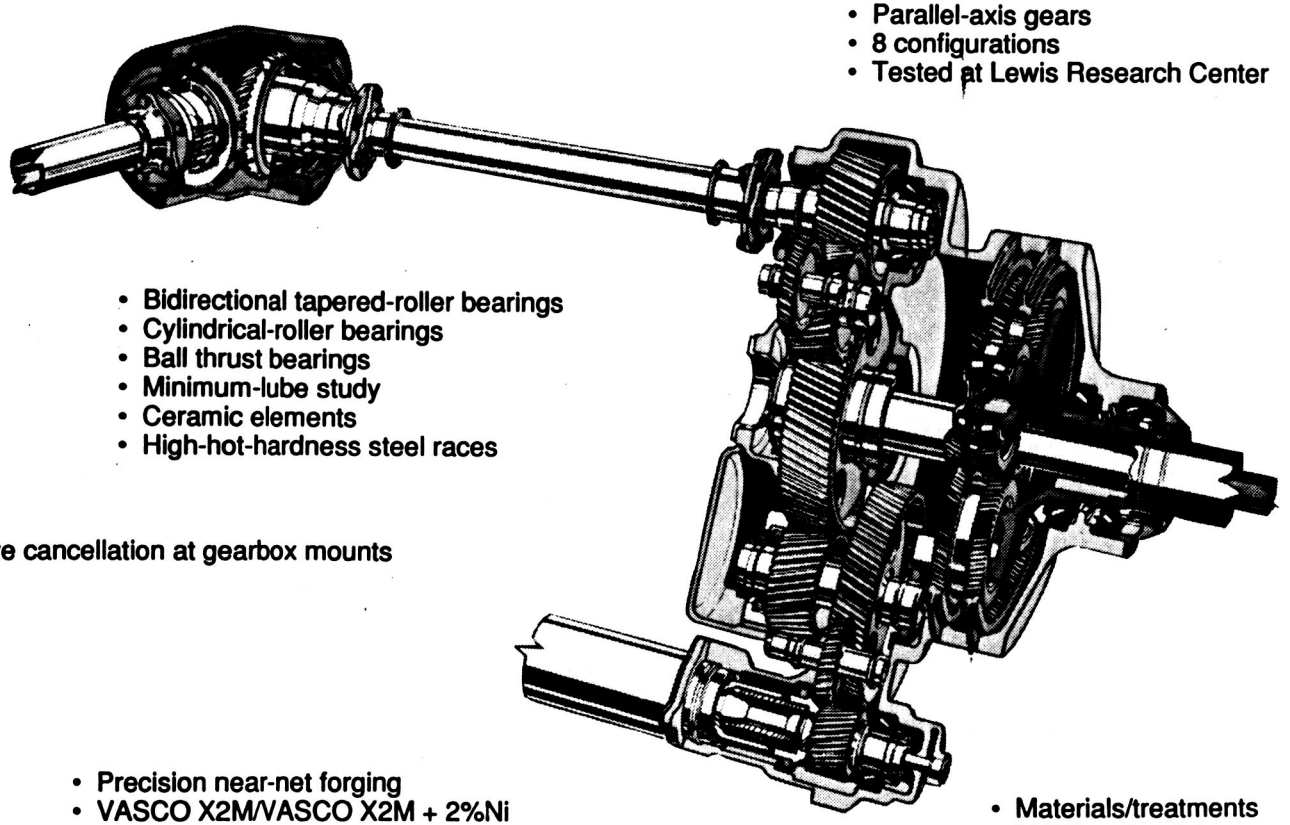

- Parallel-axis gears
- 8 configurations
- Tested at Lewis Research Center

- Bidirectional tapered-roller bearings
- Cylindrical-roller bearings
- Ball thrust bearings
- Minimum-lube study
- Ceramic elements
- High-hot-hardness steel races

- Active cancellation at gearbox mounts

- Precision near-net forging
- VASCO X2M/VASCO X2M + 2%Ni
- Single-tooth bending fatigue

- Materials/treatments
- HCR/noninvolute
- Lubrication/scoring
- Fatigue/noise

Figure 20. Planned Component Testing of A.R.T. Tactical Tiltrotor Transmission

COMPONENT DEVELOPMENT TESTING

TRANSMISSION NOISE REDUCTION

Background

Noise within many large helicopters is dominated by sound radiated at rotor transmission frequencies (Figure 21). In the CH-47, a large tandem-rotor helicopter, the predominant noise sources are those of the first-stage planetary gears in mesh with both the stationary ring and sun gears. Studies in the past[7] have identified the first-stage planetary frequencies as having both airborne and structureborne paths to interior spaces.

The major forces involved in gear noise generation arise from gear tooth meshing. These forces are transmitted structurally through the bearings to the surrounding case. This results in gear noise radiated by the transmission case as well as the fuselage due to forces transmitted through the mounting legs.

Transmission noise reduction, as defined by Boeing for the A.R.T. program, involved three general approaches: (1) evaluation of the effect of changes in gear profile, face configuration, and contact ratio, as well as gear tooth form, for both spur and helical gears; (2) passive means of noise control including damping of input and planetary gears as well as the transmission case; and (3) active control techniques. This section reports on (2) passive noise control, and (3) active control techniques.

Introduction

Overall Boeing efforts for the A.R.T. program focused on developing a rotor drive system for a tactical tiltrotor (TTR) aircraft. The TTR design is configured as a small, lightweight, highly

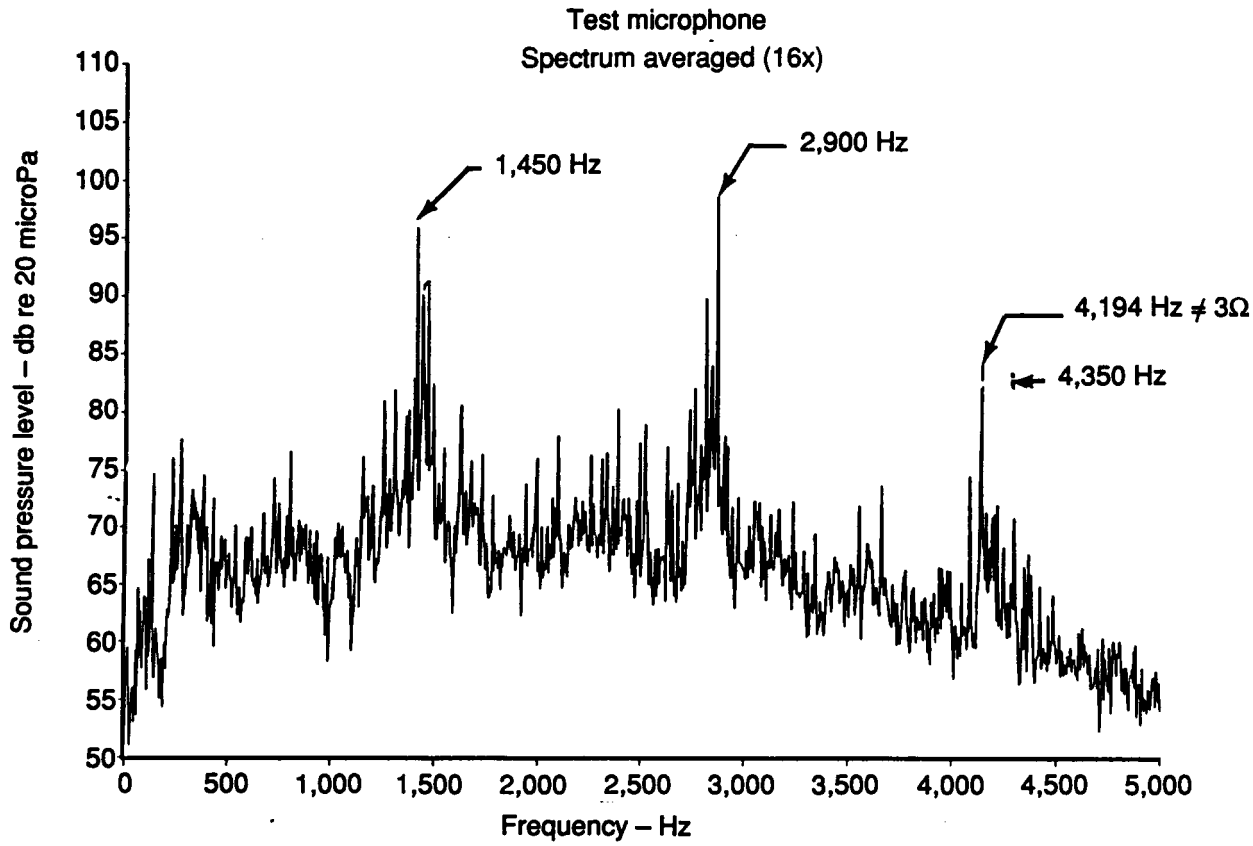

Figure 21. Transmission Noise Spectrum of CH-47 Helicopter

maneuverable attack aircraft, and a drive system which would be typical for an aircraft of this size was designed as part of the Boeing A.R.T. program. However, for ongoing noise studies it was necessary to work with an existing gearbox in order to conduct an evaluation of specific damping treatments as well as proposed active control methods. A CH-47C forward rotor transmission was chosen to demonstrate noise reduction methodology, and a test stand of composite material was designed to provide a mounting for this transmission.

In the CH-47 helicopter (Figure 22) power from the engines operating at 15,000 rpm is transmitted through right-angle gearboxes to a combining transmission in the aft portion of the fuselage. This combining transmission divides power to both forward and aft rotor transmissions through interconnecting shafts. The speed of these shafts, 6,900 rpm, is reduced in the transmission to nominal rotor operating speeds of 225 rpm. This is accomplished through a two-stage planetary system driven by an input pinion/bevel gear that also achieves a 90-degree change in direction. A cutaway drawing of the forward rotor transmission is shown in Figure 23.

Helicopter drive systems typically transmit power that ranges from 300 hp for small aircraft to 3,000 hp or more for large helicopters. The power transmitted by large helicopter rotor transmissions can be greater than for other commercial drive systems, such as trucks or other land-based vehicles, but the weight of aircraft gearboxes is always minimized in order to maximize payload. As a result, gear stresses, tooth forces, and case deflections are high. The resulting noise levels may be higher than for transmissions that transmit significantly higher levels of power but have not been subject to stringent weight restrictions. Automotive truck transmissions, for example, typically generate sound levels of 70 db(A) or less at a distance of 15 feet and their specific weight (lb/hp) is in the order of 2 to 2.5 lb/hp. Large helicopter rotor transmissions, on the other hand, have specific weights on the order of 0.4 lb/hp and can produce sound levels of 100 db(A) at a similar distance.

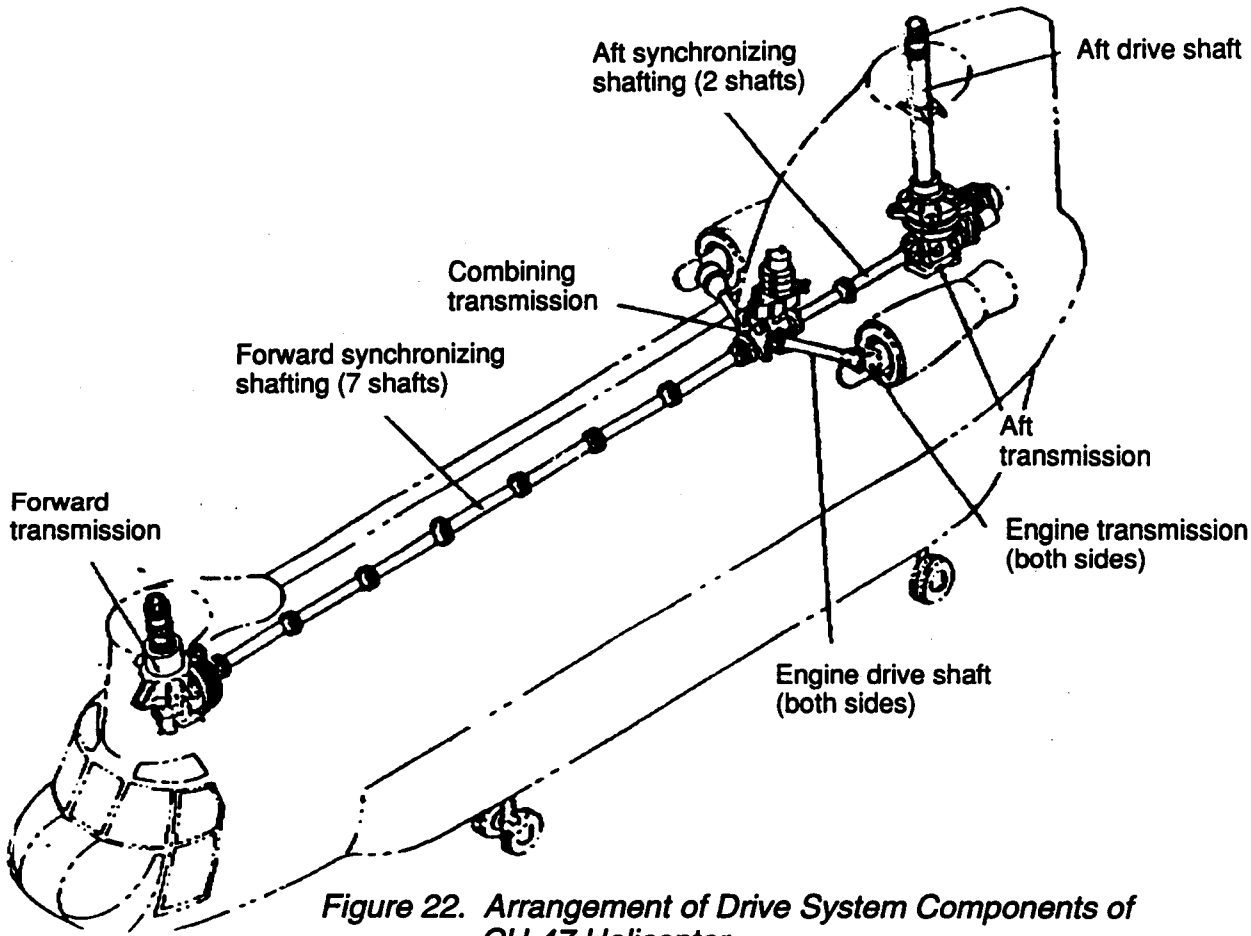

Figure 22. Arrangement of Drive System Components of CH-47 Helicopter

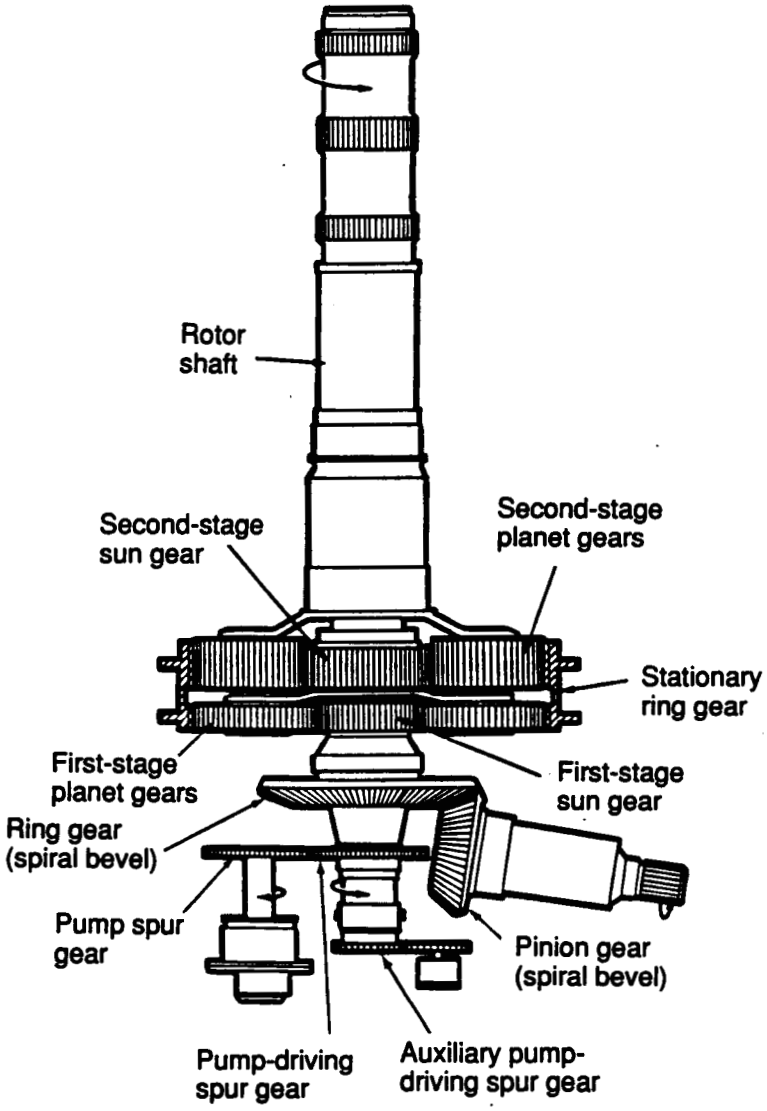

Figure 23. Major Components of CH-47 Forward Rotor Transmission

Approach

Passive Control -

Airborne Noise - Traditionally, noise reduction from airborne paths has relied on passive treatment of surfaces surrounding the transmission. The area treated by soundproofing material is limited to those surfaces that are not otherwise required to be visible for utility purposes. Cabin treatments for tandem-rotor helicopters have achieved 30 to 35-db noise reduction at speech frequencies, whereas reductions in cockpits have been limited to 20 db. This reduced acoustical performance in cockpits by passive treatments arises primarily from an inability to adequately cover all sound-radiating surfaces. Window transparencies, which comprise a large percentage of the cockpit surface, have been found to be a significant sound-radiating surface for gear noise.

For example, one cockpit noise reduction test conducted in the past on a CH-47 was limited to a noise reduction of 20 db even though 95 percent of all surfaces were covered with a 1.5 -psf absorber/barrier blanketing material. It was concluded that any additional noise reduction would have had to be achieved through elimination of remaining structureborne noise paths into the cockpit.

Structureborne Noise - Generally, rotor transmissions in large helicopters are not vibration-isolated from the structure due to stiffness requirements for large startup torques, as well as critical shaft alignment requirements. During the recent development of two Boeing helicopters, the Model 234 and Model 360, passive elastomeric transmission mounts had been investigated as a potential solution for reducing structureborne noise of rotor transmissions. Mounts were required to be stiff in reacting torques, particularly startup torques, and torsional deflections were required to be limited to 1/4 degree or less to maintain drive shaft alignment. Based on these requirements, passive mounting systems did not appear to be feasible for these installations.

A more thorough review of passive mounting systems was initiated as part of the A.R.T. program. A review of adaptability of passive mounts to the test transmission was conducted by the Lord Corporation over a period of nine months. Lord also examined other options, including proprietary Fluidlastic mounts and adaptive systems which were considered to be of less interest at the current stage of development than a passive elastomeric system. Figure 24 is a Lord Corporation plot of normalized isolator weight, noise reduction, and life as a function of horsepower. Note that as power required increases, the elastomeric mount system becomes less attractive, since the trend is toward greater mount weight and lower noise reduction. Any mount design must be stiff enough to take rotor torque loads, particularly during rotor startup and stopping. The higher the horsepower of the transmission, the larger and stiffer the mount must be, and there is a tradeoff between life, weight, and noise reduction. After extensive review, Lord confirmed earlier conclusions and did not recommend an elastomeric isolator for high-horsepower applications such as the subject transmission. Figure 25, provided by Lord, shows the reduction in transmissibility for a mounting system typical for a large helicopter: 2,500-hp transmission, 250,000 lb/in. airframe stiffness, four-blade rotor (~ 15-Hz blade passage frequency). For the available mount stiffness range, a reduction limited to 4 db in transmissibility appeared to be achievable, but this was not sufficient to warrant further consideration, further indicating that a passive isolator would not be an effective approach to noise reduction.

After this extensive investigation of the adaptability of passive mounts to large transmissions, such as the CH-47C, it was concluded that an elastomeric mount system was not attractive. However, passive measures might be applicable to smaller transmissions, such as the TTR. It was for these reasons that active control of structureborne noise was pursued.

Active Control - Active noise control is typically applied to low-frequency problems. The motivation is that passive noise control methods for low frequencies require large volumes of

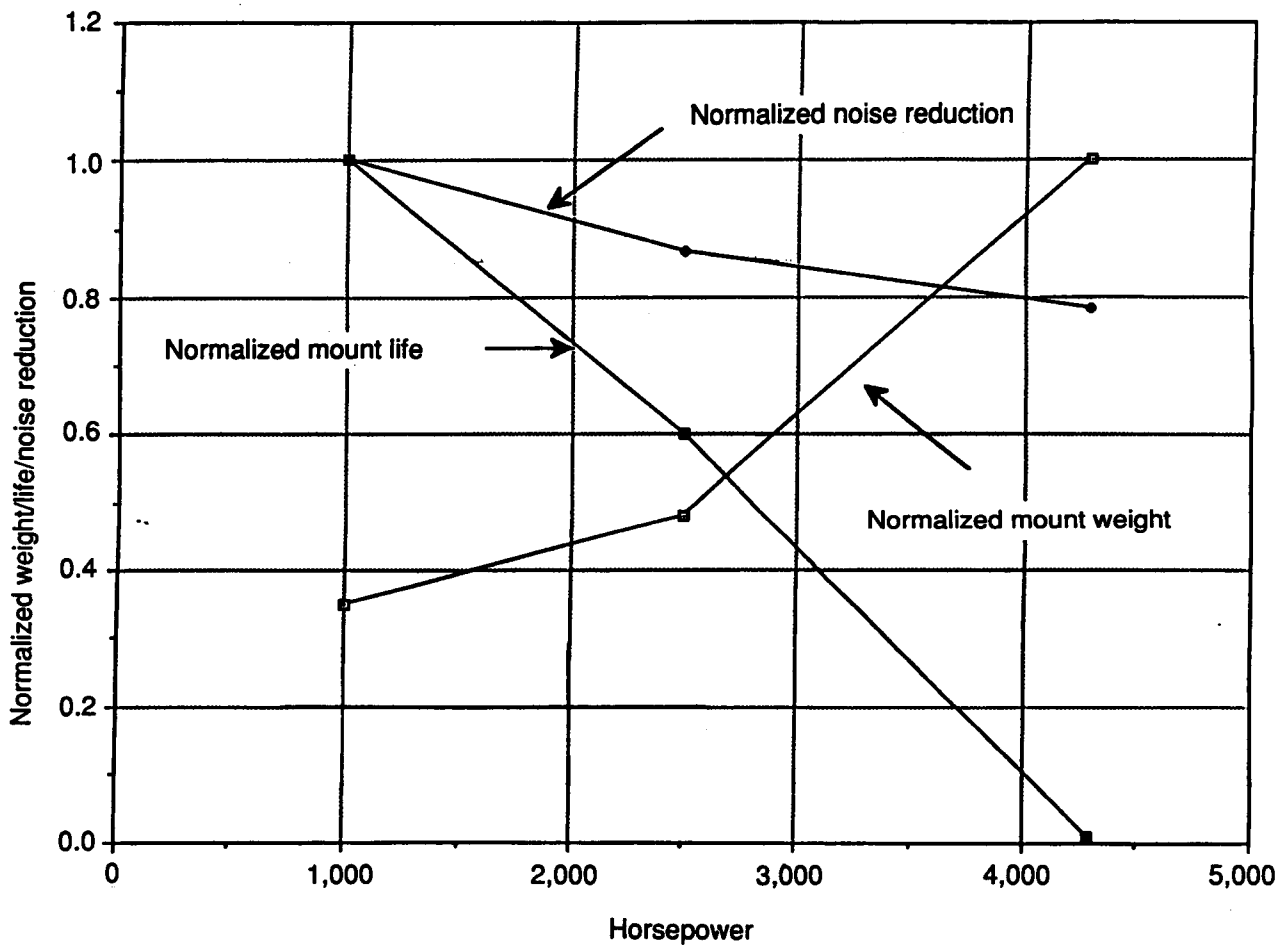

Figure 24. Normalized Weight, Life, and Noise-Reduction Trends for a Large Rotor Transmission

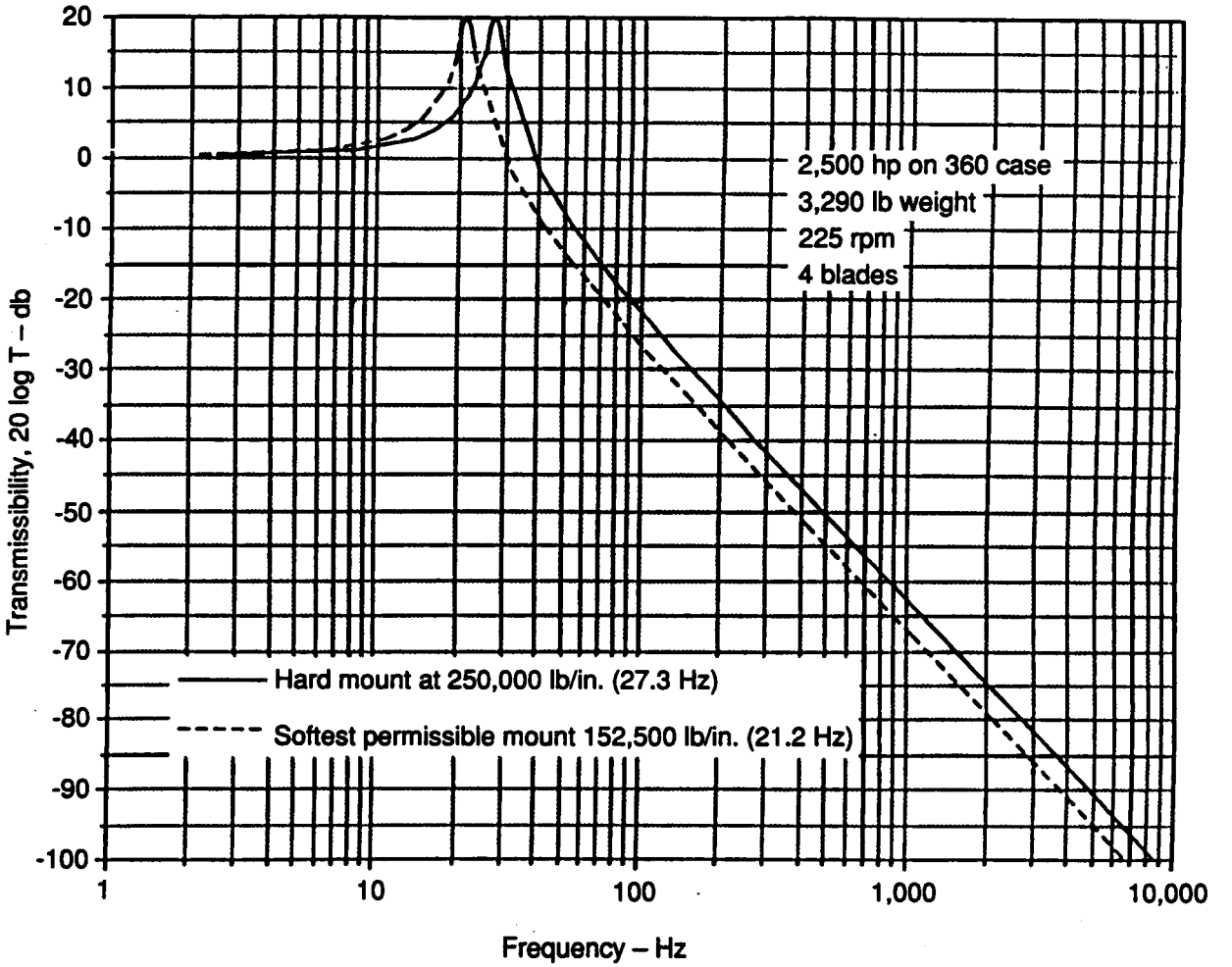

Figure 25. Potential Noise Reduction of Transmission Mount

space and/or large amounts of mass to be effective. At low frequencies an active solution may be the only workable alternative to a noisy machine.

High-frequency applications of active control are more difficult and less common. At high frequencies the wavelengths are short, the data-processing times are short, and passive noise control methods are generally considered to be effective. The utility of active noise control for high-frequency problems cannot be argued in general terms.

The particular issues that motivate this study of high-frequency active noise control are that elastomeric mounts are not feasible, an adequate amount of passive treatment cannot be applied in the helicopter cockpit, and the potential exists for weight savings by reducing the amount of passive treatments used. The objective of the initial work was to determine what is required to achieve noise reductions in the gear mesh frequency range with an active system. The active control system is considered in two parts: the actuators and sensors and the control algorithm.

Actuators and Sensors - The choice of an actuator configuration for the control of distributed-parameter systems is best viewed as a problem of superposition of fields. The control actuators (secondary sources) must be able to generate a field that is spatially similar to the field produced by the offending noise source (primary source). The field could either be an acoustic field in the airspace or a vibration field in the structure.

In the helicopter problem, the goal is to reduce the noise level in occupied spaces. It is logically possible to attack the noise problem either in the airspace[8] or in the radiating structure[9]. These approaches are discussed briefly. A third approach, and the one that is taken in the current work, is to attack the problem at the source. In the current context the source is the connection between the transmission and the fuselage structure.

Control of the interior noise with acoustic sources is a problem of modal control. The airspace dimensions are on the order of 10 feet and acoustic wavelengths at the

disturbance frequencies are on the order of 1 foot. The number of modes that should be controlled will be large, and modal spillover could be a serious problem. The number of microphones and speakers that would be required to observe and control the space would be large, and it would be difficult to avoid placing transducers in awkward positions. Direct control of the airspace is considered to be unlikely and was not pursued. Modal control of the vibration of the fuselage is unlikely for many of the same reasons.

Actuator Location - A recent paper by Hansen and Snyder[10] illustrates the difficulties of controlling acoustic radiation from a plate as a result of increasing damping, modal density, and plate dimension (as compared to an acoustic wavelength). The uncontrolled system is a rectangular plate driven by a single disturbing force and radiating into a halfspace. The optimum reduction in radiated power that can be achieved by a single control force is calculated for many control force locations. One conclusion that can be drawn from this paper is that reductions can always be achieved when the control force is near the disturbing force. Applying control forces at the connection between the transmission and the fuselage is the most viable approach. This approach was used successfully in the small-scale test and again in the full-scale testing.

Sensor Location - The choice of the sensor configuration is usually viewed as a finite approximation to some globally defined quantity such as potential energy or power. Choosing to locate the actuators at the transmission connection points suggests locating the sensors at the connection points. In this configuration the control system is trying to observe and control the power flow into the fuselage. This collocated configuration was used both in the small-scale testing and in the full-scale testing.

Controller - The controller for this study is a synchronous adaptive controller for periodic disturbances. The general subject of adaptive signal processing is discussed in the book by Widrow[11]. Adaptive techniques that are specialized to periodic disturbances were

developed independently by Chaplin[12]. NCT's methods exhibit features of both approaches. The basic notation is defined by the single-channel block diagram shown in Figure 26.

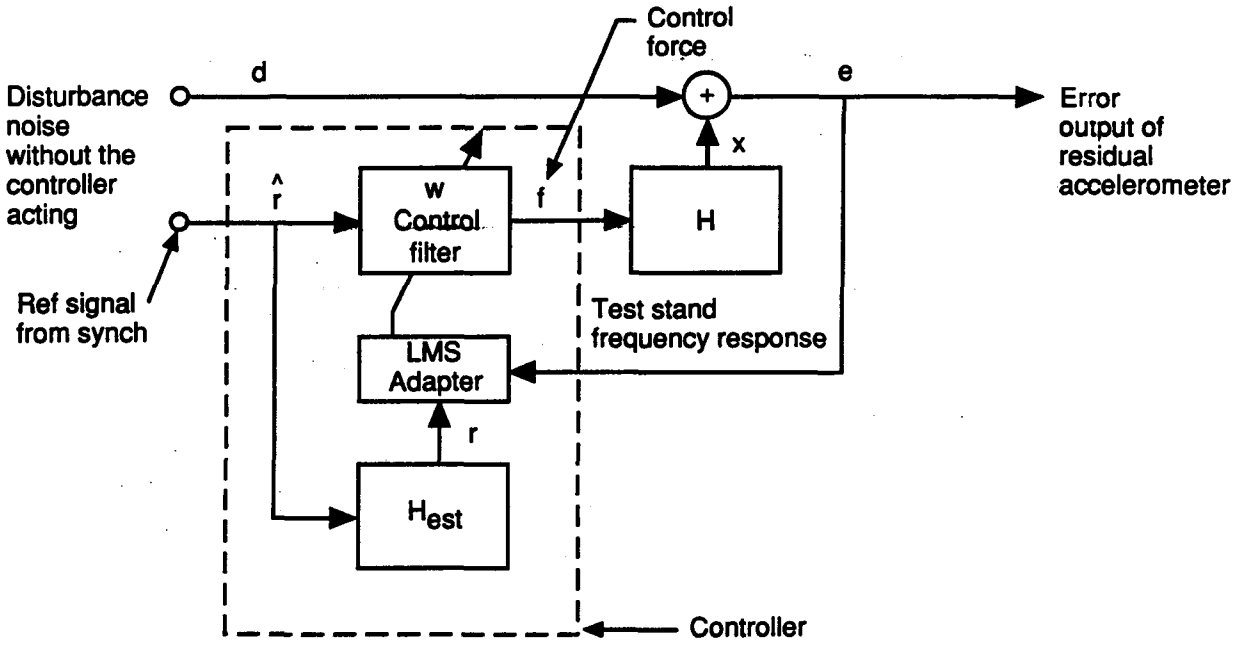

Figure 26. Block Diagram of a Single-Channel, Single-Harmonic Controller

For the A.R.T. program, the disturbance to be canceled represented a major source of noise on the CH-47C rotor transmission (Figure 27). The lower planetary gear mesh generates a fundamental frequency of 1,450 Hz at the normal rotor operating speed of 225 rpm. Associated with this fundamental frequency are sidebands related to the planetary carrier speed, 27 Hz. These sidebands sometimes are of equal or greater magnitude than that of the fundamental tone and any noise reduction measures must address them in order to achieve meaningful improvements in interior noise. For the current program, the disturbance to be canceled consisted of the lower planet gear mesh fundamental frequency (LP1) as well as two lower and two upper sidebands. Although additional sidebands can be noted in some spectra, the available controller capacity limited the program to these frequencies.

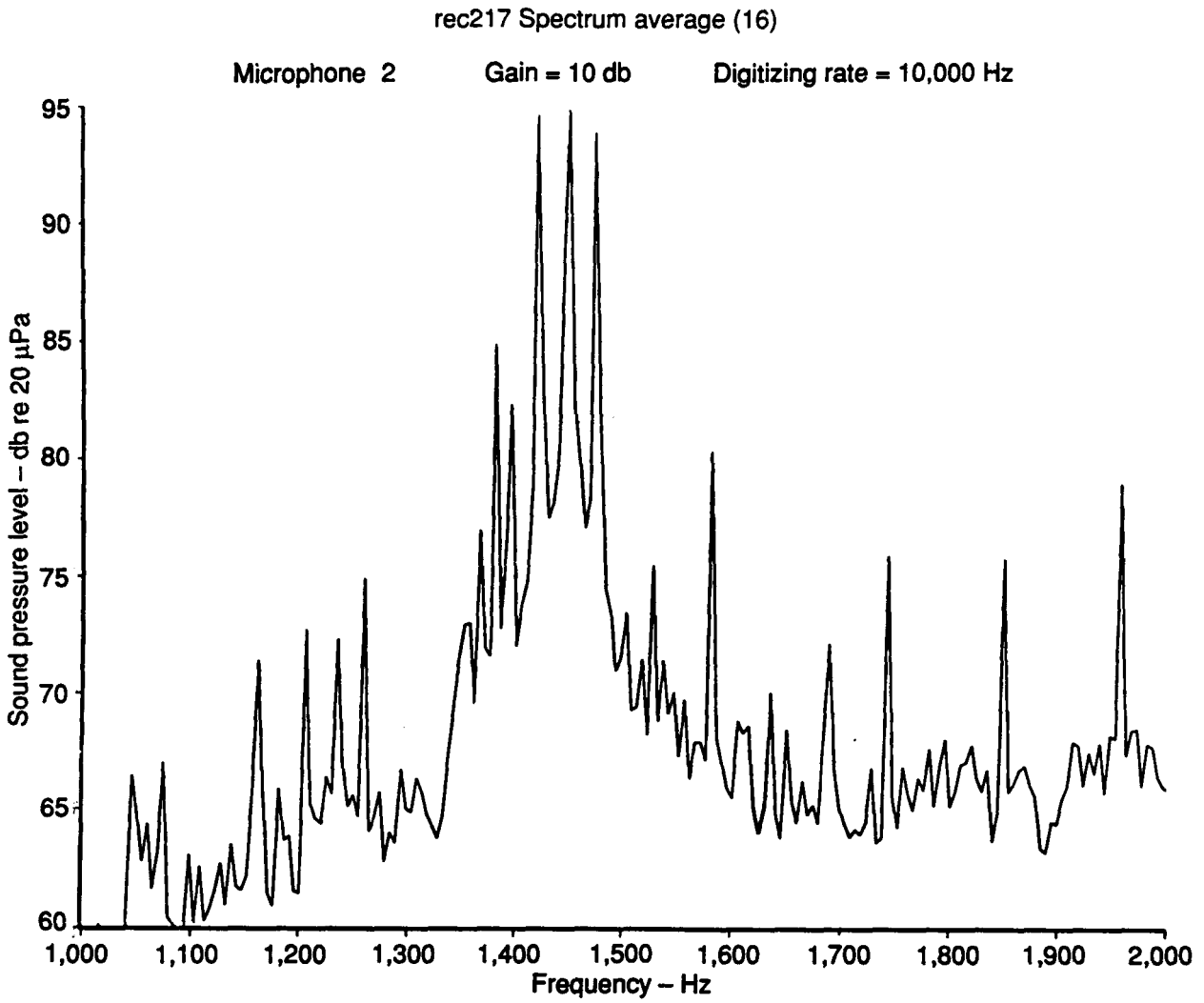

Figure 27. Transmission Gear Mesh Frequency and Sidebands

It is assumed that the disturbance to be canceled, d, can be represented by a harmonic series as shown in Figure 28. A reference signal, $r_i(n)$, is required for the *ith* harmonic to be canceled. For example, the control of the lower planet gear mesh frequency, LP1, and two lower sidebands was accomplished by choosing a fundamental that represents the spacing between LP1 and the immediately higher (or lower) sideband frequency (~27 Hz). Therefore LP1 is harmonically related to the reference frequency by

$$n = 1450/27.34 = 53\text{rd harmonic.}$$

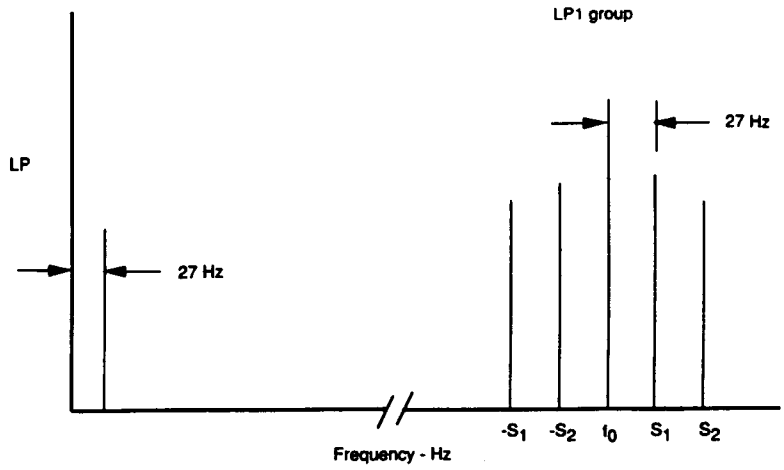

LP1 is 53rd harmonic of 27-Hz fundamental.

Figure 28. Harmonic Series Representation of Disturbance Signal

Each of these reference signals is a complex exponential,

$$\hat{f}_i(n) = e^{i\omega_i n\Delta t} .$$

The reference signals are generated using a synch signal from an optical pickup mounted on the rotor shaft. The advantages of using a synch signal over other approaches include eliminating feedback from the actuator to the reference sensor.

The output to the q*th* secondary source is generated by multiplying each harmonic of the reference signal by a complex filter weight. For each harmonic this operation can produce a sinusoid with any amplitude and phase. The weights will be adapted to achieve optional cancellation, but for the moment they are assumed to be fixed. The q*th* controller output is thus given by the expression

$$f_q(n) = \Re[\sum_{i=1}^{H} W_{qi}\hat{f}_i(n)] . \tag{5}$$

The operator, $\Re$, indicates taking the real part.

The response of the system being controlled is given by the convolution of the controller output with the appropriate impulse response. The response of the system at the p*th* sensor due to a unit impulse at the q*th* actuator is denoted by $h_{pq}(j)$. Therefore, the

response to the controller output is

$$\chi_p(n) = \sum_{q=1}^{Q} \sum_{j=0}^{\infty} h_{pq}(J) f_q(n-j) .$$

Inserting the expression for f_q and interchanging the order of the summations on i and j yields

$$\chi_p(n) = \sum_{q=1}^{NQ} \sum_{i=1}^{NH} \Re[W_{qi} \sum_{j=0}^{\infty} h_{pq}(j) \hat{f}_i(n-j)] .$$

The quantity resulting from the rightmost summation is defined as the filtered reference signal,

$$r_{pqi}(n) = \sum_{j=0}^{\infty} h_{pq}(j) \hat{f}_i(n-j) .$$

Because the reference signal $\hat{f}_i$ is a complex exponential with constant frequency, the filtered reference signal can be written as

$$r_{pqi} = e^{i\omega_i n\Delta t} H_{pq}(\omega_i) .$$

The filtered reference signal is a complex exponential multiplied by the frequency response of the system being controlled at the frequency of the disturbance.

An expression for the total error signal at sensor p can be written. The disturbance at the p*th* sensor is due to the action of the primary force and is denoted by $d_p(n)$. The

error at the p*th* sensor is the superposition of the disturbance and the response due to the secondary force, the controller output. The error for the p*th* sensor can be written as

$$e_p(n) = d_p(n) + \Re\left[r_p^T(n)\, w\right]$$

by defining,

$$r_p^T = \left[r_{p11},\ r_{p21},\ \cdots,\ r_{p,Q,1},\ \cdots,\ r_{p,1,H},\ \cdots,\ r_{p,Q,H}\right],$$

and

$$w^T = \left[w_{11},\ w_{21},\ \cdots,\ w_{Q,1},\ \cdots,\ w_{1,H},\ \cdots,\ w_{Q,H}\right].$$

The individual errors and disturbances can be combined into vectors that are as long as the number of sensors, P.

$$e^T(n) = \left[e_1(n),\ e_2(n),\ \ldots,\ e_p(n)\right]$$

$$d^T(n) = \left[d_1(n),\ d_2(n),\ \ldots,\ d_p(n)\right]$$

The weight vector remains the same and the reference sequence vectors are combined to form a matrix,

$$R^T(n) = [r_1(n), r_2(n), \ldots, r_p(n)].$$

Using the above definitions, the matrix equation for the total error becomes

$$e(n) = d(n) + \Re[R(n)\,w].$$

The errors are a function of the weights. The weights are chosen to minimize the errors in some way. A cost function, J, is defined to be the mean-squared error,

$$J = E[e^T(n)\,e(n)] = \lim_{N\to\infty} \frac{1}{N} \sum_{n=1}^{N} \sum_{p=1}^{P} e_p^2(n).$$

The weights that minimize the value of the cost function are the optimum weights. The optimum weights can be obtained by several methods. One approach is the LMS algorithm which makes use of the instantaneous gradient, the gradient of the instantaneous cost function,

$$J(n) = \sum_{p=1}^{P} e_p^2(n).$$

The derivative of this cost function with respect to one of the complex weights is

$$\frac{\partial J}{\partial w_{qi}} = 2 \sum_{p=1}^{P} e_p(n) H_{pq}^{*}(\omega_i) e^{-i\omega_i n\Delta t}.$$

As may be expected, the weights for each harmonic are independent; the gradient for each harmonic depends only on other variables at that harmonic. The gradient for all of the output channels at the *ith* harmonic can be written in vector form as

$$\frac{\partial J}{\partial w_i} = 2H^H(\omega_i) e(n) e^{-i\omega_i n\Delta t},$$

where $$w_i^T = [w_{1i}, w_{2i}, \ldots, w_{Q,i}],$$

and the superscript, H, indicates the conjugate transpose. The weights are allowed to adapt to the optimum weight vector by moving a small amount in the direction opposite of the gradient. The weight update equation for the *ith* harmonic is

$$w_{i,n+1} = w_{i,n} - 2\mu H^H(\omega_i) e(n) e^{-i\omega_i n\Delta t}. \tag{6}$$

Mu (μ) is a small, positive constant that determines the rate of adaptation.

Equations 5 and 6 constitute an adaptive controller for periodic noise. Equation 5 defines the controller output from the reference input. Equation 6 defines an LMS adaptive process for finding the optimum weights.

Small-Scale Test

Preliminary investigations of active control of transmission noise began in 1988 with the small, electric-motor-driven, planetary transmission and mounting structure shown in Figure 29. The test stand was designed and constructed by Boeing. The transmission and stand were not to scale, but the spectral content of the vibration signature was similar to that of a full-scale transmission. The tests were performed at NCT's lab. The four legs of the transmission were bolted to a 24 by 30 by 1/4-inch aluminum plate. The objective of the test was to reduce the plate vibration at the gear mesh frequency (1,170 Hz) and the associated sidebands (1,170 $\pm$26 Hz).

Control forces were applied by piezoelectric shakers (WR F7) mounted on the transmission legs inboard of the mounting bolts. The error sensors were accelerometers attached to the mounting bolts. An NCT 2000 controller was used. This controller treated the four shaker/accelerometer pairs as being independent channels. There were concerns that, since the four pairs of shakers and accelerometers were coupled by the dynamics of the structure, the controller would not be able to converge to a solution; this point will be discussed later.

The synch input to the controller was a 128-pulse/rev synch signal. Using this information, the controller generated output signals for each shaker containing the gear mesh and sideband frequencies. The magnitude and phase of each tone were adjusted automatically by the controller (in a manner similar to equation 2) to minimize the corresponding acceleration level.

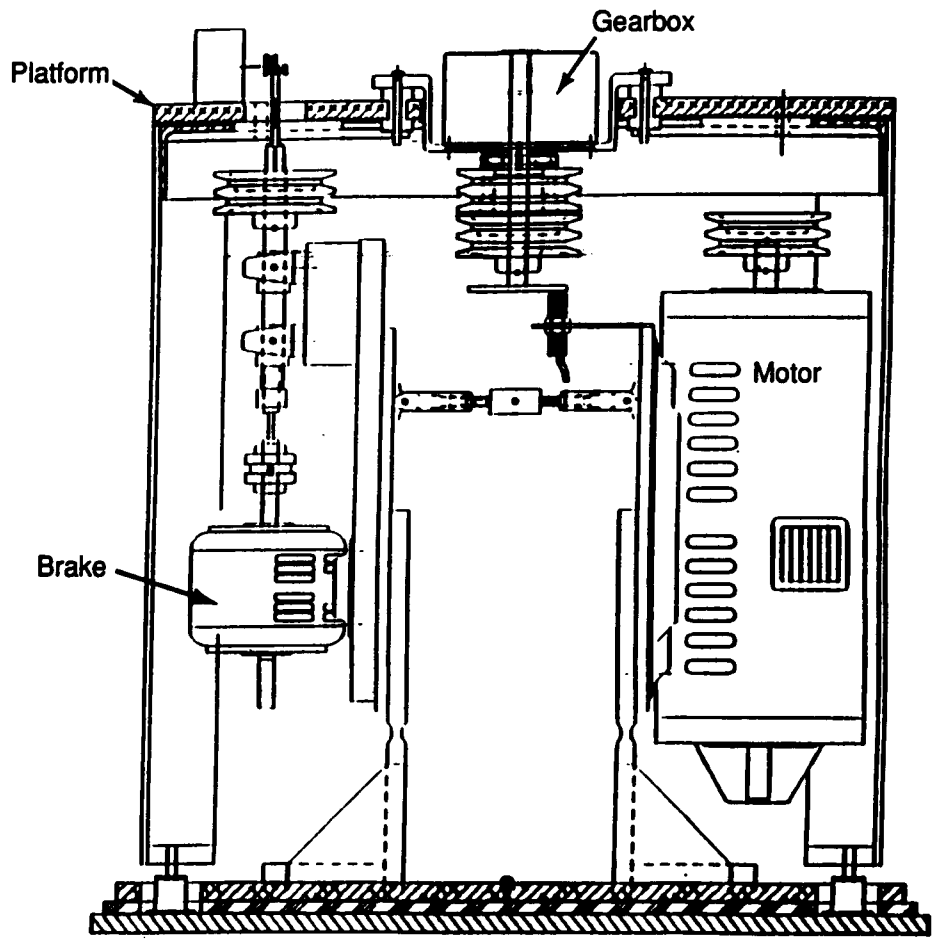

Figure 29. Small-Scale Transmission Test Stand

An example of the reductions that were achieved at one of the error accelerometers is shown in Figure 30. The gear mesh frequency and the sidebands are marked. Reductions are on the order of 5 db. Four shakers were used to minimize four accelerometers while these data were acquired. The global response of the plate is indicated by the data in Figure 31. This figure shows the uncanceled and canceled gear mesh frequency acceleration magnitudes recorded from 16 accelerometers placed randomly about the plate. Positions with high uncanceled levels show the greatest reductions. The power average over the 16 sensors is also shown at the extreme right of the figure. The average acceleration reductions are on the order of 5 db. The small-scale testing revealed the following:

1. The controller was able to cancel a disturbance consisting of a tone with sidebands, essentially an issue of controlling a high harmonic number.

2. A controller that accounts for the full matrix of interactions among channels should be used for the full-scale test. With one vertically oriented shaker on each transmission leg, a noninteracting controller could converge to a solution. In another phase of the testing, shakers were mounted in three perpendicular directions on a single leg. In this configuration the controller did not converge because of strong interactions. Although it was still in the development stage during the small-scale testing, it was decided that a controller that accounts for interactions, such as the NCT 2010, should be used for the large-scale testing.

3. Global reductions are possible using sensors and actuators that are collocated at the connection points between the transmission and the test stand. It is important that the control system is sensing and actuating in all of the significant degrees of freedom. In this case vertical (out-of-plane) motions were most significant, but this will not always be the case.

Full-Scale Test

Description of the Test Stand - The reduction in acceleration levels on the small-scale test stand led to a continued active control investigation on a full-scale basis. The full-scale test stand (Figures 32 and 33) was designed and constructed as part of the A.R.T. program and located

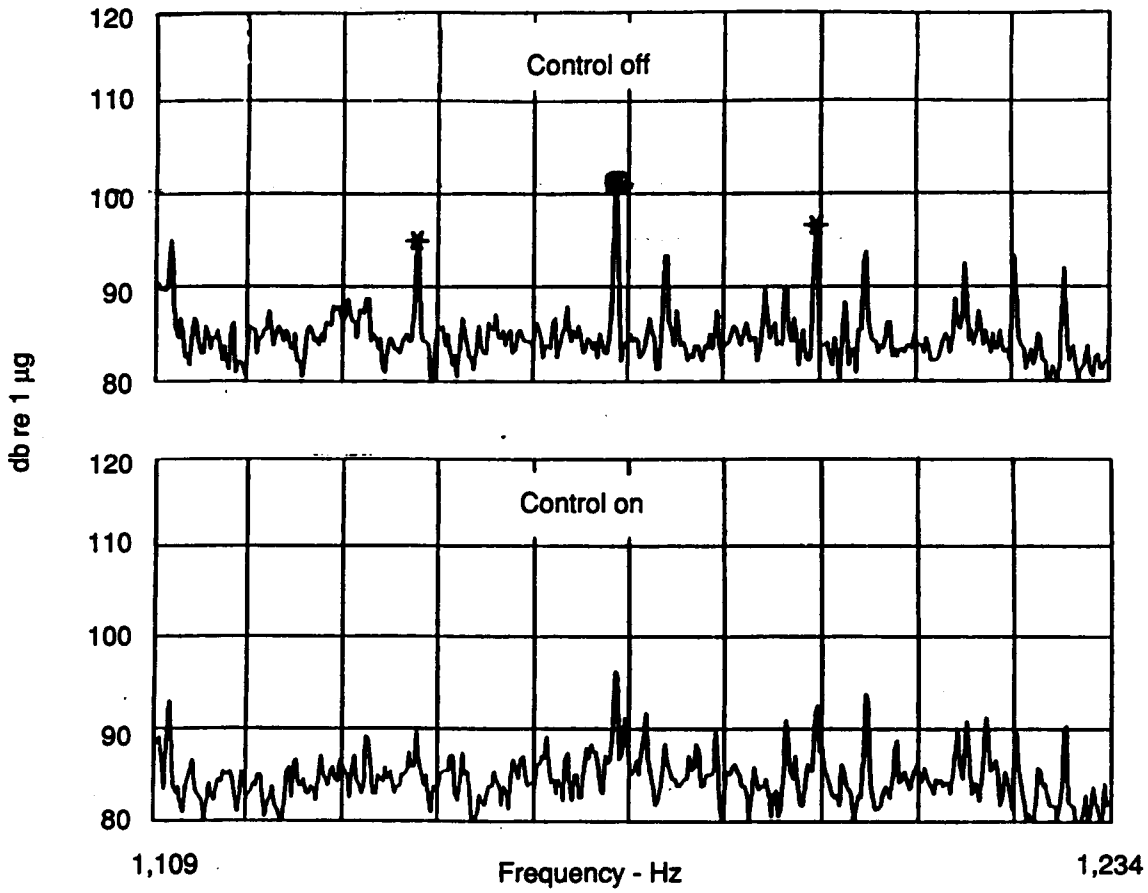

Figure 30. Measured Acceleration Levels at Leg 4 on the Small-Scale Test Stand

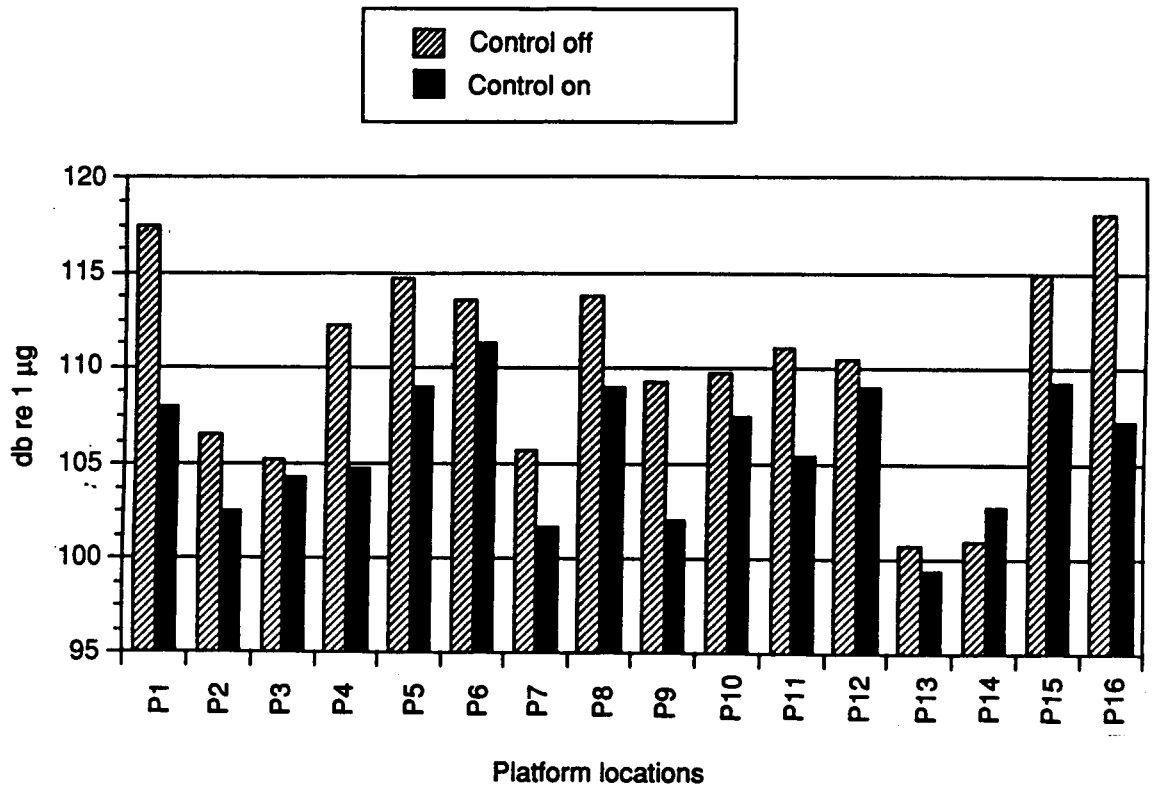

Figure 31. Measured Acceleration Levels at 16 Locations on the Small-Scale Test Stand

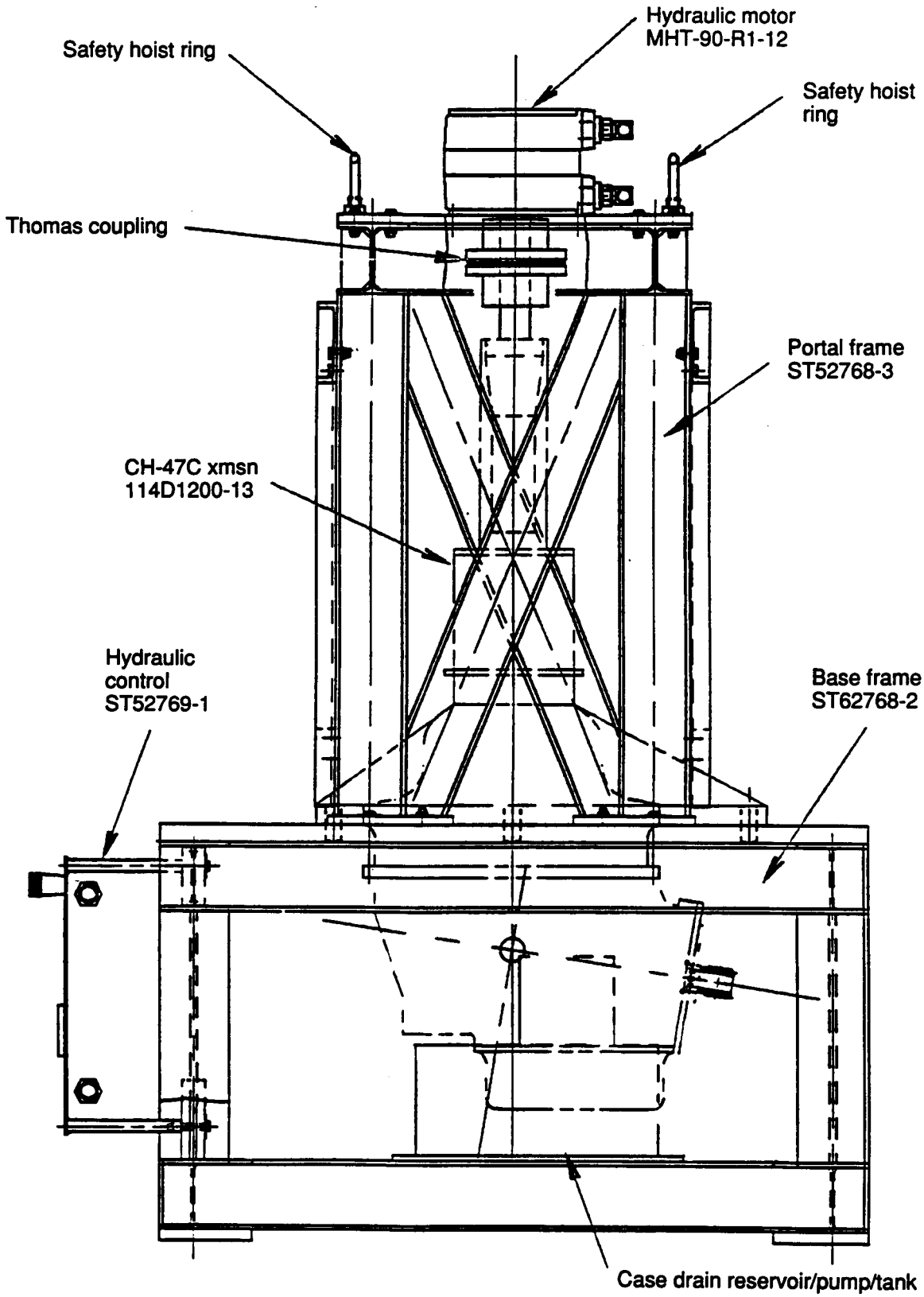

Figure 32. Side View of A.R.T. Full-Scale Noise Test Stand

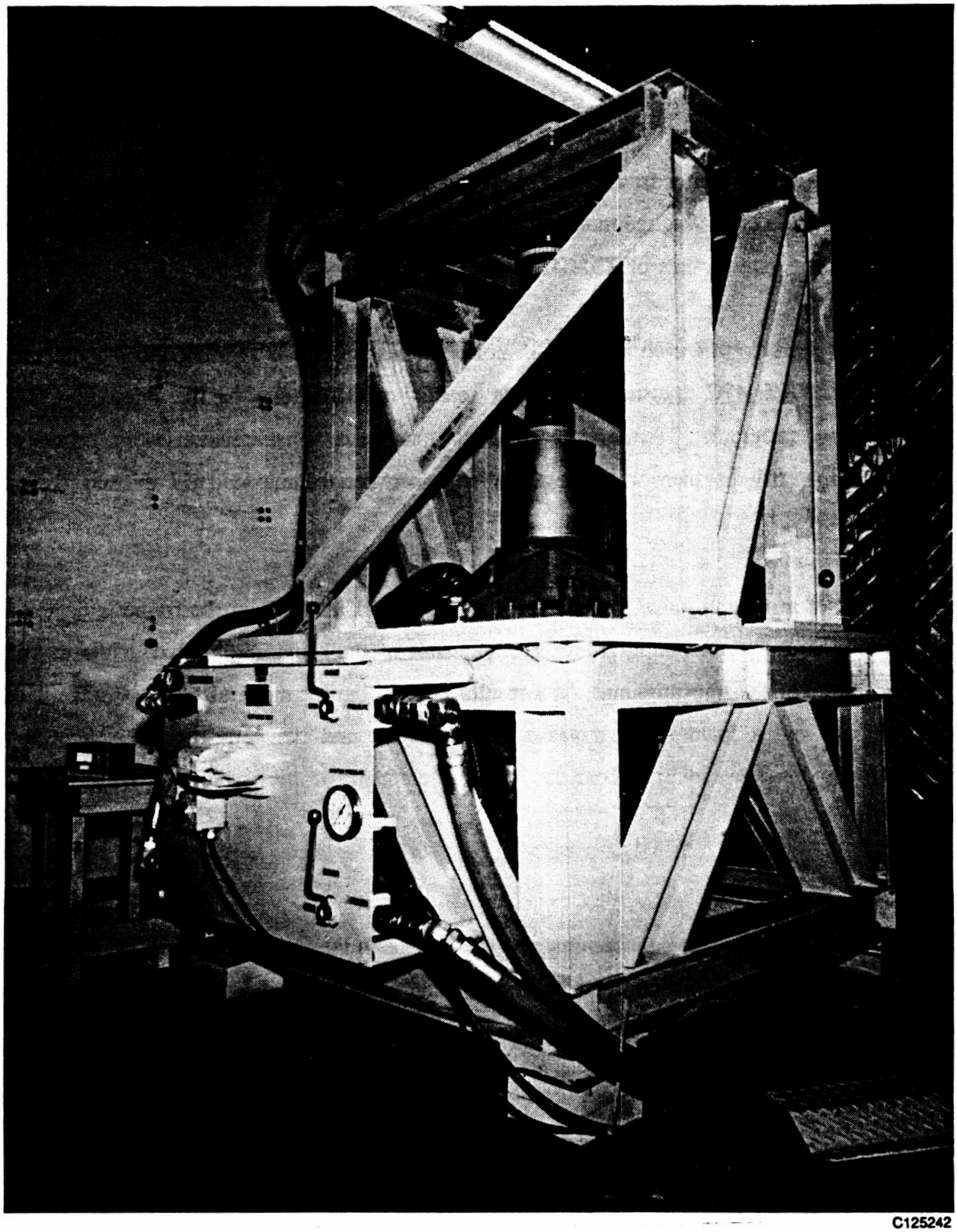

C125242

Figure 33. The A.R.T. Full-Scale Noise Test Stand

in the large acoustic test chamber of the Acoustical Laboratory. This room has acoustically treated interior surfaces to minimize reflections.

The test stand consists of a CH-47C forward rotor transmission mounted in a composite structure. The gearbox is driven by a 75-hp hydraulic motor mounted at the output shaft. The motor is capable of driving the transmission over a speed range of 0 to 300 rpm, which includes the normal operating range of 220-245 rpm.

A CH-47 gearbox was used for A.R.T. noise studies since it is representative of helicopter gearing and CH-47C transmissions were readily available due to the ongoing CH-47D modification program. The noise levels of the particular transmission used in testing were surveyed to verify that there was general similarity between the unloaded test unit and flight data (Figure 34).

A survey of test stand noise with and without acoustical material on the frame indicated that transmission noise reradiating from the framework of the stand contributed to the measured sound levels of the transmission. As a result, a sound barrier material with a surface density of 0.5 psf and a foam backing was applied to test stand structural elements to minimize structureborne noise radiating from the structural elements of the stand.

Instrumentation -

Vibration - Vibration measurements were made on the transmission and on the mounting deck. Triaxial accelerometers were located on the mounting bolts of each leg of the transmission. In addition, 12 accelerometer locations were defined on the mounting deck to determine spatial averaged vibration levels. Table 19 lists the vibration instrumentation by location. The 12 channels of triaxial accelerometers were recorded simultaneously, while the spatially distributed accelerometers were recorded in groups of four in order to accommodate other required instrumentation.

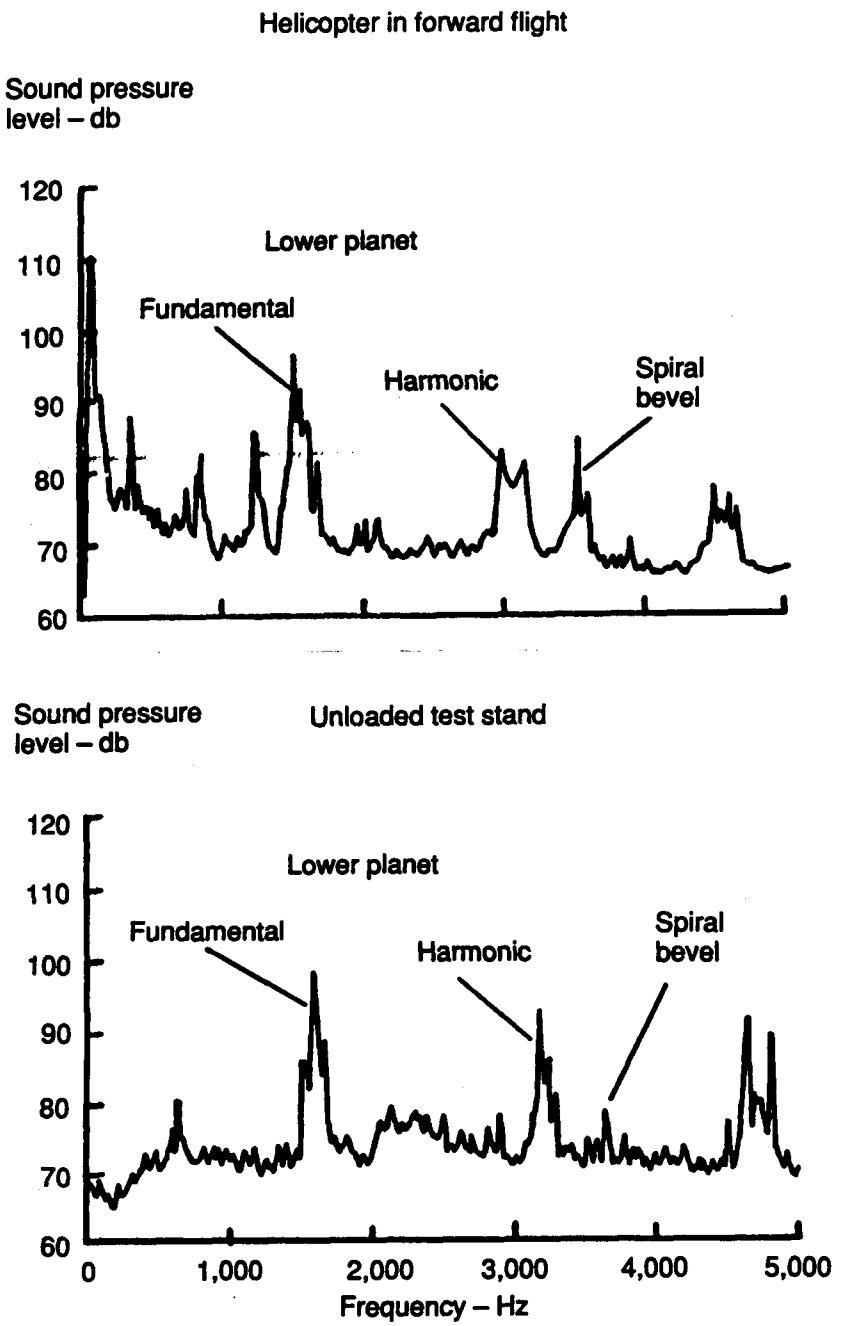

Figure 34. Comparison of Rotor Transmission Noise Data: Flight Test and Unloaded Test Stand

Acoustic - Fifteen 0.5-inch-diameter microphones were located in an array around the transmission as shown in Figure 35. The 12 microphones on a 2-meter arc from the transmission center were free-field response transducers and the three located in the near field had pressure response characteristics. The array was selected to acquire representative acoustic data at locations where the test stand had minimal influence on the noise of the transmission. No data were acquired at azimuths where the test stand control panel or case drain reservoir for hydraulic fluid was located.

Data Recording - All vibration and acoustic data, along with rotor shaft speed, run identification, and time code, were recorded simultaneously on a Honeywell 101,32-track, 1-inch magnetic tape recorder operating in the wideband and I FM mode at a tape speed of 15 inches per second. The input signals were recorded at a level of approximately 1 volt and input and output signals monitored with an oscilloscope. Calibration signals, 94 db at 1,000-Hz tone, and white noise signals of one volt rms were applied at regular intervals.

Data Analysis - Data were analyzed with an Apollo DN3500 work station equipped with an A/D converter capable of digitizing 130,000 samples per second. Data were analyzed over a frequency range of 0-5,000 Hz, eight channels at a pass. A list of all instrumentation used during the test is included in Table 19.

Test Procedure - Before taking data, the test stand was run for approximately 20 minutes in order to stabilize operating temperatures and therefore transmission speed. An oil cooler was added to the system to permit running times in excess of 30 minutes without building excessive heat levels. The CH-47 transmissions normally operate with this cooler.

Each set of test data was recorded five times to evaluate repeatability. For each test point the rotor speed was upset by significantly reducing rpm and then reestablishing the test speed. The

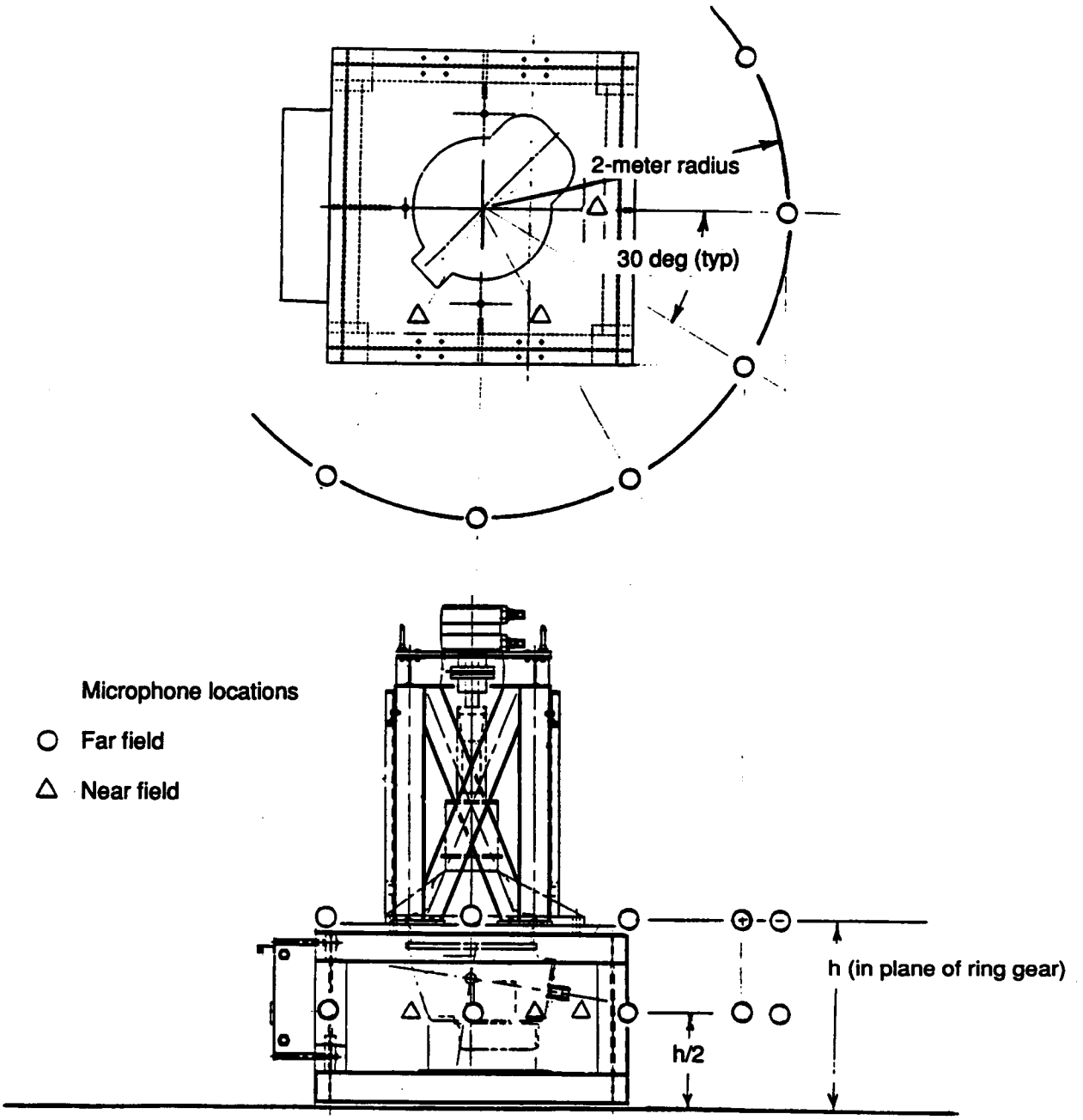

Figure 35. Microphone Locations for Full-Scale Noise Test

number and length of records were established based on the procedure outlined in the following section.

Data Sampling - Confidence limits for sampling of data were determined from preliminary running of the test stand with a set of ten records in the baseline configuration. It was desired to have sufficient records to establish a 95-percent confidence level of + 1 db. The confidence limit is given by

$$CL = t\,\sigma/n^{1/2},$$

where
- CL = confidence limit, db
- t = probability distribution
- σ = standard deviation of sample, db
- n = number of samples
- df = degrees of freedom
  = $n-1$.

Statistical significance was determined using the t distribution, sometimes call the Student t distribution. When the sample size is very large, the t and normal distributions are very similar. However, for relatively small sample sizes (small number of degrees of freedom) the t distribution is slightly flatter than the normal distribution.

The results of the survey indicated a 95-percent confidence of data within + 0.3 db for ten repeats and 95-percent confidence of the data within + 1.0 db for five records. Similarly, a level of 90-percent confidence within + 0,2 db was achieved for ten runs and a 90-percent confidence within + 0.8 db. It was decided that five repeats of each condition giving a 95-percent confidence within + 1.0 db would be sufficient to report data trends.

Baseline Test - The initial set of data was obtained without any modification to the transmission. Testing included stabilized running at constant rotor rpm as well as continuous rpm sweeps. These data were used for comparison with data from all subsequent modified configurations.

TABLE 19. INSTRUMENTATION USED FOR A.R.T. NOISE TESTS

Tape recorder	Honeywell Model 101
Preamplifiers (28)	Dynamics Model 7509 PJ
Microphone (12)	Bruel & Kjaer Type 4133
Microphone (3)	Bruel & Kjaer Type 4134
Microphone preamplifier (15)	Bruel & Kjaer Type 2619
Microphone power supply (1)	Bruel & Kjaer Type 2801
Microphone power supply (7)	Bruel & Kjaer Type 2807
Triaxial accelerometer (4)	Wilcoxon Research Type M733
Accelerometer power supply (4)	Wilcoxon Research Type P703BT
Sound level calibrator	Bruel & Kjaer Type 4230
Vibration generator (4)	Wilcoxon Research F7
Vibration generator (4)	Wilcoxon Research F8
Power amplifier (4)	Wilcoxon Research PA8
Matching network (4)	Wilcoxon Research N8H
Active cancellation system	Noise Cancellation Technologies, Inc Model 2010
Real-time analyzer	Bruel & Kjaer Type 2133
Data analysis system	Apollo work station

Residual Vibration Levels - To investigate the effect of the influence of vibration from three of the mounting legs on the fourth leg, a bolt removal experiment was conducted. With a triaxial accelerometer located on the test stand platform at the base of the aft leg,

the vibration levels with and without the aft leg mounting bolt were measured. Data with the bolt removed indicated the influence of the residual vibration due to input other than the leg under study. Results are shown in Table 20.

TABLE 20. VIBRATION WITH ONE MOUNTING BOLT REMOVED

Direction	Vibration level (g)	
	Bolt in	Bolt out
x	1.6	1_p 0.7
y	3.5	0.8
z	3.5	2.4

The influence of the vertical vibration (z direction) appeared to result from flanking paths due to the test stand upper portal structure as well as the remaining bolted mounting legs. The vertical vibration remained within approximately 1 db of the level with the bolt installed, indicating a limitation to the amount of cancellation that might otherwise be achieved unless cancellation was applied to all legs.

Effect of Bolt Torque - In an allied investigation to the residual vibration study, the effect of mounting bolt torque on deck acceleration levels was investigated. Vibration levels measured on the deck of the test stand immediately adjacent to the aft leg are essentially unaffected by mounting bolt torque. For testing, however, all bolts were tightened to 600 lb-ft, a value representative of the production aircraft installation.

Active Control - Active control of transmission structureborne noise at lower planet gear mesh frequency was performed with an NCT 2010 interactive controller and three to four piezoelectric shakers mounted on the transmission legs. Control of three axes on any one leg or one axis on all four transmission mounting legs was evaluated with the four available Wilcoxon Research F8 shakers. The simultaneous control of three axes on all four mounting legs was not feasible in view of the large expense that would have been required for the shakers and the associated

power supplies and matching networks. It should be noted that the large F8 shakers were used for experimental purposes and were not intended to represent production hardware, which would have to be optimized with regard to size and weight.

The magnitude of the required control forces was estimated from data acquired from the test stand. At a particular frequency, the vector of control forces is related to the vector of operating accelerations by

$$(f) = [Y]^{-1} (a)$$

where (f) is the vector of control forces
(a) is the vector of the operating accelerations
[Y] is the matrix of accelerations.

When the off-diagonal elements of the acceleration matrix are small compared to the diagonal elements, the matrix equation is nearly uncoupled and the following approximation can be used for the *ith* control force:

$$f_i = a_i/Y_{ii}.$$

The validity of this approximation is indicated by Figure 36. This figure shows plots of the direct acceleration in the vertical direction on leg 1 and the cross accelerations to the other three legs. The cross terms are relatively insignificant. With this approach the magnitude of the vertical control forces was estimated to be 100 pounds or less.

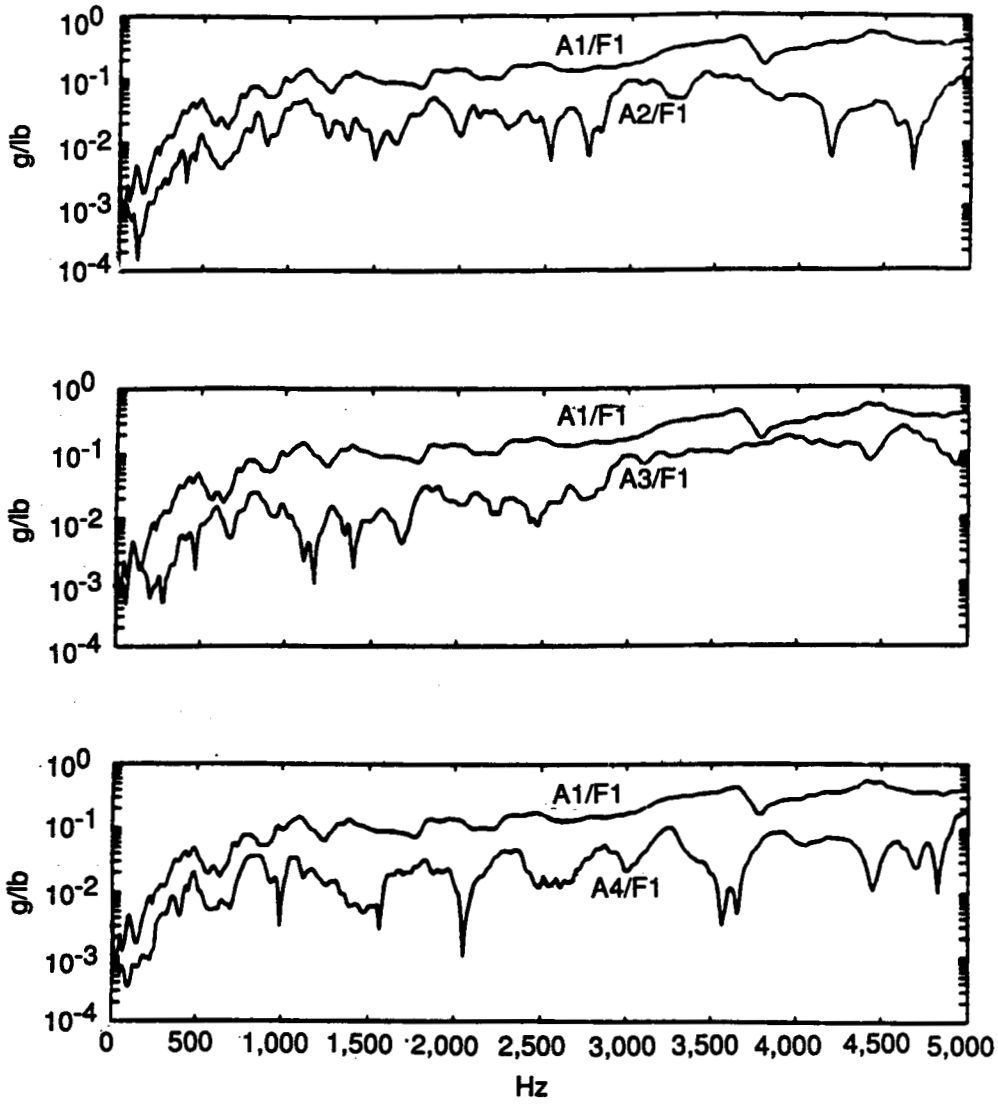

Figure 36. Comparison of Direct and Cross Accelerations Measured on the Full-Scale Test Stand

Results

Active Control - Initially, four piezoelectric shakers were used to control the same axis on each of the four legs simultaneously: for example, the vertical axis at the mounting bolt on each leg. Control of the radial and tangential axes also was evaluated separately. For each of these three control configurations, three residual or feedback accelerometer positions were tested for a total of nine control configurations. All residual accelerometers were as shown in Figure 37: (1) on the platform at the base of the leg, (2) on the mounting bolt, and (3) on the actuator pad which mounted the radial shaker. A fourth actuator configuration also was investigated: control of three axes simultaneously on the aft leg of the transmission. A triaxial accelerometer provided the feedback signals for the respective control axes.

In addition, it was decided to examine the control of two channels simultaneously on the aft mounting leg of the transmission, which typically has displayed the largest acceleration levels measured in flight. The x-y, x-z, and y-z axes were investigated by using as feedback sensors the receptive axes of a triaxial accelerometer.

A final configuration evaluated was the control of four channels of case vibration simultaneously. A summary of these control configurations is shown in Table 21. These configurations represent ten separate conditions for which active control of transmission noise was evaluated.

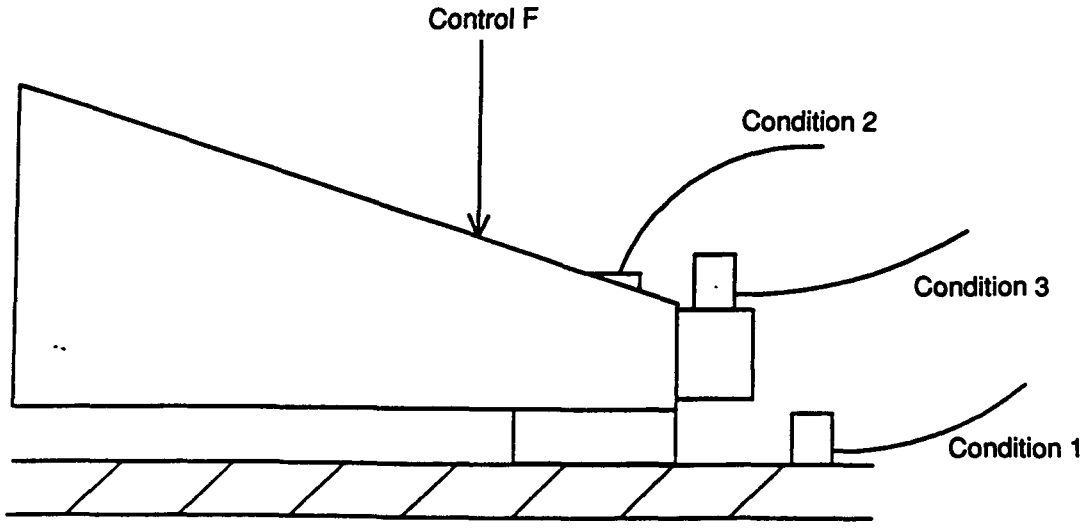

Figure 37. Location of Residual Accelerometers

TABLE 21. SUMMARY OF ACTIVE NOISE CONTROL CONFIGURATIONS EVALUATED

Configuration	No. channels	Actuator location	Control direction	Residual sensor location
1	4	All legs	Vertical	Leg
2	4	-	-	Platform
3	4	-	-	Bolt
4	4	All legs	Radial	Bolt
5	4	All legs	Tangential	Bolt
6	3	Aft leg	All axes	Bolt
7	2	Aft	Rad/tang.	Bolt
8	2	Aft	Tang./vert	Bolt
9	2	Aft	Rad/vert	Bolt
10	4	Case	Radial	Case

Figure 38 is a spectral analysis of a vertical-axis accelerometer on the bolt of one of the transmission legs during control of the four vertical axes. The lower planetary mesh frequency (LP1) centered at 1,450 Hz is the frequency group addressed by the control system. Summary bar charts included in this section indicate the change in amplitude of the maximum acceleration level in this frequency grouping. The upper graph represents a control-off case and the lower graph, control on.

Single-Axis Control - Figure 39 is a summary of the effect of active control on vertical-axis acceleration as measured on the platform, bolt, and actuator pad. In each case the accelerations were reduced to 1 g or less from initial levels of 2 g or greater (a reduction of 6-15 db). The vertical-acceleration levels on the actuator pad were higher than platform or bolt levels since the pad was essentially cantilevered off the end of the leg (Figure 37).

Figure 40 shows the impact of the same actuator configuration on platform acceleration levels. Reduction in acceleration levels averaged over the surface of the platform was

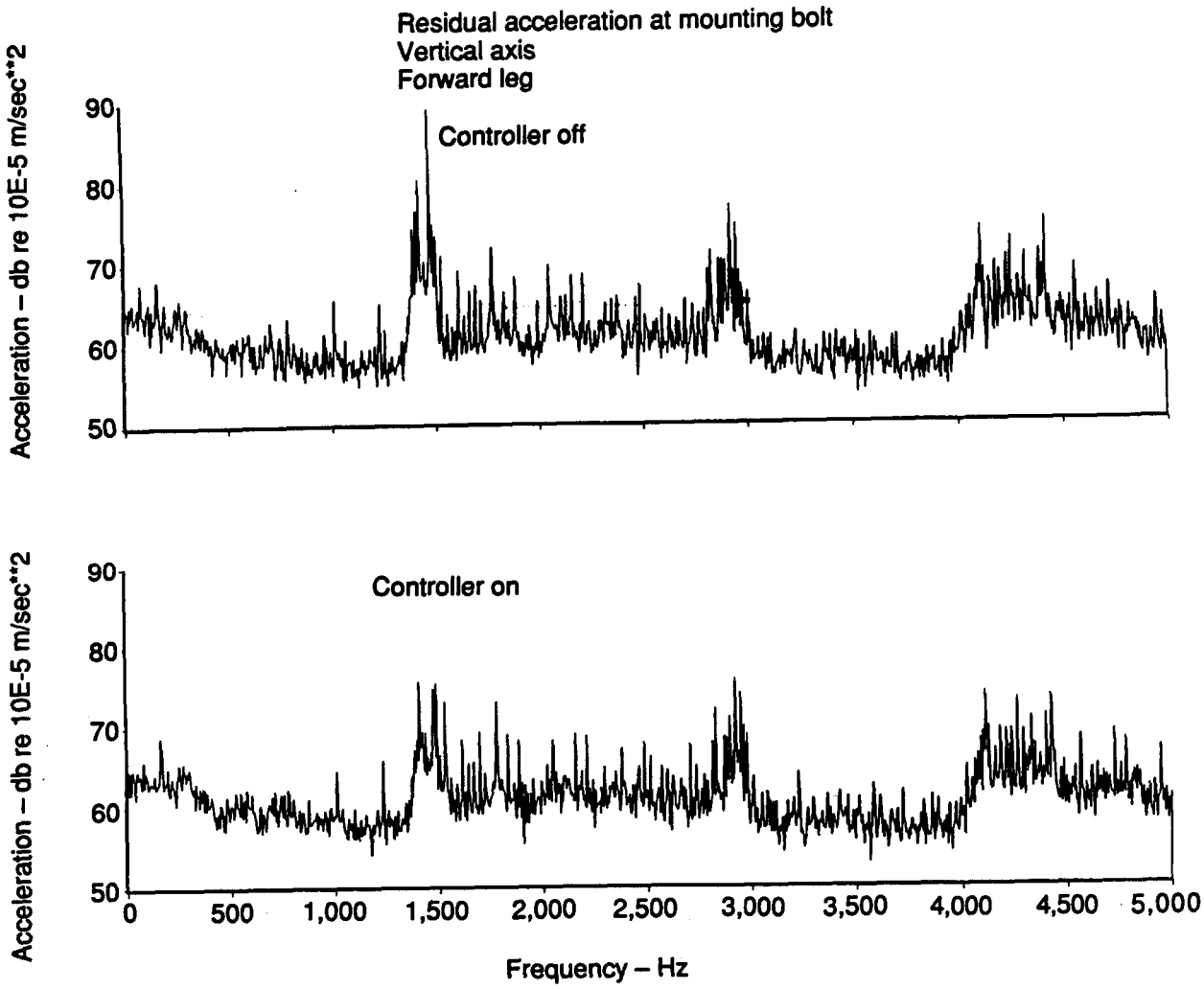

Figure 38. Typical Effect of Active Control on Vertical Axis Acceleration

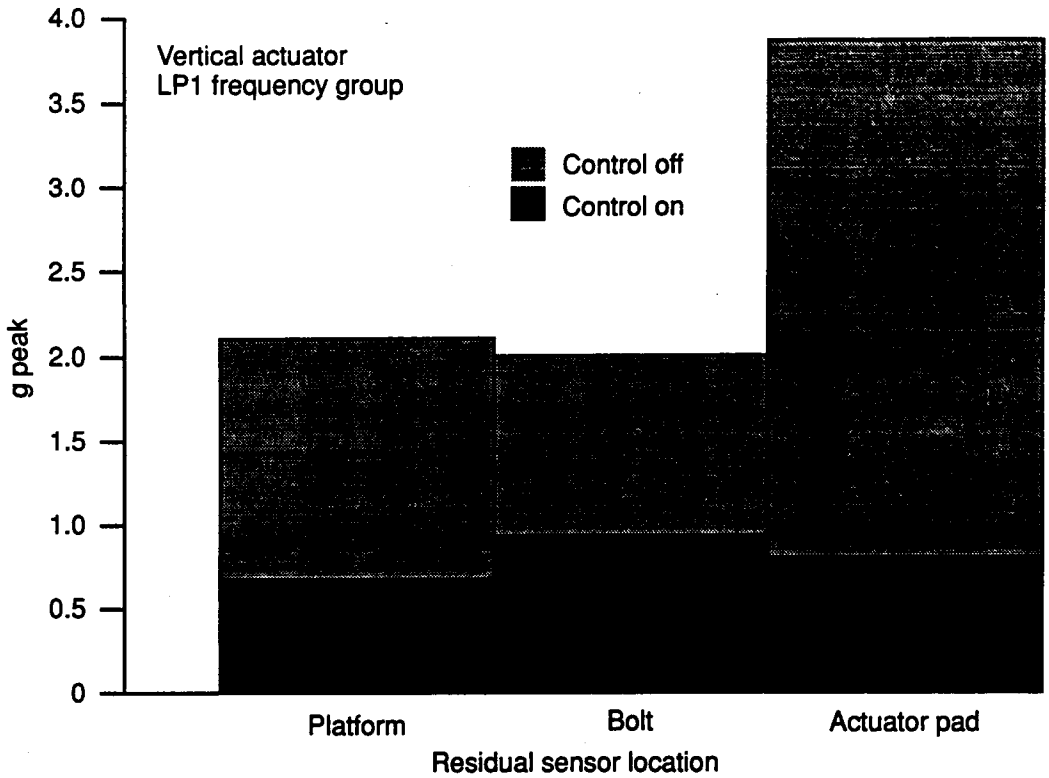

Figure 39. Averaged Residual Sensor Accelerations at Three Locations

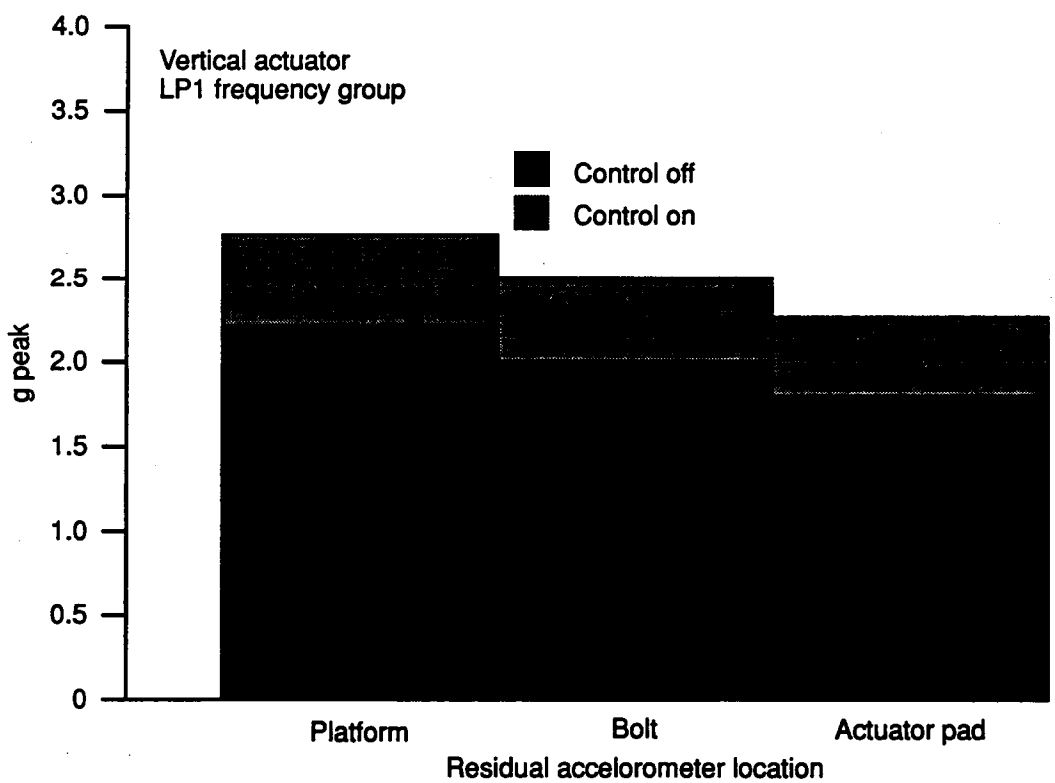

Figure 40. Averaged Platform Accelerations for Three Residual Sensor Locations

less than 2 db and was independent of the location of the residual sensor. It appears that the upper portal of the test stand may have provided a flanking path for vibration and structureborne noise and thus limited the effectiveness of the controller. Similar results were noted for all of the actuator configurations and thus only the acceleration levels of the residual sensors are reported. The test configuration with the residual sensor located on the bolt frequently demonstrated the greatest reduction in acceleration levels. In general, the application of active control to the transmission mount vertical axis demonstrated greater reductions in acceleration levels than any of the other directions evaluated. Radial-axis control showed a mixed result in reducing radial acceleration levels. With the residual sensor on the bolt, reductions up to 6-11 db were observed at several frequencies in the LP1 grouping, but levels at all frequencies were reduced. However, the configuration with the residual sensor located on the platform displayed increased acceleration levels ranging from 2-9 db at most of these same frequencies. Tangential control with the sensor on the bolt achieved up to 11-db reduction at the fundamental frequency and all LP1 sidebands were reduced as well.

Two-Axis Control - Simultaneous active control of two axes was evaluated on the aft leg of the transmission for all combinations of axes and for residual sensors on the bolt and platform. The results were not as impressive as demonstrated for single-axis control and again achieved mixed results in that, while the acceleration levels for some configurations were reduced, others were increased, although the increase in amplitude tended to be minimal in comparison with the reductions.

Three-Axis Control - The results of three-axis control on the aft leg of the transmission were similar to those of the two-axis control in that levels were generally reduced with the residual sensor located on the bolt and tended to increase when the sensor was located on the platform. The aft leg was the only location evaluated for three-axis control.

Control of Airborne Noise - Actuators were mounted on the lower case of the transmission as shown in Figure 41 in an effort to reduce the direct radiation. A previous Boeing study showed that stiffening plates applied to these locations reduced radiated noise. Prior NASTRAN vibration modeling and testing[7] also indicated that there were hotspots on the case.

A survey of vibration levels of the lower transmission case was made with a hand-held accelerometer as an aid in locating the four available shakers. The locations selected displayed vibration levels of 3.8-7.5 g, although there were a few other locations displaying levels of 3.8 g or higher. Since the program was limited to four vibration shakers, locations were chosen based on accessibility to the large shakers.

The reduction in case accelerations is shown in Figure 42. No reduction in sound pressure level was measured. It is thought that, while local reductions in case vibration were achieved, these localized reductions represented only a small area of the case with respect to radiated sound, and thus measured sound levels were dominated by the remaining unsilenced regions on the case.

Ring Gear Modification - The dominant noise source within the CH-47 rotor transmission, as noted previously, is the first stage of the dual planetary system employed to reduce input rpm from 6,900 to 225, the main rotor frequency. The planetary first stage has a relatively high pitch-line velocity compared to the second stage and, along with the high transmitted loads, therefore generates high noise levels within the planetary system. Forces at the gear mesh frequency (approximately 1,450 Hz) are transmitted to the gear case through a stationary ring gear which forms an integral part of the transmission housing in joining the upper and lower covers (Figure 43). The baseline ring gear has upper and lower lugs which rigidly join the upper and lower covers respectively (Figure 44 left). A modification was made to this gear to eliminate one of the paths of structureborne noise ((Figure 44 right). An elastomeric insert also was

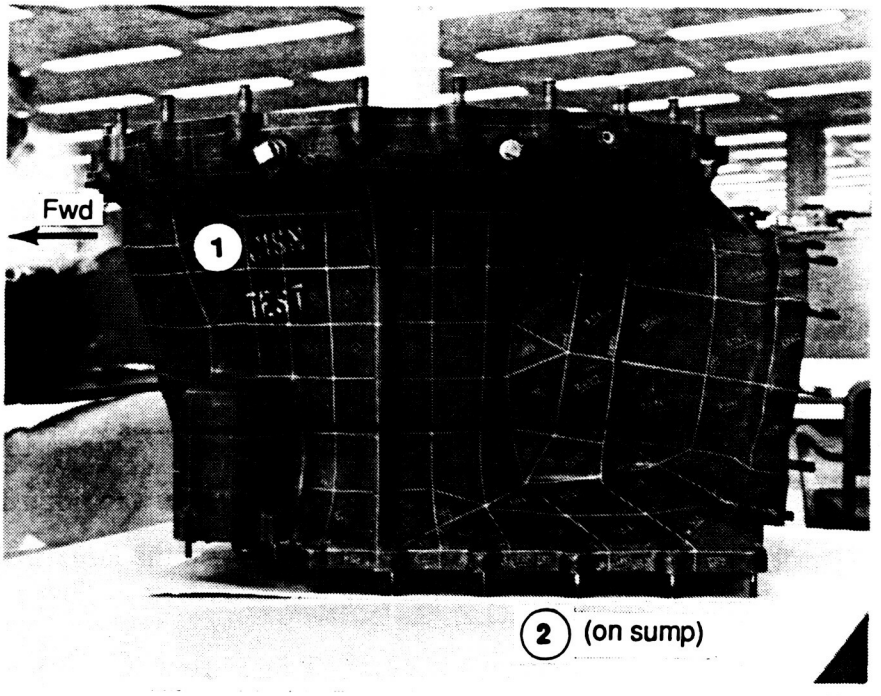

182376

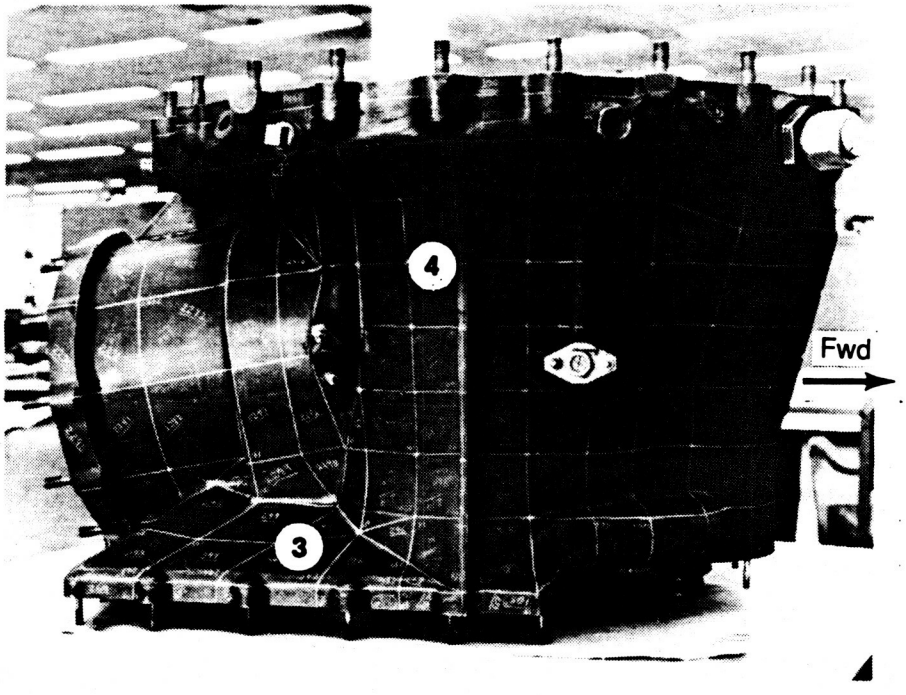

182374

Figure 41. Locations of Shakers on Lower Case of Transmission

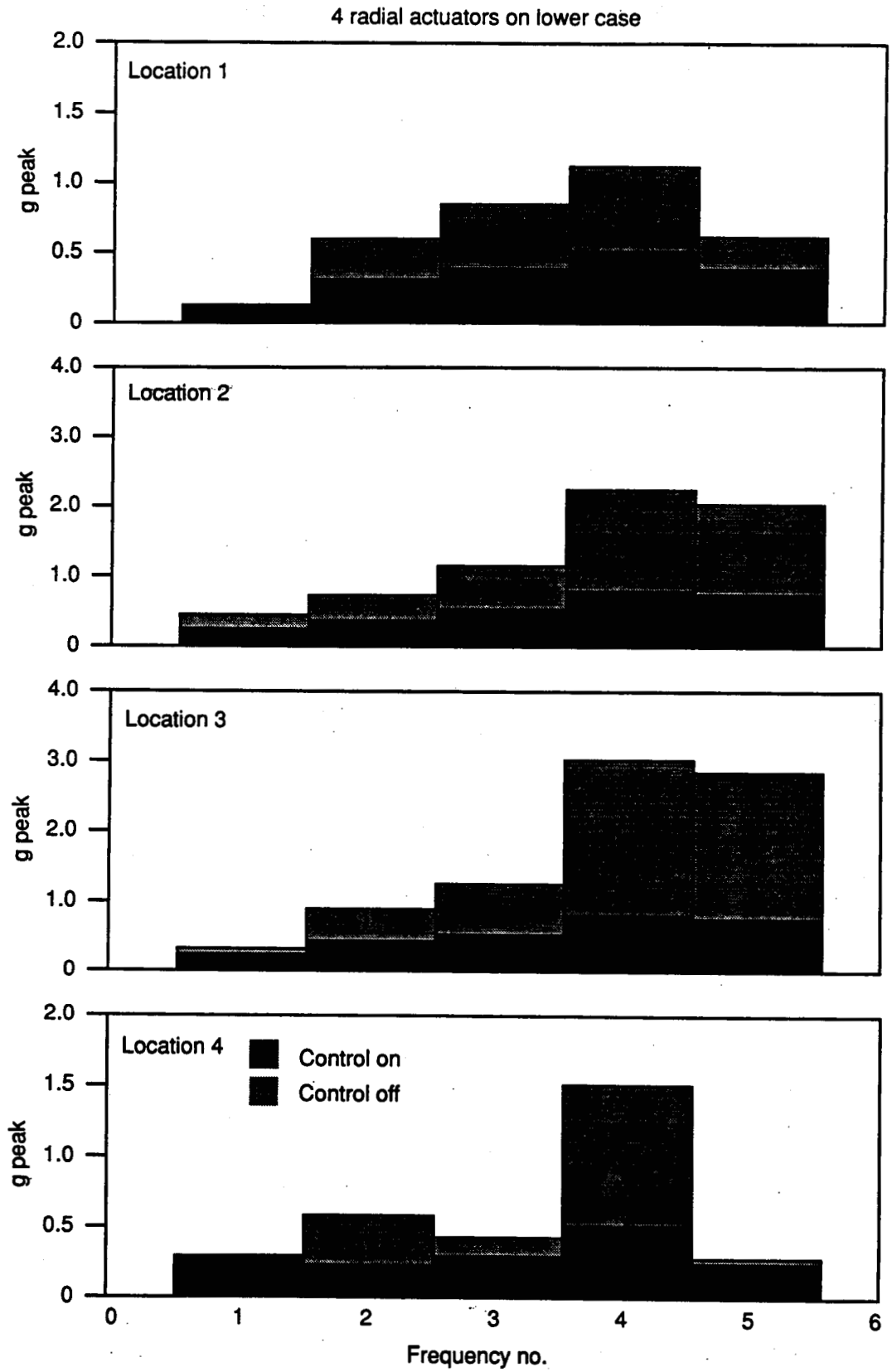

Figure 42. Effect of Active Control on Accelerations of Lower Case

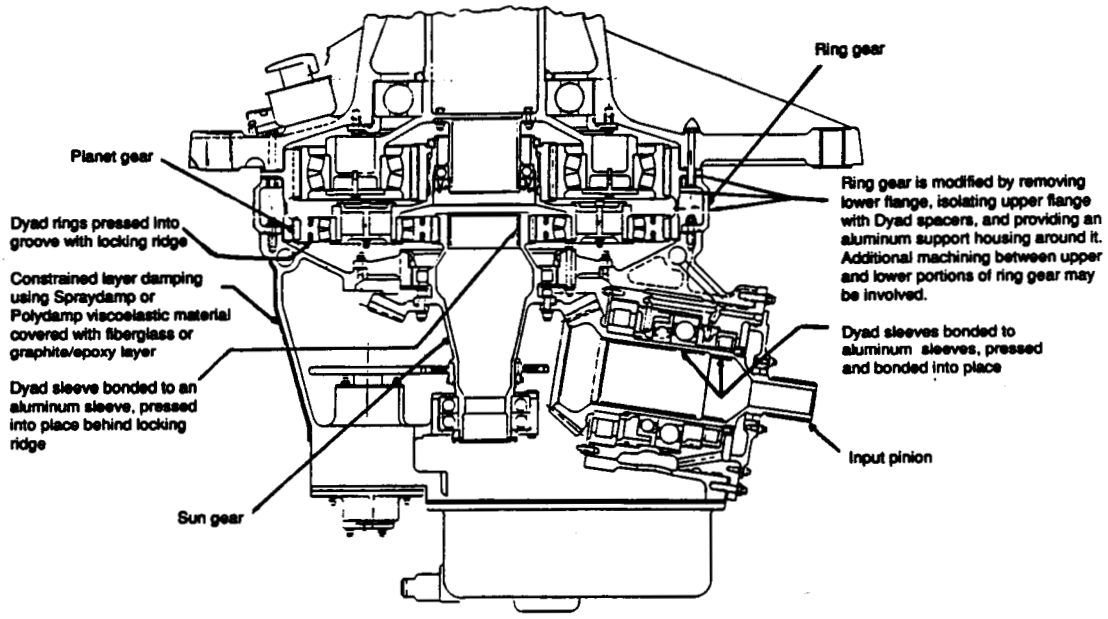

Figure 43. Added Transmission Damping

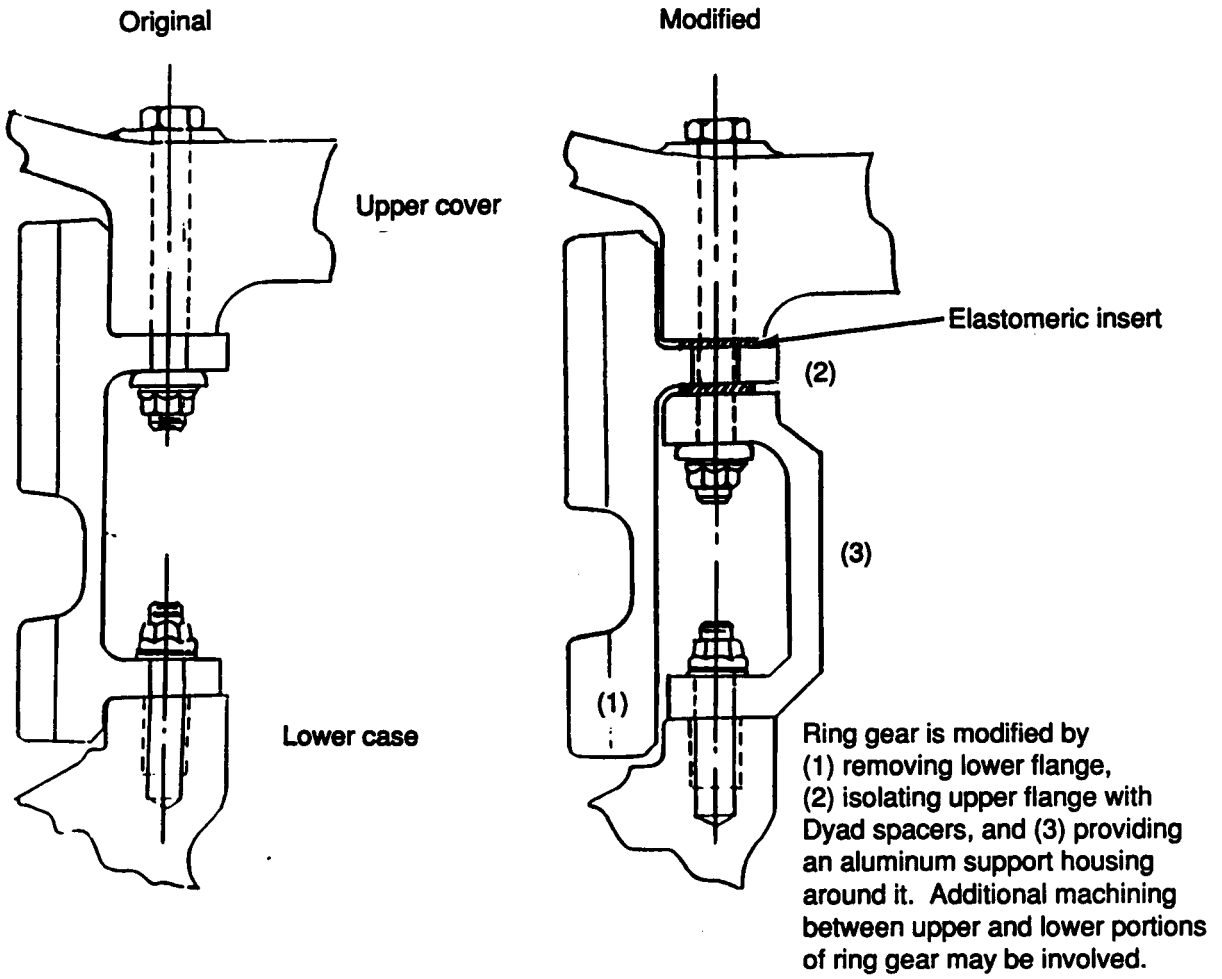

Figure 44. Ring Gear Modification

applied at the bolted connection to the upper cover. The viscoelastic material was Dyad O 60. At the completion of the baseline series of tests, the transmission was disassembled, the modified ring gear installed, and ring gear bolts torqued to specified values. It was noted that the elastomeric material took a permanent set after several hours and the bolts were retorqued to the initial values. Several iterations were required to stabilize the torque values.

It should be noted that prior Boeing experience with transmission assembly effects on self-generated noise levels indicates that assembly tolerance by itself can vary transmission noise by noticeable amounts. The current test program did not address this issue, however, and no Boeing data exist to document the effect.

A summary chart of the effect of ring gear modification as well as gear and case damping is shown in Figure 45 for three representative rotor speeds. Only a modest reduction in sound level was achieved with modifications to the transmission. At 245 rpm for the condition of the modified ring gear plus damping the levels actually went up slightly.

Each modification to the transmission required a complete disassembly of the gearbox, and the final configuration change included installation of first-stage planetary gears from another transmission, among other changes. These gears previously had been modified by the installation of damping material. The sound levels related to this configuration change may have been due more to the new gear mesh than the added damping which the modification was designed to provide.

Damping -

Static Tests - Tests were conducted on selected CH-47C forward rotor transmission gears to evaluate the effect of applied damping on the decay of gear noise and vibration. A

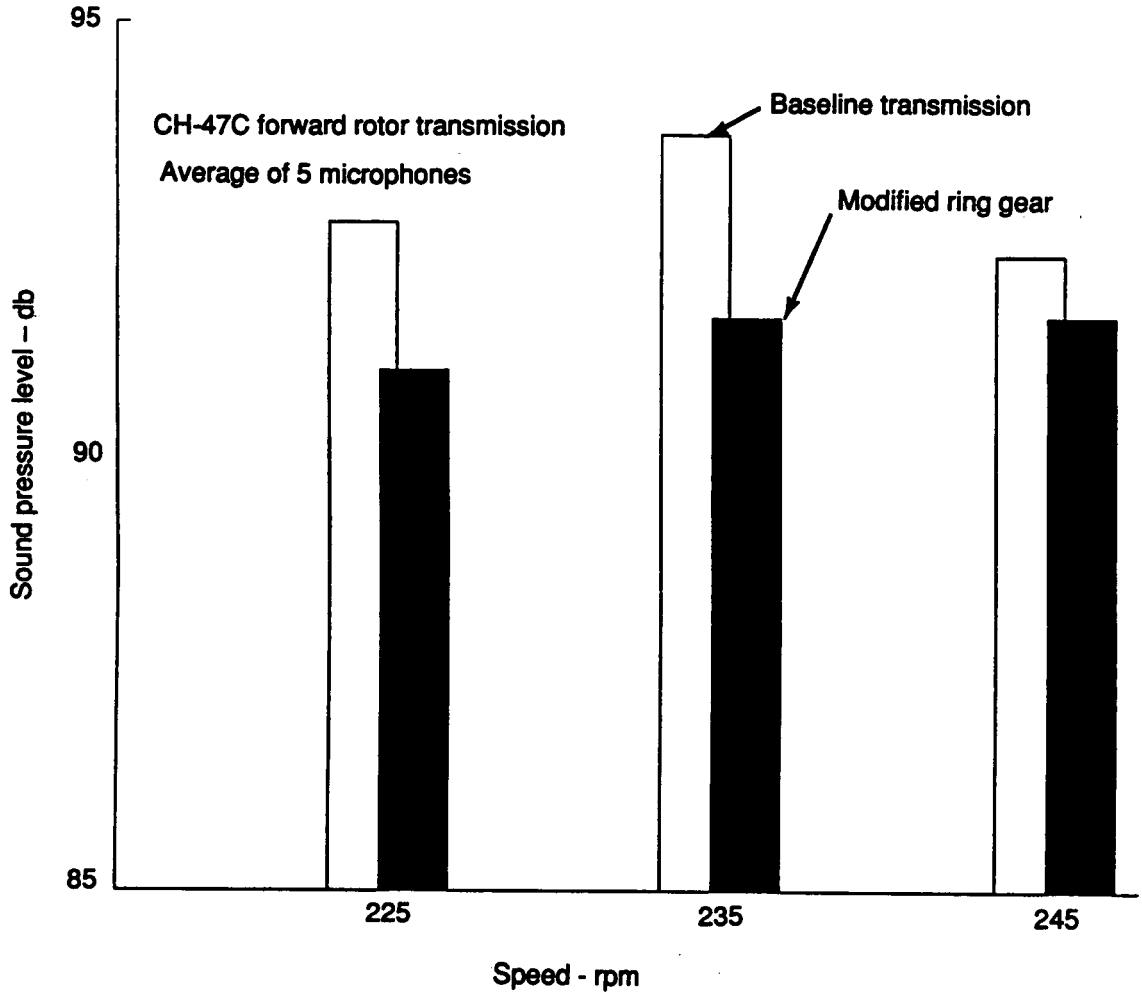

Figure 45. Comparison of Sound Levels of Baseline and Modified Ring Gears

planetary gear and an input pinion gear were freely suspended and records of the acoustic and vibratory decay acquired on a Bruel and Kjaer 2133 dual-channel digital-frequency analyzer. Successive layers of damping tape were applied and the effect on noise and vibration at a typical bearing location recorded. Figure 46 illustrates the effect of added damping on the input pinion gear, indicating that damping of the gear would be beneficial in reducing noise. Similar results were obtained for a first-stage planet gear when damping tape was applied.

Design of Damped Gears - Thirteen sketches of candidate designs for damping of gears were prepared. The sketches included constrained-layer damping, frictional damping, and oil-film damping. The gears considered were the input pinion gear, sun/bevel, first-stage planetary gear, as well as the gear case, since these gears and the case were involved with the generation and/or propagation of noise at first-stage planetary gear mesh frequency. The damping approach and application were:

Constrained-layer damping:	Input pinion (2)
	Transmission housing
	Sun/bevel gear (2)
	Stationary ring gear
	First-stage planetary gear
Frictional damping:	Input pinion
	Sun/bevel gear
	Stationary ring gear
	First-stage planetary gears
Oil-film damping:	Input pinion
	Sun/bevel gear

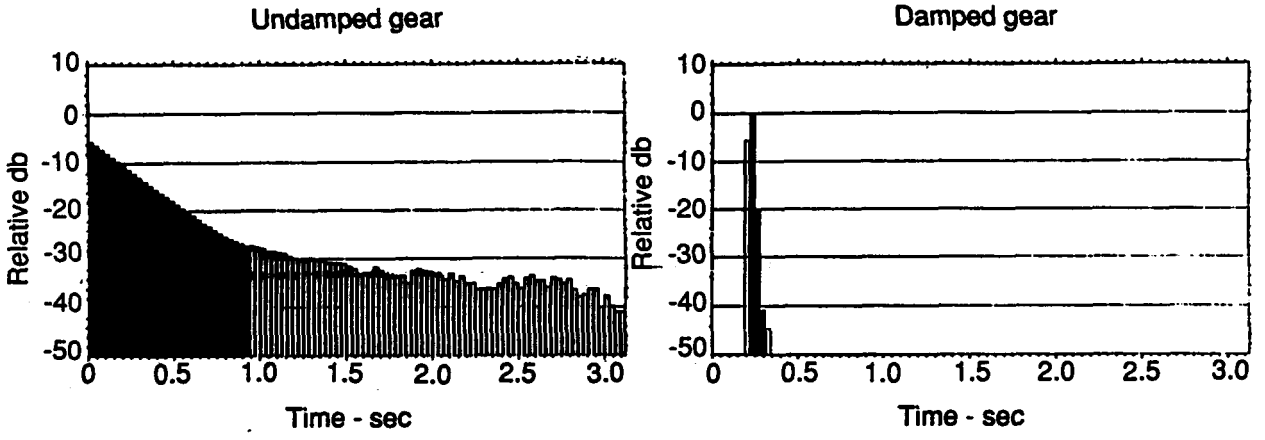

Reverberation time (sec)
Gear configuration

Frequency	Undamped	Undamped bearing installed	Damped bearing installed
A	2.7	0.20	0.09
1,250 Hz	—	0.12	0.09
1,600 Hz	2.4	0.13	0.10

Figure 46. Effect of Damping on Input Pinion Gear

The selected damping designs all used constrained-layer damping and included the input pinion gear (two locations), the sun gear, and all first-stage planetary gears (see Figure 43). The lower case was covered with a composite material which encapsulated sheet Dyad O material. The mounting legs of the upper cover had a viscoelastic damping material manufactured by the 3M Company applied. The material was 3M ISD110, applied to an aluminum constraining layer and bonded to both sides of the vertical webs as well as the horizontal surfaces of each mounting leg (Figure 47).

Ring Gear Plus Damping of Components - At the completion of the testing with the modified ring gear, the transmission was disassembled for a second time and the damped gears installed and the upper and lower case damping applied. The damped spiral bevel input pinion, sun gear, and each of the first-stage planetary gears were installed. It should be noted that this configuration change included installation of first-stage planetary gears from a different transmission, and each of the gears had been modified by the installation of damping material. The sound levels related to this configuration change may have been influenced as much by the new mesh between gears from a different transmission as from the added damping which the modifications were designed to provide. No documentation exists for this effect. This final configuration exhibited sound levels slightly higher than those of the ring gear modification alone; Figure 48 compares the two configurations. As was the case for the ring gear modification alone, the change in sound level was not considered to be significant.

Figure 49 compares sound pressure levels of the three configuration tested.

Conclusions

Passive Control - A review of the applicability of passive mounting systems for large helicopter transmissions confirmed earlier studies that only minimal reduction in structureborne noise (transmissibility) could be expected for a rotor transmission of the weight and horsepower

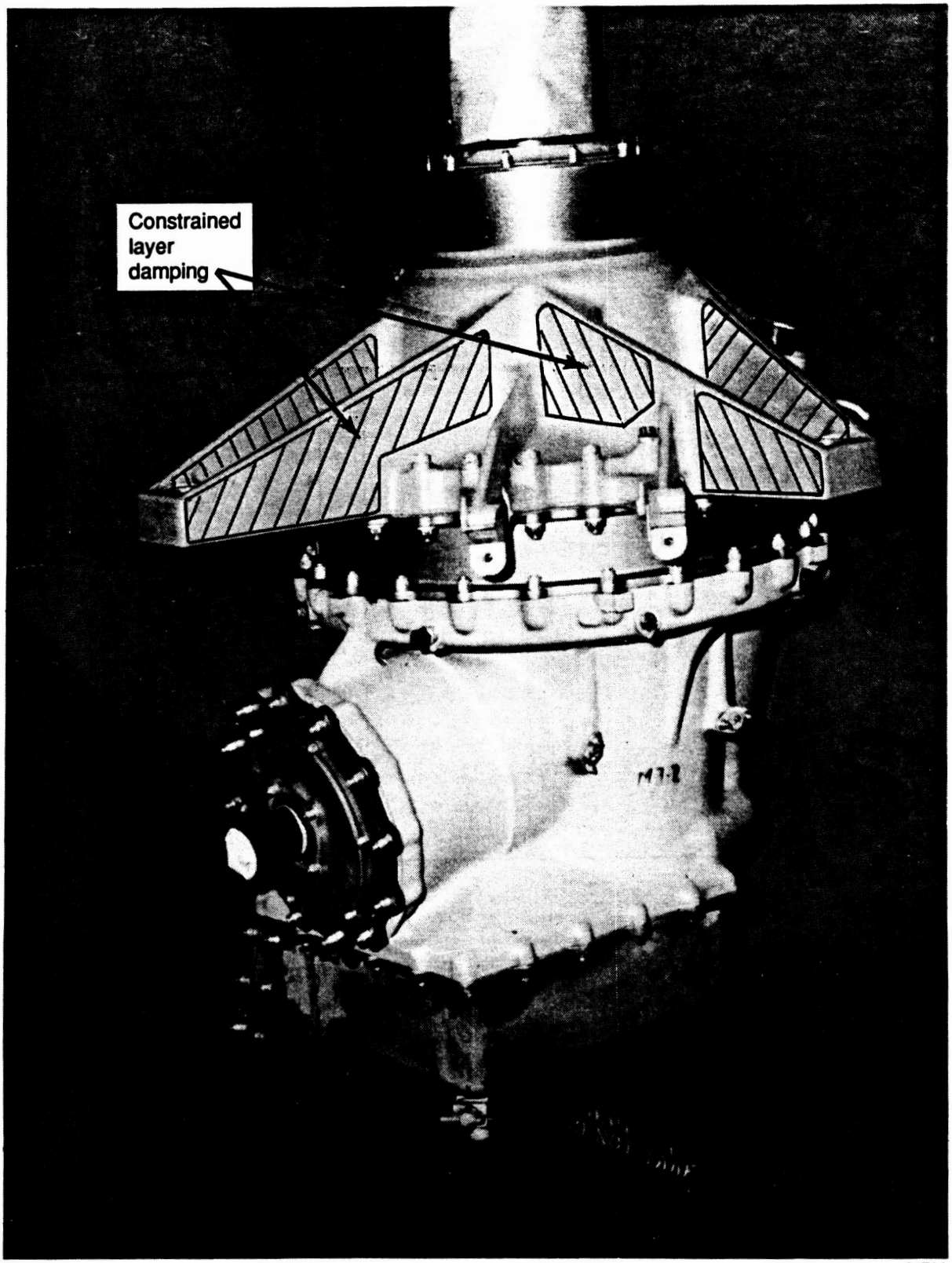

64714

Figure 47. Damping Areas of Mounting Legs

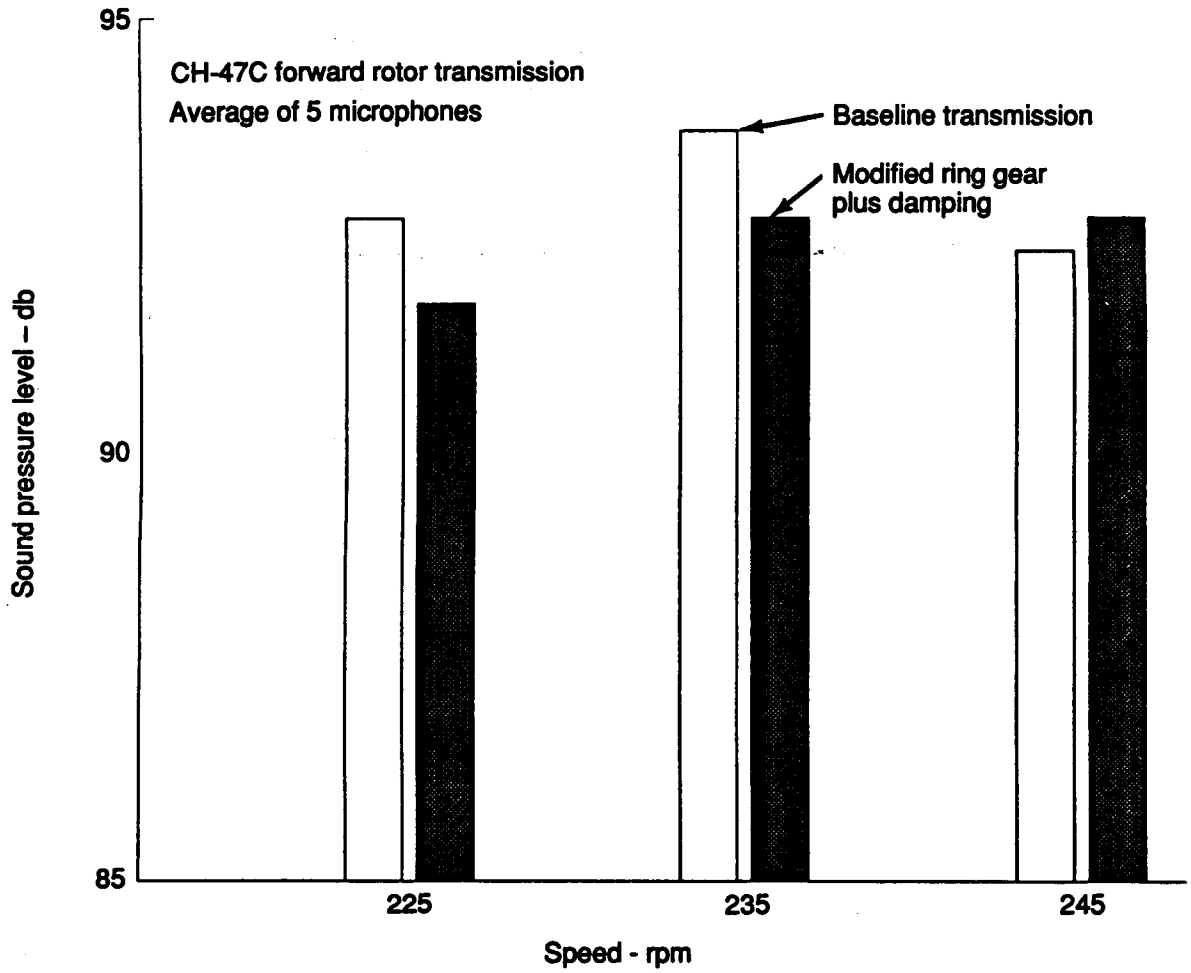

Figure 48. Comparison of Sound Levels of Baseline and Damped Configurations

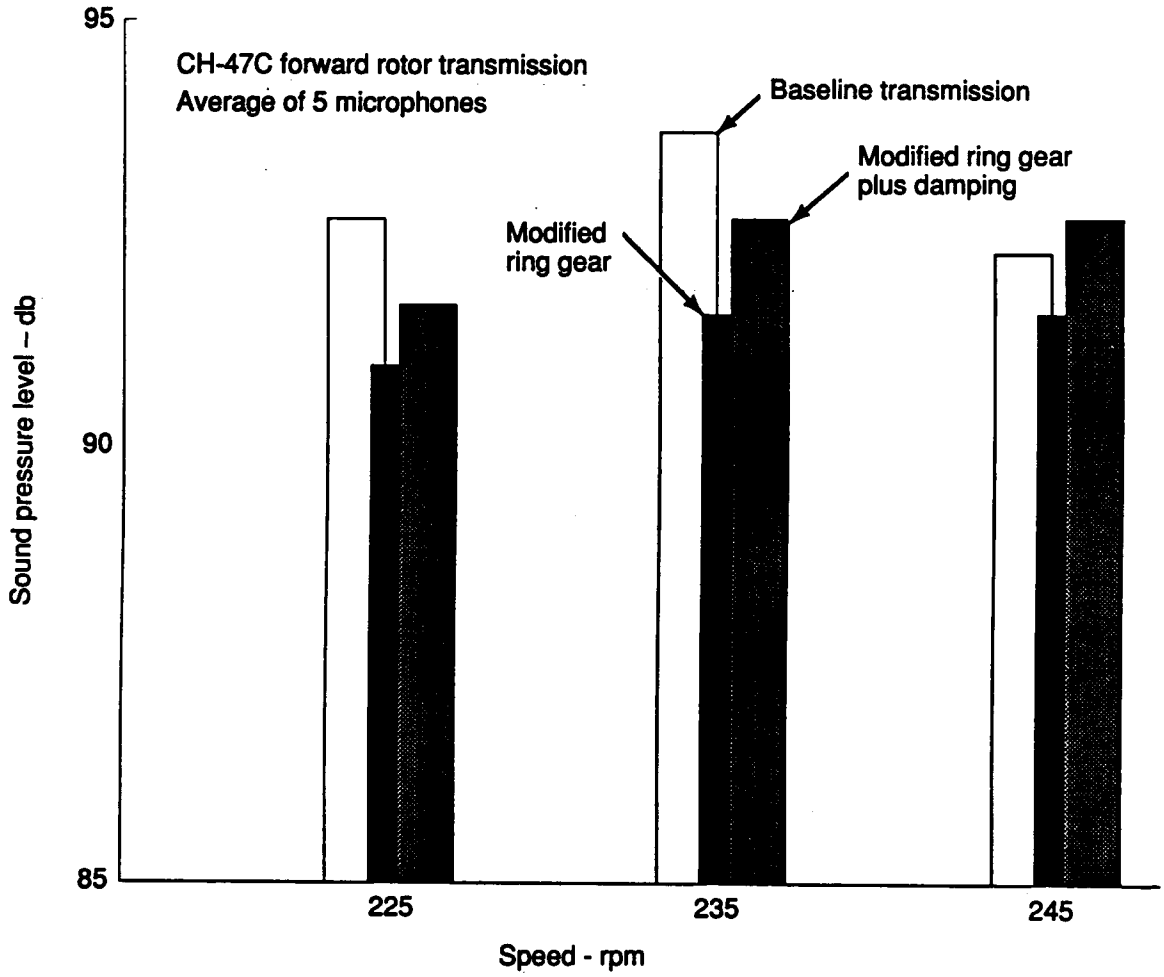

Figure 49. Summary Comparison of Three Transmission Configurations Tested

category of the CH-47. The tradeoff between mount life, weight, and noise reduction indicated that a passive isolator would not be an effective approach to noise reduction. However, the application of passive control to transmissions smaller than the CH-47 appears to be viable.

Active Control - The initial testing with a small-scale transmission proved that a controller could successfully cancel a disturbance consisting of a tone with sidebands at frequencies of lower planet gear mesh of the CH-47 transmission (~ 1,450 Hz). Before this, most active control had dealt with frequencies well below 1,000 Hz, and the achievement of a noise reduction, including sidebands above 1,000 Hz, was considered significant. The availability of a controller that accounts for interactions among channels was considered an important part of the test.

The full-scale test demonstrated reduction of 6-15 db in the vertical axis, the major vibration axis of in-flight transmission vibration. Multiaxis control did not produce the same magnitude reductions. The mass of the actuators appeared to have contributed as much as 10 db of the 15-db total reduction.

The four case-mounted shakers demonstrated a reduction in vibration but were not effective in reducing radiated noise. It appears that the remaining radiating surfaces overpowered those regions that were effectively reduced in vibration.

Ring Gear Modification - The ring gear modification resulted in a modest reduction in radiated noise and vibration. Although one of the two major paths for structureborne noise was eliminated, the remaining path appeared to have contributed significantly to the airborne noise radiation. An elastomeric material between the joining surfaces prevented metal-to-metal contact, but the thinness of the material (0.050 inch) along with the high torque values required to join the upper cover and ring gear (600 lb-ft) minimized any noise reduction due to this material. An effective noise reduction in this area would require significant isolation at all mating surfaces.

Damped Gears and Case - The damping of gears and case also displayed mixed results. The disassembly of the gearbox that was required to install the modified gears resulted in slight tolerance changes between mating gears; in the past this has been noted to result in noise level changes even though no internal modifications have been made. While no documentation of this effect exists, prior experience has indicated a variation in production gearbox noise levels. Part of the increased noise with the damping treatment installed may have resulted from this reassembly effect.

The largest magnitude reduction in structureborne noise was at the transmission mounting legs in the vertical direction. While no meaningful noise reduction in sound level was measured, it appears that reductions in structureborne noise up to 10 db or more at frequencies up to 1,500 Hz are possible. The reduction of a fundamental gear mesh frequency and its sidebands has been demonstrated, but reduction at the harmonic frequencies (2,900, 4,350 Hz) would require a controller of substantially greater capacity and speed.

HYBRID BIDIRECTIONAL TAPERED-ROLLER BEARINGS

The selected A.R.T. drive system makes extensive use of single helical gears. The use of thrust-type bearings is required to react the thrust produced by these single helical gears. Boeing selected a bidirectional tapered-roller bearing to react the thrust and radial load at one end of each shaft. The other end of the shaft was supported by a cylindrical-roller bearing that reacts the radial load and allows for axial growth due to loads and thermal growth.

Bidirectional tapered-roller bearings have been developed by The Timken Company for use in turbine engines to react only thrust loads. The design concept has been expanded for use in the A.R.T. transmission to react both radial and thrust loads. This type of bearing offers high load and speed capability within a single-row bearing and can also handle combined thrust and radial loads produced by the gear reaction in two directions. In addition, the problems of preloading a set of tapered-roller bearings and varying preload setting due to thermal growth will be eliminated by this concept. An initial bearing setting is provided by the bearing manufacturer, much like that of unmounted radial clearance for ball and roller bearings. The proposed bearing design was also tested as a hybrid which incorporates ceramic rollers and polyether-ether-ketone (P.E.E.K.) composite cages to reduce dynamic loads, increase performance under marginal or oil-off operation, and increase the fatigue life of this type of bearing.

The Timken Company was chosen as a subcontractor to Boeing Defense & Space Group, Helicopters Division, for the design, fabrication, and testing of a hybrid bidirectional tapered-roller bearing for the advanced rotorcraft transmission. A hybrid directional tapered-roller bearing was designed, fabricated, and tested with an envelope of 2.5591-inch bore, 4.3307-inch outside diameter, and 0.9843-inch width, made from CBS600 VIMVAR steel for the inner race, outer race, cone and cup ribs, with silicon nitride tapered rollers and a machined-steel, silver-plated cage. Material variations consisted of a zirconia cup rib and a P.E.E.K. cage. The hybrid bearing operated successfully with combined radial and thrust loads at speeds up through

25,300 rpm (1.64 MDN (M=millions, D=diameter of bearing bore in millimeters, N=shaft speed in rpm)) with a synthetic lubricant per DOD-L-85734 supplied at a rate of 3 pints per minute. The hybrid bearing operated successfully with reversing axial loads while carrying a radial load through 23,000 rpm (1.50 MDN). Oil-off testing verified that the hybrid bidirectional tapered bearing can operate at 12,000 rpm (0.78 MDN) for 60 minutes without damage. Endurance tests achieved 7.1, 8.3, and 11.9 times L-10 life for the hybrid bearing. A bearing performance run was completed with 5.0- and 7.5-centiStoke (cSt) synthetic lubricants which illustrated the higher viscosity lubricant results with higher bearing temperature and torque. Details of the work conducted by The Timken Company follow.

The development of the bidirectional bearing for this program is intended for use in a tactical tiltrotor (TTR) aircraft. The bearing is shown on the transmission engine input shaft in Figure 50. The bearing development testing in this program used the application loads, speeds, and temperatures relevant to this bearing position.

NOTE: This section of the report was prepared originally by The Timken Company, a subcontractor to The Boeing Company, Helicopters Division. Boeing would prefer to provide the customer with a report that is consistent in style and format throughout. However, in the interest of reducing the cost of production of this report, Boeing is using all illustrations provided by Timken in their original form.

Bearing Design

The bearing evaluated in this program was a ribbed-cup, bidirectional, tapered-roller bearing design. The size of the bearing was established by Boeing to be applied to the input shaft of the Advanced Rotorcraft Transmission.

Two bearing configurations were then designed. Configuration I was a conventional ribbed-cup, bidirectional, tapered-roller bearing, with the races and rollers fabricated form CBS600

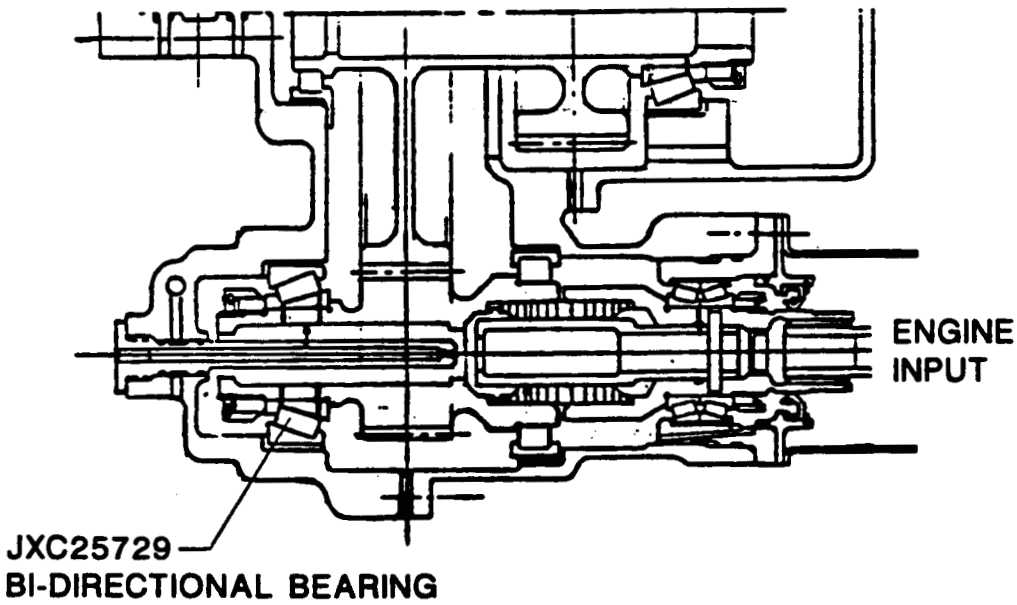

Figure 50. Transmission Input Shaft

VIMVAR steel and the cage machined from SAE 4340 VAR and silver-plated (AMS2410G) (Figure 51). Bearing configuration II (Figure 52) is the same bearing design with the following materials:

a. The inner and outer races and cone rib were fabricated from CBS600 VIMVAR steel.

b. The rolling elements were fabricated from Noralide NBD-200 silicon nitride. These rollers were ground by Professional Instruments Company, Minneapolis, MN. Split Ballbearing of Lebanon, NH, fluorescent-penetrant inspected the rollers according to MIL-STD-6866, Type I, Method D.

c. The cup rib was fabricated from Norzide Grade YZ-110HS zirconia.

d. The cage was fabricated from polyether-ether-ketone (P.E.E.K) polymer reinforced with 30-percent carbon fibers. The cages were molded by Dexter Composites Division, Cleveland, OH.

All the bearing components are shown in Figure 53.

The bearing design is a bidirectional concept (Figure 54) which can resist a combination of radial and thrust load in either the major or minor direction. This is a tapered bearing that can be mounted in an application without a mating tapered bearing on the same shaft, as shown in Figure 50.

The results of the bearing fatigue life calculations are shown in Table 22. The calculated fatigue lives are shown for the helicopter hover mode, the airplane cruise mode, and a cubic mean load condition for a 5.0-cSt and 7.5-cSt viscosity lubricant. The adjusted life is based on The Timken Company C(90) rating, a load zone adjustment, the ASME lubrication adjustment factor, and a material enhancement factor of 10 for the VIMVAR steel.

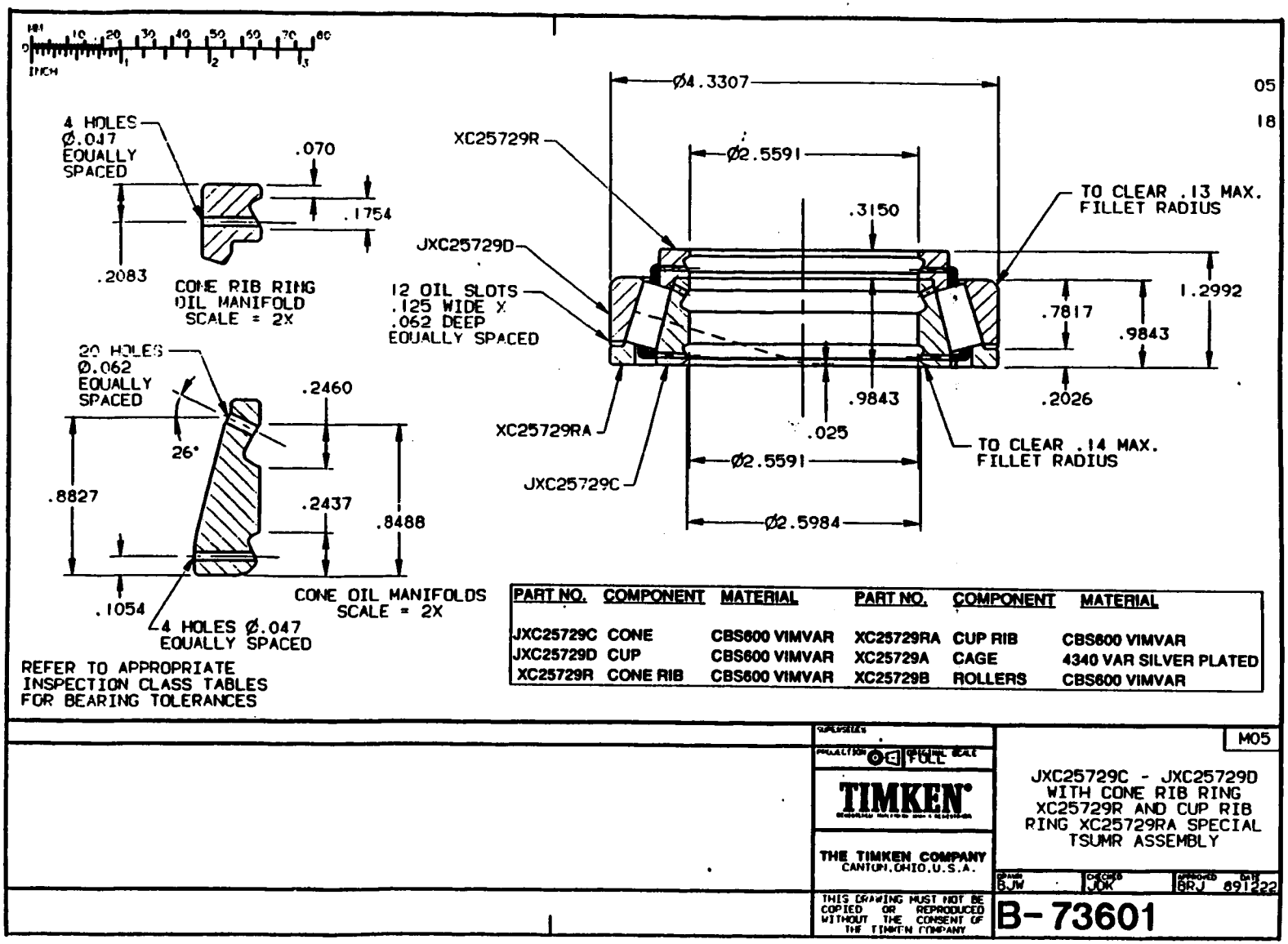

Figure 51. Conventional Bidirectional Bearing JXC25729

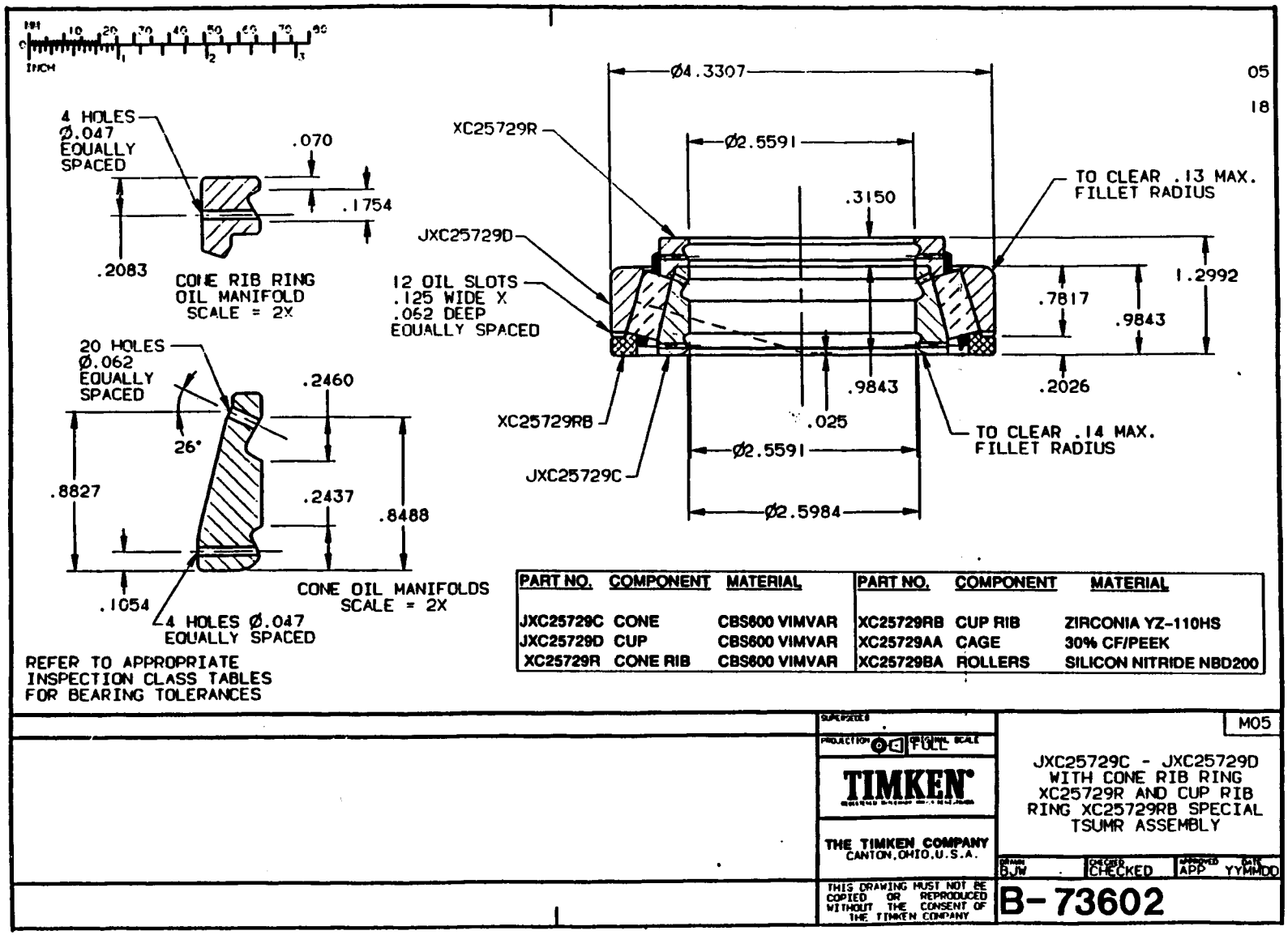

Figure 52. Hybrid Bidirectional Bearing JXC25729

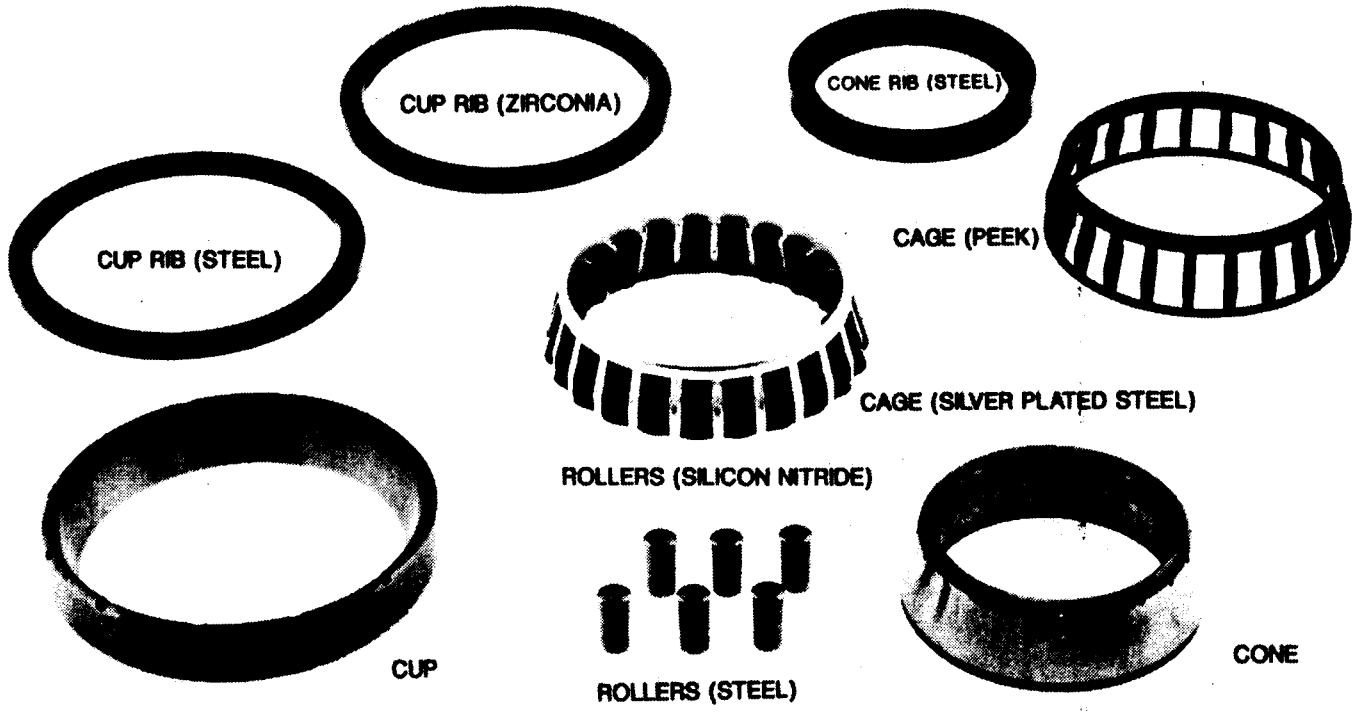

Figure 53. Components of Bidirectional Bearing

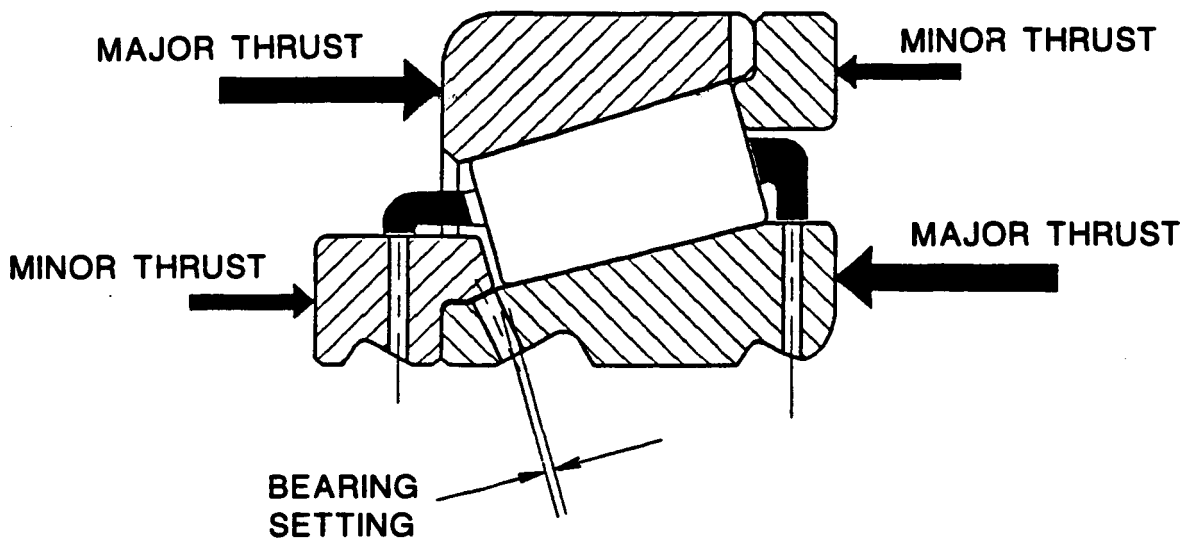

Figure 54. Concept of Bidirectional Bearing

TABLE 22. RESULTS OF BEARING FATIGUE LIFE CALCULATIONS

Load condition	Lube factor		Adjusted life (hours)*
	Cone	Cup	
	5.0-cSt lubricant at 300°F		
Hover (helicopter mode)	1.37	1.56	2,437
Cruise (airplane mode)	0.85	1.13	2,126
Cubic mean load (hover/helicopter)	1.53	1.68	9,966
	7.5-cSt lubricant at 300°F		
Hover (helicopter mode)	2.14	2.25	3,643
Cruise (airplane mode)	1.90	2.03	4,268
Cubic mean load (hover/helicopter)	2.22	2.29	13,923

Maximum power = 2,424 hp at 23,000 rpm
Cubic mean load = 0.66 x maximum power

*Adjusted life based on:
a. Load-zone-adjusted L-10 life
b. ASME lubrication factor
c. Material factor

Design Code for Performance

A computer model was prepared to address the following areas:

a. Analysis of the conventional material versus hybrid

b. Effects of the ceramic steel bearing

c. Performance under the tested speeds and loads

d. Details of stress for the test conditions.

Based on the results of the test runs, this program can be used to calculate the expected results as well as the bearing performance by modifying the geometric parameters.

Bearing Fabrication

The bearings fabricated and tested in this program were 11 conventional and 12 hybrid bearings. In a few test runs components within the bearing were changed to determine the operating differences, i.e., steel cages were replaced with P.E.E.K. cages while retaining all other components.

Test Rig

The Timken Company provided the test rig for this program. The test rig was a universal high-speed test rig modified to accept the size bearing developed for this program and to monitor the following conditions:

- Speed: up to 25,300 rpm (overspeed)
- Load: combined radial and thrust; major-minor thrust condition
- Measurements: cage speed to determine skidding; bearing and oil temperatures; oil flows; torque
- Special tests: rig modified to conduct modified oil flows and oil-off tests on selected test bearings.

Testing

This test program was intended to evaluate a wide range of operating conditions and to determine any limitations for this type of bearing design. The overall testing outline is shown in Table 23, with the specific test conditions shown in Table 24. The conventional (all-steel) bearing was tested first, followed by the hybrid bearing. The initial test runs of the conventional bearing were to establish the oil flow rates required to operate the bearings within the constraints established by Boeing, which included a maximum operating temperature of 400°F.

After the flow rates were established the major-minor thrust conditions were tested with the emphasis in this phase directed to the bearing setting. The major-minor load operating conditions are tabulated in Table 25. In the slow and rapid major-minor sequence the bearing operating conditions were stabilized before starting the reverse-thrust operation. The successful operation of the bearing in minor thrust is directly related to the internal bearing setting which dictates the roller small end/cone rib contact pattern. The overload and overspeed conditions were tested after the major-minor runs.

The hybrid bearing configurations were tested in the same sequence as the conventional bearings. The hybrid bearings were categorized into various configurations:

a. Silicon nitride rollers/steel cup rib/steel cage
b. Silicon nitride rollers/zirconia cup rib/steel cage
c. Silicon nitride rollers/zirconia cup rib/P.E.E.K. cage

These variations were tested to evaluate the bearing performance and to compare the interaction of materials.

The endurance runs were operated with the hybrid combination of steel races, silicon nitride rollers, zirconia cup ribs, and steel silver-plated cages with the conditions as shown in Table 24.

TABLE 23. TEST OUTLINE FOR A.R.T. BEARINGS

I.	All-steel bearings	
	A.	Combined radial and thrust loads
	B.	Establish flow rate to bearing
	C.	~~Major/minor load sequence~~ - slow cycle
	D.	Major/minor load sequence - rapid cycle
	E.	125% overload
	F.	110% overspeed
II.	Hybrid bearing	
	A.	Combined radial and thrust loads
	B.	Establish flow rate to bearing
	C.	Major/minor load sequence - slow cycle
	D.	Major/minor load sequence - rapid cycle
	E.	125% overload
	F.	110% overspeed
	G.	Endurance
III.	Oil-off	
	A.	All-steel bearing
	B.	Hybrid bearing
IV.	Lubricant comparison	
	A.	5.0-cSt vs 7.5-cSt oil

TABLE 24. BEARING TEST CONDITIONS

Factor	Condition					
	Idle	Normal	Normal	Overload	Overspeed	Endurance
Speed, rpm	12,000	18,000	23,000	23,000	25,300	23,000
MDN	0.78	1.17	1.50	1.50	1.64	1.50
Radial, lb	1,700	2,500	3,300	4,100	3,300	4,800
Major thrust, lb	1,100	1,550	2,020	2,550	2,020	3,000
Oil flow, pt/min	3.0	3.0	3.0	3.0	3.0	4.5
Oil inlet temp, °F	180	180	180	180	180	180

Test run duration:
Each test ran 1.5 hours after the bearing's temperature and torque were stabilized. Endurance runs were stopped after a 1-L-10 spall occurred or the run was suspended.

New bearing break-in:
New bearings were broken in by starting at 3,000 rpm, then increasing the speed 3,000 rpm in one-half-hour increments. The loads were increased proportionally.

TABLE 25. MAJOR/MINOR LOAD OPERATING CONDITIONS

Speed (rpm)	Major Radial (lb)	Major Thrust (lb)	Minor Radial (lb)	Minor Thrust (lb)	Cycle[1,2]
12,000	1,700	1,100	900	300	Slow
18,000	2,500	1,550	1,300	400	Slow Rapid
23,000	3,300	2,020	1,600	500	Slow Rapid

1. Slow cycle
   5 minutes major loads
   5 minutes minor load
   4 repetitions

2. Rapid cycle
   110 seconds major loads
   10 seconds minor loads
   25 repetitions

The loads were increased to reduce the calculated L-10 bearing life, thus shortening the test time. The goal was to achieve a ten-times-L-10 test bogey.

Minimum-lubrication requirements were conducted as part of the initial lubrication requirements in the first phase of testing. The oil flow was reduced until excessive bearing temperatures occurred. The minimum oil flow was conducted in the major load condition as this was the condition that generated the maximum heat. The oil supply to the bearing was established as 3 pints per minute to maintain an acceptable operating temperature at 23,000 rpm.

The oil-off testing was conducted at 5,400 and 23,000 rpm for the conventional bearings and at 12,000, 18,000, and 23,000 rpm for the hybrid bearings. The hybrid bearing configurations tested were the silicon nitride rollers/steel cup rib/steel silver-plated cage and silicon nitride rollers/zirconia cup rib/steel silver-plated cage.

Performance data for the all-steel conventional bearing and the hybrid bearing are shown in Tables 26 and 27, respectively. The bearing parameters listed are for the operating conditions applied to the bearings through the test program. The film thickness and lambda ratio values were calculated for the 5.0-cSt viscosity lubricant.

Comparative test runs with a 5.0-cSt (DOD-L-85734) and a 7.5-cSt (DERD 2487) oil were conducted as part of this contract.

Materials Tested

This program was directed toward the evaluation of a bidirectional tapered-roller bearing in a conventional and hybrid design. The conventional and hybrid designs were made to the same envelope dimensions; however, the roller, cup rib, and cage materials differed in the two configurations. The conventional design and materials are shown in Figure 51, with the hybrid design shown in Figure 52. The bearings tested were in various combinations of the

TABLE 26. PERFORMANCE DATA FOR JEX25729 ALL-STEEL BEARING

Factor	Normal	Normal	Normal	Overload	Overspeed
Speed, rpm	12,000	18,000	23,000	23,000	25,300
MDN	0.78	1.17	1.50	1.50	1.64
Radial, lb	1,700	2,500	3,300	4,100	3,300
Major thrust, lb	1,100	1,550	2,020	2,550	2,020
Cage rpm	5,419	8,129	10,387	10,387	11,426
Roller rpm	59,215	88,823	113,469	113,469	124,846
Centrifugal force, lb					
Roller	27.4	61.6	100.6	100.6	121.7
Cup race/roller body	26.3	59.1	96.5	96.5	116.8
Cup rib/roller LE	8.0	18.0	29.4	29.4	35.6
Hertzian stress, psi x 1,000					
Cone/roller	132.0	158.0	181.0	202.0	181.0
Cup/roller	124.0	151.0	176.0	194.0	178.0
Roller LE/cup rib	15.0	18.0	20.0	21.0	21.0
EHD film thickness, microinches					
Temperature, °F	250	300	350	360	370
Cone/roller	9.1	8.1	7.1	6.6	6.9
Cup/roller	9.7	8.7	7.5	7.0	7.3
Lambda ratio					
Cone/roller	1.6	1.4	1.2	1.1	1.2
Cup/roller	1.7	1.5	1.3	1.2	1.2

TABLE 27. PERFORMANCE DATA FOR JEX25729 HYBRID BEARING

Factor	Normal	Normal	Normal	Overload	Overspeed	Endurance
Speed, rpm	12,000	18,000	23,000	23,000	25,300	23,000
MDN	0.78	1.17	1.50	1.50	1.64	1.50
Radial, lb	1,700	2,500	3,300	4,100	3,300	4,800
Major thrust, lb	1,100	1,550	2,020	2,550	2,020	3,000
Cage rpm	5,419	8,129	10,387	10,387	11,426	10,387
Roller rpm	59,215	88,823	113,469	113,469	124,846	113,469
Centrifugal force, lb						
Roller	11.1	25.0	40.8	40.8	49.3	40.8
Cup race/roller body	10.7	24.0	39.1	39.1	47.3	39.1
Cup rib/roller LE	3.2	7.3	11.9	11.9	14.4	11.9
Hertzian stress, psi x 1,000						
Cone/roller	144.0	173.0	198.0	221.0	198.0	240.0
Cup/roller	133.0	160.0	185.0	206.0	186.0	222.0
Roller LE/cup rib	16.0	18.0	20.0	22.0	21.0	23.0
EHD film thickness, microinches						
Temperature, °F	250	300	350	360	370	350
Cone/roller	9.2	8.3	7.2	6.7	7.0	7.0
Cup/roller	9.9	8.8	7.7	7.2	7.4	7.4
Lambda ratio						
Cone/roller	1.6	1.4	1.2	1.1	1.1	1.2
Cup/roller	1.7	1.5	1.3	1.2	1.2	1.3

conventional and hybrid designs; for example, the conventional bearing was tested first with radial and major thrust loads to determine the initial oil flow requirements. The hybrid design was then tested with the cone and cup always being CBS600 and the other component combinations being:

a. Silicon nitride rollers/steel cup rib/steel silver-plated cage

b. Silicon nitride rollers/steel cup rib/P.E.E.K. cage

c. Silicon nitride rollers/zirconia cup rib/P.E.E.K. cage

A total of 43 test runs was conducted; see Appendix B for a detailed list.

Results and Discussion

The test program outlined in Table 23 was followed. The testing started with the all-steel bearing, also referred to as the conventional bearing, by applying the combination radial and thrust loads. The loads were determined by Boeing to simulate the bearing loads of the transmission input shaft. The first run was a shakedown run to establish the initial operating characteristics of the bearings through 23,000 rpm. The bearing performance was monitored via temperatures of the cup outside diameter, rib outside diameter, oil out through the cup slots when open, oil out at the cup rib inside diameter, and the total torque of all four bearings measured by the torque table of the test head (Figure 55).

A more-than-adequate supply of oil was provided to the bearings in the shakedown run; however, in the next phase of testing the oil was reduced to a minimum level to maintain acceptable bearing performance and to establish the flow rate that will be used throughout the remaining test phases. The maximum practical operating temperature of the output oil was set at 400°F at the outset of the program by Boeing. The speed levels tested were 12,000, 18,000, 23,000, and 25,300 rpm, with increasing load levels at each speed as outlined in Table 24.

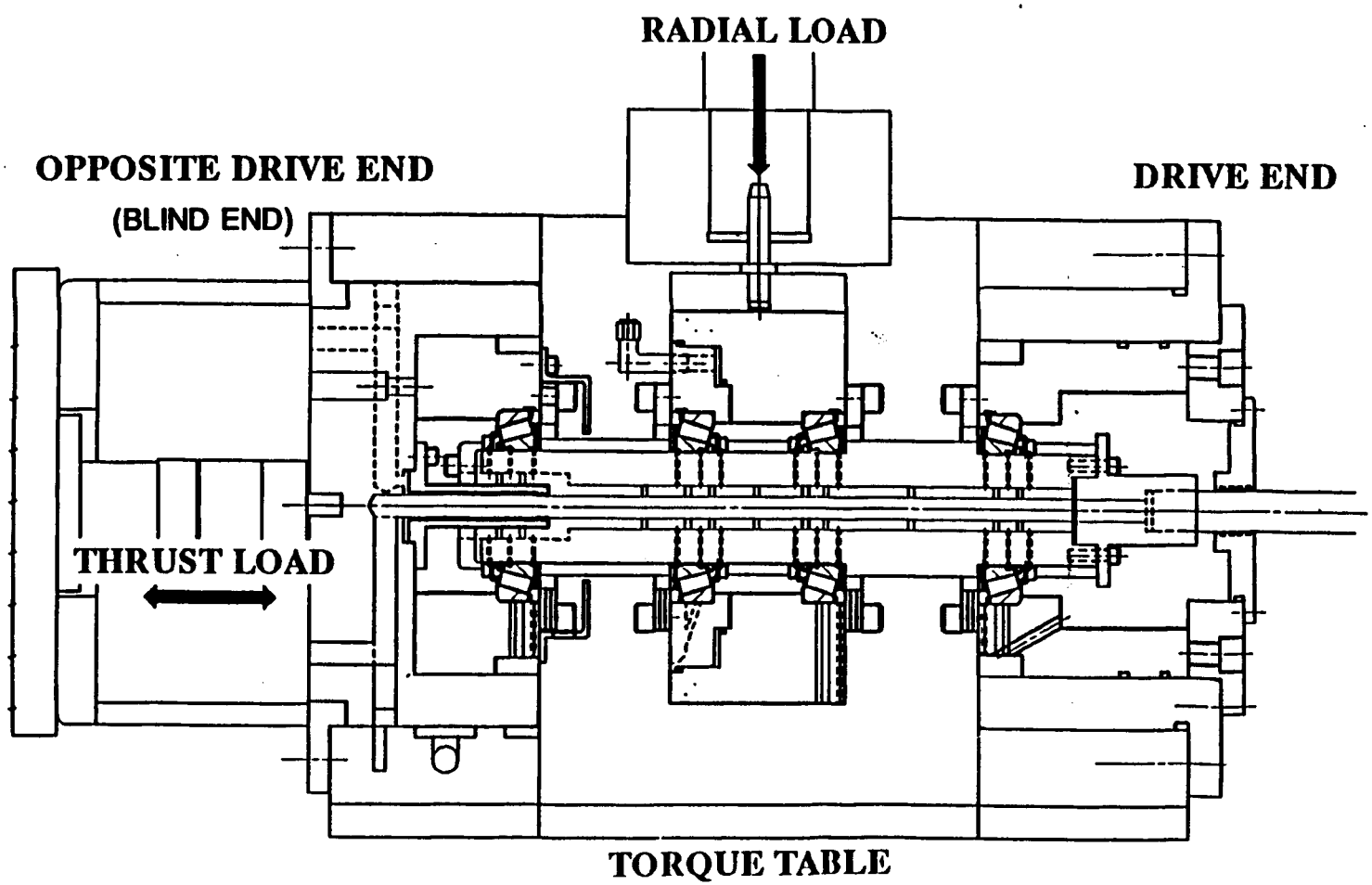

Figure 55. Cross Section of Test Head

The cup was designed with 12 slots in the front face as shown in Figures 51 and 52 to allow oil to leave the bearing and not generate additional heat by trapping oil at the cup rib. In the course of the many test runs these slots were either open or closed to compare the bearing performance. When the slots were used to allow the oil to flow out of the bearing, corresponding holes were required in the housing to carry the oil away from the cup. This may require a more complex housing than may prove practical, and for this reason bearing performance data were collected with and without the slots open. The oil flow requirements established for the bearing were with the slots closed since this may be the more practical for transmission housing fabrication. The temperature response of the test bearing cup outside diameter, rib outside diameter, and oil out at the cup rib is shown in Figures 56, 57, and 58, respectively. These oil flow rates varied from 0.5 pt/min at 12,000 rpm to 3.5 pt/min at 25,300 rpm. Based on the bearing temperature, a 3.0-pt/min oil flow rate per bearing was selected as the normal rate to use throughout the tests.

A comparison of the temperatures and torques with the cup slots open and closed for the all-steel bearing is shown in Figure 59, which illustrates the point that less heat and torque are generated when the oil is allowed to exit through the slots in the cup. Figure 60 is the same comparison of temperature and torque with and without the cup slots closed for the hybrid bidirectional bearing with silicon nitride rollers and a steel cup rib. The same results occurred, with the bearings generating less heat and torque with the slots open. This hybrid data can be compared with the all-steel bearing data of Figure 59. The temperature response of the hybrid bearings is lower than the all-steel and the torque in some conditions is higher. The torque response is for all four bearings in the test unit; also, in all test runs other than the endurance runs the center loading bearings (Figure 55) are the all-steel design. Figure 61 illustrates the operating parameters for the hybrid bearing with silicon nitride rollers, a zirconia rib, and silver-plated steel cage on the top chart and the same combination except with a P.E.E.K. cage replacing the steel cage on the bottom chart. The hybrid bearing with a zirconia rib and steel cage operated at higher temperatures than the all-steel bearing as well as the hybrid bearing with a steel cup rib. The hybrid with a zirconia rib and P.E.E.K. cage operated at higher temperatures than the

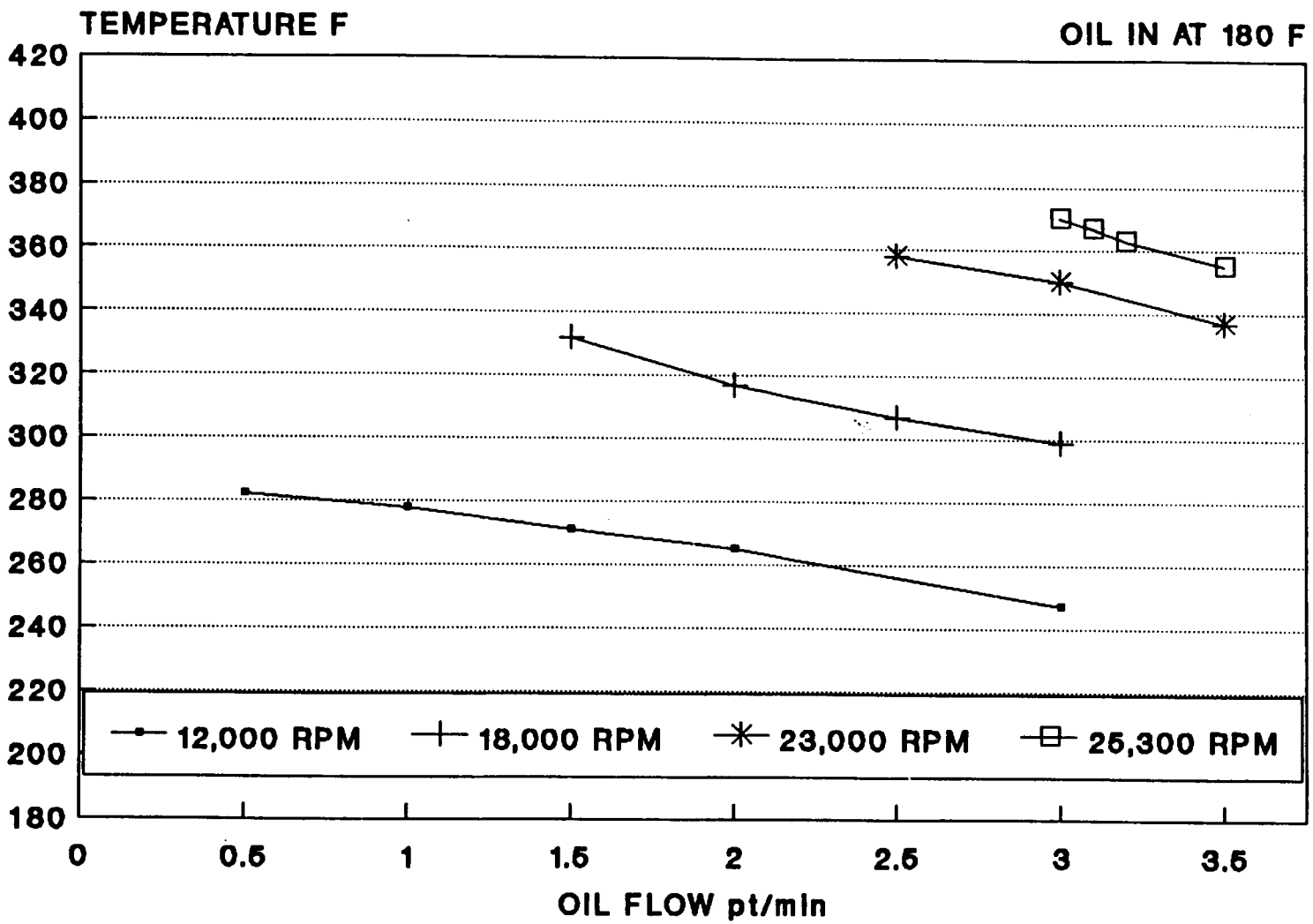

Figure 56. Cup O.D. Temperature Versus Oil Flow, All-Steel Bearing, Cup Slots Closed

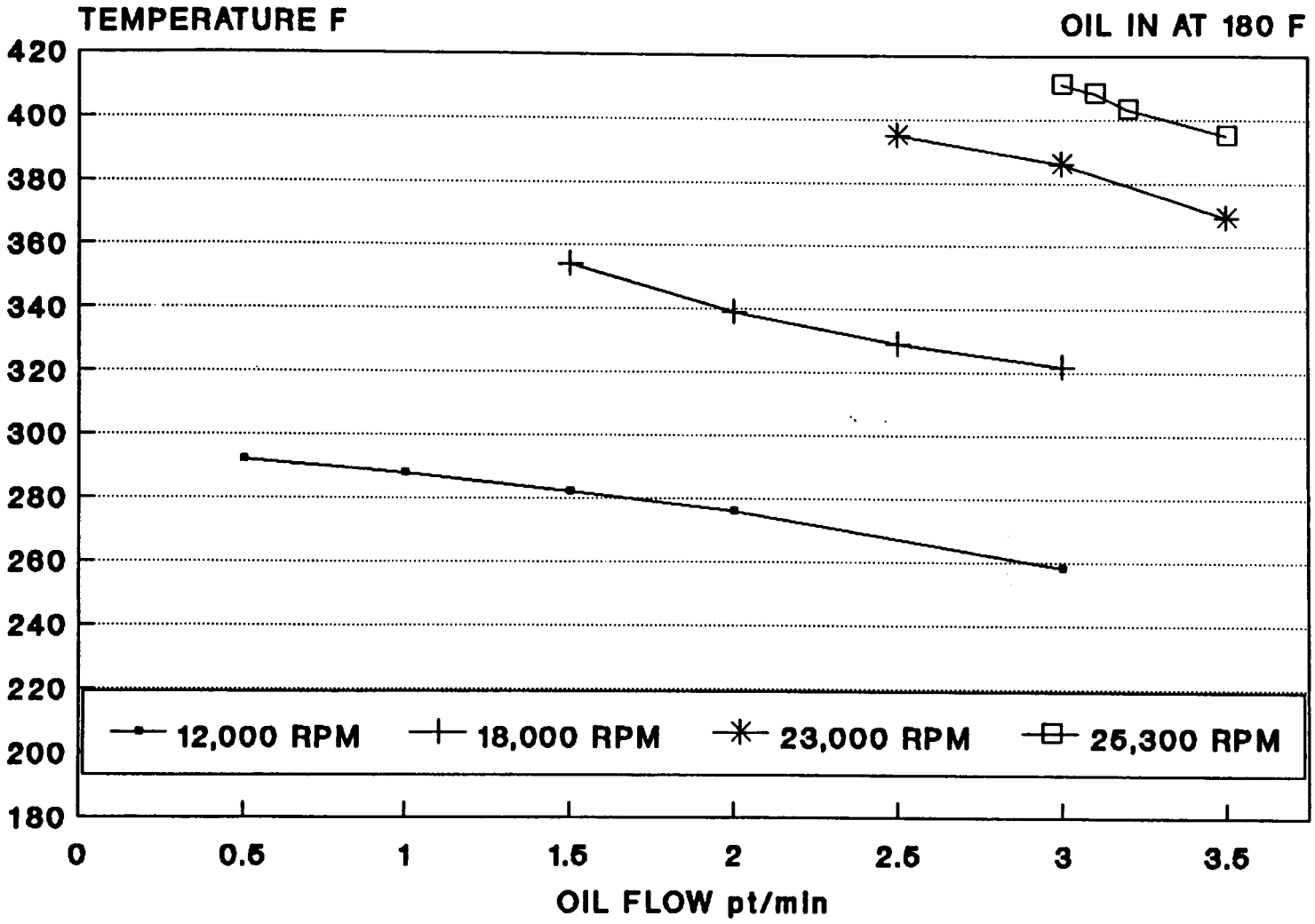

Figure 57. Rib O.D. Temperature Versus Oil Flow, All-Steel Bearing, Cup Slots Closed

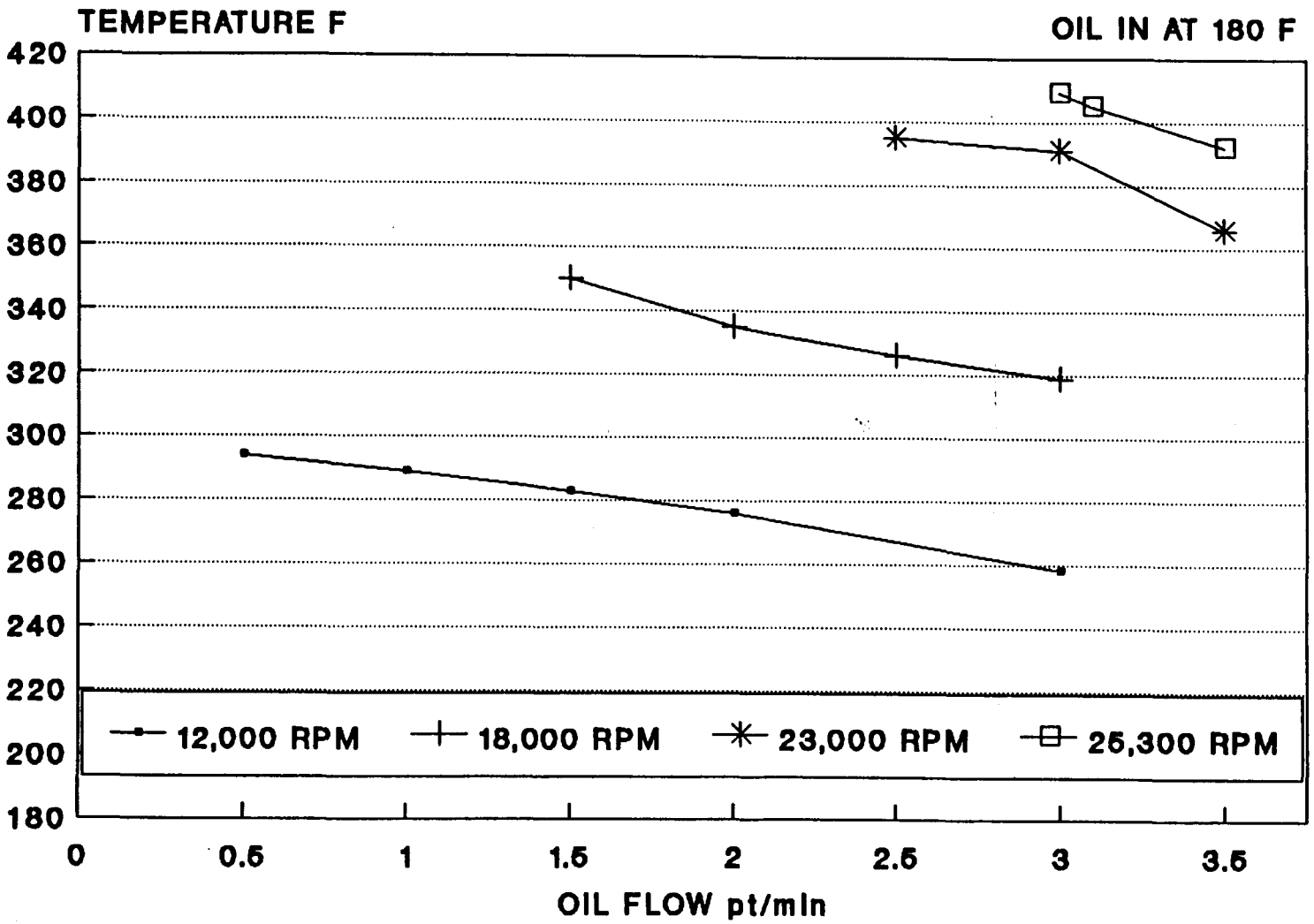

Figure 58. Oil-Out Temperature Versus Oil Flow, All-Steel Bearing, Cup Slots Closed

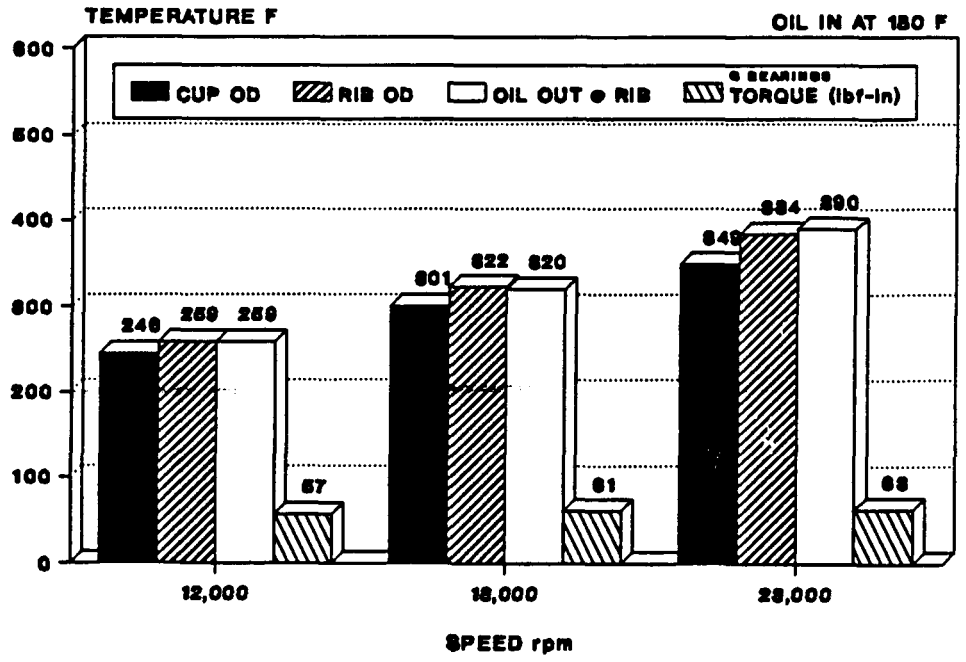

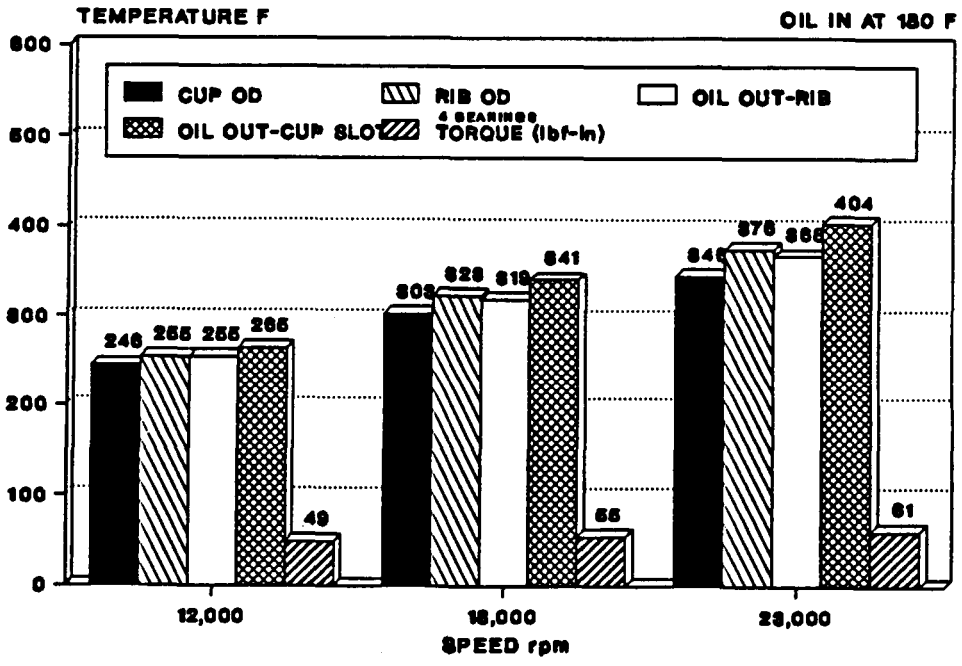

Figure 59. Temperature Versus Speed at 3 Pt/Min, All-Steel Bearing, Cup Slots Closed (Top) and Open (Bottom)

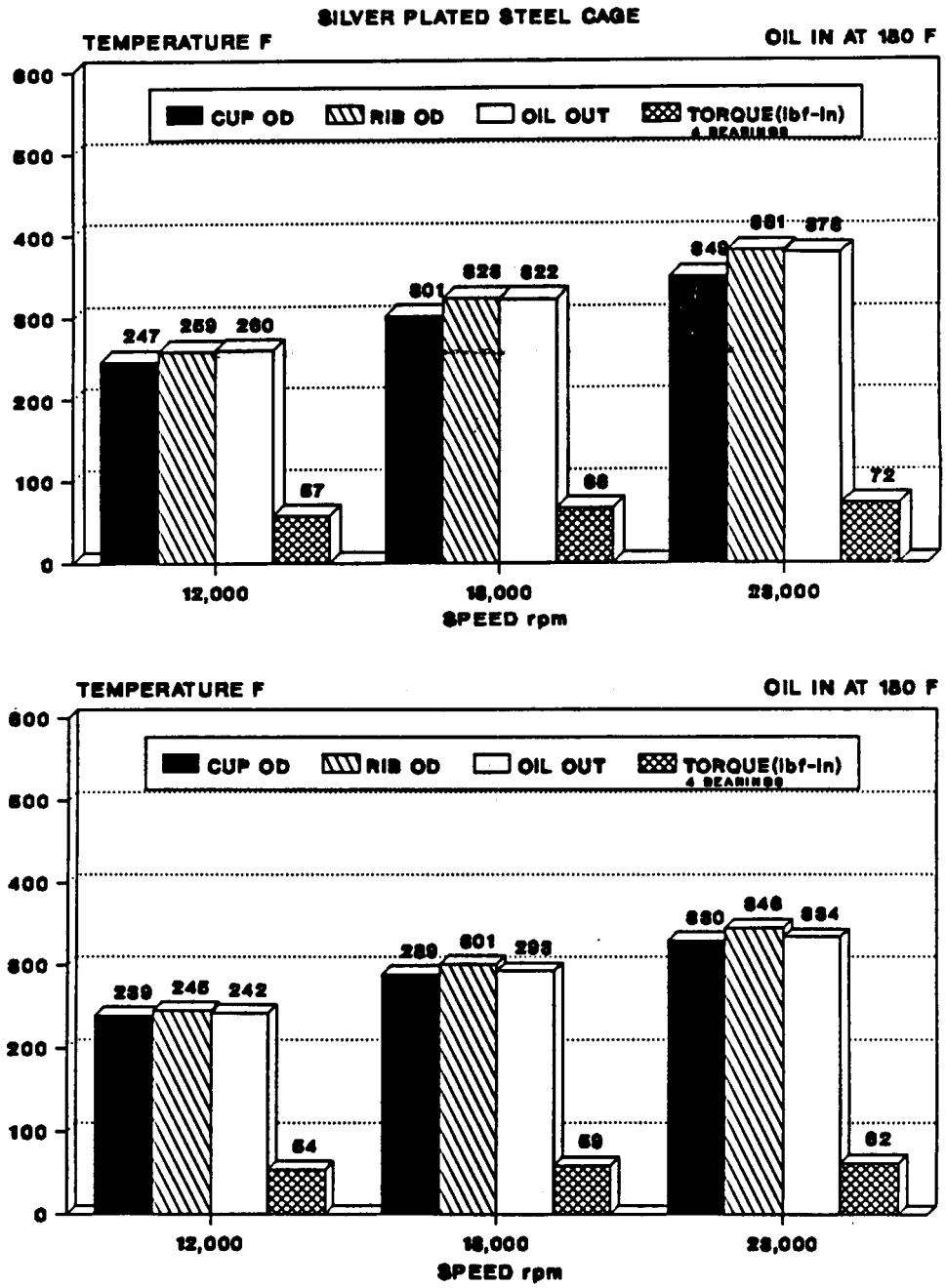

Figure 60. Temperature Versus Speed at 3 Pt/Min, Hybrid Bearing With Silicon Nitride Rollers and Steel Cup Rib, Cup Slots Closed (Top) and Open (Bottom)

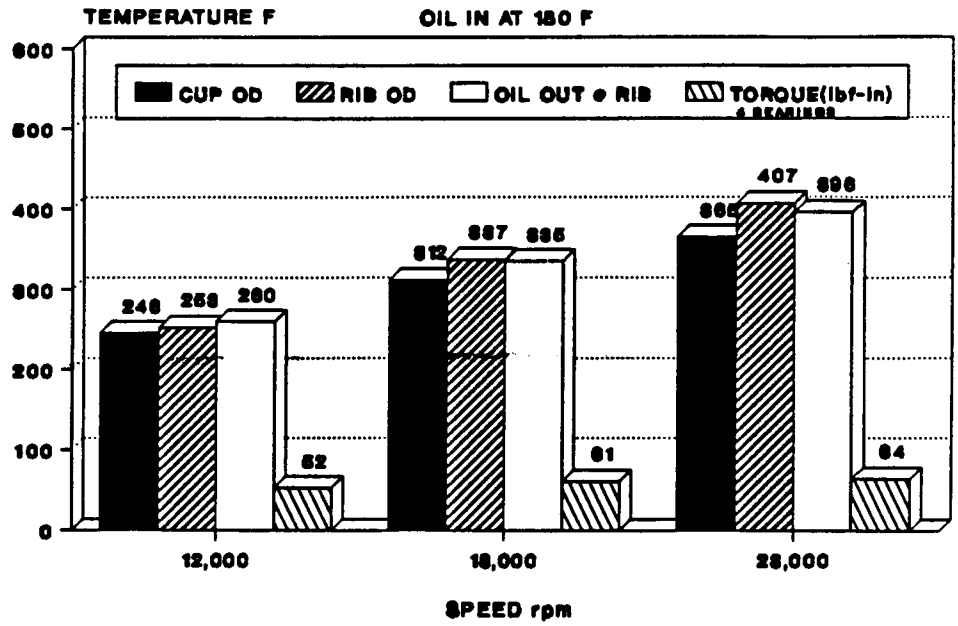

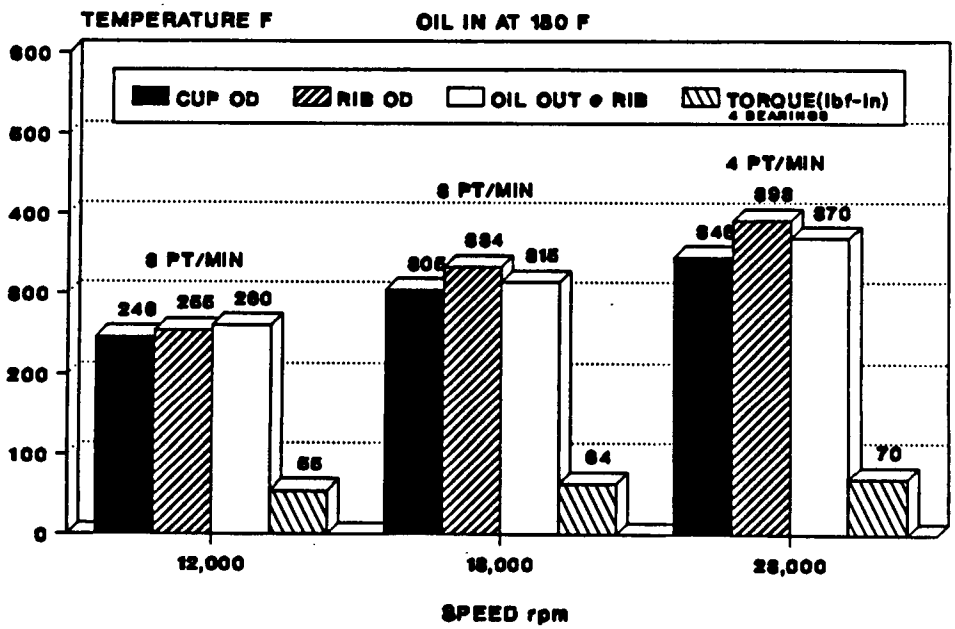

Figure 61. Temperature Versus Speed at 3 Pt/Min, Cup Slots Closed, Hybrid Bearing With Silicon Nitride Rollers and Zirconia Rib, Steel Cage (Top) and P.E.E.K. Cage (Bottom)

other bearing configurations; however, as indicated, the 23,000-rpm run was supplied with 4 pt/min of oil to keep the temperatures below 400°F.

The 23,000-rpm normal, 125-percent overload, and 110-percent overspeed bearing response is shown in Figure 62 for the all-steel bearing with the cup slots closed and maintaining a 3-pt/min oil flow to the bearings. In this condition the temperature was allowed to exceed 400°F in the overspeed condition. The results of the hybrid bearing overload and overspeed are shown in Figure 63, where the hybrid bearing design used the silicon nitride rollers, zirconia rib, and steel cage with the closed cup slots at the top and the same configuration with a P.E.E.K. cage at the bottom. The hybrid bearing did operate at lower temperatures at 23,000 rpm but higher at the overload and overspeed; however, the zirconia rib and steel cage ran with less torque. Additional oil was supplied to the hybrid bearing using the P.E.E.K. cage for the overload and overspeed runs.

Major-minor thrust runs were conducted with two cycles as outlined in Table 25. The slow cycle was applied at 12,000, 18,000, and 23,000 rpm and the rapid cycle was applied to the bearings at 18,000 and 23,000 rpm. Bearing setting is the critical factor in operating the bearing successfully in the major-minor thrust conditions. Numerous bearing settings were tested to establish the setting range for successful bearing performance. Temperature and torque versus time are graphically shown in Figures 64 through 67 of the slow cycle for the bearing configurations of the (1) all-steel, (2) silicon nitride rollers-steel cup rib-steel cage, (3) silicon nitride rollers-zirconia cup rib-steel cage, and (4) silicon nitride rollers-zirconia cup rib-P.E.E.K. cage, respectively. Figures 68 through 71 illustrate bearing temperature and torque response for the rapid-cycle major-minor thrust at 18,000 and 23,000 rpm with the same bearing configurations. The bearing temperature and torque are directly responsive to the direction of the thrust load as illustrated in these graphs (see Figure 54). The major load is carried by the cup race-roller body-cone race and roller large end-cup rib, with the race contacts responsible for the heat generation. In the minor thrust direction the bearing component contacts are primarily the roller large end-cup rib, roller small end-cone rib, and a small load zone of the

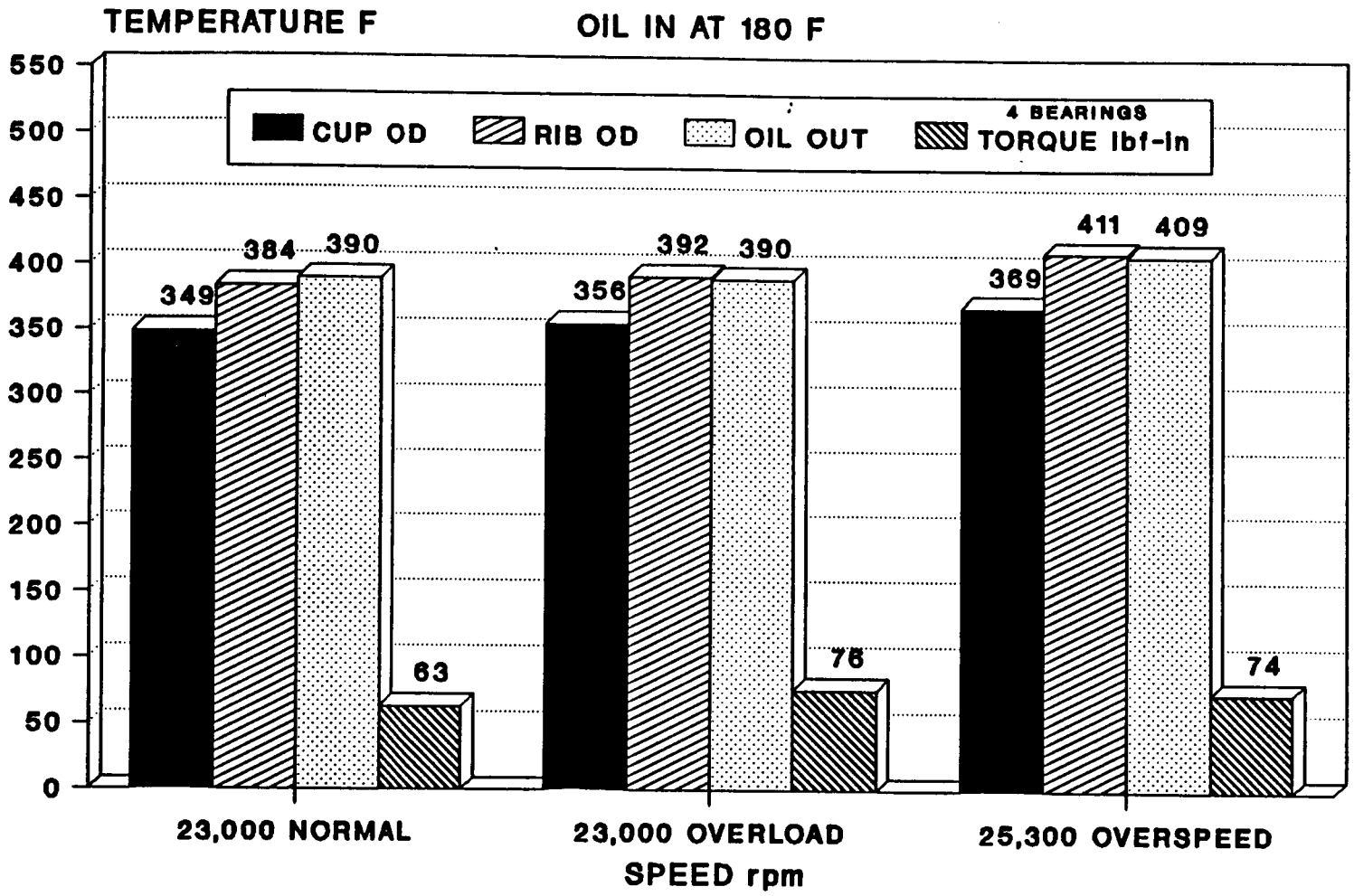

Figure 62. Temperature at Overload and Overspeed at 3 Pt/Min, All-Steel Bearing, Cup Slots Closed

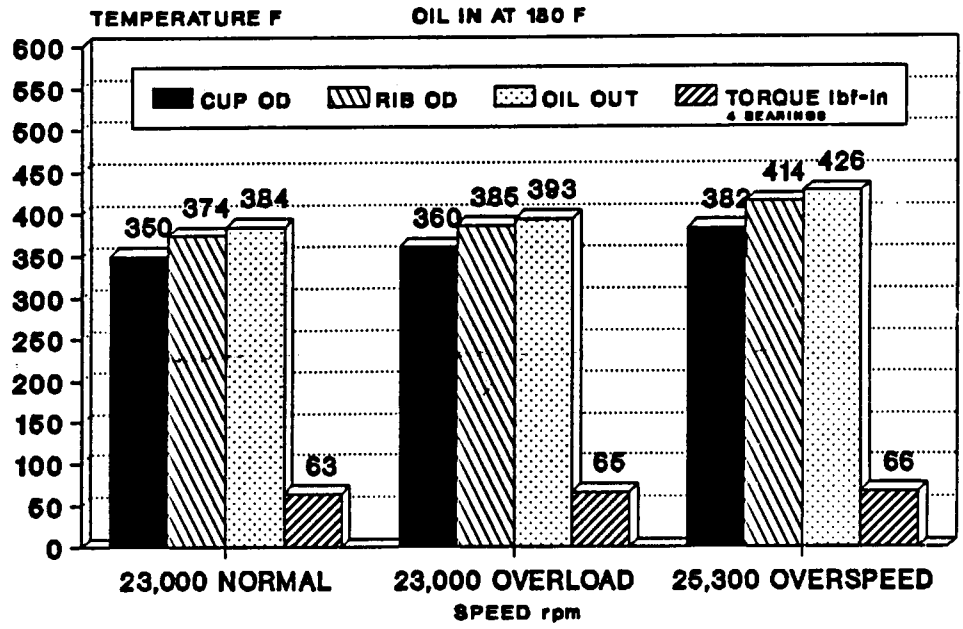

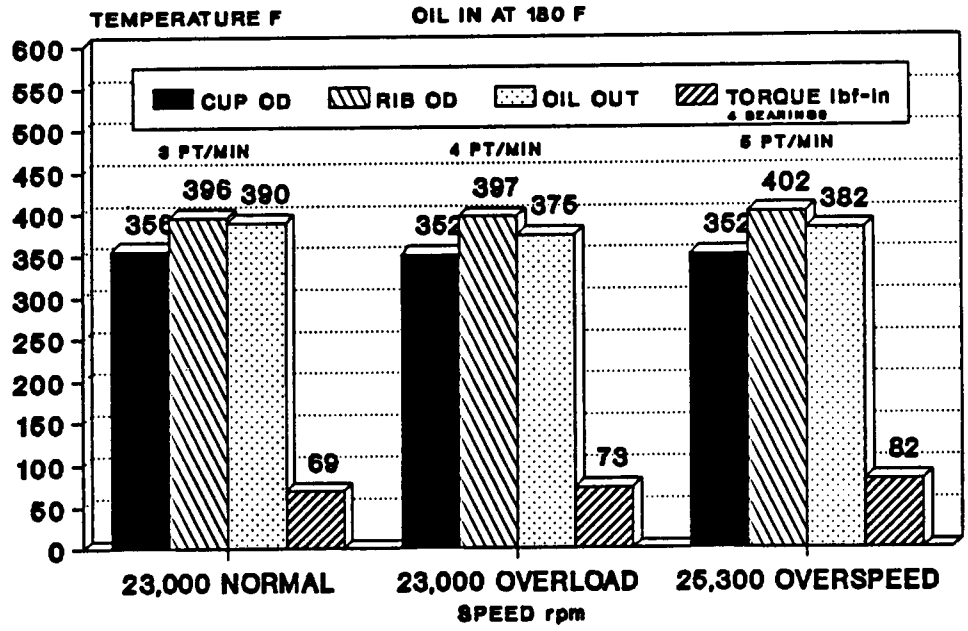

Figure 63. Temperature at Overload and Overspeed, Cup Slots Closed, Hybrid Bearing With Silicon Nitride Rollers and Zirconia Rib, Steel Cage (Top) and P.E.E.K. Cage (Bottom)

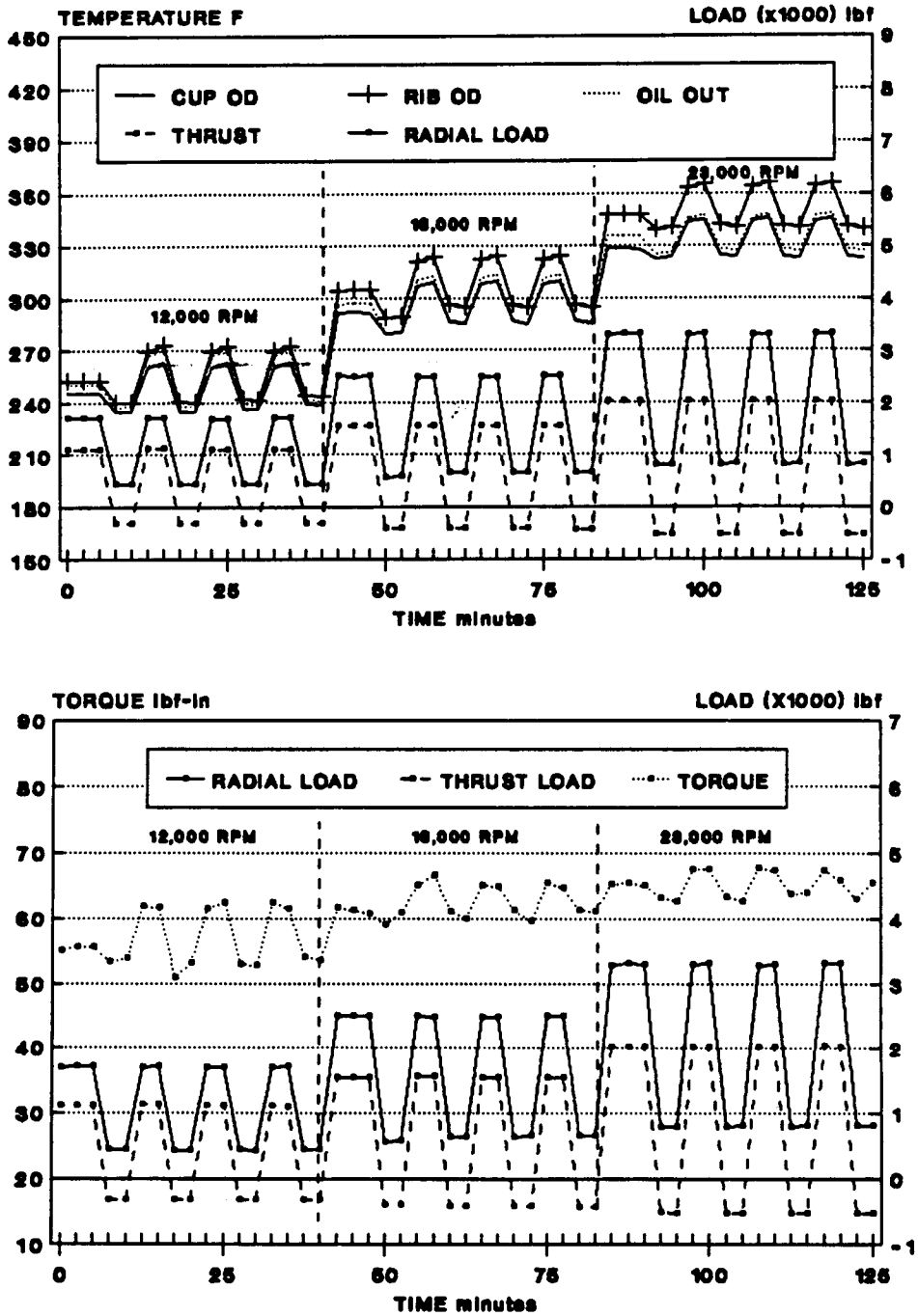

Figure 64. Temperature, Torque, and Load Versus Time, All-Steel Bearing, Major-Minor Thrust

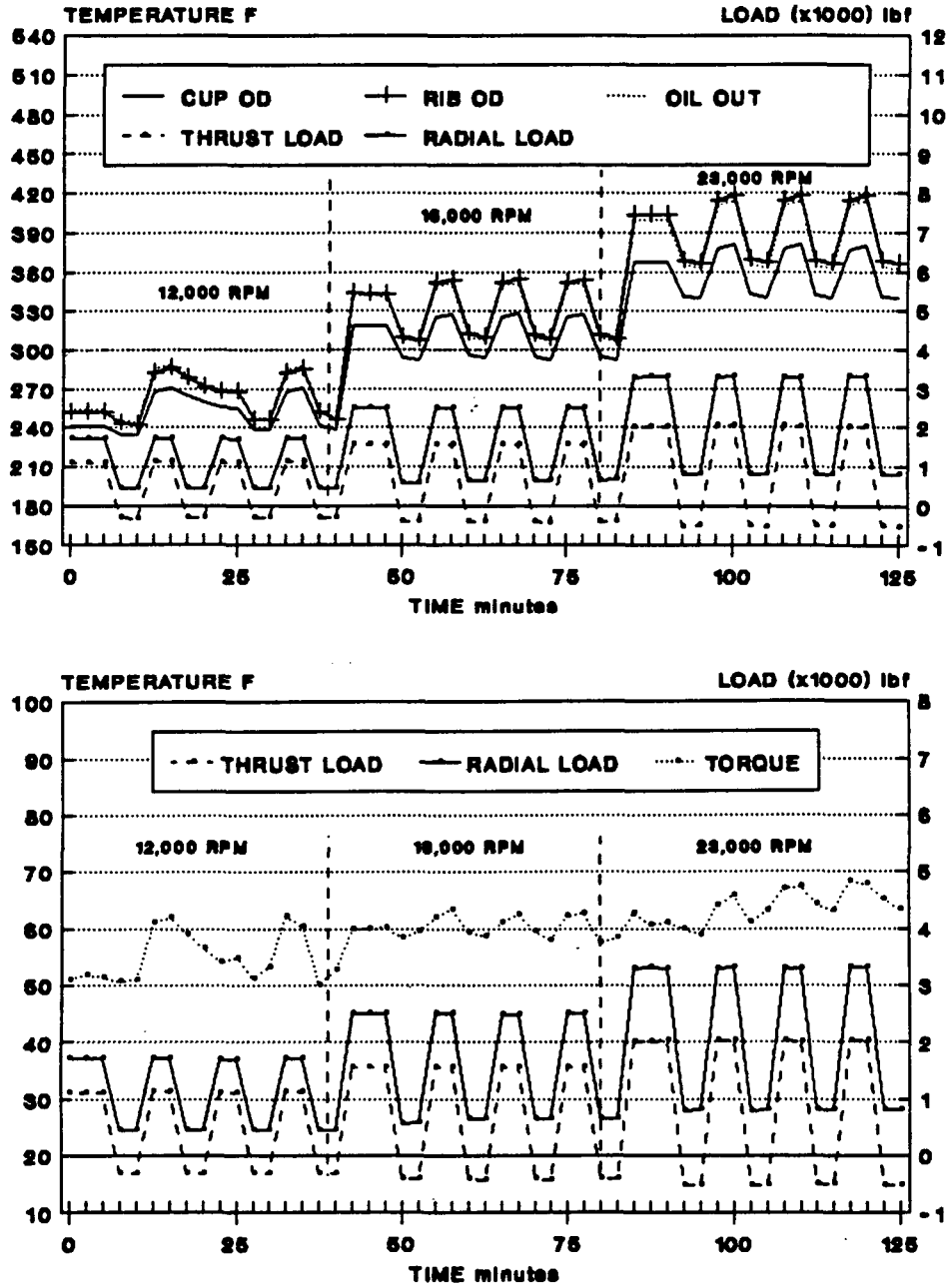

Figure 65. Temperature, Torque, and Load Versus Time, Hybrid Bearing With Silicon Nitride Rollers and Steel Cup Rib, Major-Minor Thrust

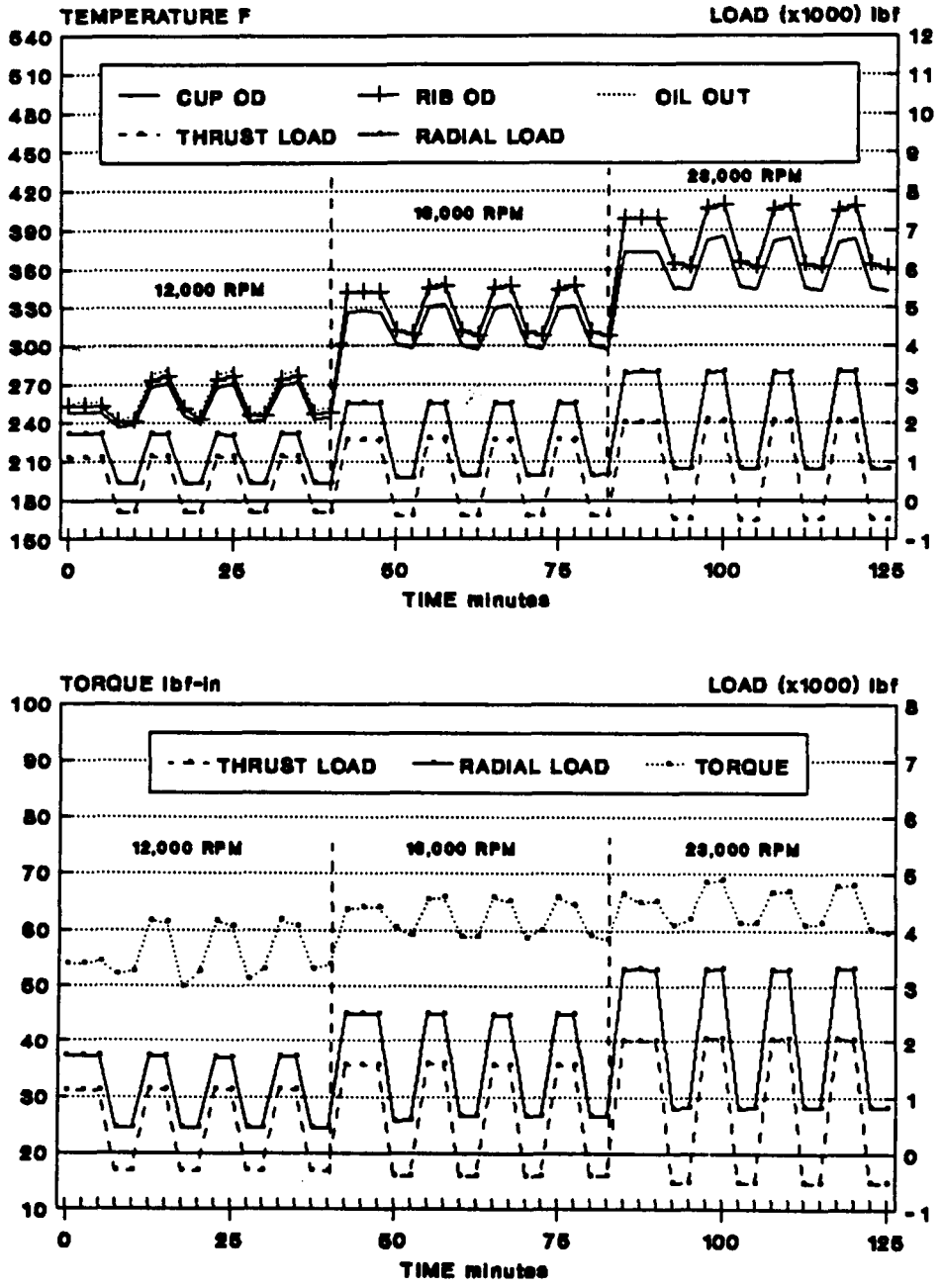

Figure 66. Temperature, Torque, and Load Versus Time, Hybrid Bearing With Silicon Nitride Rollers and Zirconia Cup Rib, Major-Minor Thrust

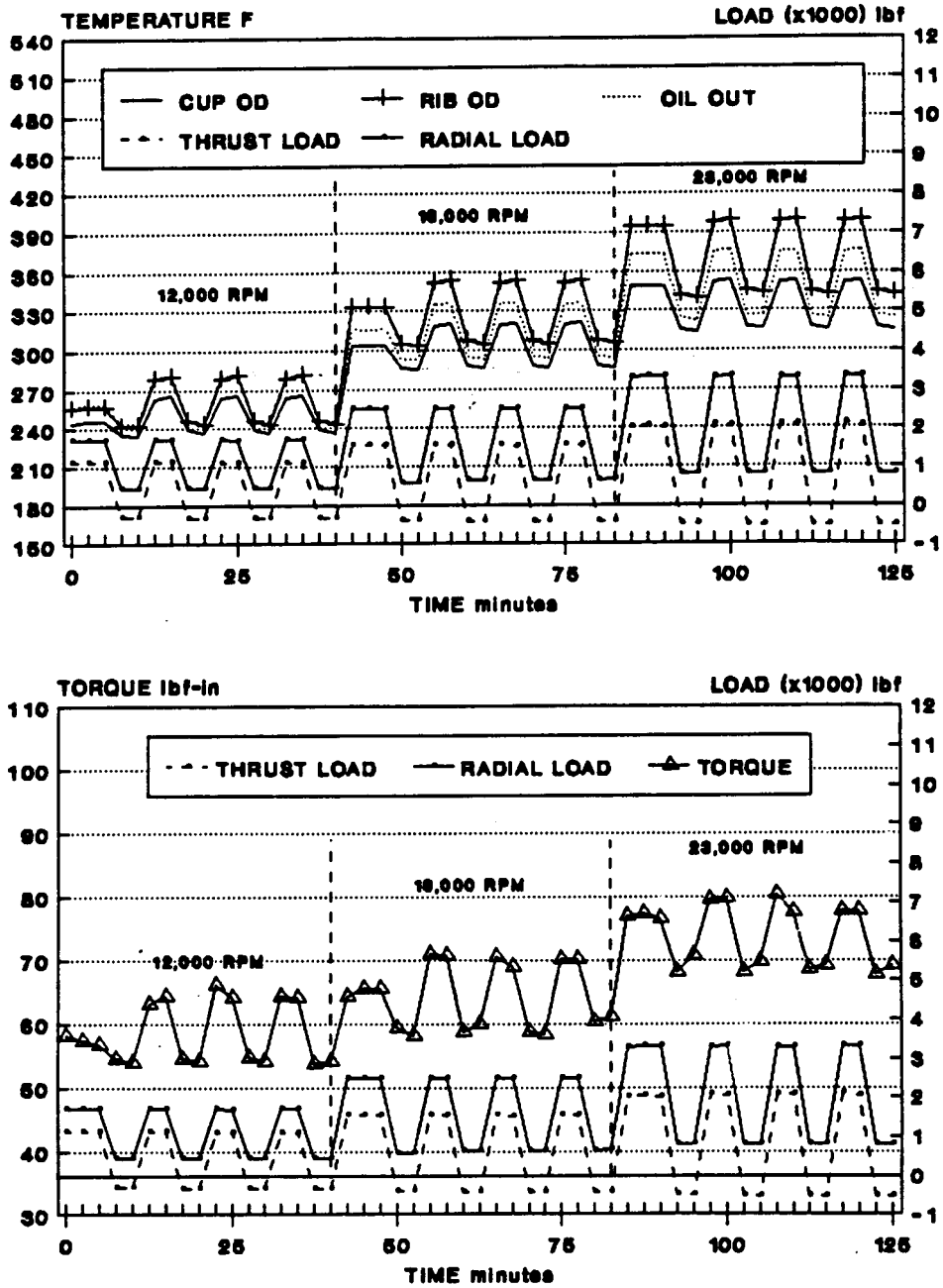

Figure 67. Temperature, Torque, and Load Versus Time, Hybrid Bearing With Silicon Nitride Rollers, Zirconia Cup Rib, and P.E.E.K. Cage, Major-Minor Thrust

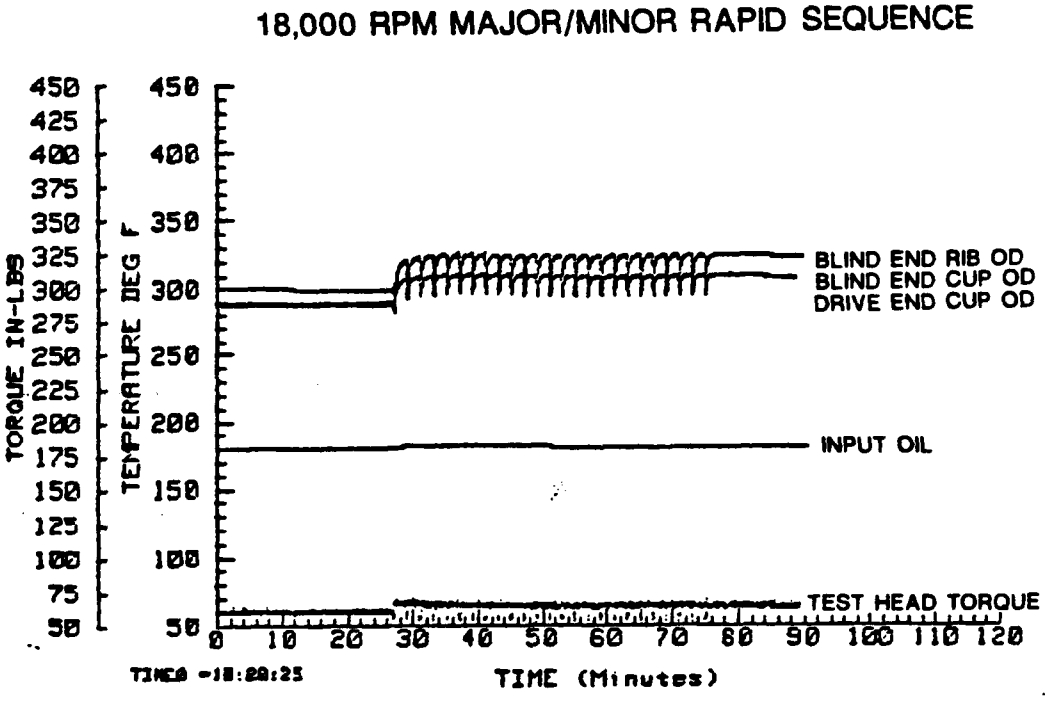

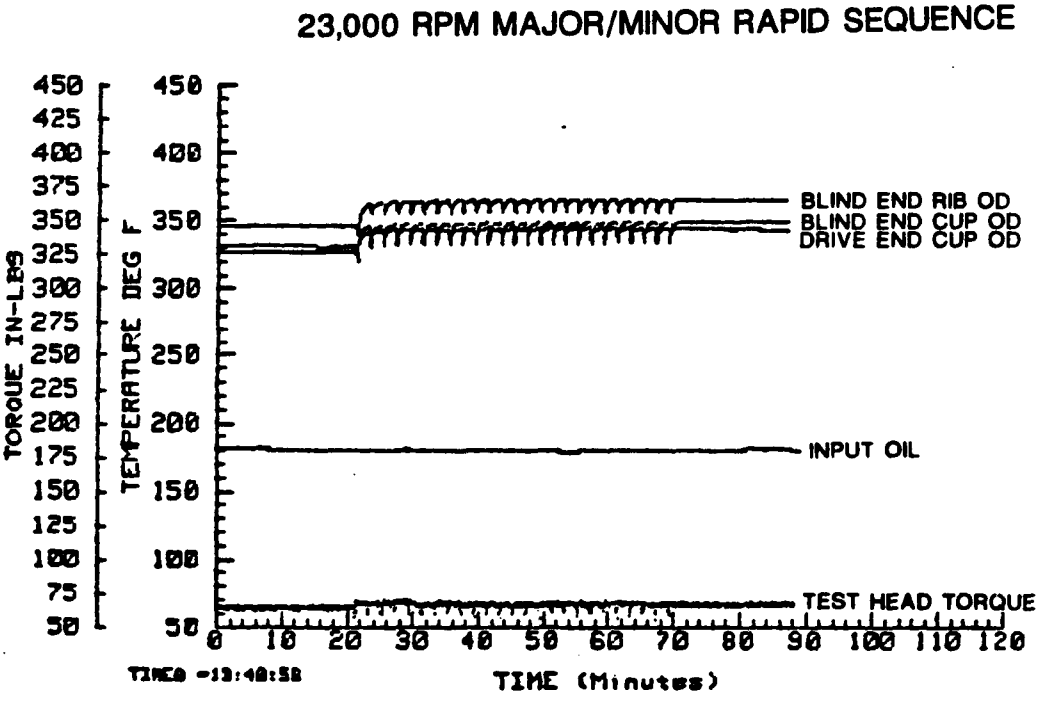

Figure 68. Temperature and Torque Versus Time in Rapid-Sequence Major-Minor Thrust, All-Steel Bearing

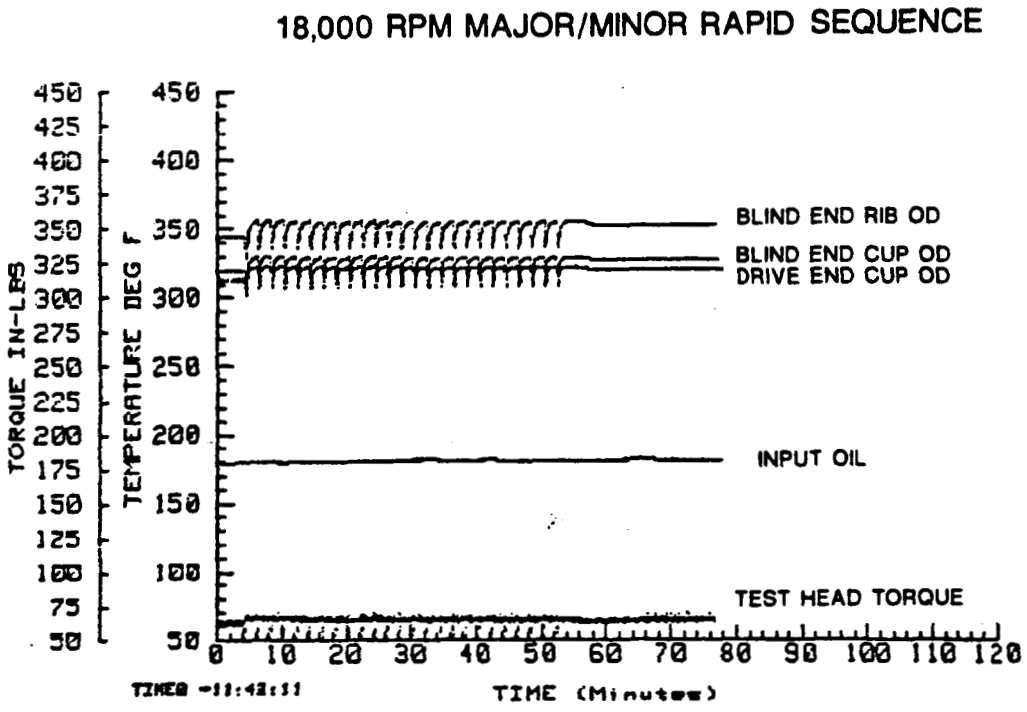

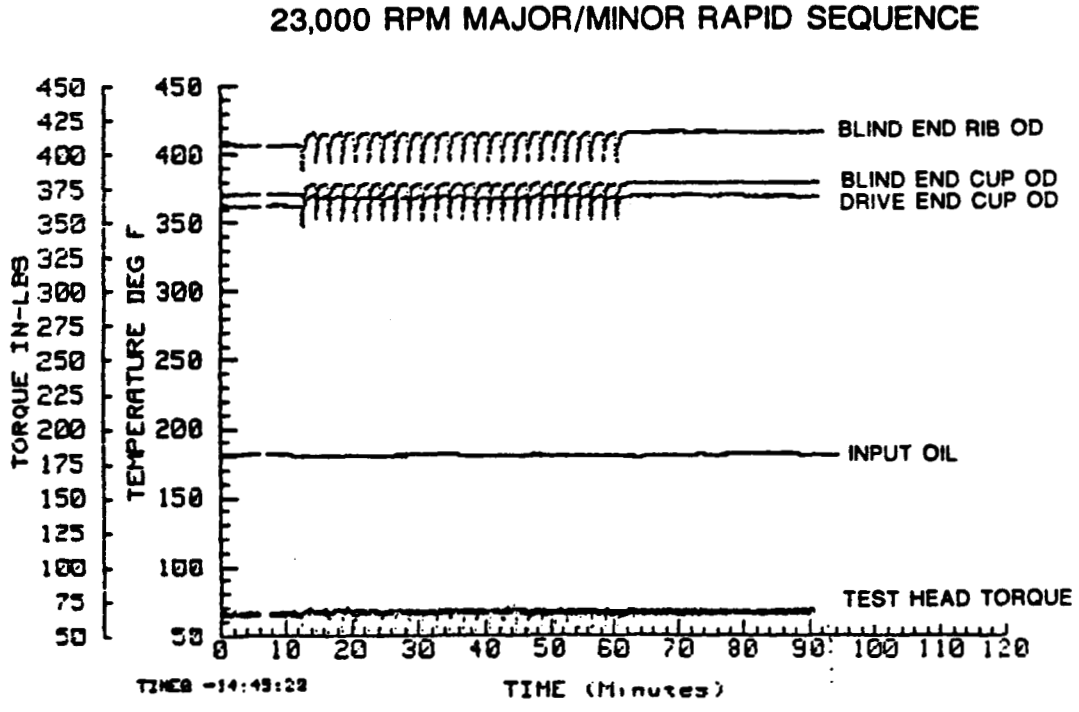

Figure 69. Temperature and Torque Versus Time in Rapid-Sequence Major-Minor Thrust, Hybrid Bearing With Silicon Nitride Rollers and Steel Cup Rib, Cup Slots Closed

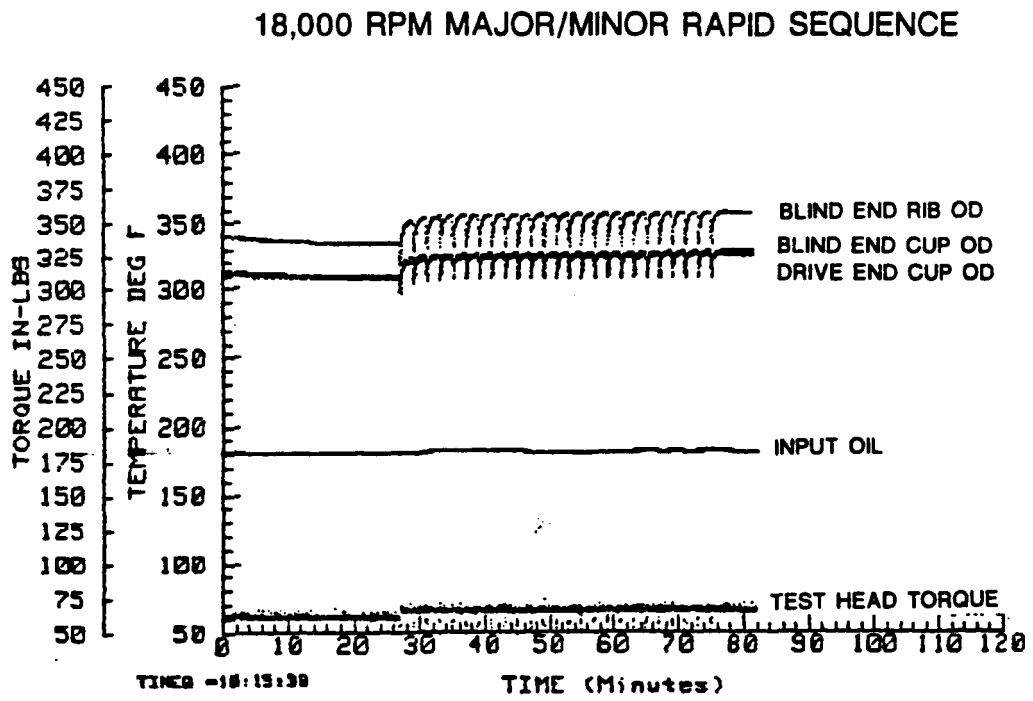

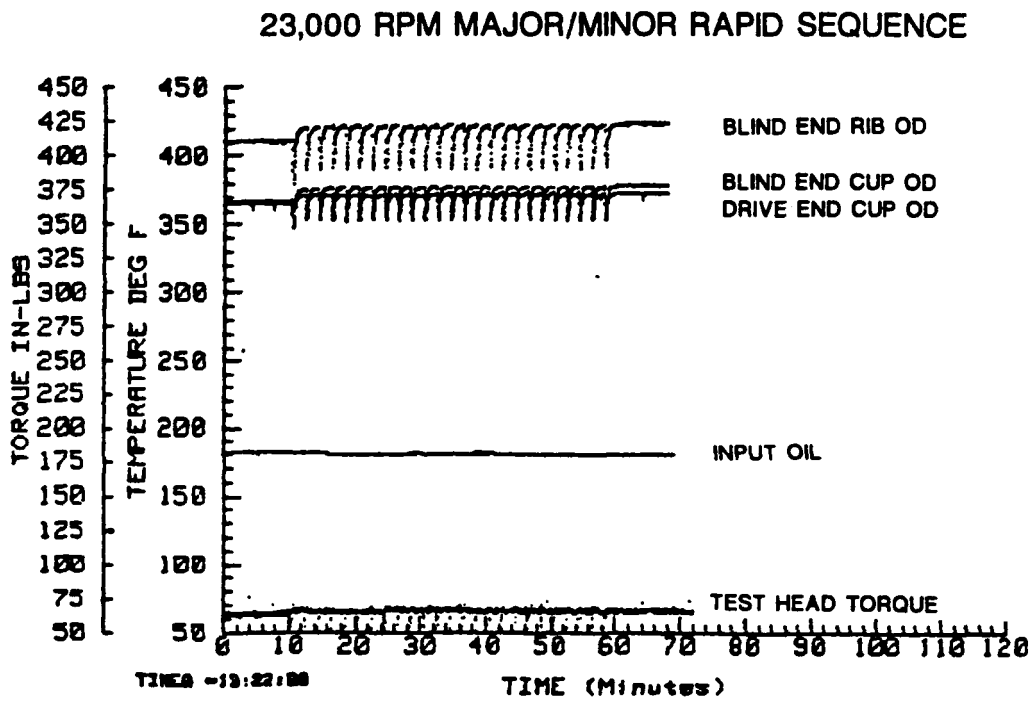

Figure 70. Temperature and Torque Versus Time in Rapid-Sequence Major-Minor Thrust, Hybrid Bearing With Silicon Nitride Rollers and Zirconia Cup Rib, Cup Slots Closed

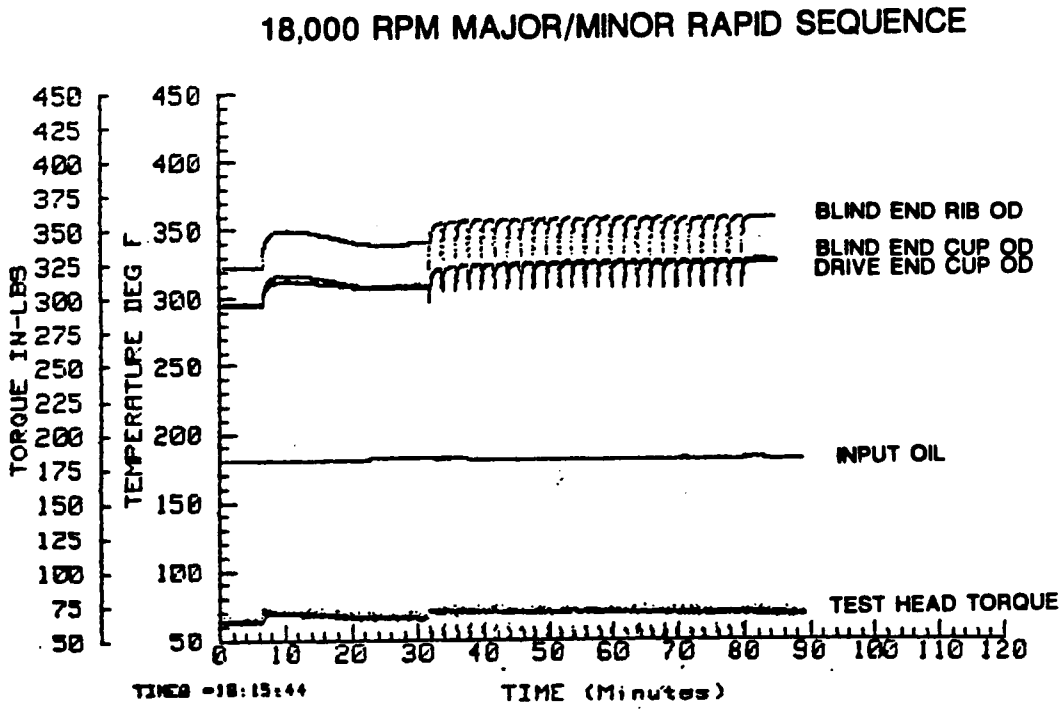

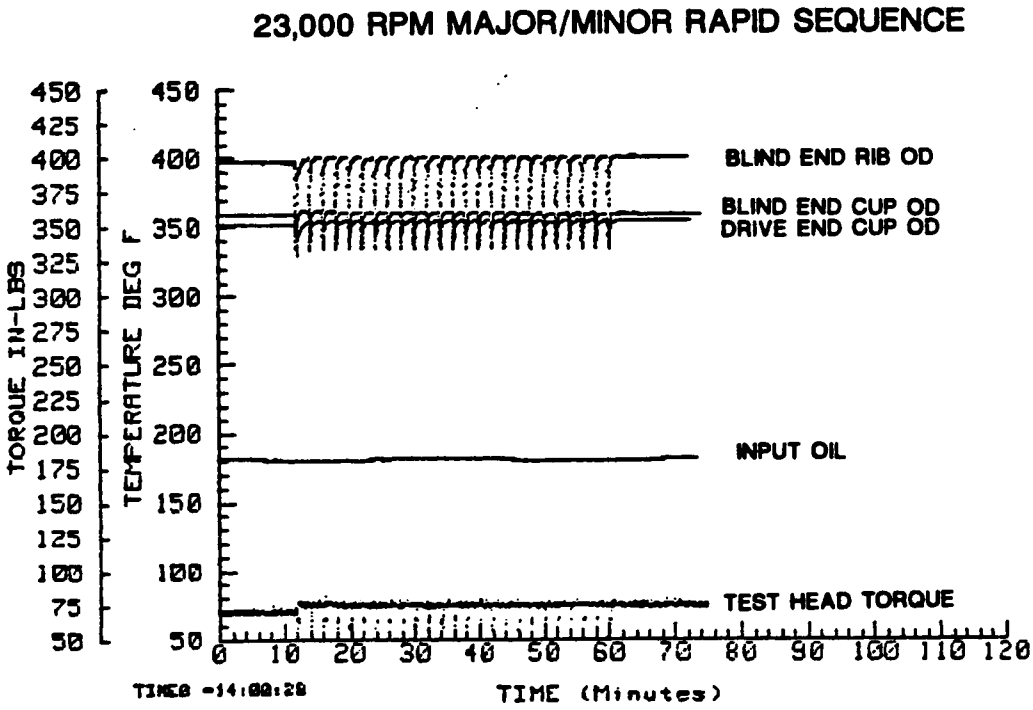

Figure 71. Temperature and Torque Versus Time in Rapid-Sequence Major-Minor Thrust, Hybrid Bearing With Silicon Nitride Rollers, Zirconia Cup Rib, and P.E.E.K. Cage, Cup Slots Closed

roller body-cup and cone race. Because of the contacting components and the magnitude of load the bearings generate less heat in the minor direction than in the major direction, thus explaining the lower temperatures and torques.

The cage speed was monitored when the bearings were operated in the major-minor thrust conditions to determine if skidding occurred. The cage speed was found to slow through the transition from the major-to-minor and minor-to-major reversals. A reduction of 2 to 11 percent was measured during the transition before the cage regained a stable speed. The time of transition was 1 to 2 seconds. The slowest stabilization occurs in the major-to-minor reversal and the fastest stabilization for the minor-to-major reversal. This indicates that skidding does occur during transition.

Figures 72 and 73 are photographs of bidirectional hybrid bearing no. 14 with silicon nitride rollers, a zirconia cup rib, and a steel cage. This bearing has completed the following:

<u>Hours of Operation</u>

128 hours at more than 12,000 rpm
65 hours at 23,000 rpm
5 hours at 25,300 rpm

<u>Thrust Reversals</u>

248 total thrust reversals
168 with a steel cage
62 with a P.E.E.K. cage
168 thrust reversals at 23,000 rpm
87 with a steel cage
29 with a P.E.E.K. cage

Figure 72. Hybrid Bearing No. 14 Cone, Cone Rib, Rollers, and Cage

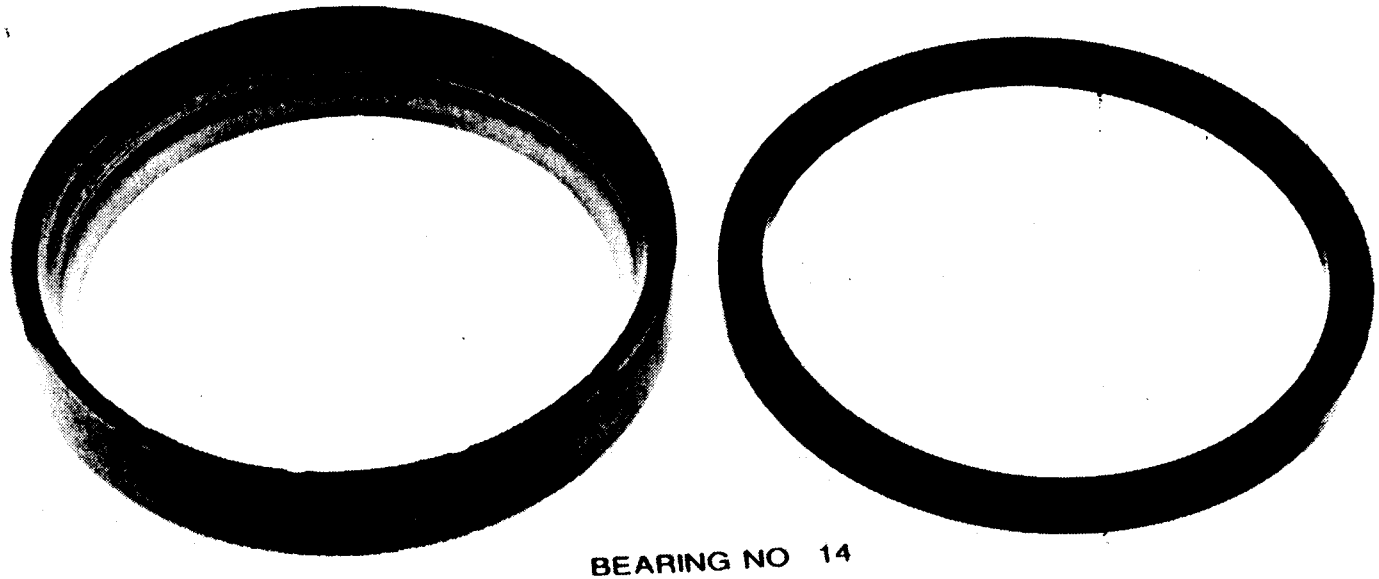

Figure 73. Hybrid Bearing No. 14 Cup and Zirconia Cup Rib

The bearing components were closely examined at the conclusion of these tests, with all components in very good condition except for the zirconia cup rib. Figures 74 and 75 are photomicrographs of the zirconia cup rib face and face o.d. radius, respectively. The zirconia cup rib from bearing no. 14 is shown in Figure 74; the top view is of the rib face outside the roller end contact area and the lower is of the contact area. The zirconia surface contacting the roller end has become crazed and deteriorated. Figure 75 shows where chips have broken out of the rib face O.D. of the zirconia cup rib for bearings no. 13 and 14. The roller contact area is the darker band on the rib face, with the chips starting to break out at the edge of the contact. These chips were located in the maximum-load-zone area of the roller race contacts. The load zone contact was detectable, representing the combined radial and thrust conditions; however, no misalignment condition existed that would generate an edge stress effect. Also, the roller end-rib contact zone was well within the rib face flat, eliminating any possibility of truncation.

The success of completing a major-minor thrust run was dependent on the mounted setting of the bidirectional bearing. The setting is determined by the clearance at the roller small end and cone rib face, as illustrated in Figure 54. The emphasis of the testing has been to find an acceptable range of bearing setting to have damage-free bearings in the major-minor operating mode. The setting range differs between the conventional all-steel and the hybrid bearings. The settings determined by testing are:

Bearing settings for major-minor thrust operation

	Conventional	Hybrid
Minimum	0.0011 inch	0.0002 inch
Maximum	0.0027 inch	0.0034 inch

The conventional all-steel bearing is more sensitive to setting than the hybrid configuration. The silicon nitride roller is the major difference, as both the steel rib and zirconia rib were successfully operated in the hybrid configuration. The bearing movement was measured at operating conditions as illustrated in Figure 76 for both the conventional and hybrid bearings.

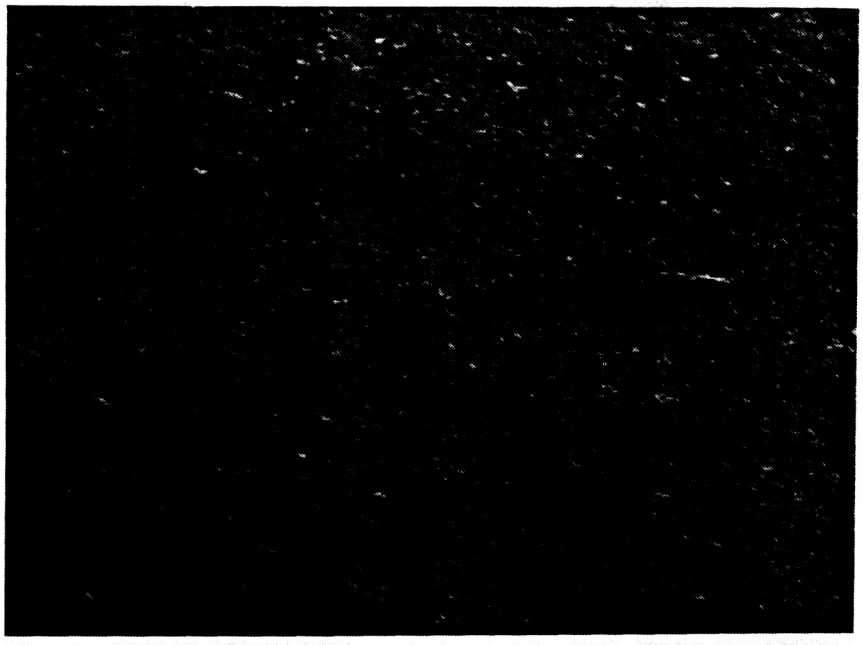

OUTSIDE ROLLER END/RIB CONTACT AREA 200X

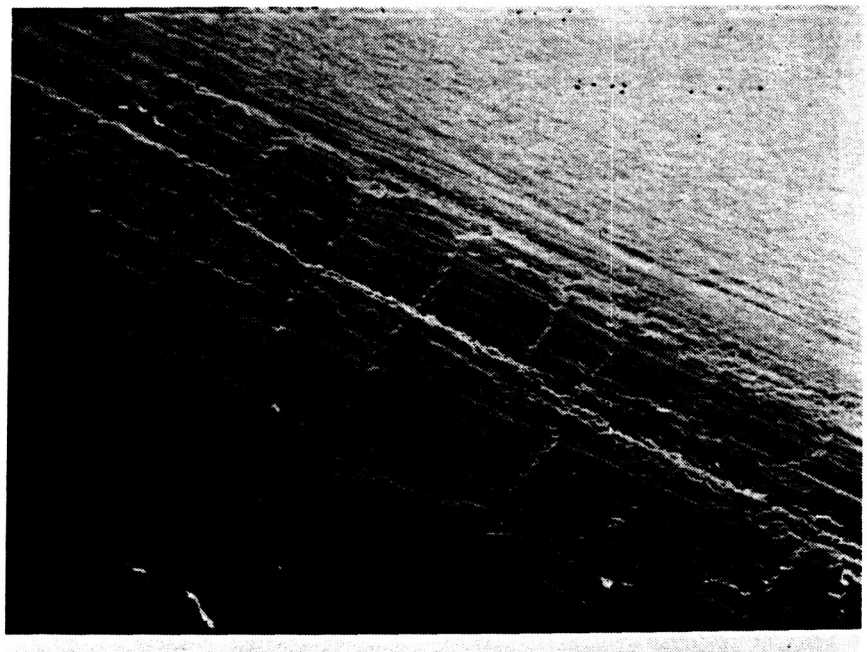

INSIDE ROLLER END/RIB CONTACT AREA 200X

Figure 74. Zirconia Rib Face Surface Outside and Inside Roller End/Rib Contact Area

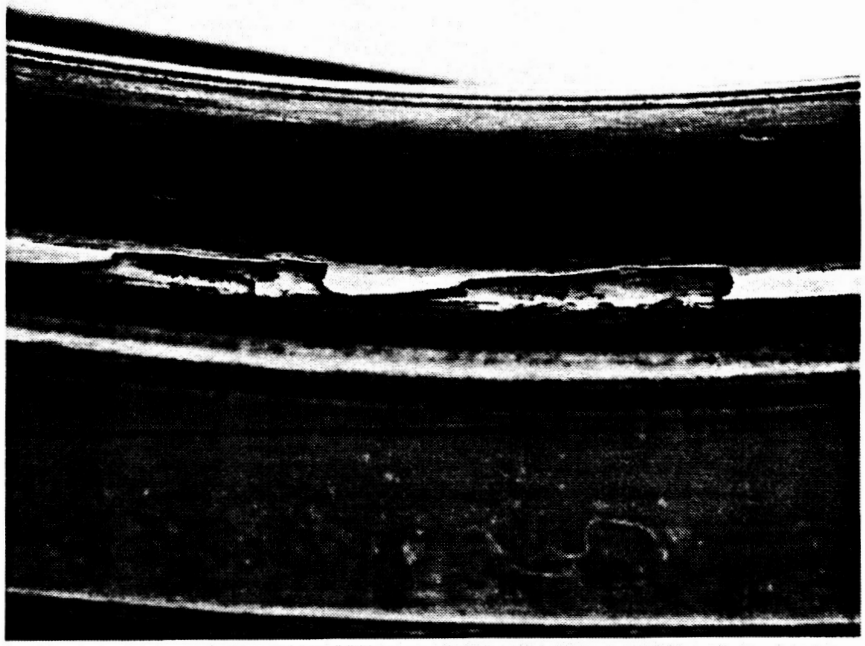

BEARING NO. 13 ZIRCONIA RIB 10X

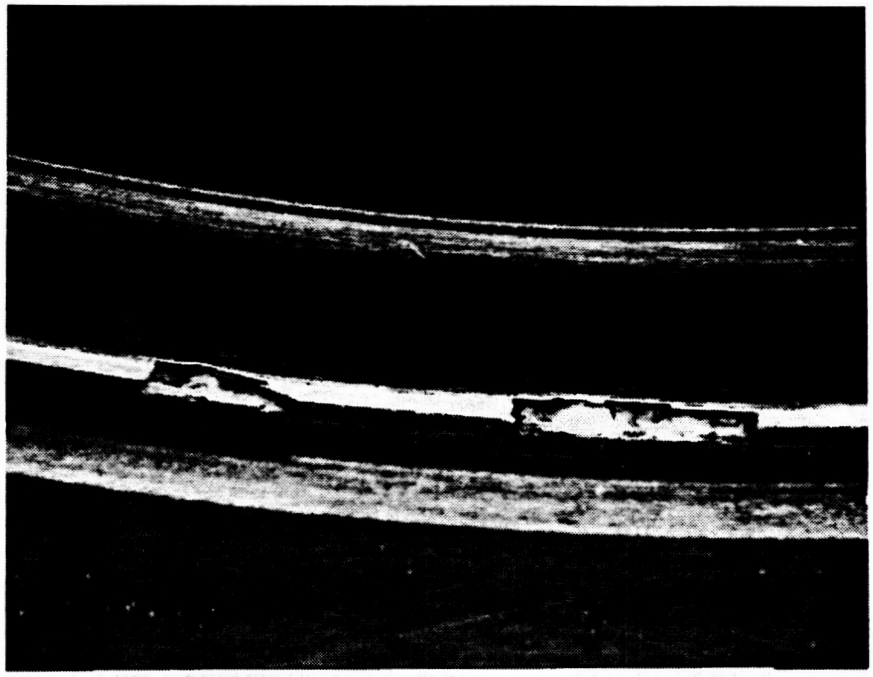

BEARING NO. 14 ZIRCONIA RIB 10X

Figure 75. Chipped Area on Outside Diameter of Zirconia Rib Faces

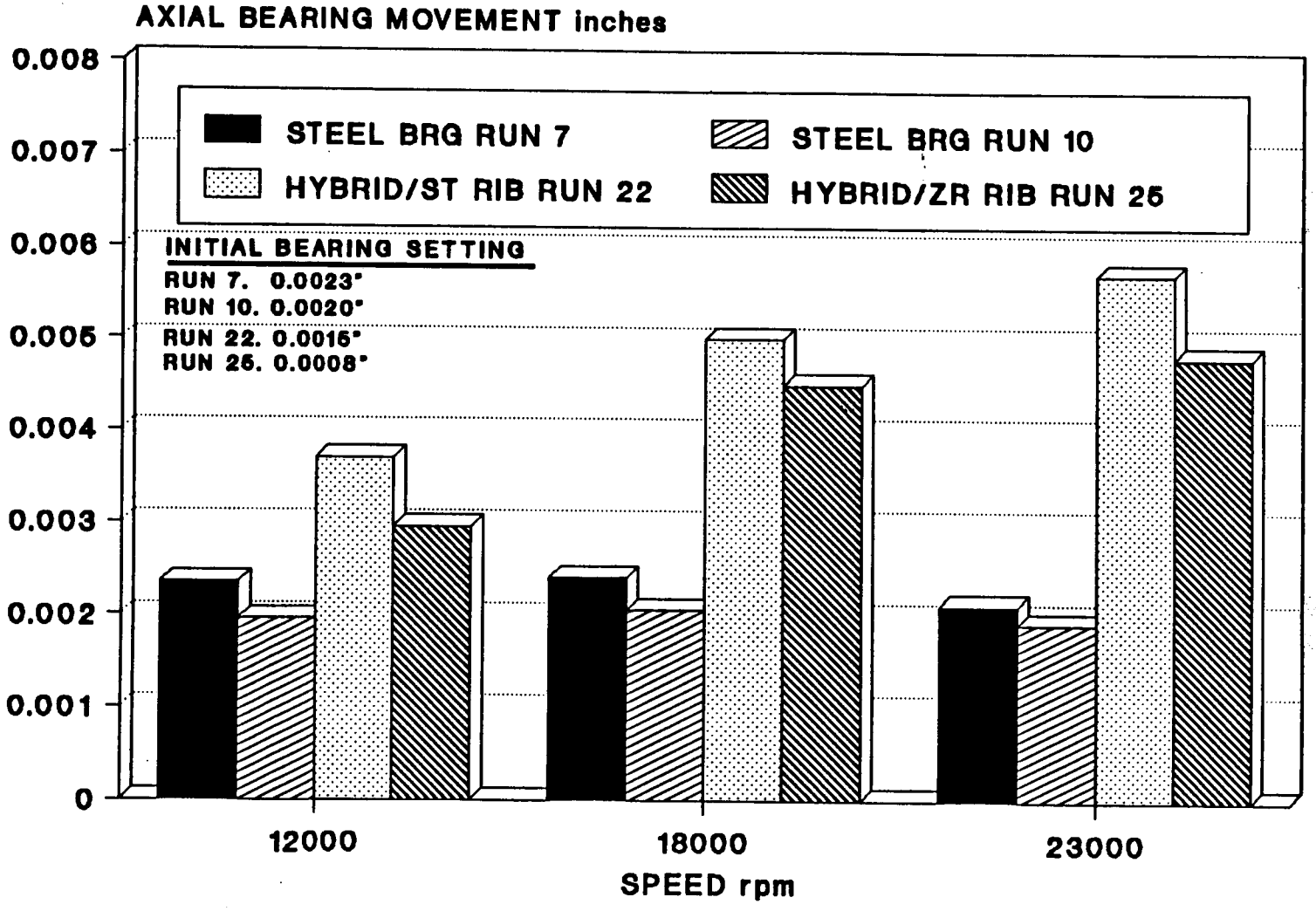

Figure 76. Bearing Movement for Major-Minor Thrust at Operating Speed, Load, and Temperature

The bearing movement was monitored as the major-minor thrust was applied and, as the results show, the bearings with the silicon nitride rollers have greater movement than the conventional bearing and did not become damaged. This greater operating range can be attributed to the material properties of the silicon nitride. The greater range is an advantage when setting up the bearing, especially in a production environment, as the operator is not required to set up to a very tight dimension.

Endurance testing was performed with three sets of two bearings each of the hybrid configuration of silicone nitride rollers, zirconia cup ribs, and silver-plated steel cages. The bearings were tested at the condition shown in Table 24 at 23,000 rpm to reduce the calculated L-10 life, thus reducing the actual testing time. The calculated L-10 life was based on parameters of the all-steel bearing as agreed by Boeing and The Timken Company, rather than using the material properties of silicon nitride in equations that were developed for steel bearings. The testing of the three sets of bearings resulted in two damaged bearings at 8.3 and 7.1 times the L-10 level, respectively, with testing of the third suspended at 11.9 times L-10 life. The bearings were mounted in pairs at the shaft center two positions and the end positions. The individual runs were stopped and both bearings removed when one bearing in the set became damaged; then a new set was installed.

Figure 77 is a plot of the 8.3-times-L-10 run showing the temperature and torque versus time for the bearing at the drive center and opposite drive center positions. Inspection of the bearing components showed that one silicon nitride roller was damaged by surface deterioration; all other rollers were in very good condition. The cone, cone rib, rollers, and cage are shown in Figure 78, cup and cup rib in Figure 79, and the damaged roller in Figure 80. The damaged roller was within the size range of the other rollers in this set and no dimensional disparities were found that would have caused this damage. The resulting damage of the cone and cup race may be of interest to concerned users of hybrid bearings in aerospace applications for the fact that, first, the silicon nitride roller did not break apart as may have been suspected, and second, the silicon nitride roller surface generated gross wear on the steel races, causing steel particles to be mixed

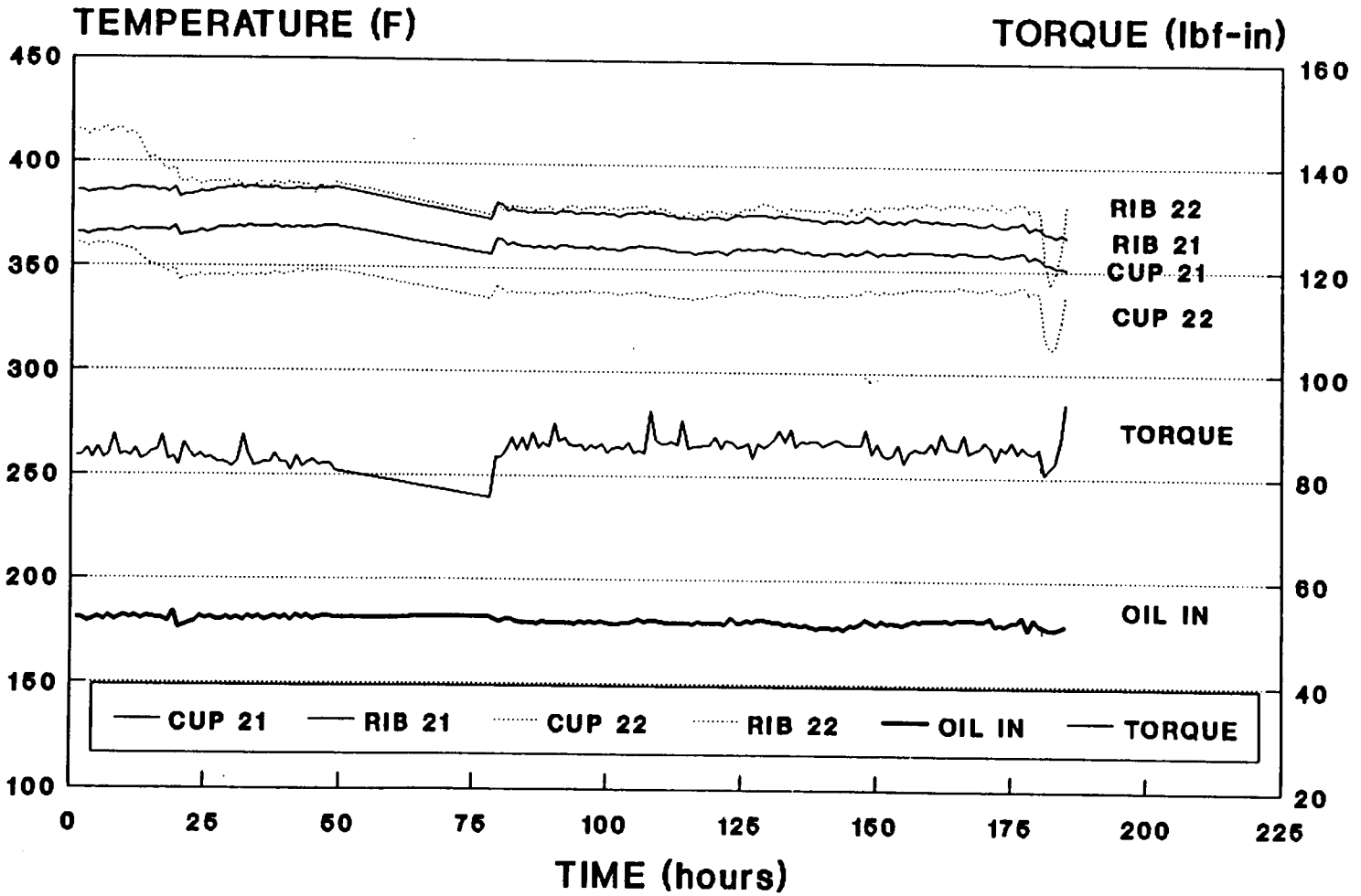

Figure 77. Endurance Temperature and Torque Versus Time for Hybrid Bearings No. 21 and 22 in the DC and BC Positions; 8.3 Times L-10 Life With BC Damage

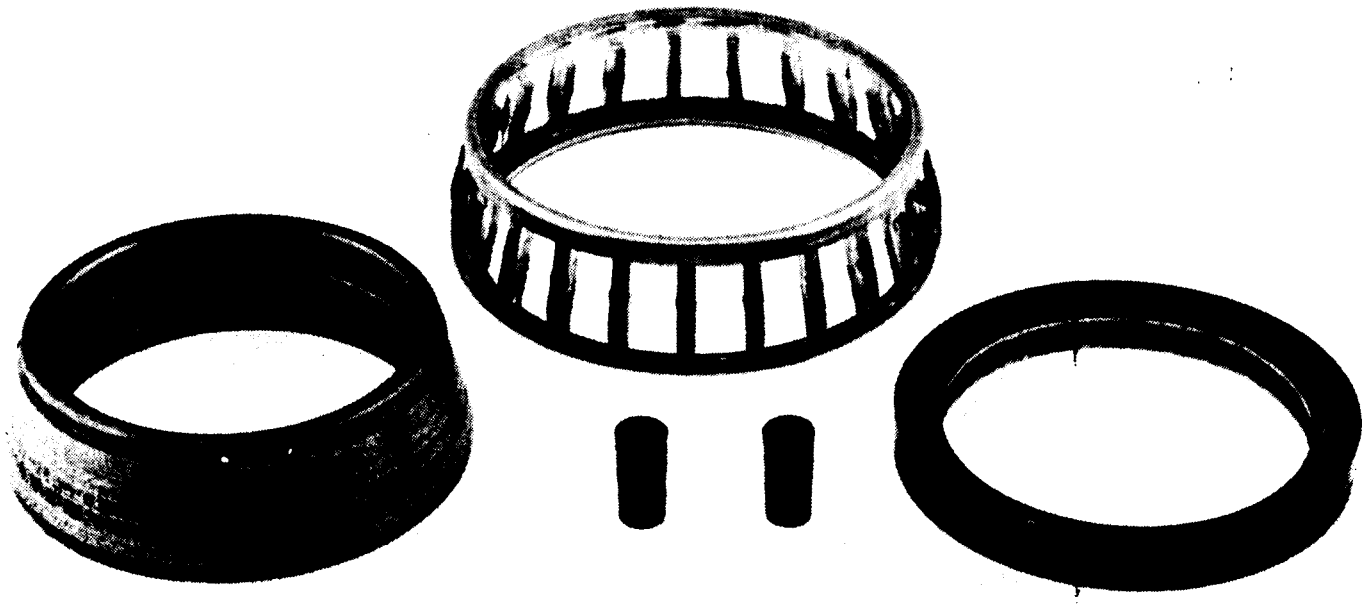

BEARING NO H22

Figure 78. Hybrid Bearing No. 22 Cone, Cone Rib, Rollers, and Cage

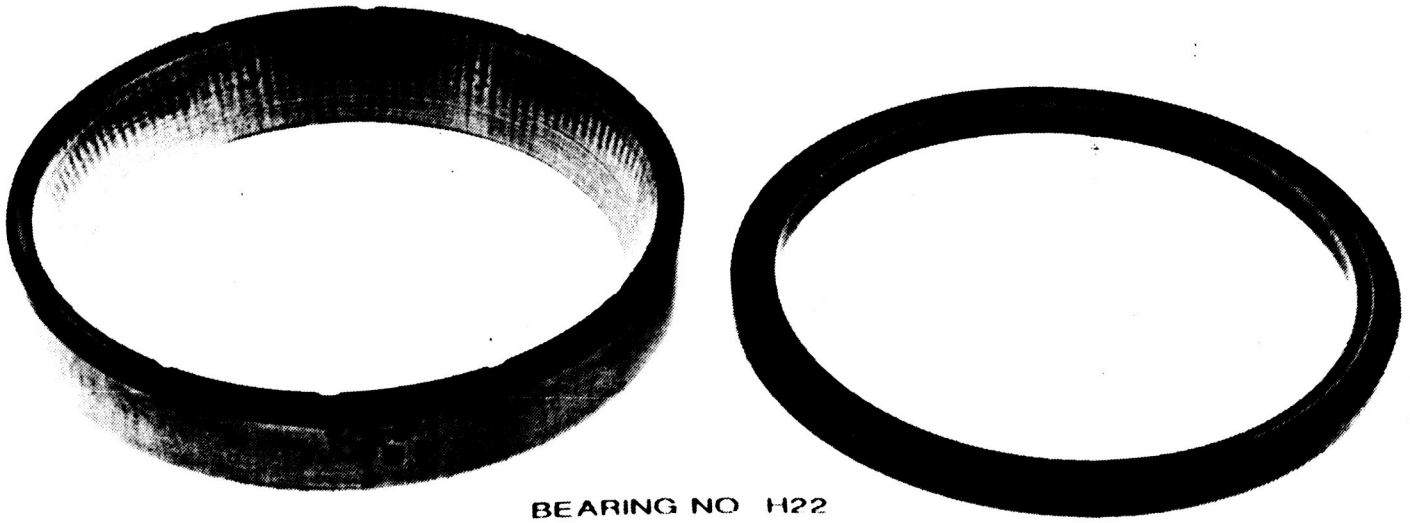

Figure 79. Hybrid Bearing No. 22 Cup and Zirconia Cup Rib

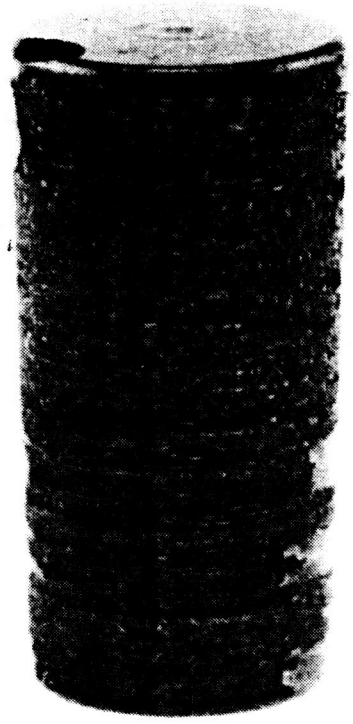

Figure 80. Hybrid Bearing No. 22 Silicon Nitride Roller

into the oil system and thus allowing chip detectors to signal an alarm. Approximately 890 milligrams of flakes (particles) were recovered from the oil filter; all were magnetic. Perimeter sizes range down from the largest flakes being square-shaped, approximately 0.020 inch on a side. The majority (90 percent) of the particles are under 0.008 inch, with only approximately 2 percent of the flakes being in the range of 0.016 to 0.020 inch.

Endurance running continued with a new set of bearings which achieved 7.1 times L-10 life, as illustrated in Figure 81. The opposite drive end center bearing became noisy and was found to have a spalled cup when removed from the test rig. The spalled area extended for the full length of the race through an arc of 150 degrees. The zirconia cup rib had chips break out of the face o.d. radius as well as at the face i.d. radius, as illustrated in Figure 75.

Figure 82 shows the performance data of hybrid bearings 24 and 25 which achieved 11.9 times L-10 life, when the test was suspended. No damage was observed on the components other than the chipped zirconia cup rib similar to the previously tested zirconia cup ribs discussed above. Figures 83 and 84 are photographs of hybrid bearing no. 25 showing the tested cone, cone rib, and cage roller assembly and the cup and zirconia cup rib, respectively. In all the test runs some degree of fretting was observed at the cone bore. The fretting can be attributed to the reduction of contact area between the bore and shaft due to the oil manifolds in the cone bore. A redesign of these manifolds to increase the contact area at the cone bore and shaft interface should be addressed in the next generation of bearing design.

Posttest bearing component profile traces for the cone race, cup race, roller race, roller large end spherical radius, and the cup rib face are shown in Figures 85 through 89, respectively. These figures are a comparison of the conventional all-steel (top), the hybrid with the steel cup rib (middle), and the hybrid with the zirconia cub rib (bottom). All components were pretest-inspected and within tolerances. Figure 86 shows that the cup races for bearings no. 2 and 12 have a high spot on the right side (cup large end) of the trace; this is an indication of the carbon buildup out of the contact zone. Carbon buildup has been observed on the bearing components

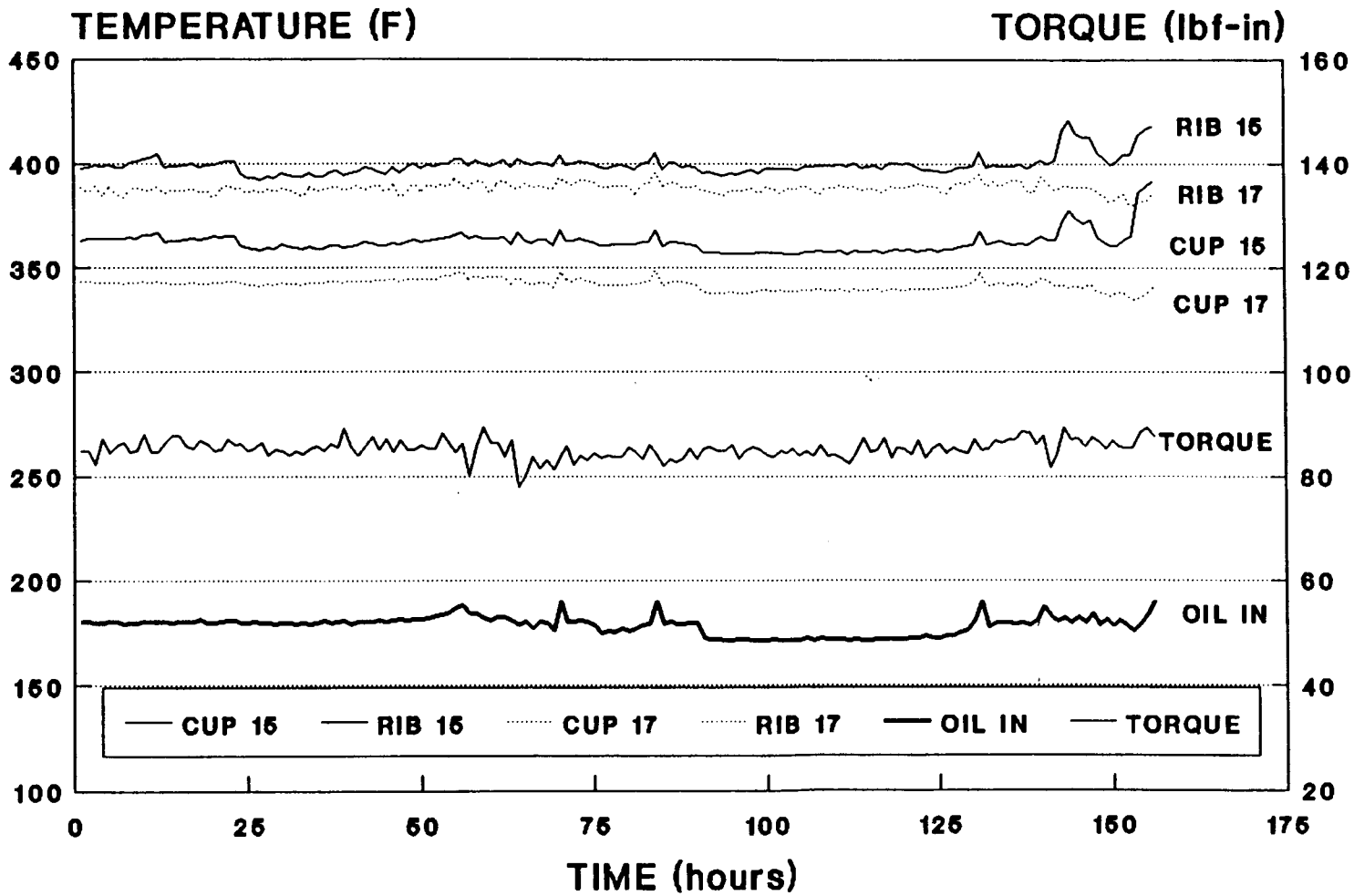

Figure 81. Endurance Temperature and Torque Versus Time for Hybrid Bearings No. 15 and 17 in the DC and BC Positions; 7.1 Times L-10 Life with DC Damage

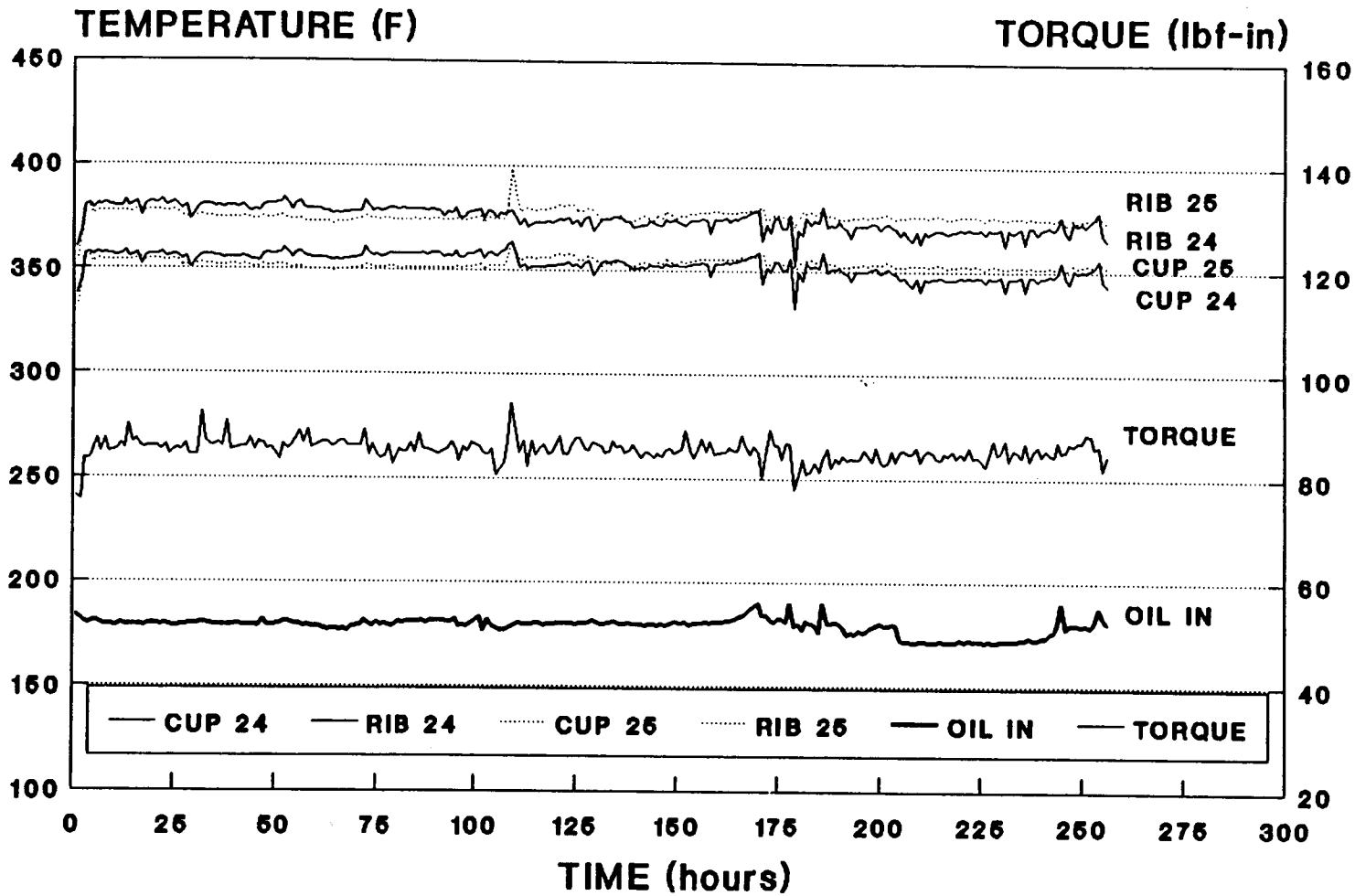

Figure 82. Endurance Temperature and Torque Versus Time for Hybrid Bearings No. 24 and 25 in the DE and BE Positions; 11.9 Times L-10 Life With Test Suspended

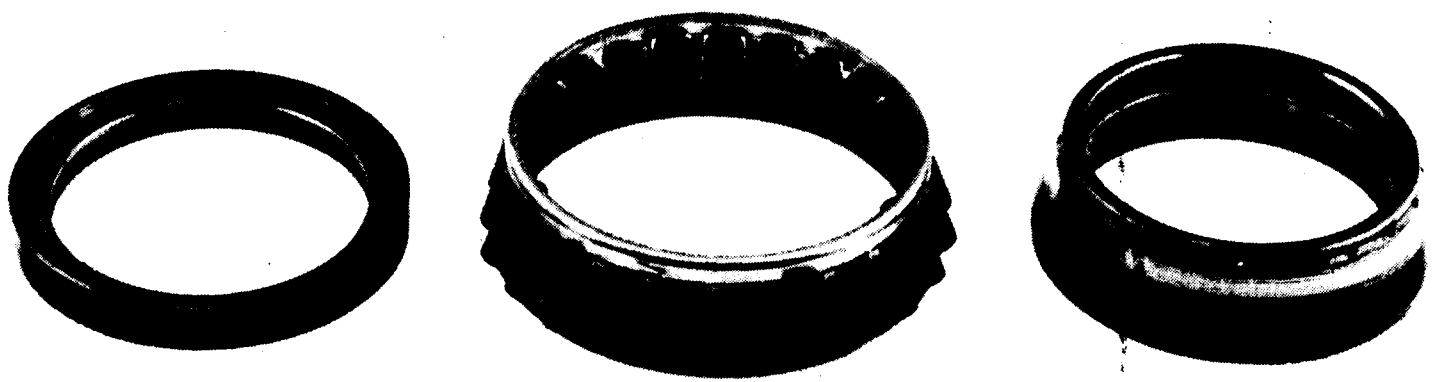

BEARING NO. H25

Figure 83. Hybrid Bearing No. 25 Cone, Cone Rib, Rollers, and Cage After 11.2 Times L-10 Life Endurance Test

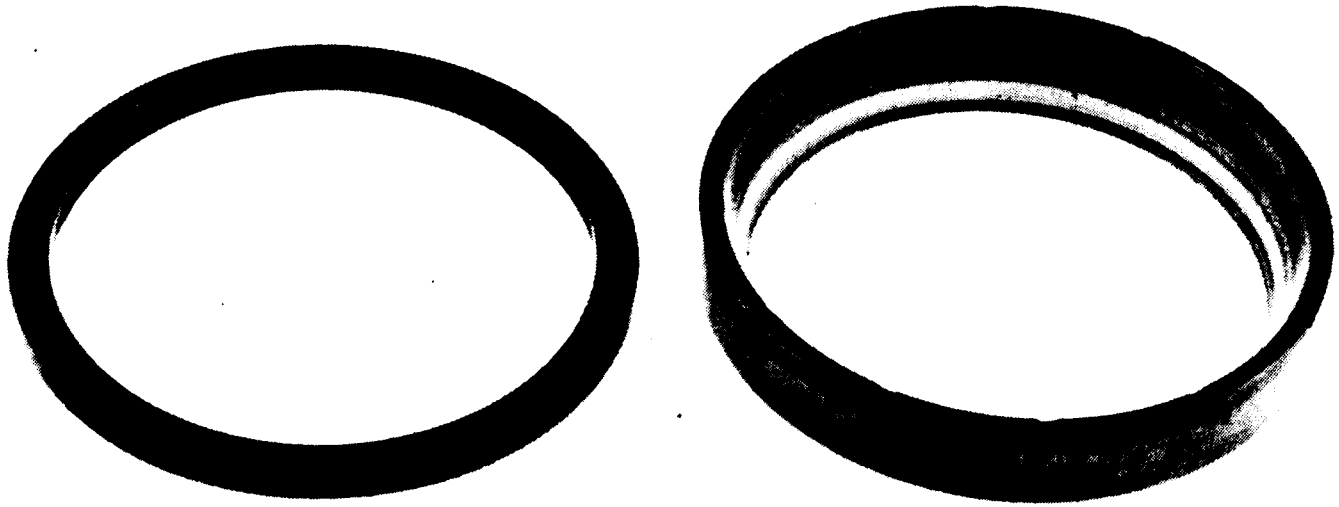

BEARING NO. H25

Figure 84. Hybrid Bearing No. 25 Cup and Zirconia Rib After 11.2 Times L-10 Life Endurance Test

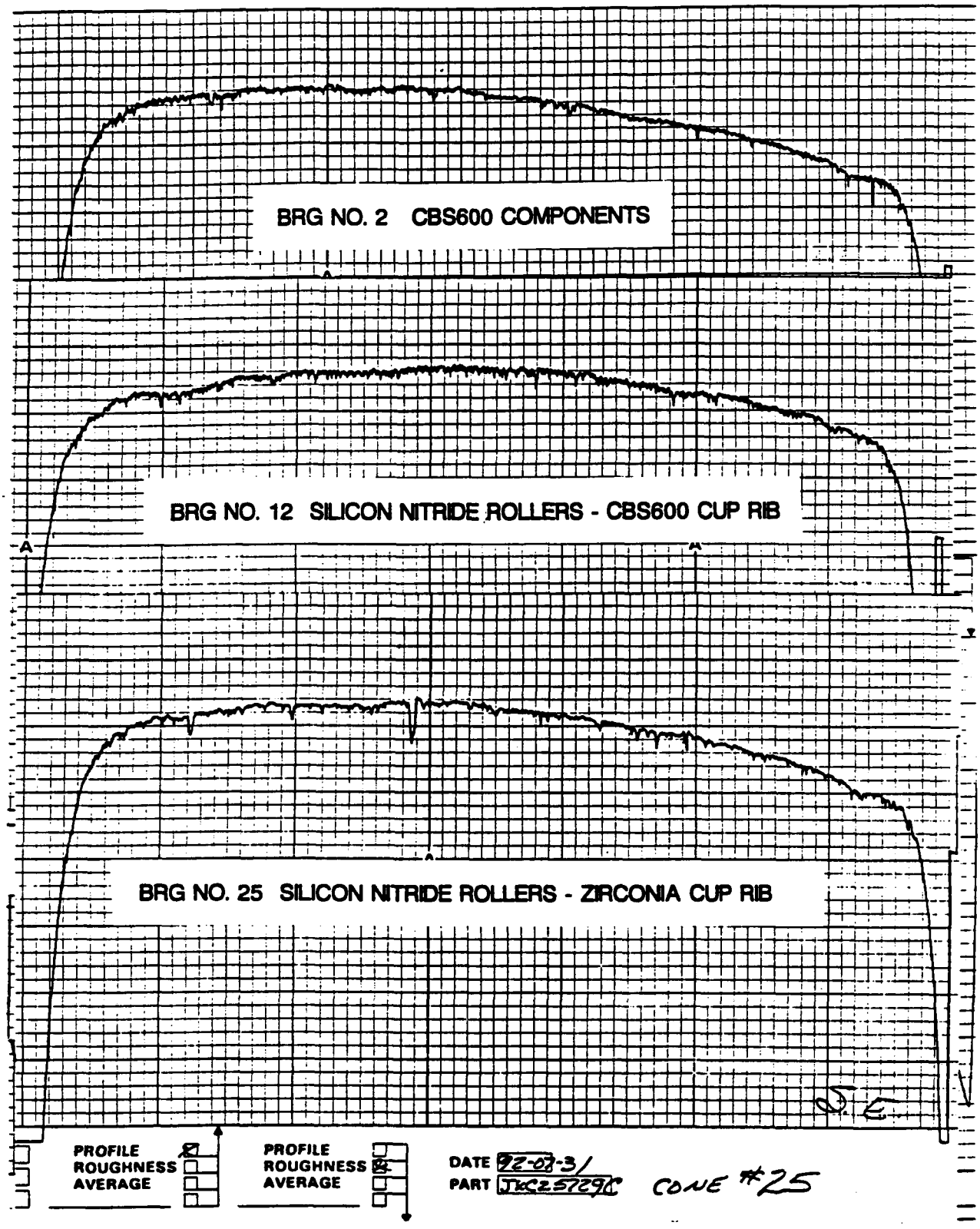

Figure 85. Posttest Cone Race Profiles of Conventional and Hybrid Bearings

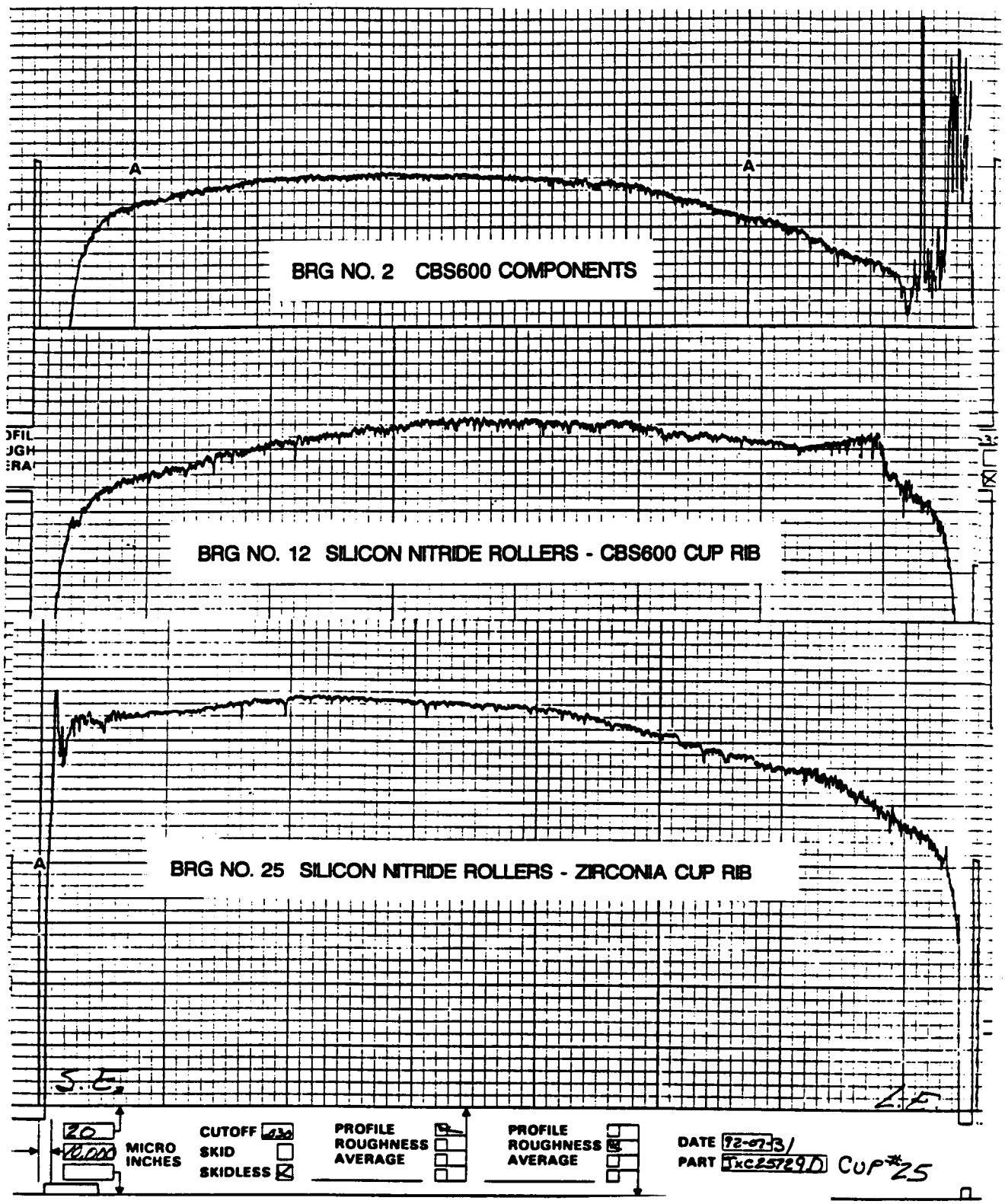

Figure 86. Posttest Cup Race Profiles of Conventional and Hybrid Bearings

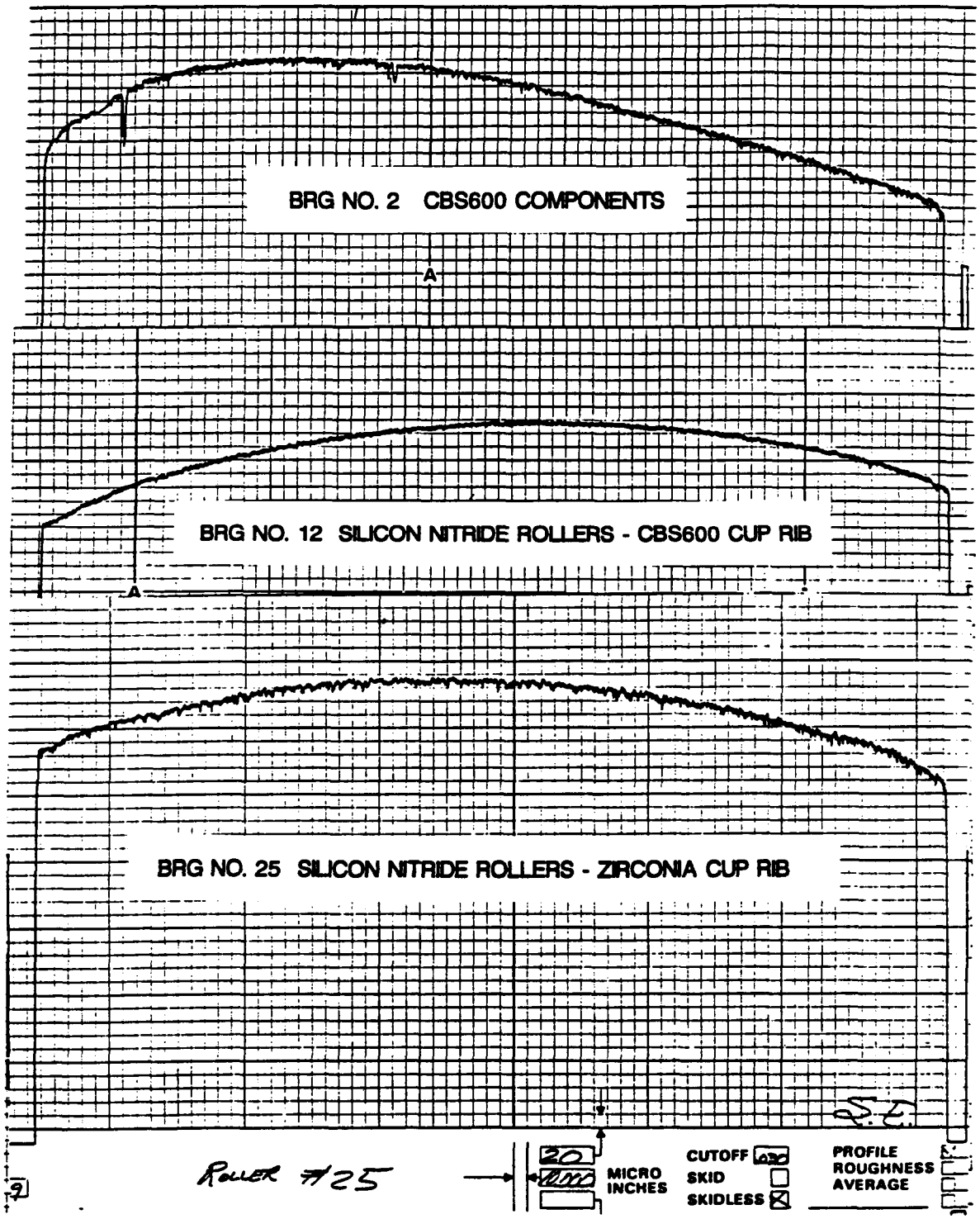

Figure 87. Posttest Roller Race Profiles of Conventional and Hybrid Bearings

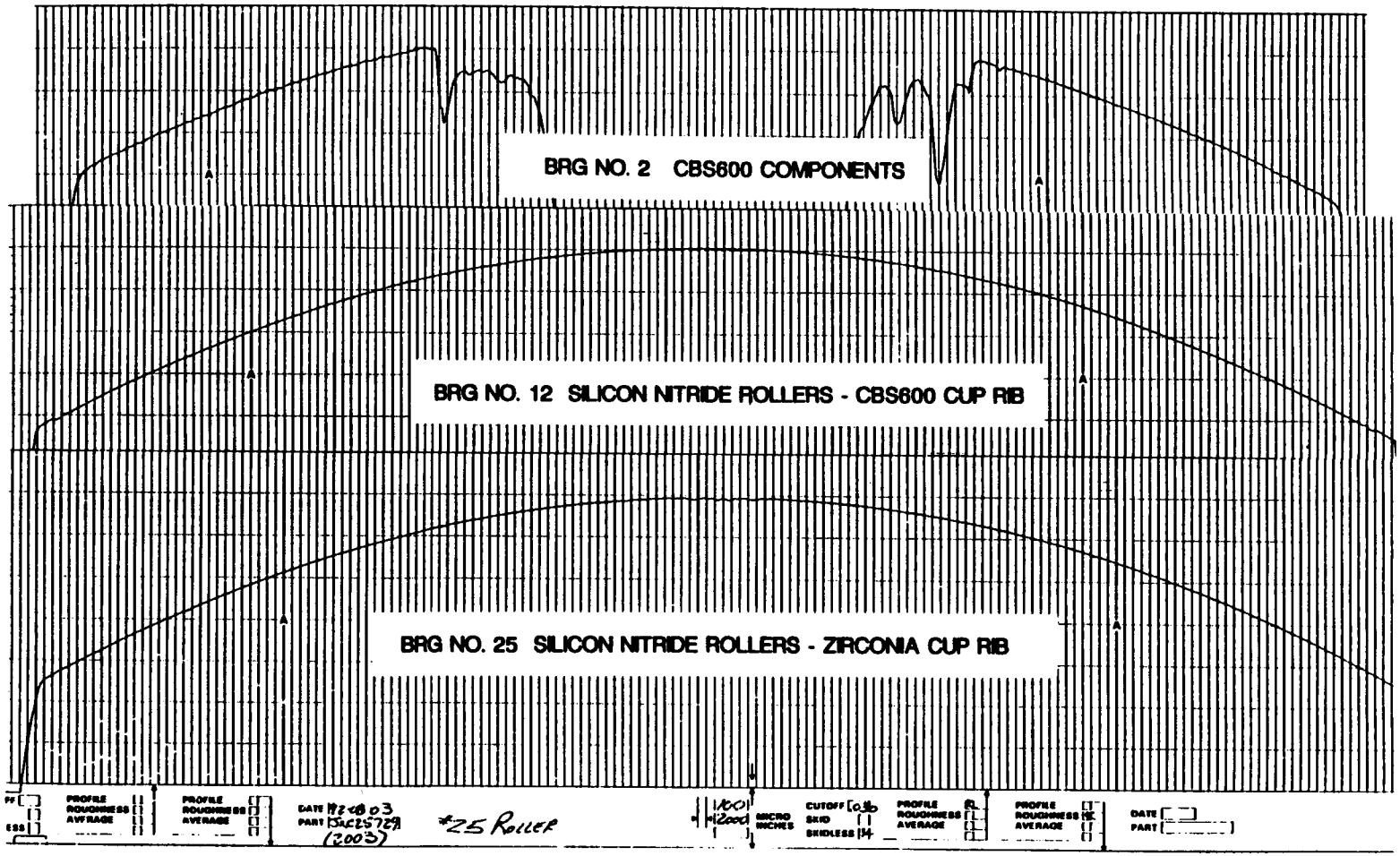

Figure 88. Posttest Roller Large-End Spherical-Radius Profiles of Conventional and Hybrid Bearings

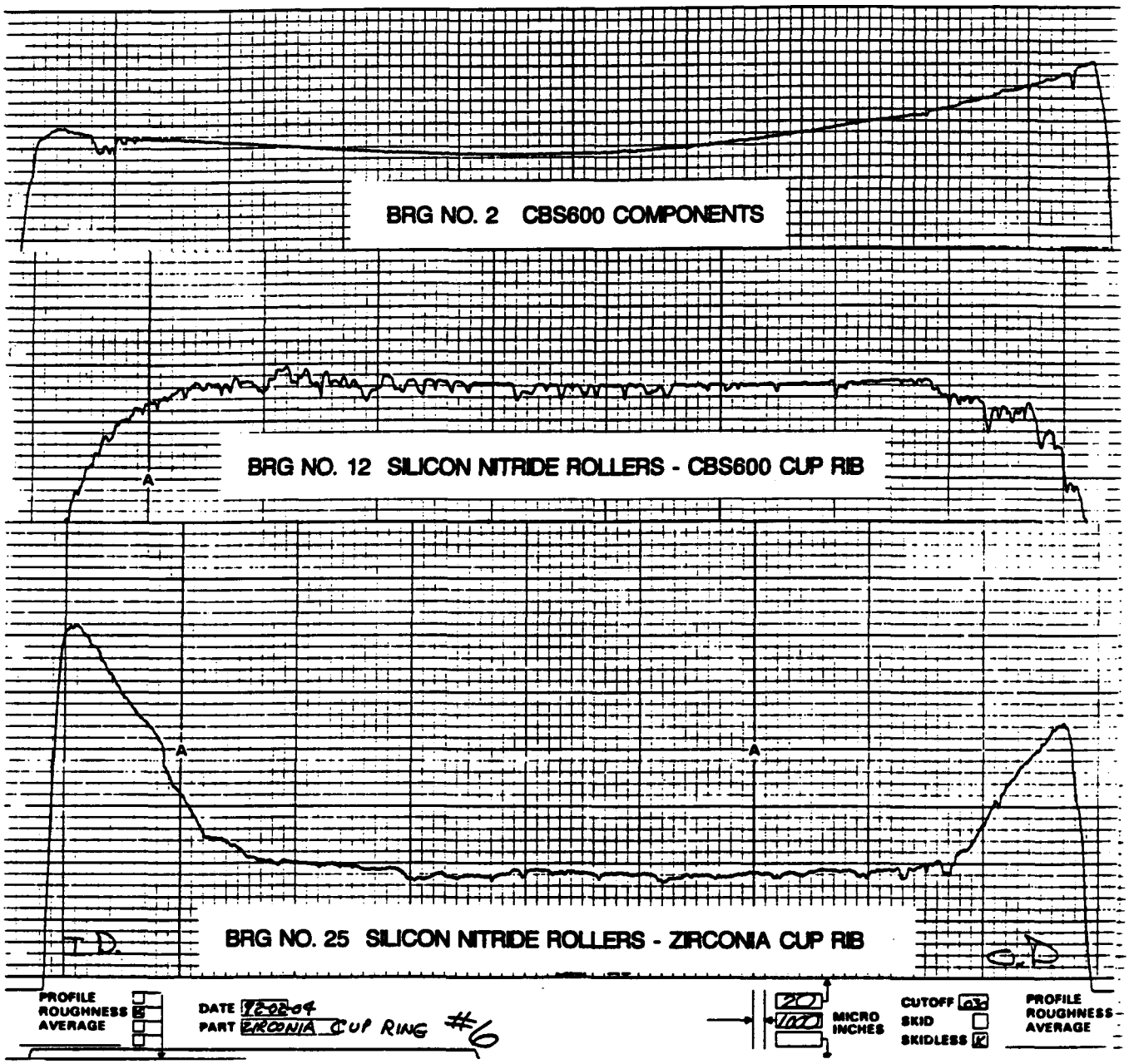

Figure 89. Posttest Cup Rib Face Profiles of Conventional and Hybrid Bearings

throughout this development program, with the heaviest deposits observed on the cup rib face. A posttest trace indicated a 0.00032-inch carbon layer on a rib face. Figures 87 and 88 are the profiles of the roller bodies and roller spherical large end, respectively.

The final figure in this group of component traces is Figure 89, illustrating the rib face profile for the all-steel CBS600 cup rib, the CBS600 steel cup rib which ran in the hybrid bearing, and the zirconia rib from the endurance test bearing no. 25 which was suspended at 11.9 times L-10. The zirconia rib face shows a heavy wear pattern, while the steel rib from bearing no. 2 shows moderate wear and the steel rib from the hybrid bearing shows very little wear. These three rib profiles are representative of runs with similar components. The compatibility of the silicon nitride rollers and the zirconia rib is questionable for these two material combinations. The CBS600 cup rib performed with an acceptable wear when operating with the silicon nitride rollers. The silicon nitride rollers have not shown any wear of the large end whether operating against the CBS600 steel rib or the zirconia rib. Oil-off runs were completed at speeds of 5,400, 12,000, 18,000, and 23,000 rpm. The bearing operating parameters were stabilized at the operating loads and speeds before shutting off the oil supply to the test bearing. All oil-off bearings were mounted at the opposite drive end position (Figure 55). The hybrid bearing with the CBS600 cup rib was tested first at 23,000 rpm, achieving a 95-second oil-off run time (Figure 90). The next oil-off run used the hybrid zirconia cup rib running at 12,000 rpm; this bearing operated for 90 seconds oil-off (Figure 91). The third oil-off test run was at a slower speed of 5,400 rpm with an all-steel bearing to see how the conventional bearing would perform at a speed more typical of the current helicopter transmission application using a tapered-roller bearing; the results of this run are shown in Figure 92. The bearing operated for 62 minutes oil-off, at which time oil was supplied to the bearing with the bearing returning to preoil-off operating conditions. The posttest condition of the cone, cone rib, and roller cage assembly is shown in Figure 93 and the cup and cup rib in Figure 94. These components showed no signs of damage.

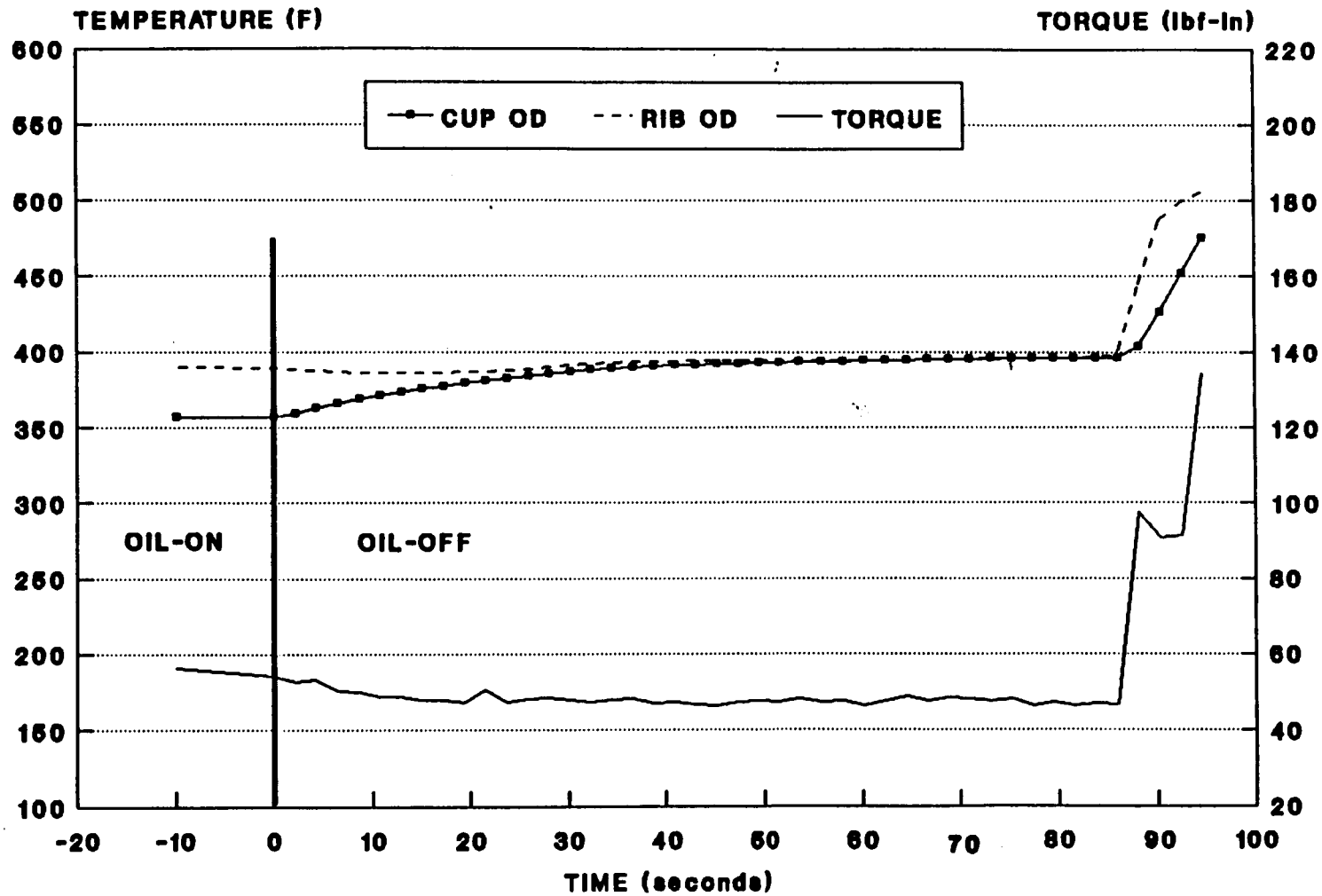

Figure 90. Temperature and Torque Versus Time in Oil-Off Test of Hybrid Bearing With Silicon Nitride Rollers and Steel Rib at 23,000 rpm

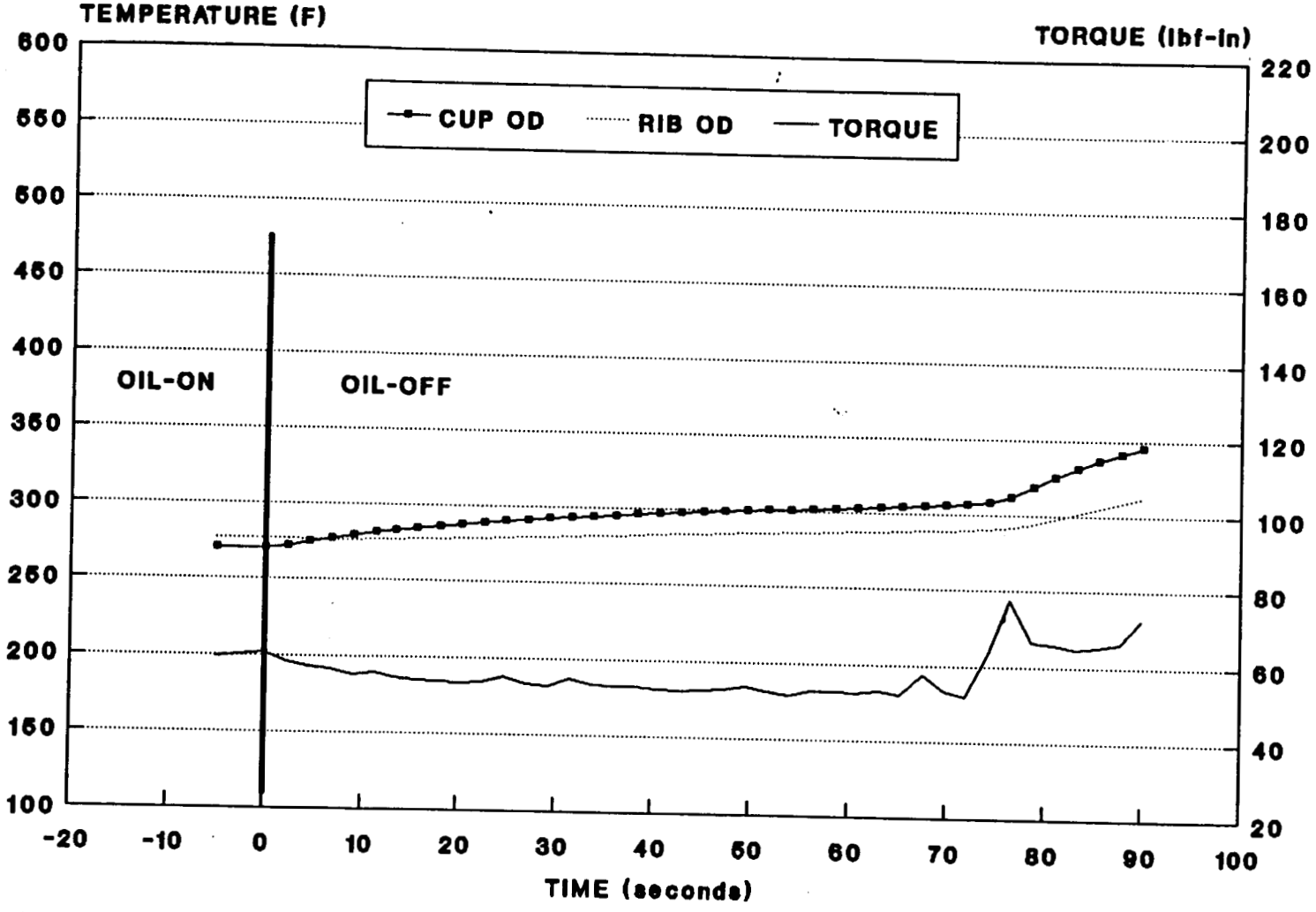

Figure 91. Temperature and Torque Versus Time in Oil-Off Test of Hybrid Bearing With Silicon Nitride Rollers and Zirconia Rib at 12,000 rpm

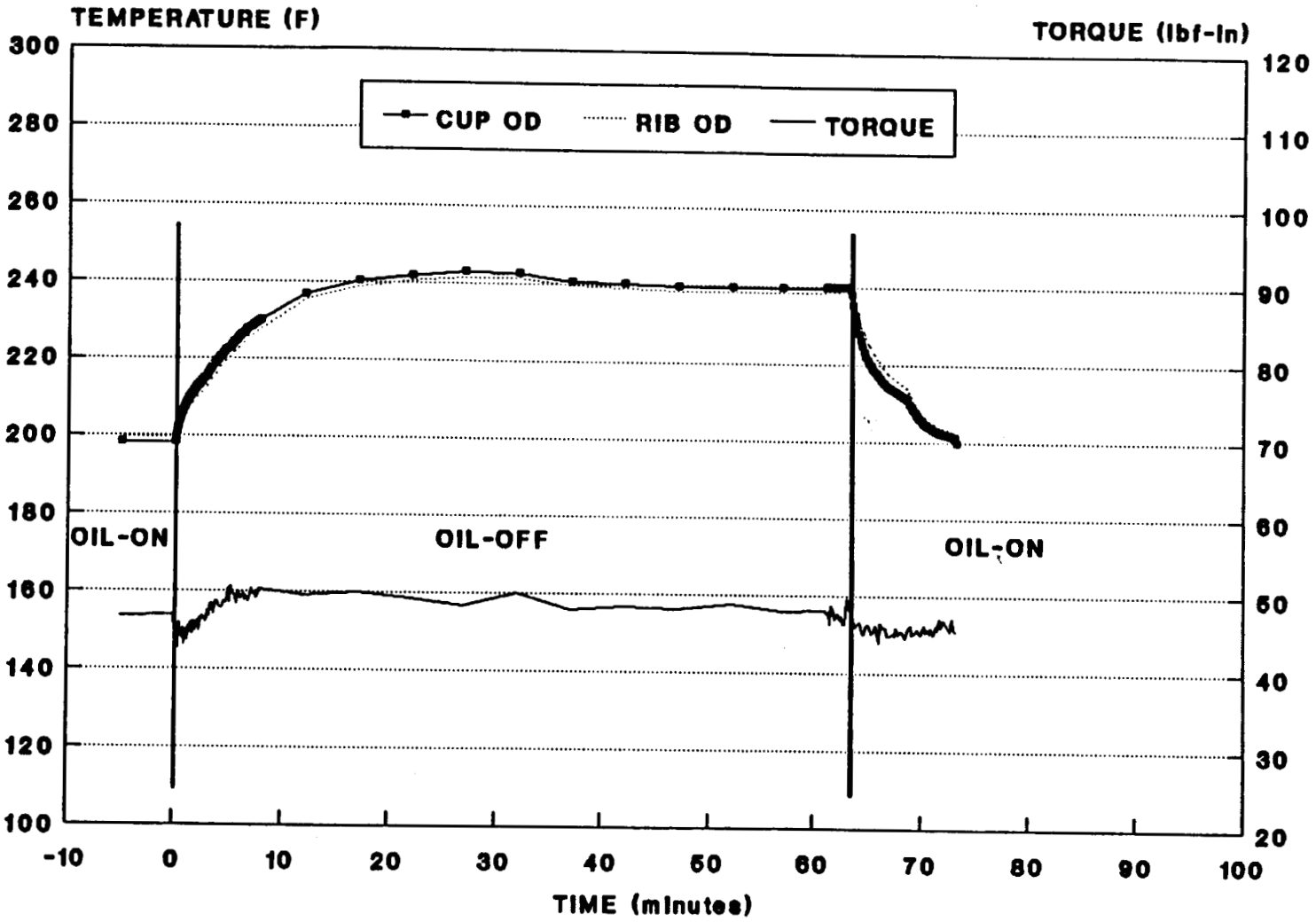

Figure 92. Temperature and Torque Versus Time in Oil-Off Test of All-Steel Bearing at 5,400 rpm

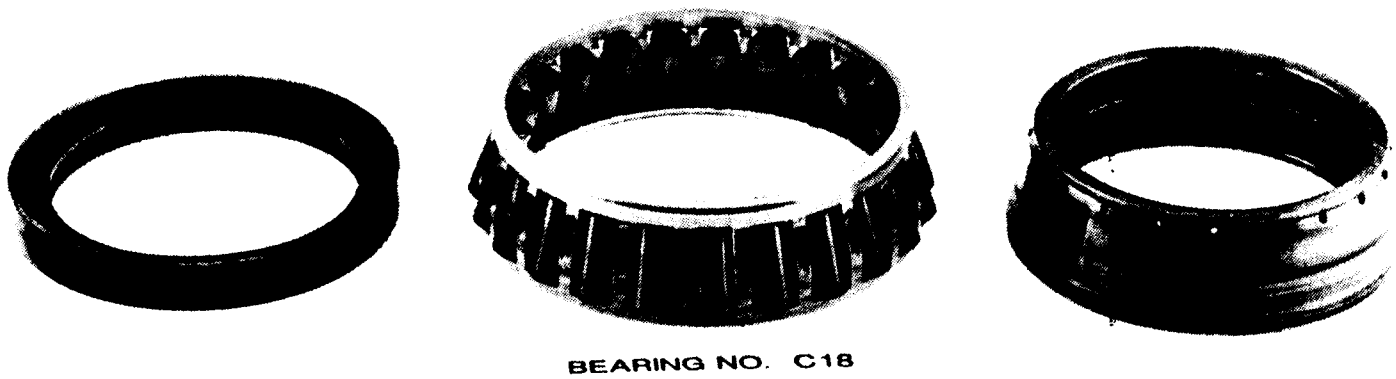

Figure 93. Conventional Bearing No. 18 Cone, Cone Rib, Rollers, and Cage After 62 minutes in Oil-Off Test at 5,400 rpm

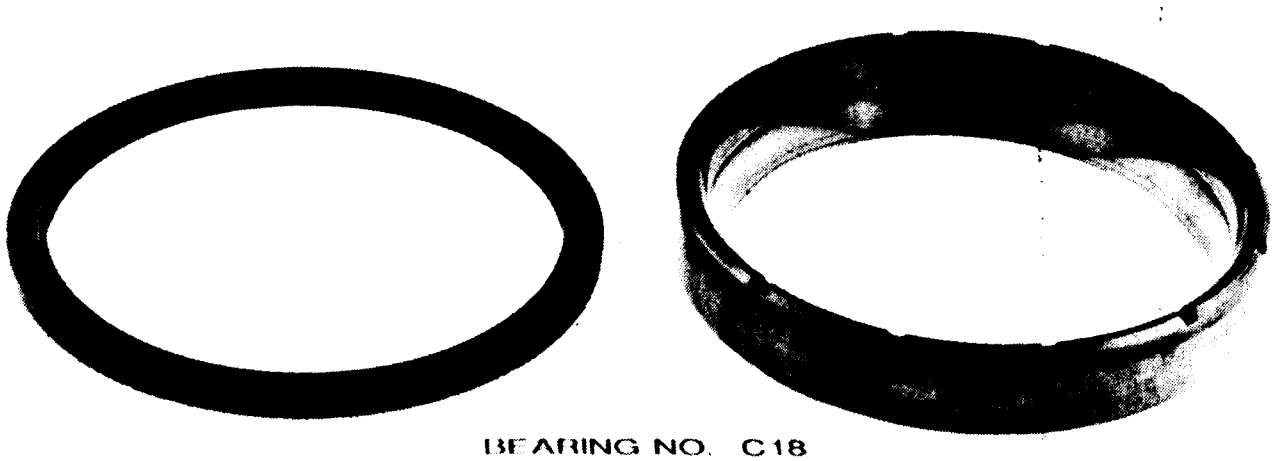

Figure 94. Conventional Bearing No. 18 Cup and Cup Rib After 62 Minutes in Oil-Off Test at 5,400 rpm

The next oil-off run was at 12,000 rpm with a hybrid bearing with a CBS600 cup rib. This bearing operated for 60 minutes followed by the return of oil to the bearing, at which time the operating temperature and torque were lower than the preoil-off stabilized conditions (Figure 95). The bearing components were in very good condition, as shown in Figures 96 and 97. The last oil-off run was at 18,000 rpm with a hybrid bearing with a CBS600 steel cup rib. The oil-off time for this run was 90 seconds, as shown in Figure 98. The bearing damage encountered on this short oil-off run was at the roller end rib contact. The rib damage caused an increase in bearing temperatures and torque. The silicon nitride roller large end had material pickup from the steel rib; however, when this material was removed from the roller end there were no visible signs of damage to the roller.

An observation of the bearing damage of the shortened oil-off runs was contact of the roller small end against the cone rib. Therefore, the mounted bearing setting was increased from 0.0033 to 0.0095 inch on the second run at 12,000 rpm. The 18,000-rpm run had a bearing setting of 0.0093 inch and operated for 90 seconds before the cup rib became damaged.

Bearing performance was measured and compared with two oils of different viscosities. The first oil was Exxon ETO 25, a 5.0-cSt oil used throughout the test program. The second oil was Exxon ETO 274, a 7.5-cSt oil. Both are synthetic oils with an additive package to minimize oxidation and to operate in a high-temperature and high-load environment. ETO 25 has been approved against DOD-L-85734 specifications and ETO 274 has been approved against DERD 2487 specifications. The results of this test are illustrated in Figure 99. Higher bearing operating temperatures were observed with the higher viscosity oil, as well as higher torque readings. All operating conditions were equal for both test runs. The results of this comparative test were as expected.

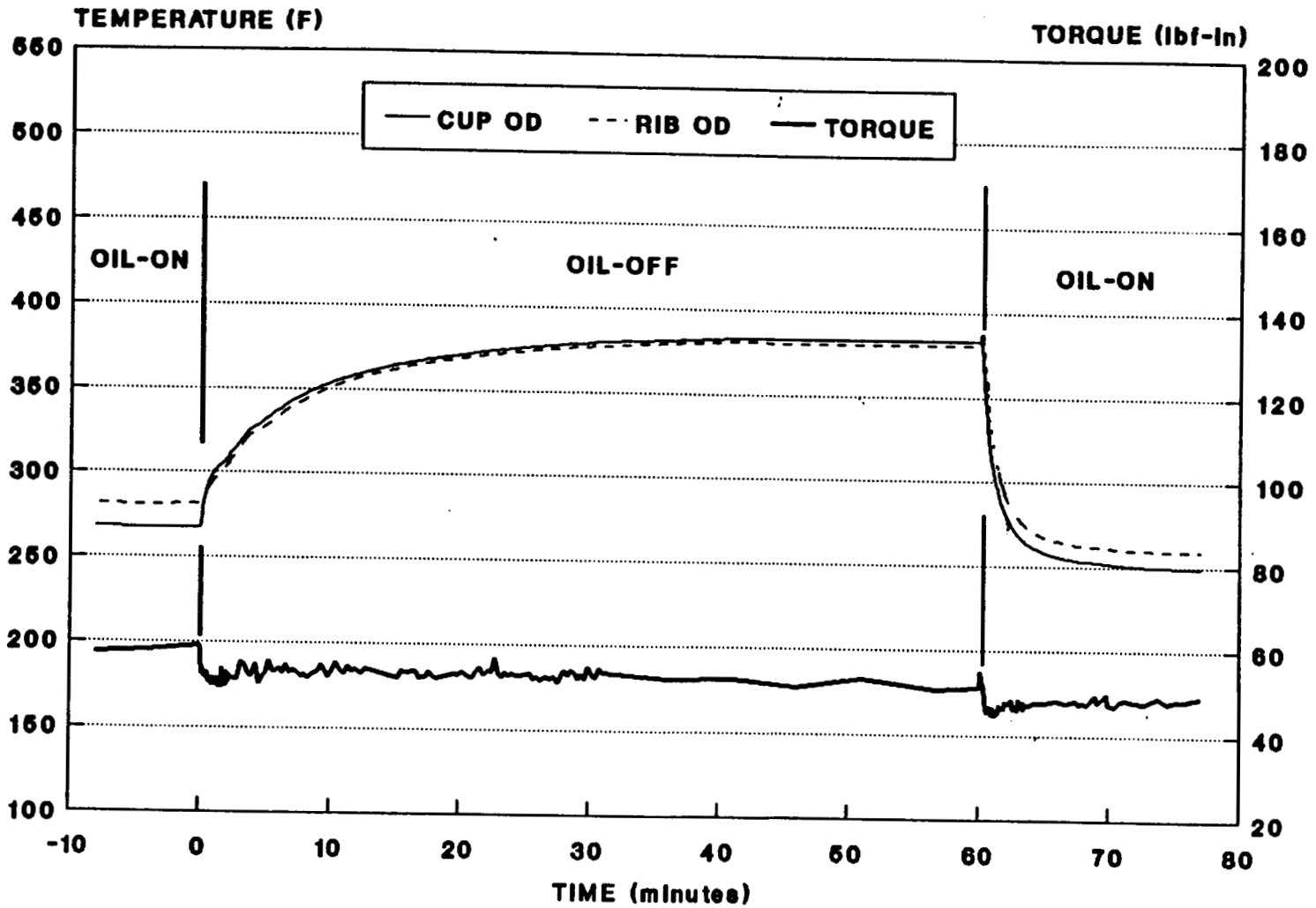

Figure 95. Temperature and Torque Versus Time in Oil-Off Test of Hybrid Bearing With Silicon Nitride Rollers and Steel Rib at 12,000 rpm

Figure 96. Hybrid Bearing No. 12 Cone, Cone Rib, Rollers, and Cage After 60 Minutes in Oil-Off Test at 12,000 rpm

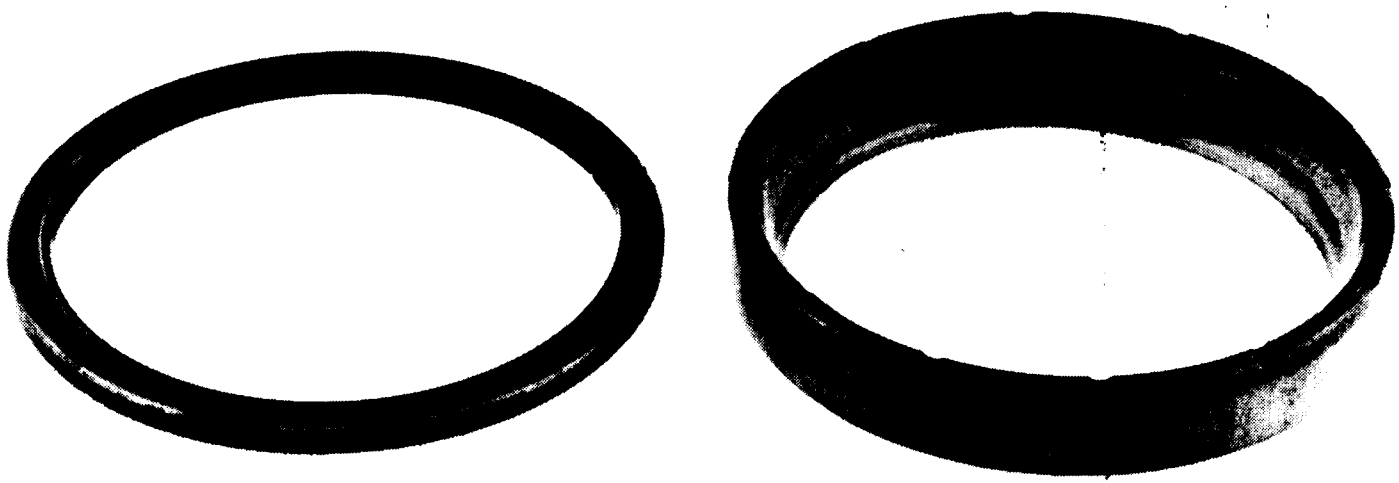

BEARING NO. H12

Figure 97. Hybrid Bearing No. 12 Cup and Cup Rib After 60 Minutes in Oil-Off Test at 12,000 rpm

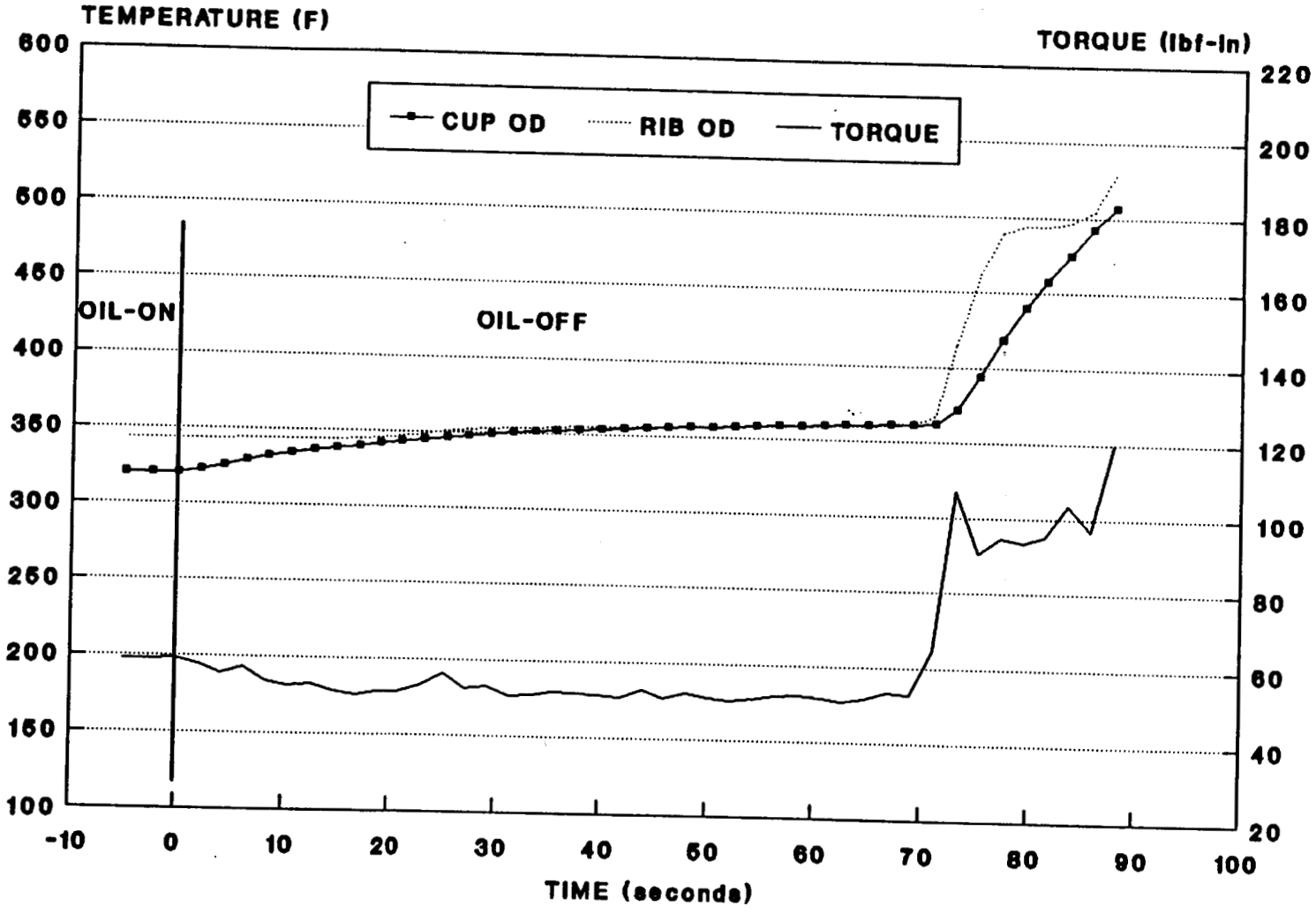

Figure 98. Temperature and Torque Versus Time in Oil-Off Test of Hybrid Bearing With Silicon Nitride Rollers and Steel Rib at 18,000 rpm

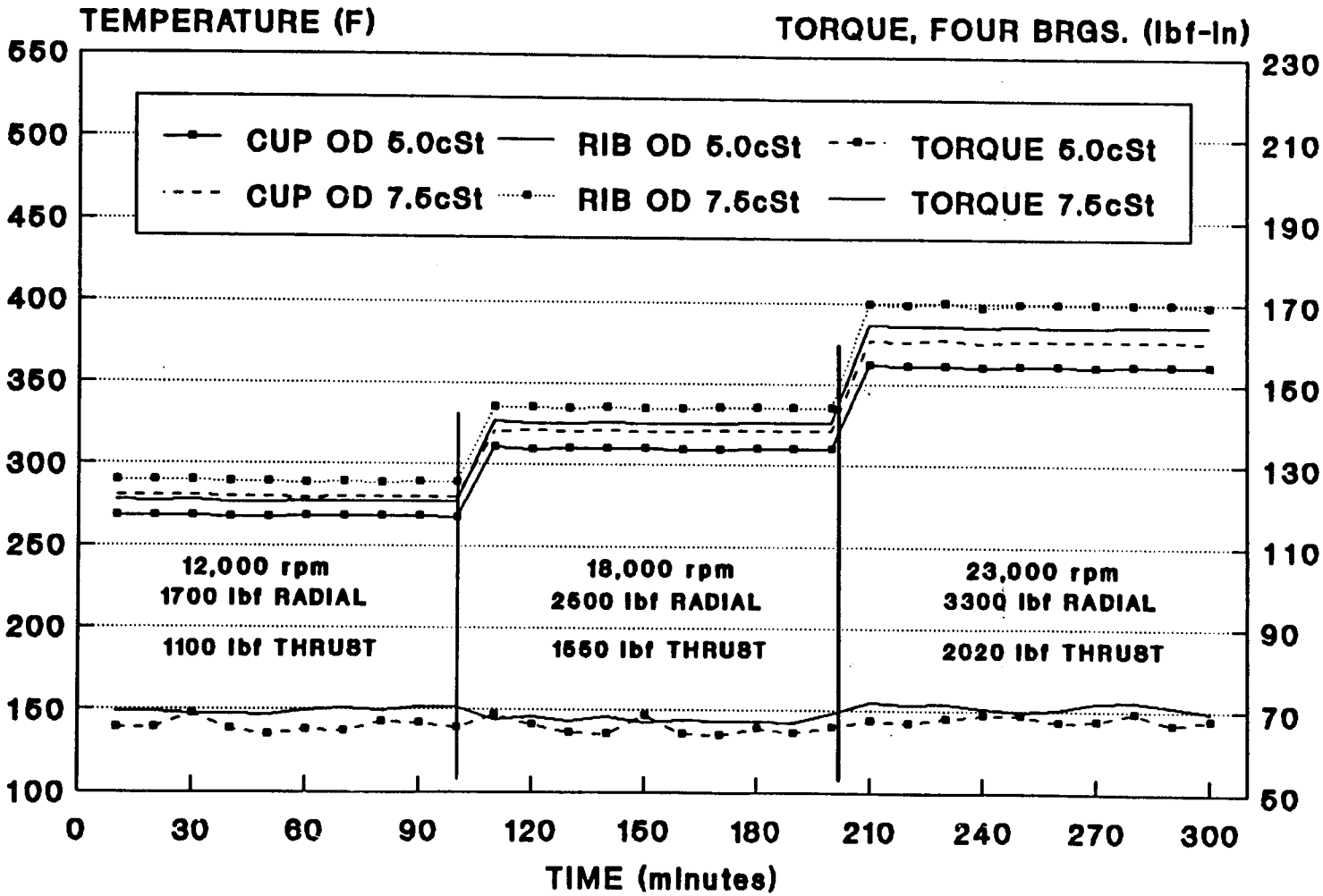

Figure 99. Speed, Temperature, and Torque Versus Time for 5.0- and 7.5-Centistoke Oil

Conclusions

The single-row tapered bidirectional bearing test was successful in proving the concept. The test accomplished the goal of operating the conventional all-steel and hybrid designs in the combined radial load with major and minor thrust load conditions at the advanced-rotorcraft operating criteria.

The conventional and hybrid bearings demonstrated the ability to carry the A.R.T. radial and major thrust load combination up through 23,000 rpm (1.50 MDN).

The conventional and hybrid bearings demonstrated the ability to carry the A.R.T. radial and minor thrust load combination up through 23,000 rpm (1.50 MDN).

The conventional and hybrid bearings can operate at 25,300 rpm (1.64 MDN) with 3.0 pt/min of DOD-L-85734 lubricant.

The conventional and hybrid bearings can operate at 125-percent overload and 110-percent overspeed.

The conventional and hybrid bidirectional bearings operated with less heat generation when the oil exited the bearings through the cup front face slots.

The hybrid bearing (silicon nitride rollers, CBS600 cup rib, steel cage) operated at a lower temperature than the conventional bearing.

The zirconia rib became crazed and deteriorated in the roller contact path.

The hybrid bidirectional bearing with the P.E.E.K. cage generated a higher bearing temperature than with the steel silver-plated cage.

The hybrid directional bearing operated successfully with a wider range of settings than the conventional bidirectional bearing.

The hybrid bidirectional bearing achieved 7.1, 8.3, and 11.9 times L-10 life.

Oil-off testing achieved 60 minutes at 12,000 rpm for the hybrid design and 62 minutes at 5,400 rpm for the conventional steel design.

The bidirectional bearings operated at lower temperatures and torque with the 5.0-cSt versus the 7.5-cSt oil.

The damage to the silicon nitride roller was not total fracture and the mating steel raceways wore, providing debris that could be identified by a chip detector.

Fretting in the cone bore was attributed to the reduction of cone bore surface area due to the oil manifolds.

IMPROVED BEARING TECHNOLOGY

Significant improvements in bearing technology are required to achieve the goals of weight reduction and increased MTBR's as demanded by the A.R.T. program. The work conducted for this task supplements the work previously completed on developing the bidirectional tapered-roller bearing and also includes the following additional work:

1. Improved life-prediction theory (SKF new-life theory)
2. Interaction of surfaces of rolling-element materials
3. Optimized design of hybrid ball and roller bearings.

Two computer programs, PC-SHABERTH and PC-CYBEAN, were modified by MRC Bearings of SKF to incorporate the new bearing-life theory and the traction properties of various material combinations to better predict the service life of transmission bearings. With this life model, it was hoped that bearing fatigue lives could be optimized to achieve the desired goal of a 5,000-hour MTBF gearbox. The difference between the SKF new life formulation and the most commonly used Lundberg-Palmgren (AFBMA) life formulation is that the new theory established a fatigue limit stress and a modified stress volume for calculating the bearing life. With this new life formulation, the effects of the following conditions can also be included in the life prediction:

1. Shear stresses due to traction
2. Hoop stress due to fit-up and rotation
3. Residual stresses
4. Lubricant contamination.

Although none of the above factors can be included in the current life-prediction methodology, it is a known fact that all of these factors have a significant effect on the actual life of bearings. This new life theory does provide the capability to better predict bearing lives in future helicopter transmissions.

In support of this work, traction tests were performed under stress, temperature, lubrication, and surface-roughness conditions which simulated those of the A.R.T. transmission bearings. All traction tests were performed at a maximum Hertz stress of 294,000 psi, which corresponds to the stress of the heaviest loaded roller in a typical helicopter transmission application.

Implementation of Theory of Improved Bearing Life

Background - The new SKF fatigue-life theory for rolling-element bearings was introduced in a 1984 paper by Ioannides and Harris[13]. The key concept embodied in the new SKF life theory is the applicability of a fatigue limit stress. If the operating stress remains below the fatigue life limit for all rolling-element/raceway contacts in the bearing, the bearing can have infinite fatigue life provided it is properly lubricated and protected from contamination. The existence of a fatigue limit stress has been confirmed by recently published data[14] for endurance testing or heavily-loaded 6309 deep-groove ball bearings accurately manufactured from clean homogeneous steel.

A simplified version of the new SKF life theory has been included in the recently released edition of the SKF General Catalog. The catalog implementation of the new life theory is not suitable for aerospace bearing applications due to the following limitations:

1. It does not consider the effect of rolling-element centrifugal forces on the rolling-element load distribution. At high speed, the load on a rolling element due to centrifugal force can be greater than that due to the applied load.

2. The effect of shear stresses due to traction between the rolling elements and raceways is not explicitly considered.

3. The effect on life of hoop stresses due to fit-up, rotation, and residual stress is not quantifiable.

The new SKF life theory has also been incorporated into a sophisticated set of mainframe computer programs at ERC. However, due to the complexity of the calculations, the amount of computer time required to execute these programs is very long. Clearly, an implementation of the new life theory was needed which was intermediate in sophistication between the SKF catalog method and the ERC mainframe programs. This report documents the technical approach and formulation used to incorporate the new life theory in the PC-SHABERTH computer program for ball bearings. A similar approach was used for roller bearings.

Appendix C contains a complete listing of the computer program developed to calculate ball-bearing and roller-bearing life according to the new SKF life theory in PC-SHABERTH.

Analytical Approach - The approach taken in this implementation is to establish a ratio between fatigue life calculated using Lundberg-Palmgren theory and life calculated using the new life theory. The Lundberg-Palmgren formulation is expressed by equation 7. Similarly, the new life theory formulation is expressed by equation 8.

$$\ln \frac{1}{S} \sim N^{e} \tau_{O}^{C} \frac{V}{z_{o}^{h}} \tag{7}$$

$$\ln \frac{1}{\Delta S_i} \sim N^{e} (\tau_i - \tau_L)^{c} \left(\frac{\Delta V_i}{z_i^{h}} \right). \tag{8}$$

where c = empirical constant = 31/3 for ball bearings of SKF standard steel

e = empirical constant (Weibull slope) = 10/9 for ball bearings of SKF standard steel

h = empirical constant = 7/3 for ball bearings of SKF standard steel

N = number of stress cycles endured

S, ΔS_i = probability of survival

V = stressed volume

ΔV_i = volume of material for which stress limit is exceeded

z_i = depth below surface where ΔV_i is located

z_o = depth of maximum orthogonal shear stress

τ_i = stress at z_i

τ_L = fatigue limit stress

τ_o = maximum orthogonal shear stress.

If subscript 1 is used to refer to the Lundberg-Palmgren theory and subscript 2 to refer to the new life theory, the following equation can be written:

Assuming $\tau_2 > \tau_L$,

$$N_1^e \ \tau_1^c \left(\frac{V_1}{z_1^h}\right) = N_2^e \ (\tau_2 - \tau_L)^c \left(\frac{\Delta V_2}{z_2^h}\right). \tag{9}$$

Equation 3 can be rewritten as

$$\left(\frac{N_1}{N_2}\right)^e = \left(\frac{z_1}{z_2}\right)^h \left[\frac{(\tau_2 - \tau_L)}{\tau_1}\right]^c \left(\frac{\Delta V_2}{V_1}\right). \tag{10}$$

In the Lundberg-Palmgren formulation, the stressed volume V_1 is given by

$$V_1 = 2\pi R \ (2a) \ (z_1) \tag{11}$$

where R = radius from bearing centerline to raceway surface

$2a$ = length of contact ellipse

$z_1 = z_o$.

For the new life theory, it will be assumed that

$$\Delta V_2 = 2\pi R\ (2a)\ (\Delta z_2) \tag{12}$$

where Δz_2 = summation of the depth increments for which the calculated stress exceeds the stress limit;

i.e., $\tau_2 > \tau_L$.

Making use of equations 11 and 12, equation 10 can be rewritten as

$$\left(\frac{N_1}{N_2}\right)^e = \left(\frac{z_1}{z_2}\right)^h \left[\frac{(\tau_2 - \tau_L)}{\tau_1}\right]^c \left(\frac{\Delta z_2}{z_1}\right). \tag{13}$$

Further, by simplifying equation 13 and substituting values for the empirical exponents e, c, and h,

$$\Phi = \left(\frac{N_2}{N_1}\right) = \left(\frac{z_2}{z_1}\right)^{2.1} \left[\frac{\tau_1}{(\tau_2 - \tau_L)}\right]^{9.3} \left(\frac{z_1}{\Delta z_2}\right)^{0.9} \tag{14}$$

where $L_2 = \phi L_1$. (15)

The ratio ϕ must now be incorporated into the life-calculation formulation used in PC-SHABERTH. For a ball bearing, the life of a raceway is calculated using the following general equation:

$$L_m = \left(\frac{Q_{cm}}{Q_{eqvm}} \right)^3 \tag{16}$$

where

L_m	=	life of raceway (revs x 10^6)
m	=	1, 2 for outer and inner raceway, respectively
Q_{cm}	=	raceway dynamic capacity
Q_{eqvm}	=	equivalent dynamic load.

The raceway dynamic capacity, Q_{cm}, is calculated in pounds using equation 17,

$$Q_{cm} = 7080 \left[\frac{2f_m}{(2f_m - 1)} \right]^{0.41} \left[\frac{(1 + c_m\gamma)^{1.39}}{(1 - c_m\gamma)^{1/3}} \right] (Z)^{-1/3} \left[\frac{\gamma}{\cos\alpha} \right]^{0.3} (D)^{1.8} \tag{17}$$

where subscript	m	=	1,2 for outer and inner raceway, respectively
	c_1	=	1 (outer raceway)
	c_2	=	-1 (inner raceway)
	D	=	ball diameter (in.)
	d_m	=	bearing pitch diameter (in.)
	f_m	=	r_{gm}/D
	r_{gm}	=	raceway groove radius (in.)
	Z	=	number of balls
	α	=	nominal contact angle
	γ	=	$D \cos\alpha/d_m$.

The equivalent dynamic load, Q_{eqv}, is given by equation 18 for a ball bearing.

$$Q_{eqv} = \left[\frac{1}{Z} \sum_{j-1}^{j-z} Q_{mj}^{p} \right]^{1/p} \tag{18}$$

where	Q_{mj}	=	contact load at raceway m for ball j
	p	=	3 for rotating ring
		=	10/3 for nonrotating ring.

Combining equations 16 and 18:

$$L_m = \left[\frac{Q_{cm}}{\left(\frac{1}{Z} \sum_{J-1}^{J-Z} Q_{mj}^{p} \right)^{1/p}} \right]^3 . \tag{19}$$

Equation 19 can be rewritten as

$$L_m = \left[\frac{1}{Z} \sum_{j-1}^{j-z} \left(\frac{Q_{mj}}{Q_{cm}} \right)^p \right]^{-3/p} . \tag{20}$$

For an individual ball/raceway contact, the life, L_{mj}, is given by:

$$L_m = \left(\frac{Q_{cm}}{Q_{mj}} \right)^3 . \tag{21}$$

Substituting equation 21 into equation 20 yields

$$L_m = \left[\frac{1}{Z} \sum_{j-1}^{j-z} (L_{mj})^{-p/3} \right]^{-3/p} . \tag{22}$$

Introducing the ratio ϕ defined in equations 14 and 15, equation 22 can be rewritten as:

$$L_{1m} = \left[\frac{1}{Z} \sum_{j-1}^{j-z} (\phi_j L_{mj})^{-p/3} \right]^{-3/p} . \tag{23}$$

The final equation used in PC-SHABERTH to calculate ball-bearing raceway life in hours according to the new life theory is given by 24.

$$L_{2m} = L_{1m} \; (a_{2m}) \left(\frac{1745}{\omega_{DIFF}} \right) \left(\frac{EP_{STEEL}}{EP_m} \right)^{6.3} CONTFC_m \tag{24}$$

where a_{2m} = material constant for ring material using new life theory

ω_{DIFF} = absolute value of the difference in raceway speeds (radians/sec)

EP_{STEEL} = effective modulus of elasticity of steel (psi)

= 32.5274×10^6 psi

EP_m = effective ball/raceway modulus of elasticity (psi)

$$= \frac{2}{\left[\frac{(1 - v_1^2)}{E_1} + \frac{(1 - v_2^2)}{E_2} \right]}$$

E_1, E_2 = modulus of elasticity of ball and raceway, respectively (psi)

v_1, v_2 = Poisson's ratio for ball and raceway materials, respectively

$CONTFC_m$ = contamination factor.

The factor a_{2m} was included in case it was found necessary to adjust the calculated lives for different bearing materials. Calculations made to date for standard bearing ring materials (52100, M50, and M50 NiL steel) have not indicated a need to change a_{2m} from its default value of one.

The term $(1745/\omega_{DIFF})$ in equation 24 converts the calculated life from millions of revolutions to hours. The term $(EP_{STEEL}/EP_m)^{6.3}$ adjusts the life when materials other than standard bearing steel are used for the balls and/or raceways. This adjustment factor, based on the ratio of the effective elastic modulus of standard bearing steel to the effective elastic modulus for the ball/raceway material combination actually used, is necessary because implicit in the dynamic capacity equation 17 is the use of an assumed effective modulus of elasticity. For standard bearing steel, the effective modulus is 32.5274×10^6 psi based on an elastic modulus of 29.6×10^6 psi and Poisson's ratio of 0.3.

The effective modulus life-adjustment factor has been included in PC-SHABERTH for many years for the calculation of life using Lundberg-Palmgren theory. This adjustment factor is still needed in calculating life according to the new SKF theory because the method derived involves ratioing from the Lundberg-Palmgren life.

The contamination life factor ($CONTFC_m$) reduces the calculated life based on the ratio of the filter rating to the calculated raceway EHD film thickness. A curve fit was used to determine the contamination factor based on the data of Sayles and Macpherson[15]. The maximum value of the contamination factor is one, indicating no life reduction due to contamination. In general, the coarser the lubricant filter used is, the higher the filter rating and the smaller the value of the contamination factor and the larger the reduction in life.

The overall bearing life is calculated by statistically combining the raceway lives using equation 19.

$$L_{BEARING} = (L_{INNER\ RING}^{-e} + L_{OUTER\ RING}^{-e})^{-1/e} \tag{25}$$

where e = Weibull plot slope = 10/9 for ball bearings.

Calculation of Stresses - The ratio ϕ, given by equation 14, related the fatigue life calculated using the new life theory to fatigue life calculated using Lundberg-Palmgren theory. To calculate the value of ϕ at each ball position, it is necessary to determine the stresses at and below the raceway contact surfaces.

J. O. Smith and C. K. Liu[16] obtained a closed-form solution for the case of line contact between two bodies subjected to combined normal force and friction force due to lateral sliding. In ball bearings, elliptical-point contacts occur between the balls and raceways. Figures 100 and 101 illustrate the normal stress distribution for an elliptical point contact and a line contact, respectively.

NOTE: This section of the report was prepared originally by MRC Bearings of SKF, a subcontractor to The Boeing Company, Helicopters Division. Boeing would prefer to provide the customer with a report that is consistent in style and format throughout. However, in the interest of reducing the cost of production of this report, Boeing is using all illustrations provided by MRC Bearings in their original form.

In Figures 100 and 101, the y-axis is in the direction of rolling. If the contact ellipse in Figure 100 is divided into a number of slices parallel to the y-axis, the center slice where the maximum normal stress occurs approximates part of a line contact. The formulation of Smith and Liu will therefore provide a good approximation of the stresses at and below the contact surface.

In implementing the new life theory in PC-SHABERTH, a reasonable compromise must be made between computational accuracy and program execution speed. Since the stresses must be

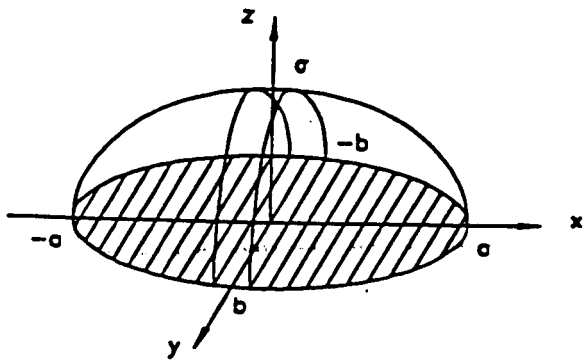

$$\sigma = \sigma_{MAX}\left[1 - \left(\frac{x}{a}\right)^2 - \left(\frac{y}{b}\right)^2\right]^{1/2}$$

$$\sigma_{MAX} = \frac{3Q}{2\pi ab}$$

Figure 100. Point Contact Normal Stress Distribution

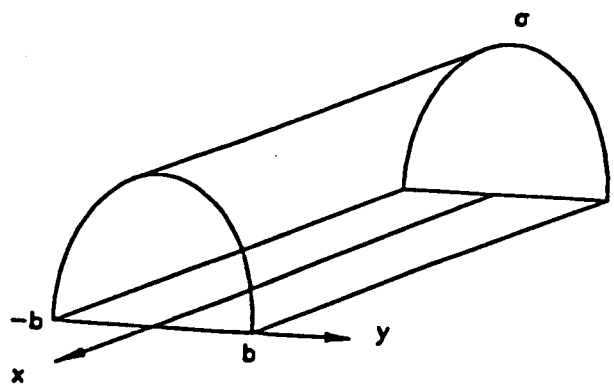

$$\sigma = \sigma_{MAX}\left[1 - \left(\frac{y}{b}\right)^2\right]^{1/2}$$

$$\sigma_{MAX} = \frac{2Q}{\pi \ell b}$$

Figure 101. Line Contact Normal Stress Distribution

calculated at the outer and inner raceways for each ball in the bearing, a relatively simple stress-calculation method is needed to prevent excessive execution time. The approach adopted is to calculate the stresses using the formulation of Smith and Liu at evenly spaced points along the y-axis (from - 2b to 2b) for evenly spaced values of the depth below the surface z (from 0 to 6b).

The equations for the stresses at any depth z below the surface are as follows:

$$\sigma_x = \frac{-2vP_{MAX}}{\pi}\left\{z\left[(b^2 + y^2 + z^2)\ \frac{\phi_1}{b} - \frac{\pi}{b} - 2y\,\phi_2\right] + \mu\left[(y^2 - b^2 - z^2)\ \phi_2 + \frac{\pi y}{b} + (b^2 - y^2 - z^2)\ \frac{y}{b}\,\phi_1\right]\right\} \tag{26}$$

$$\sigma_y = \frac{-P_{MAX}}{\pi}\left\{z\left[\frac{(b^2 + 2z^2 + 2y^2)}{b}\ \phi_1 - \frac{2\pi}{b} - 3y\,\phi_2\right] + \mu\left[(2y^2 - 2b^2 - 3z^2)\ \phi_2 + \frac{2\pi y}{b} + 2(b^2 - y^2 - z^2)\ \frac{y}{b}\,\phi_1\right]\right\} \tag{27}$$

$$\sigma_t = \frac{-P_{MAX}}{\pi}\left[z(b\phi_1 - y\phi_2) + \mu z^2\phi_2\right] \tag{28}$$

$$\tau\sigma_z = \frac{-P_{MAX}}{\pi}\left\{z^2\,\phi_2 + \mu\left[(b^2 + 2y^2 + 2z^2)\ \left(\frac{z}{b}\right)\phi_1 - 2\pi\left(\frac{z}{b}\right) - 3yz\phi_2\right]\right\} \tag{29}$$

where $M = [(b + y)^2 + z^2]^{1/2}$

$N = [(b - y)^2 + z^2]^{1/2}$

P_{MAX} = maximum normal stress (psi)

y = coordinate from center of contact in direction of rolling (in.)

z = depth below contact surface (in.)

μ = friction coefficient

v = Poisson's ratio .

$$\phi_1 = \frac{\pi\ (M + N)}{MN[2MN + 2y^2 + 2z^2 - 2b^2]^{1/2}}$$

$$\phi_2 = \frac{\pi\,(M - N)}{MN[2MN + 2y^2 + 2z^2 - 2b^2]^{1/2}}$$

A special set of equations is used to evaluate the stresses at the contact surface (z = 0):

$$\sigma_x = \begin{cases} -2\nu P_{MAX}\,\mu\left[\frac{y}{b} - \left(\frac{Y^2}{b^2} - 1\right)^{1/2}\right] for\ y \geq b \\ -\nu P_{MAX}\left[2\left(1 - \frac{Y^2}{b^2}\right)^{1/2} + 2\mu\left(\frac{y}{b}\right)\right]\ for\ |y| \leq b \\ -2\nu P_{MAX}\,\mu\left[\frac{y}{b} + \left(\frac{y^2}{B^2} - 1\right)^{1/2}\right] for\ y \leq -b \end{cases} \tag{30}$$

$$\sigma_y = \begin{cases} -2\mu P_{MAX}\left[\frac{y}{b} - \left(\frac{Y^2}{b^2} - 1\right)^{1/2}\right] for\ y \geq b \\ -P_{MAX}\left[\left(1 - \frac{Y^2}{b^2}\right)^{1/2} + 2\mu\left(\frac{y}{b}\right)\right]\ for\ |y| \leq b \\ -2\mu P_{MAX}\left[\frac{y}{b} + \left(\frac{y^2}{b^2} - 1\right)^{1/2}\right] for\ y \leq -b \end{cases} \tag{31}$$

$$\sigma_z = \begin{cases} -P_{MAX}\left(1 - \frac{y^2}{b^2}\right)^{1/2} & for\ |y| \le b \\ 0\ for\ y \ge b\ plus\ y \le -b \end{cases} \tag{32}$$

$$\tau_{zy} = \begin{cases} -\mu P_{MAX}\left(1 - \frac{y^2}{b^2}\right)^{1/2} & for\ |\ y\ | \le +b \\ 0\ for\ y \ge b\ plus\ y \le -b. \end{cases} \tag{33}$$

Equations 26 through 33 give the stresses due to the normal Hertzian stress plus the frictional shear stress caused by lateral sliding. In PC-SHABERTH, the contact ellipse is divided into as many as 21 slices. The lateral sliding velocity is calculated at the center of each slice. The value of the friction coefficient μ used in computing the stresses is the average friction coefficient for the contact given by equation 34.

$$\mu_{AVG} = \frac{\sum_{k-1}^{k-21} |f_k|}{Q} \tag{34}$$

where f_k = friction force on slice k

Q = ball/raceway contact force.

Alternatively, an input value of friction coefficient can be used in computing the stresses.

In addition to the normal stress and the frictional shear stress, it is required to consider the effect on life of fit-up stress, stress due to rotation, and residual stress. These are all hoop stresses which act in the y direction in the chosen coordinate system. Using the principle of superposition, a term can simply be added to the normal stress calculated in the y direction using equation 27 or 31.

$$\sigma_y' = \sigma_y + \sigma_{HOOP} \tag{35}$$

where $\sigma_{HOOP} = \sigma_{ROT} + \sigma_{FIT} + \sigma_{RES}$

σ_{ROT} = hoop stress due to ring rotation

σ_{RES} = residual stress due to heat treatment, material processing, and manufacturing.

For practical purposes, the hoop stresses due to rotation and fit-up can be considered constant values for the subsurface region of interest. The residual stress can vary significantly over the subsurface region depending on the material and manufacturing process. The current formulation for hoop stress assumes a constant value of residual stress. However, if the variation of residual stress with depth below the surface is significant, the computer program could be modified to allow input of the residual stress values versus depth and then use curve fitting or linear interpolation to determine the residual stress at the desired depth.

The hoop stress due to ring rotation is calculated using equation 36 from Roark[17].

$$\sigma_{ROT} = \frac{1}{8}\rho\left(\frac{\omega^2}{386.4}\right)\left[(3+v)\left(R^2 + R_0^2 = \frac{R^2R_0^2}{r^2}\right) - (1+3v)r^2\right] \tag{36}$$

where R = outer radius of ring (in.)

R_0	=	inner radius of ring (in.)
r	=	radius for which stress is computed
v	=	Poisson's ratio
ρ	=	density (lb/in.^{3})
ω	=	rotational speed (rad/sec).

The formulation for the fit-up hoop stress was derived from Seely & Smith[18]. Consider the fit-up of the two rings shown in Figure 102.

If the two rings are mounted with a radial interference of δ, the resultant interface pressure between the two rings is given by equation 37.

$$P_s = \frac{\delta}{R_2 \left\{ \frac{1}{E_2}\left[\frac{(R_3^2 + R_2^2)}{(R_3^2 - R_2^2)} + v_2 \right] + \frac{1}{E_1}\left[\frac{(R_2^2 + R_1^2)}{(R_2^2 - R_1^2)} \; v_1 \right] \right\}} \tag{37}$$

where	E_1, E_2	=	modulus of elasticity of rings 1 and 2
	P_s	=	radial pressure acting at interface between rings 1 and 2
	v_1, v_2	=	Poisson's ratio of rings 1 and 2.

For the fit-up of an inner ring on a shaft, the resultant hoop stress (tangential) can be calculated using equation 38.

$$\sigma_{FIT_{TR}} = P_S \left[\frac{R_2^2}{(R_3^2 - R_2^2)} \right] \left[\left(\frac{R_3^2}{R^2} \right) + 1 \right] \tag{38}$$

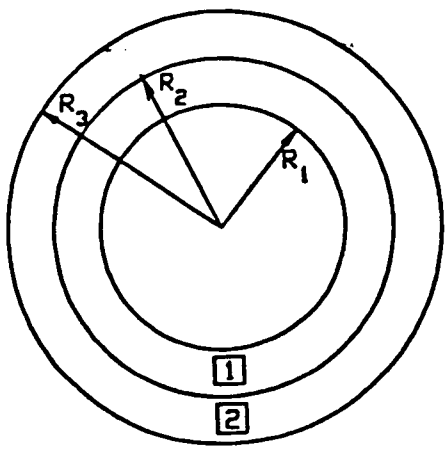

Figure 102. Diagram for Fit-Up of Two Concentric Rings

where R = radius to point of interest on inner raceway

R_2 = bore radius of inner ring

R_3 = outer radius of inner ring.

As can be seen from equation 38, the maximum tensile fit-up stress occurs at the bore of the bearing inner ring.

For the interference fit of an outer ring in a housing, the resultant compressive hoop stress is calculated by equation 39.

$$\sigma_{FIT_{OR}} = -P_S \left[\frac{R_2^2}{(R_2^2 - R_1^2)} \right] \left[1 + \frac{R_1^2}{R^2} \right] \tag{39}$$

where R_1 = inner radius of outer ring

R_2 = outer radius of outer ring

R = radius to point of interest on outer raceway.

Now that equations have been developed for the normal stresses (σ_x, σ_y, σ_z) and the shear stress (τ_{yz}), the principal stresses, maximum shear stress, octahedral shear stress, and Von Mises stress can be determined for any point at or below the contact surface. According to Seely & Smith[19], σ_x is a principal stress designated as σ_3. The other two principal stresses can be determined using Mohr's circle.

$$\sigma_3 = \sigma_x \tag{40}$$

$$\sigma_1 = \frac{(\sigma_y + \sigma_z)}{2} + \frac{\left[(\sigma_y - \sigma_z)^2 + 4\tau_{yz}^2\right]^{1/2}}{2} \tag{41}$$

$$\sigma_2 = \frac{(\sigma_y + \sigma_z)}{2} - \frac{\left[(\sigma_y - \sigma_z)^2 + 4\tau_{yz}^2\right]^{1/2}}{2} \tag{42}$$

The maximum shear stresses can be determined from the principal stresses using equations 43 through 45.

$$\tau_{MAX_1} = \frac{1}{2}\ (\sigma_1 - \sigma_2) \tag{43}$$

$$\tau_{MAX_2} = \frac{1}{2}\ (\sigma_2 - \sigma_3) \tag{44}$$

$$\tau_{MAX_3} = \frac{1}{2}\ (\sigma_1 - \sigma_3) \tag{45}$$

The maximum octahedral shear stress t_G can also be determined from the principal stresses using equation 46.

$$\tau_G = \frac{1}{3}\left[(\sigma_1 - \sigma_2)^2 + (\sigma_2 - \sigma_3)^2 + (\sigma_3 - \sigma_1)^2\right]^{1/2} \tag{46}$$

The Von Mises stress σ_{VM}, which is the equivalent stress based on the distortion energy failure theory, is given by equation 47.

$$\sigma_{VM} = \left(\frac{1}{2^{1/2}}\right)\left[(\sigma_1 - \sigma_2)^2 + (\sigma_2 - \sigma_3)^2 + (\sigma_3 - \sigma_1)^2)\right]^{1/2} \tag{47}$$

Comparing equations 46 and 47, it is clear that

$$\sigma_{VM} = \tau_G\left(\frac{3}{2^{1/2}}\right) = 2.1213\tau_G. \tag{48}$$

Selection of Fatigue Stress Criterion - In equation 8, which is the basic equation for the new life theory, the values of the stress parameter τ_1 and the fatigue limit stress τ_L are dependent on the fatigue failure hypothesis selected. There are many different failure theories; but the two most commonly applied to bearing fatigue life are the maximum orthogonal shear stress (also called maximum alternating shear stress) and the maximum Von Mises stress, which is the equivalent stress based on the maximum energy of distortion theory. Broszeit and Zwirlein[20] state that the Von Mises stress criterion provides the best representation of the extent of material stressing in the case of dynamically loaded rolling elements. The Von Mises stress also has the advantage of being a scalar quantity that is straightforward to calculate. For these reasons, the Von Mises stress was selected as the fatigue stress criterion to use in this implementation of the new life theory.

In the paper by Ioannides and Harris[13], the value deduced for the fatigue limit stress based on the maximum orthogonal shear stress was 350 N/mm^2 (50,763 psi) for properly made bearings of AISI 52100 steel. The corresponding fatigue limit stress for 52100 steel based on the Von

Mises stress is given in Reference 13 as 606 N/mm^2 (87,893 psi). Based on recent work [21,22] involving the correlation of calculated bearing life to field test data for Pratt & Whitney Aircraft - Florida and Pratt & Whitney - Canada gas turbine engine mainshaft ball bearings, a fatigue limit stress of 290 N/mm^2 (42,061 psi) was deduced for VIMVAR M50 steel using the maximum orthogonal shear stress criterion. The corresponding fatigue limit stress for VIMVAR M50 steel based on the Von Mises stress criterion is 502 N/mm^2 (72,809 psi) using the same ratio (1.73) as for 52100 steel.

Calculation of the ϕ Ratio - The ϕ ratio, which relates the life calculated using the new SKF theory to the Lundberg-Palmgren life, is defined by equation 14 which is repeated for convenience below:

$$\phi = \left(\frac{L_2}{L_1}\right) = \left(\frac{z_2}{z_1}\right)^{2.1} \left[\frac{\tau_1}{(\tau_2 - \tau_L)}\right]^{9.3} \left(\frac{z_1}{\Delta_{z_2}}\right)^{0.9} . \tag{14}$$

The parameter z_1 is the depth to the maximum orthogonal shear stress for the Lundberg-Palmgren formulation, i.e., for the case of normal Hertzian pressure only. The value for z_1 can be found by solving a cubic equation (49) for the auxiliary parameter t and then substituting this value into equation 50.

$$\frac{b}{a} = [(t^2 - 1) \quad (2t - 1)]^{1/2} \tag{49}$$

$$z_1 = \frac{b}{[(t + 1) \quad (2t - 1)^{1/2}]} \tag{50}$$

In PC-SHABERTH, equation 49 is solved using a subroutine (ROOT3) which obtains a closed-form solution of a cubic equation. The value of z_1 is then obtained from equation 50.

Since the Von Mises stress was chosen as the fatigue stress criterion in this implementation of the new life theory, τ_1 is the maximum Von Mises stress at depth z_1 considering normal stress only. Thus, the value for τ_1 is obtained by evaluating equations 26 through 29 [with $z = z_1$, the friction coefficient $\mu = 0$, and $y = 0$], then evaluating the principal stress using equations 40 through 42 and finally using equation 47 to calculate the Von Mises stress. Note that setting $y = 0$ in equations 26 through 29 is based on the observation that the maximum Von Mises stress occurs there in the frictionless case.

The value of τ_2 in equation 14 is the maximum Von Mises stress considering the total stress field; normal stress, frictional shear stress, and hoop stress due to fit-up, rotation, and residual stress. The technique used to determine τ_2 is to evaluate the Von Mises stress at evenly spaced depth increments from $z = 0$ to $z = 6b$ for values of y varying from -2b to 2b in evenly spaced increments. Currently, the increments used for both y and z values are b/10. The value of z_2 in equation 14 is the z coordinate where τ_2 occurs. The value of Δz_2 is determined by adding up all the depth increments for which the maximum Von Mises stress exceeds the fatigue stress limit τ_L.

Incorporation of Fluid-Lubricated Traction Data Into PC-SHABERTH - The PC-SHABERTH program was updated to allow the optional input of a friction coefficient versus percent slip curve (sliding velocity/rolling velocity x 100) for fluid lubrication. The previous calculation method using "built-in" traction versus slip curves for four standard lubricants (mineral oil, MIL-L-7808, polyphenyl ether, and MIL-L-23699) is still available. However, if traction test data (such as that generated in this contract) are available, the user can define the traction coefficient at the rolling element/raceway contacts as a function of slide-to-roll ratio (SRR). There are currently two choices for the friction curve shape:

1. The friction coefficient increases linearly with sliding velocity until it reaches a maximum value (μMAX). The required input values are μMAX and SRR_c.

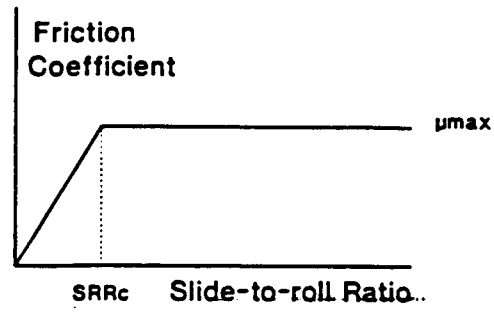

2. The friction coefficient increases linearly with sliding velocity up to a cutoff value of slide-to-roll ratio (SRR_c) and thereafter increases exponentially, asymptotically approaching a maximum value (μMAX). The required input values are μ_c, SRR_c, μMAX, and K (an exponent controlling how quickly μMAX is approached with increasing sliding velocity).

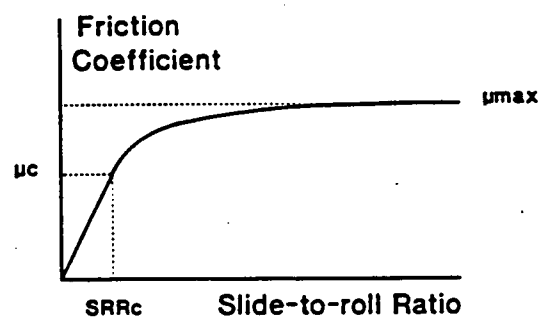

Figure 103 shows that the first friction curve option provides a reasonable approximation to the actual friction data for the room-temperature test of a silicon nitride ball and an M50 NiL disk using MIL-L-23699 lubricant. The curve fit shown was obtained for μMAX = 0.063 and SRR_c = 0.0046.

Figure 104 shows that the second friction curve option provides a good approximation to the experimental data for 280°F test of a silicon nitride ball and an M50 NiL disk using MIL-L-

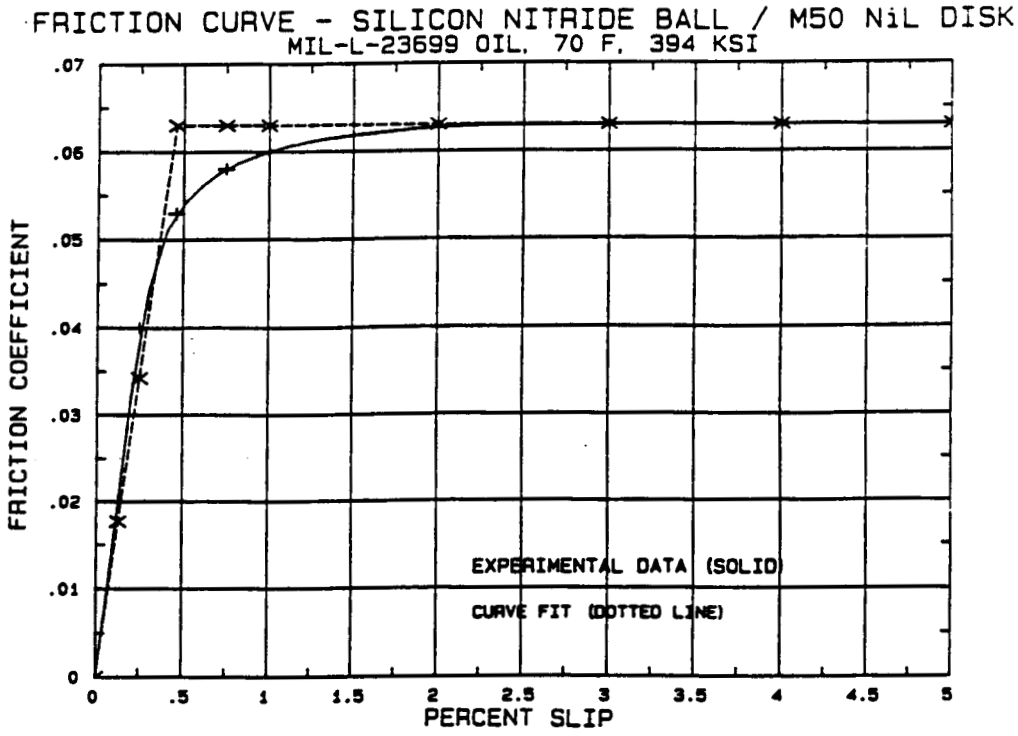

Figure 103. Friction Curve Fit for μMAX - 0.063 and SRRc = 0.0046

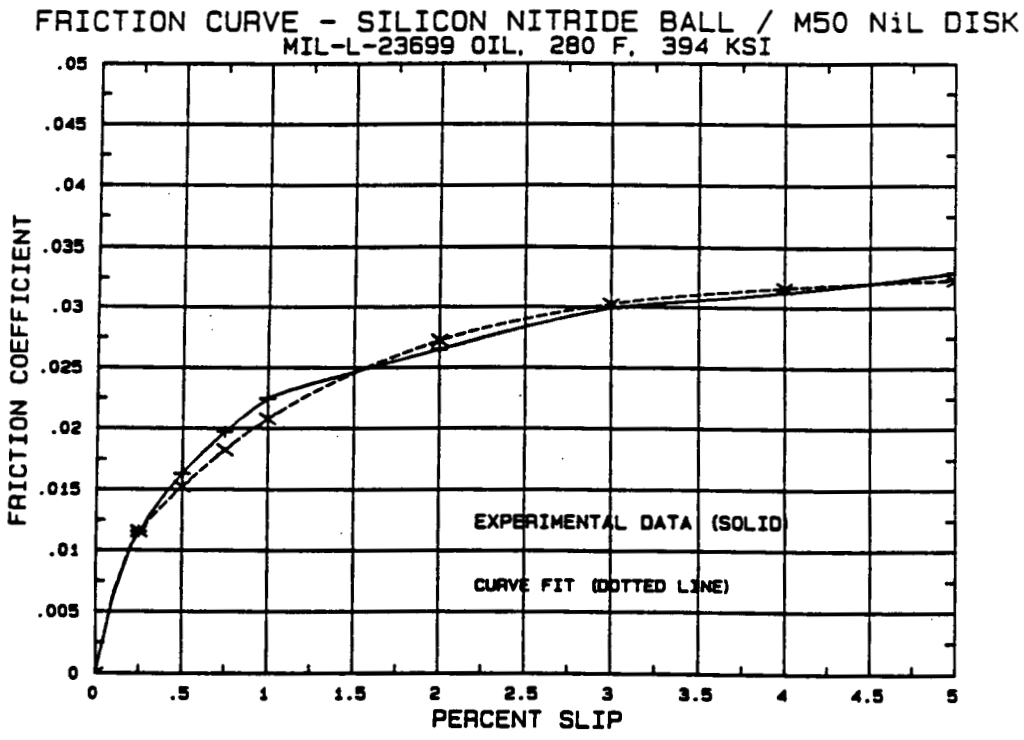

Figure 104. Friction Curve Fit for μMAX = 0.033, μc = 0.020, SRRc = 0.0064, and K = 60

23699 lubricant. The curve fit shown was obtained for $\mu MAX = 0.033$, $\mu_c = 0.020$, $SRR_c = 0.0064$, and K =60.

Analysis of Reference Bearings - A skidding analysis was performed using PC-CYBEAN2 for the MR315C2 cylindrical roller bearing and its predecessor, the 114DS665 bearing. Both bearing designs are very similar except that the MR315C2 design incorporates silicon nitride rollers instead of steel rollers and a carburized M50 NiL inner ring instead of through-hardened M50 steel. Also, the ceramic rollers are square (25-mm diameter by 25-mm length), while the steel rollers are rectangular (25-mm diameter by 24.8-mm length). Both bearing designs feature two-point, out-of-round outer rings for which the difference between the maximum and minimum free-state outer diameters is 0.024 to 0.027 inch.

Figure 105 is a plot of percent cage slip versus applied radial load for the two bearing designs. The analysis indicates that for both designs the out-of-round is sufficient to preclude any significant skidding. Interestingly, the MR315C2 design is predicted to have slightly higher values of cage slip under light loads even though the ceramic rollers have approximately 60 percent lower centrifugal forces acting on them. This is due primarily to the fact that the calculated operating clearance for the MR315C2 bearing is considerably higher (0.0040 inch versus 0.0025 inch) because of the low coefficient of thermal expansion of the ceramic rollers. For the MR315C2 design, based on an assumed uniform operating temperature of 260°F, an increase in the internal bearing clearance of 0.00175 inch was calculated due to the difference in thermal expansion coefficients of the steel rings (6.244×10^{6} 1/°F) and ceramic rollers (1.61×10^{-6} 1/°F). The higher bearing operating clearance results in lower roller pinch forces due to the out-of-round and therefore more cage slip for the MR315C2 design.

Appendix D contains PC-CYBEAN2 output listings for the MR315C2 and 114DS665 bearings for an applied radial load of 1,000 pounds.

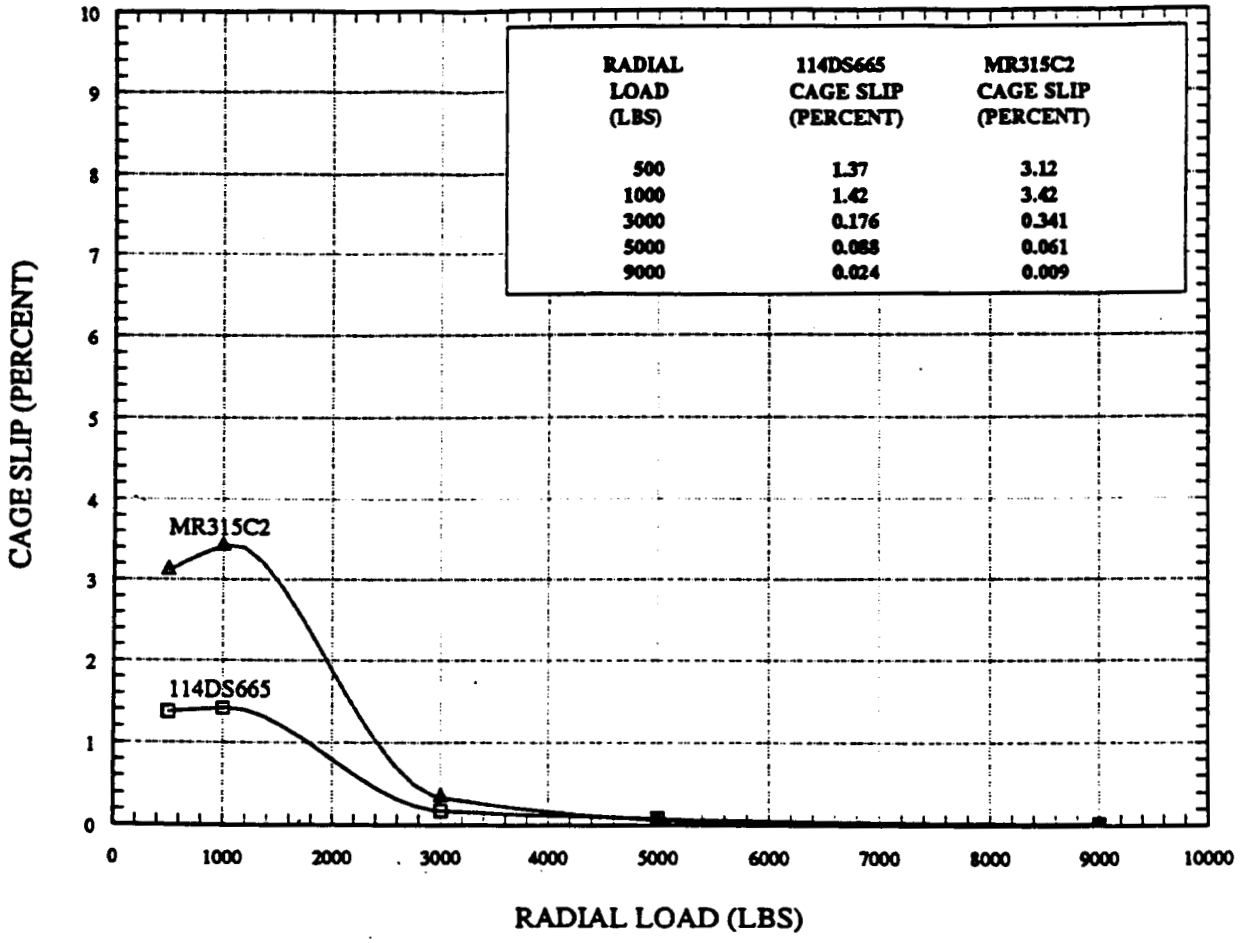

Figure 105. Skidding Analysis Results Using PC-CYBEAN2

Four MR315C2 cylindrical roller bearings were fabricated at MRC Bearings and supplied to Boeing for full-scale transmission testing. The bearings are similar in design to Boeing part number 145DS665 (SKF N315VAG) which is used on the CH-47C/D helicopter transmission input pinion shaft.

The MR315C2 bearing incorporated NBD-100 silicon nitride rollers. The ceramic rollers were finish-machined in the MRC Philadelphia plant from rough-ground blanks purchased from CERBEC. The inner rings were fabricated from M50 NiL steel in the MRC Special Products shop. The outer rings, which are two-point out-of-round (0.024 - 0.027 inch), were also manufactured in the MRC Special Products shop. The silver-plated AMS 6414 steel cages were produced at the SKF Shippensburg plant.

Figure 106 is a drawing of the MR315C2 bearing.

Friction Testing

Background - MRC's statement of work for the A.R.T. program specified that friction testing be performed for the specific materials and lubrication conditions expected in service. MRC Bearings previously developed a ball-on-disk traction test machine capable of evaluating the frictional performance of various material and lubricant combinations. The ball-on-disk test rig provides an efficient way to simulate the traction characteristics of rolling-element bearing contacts. The MRC traction test machine measures traction force and ultimately friction coefficient at the ball-disk interface as the amount of relative slip is varied.

A total of 29 traction tests were performed involving two different ball materials (M50 and silicon nitride) and three different disk materials (Armoloy TDC-coated M50, M50 NiL, and VASCO X2). The traction tests covered the temperature range from 70 to 400°F with MIL-L-23699 oil. Unlubricated traction tests were also run for the various material combinations at room temperature. For each test, a plot of traction coefficient versus percent slip was generated.

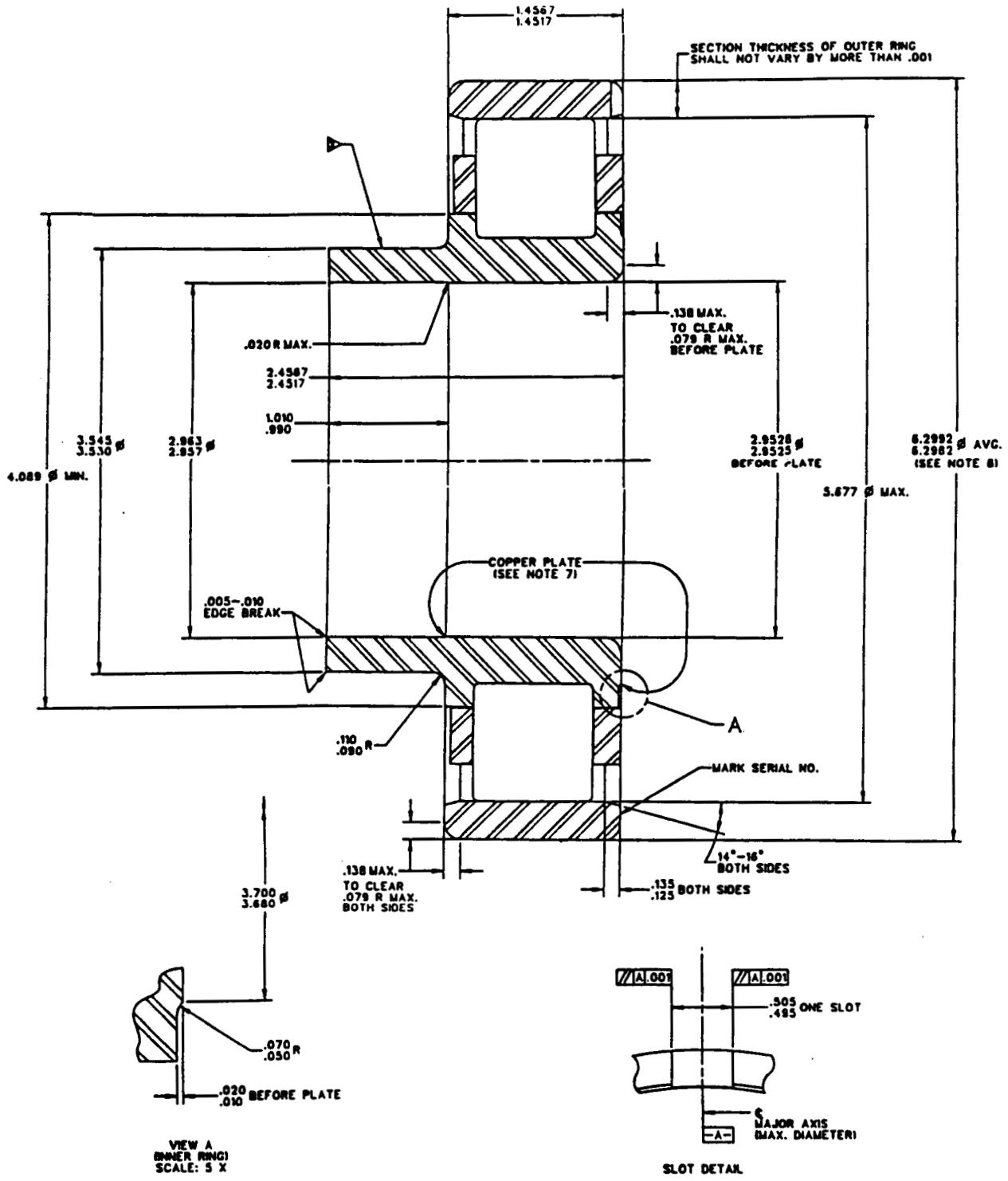

Figure 106. MRC Test Bearing MR315C2 (Sheet 1 of 2)

FILE NO. D74937 REV.

ENGINEERING DATA		
CUSTOMER		BOEING HELICOPTER
CUSTOMER PART NUMBER		–
CUSTOMER FSCM NUMBER		77277
GRADE (U.O.S.)		RBEC 5
NO. & SIZE OF ROLLERS (DIA. X LENGTH) (mm)		12–7.5 X 7.5
PITCH DIAMETER (REF.)		4.6850
RADIAL CLEARANCE		.0025–.0030
MIN. ALLOWABLE END FLOAT		.180
ROLLER TO INNER RING END CLEARANCE		.0007–.0022
DIAMETRAL CAGE CLEARANCE	PILOT	.013–.023
CAGE POCKET CLEARANCE	AXIAL	.008–.013
	CIRCUMFERENTIAL	.008–.013
CAGE FACE TO BEARING FACE CLEARANCE (MIN.)		.001

RING		
RACEWAY SIDEWALL ANGLE		0°08'–0°45'
SURFACE FINISH (AA) MAX. (BEFORE PLATING)	BORE	13
	OD	13
	RING FACES	16
	RACEWAYS	4
	RACEWAY SIDEWALLS	10
	CAGE PILOT SURFACE	13
	FACE SLOT WALLS	125

ROLLER		
SURFACE FINISH (AA) MAX.	OD	4
	CROWN	4
	END FACES	8
	CORNERS	32
DIAMETER VARIATION PER BEARING NOT TO EXCEED		.000250
LENGTH VARIATION PER BEARING NOT TO EXCEED		.0002
END FACE RUNOUT WITH OD		.00020
CORNER RUNOUT WITH OD		.001
CROWN RUNOUT WITH OD		.00020

CAGE		
TYPE		1 PC. MACH. NON-SEP.
RETENTION		BENT TANG
PILOT SURFACE		BORE
PLATING	THICKNESS	.001–.002
	SPECIFICATION	AMS 2412
SURFACE FINISH (AA) MAX. (BEFORE PLATING)	BORE	32
	OTHER SURFACES	63
WIDTH (MAX.)		1.412
UNBALANCE @ 500 RPM NOT TO EXCEED (g–cm)		5
FACES TO BE PARALLEL WITHIN		.002
OD TO BE CONCENTRIC WITH BORE WITHIN		.002
CAGE POCKET CORNER RADIUS		.035–.045

HEAT	OUTER RING	INNER RING	ROLLER	CAGE
SPECIFICATION	AMS 6491	AMS 6278	NBD 100	AMS 6414
HARDNESS	Rc 60 MIN.	SEE NOTE 6	–	Rc 28–38
STABILIZATION	600°F	600°F	–	–

INSPECTIONS	OUTER RING	INNER RING	ROLLER	CAGE
MAGNETIC PARTICLE	100%	100%	–	–
NITAL ETCH	100%	100%	–	–
EDDY CURRENT	100%	100%	–	–
FLUORESENT PENETRANT	–	–	–	100%
VISUAL	100%	100%	100%	100%
HARDNESS	100%	100%	–	–
DYE PEN	–	–	100%	–

1 POSSESSION OF THIS SERVICE DRAWING CONFER NO RIGHTS TO USE THE INFORMATION CONTAINED ON THE FACE HEREON FOR MANUFACTURING PURPOSES, AND MRC BEARINGS MAKES NO WARRANTY THAT SUCH INFORMATION IS COMPLETE OR THAT ANYTHING REPRESENTED HEREON IS FIT FOR ANY PARTICULAR PURPOSE.

2 ▷ MARK MRC IDENTIFICATION, CUSTOMER PART NO. & SERIAL NO. WHERE SHOWN.

3 ALL DIMENSIONS ARE IN INCHES AND APPLY AFTER PLATING U.O.S.

4 BREAK EDGES .005–.015 U.O.S.

5 SURFACE FINISH 90 AA MAX. U.O.S.

6 HEAT TREATING AND CARBURIZATION OF INNER RING SHALL YIELD THE FOLLOWING CHARACTERISTICS:

- SURFACE HARDNESS Rc 60–64
- EFFECTIVE CASE HARDNESS Rc 58 MIN. AT A DEPTH OF .020–.035
- CORE HARDNESS Rc 38–47

7 COPPER PLATE INNER RING .0001–.0003 THICK PER AMS 2418 WHERE SHOWN.

8 THE FREE STATE DIFFERENCE BETWEEN THE MAX. AND MIN. OD MUST BE .024–.027 .

9 RACEWAYS, CAGE RIDING RING LANDS AND ROLLERS MUST BE FREE FROM EVIDENCE OF NITAL ETCH.

10 SURFACE FINISH OF RACEWAYS MUST BE 100% INSPECTED.

11 MRC BEARINGS SHALL MAINTAIN RECORDS OF MILL HEAT AND HEAT TREATMENT.

12 NO PORTION OF THE CAGE MAY PROTRUDE BEYOND RING FACES WITHOUT SPECIFIC APPROVAL OF THE BOEING HELICOPTER ENGINEERING DEPARTMENT.

13 PACKAGE PER BOEING DOCUMENT, M1001, P-58, CAT. II.

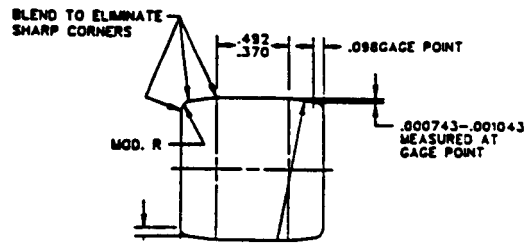

REVISIONS	DRAWN JWP	DATE 02/14/91	GRUMMAN AEROSPACE BEARINGS	MRC BEARINGS JAMESTOWN, NEW YORK 14701
	CHECK MR	DATE 02/20/91	PART NO. 6P/10	CYLINDRICAL ROLLER BEARING MRC MR315C2
	APPROVED	DATE 2/20/91		
	CAD NO MANUAL CHANGES		SIZE D / CODE IDENT NO. 38443	FILE NO. D74937 / REV
			SCALE: 2 X	SHEET 1 OF 1 / DIR 13

Figure 106. MRC Test Bearing MR315C2 (Sheet 2 of 2)

At the request of Boeing, three additional traction tests were performed with a new lubricant. DOD-L-85734 oil, which will be used in the A.R.T. program transmission testing. The tests were run with a silicon nitride ball and an M50 NiL disk at temperatures of 70°F, 280°F, and 400°F.

Brief Overview of Traction in a Rolling/Sliding Contact - The use of traction testing to evaluate materials and lubricants provides frictional information which is used to predict bearing heat-generation rates. It is also an excellent way to evaluate the material response to normal and tangential contact stress. The development of a tangential stress as the contacting bodies depart from pure rolling to incipient sliding and gross slip is an essential feature of the testing process.

Two rolling bodies can depart from a "free" or "pure" rolling condition if they are called upon to transmit a tangential force (T). If the tangential force (traction) is less than the limiting traction force ($T < \mu P$, where μ and P are traction coefficient and normal load, respectively), the two bodies will not give rise to gross sliding, but rather to creep resulting in a contact that is divided into "stick" and "slip" regions [23]. The strain in the stick region is likely to be controlled by elastic properties for an unlubricated surface. Also, the difference between the tangential strains in the two bodies in the "stick" regions lead to an apparent slip where in one revolution the distance covered is slightly greater than the undeformed perimeter of a circular body. The strain in the "slip" region is controlled by the local coefficient of friction and normal load. The size of the slip and stick regions is a function of the tangential force (T). A small tangential force causes microslip at the trailing edge of the contact. As the tangential force increases, the slip extends forward until $T = \mu P$; then the slip region reaches the leading edge of the contact and gross sliding occurs.

The initial slope of the traction curve in Figure 107 reflects the elastic response (shear modulus) of the material in the contact region. For clean interfacial conditions, the strain-affected zone extends below the surface (near-surface region) and the initial slope reflects the shear modulus

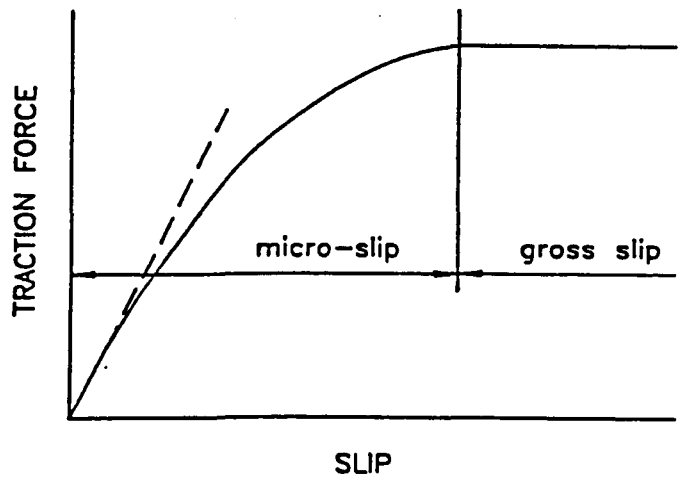

Figure 107. Schematic Representation of a Traction-Versus-Slip Curve (Creep) for Unlubricated Surfaces

of the bulk materials. For other than clean conditions (e.g., liquid or solid forms, oxides, compacted islands of oxides, wear debris), the stiffness of the third-body material will contribute to a portion of the actual initial small strain response. For large strains, of course, the shear properties of the third-body material will control the resulting tractive stress. Thus, it is possible to use the initial slope of a traction-versus-slip curve to obtain the shear modulus of the strain-affected zone [24] or even an effective viscosity of a solid film [25,26]. An effective shear modulus (G), obtained from Reference 24, is :

$$G = pmhPO/(4a)$$

where m = initial slope

h = depth of strain-affected zone

PO = maximum Hertz contact pressure

a = contact half-width in rolling direction.

For high strain conditions (gross sliding throughout the contact) the maximum tractive force, as shown in Figure 107, is determined by the shear strength of the third-body material. The shear strength is a function of the interfacial conditions within the contact (e.g., pressure, temperature, shear rate, etc) as well as the composition and local distribution of the third-body material at a given instant in time.

The entire traction curve, then, from initial slip to maximum tractive force, reflects deformation properties arising from a zone below the surface to the shear plane which gives rise to the traction response. If the tribological conditions within the bearing can be simulated, then appropriate traction testing can provide a useful means for evaluating the performance of materials and lubricants.

MRC Bearings High-Temperature Traction-Testing Machine - MRC Bearings developed the high-temperature traction-test device for the purpose of evaluating materials and lubricants in

complex environments. This test apparatus allows the study of the traction force generated between a single ball and a flat disk as a function of speed, contact stress, degree of slip, temperature, lubricant, and material. A schematic of the test apparatus is shown in Figure 108, top. During testing, the ball drive axis is positioned at an angle to the disk to provide a uniform slip velocity (no spin) across the circular area of contact. The ball and disk configuration is shown in more detail in Figure 108, bottom.

For high-temperature testing, the specimens are enclosed in an inner and outer chamber and can be heated to temperatures as high as 816°C (1,500°F). The chamber is heated by electric resistance heating plates located on the top and bottom of the inner chamber. This chamber is constructed from 300-series stainless steel and has close-clearance openings for the disk and ball spindles. The outer chamber is a boxlike structure encompassing the inner chamber. This is used for insulation purposes. Two thermocouples are used to monitor and control the temperature of the heating plates and the test chamber. The temperature reading is displayed on a seven-segment liquid-crystal display mounted on the data acquisition system. This allows accurate control.

The test ball is attached to a drive quill made from a high-tungsten, low-thermal-expansion material (see Figure 108). The quill is mounted by way of a tapered seat fitted into a rigid, high-speed spindle assembly. The spindle is mounted on a pair of dovetail slides and a sine plate so that any desired contact geometry can be established at any disk track radius. This also permits several test runs to be made on each ball and disk specimen. The entire ball drive and positioning system is pivoted about a vertical axis on hydrostatic bearings so that transverse force (traction) at the ball/disk contact can be measured by a restraining load cell. The disk is mounted on a vertically oriented shaft restrained radially by hydrostatic bearings. A servo-actuated deadweight loading system, acting through a lever system, forces the disk upward against the ball.

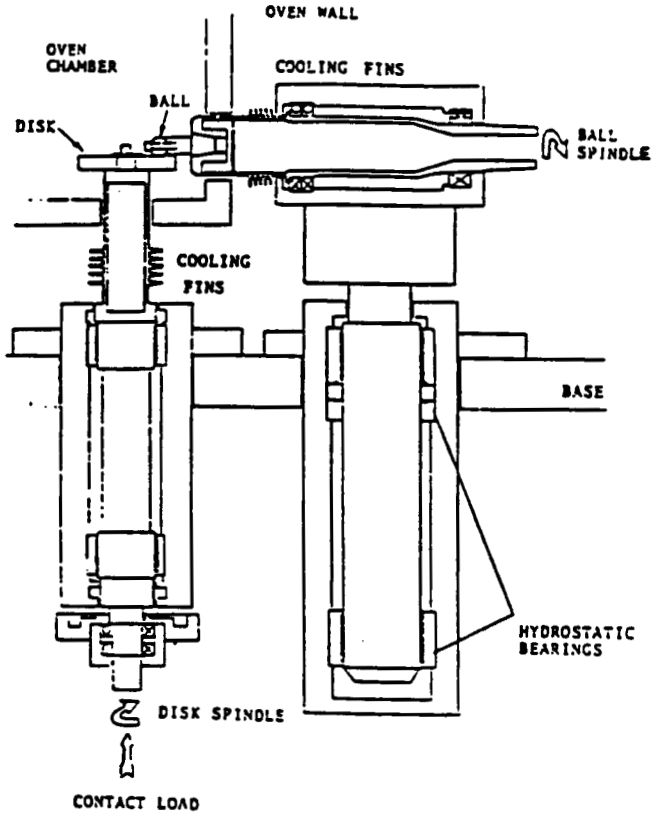

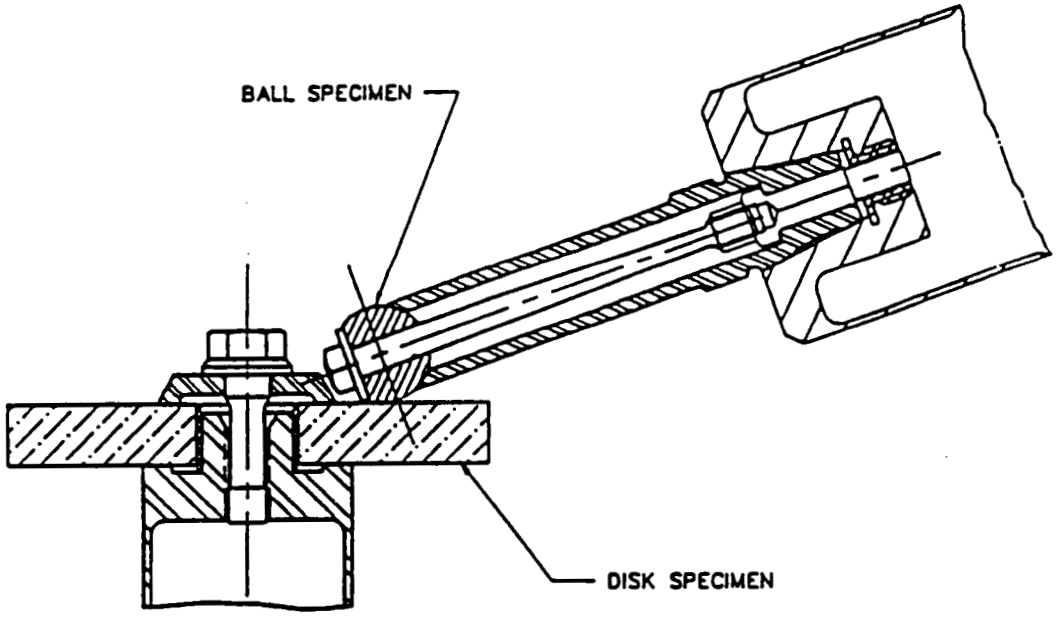

Figure 108. The MRC High-Temperature Traction-Testing Machine and Ball-on-Disk Test Arrangement

The disk and ball shafts are driven by independent motors. The ball shaft is driven by a 2-horsepower, variable-frequency motor allowing a ball shaft speed up to 7,200 rpm. The disk shaft is directly coupled to a 3-horsepower, variable-frequency motor providing speed up to 3,600 rpm. The shaft speeds are measured by multitooth inductive tachometers.

A specially designed and constructed electronic control and data acquisition system is used for the high-temperature traction tester. For real-time monitoring of the traction force and sliding (slip) velocity in the contact, the outputs of the speed sensors are fed into circuits which provide a signal that is proportional to the slide/roll ratio (the difference between ball and disk surface velocities divided by one-half the sum of the surface velocities).

The slide/roll ratio signal and the traction load cell output signal are fed to an X-Y plotter as the X and Y axes, respectively. A real-time plot of traction force versus slip is created and allows the operator to control the input rolling/sliding velocity ratio and monitor traction response.

Traction force versus slide/roll ratio data are collected and analyzed via a microcomputer-based data-acquisition system. The system is built around an IBM PC/XT computer and a Hewlett-Packard 3497A data acquisition/control unit. The voltage output of the traction force load cell as well as the ball and disk rpm are digitally recorded at a rate of two to three signals per second. A computer program (TRACTOR) directs the digital data to a hard-disk file for permanent storage along with a time-of-day stamp.

After a test is concluded, the raw data are processed further by means of computer programs. A program named PROCESS converts the time-of-day stamp into duration of test (in seconds) and the load cell voltage is converted into traction force (in pounds). Further computation is done using program PREPLOT to take into account the geometric conditions of the test hardware to compute linear surface velocities from shaft rotation speeds to determine the slide/roll ratio or percent slip. The slide/roll (ζ) is defined by:

$$\zeta = 2\,(V_D - V_B)/(V_D + V_B)$$

where V_D is the disk surface velocity at the point of contact and V_B is the ball surface velocity. This ratio is positive when the disk surface is moving faster than the ball surface and negative when the disk surface is moving slower than the ball surface.

A final computation is made by program FORCE2TRACTION which converts traction force into a traction coefficient by dividing by the contact load. Both traction force and traction coefficient can be plotted as a function of slide/roll ratio by any of a number of commercially available plotting-software packages.

Test Parameters - The contract for the A.R.T. program specified that three traction tests be performed for each of the following material combinations:

Ball	Disk
M50	M50 with Armoloy TDC coating
M50	M50 NiL
M50	VASCO X2
Silicon nitride	M50 with Armoloy TDC coating
Silicon nitride	M50 NiL
Silicon nitride	VASCO X2

The ball specimens used in the traction testing were fabricated from 13/16-inch-diameter Grade 10 balls. The silicon nitride balls were made of Norton NBD-100 material. The disk test specimens had an outside diameter of 3.75 inches and a thickness of 0.5 inch.

The traction tests were to be performed under stress, temperature, lubrication, and surface-roughness conditions which simulate those of the selected transmission bearing in operation. The bearing selected for this program is a cylindrical-roller bearing (Boeing part number 114DS665, SKF N315VAG) used on the Boeing CH-47C/D helicopter transmission input pinion shaft. All of the traction tests were performed at a maximum Hertz stress of 294,000 psi, which

corresponds to the stress on the heaviest loaded roller under single-engine operation. For the traction tests run with M50 balls, a contact load of 83 pounds produced the desired stress. To keep the same stress level with the ceramic balls, the contact load was reduced to 58 pounds because of the higher effective modulus of elasticity of silicon nitride.

The surface finishes of all the test specimens were measured before testing. The table below provides the surface finishes measured at MRC for the disk specimens using a Taylor-Hobson surface-profile tracing machine:

Surface Finish (microinches)

Disk	Top	Bottom
TDC-coated M50 no. 1	2.60	2.73
TDC-coated M50 no. 2	3.48	3.60
TDC-coated M50 no. 3	2.80	3.24
M50 NiL no. 1	2.16	1.81
M50 NiL no. 2	2.46	2.31
M50 NiL no. 3	1.78	1.87
VASCO X2 no. 1	2.93	2.57
VASCO X2 no. 2	2.47	2.15
VASCO X2 no. 3	3.16	3.16

As indicated, all of the disk specimens had surface finishes less than 4 microinches. All of the ball test specimens had measured surface finishes less than 0.5 microinch.

All of the traction tests were run at a rolling speed (disk peripheral velocity) of 250 inches/second. The temperature of the cylindrical chamber enclosing the ball and disk was controlled to produce a range of lambda (film thickness/composite surface roughness) values representative of engine operation. For reference, the 114DS665 CRB was calculated to have a lambda value of 0.8 at the inner race for typical engine operating conditions (15,000 rpm,

260°F). The lambda values calculated for the ball-on-disk test rig at various traction-test temperatures are summarized below:

Temperature (°F)	Lambda
70	9.71
150	2.71
200	1.53
280	0.80
350	0.51
400	0.39

Mobil Jet II lubricant meeting the MIL-L-23699 specification was drip-fed onto the disk near the ball/disk contact at the rate of approximately one drop per second. This oil drip rate was found to provide ample lubrication at the ball/disk contact resulting in full EHD film formation.

Discussion of Results - Table 28 contains a summary of all 32 traction tests performed to date for the A.R.T. program. For the initial material combination examined (M50 ball/TDC-coated M50 disk), traction testing was performed at a variety of different temperatures ranging from room temperature to 400°F. For the remaining material combinations examined, traction tests were run at room temperature, 280, and 400°F with Mobil Jet II lubricant. The lambda values calculated for these temperatures were approximately 10, 0.8 and 0.4, respectively. For all the material combinations, unlubricated traction tests were also performed at room temperature to assess the friction levels for an oil-off condition.

Appendix E shows plots of traction coefficient as a function of percent slip for each of the tests run. As can be seen from the plots, the traction curves for each test were traced several times from +5 to -5 percent slip (positive slip implies the disk surface is moving faster than the ball surface and negative slip vice versa).

TABLE 28. BOEING A.R.T. TRACTION TESTING SUMMARY

Test	Date	Ball	Disk	Disk side	Track diameter (in.)	Lubricant	Temp (°F)	Initial maximum traction coefficient	Run-in maximum traction coefficient
BART1	4-10-90	M50-1	M50-1 TDC	Top	3.30	Mobil Jet II	70	0.064	0.064
BART2	4-10-90	M50-1	M50-1 TDC	Top	3.30	Mobil Jet II	280	0.054	0.050
BART3	4-10-90	M50-2	M50-1 TDC	Top	3.00	Mobil Jet II	280	0.049	0.046
BART4	4-11-90	M50-3	M50-1 TDC	Top	2.75	Mobil Jet II	200	0.050	0.048
BART5	4-11-90	M50-4	M50-1 TDC	Top	2.50	Mobil Jet Ii	75	0.063	0.063
BART6	4-12-90	M50-5	M50-1 TDC	Top	2.50	Mobil Jet II	150	0.054	0.051
BART7	4-12-90	M50-6	M50-1 TDC	Bot	3.30	None	70	0.610	0.520
BART8	4-12-90	M50-7	M50-1 TDC	Bot	3.00	Mobil Jet II	350	0.064	0.040
BART9	4-16-90	M50-8	M50 NiL-1	Top	3.30	None	70	0.580	0.500
BART10	4-16-90	M50-9	M50 NiL-1	Top	3.00	Mobil Jet II	70	0.063	0.063
BART11	4-16-90	M50-9	M50 NiL-1	Top	2.75	Mobil Jet II	280	0.031	0.029
BART12	4-18-90	M50-4	M50-1 TDC	Bot	2.75	Mobil Jet II	400	0.080	0.036
BART13	4-18-90	M50-9	M50 NiL-1	Top	2.50	Mobil Jet II	400	0.028	0.022
BART14	4-19-90	M50-11	VASCO X2-1	Top	3.30	None	70	0.620	0.550
BART15	4-19-90	M50-10	VASCO X2-1	Top	3.00	Mobil Jet II	70	0.063	0.063
BART16	4-19-90	M50-10	VASCO X2-1	Top	2.75	Mobil Jet II	280	0.047	0.044
BART17	4-19-90	M50-10	VASCO X2-1	Top	2.50	Mobil Jet II	400	0.066	0.045
BART18	4-20-90	C1	M50-2 TDC	Top	3.30	None	70	0.550	0.410
BART19	4-20-90	C2	M50-2 TDC	Top	3.00	Mobil Jet II	70	0.064	0.064
BART20	4-20-90	C2	M50-2 TDC	Top	2.75	Mobil Jet II	280	0.077	0.031
BART21	4-20-90	C2	M50-2 TDC	Top	2.50	Mobil Jet II	400	0.091	0.026
BART22	4-21-90	C3	M50 NiL-2	Top	3.30	None	70	0.490	0.400
BART23	4-21-90	C4	M50 NiL-2	Top	3.00	Mobil Jet II	70	0.063	0.063
BART24	4-21-90	C4	M50 NIL-2	Top	2.75	Mobil Jet II	280	0.035	0.033
BART25	4-21-90	C4	M50 NiL-2	Top	2.50	Mobil Jet II	400	0.051	0.021
BART26	4-23-90	C5	VASCO X2-2	Top	3.30	None	70	0.500	0.470
BART27	4-23-90	C6	VASCO X2-2	Top	3.00	Mobil Jet II	70	0.063	0.063
BART28	4-23-90	C6	VASCO X2-2	Top	2.75	Mobil Jet II	280	0.040	0.037
BART29	4-23-90	C6	VASCO X2-2	Top	2.50	Mobil Jet II	400	0.063	0.025
BART30	2-7-91	C7	M50 NiL-3	Top	3.00	DOD-L-85734	70	0.059	0.059
BART31	2-8-91	C7	M50 NiL-3	Top	2.75	DOD-L-85734	280	0.032	0.032
BART32	2-8-91	C7	M50 NiL-3	Top	2.50	DOD-L-85734	400	0.030	0.029

For the room-temperature lubricated tests, the traction curves for all material combinations are virtually identical. This is as one would expect, because at room temperature the oil film formed is thick enough to ensure that there is virtually no contact of the ball and disk surfaces. Good repeatability of the traction test rig is therefore demonstrated by these results.

The lubricated traction test run at temperatures of 280°F or higher exhibit a run-in effect. The friction coefficients observed during the first traction curve trace are higher than those of subsequent traces. This run-in effect becomes more pronounced with increasing temperature.

Table 29 summarizes the maximum friction coefficients measured after run-in for the various material combinations evaluated under the test conditions common to all.

In nearly all cases tested, the traction coefficient decreased with increasing temperature. Figure 109 illustrates this trend for M50 ball/TDC-coated M50 disk combination for which the most complete set of traction versus temperature data was obtained. The values plotted represent the maximum friction coefficients measured after run-in effects. As can be seen from Figure 109, the maximum friction coefficient consistently decreases with increasing temperature. The only exception to this trend noted in the data of Table 28 is for the M50 ball/VASCO X2 disk combination, where the maximum friction coefficient increased very slightly from 280°F (0.044) to 400°F (0.045).

The trend of decreasing friction coefficient with increasing temperature was not anticipated before the actual testing. It was expected that as the temperature increased, the EHD film thickness would decrease, resulting in lower lambda values and consequently more surface asperity contact and higher friction coefficients. However, since this same trend has been observed for Mobil Jet II lubricant by Tevaarwerk in Reference 27 and for Mobil RL-714 lubricant in Reference 28, it is believed that this effect is real.

TABLE 29. MAXIMUM FRICTION COEFFICIENTS IN BOEING A.R.T. TRACTION TESTING

Materials ball/disk	Unlubricated	Lubricated		
		70°F	280°F	400°F
M50 / M50 + TDC	0.52	0.064	0.046	0.036
M50 / M50 NiL	0.50	0.063	0.029	0.022
M50 / VASCO X2	0.55	0.063	0.044	0.045
Si3N4 / M50 + TDC	0.41	0.064	0.031	0.026
Si3N4 / M50 NiL	0.40	0.063	0.033	0.021
Si3N4 / VASCO X2	0.47	0.063	0.037	0.025

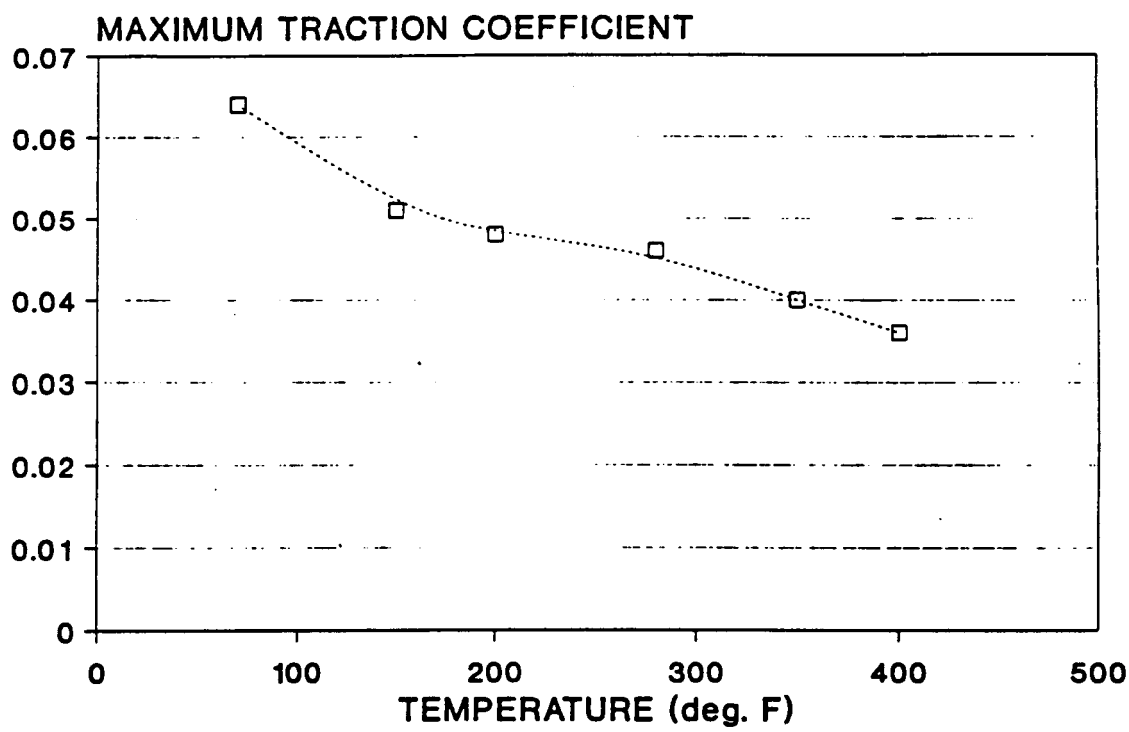

Figure 109. Peak Traction Coefficient Versus Temperature for M50 Ball/TDC-Coated M50 Disk

In the lubricated tests, the lowest maximum friction coefficient measured was 0.021 for the ceramic ball/M50 NiL disk combination at 400°F. Of the three disk materials tested, M50 NiL produced the lowest friction coefficient in all but one case; with the ceramic ball at 280°F, TDC-coated M50 had a slightly lower friction coefficient (0.031 versus 0.033). The relative ranking of TDC-coated M50 and VASCO X2 with respect to friction was not consistent; it varied with the ball material and the temperature. The friction coefficients measured for the three disk materials were lower with the ceramic ball than the M50 ball in all but one case: M50 NiL disk at 280°F.

The traction coefficients measured in the unlubricated test were generally an order of magnitude higher than observed for the lubricated tests. The highest maximum traction coefficient observed after run-in was 0.55 for the M50 ball/VASCO X2 disk, while the lowest was 0.40 for the ceramic ball/M50 NiL disk. The unlubricated traction coefficients were lower for all three disk materials with the ceramic ball. The ranking of the disk materials from lowest traction coefficient to highest was consistent for both ball materials in the unlubricated tests: M50 NiL, TDC-coated M50, and VASCO X2, although the magnitude differences were not large.

Three additional ball-on-disk friction tests were performed with DOD-L-85734 lubricant, which is an improved version of MIL-L-23699 that will be used for all Boeing A.R.T. testing. The friction tests were performed with a silicon nitride ball and an M50 NiL disk at three different temperatures (70, 280, and 400°F). The resulting traction-versus-slip curves are included in Appendix E and are quite similar to those obtained previously with the MIL-L-23699 lubricant. The table below lists the maximum friction coefficients recorded with the two different lubricants. The data indicate that the DOD-L-85734 lubricant results in a slightly lower friction coefficient at room temperature and a higher friction coefficient at 400°F.

Maximum Friction Coefficient

Temperature (°F)	MIL-L-23699	DOD-L-85734
70	0.063	0.059
280	0.033	0.032
400	0.021	0.029

Summary and Conclusions - A total of 32 traction tests were performed involving two different ball materials (M50 and silicon nitride) and three different disk materials (Armoloy TDC-coated M50, M50 NiL, and VASCO X2). The traction tests were performed under stress, temperature, lubrication, and surface-roughness conditions which simulate those of a selected cylindrical-roller bearing (Boeing part number 114DS665, SKF N315VAG) used on the CH-47C/D helicopter transmission input pinion shaft. The traction tests covered the temperature range from 70°F to 400°F. The first 29 traction tests were performed with Mobil Jet II oil meeting the MIL-L-23699 specification; the last three tests were performed with DOD-L-85734 oil. Unlubricated traction tests were also run for the material combinations at room temperature. For each test, a plot of traction coefficient versus percent slip was generated.

The following conclusions and observations were made based on the traction test results:

- M50 NiL provided the lowest friction of the three disk materials tested. The relative ranking of the other two disk materials with respect to friction varied with the test conditions.

- The friction coefficients were generally lower with the ceramic ball than with the M50 ball.

- At room temperature (lambda of approximately 10), the lubricated traction curves were virtually identical for all the material combinations tested.

- Friction coefficients generally decreased with increasing temperature in spite of the lower calculated lambda values.

- A run-in phenomenon was observed at elevated temperatures resulting in the highest friction coefficients occurring during the first trace of the traction curve.

- In the unlubricated tests, the peak friction coefficients were an order of magnitude higher than those observed with oil lubrication. The friction coefficients were lower with the ceramic ball than the M50 ball. M50 NiL provided the lowest unlubricated friction, followed in turn by TDC-coated M50 and VASCO X2.

- Use of the DOD-L-85734 lubricant resulted in a slightly lower friction coefficient at room temperature and a slightly higher friction coefficient at 400°F than MIL-L-23699 lubricant.

TRANSMISSION LUBRICATION STUDY WITH HYBRID BEARINGS

Hybrid (ceramic) rolling-element bearings have the potential for great improvement in bearing performance for future transmissions. These benefits include longer fatigue life, good performance under marginal lubrication, and reduced weight (approximately 22 percent per bearing). Rolling-element centrifugal loads can be reduced significantly by simply changing from steel to ceramic; for very high-speed bearings, this can yield a major improvement in bearing fatigue life.

A hybrid ceramic bearing is a combination of ceramic rolling elements with metallic races. The silicon nitride (Si_3N_4) material (ceramic) which is used to fabricate rolling elements (balls or rollers) has basic properties as shown in Table 30. The basic properties of Si_3N_4 are greatly different from those of bearing steels and therefore it is important to understand the impact of rolling elements made from this material. Some of the key factors to be considered are described in the following paragraphs.

Density

The density of silicon nitride is 40 percent of that of bearing steels. This low density significantly reduces the centrifugal forces of the rolling elements on the outer ring in high-speed operations. Since the rolling-element centrifugal loading is directly proportional to its weight, using Si_3N_4 rolling elements offers the potential for significant improvement in high-speed bearing performance. The low density results in an average weight reduction of approximately 22 percent for each bearing.

TABLE 30. PROPERTIES OF AN ADVANCED SILICON NITRIDE CERAMIC BEARING MATERIAL

Property of Si_3N_4	SAE units	Metric units
Density	0.117 lb/in.^{3}	3.2 gm/cm^3
Hardness	HV_{10kg} 1,700 (HRC 78)	
Elastic modulus	46 x 10^6 psi	320 GPa
4-point bend strength, mean	116,000 psi	800 MPa
Weibull modulus	9.7	9.7
Hertz compressive strength	4,060,000 psi	28 GPa
Fracture toughness	3,700 psi-in.$^{1/2}$	4.1 MPa-m$^{1/2}$
Poisson's ratio	0.26	0.26
Temperature capability	1,800°F	1,000°C
Thermal expansion coefficient		
-274 to 68°F (-170 to 20°C)	0.24 x 10^{-6}/°F	0.43 x 10^{-6}/°C
68 to 932°F (20 to 500°C)	1.24 x 10^{-6}/°F	2.23 x 10^{-6}/°C
68 to 1,832°F (20 to 1,000°C)	1.61 x 10^{-6}/°F	2.9 x 10^{-6}/°C
Thermal conductivity		
(100°C)	203 W/m-K	29.3 Btu-in./ft^2-h-°F
(500°C)	147 W/m-K	21.3 Btu-in./ft^2-h-°F
(1,000°C)	107 W/m-K	15.5 Btu-in./ft^2-h-°F

Hardness

The hardness of Si_3N_4 is so high that it cannot be measured on the common Rockwell C scale. Silicon nitride is about twice as hard as bearing steels when compared using microhardness scales. High hardness improves wear resistance, which reduces the damaging effects of repeated surface contacts.

Elastic Modulus

The elastic modulus of Si_3N_4 is about 50 percent greater than that for steel. This results in smaller ball-to-race contact footprints and therefore higher contact stresses. This is a particular problem for hybrid bearings where the load capacity is limited by the lower compressive strength of the steel races. Caution must be exercised when using ceramic hybrid bearings in heavily loaded applications. The calculated static load capacity of a ball bearing is reduced by about 40 percent when steel balls are replaced with ceramic balls and no other design changes are made. When necessary, this effect can be compensated for by using raceways with tighter ball conformance.

Tensile Strength

The tensile strength of Si_3N_4 is low compared to other structural materials and a fraction of the strength of bearing steels. It is important to minimize the tensile stresses on ceramic components.

Hertz Compressive Strength

The Hertz compressive strength of Si_3N_4 is much higher than that of conventional bearing materials, resulting in very high load capacities for full ceramic bearings. (The load capacity of hybrid bearings is limited by the steel races.)

Fracture Toughness

The fracture toughness of Si_3N_4 is significantly less than that of M50 bearing steel, meaning Si_3N_4 is much less resistant to brittle failure than M50.

Temperature Capability

Si_3N_4 can operate to temperatures of about 1,800°F. The more common high-temperature bearing materials like M50 and BG42 begin to lose hardness and performance after prolonged exposure to temperatures above 800°F.

Thermal Expansion

Si_3N_4 expands at about 20 percent of the rate of most materials used for shafts and housings.

Corrosion Resistance

Si_3N_4 is virtually chemically inert, a dramatic improvement over conventional materials.

Fatigue Life

The rolling-contact fatigue life of high-quality Si_3N_4 is superior to even the best bearing steels. Rolling-contact fatigue tests run at high contact stresses show Si_3N_4 fatigue lives at least ten times better than M50. One of the major advantages of Si_3N_4 over other ceramics is that in fatigue it fails by spalling, similar to steel, while other ceramics fail catastrophically.

The fatigue life of a ceramic hybrid bearing is generally limited by the metallic races. The stress on the metallic race may be higher with ceramic rolling elements due to the smaller

contact footprint, thereby reducing the bearing fatigue life. In most applications, the rolling-contact fatigue life will be reduced by converting to a ceramic hybrid bearing.

Fabrication and Testing

A comparison of ceramic and steel properties is shown in Table 31. The one concern not addressed above is the nonmagnetic property of ceramic. This could result in the development of new methods for detecting bearing failures. Currently, magnetic plugs are used to detect particles generated by a bearing fatigue failure.

The main reason for using hybrid bearings in the A.R.T. transmission was primarily to take advantage of the potential of operating these bearings at reduced oil flow rates and therefore reduce the lubrication system weight.

The hybrid bearing concept was tested in a CH-47 engine transmission and compared with test data from standard bearing operation. Extensive testing was conducted to evaluate the hybrid bearings over a wide range of operating conditions. Included in these tests was the reduction in oil supply, the use of three types of lubricants with different viscosities, and the determination of heat-generation rates.

A complete set of hybrid bearings was designed to replace two cylindrical-roller and one ball thrust bearing on the CH-47 engine transmission input pinion. The large cylindrical-roller bearing was designed and fabricated under the MRC program described earlier. The basic parameters for this bearing are summarized in Table 32. This bearing incorporated the low traction properties of M50-NiL and NBD100 silicon nitride rollers. A photograph of the final assembly of this hybrid bearing is shown in Figure 110.

In addition to this bearing, the outboard bearing was also fabricated with silicon nitride rollers. This bearing was fabricated by Split Ballbearing as shown in Figure 111. To complete the input

TABLE 31. COMPARISON OF CERAMIC AND STEEL PROPERTIES

Property	Si_3N_4	Bearing steels
Density	0.117 lb/in.^{3}	0.28 lb/in.^{3}
Hardness	HV_{10kg} 1,700 HRC 78	HV_{10kg}655-763* HRC 58-63*
Elastic modulus	45 x 10^6 psi	29 x 10^6 psi
Temperature capability	1,800°F	350-1,000°F*
Corrosion resistance	Excellent	Poor
Magnetism	Nonmagnetic	Ferromagnetic

* Depends on specific material

TABLE 32. HYBRID CYLINDRICAL-ROLLER BEARING

Bearing designation:	MR315C2
Application:	CH-47C/D engine transmission input pinion
Materials:	Inner ring - M50 NiL steel (carburized) Outer ring - M50 steel Rollers - NBD 100 silicon nitride Cage - silver-plated AMS 6414 steel
Basic geometry:	Number of rollers = 12 Roller diameter = 25 mm Clearance = 0.0635-0.0672 mm (0.0025-0.0030 in.) Bore diameter = 75 mm (2.9528 in.) Outer diameter = 160 mm (6.2992 in.) Pitch diameter = 119 mm (4.685 in.)
Design features:	One-piece machined inner land riding cage Two-point out-of-round outer ring

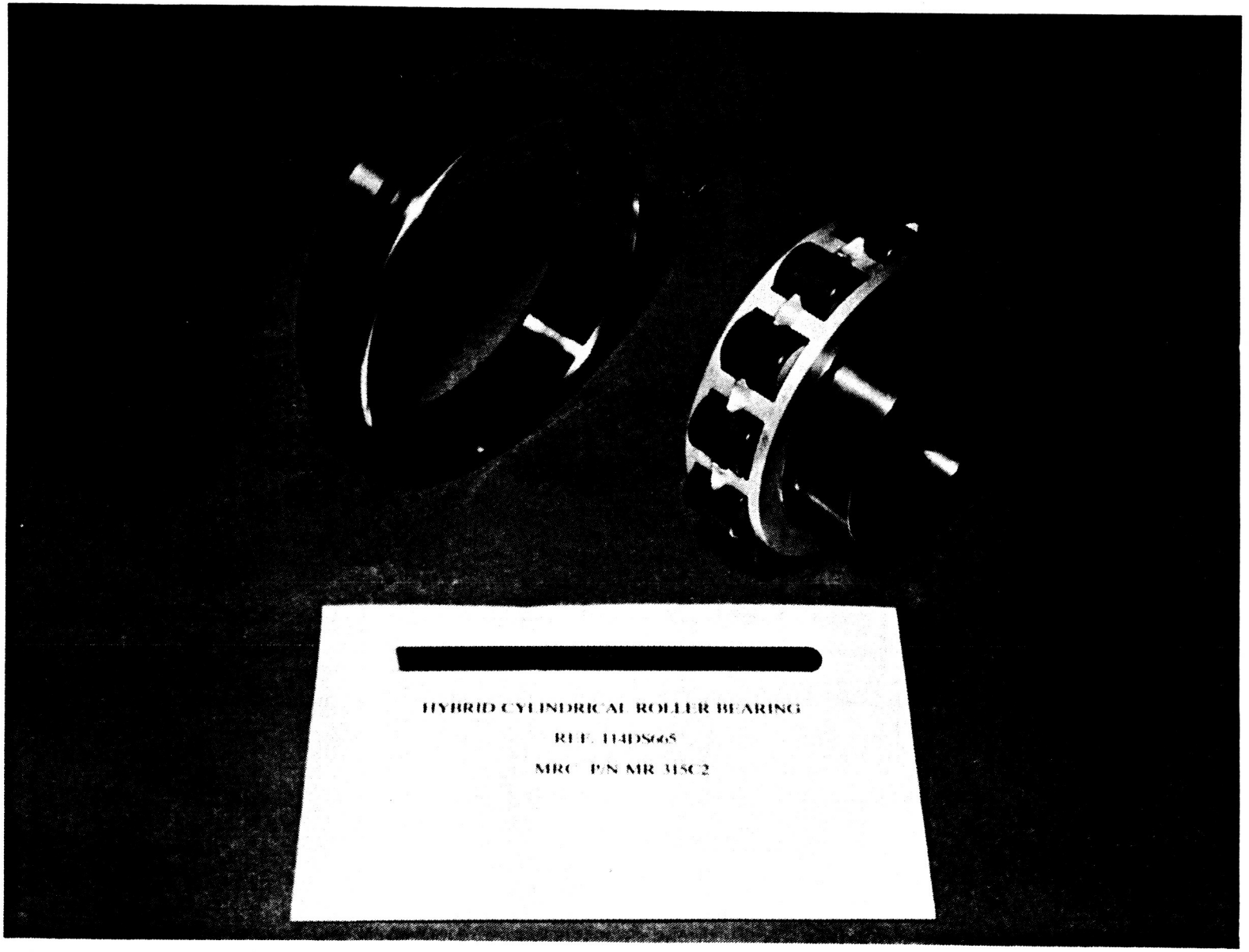

Figure 110. Hybrid Cylindrical-Roller Bearing MR315C2

C132329

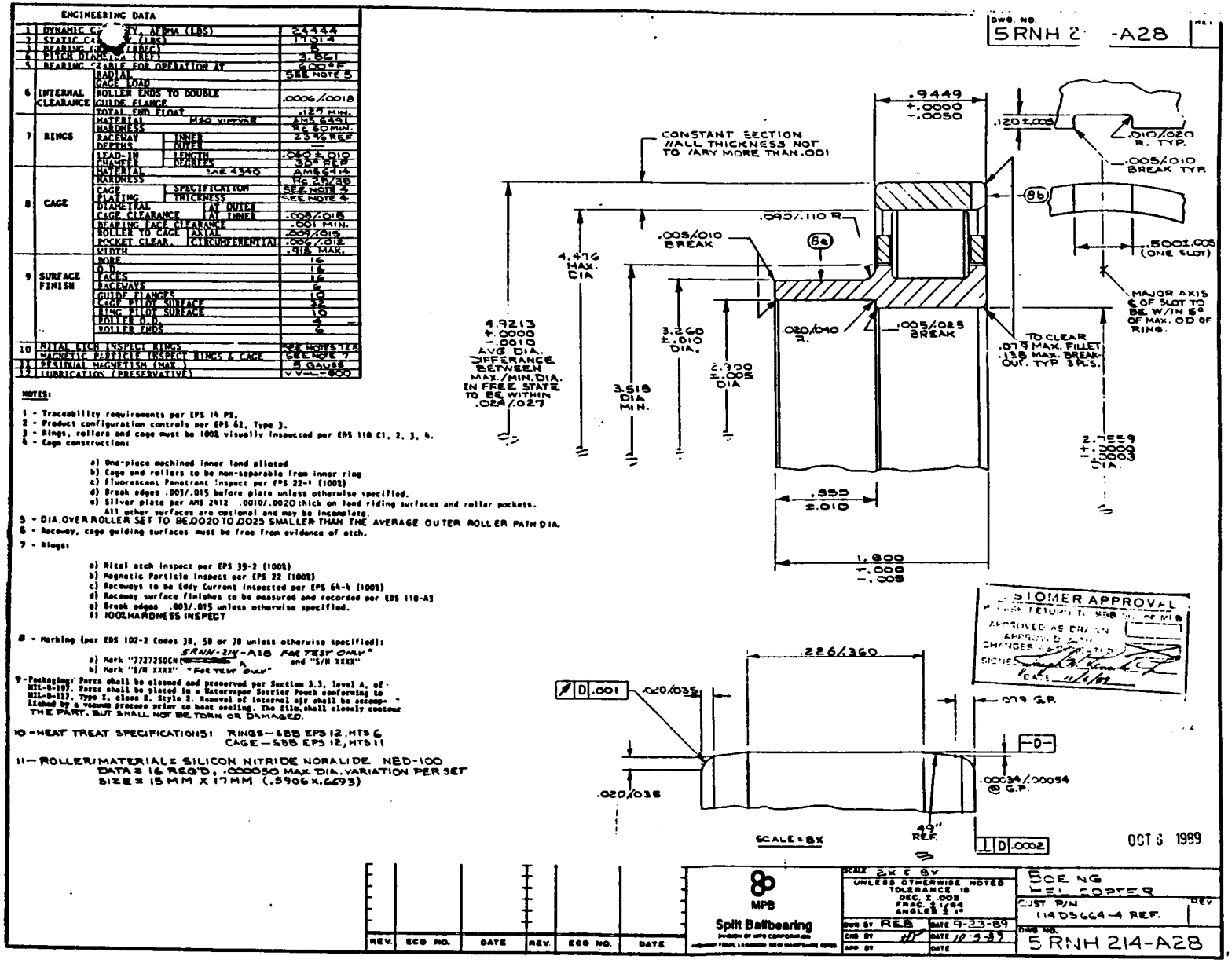

Figure 111. Hybrid Outboard Cylindrical-Roller Bearing 5RNH214-A28 Manufactured by Split Ballbearing

pinion bearings, the ball thrust bearing was also designed as a hybrid. In addition to the ceramic balls, the races were thin dense chrome-plated (TDC) and an added coating of Dicronite was applied. These coatings were added in an attempt to extend the oil-off operations of the ball thrust bearing; this configuration is shown in Figure 112. Finally, a second ball thrust bearing was designed as a full-complement hybrid bearing. This design eliminated the retainer and added two additional balls (Figure 113). This configuration resulted in a higher capacity and lighter weight. The main concern was the ability of a full-complement ball thrust bearing to operate at very high speeds (15,000 rpm or 1.05×10^6 DN). The complete assembly of the three bearings and the input pinion is shown in Figure 114.

The testing of the hybrid bearings was conducted in an instrumented CH-47 engine transmission as shown in Figure 115. This transmission operates at an input speed of 15,066 rpm at a maximum power of 4,600 hp. All bearings in this transmission were thermocoupled to record operating temperatures, along with oil inlet and outlet temperatures. The test parameters that were varied included torque and oil flow. In addition to the hybrid bearings, tests were also conducted on the standard bearing design in order to compare performance differences.

The basic test program was established to evaluate several parameters that determine the lubrication requirements of a high-speed bearing assembly. These parameters were as follows:

- Standard versus hybrid design
- Oil flow versus torque
- Type of lubricant.

The selection of the type of lubricant used in a transmission is very important. The lubricant must possess properties that develop high oil films (high viscosity) while minimizing the power loss due to churning and viscous shear (low viscosity). The oil must also have properties to maintain the durability of the gear teeth under high contact pressure and sliding velocity (high Ryder gear rating) and provide adequate oil film thickness to ensure good bearing fatigue life.

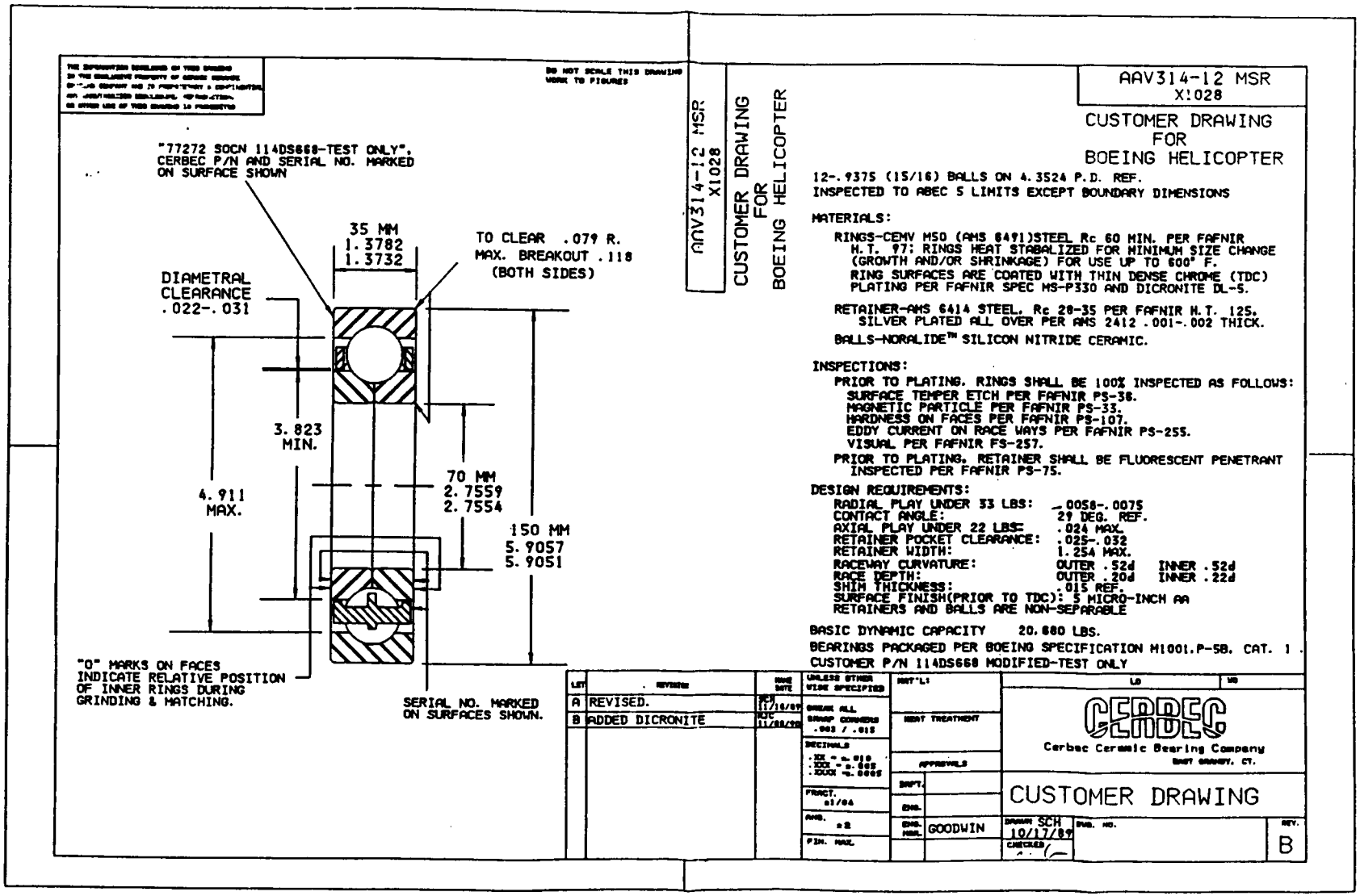

Figure 112. Hybrid Ball Thrust Bearing AAV314-12 MSR X1028 Manufactured by CERBEC

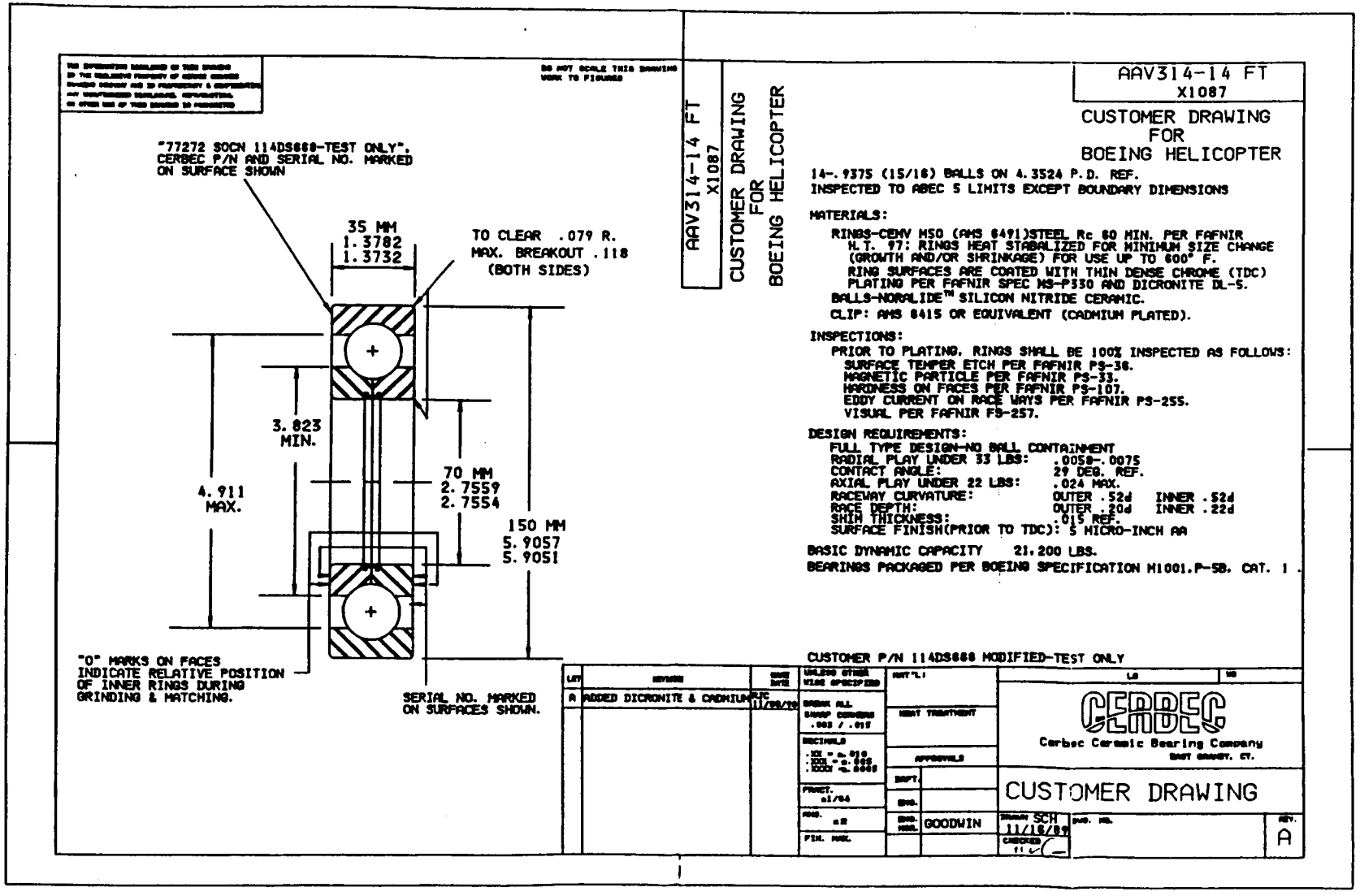

Figure 113. Full-Complement Hybrid Ball Thrust Bearing AAV314-14 FT X1087 Manufactured by CERBEC

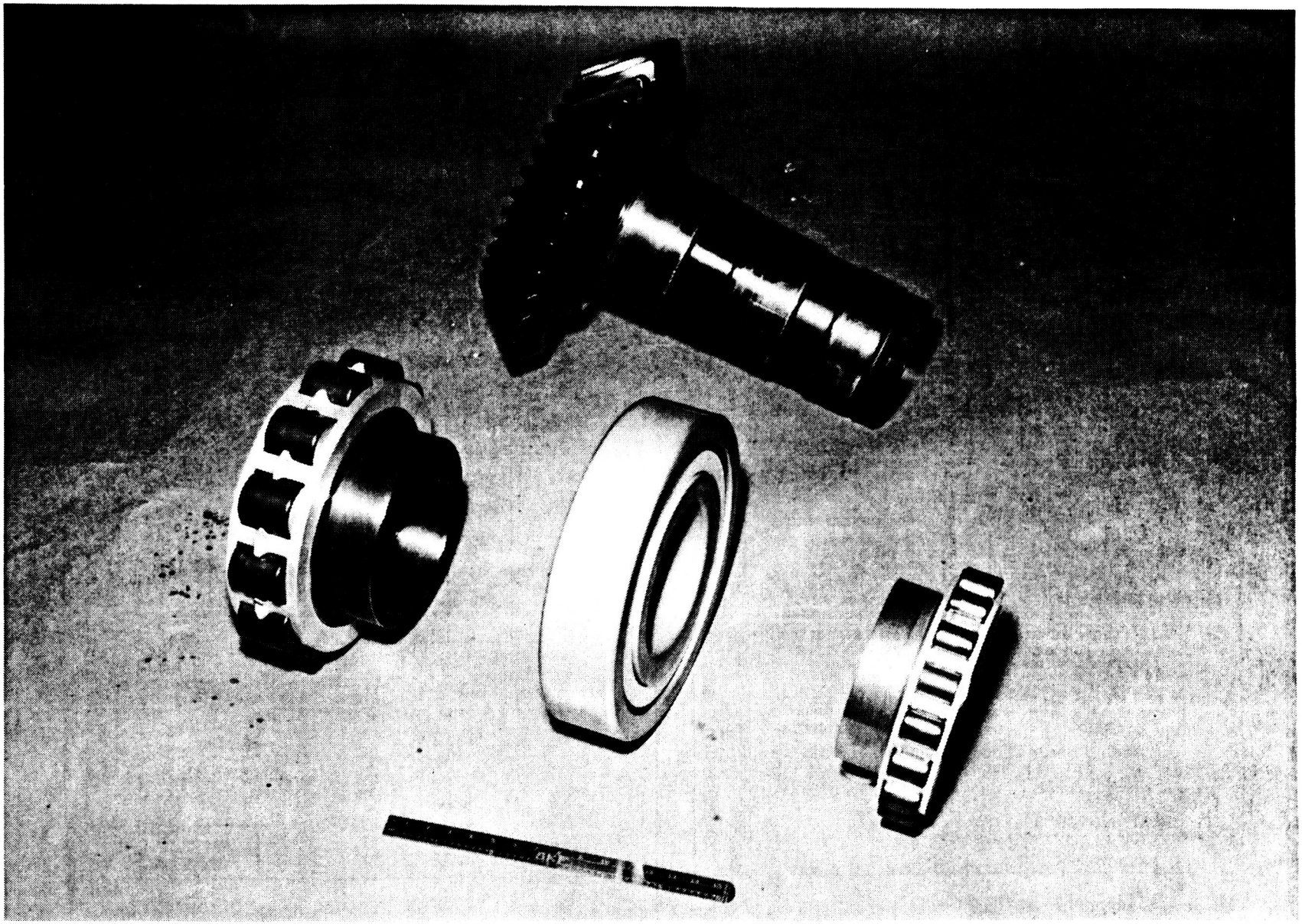

C132330

Figure 114. Input Pinion With Three Test Bearings

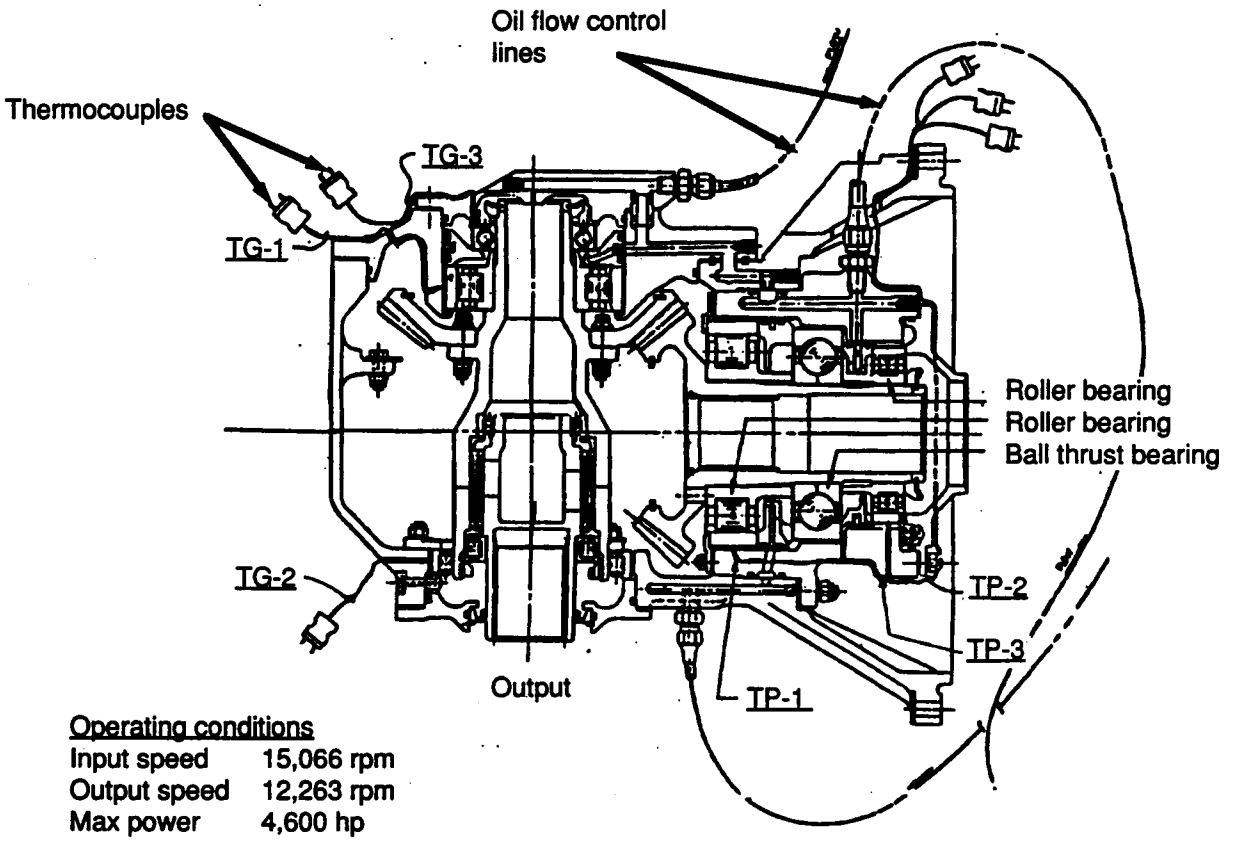

Figure 115. Test Transmission and Instrumentation

During a search of available lubricants, three lubricants were selected based upon their use in transmission applications. The three lubricants and several basic properties of each are shown in Table 33. The oils range from a low viscosity of 3.4 cSt to a high of 7.75 Cst at 210°F. The three oils are approximately 50-percent different in their viscosities. Also, the Ryder gear ratings for these oils range from 2,200 to 4,000 lb/in. These oils provide the desired range of properties that were required for the program.

Oil flow requirements for the bearings in a transmission are usually determined by minimum orifice size and not by required flow. Therefore, most bearings receive more oil than is required to maintain thermal stability. In addition, if the operating temperature limits for bearings could be increased from the current limit of approximately 300°F to 350 or 400°F, the oil system capacity could be reduced significantly by reducing oil flow to all bearings. The purpose of this test was to determine how low the oil flow could be reduced and still maintain stable operating temperatures on all bearings. For this program, the oil flow was reduced by decreasing the oil pressure to the oil lubricators within the existing transmission. Oil flow and torque were varied to determine the bearing outer race operating temperature. The results of one series of tests at a constant oil flow for a ball and roller bearing are shown in Figures 116 and 117.

Finally, the test program was repeated for the same parameters except that the standard ball and roller bearings were replaced with hybrid ball and roller bearings on the input pinion shaft. Based upon earlier traction test data, it was expected that the internal friction losses would be lower, resulting in lower bearing operating temperatures. By repeating the same factors of type of lubricant, oil flow, and torque, the effect of the hybrid design would be evaluated. The results of these tests for the hybrid bearing designs are shown as the dotted lines on Figures 116 and 117. A review of these data indicates that the hybrid ball and roller bearings operated at lower outer race temperatures than a standard bearing under the same operating conditions. The only exception appears to be at the very low torque range (less than 5,000 in.-lb) for the DOD-L-85734 and ETO 274 oils; at these points, it appears that the hybrid bearing temperatures were

TABLE 33. OILS TESTED

Oil	Viscosity at 210°F (cSt)	Ryder gear rating (lb/in.)
MIL-L-7808	3.4	~2,200
DOD-L-85734	5.3	4,000
ETO 274	7.75	3,200

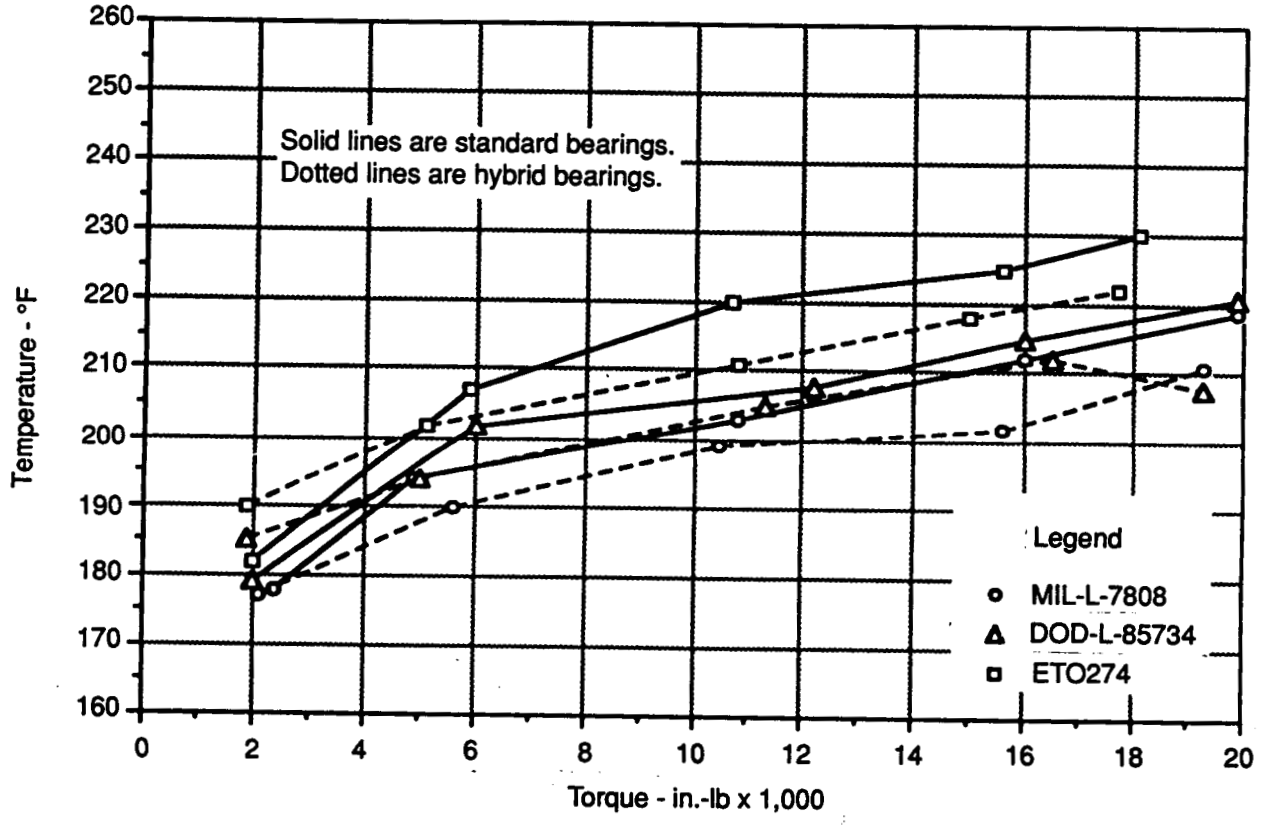

Figure 116. Comparison of Different Oils With Standard and Hybrid Ball Thrust Bearings

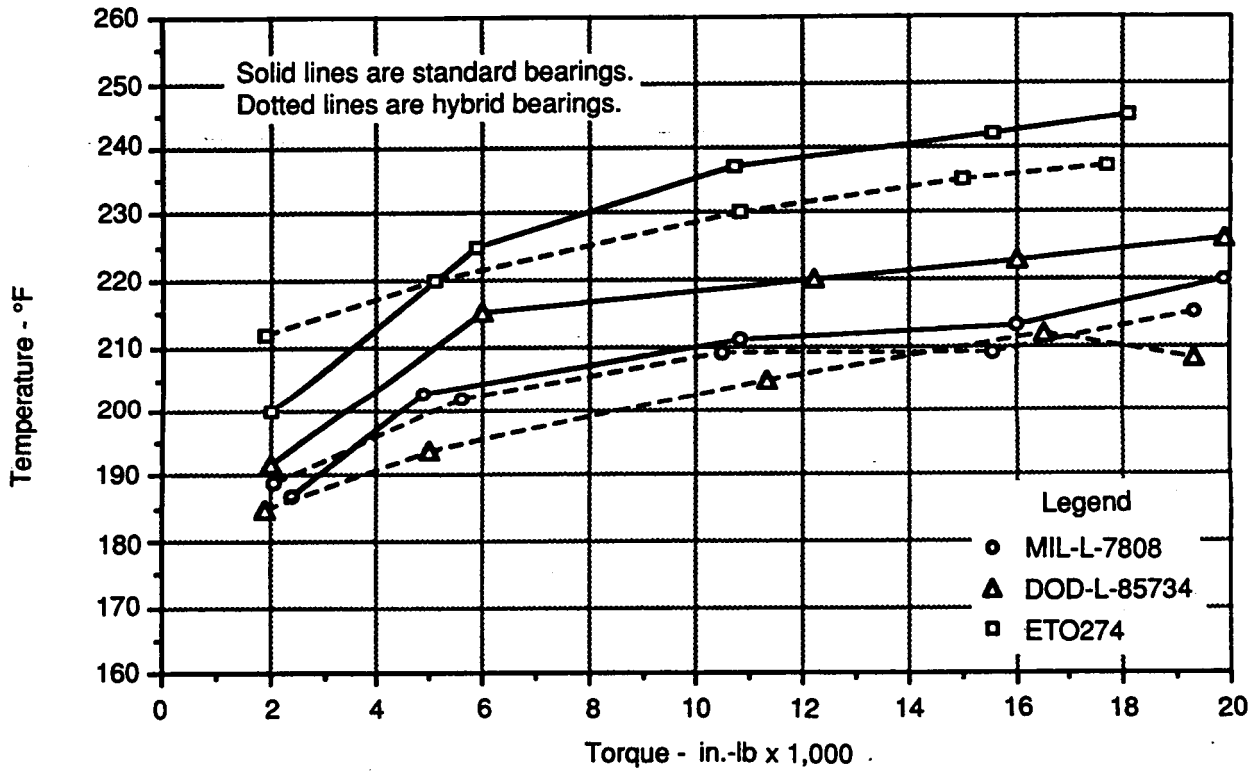

Figure 117. Comparison of Different Oils With Standard and Hybrid Roller Bearings

slightly higher than the standard bearings. This could be the result of increased skidding as predicted by the MRC analysis of the hybrid roller bearing under light loading.

The final test conducted under this task was the evaluation of the loss-of-oil performance of hybrid bearings. This test was conducted on the CH-47 engine transmission and was initially planned to cut the oil supply to only the input pinion bearings and determine the time to thermal seizure. After many tries and reduction in oil supply to the output gear bearings, clutch, and gear mesh, it became apparent that small quantities of oil in the system are sufficient to maintain thermal stability. In most cases, bearing temperatures in excess of 450°F were achieved and stable operation continued. With the use of high-temperature bearing and gear steels (M50 and VASCO-X2), these operating conditions could be maintained for some time. Long-term operation at these conditions will result in surface distress and eventually bearing and gear failure.

To perform the oil-off test, the total oil supply to the entire gearbox was cut off to obtain a failure of the ball thrust bearing on the input pinion. The temperature plot for this test is shown in Figure 118. A very gradual rise in temperature was noted until approximately 8.5 minutes into the run, when both a change in sound and a sharp rise in bearing temperature occurred. The test was stopped at this point and the bearings were inspected. The primary failure was the ball thrust bearing on the input pinion (Figure 119).

This same test was repeated with hybrid bearings on the input pinion. The results of this test were not as expected and ended in a failure after only 3.5 minutes, as shown in Figure 120. A review of the bearings showed that the ball thrust bearing was the primary failure (Figure 121). Inspection of the bearing indicated that the ceramic balls were in very good condition but the inner raceway was severely worn. The failure mechanism was slightly different than the welding that occurred when using steel balls and raceways. The cause of the relatively short running time could not be determined. The only possible cause could be the use of new hardware used in this transmission to replace all parts that were damaged during the first oil-off

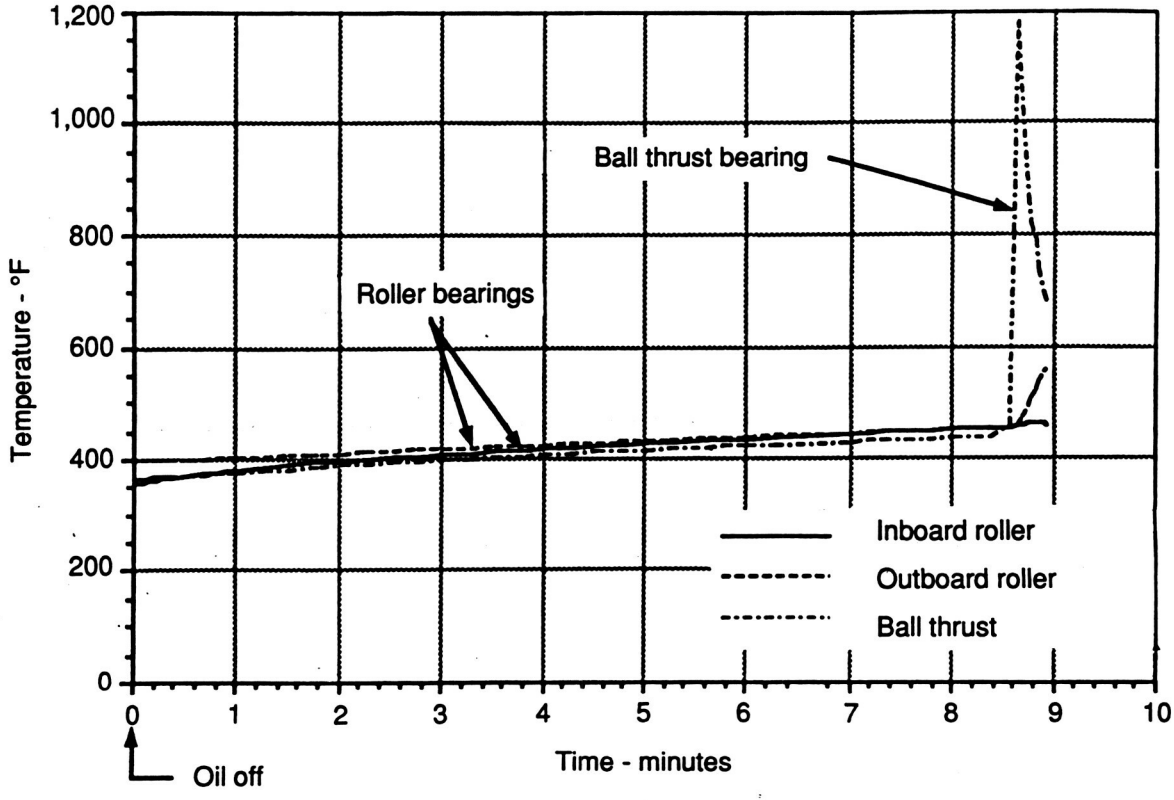

Figure 118. Oil-Off Test of Standard Ball and Roller Bearings

C135824

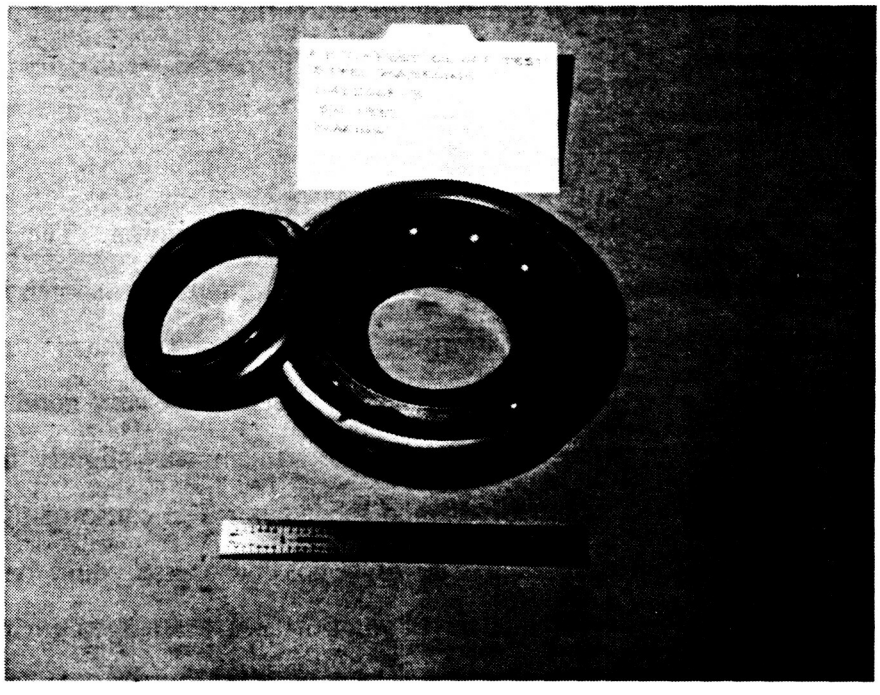

Figure 119. Failed Input Pinion Standard Ball Thrust Bearing From Oil-Off Test

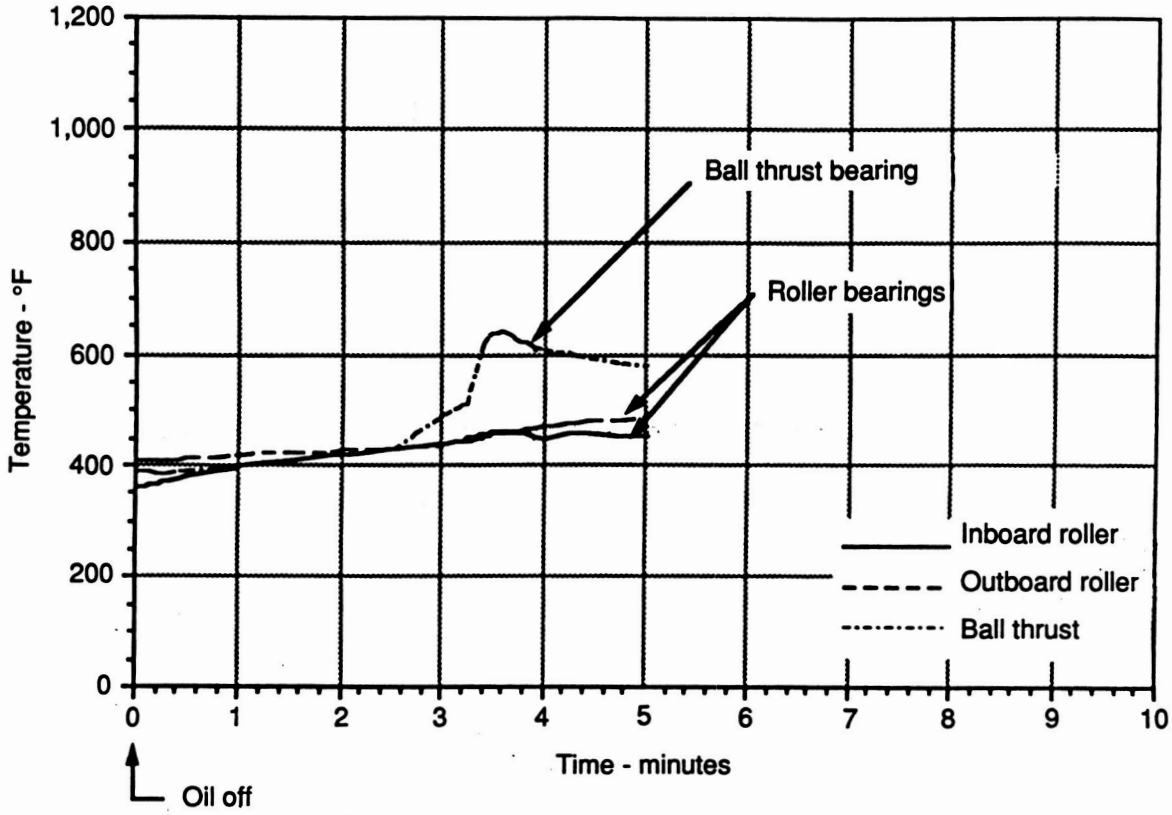

Figure 120. Oil-Off Test of Hybrid Ball and Roller Bearings

C135807

Figure 121. Failed Input Pinion Hybrid Ball Thrust Bearing From Oil-Off Test

test. Although this test was not very successful, it is still expected that hybrid bearings should improve the performance of bearings during oil-off testing. Other tests conducted by other sources have indicated significant improvement during oil-off operation.

In summary, hybrid bearing test results indicate that good marginal lube performance and reduced friction can be achieved. Temperature data were generated for both hybrid ball and roller bearings and compared to standard steel bearings for three different lubricants and at various loads. Generally, the hybrid bearings operated at lower temperatures except for the very low load conditions. Under these very low loads, hybrid bearings appear to have higher skidding which could result in the slightly higher temperatures. Similar tests were conducted for reduced oil flow rates and resulted in similar data. These tests indicated that a reduction in the lubrication flow rates to all bearings is achievable when using hybrid bearing designs. In combination with lighter weight, longer fatigue life, and corrosion resistance, it is expected that the use of hybrid bearings can make a significant impact toward achieving the design goals of the advanced rotorcraft transmission.

PRECISION NEAR-NET-FORGED SPUR GEARS

Precision, near-net-shape forging of helicopter gears offers several advantages in the design of advanced rotorcraft transmissions because this process has shown the potential for:

1. Reducing machining, material, and energy requirements
2. Increasing fatigue life
3. Improving the tooth-bending endurance limit.

These potential benefits are expected to contribute directly to reducing weight and extending service life of the A.R.T. gears.

The key to successful precision forging is the design and manufacture of the forging dies to precise dimensions. Corrections must be built into the forging dies to accommodate the distortions and thermal changes that occur during the forging process. The process developed by the Eaton Corporation results in the final forged gear being within several thousandths of an inch of the predicted value and final machining dimensions. This process produces a forged gear blank that is equivalent to a rough-machined gear before final grind. This is achieved without any machining and could be a significant cost reduction in the machining cost of helicopter gears.

The Manufacturing Technologies Center of Eaton Corporation was selected by Boeing to produce spur gears for testing in the advanced rotorcraft transmission program. The production of the spur gears, with 32 teeth and a 6-inch pitch diameter, was accomplished in two phases. Phase I involved the forging and finishing of five near-net forged spur gears and five conventionally forged nontooth spur gear blanks. These gears were made out of VASCO X2M steel. Phase II involved the forging and finishing of five near-net spur gears made from a modified VASCO X2M steel containing between 2.0 and 2.5-percent Ni.

The gears were forged at Eaton's Forge Division in Marion, Ohio. The gears were then finish-machined and heat-treated by outside vendors (Summit Gear/Kurt Manufacturing and Litton Industries).

The Phase I gears were forged in November 1989. They were sent to Summit Gear in January 1990 and the finished gears were sent to Boeing in August 1990. The Phase II gears were forged in August 1990 and the finished gears were sent to Boeing in December 1991.

The following tasks will be used to describe the production process used in making these spur gears.

The process of making a spur gear, near-net or conventional, includes:

1. Design of the involute profile of the finished gear tooth
2. For a near-net gear, modify this profile for the forging punch and die
3. Generate the necessary tooling drawings
4. Produce the required tools
5. Inspect tooling
6. Calculate billet dimensions
7. Produce the required number of billets
8. For forging operation, heat the billets, upset-preform, and finish-forge
9. Heat-treat the forgings
10. Rough-machine the forgings
11. Final machining, grinding, and heat-treating of the forgings
12. Final inspection of the finished gears.

The following is a detailed description of the pertinent processes.

Process Development

Eaton's computer program GearDi was used to calculate and plot the coordinate points for the involute profile of the finished spur gear, as shown in Figure 122 and in Appendix F. The finished spur gear tooth data came from drawing number SK32174 as supplied by Boeing. This profile was then merged into Eaton's CAD system to produce the required part and tooling drawings.

A near-net gear forging is essentially a net-shape product with a small amount of removable or machining stock (an envelope) added to the finished gear dimensions. This allows the near-net part to be finish-machined with a minimum removal of material, thus preserving the grainflow pattern in the tooth area introduced by the forging process.

To design a near-net gear, the finished-part drawing is modified, via CAD, to include this envelope. This modification then becomes the finished near-net forging drawing, as shown in Figure 123. This drawing is then modified to produce the lower die drawing. This is done by accounting for the increase in part size when it is at forging temperatures (cold size times 1.0155).

The upper punch has the same plan view profile as the lower die except it is reduced in scale to allow for punch-to-die clearance. Therefore the lower die drawing is modified, by scaling back the dimensions, to produce the upper punch drawing.

In short, the finish part drawing leads to the finish forge drawing which leads to the lower die drawing which leads to the upper punch drawing. This may seem complex, but all of these profiles are merely scaled versions of the original finished involute profile.

A short description of the forging process, which is illustrated in Figure 123, may help clarify the above. The hot preformed billet is forged in two steps (preform to finish forge), by the

NOTE: This section of the report was prepared originally by the Eaton Corporation, a subcontractor to The Boeing Company, Helicopters Division. Boeing would prefer to provide the customer with a report that is consistent in style and format throughout. However, in the interest of reducing the cost of production of this report, Boeing is using all illustrations provided by Eaton in their original form.

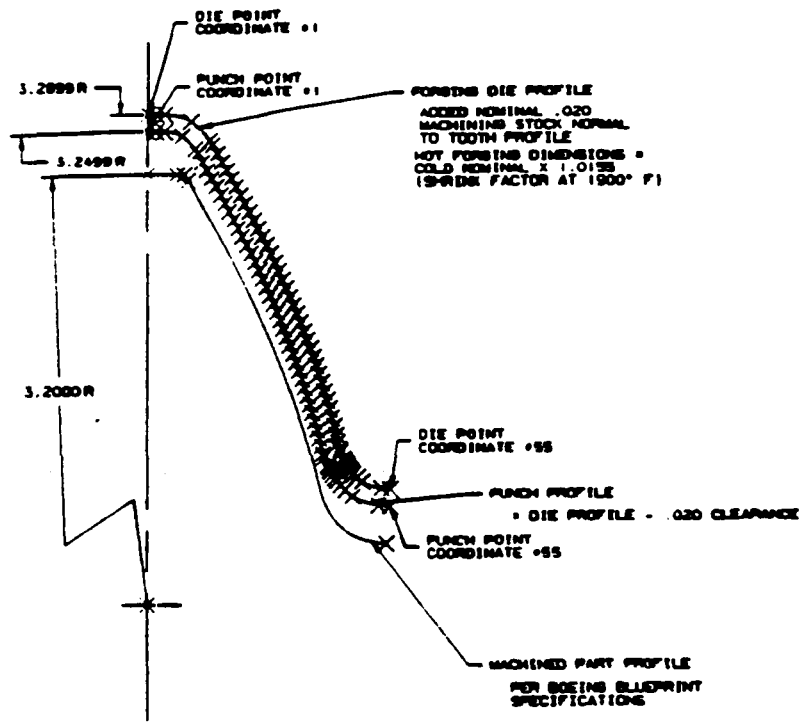

Figure 122. Tooth, Die, and Punch Profiles

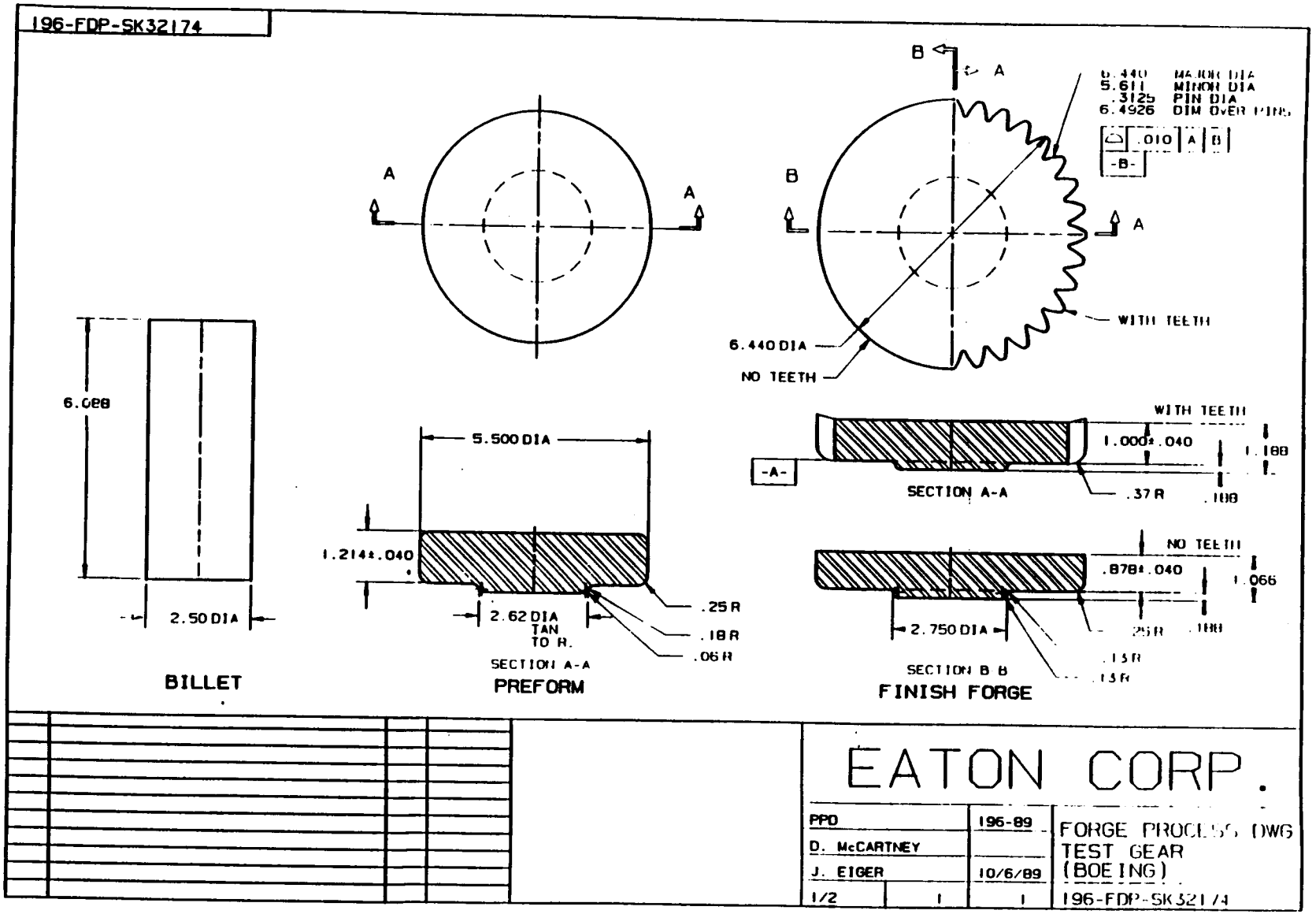

Figure 123. Finished-Part Forge Drawing

upper punch, into the lower die. This forging, upon cooling, becomes the finished forged part which is then machined into the finished part.

Design of Forging Tooling

Once all of the near-net profiles are generated, the remaining tooling designs can proceed. The lower near-net die, in conjunction with the compression ring, is designed to withstand the maximum forging load with minimum elastic deflection. This produces a part as close as possible to the unstrained die dimensions. The compression ring is just that: a ring with an inner diameter slightly smaller than the outer diameter of the lower die which, after being heated and placed over the die, contracts, putting the die into compression. This compression offsets most of the expanding (tension or hoop stress in the ring) forces that the forging loads place on the die. When the die undergoes this expansion it returns to a neutral stress state and to its original size, producing the original desired part profile. The near-net profile is formed into the lower die by the EDM electrode process.

The upper punch is designed to withstand the maximum axial compressive load received during forging. It has the same profile as the lower die except it is scaled back to allow for clearance between the punch and the die. This clearance also permits the part to forge with a small amount of flash. The upper punch is formed by the wire EDM process.

The conventional forging tooling is vastly simpler in design. It is designed in an identical manner to the near-net tooling except without the tooth profile, as shown in the tooling drawings in Appendix G.

The near-net and conventional tooling are designed to fit into standard toolholders used in the forging presses at Eaton's Forge Division in Marion, Ohio.

Manufacture of Forging Tooling

With all of the preceding calculations completed, the task of producing the tooling could proceed. The design work was done in house and the tooling manufacture was subcontracted to local machining, grinding, heat-treating, and EDM vendors. The preform and finish-forging tooling was identified with the appropriate detail numbers.

Billet Design - The billet must be carefully designed in order to produce a forging that properly fills the die without excessive flash while adhering to proven upset ratios to gain the benefits of the forging process. The billet upset ratio is a ratio of the billet's initial height before upsetting to its final height after upsetting, based on its initial diameter. Standard length-to-diameter ratios were applied to the billet used for the test gears.

The billet volume was obtained from calculations of the finish forge gear volume. The upset ratio was then applied to this volume, in conjunction with nominal available bar stock sizes, to arrive at the billet's starting dimensions (6.088 by 2.5 inches in diameter). The same billet size was used for the toothed and nontoothed forgings; this practice greatly simplifies the design and forging processes. The conventional (nontooth) gear blank tooling was then designed around this single-size billet.

Forging of Near-Net-Shape Test Gear

Near-net forging differs from conventional forging in that the forging loads progressively increase as the complexity or detail increases in the part to be forged. In other words, due to the dynamics of metal flow in forgings, the sharper the corner is, the harder it is to fill. The near-net forgings required considerably more tonnage than the conventional pancake forgings. This increase in forging loads translates into increased stresses for the forging dies, particularly in the tooth tip and root areas. A properly designed preforming operation will reduce the amount of plastic deformation in the final near-net forging. Proper preforming also reduces the

stresses which in turn reduces the tooling elastic deflection. This reduced deflection then produces a finished part closer to the designed dimensions.

Forging of the gears took place at Eaton's Forge Division in Marion, Ohio. The forging was done in a 1,600-ton mechanical press and the forging station is shown in Figure 124. The forging process is as follows:

- Billets are loaded into a nitrogen-atmosphere, gas-heating conveyor unit
- The billets are heated to forging temperature (optically checked)
- Forging dies are sprayed with graphite lubricant
- Billets are manually loaded into the preform station and upset forged (Figure 125)
- Preform is transferred to the final forge station and forged (Figure 126)
- The finished forging is removed and placed on a cooling pallet
- Finished forging is inspected (Figure 127).

Sample billets of AISI 8620 steel are used to set the press to the proper stroke. A dimensional inspection can be made while the gears are still hot by using a special caliper that is calibrated to measure steel at forging temperatures. The 1,600-ton press used is equipped with a microadjusting hydraulically controlled bolster. This type of bolster permits extremely fine vertical adjustments, which in turn allows forgings to be produced that properly fill the die, yet are virtually flashless. When the initial sample billets pass dimensional and visual inspection the VASCO material is then forged. The bolster is adjusted to accommodate for the increased tonnage required for the VASCO material, thus producing the filled, virtually flashless forgings shown in Figure 128.

The billets used in forging the gears were identified with individual serial numbers. These numbers were retained after the gears were forged by re-marking each gear as it was removed from the finish forge die. These serial numbers can be seen in Figure 128.

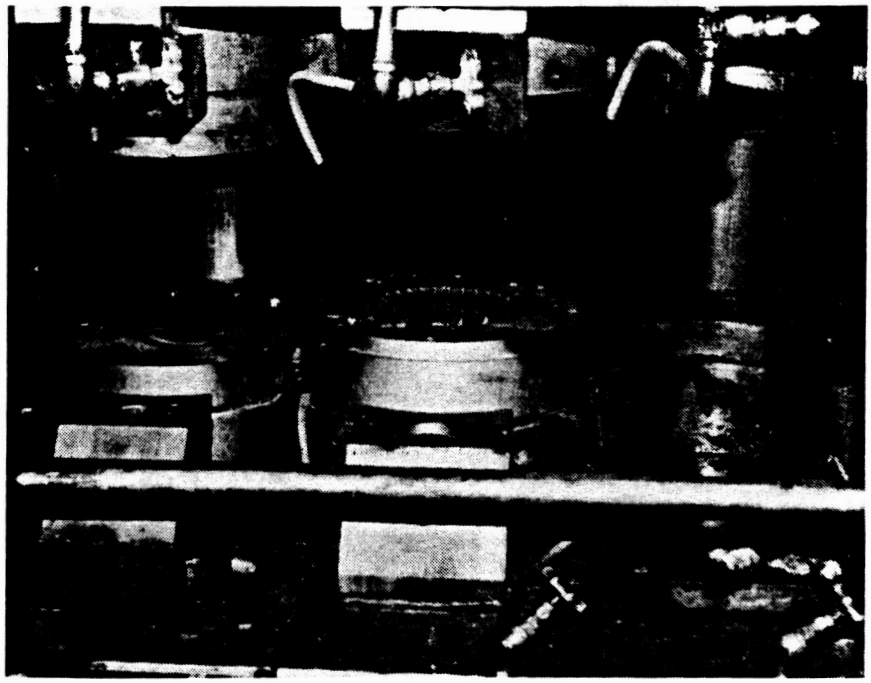

Figure 124. Forging Station

Figure 125. Heated Billet Loaded Into Preform Station

Figure 126. Preform Transferred to Final Forge Station

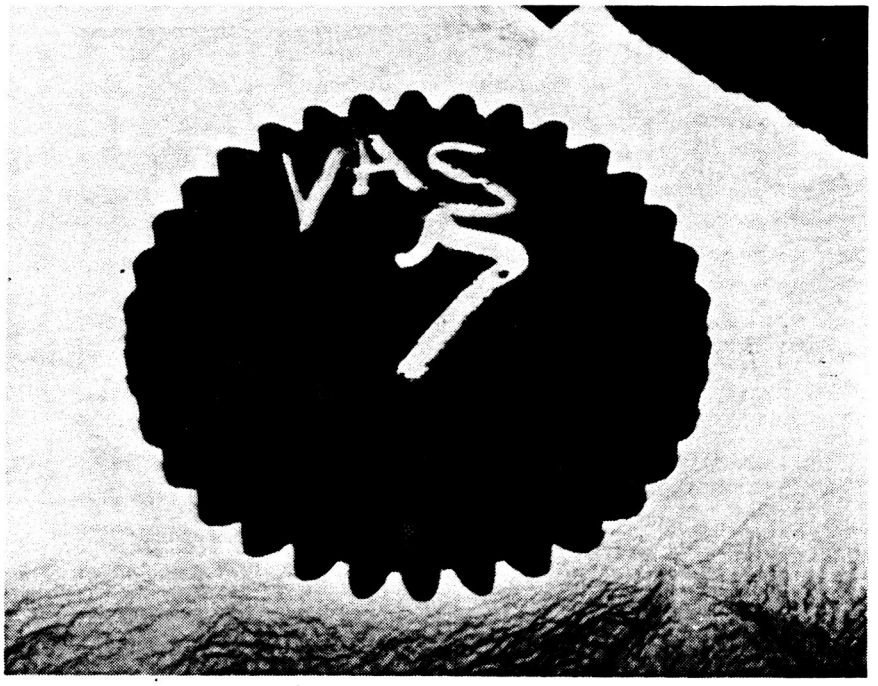

Figure 127. Finished Forged Gear

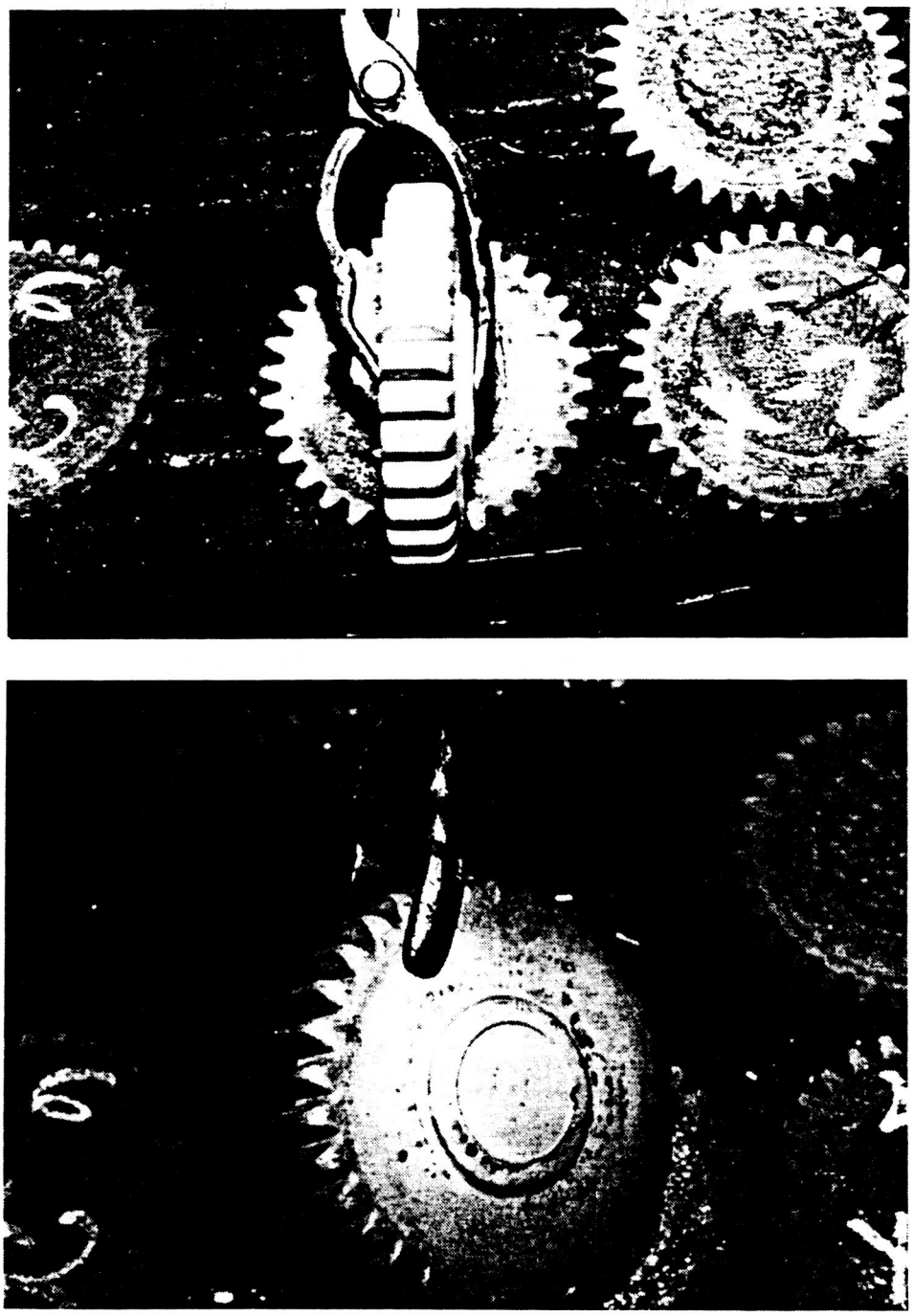

Figure 128. Still-Hot Near-Net Gear Forgings

Forging of Conventional Baseline Gear Blank

The forging of the conventional gear blank followed exactly the same procedure as the near-net gears except that the process required less tonnage. As with the near-net gears, each forging retained its original serial number before and after forging.

Finishing of Test Gears

After the gears were forged they were annealed and then sent to be rough-machined by B&G Machine Company. The rough machining consisted of reducing the forging thickness to 0.425 inch and turning the bore to 1.750 inches for the Phase I gears. Due to a carburizing problem in Phase I, the Phase II gears were reduced in thickness to only 0.525 inch and turned to the same bore size as Phase I. The rough-machining process sheet for Phase I is shown in Figure 129.

After rough machining the gears were inspected and sent to Summit Gear for final processing in accordance with the specifications on Boeing engineering drawing SK32174.

Inspection of Test Gears

The dimensional inspection data are shown in Tables 34 and 35 respectively. The profile and lead charts are too large to reproduce here, but they are available.

Testing and Evaluation

When gears are manufactured from conventional forged blanks, the gear teeth are actually cut into and across the forging flow lines. This does not provide for any material grain orientation along the tooth profile and root radius, as shown in Figure 130. Conversely, when a gear blank is near-net-shape forged, the rough shape of the gear teeth is produced in the forging operation.

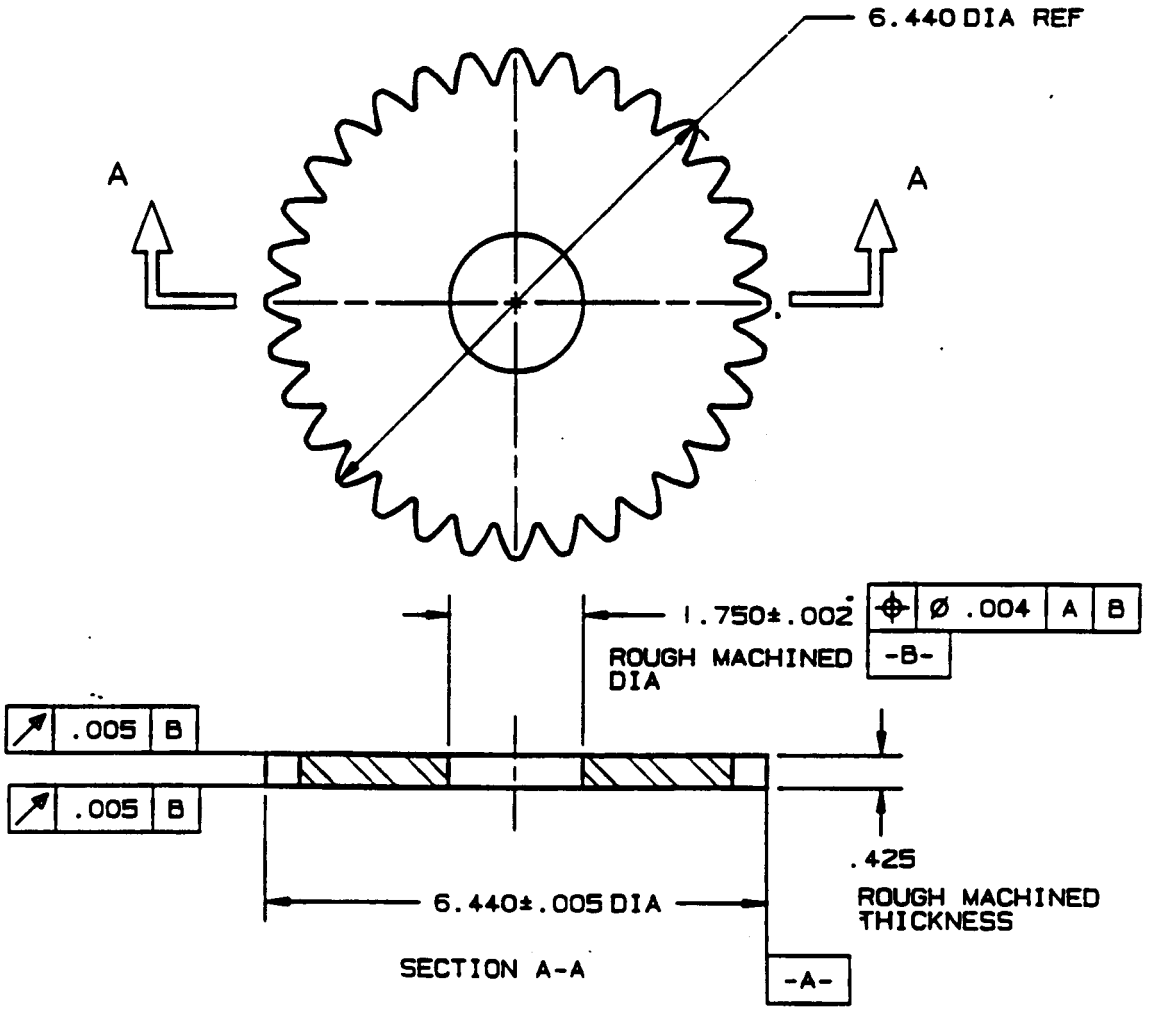

SEMI FINISH

Figure 129. Process Sheet For Rough Machining Near-Net Gear

TABLE 34. DIMENSIONAL INSPECTION OF BOEING GEARS (PHASE I) BY EATON CORPORATION

Gear serial no.	Major dia (in.)	Root dia (in.)	Over pins (in.)	Hole dia (in.)	Thickness (in.)
Specifi-cations	6.400 6.395	5.571 5.551	6.5131 6.5092	1.881 1.876	0.380 0.375
C2	6.3990	5.5543	6.5100	1.8760	0.378
C3	6.3990	5.5527	6.4990	1.8762	0.379
C5	6.3990	5.5548	6.5125	1.8762	0.380
C6	6.3990	5.5555	6.5105	1.8760	0.379
C8	6.3990	5.5514	6.5105	1.8764	0.379
N4	6.3990	5.5519	6.5105	1.8762	0.379
N6	6.3995	5.5523	6.5105	1.8763	0.379
N8	6.3990	5.5551	6.5105	1.8764	0.380
N9	6.3990	5.5435	6.5070*	1.8760	0.378
N18	6.3990	5.5517	6.5105	1.8760	0.379

* Dimensional deviation to Boeing specifications
Visual inspection notes:
C2: tooth surface cleanup
C6: oversize tooth edge radius
C8: oversize tooth edge radius

TABLE 35. DIMENSIONAL INSPECTION OF FINISHED-MACHINED NEAR-NET GEARS (PHASE II) BY EATON CORPORATION FOR BOEING

Gear serial no.	Major dia (in.)	Root dia (in.)	Pin dia (in.)*	Over pins (in.)	Hole dia (in.)	Thickness (in.)
Specs	6.400 6.395	5.571 5.551	0.3456	6.5131 6.5092	1.881 1.876	0.380 0.375
20	6.395	5.556	0.3450	6.500	1.875	0.377
21	6.396	5.558	0.3450	6.500	1.875	0.379
22	6.398	5.556	0.3450	6.498	1.875	0.376
23	6.395	5.558	0.3450	6.499	1.875	0.378
24*	6.395	5.531**	0.3450	6.495	1.877	0.379
25	6.397	5.556	0.3450	6.500	1.875	0.377

* Machining line near tip of tooth on all teeth
** Root diameter is undersize.

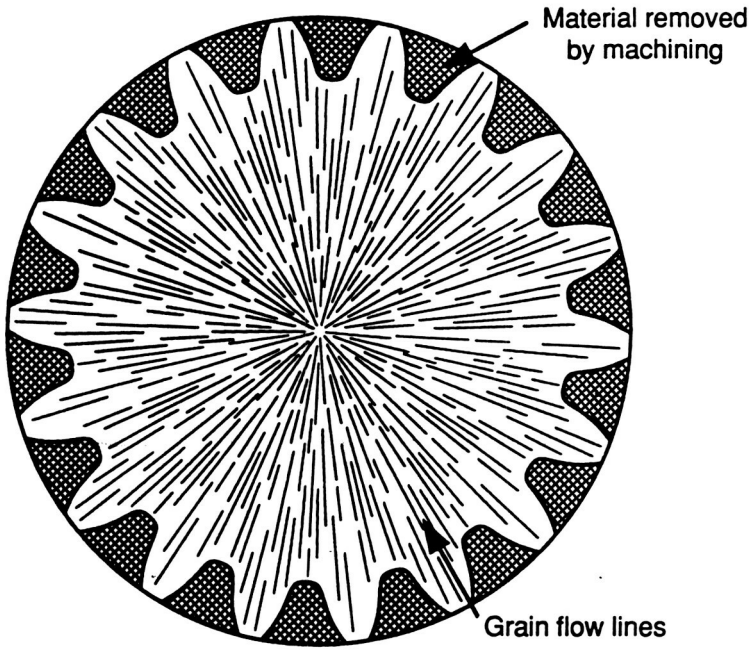

Pancake forging used and gear
teeth cut into rim

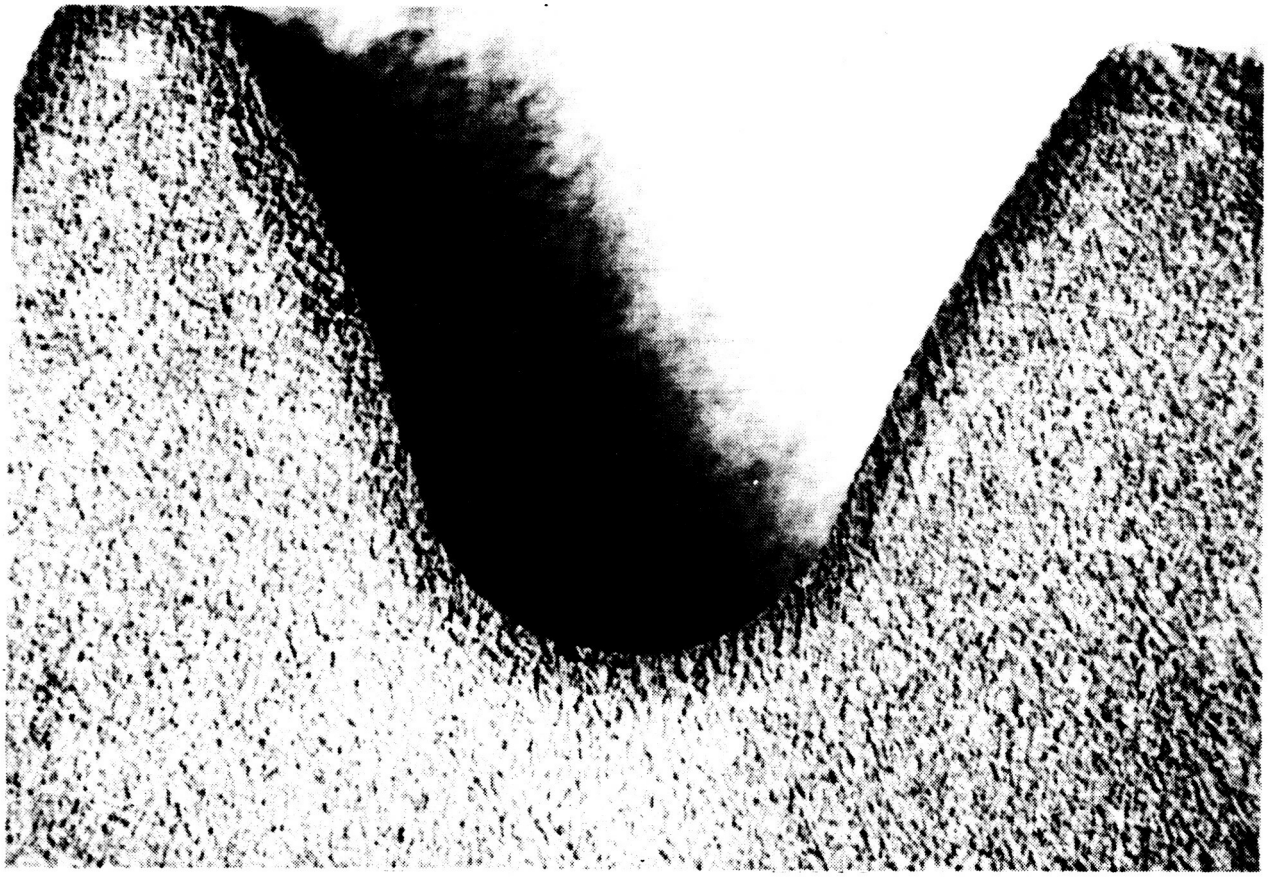

Figure 130. Standard Forged Gears

Therefore the material grain flow is around the contour of the gear teeth themselves, as shown in Figure 131. It is this conformity of the forging flow lines which should provide for the improvement in fatigue characteristics, most notably in bending but also in surface fatigue.

The approach for achieving the objective of this task was to develop, design, and manufacture tooling compatible with the standard Boeing single-tooth fatigue-test gears, manufacture a representative batch of test gears, inspect the geometry and metallurgy of the gears, and test their bending-fatigue load capacity relative to the capacity of similar, conventionally manufactured gears. In addition, a batch of test gears was manufactured from an advanced VASCO steel with a nickel additive for improved fracture toughness and basic load capacity. A large data base from prior testing of standard test gears was available and provided a good statistical comparison.

To evaluate the possible influence of the near-net forging process and the addition of nickel, single-tooth bending-fatigue tests were conducted. Spur gear test specimens were fabricated out of conventional X2M, near-net-forged X2M, and near-net-forged X2M with nickel. These specimens are 32-tooth spur gears which have had 16 teeth removed to provide access to eight of the remaining gear teeth for applying and reacting loads. The gear tooth bending-fatigue tests were conducted on the Boeing single-tooth bending-fatigue test fixture. The test fixture is shown with a typical test specimen installed in Figure 132. The load is applied to the highest point of single-tooth contact (HPSTC) on the test tooth by a load anvil mounted to an instrumented load link. Most of the load is reacted out of the gear by a tooth which is in contact with a reaction anvil 135 degrees away from the test tooth. Some of the load is reacted out through gear clamp-up friction. By rotating the specimen by increments of 90 degrees, a total of four teeth are accessible for testing while the other four accessible teeth are used as reaction teeth.

The typical procedure of maintaining a small minimum load was followed for this program so that the load ratio was close to, but not exactly, zero. The results of the tests are expressed in terms of the maximum tooth root stress as calculated from the applied load at the HPSTC using

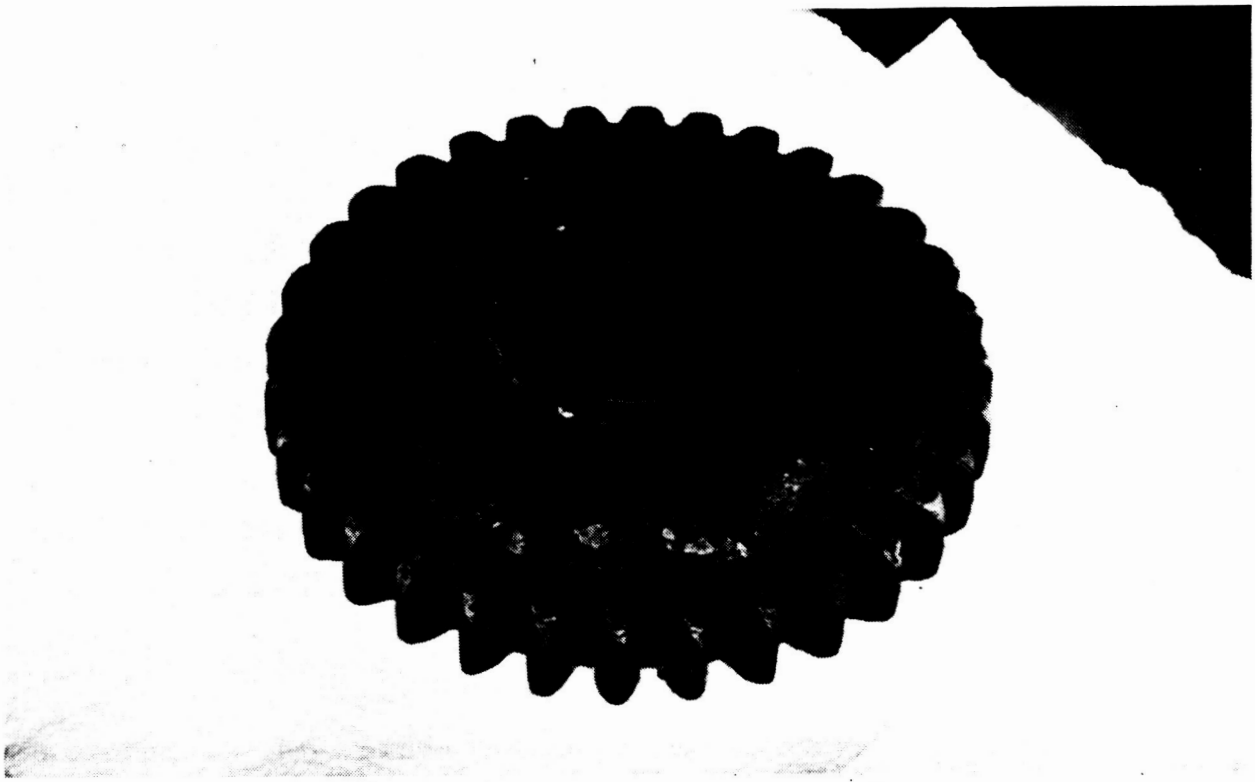

Near-net-shape forged gear with forged teeth

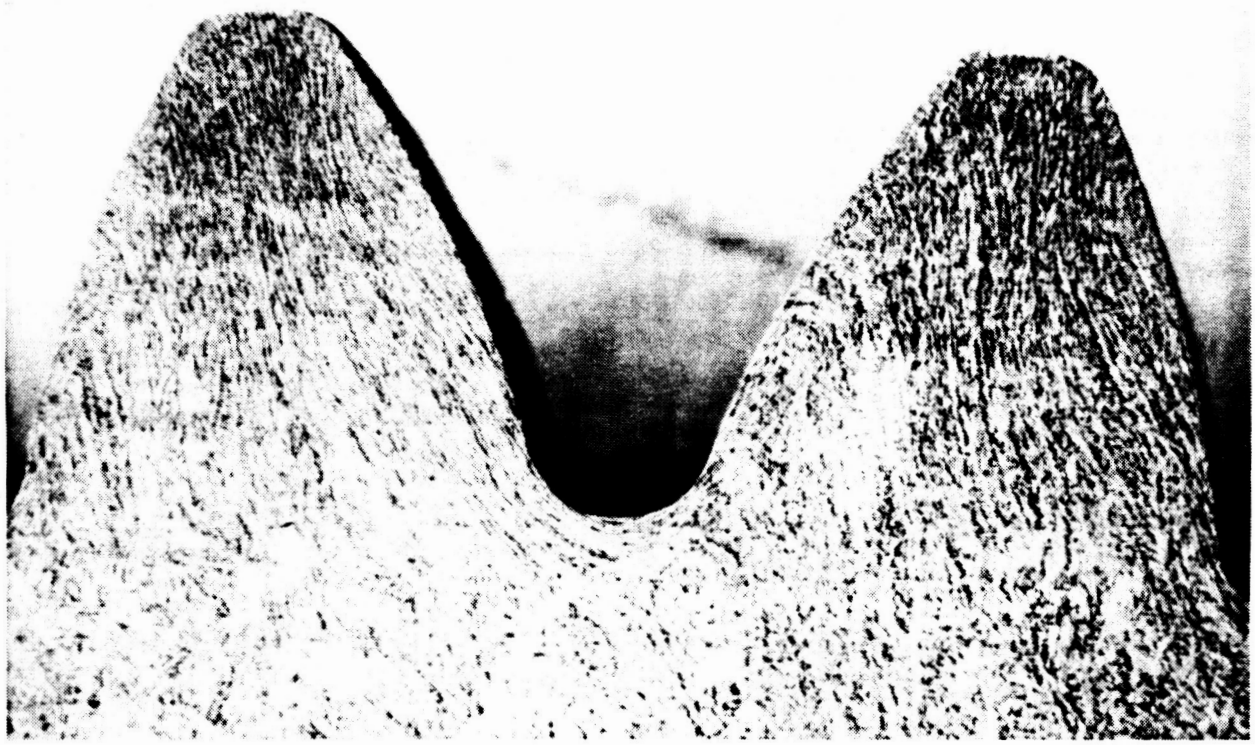

Improved grain flow

Figure 131. Near-Net-Shaped Forged Gears

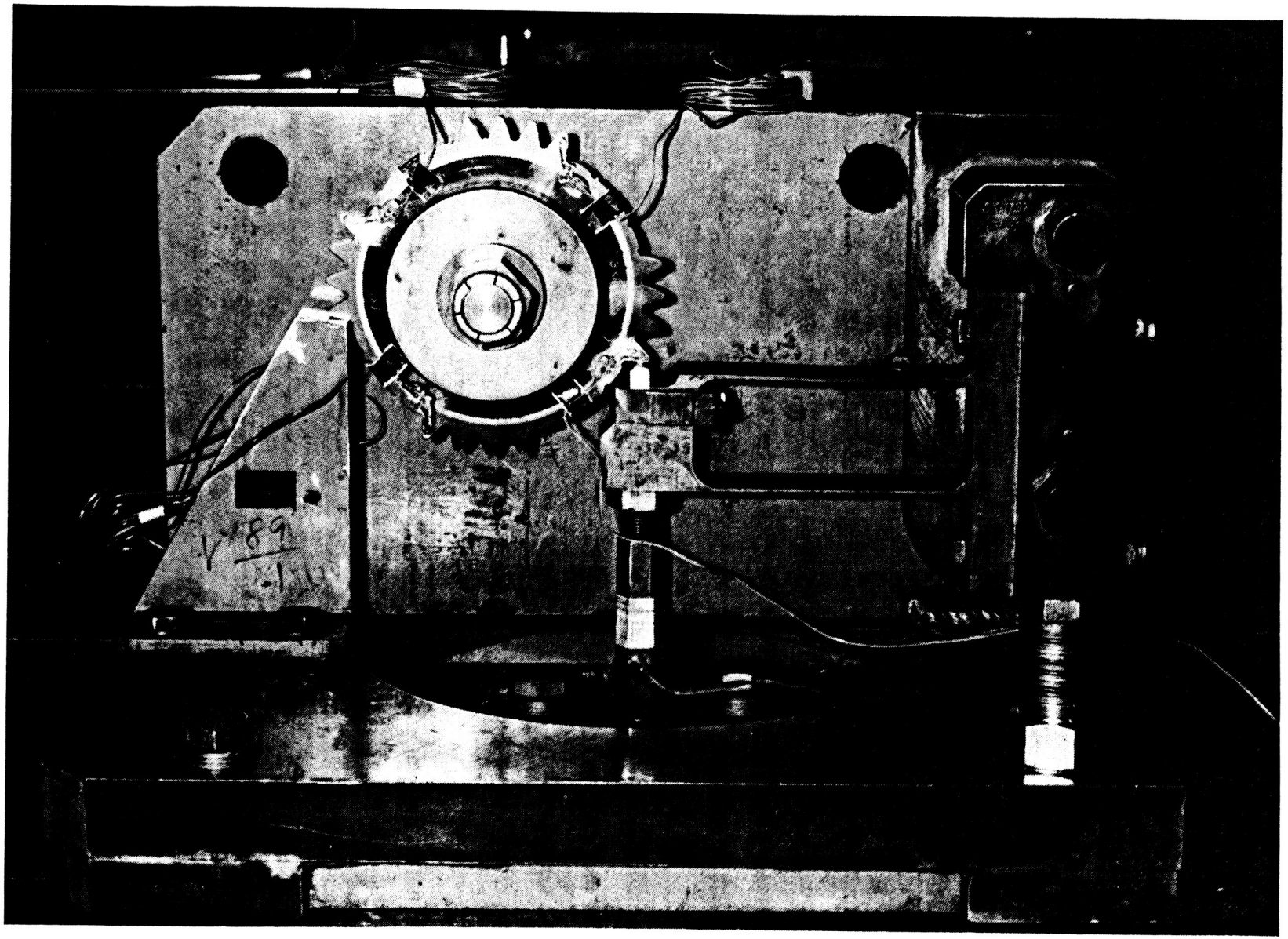

Figure 132. Single-Tooth Bending-Fatigue Test Setup

C125266

an AGMA equation. This maximum tooth root stress is a highly localized, concentrated stress. During the test program, a "master" gear instrumented with strain gages (Figure 133) at the location of this concentrated stress is periodically used to assure that the test fixture is aligned properly and to verify the validity of the AGMA equation.

The results of the testing are shown in the form of stress versus cycles (S-N) curves in Figures 134 through 137. The results for conventional X2M, near-net-forged X2M, and near-net-forged X2M with nickel are shown in Figures 134 through 136, respectively. Figure 137 shows a comparison of all the data. The S-N curves are in terms of the concentrated maximum gear tooth stress. As can be seen from the plots, this concentrated stress can reach rather high magnitudes. Because of the high value of the concentrated stress, test results can be very sensitive to local material conditions. As a result, data scatter can be high. On some specimens, early failures are suspected to be the result of improper edge breaks in the stress concentration region. These data points are identified on the figures.

Examination of these gears indicated that early fatigue failures were greatly influenced by the edge break on the gear teeth. The standard gear design specified an edge break to a radius or chamfer of 0.010/0.020 inch and visual inspection of this dimension is satisfactory. A typical edge break on a gear tooth is shown in Figure 138 and shows significant variation along the edge of the tooth. This variation resulted in the fatigue origin to be located at the edge of the tooth and not in the center. Data for the conventional gears (Figure 134) and the near-net-forged X2M gears (Figure 135) show a number of low data points which were suspect due to edge break effects.

The design requirements for edge breaks were changed and the final set of gears was produced with CNC-milled or ground radii edge breaks for the full length of the gear tooth as shown in Figure 139. The data from these gears (Figure 136) did not have the same scatter and the fatigue origin was located in the center of the gear and not at the edge of the gear. These findings indicate that careful attention should be taken to ensure that the gear is properly

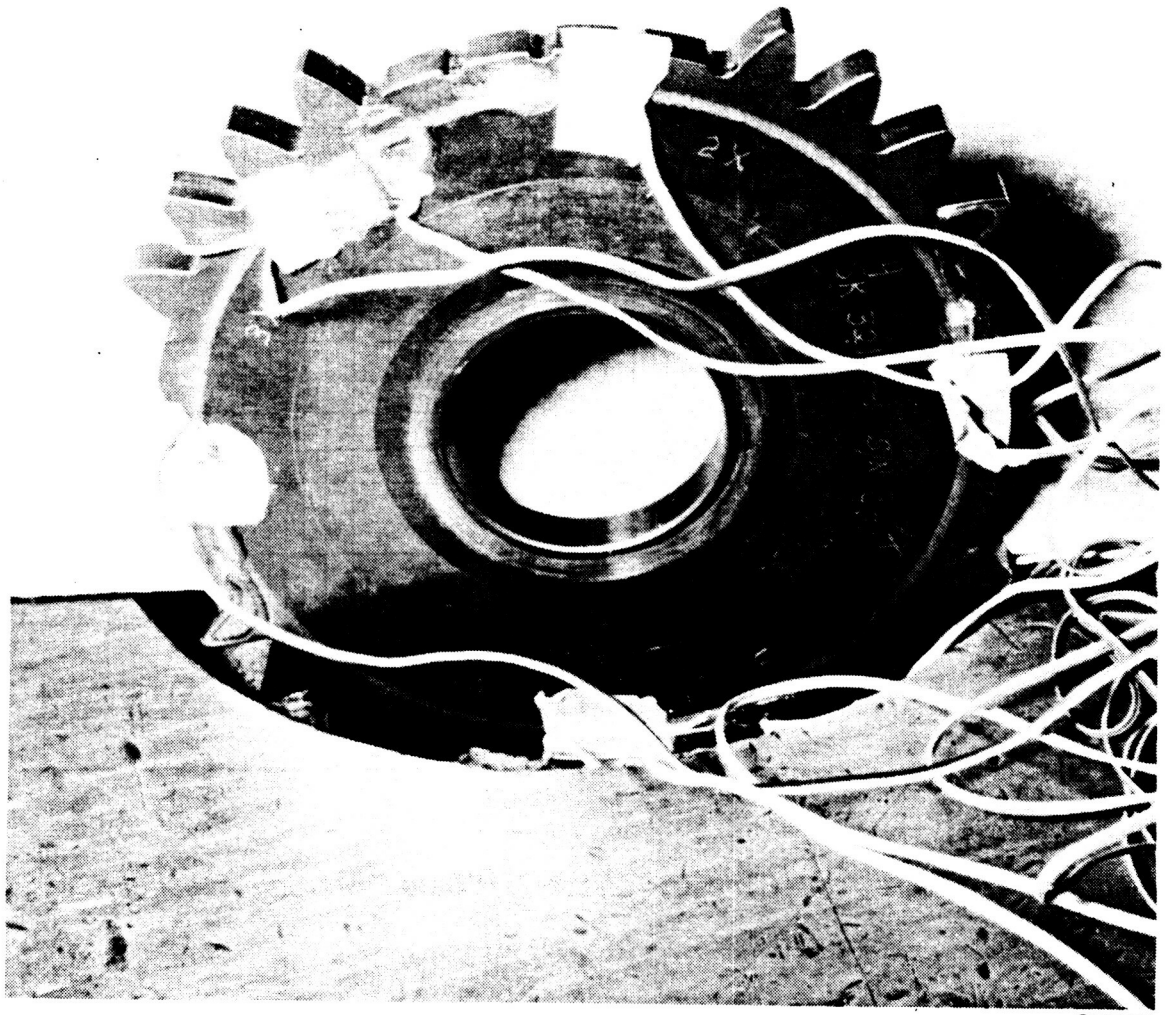

C125270

Figure 133. Master Instrumented Gear

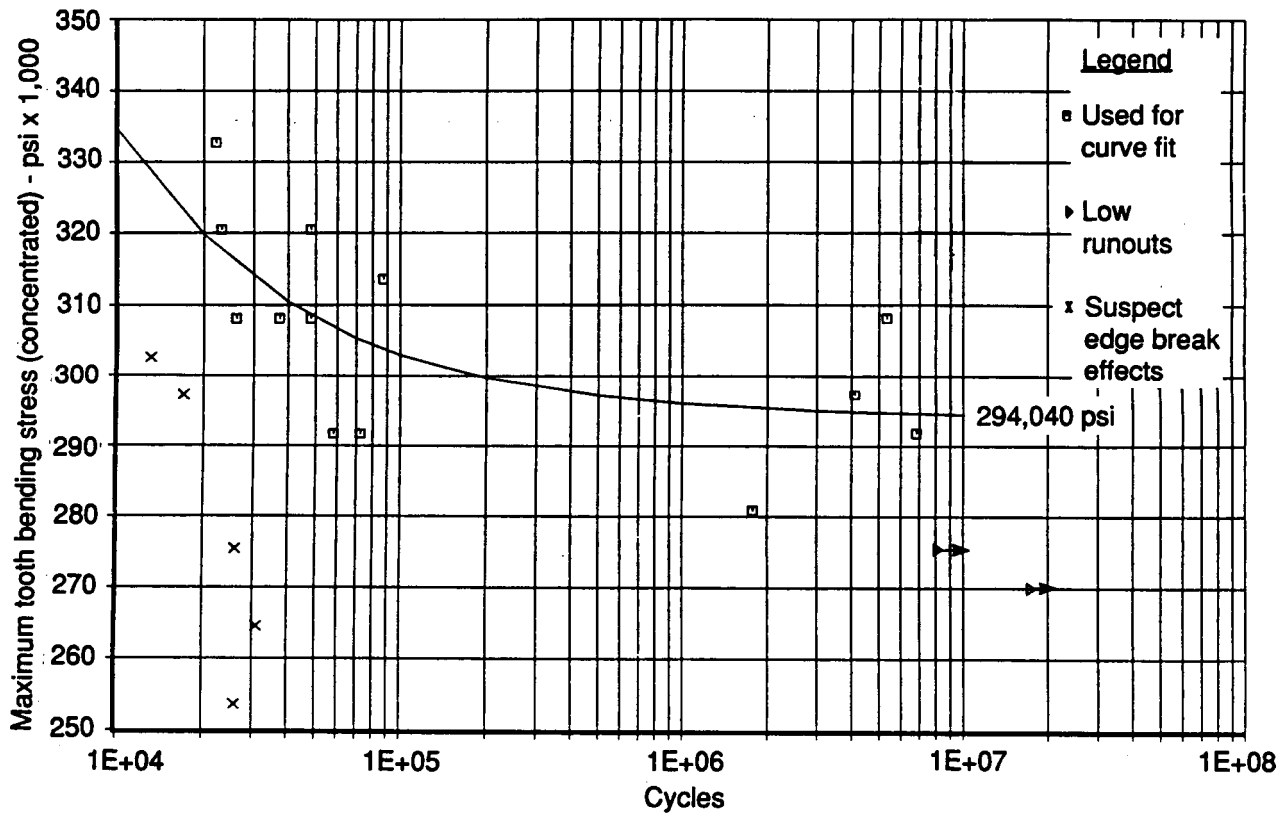

Figure 134. Single-Tooth Bending-Fatigue Test Data From Conventional X2M Gears

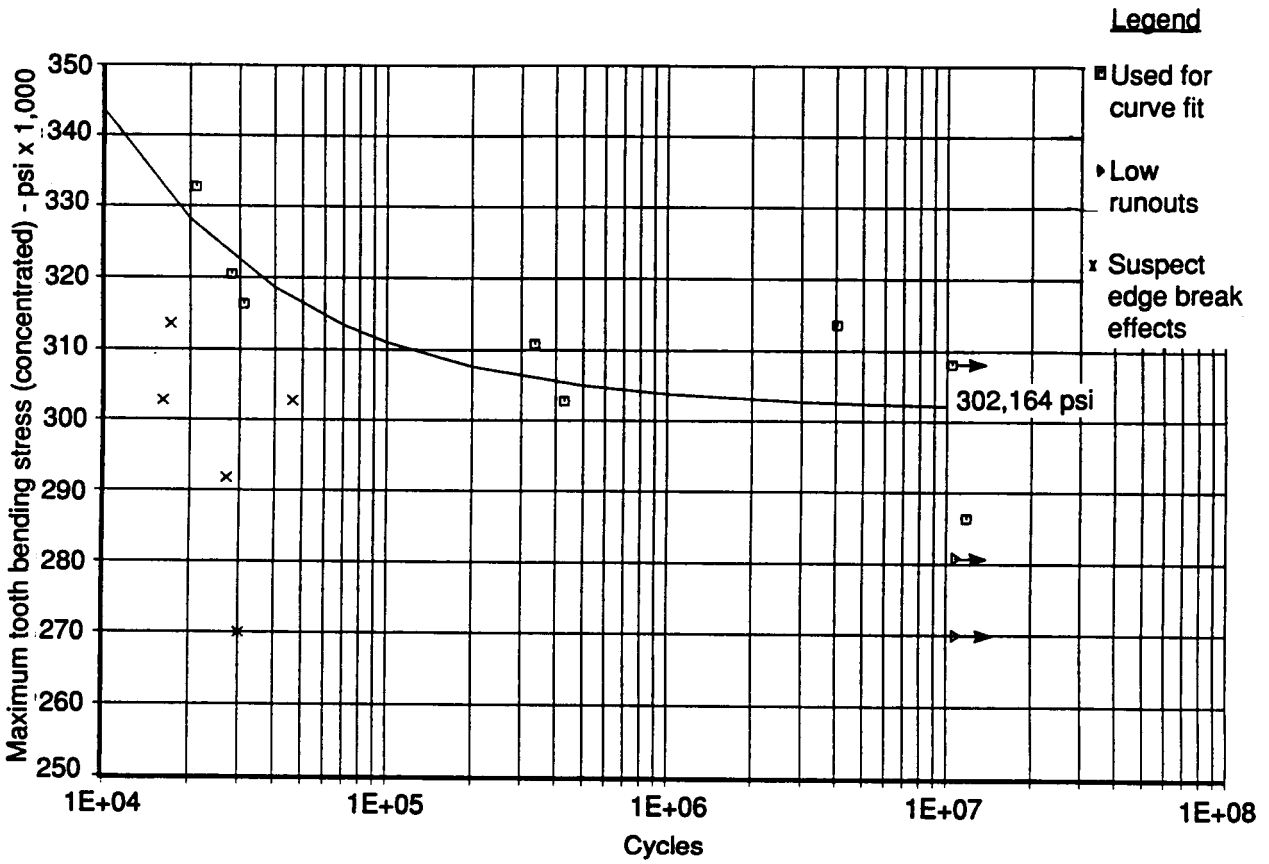

Figure 135. Single-Tooth Bending-Fatigue Test Data From Near-Net-Forged X2M Gears

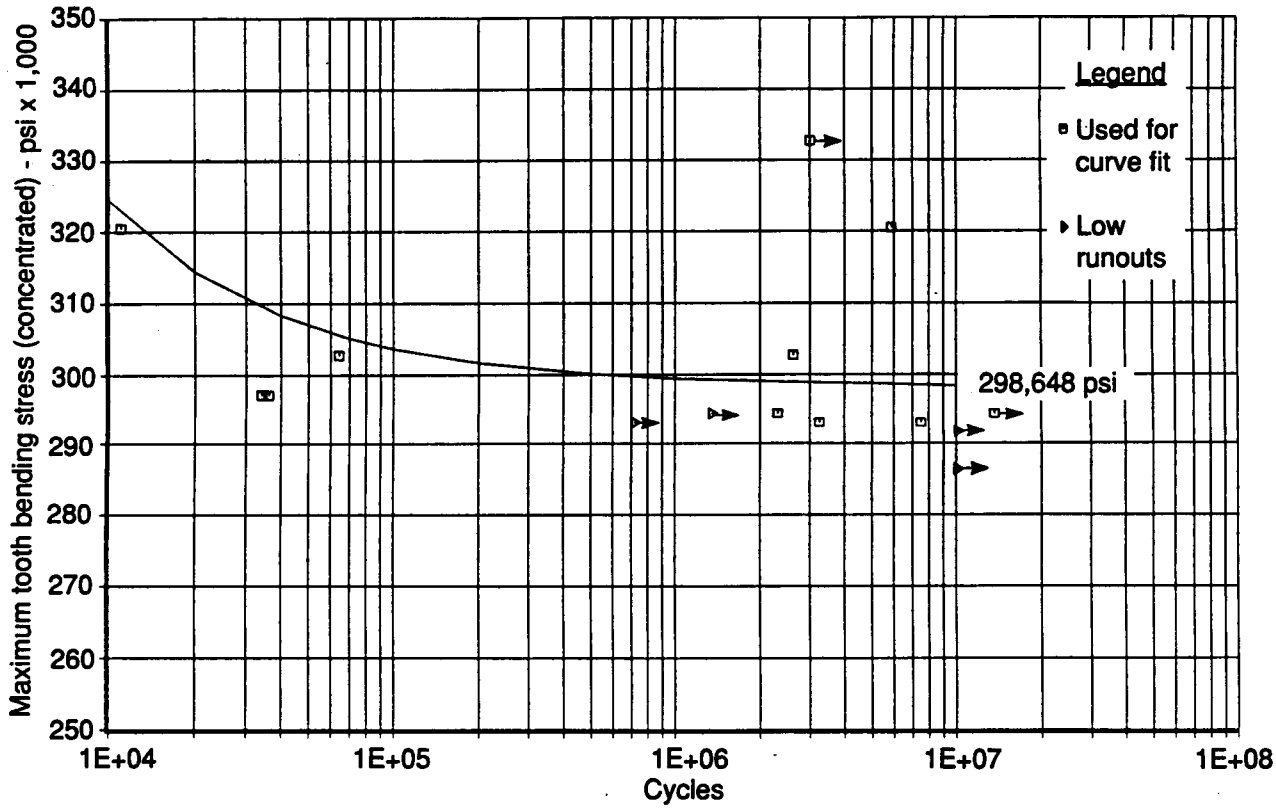

Figure 136. Single-Tooth Bending-Fatigue Test Data From Near-Net-Forged X2M Gears With Nickel

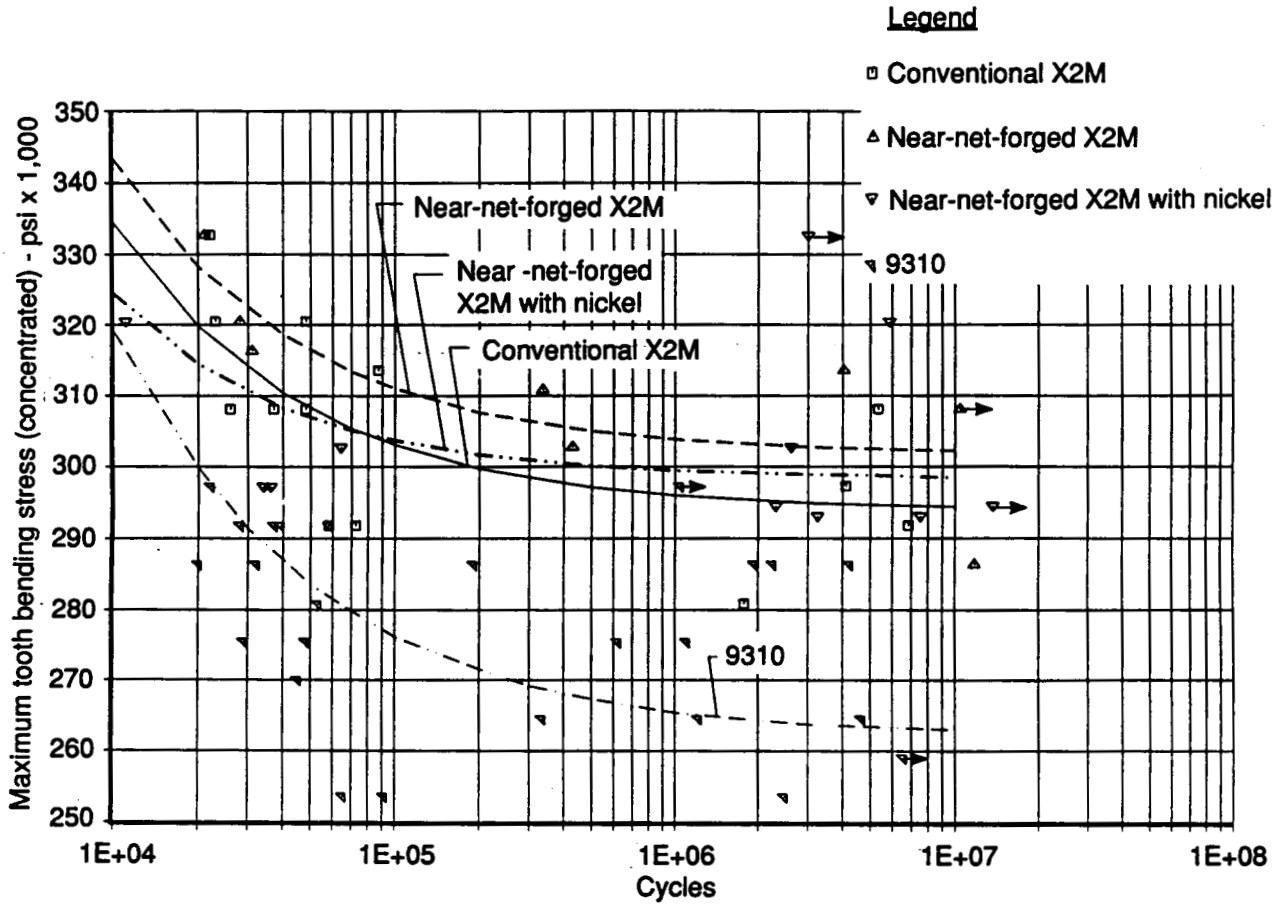

Figure 137. Single-Tooth Bending-Fatigue Test Data Summary

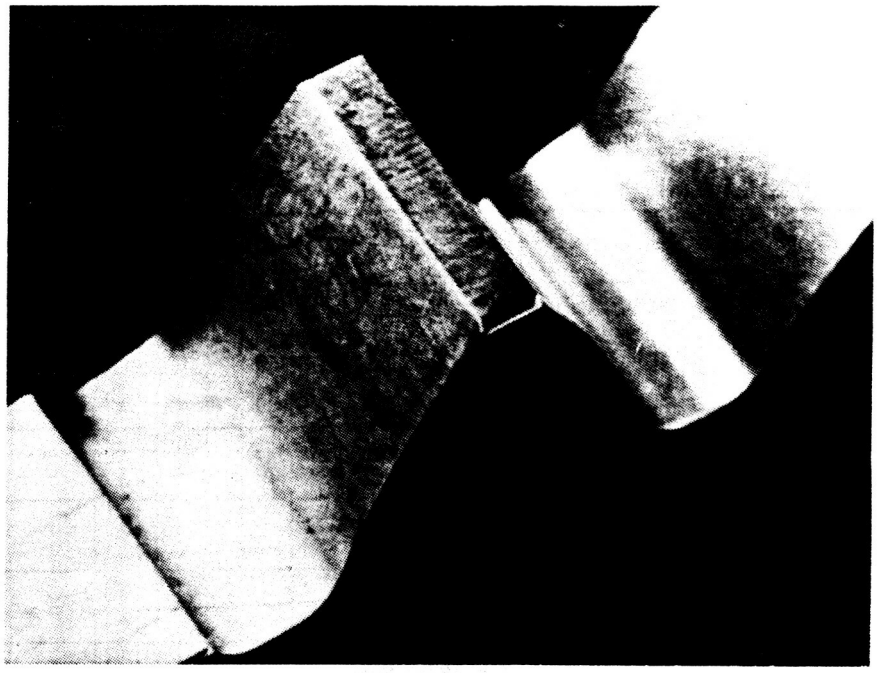

0.01/0.02-in. break sharp
edge (radius or chamfer)
visual inspect only

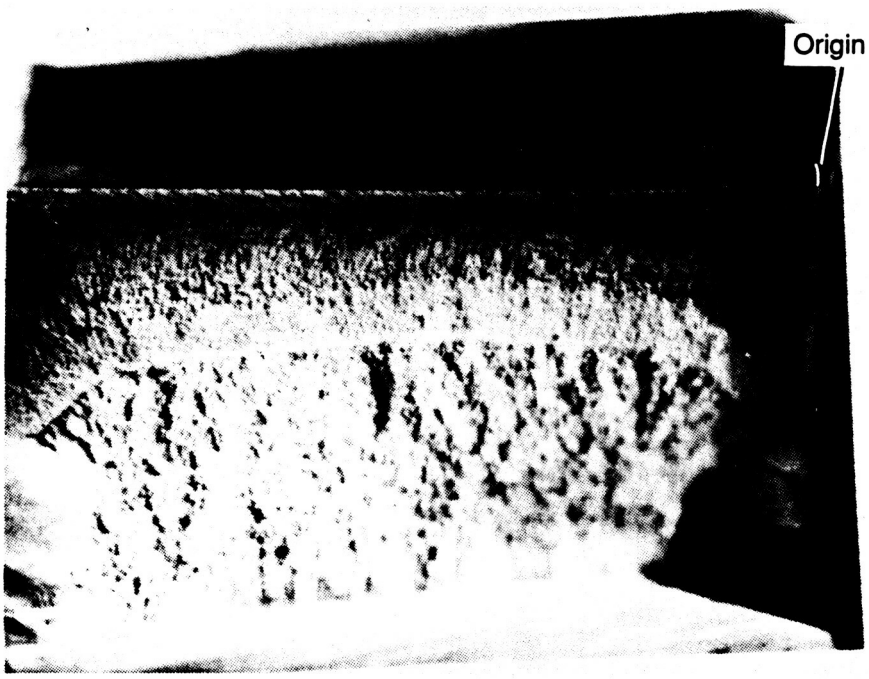

Fatigue origin

Figure 138. Effect of Edge Break on Fatigue Origin: Typical Edge Break

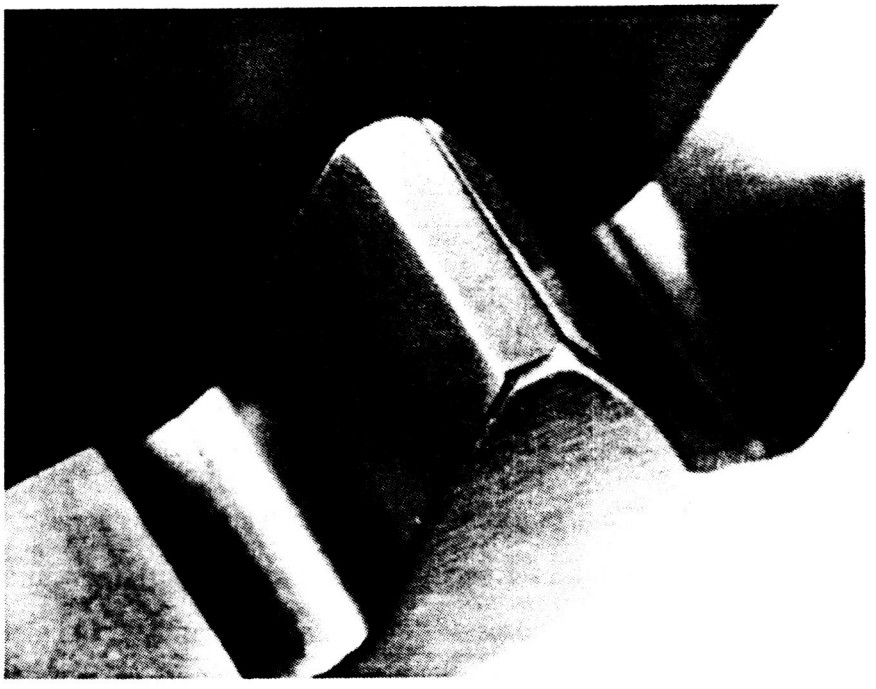

0.01/0.02-in. break by CNC
milling or grinding (radii)
full length of tooth

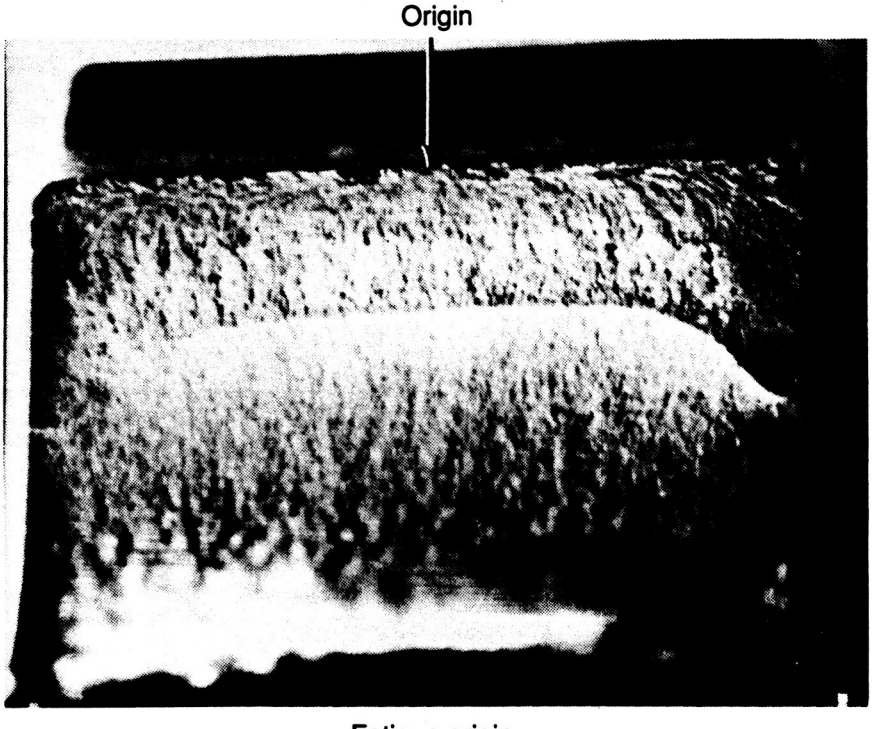

Fatigue origin

Figure 139. Effect of Edge Break on Fatigue Origin: Machined Edge Break

designed and manufactured to achieve its expected stress limits. This example of inadequate control on edge breaks could make a significant difference in the fatigue life of the gear.

Referring to the data and curve fits presented separately in Figures 134, 135, and 136, the highest endurance limit was calculated for near-net-forged X2M (302,164 psi, Figure 135), the next highest endurance limit was calculated for near-net-forged X2M plus nickel (298,648 psi, Figure 136), and the lowest endurance limit was calculated for conventional X2M (294,040 psi, Figure 134). These differences are small, especially when the data scatter is considered. This is more obvious in Figure 137 where the three curves and the data used for the curve fits are compared on the same plot. The data for all three material conditions appear to fall in the same scatter band. To firmly establish a difference in endurance limit, a larger number of specimens would have to be tested. For the purposes of this program, it can be concluded that there is not a significant difference in fatigue strength.

This test program did prove that the near-net-forged process could be used without any negative effect on the bending properties and still take advantage of the process for manufacturing cost reduction. Included in Figure 137 are data for conventional 9310 steel gears based on prior data. When compared to the standard 9310 steel gears, a significant increase in bending stress was achieved for all versions of the X2M steel gears. The bending stress was increased by approximately 50,000 psi or 20 percent. This type of increase can make a significant difference in gear sizing for achieving the same power limits.

SPUR GEARS WITH HIGH-PROFILE CONTACT RATIO, NONINVOLUTE TOOTH FORM

Introduction

The load capacity of a gear set is a function of many factors, including material, heat treatment, and tooth geometry, among many others. Improving the load capacity thus requires a change to be made to one or more of these factors such that the net result is a net gain in capacity. Unfortunately, this concept is deceptively simple. In many cases, changing a single factor for the better may make another factor worse, and the net result may not be as favorable as initially thought.

This situation is the case with high profile contact ratio (HCR) noninvolute tooth form (NIF) gearing (HCRNIF). Previous testing has demonstrated improvements in noise level and surface load capacity with no significant change in bending-load capacity. However, this testing also indicated that the scoring-load capacity of the HCRNIF gears may not be equal to that of conventional gears.

Since both the weight and reliability of a helicopter gear system can be improved substantially by increasing the inherent load capacity of a gear set, the possibility that HCRNIF gears could be developed to provide a substantial net improvement in overall system capacity is a very attractive one. Furthermore, since noise is an ever-present problem for very high power-to-weight ratio helicopter gear drives, the low-noise properties of HCRNIF gears combined with their higher load capacity are doubly attractive.

Objective

The objective of this program was to design, build, and test a set of spur gears that use a noninvolute, high profile contact ratio tooth form to provide a relatively constant-curvature

radius along the tooth profile while yielding a profile contact ratio of at least 2:1. This configuration allows the use of a high reduction ratio in a single stage while simultaneously minimizing noise generation and improving surface load capacity.

This program was directed at investigating three specific properties of HCRNIF gears as compared to similarly sized, standard contact ratio gears:

1. Scoring-load capacity
2. Noise level
3. Load sharing among teeth in mesh.

Program

The test program was aimed at investigating the overall performance of high profile contact ratio, noninvolute form gearing, its relative noise characteristics, and its load capacity as compared to a set of conventional, standard contact ratio gears at the same reduction ratio and center distance. Testing was conducted in the Boeing Gear Research Test Facility (Figure 140) on one of the gear test rigs configured for testing overhung gears on 10-inch centers (Figure 141).

The advantages of the HCRNIF configuration are twofold. First, since the profile contact ratio for the HCRNIF gears is above two (generally about 2.15 to 2.250), there are always at least two pairs of teeth in contact, and for a small portion of the mesh cycle three pairs of teeth are in contact to share the total transmitted torque, as Figure 142 shows. In contrast, standard gears with a profile contact ratio between one and two always have at least one pair of teeth in contact and, for a small portion of the mesh cycle as Figure 143 shows, they have two pairs of teeth in contact to share the full transmitted torque. The more teeth available to share the total load, the lower the stress levels should be on any single tooth; thus the HCRNIF gears should be capable of transmitting more power for a given weight. Second, the shape of the HCRNIF teeth results

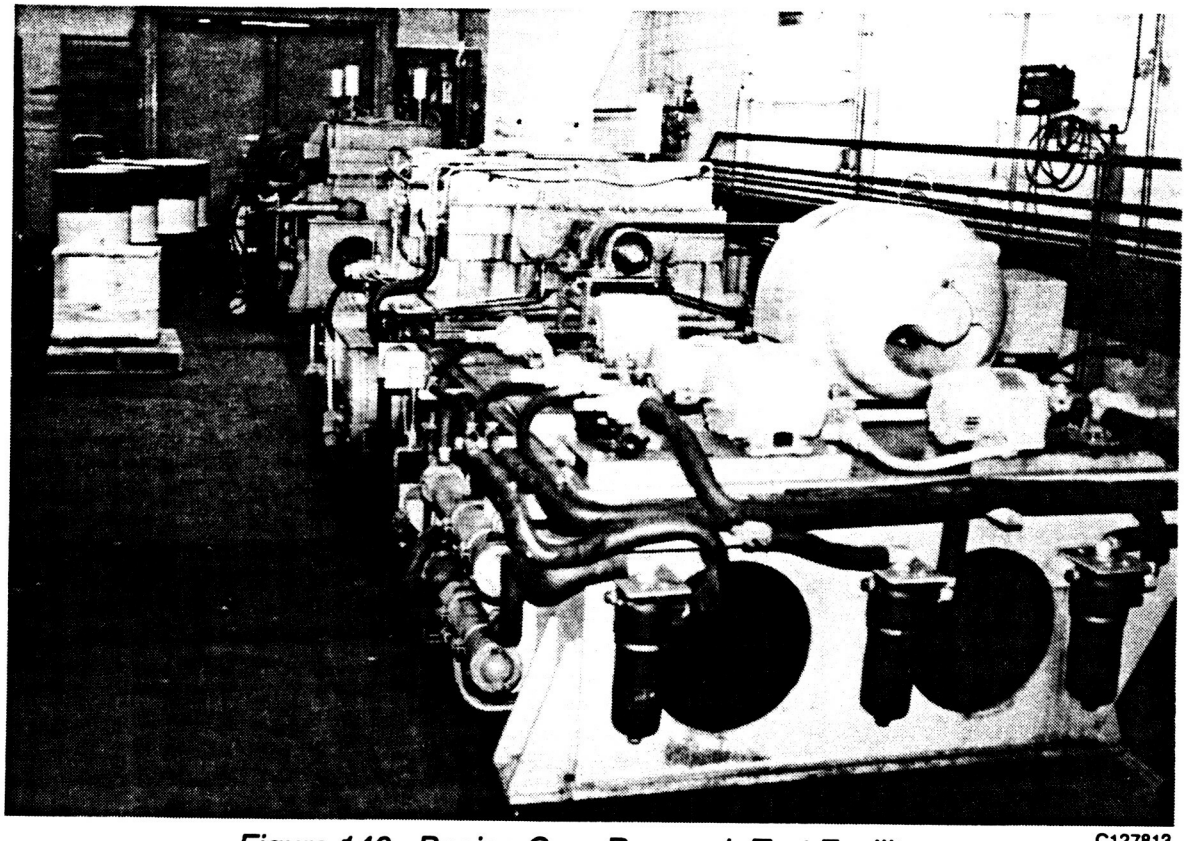

Figure 140. Boeing Gear Research Test Facility C127813

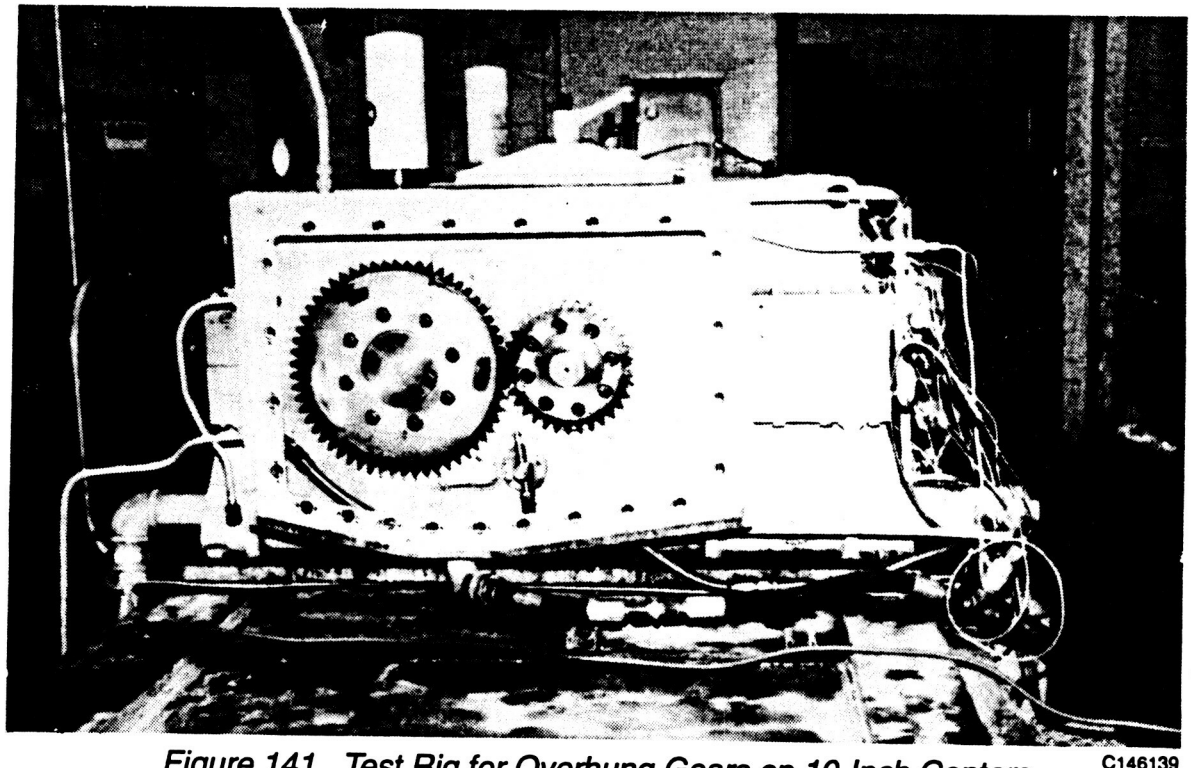

Figure 141. Test Rig for Overhung Gears on 10-Inch Centers C146139

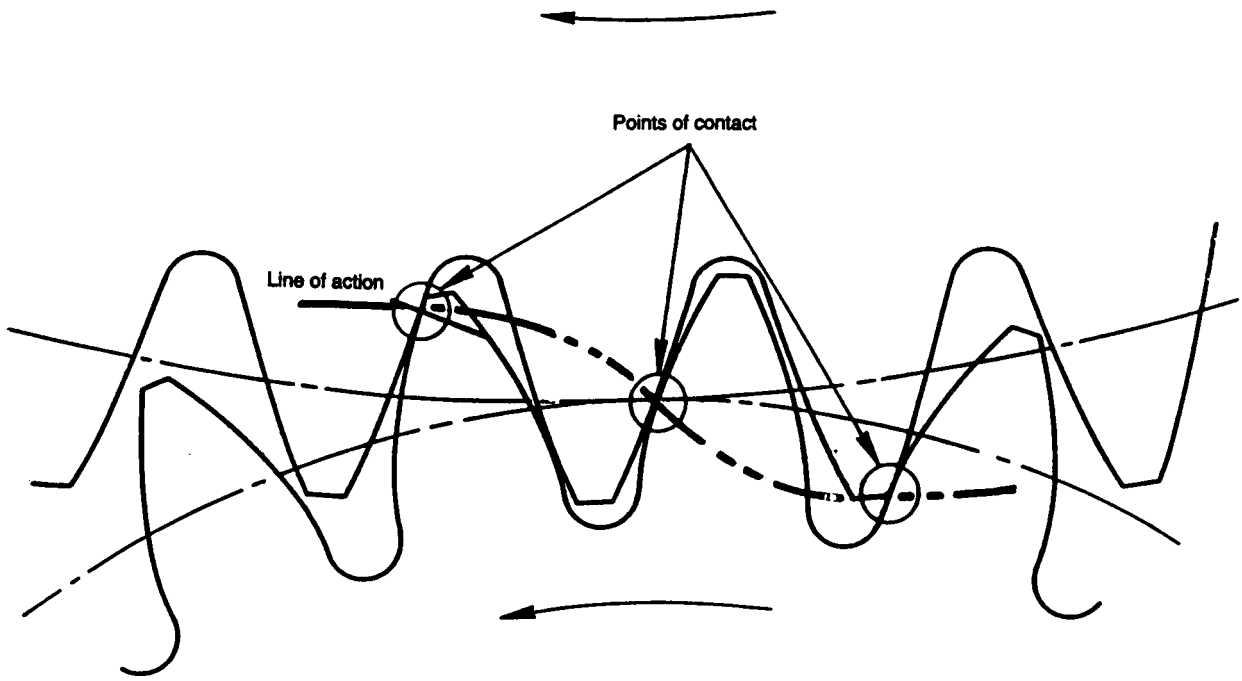

Figure 142. Spur Gears With High Contact Ratio, Noninvolute Tooth Form

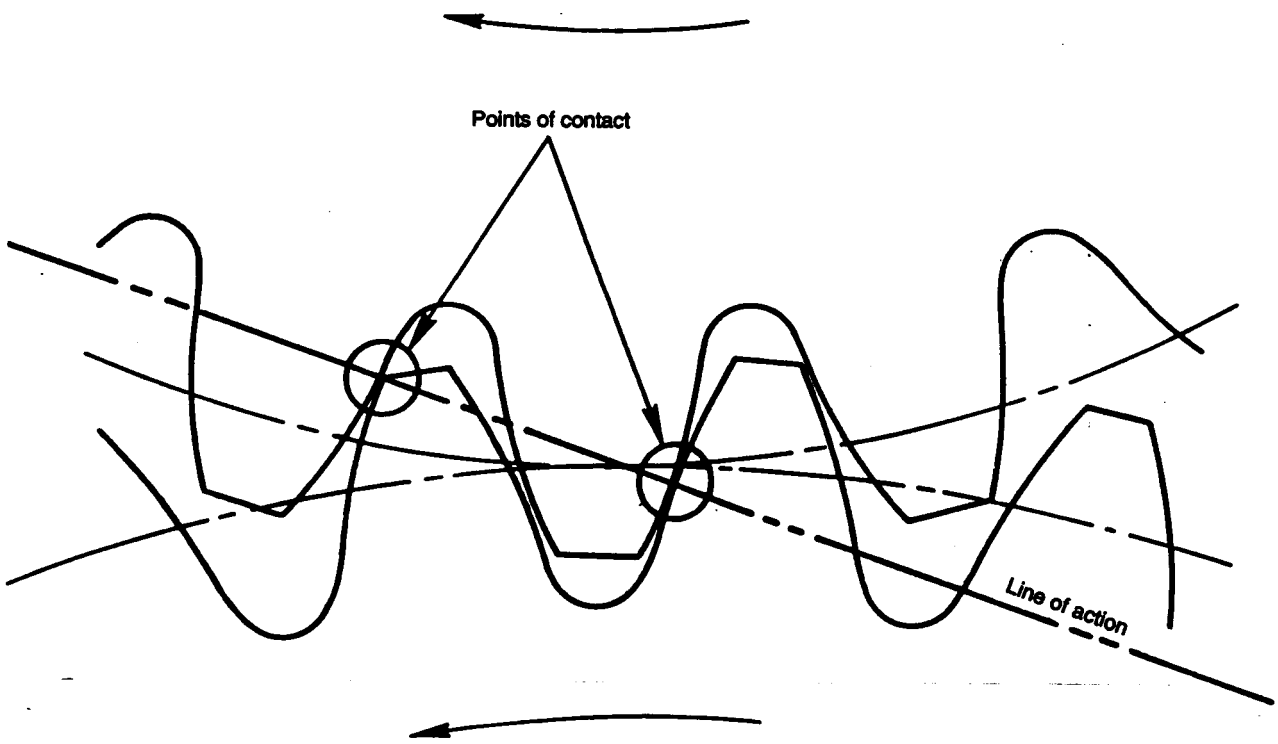

Figure 143. Spur Gears With Standard Involute Tooth Form

in lower contact stress levels for a given load so that a further improvement in the total power transmitted can be achieved. This benefit is less obvious since the overall shape of the noninvolute teeth is not substantially different visibly from that of conventional involute teeth.

Design

Two sets of spur gears, similar to those used in the planetary system testing for the heavy-lift helicopter (HLH), were designed to operate on the 10-inch center distance gear research test rig in the overhung configuration. One set of gears had a standard involute tooth form and proportions while the second used the high contact ratio, noninvolute tooth form (HCRNIF). The reduction ratio was approximately the same as the HLH sun/planet mesh.

Previous NASA testing of small gears with this tooth form indicated that their surface load capacity (surface durability) was substantially higher than that of conventional involute gears and that their bending-load capacity (at equal torque loading) was at least equal to and actually slightly greater than that of standard involute gears. The scoring resistance of the HCRNIF gears in the NASA tests appeared to be lower than that of equivalent standard gears. The lower scoring-load capacity performance may have been due to inadequate profile modification on the small test gears. This design effort therefore concentrated on modifying the HCRNIF gears so that their scoring-load capacity could be improved.

All design parameters (except face width, which was reduced to be compatible with the test rig) for the test gears used in this program are representative of typical Boeing design practice for main power transmission gears. For both the standard baseline and the HCRNIF gears, engineering drawings which are simultaneously compatible with the requirements of the test rigs and representative of typical helicopter practice were prepared to facilitate the manufacture of the test gears.

Table 36 defines the basic tooth geometry for the test gears used in this program. Except for their pressure angles, tooth height, and gear tooth shape, the two sets of test gears are virtually identical in their basic proportions. Figure 144 shows a comparison of the actual tooth forms for both types of test gears (as obtained from projections of the actual teeth).

Since the HCRNIF gears are not involute in form, additional data must be provided on the engineering drawings for these gears to obtain the tooth shape required. Although the mathematics that describe the noninvolute form used are quite complex, the desired result can be expressed as a series of X-Y coordinates which uniquely define the tooth surface. These coordinates (Figure 145) were calculated by a Boeing-developed computer program and added to the drawing. Since a CNC gear tooth grinder was used to finish the gear teeth, these coordinates are sufficient to fully define the gear tooth shape.

In addition to information which allows the tooth form to be manufactured, the drawing must also provide information that will allow the HCRNIF gear teeth to be inspected to be sure that they meet the theoretical requirements. Lead, pitch, total index, and runout can be checked on the HCRNIF gears in the same manner as is done for conventional involute gears since these inspections are not dependent upon the tooth form. Checking the profile shape is, however, another matter. While it may be possible simply to check the coordinates of a tooth with a coordinate-measuring machine, this would be an imperfect test at best.

However, advantage can be taken of the fact that an involute check on a conventional gear is not actually a check of its profile as such but rather of the deviation between the actual physical gear tooth shape being checked and the theoretical involute curve. This being the case, if a perfect involute gear were subjected to an involute check on a conventional involute-checking machine, it would yield a straight-line output (i.e., the difference between the actual tooth shape and the theoretical involute shape would be zero). A conventional involute chart is thus a plot of the deviation between the tooth being inspected and its theoretically perfect involute shape and not a plot of the involute itself. The computer program used to calculate the HCRNIF tooth shape

TABLE 36. TEST GEAR CONFIGURATION

	Standard baseline		HCRNIF	
Parameter	Pinion	Gear	Pinion	Gear
Part number	SK32344	SK32345	SK32346	SK32347
Number of teeth	33	58	33	58
Center distance (in.)	10	10	10	10
Face width (in.)	0.50	0.50	0.50	0.50
Diametral pitch	4.55	4.55	4.55	4.55
Pressure angle (deg)	25	25	21	21
Pitch diameter (in.)	7.2527	12.7473	7.2527	12.7473

Standard contact ratio, involute form (SCRIF)

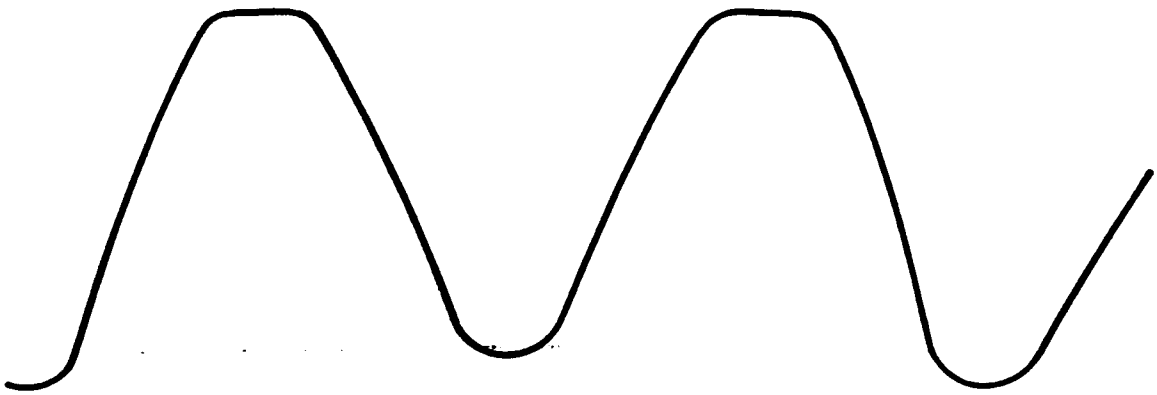

High contact ratio, noninvolute form (HCRNIF)

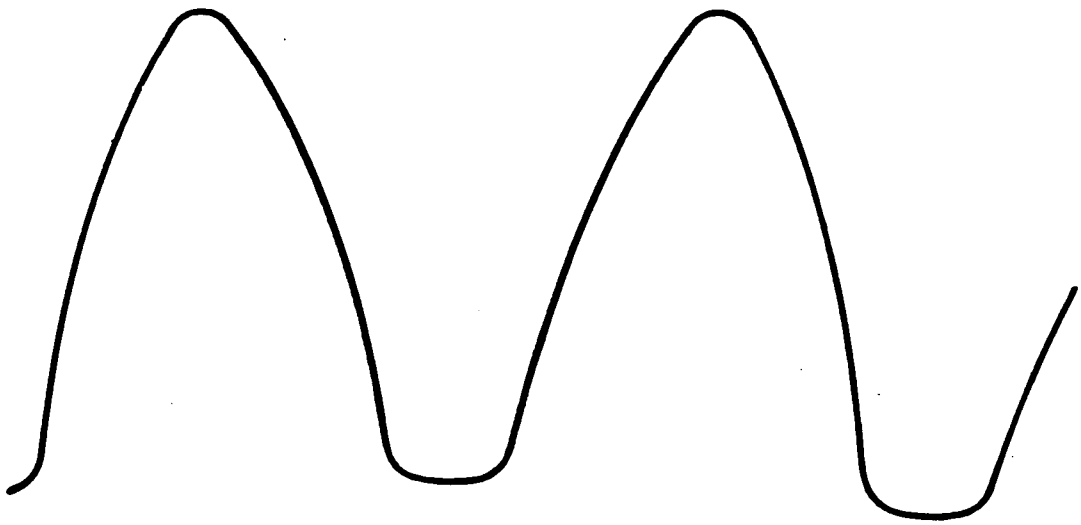

Note: Enlarged tracing made from actual gear teeth

Figure 144. Comparison of Standard Involute Tooth Form and HCRNIF Gear Tooth Profiles

Nominal tooth thickness
Profile coordinate system
Note: Origin is at intersection of tooth space centerline and pitch circle.

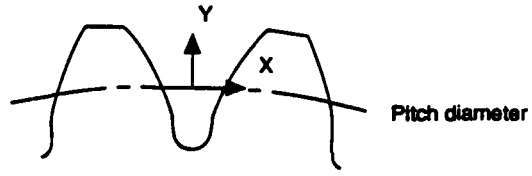

Pinion X	Pinion Y	Gear X	Gear Y
0.39456	0.38134	0.36196	0.32361
0.36594	0.34395	0.33968	0.28838
0.33932	0.30753	0.31894	0.25431
0.31459	0.27208	0.29964	0.22139
0.29164	0.23762	0.28170	0.18961
0.27036	0.20415	0.26504	0.15895
0.25065	0.17166	0.24957	0.12939
0.23241	0.14015	0.23531	0.10089
0.21567	0.10955	0.22210	0.07344
0.20022	0.07990	0.20988	0.04704
0.18598	0.05118	0.19857	0.02164
0.17286	-0.02337	0.18812	-0.00278
0.16078	-0.00357	0.17747	-0.02890
0.15082	-0.02704	0.16774	-0.05388
0.14159	-0.04986	0.15884	-0.07777
0.13304	-0.07205	0.15072	-0.10063
0.12513	-0.09365	0.14331	-0.12249
0.11780	-0.11470	0.13660	-0.14345
0.11111	-0.13524	0.13047	-0.16352
0.10494	-0.15528	0.12489	-0.18277
0.09923	-0.17487	0.11979	-0.20126
0.09397	-0.19404	0.11514	-0.21905
0.08912	-0.21283	0.11089	-0.23619
0.08464	-0.23128	0.10700	-0.25276

22432 (145) 12/1093 wb

Figure 145. Coordinates of HCRNIF Tooth Form

also calculates the deviation of the HCRNIF shape from a theoretical involute at every point along the profile. With this information, a gear tooth control chart can be defined for the HCRNIF gears.

A conventional gear drawing will contain a gear tooth control chart (sometimes called a K-chart) which defines the tip and flank modifications applied to the theoretical involute shape to accommodate tooth deflections. In a similar manner, the HCRNIF gear drawings contain profile control charts which not only show the tip and flank modifications to accommodate tooth deflections, but also show the deviations of the HCRNIF teeth from their theoretical shape. The HCRNIF gear tooth control charts are thus composite charts. With this information, the HCRNIF gears can be inspected on a conventional involute checker to determine if the tooth shapes are acceptable. The gear tooth control charts used for the test pinions and gears are shown in Figures 146 and 147, respectively. Note from these figures that the modifications on both the conventional pinion and its mating gear are relatively small *negative* values (as is typical), while the modifications on the HCRNIF pinion and gear are relatively *large positive and negative* values. The involute charts which result are interesting, as Figures 148 and 149 clearly show. Figure 148 is a typical involute chart for a baseline gear, while Figure 149 is a typical "involute" chart for a corresponding HCRNIF gear. Note carefully the change in scale between the baseline gear (0.00020 inch per division) and the HCRNIF gear (0.00050 inch per division).

Fabrication

Five sets of each type of gear were fabricated (five HCRNIF pinions, five standard pinions, five HCRNIF gears, and five standard gears). The gears were manufactured from BMS 7-223 Type III (VASCO X2M) steel in accordance with Boeing's normal practice so that they were fully representative of actual helicopter main power transmission gears. A complete inspection data history (lead, profile, spacing, runout, and finish) was compiled for each gear set. Test slugs were included in the heat-treat lot with these gears so that their metallurgical characteristics

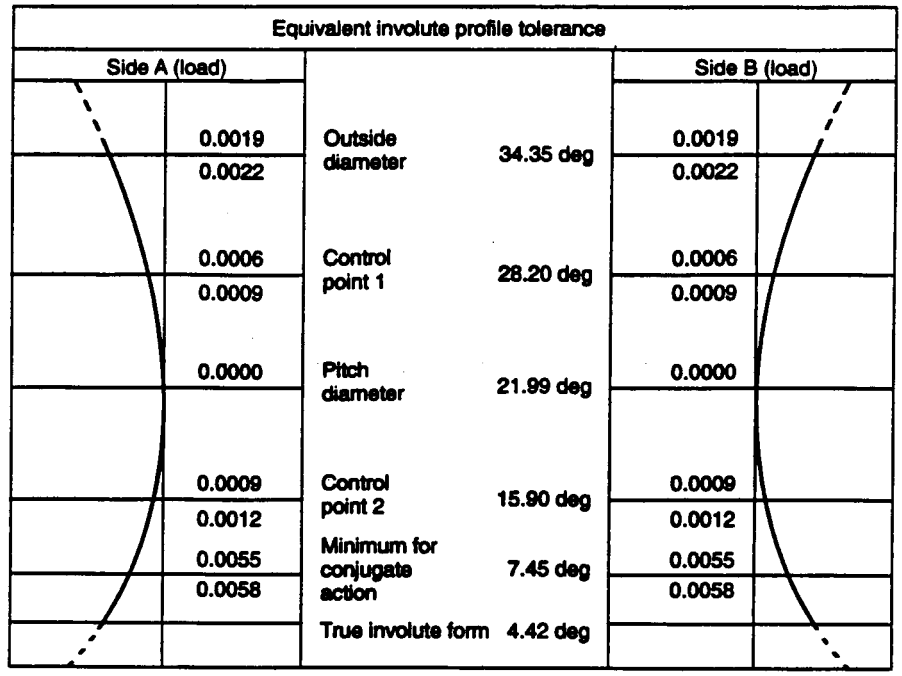

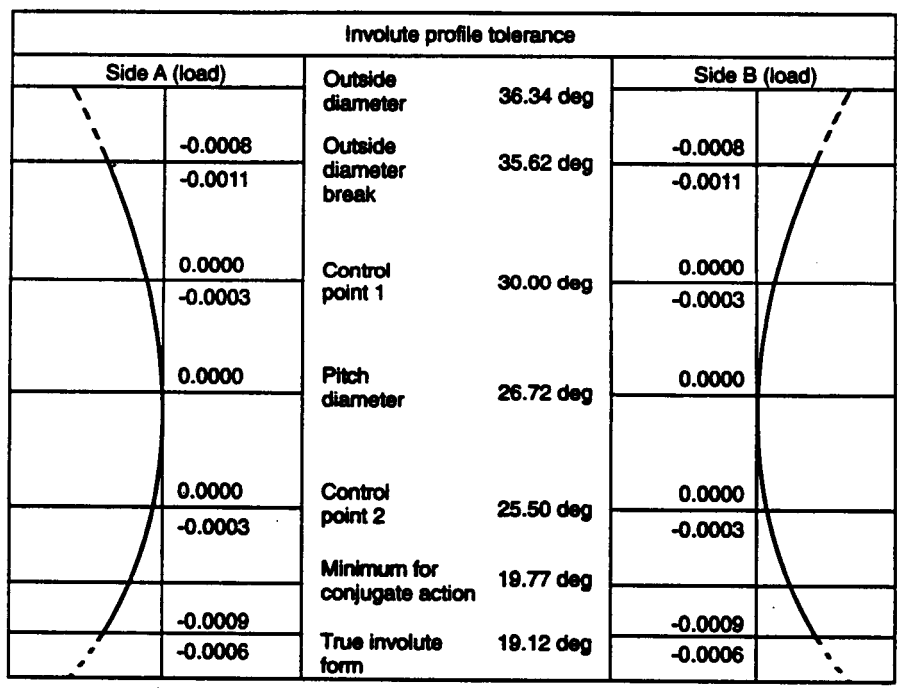

22432 (146) 12/9/93 JW

Figure 146. Tooth Control Charts for Test Pinions

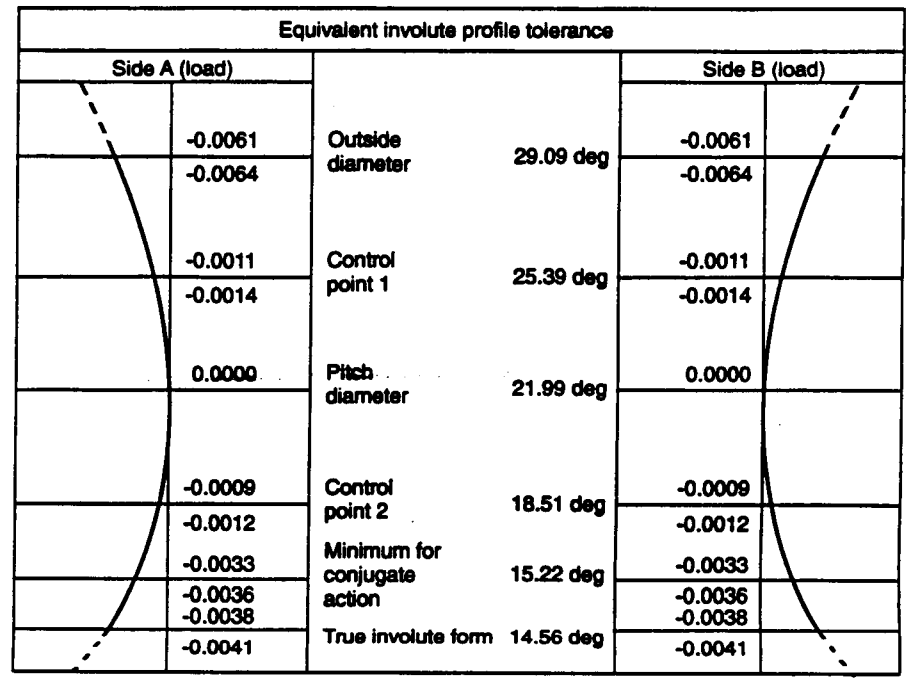

HCRNIF

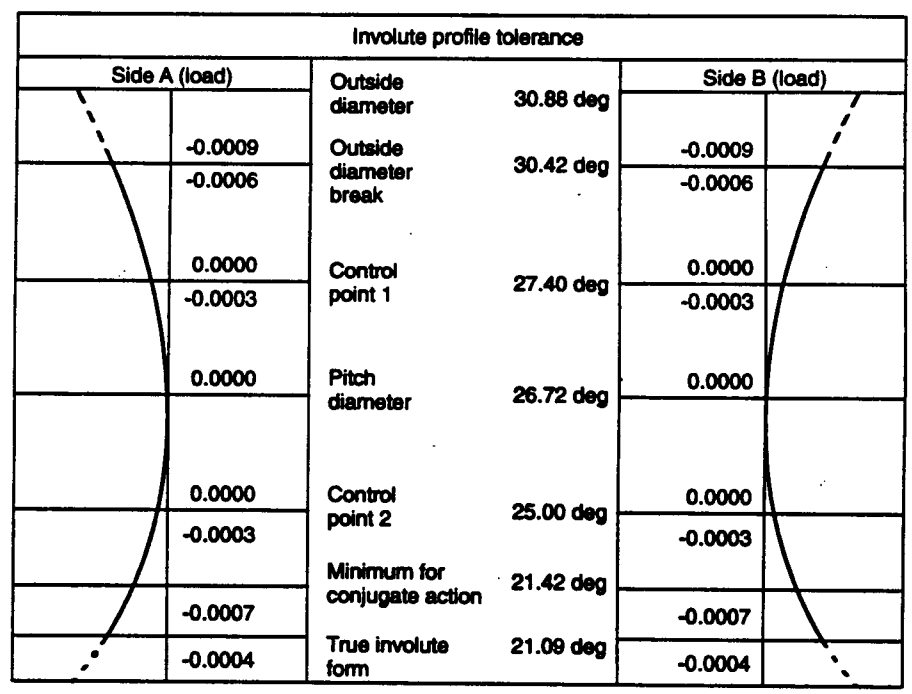

Standard baseline

22432 (147) 12/9/93 JW

Figure 147. Tooth Control Charts for Test Gears

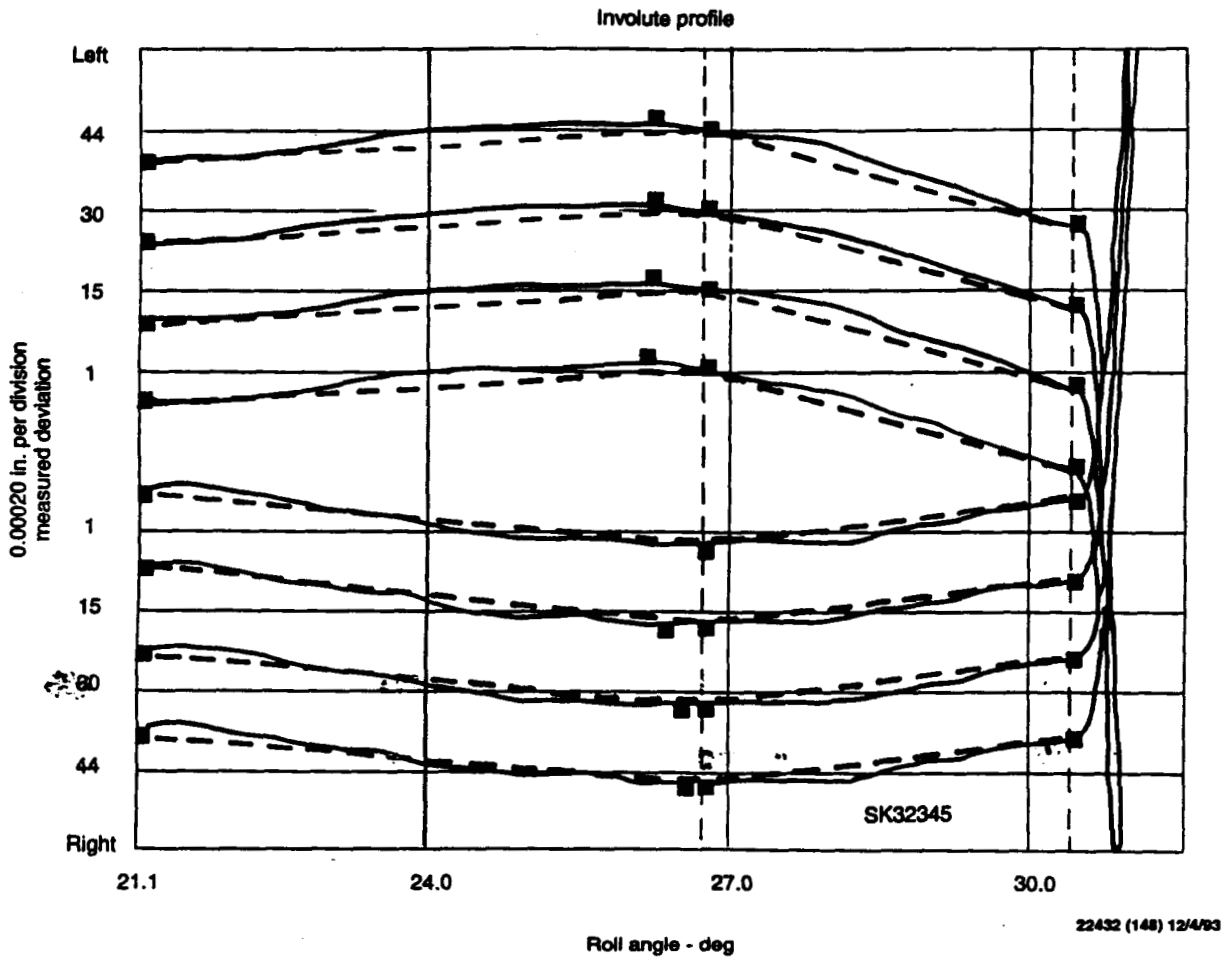

Figure 148. Typical Involute Chart for a Baseline Gear

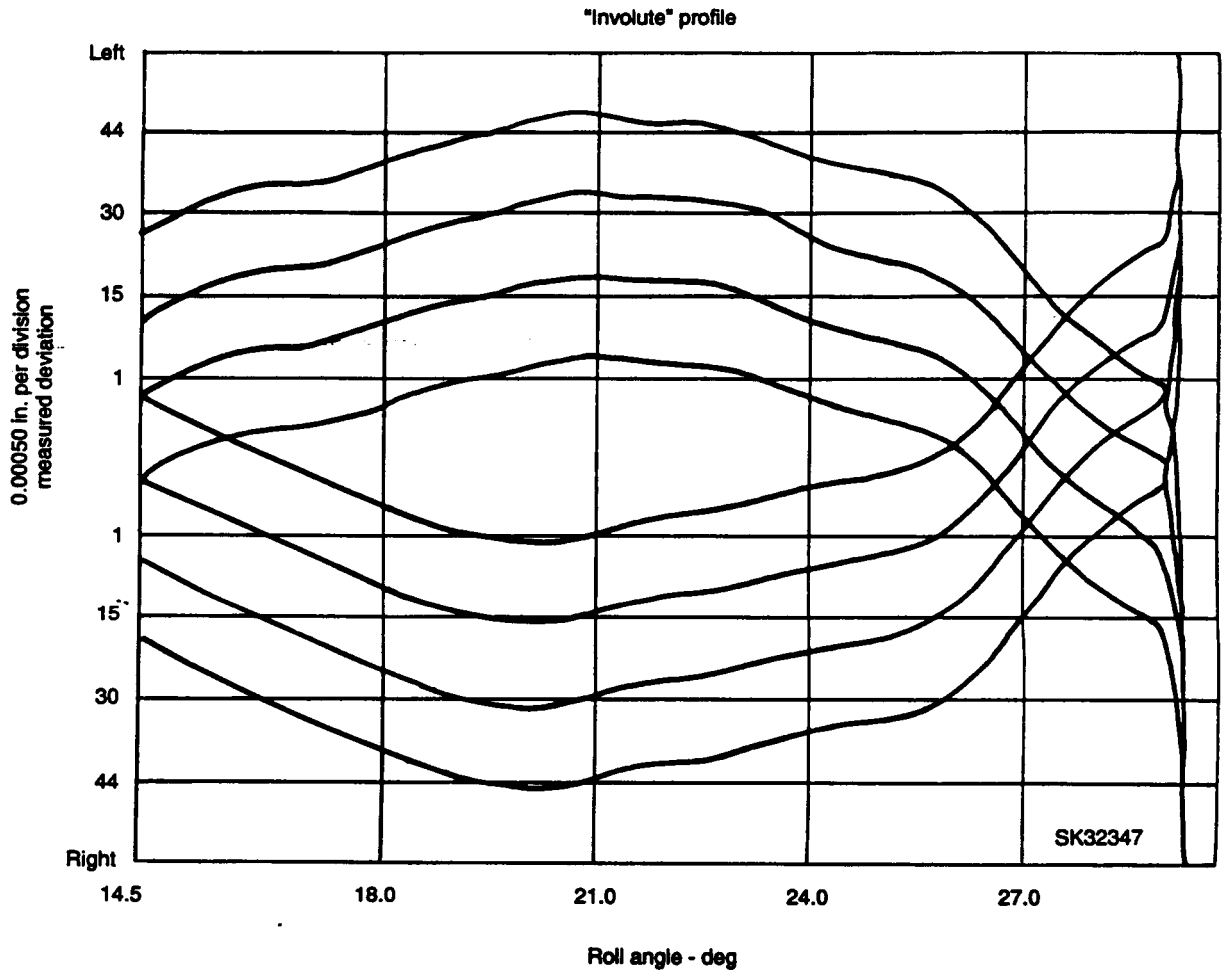

Figure 149. Typical "Involute" Chart for an HCRNIF Gear

could be defined. Although the HCRNIF gears use a tooth form that is different than that used on virtually all helicopter gears, this deviation did not significantly affect either the manufacturing methods required or the inspection techniques employed.

The HCRNIF gears were rough-cut with a conventional involute hob (configured for the lower pressure angle and increased whole depth characteristic of HCR gears) as the NIF deviation from an equivalent theoretical involute is small (on the order of a few thousandths of an inch). The baseline gears employed a standard contact ratio involute tooth form; thus they were manufactured in the normal manner (rough-hobbed, heat-treated, finish-ground), with no special provisions required.

The noninvolute tooth form was defined by Boeing in terms of X-Y coordinates for the required profile. These coordinates were then input to a CNC form wheel dresser used directly by the gear manufacturer on a gear tooth form-grinding machine. A similar process was used for the standard involute gears and they were ground on the same machine.

All test gears were manufactured in a manner that essentially duplicated the processes used for current Boeing production gears so that the test results can be readily compared with expected performance of actual future production parts.

Complete gear tooth geometry (lead, profile, spacing, runout, and finish) and metallurgical (case hardness, case depth, core hardness, microstructure) inspection data were compiled and evaluated for each gear set. Except for one problem with some of the HCRNIF gears, the resultant gears were within the engineering drawing requirements except for minor deviations that were judged to be acceptable within the context of normal helicopter production gears of similar size and type.

The only significant problem encountered in the manufacture of the test gears was case/core separation on the HCRNIF pinions. This phenomenon can occur when thin cross sections, such

as the corners of the tips of gear teeth, are carburized. To guard against this problem, Boeing production gears incorporate large, rounded chamfers at the corners of the gear teeth. Because of the relatively narrow face width of the test gears, these large chamfers were not applied and some case/core separation, as shown in Figure 150, did occur.

Case/core separation occurs when the gears are quenched. During that process, the narrow tooth corners cool much more quickly than the tooth body and the case in these locations can pull away from the core material. When this occurs, the separated corner is held to the tooth by a very thin surface skin. Because this skin is so thin, a slight impact will cause the tooth corner to completely separate from the tooth. Careful examination of Figure 150 shows this thin skin on both the tooth itself and the small corner that separated from the tooth.

Although this appears to be a crack mechanism, it is not since the corner is already separated during the heat-treatment process. A small impact to the tooth is generally sufficient to fracture the thin skin holding the corner to the tooth. This was done on the test gears (using a short length of two-by-four) to remove those tooth corners that were so affected, after which the edges of the teeth were polished to remove sharp corners. Once the corners were removed as described, no further propagation occurred and the testing proceeded normally.

Test Definition

The testing conducted as part of this program concentrated on the scoring-load capacity and the noise characteristics of the HCRNIF gears since their bending and surface-load capacity has already been established. All testing was conducted in the Boeing Gear Research Test Facility, (Building 3-12, Test Cell 9) on one of the test rigs which had been configured to test spur gear sets operating in the overhung mode. This mode provides ready access to the test gears which greatly facilitates the short test run times associated with scoring and noise testing.

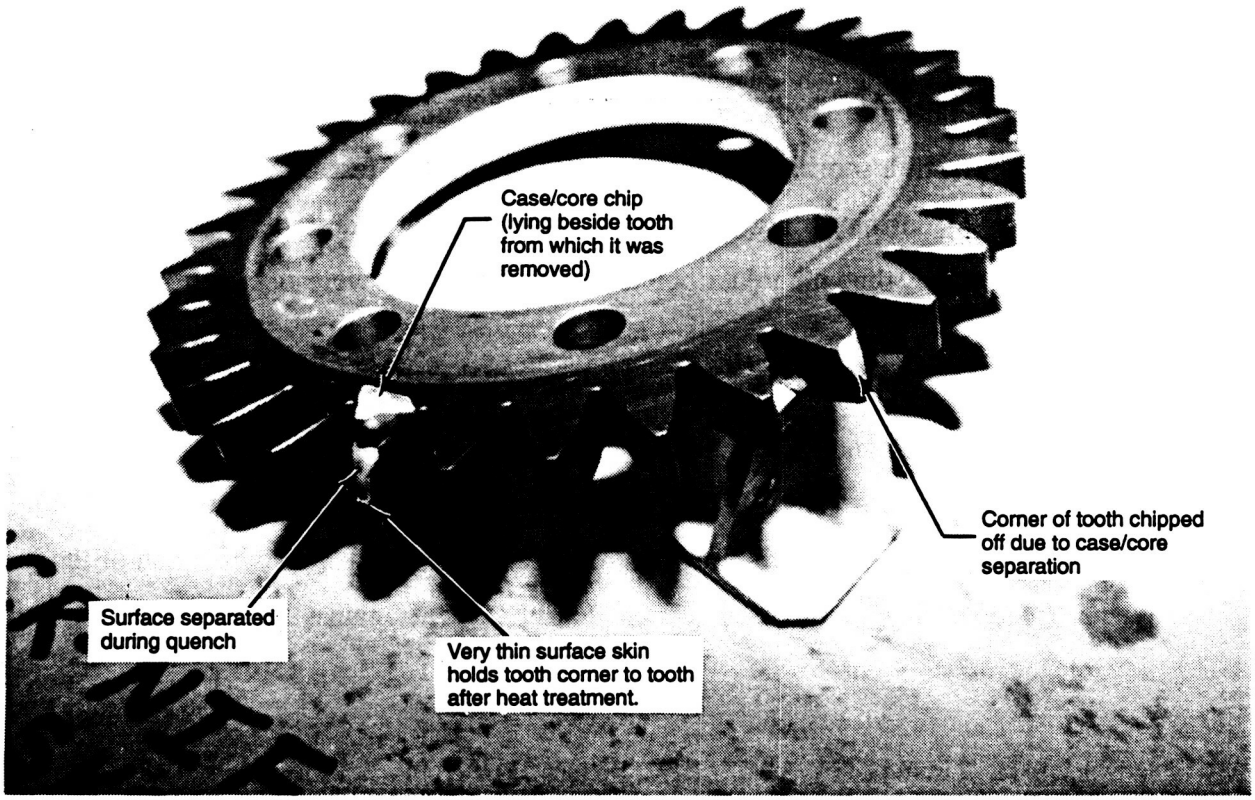

C141152 NO.15

Figure 150. Separation of Case and Core as a Result of Carburizing and Quenching

Noise Testing - Before running any load-capacity testing, each type of gear set (i.e., standard baseline and HCRNIF) was run in the gear research test rig at three different load conditions to define its relative sound characteristics. The test gear setup was identical to that used for the load testing, with the exception of the addition of a microphone to measure the noise levels. Subsequent to the noise testing, the gears were used in the scoring-test program; thus no new gears were required specifically for the noise testing.

Scoring-Load Capacity Testing - A total of 18 scoring tests (nine standard baseline and nine HCRNIF) were run. Each test was run in essentially the same manner in that increasing load levels were applied until a scoring failure occurred. Each set of test gears normally yields two data points; however, during testing, one side of one pinion of each type was damaged before any data were collected; thus nine data points per configuration were obtained rather than the expected ten.

Strain Survey - One pinion and gear set of each type was instrumented with strain gages and then rotated slowly through mesh at a wide range of load conditions so that the stresses in the tooth roots could be measured. Examination of the stress levels thus yielded a comparison of the load-capacity and load-sharing capabilities of the HCRNIF teeth against those of the equivalent standard contact ratio involute teeth.

Gear Loading

The test rig uses a closed-loop, locked-in-torque loading system. For reference purposes, the calculated bending stresses, contact stresses, and flash temperatures for the standard contact ratio test gears, as functions of test pinion torque, are shown in Figures 151, 152, and 153, respectively. The strain survey loading was selected to simulate the stress levels that would be encountered in a typical helicopter application, while the scoring loads were applied to induce failure so that a capacity comparison could be made.

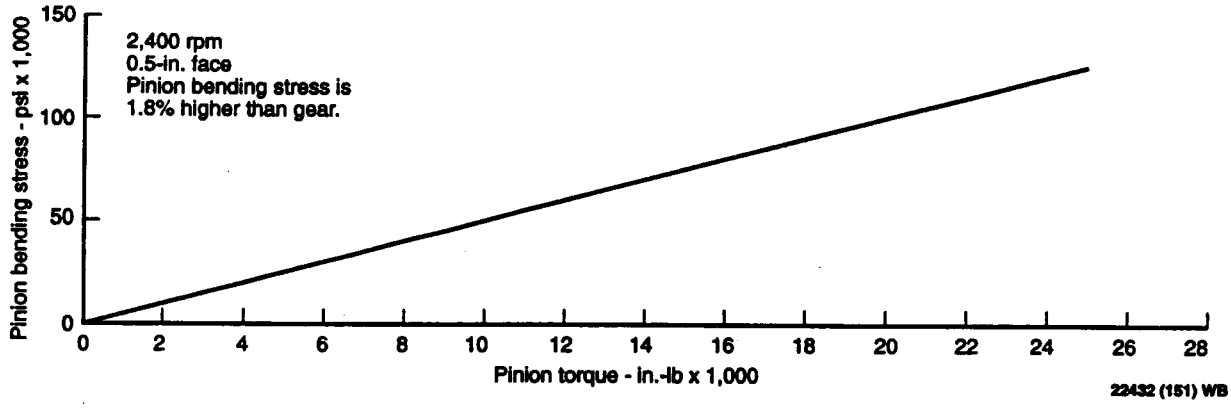

Figure 151. Calculated Bending Stress of Standard Contact Ratio Test Gears

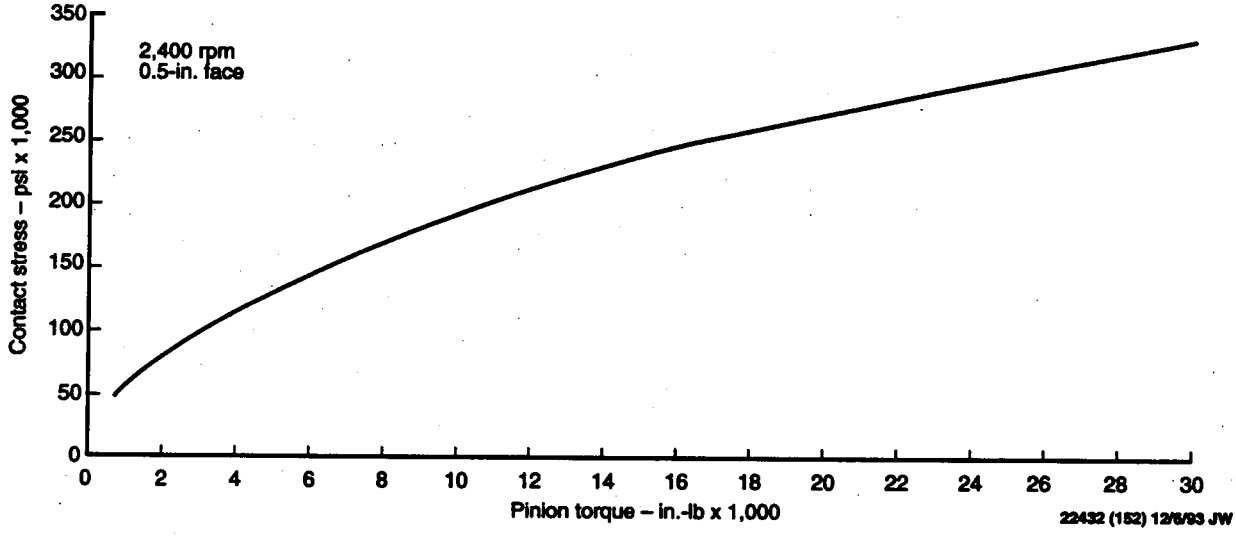

Figure 152. Calculated Contact Stress of Standard Contact Ratio Test Gears

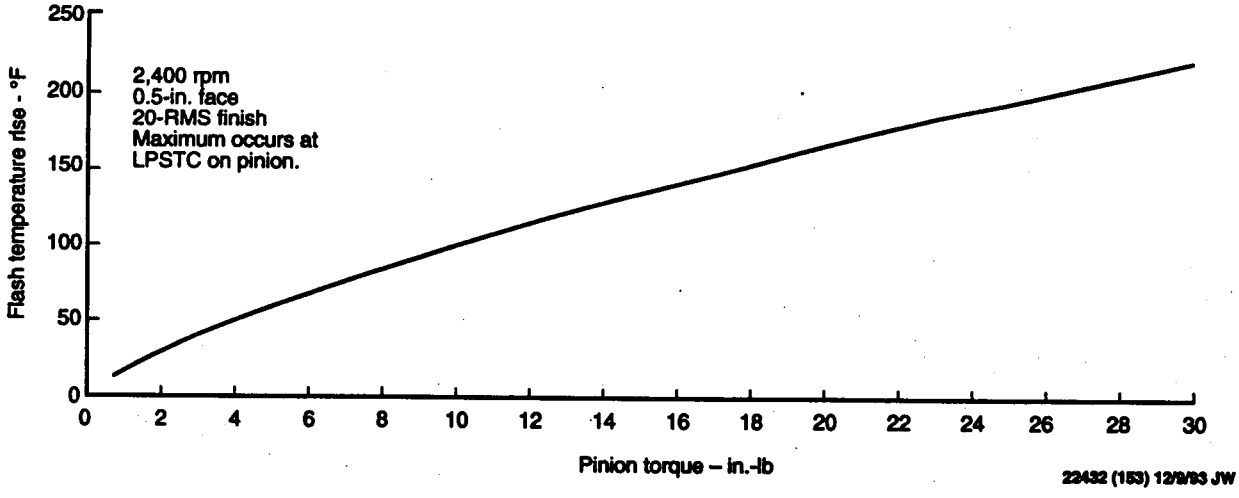

Figure 153. Flash Temperature Rise of Standard Contact Ratio Test Gears

All the test gears were loaded in the same manner. The loading system used in the test rig is closed-loop, locked-in torque. The torque load is applied by using a lever system to rotate a split coupling such that the desired amount of torque is locked into the system. With care, this allows the test torque to be accurately controlled. The load application procedure used for all test runs was the same and is defined in Table 37.

Test Procedures

Scoring - One of the two gear research test rigs was configured in the 10-inch-center distance, overhung configuration. Before the start of any testing, the strain-gaged torque shaft was calibrated to normal Boeing standards. The primary belt drive was set to provide a test gear speed of 2,400±200 rpm. All test gearbox oil tanks were flushed and refilled with DOD-L-85734 oil (in this case, Exxon ETO-25). The oil jet to the test gear was positioned on the outlet side of the mesh, as Figure 154 shows.

The oil pressure and temperature to both slave gearboxes were set and maintained at 40±10 psi and 135±20°F, respectively, for all test runs. The oil pressure and temperature to the test gears were set and maintained at 35±10 psi and 195±5°F, respectively, for the initial test runs. The size of the orifice of the test gear oil jet was initially selected to provide 0.32±0.05 gpm flow to the test gears at the cited pressure and temperature settings.

As the testing progressed, however, scoring runs at higher loads than originally anticipated dictated a change in the size of the oil jet orifice such that the flow was increased to 0.67 gpm, at which level the pressure was 28 psi while the oil temperature was maintained at 195±5°F.

Oil inlet temperature is a critical factor in the conduct of scoring tests, and the construction of the test rig allows this parameter to be accurately controlled. The bearings that support the shafts are housed in the slave box immediately behind the test gear housing; thus the test section oil system feeds only the test gears and no other members (not even a seal). This effectively isolates

TABLE 37. TORQUE APPLICATION PROCEDURE

1.	Apply required torque during stabilization period.
2.	Rotate shafts at least two complete turns by hand with main drive motor off but with all lube systems running.
3.	Recheck and readjust torque within +5 percent of target value.
4.	Run main drive motor for 20 to 40 seconds and recheck torque.
5.	If torque is within +5 percent of target, proceed with test run. If torque is not within +5 percent of target, repeat steps 2 through 4 until this requirement is met.

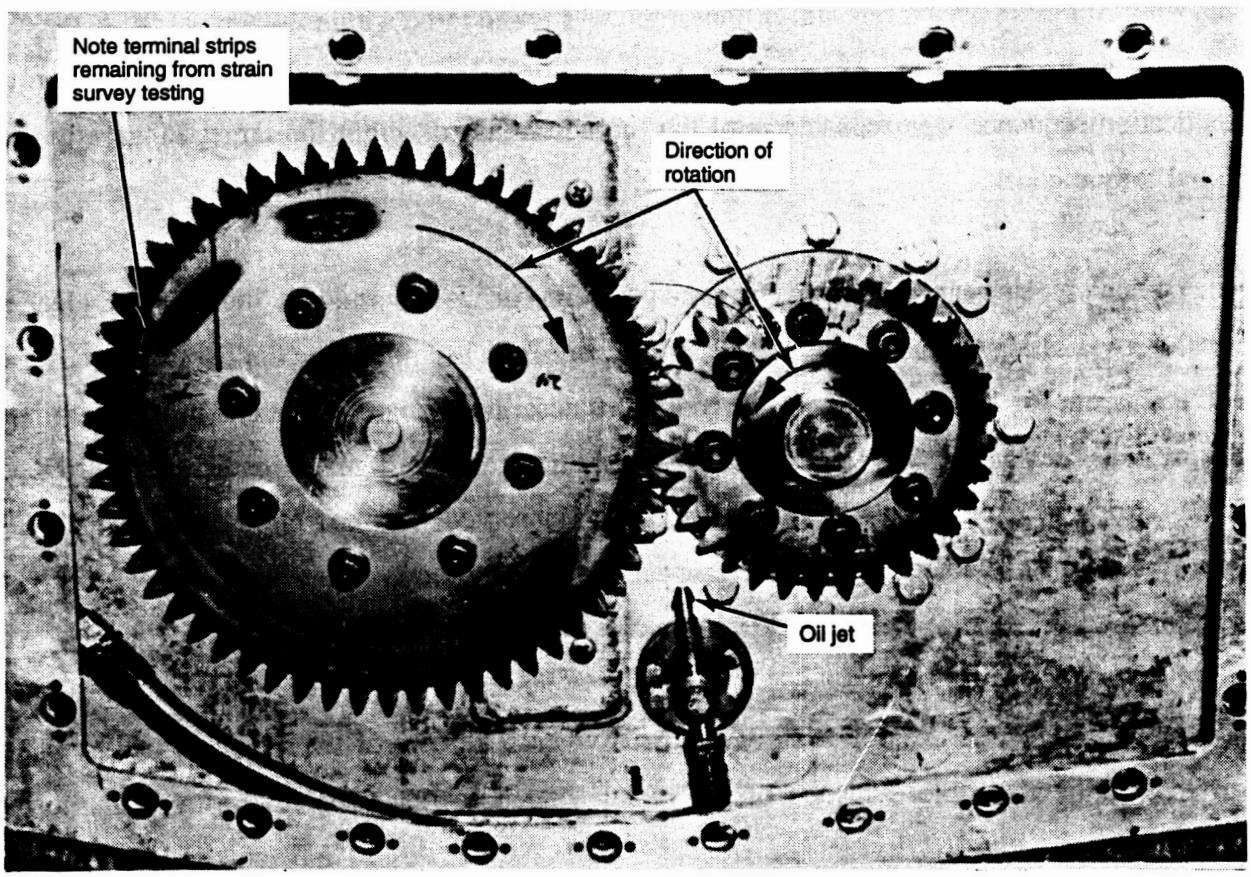

C142680 NO.9

Figure 154. Configuration of Gear Test

the test gears so that their capacity can be determined accurately. In addition, in order to provide precise temperature control of the test gear oil supply, the test gear oil sump is heavily insulated, and a very large, in-line oil heater applies heat as required just before the oil reaches the jet that feeds the test gears.

Before any test runs were conducted, the lubrication systems for all boxes were run, with the main drive motor off and the gears stationary but in the oil stream, with appropriate control exercised on heating, cooling, and flow to establish stabilized operation at the desired pressure, temperature, and flow conditions. Torque was applied during the stabilization period and the torque reading was rechecked and reset, if required, immediately before each test run.

Since the torque on this rig was applied statically, it was necessary to check it after the stand had run for a short period of time. If the torque was found to be within the target range, the test run was allowed to proceed. If the torque was found to be outside of the target range, the torque application sequence was repeated until the torque remained within the target range after the initial torque check.

The planned scoring-test procedure consisted of a series of 15-minute-long, incrementally loaded runs. An initial load estimated to be below the scoring-failure point was applied to the gear set and it was run for 15 minutes under the conditions described above. At the end of the 15-minute run, a visual evaluation was conducted of the condition of the test gears' loaded tooth surfaces. If no scoring in excess of the failure criterion was observed, the next higher incremental load was applied and the 15-minute run and inspection sequence were repeated. This procedure was continued until a scoring failure was achieved.

A scoring failure was deemed to have occurred when 5 percent of the available tooth contact surface exhibited visible evidence of the radial scratch marks associated with such scoring failure.

Static Strain Survey - One pinion and one gear of each type were instrumented with a total of eight strain gages in the root and fillet locations, respectively. The test was conducted statically (i.e., slow rotation); thus direct wire hookups (no sliprings or telemetry) were used. Data were recorded for later analysis with a MEGADAC 2000.

Root Gages - Two root gages were applied in each of four adjacent tooth spaces as Figure 155A shows. The "O" gage in each tooth space was applied 0.125 inch in from the side of the gear on which the serial number is marked; the "I" gages were applied 0.125 inch in from the opposite side of the gear as Figure 156 shows. The gages were applied along the fillet curve such that the right end of the active gage surface was tangent to the left side of the centerline of the tooth space when the gear is viewed from the side on which the serial number is marked. The gages were identified as "1RO," "1RI," "2RO," "2RI," etc, proceeding in a counterclockwise manner as Figure 156 shows. Care was exercised to insure that no wiring, adhesive, etc, extended up the tooth profile beyond the TIF diameter. Material that extends beyond this point would interfere with the proper engagement of the gears when installed and the gages would thus be destroyed.

Fillet Gages - Two fillet gages were applied in each of four adjacent tooth spaces, 180 degrees away from the root gages, as Figure 155B shows. The "O" gage in each tooth space was applied 0.125 inch in from the side of the gear on which the serial number is marked and the "I" gages were applied 0.125 inch in from the opposite side of the gear, as Figure 156 shows. The gages were applied along the fillet curve such that the left end of the active gage surface was just below the TIF diameter when the gear is viewed from the side on which the serial number is marked. The gages were identified as "1FO," "1FI," "2FO," "2FI," etc, proceeding in a counterclockwise manner as Figure 156 shows. As was the case with the root gages, care was exercised to insure that no wiring, adhesive, etc, extended up the tooth profile beyond the TIF diameter.

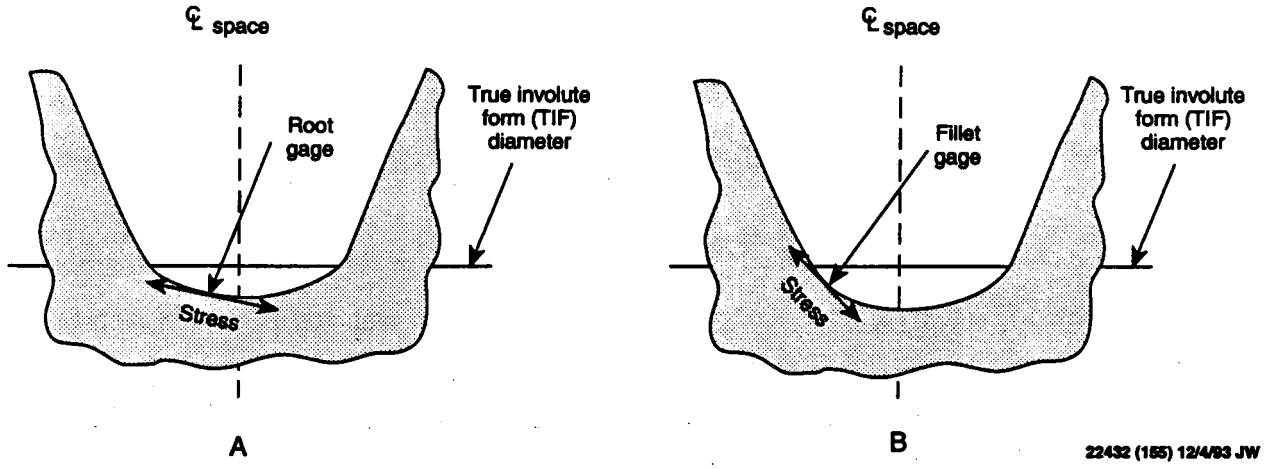

Figure 155. Locations of Strain Gages in Tooth Roots and Fillets

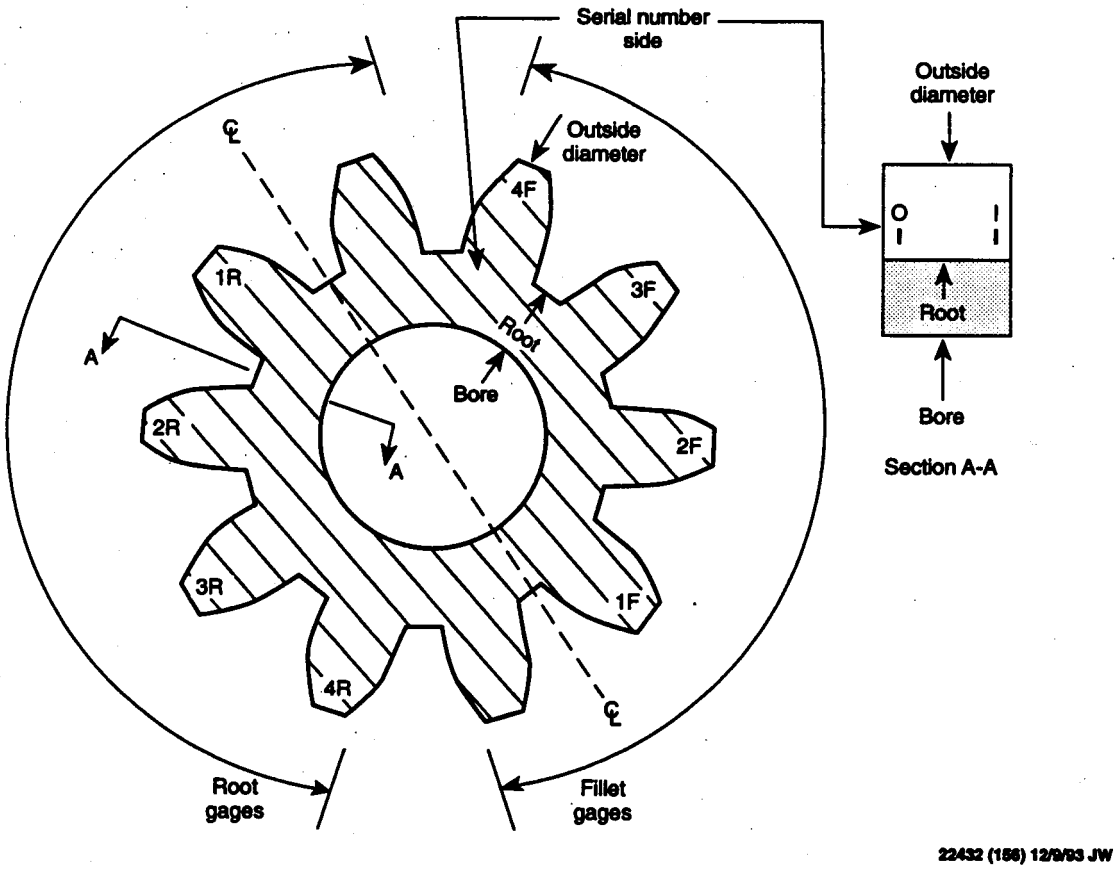

Figure 156. Locations and Identification of Strain Gages Around the Gear

Gage Placement - In order to insure that the gages were accurately placed, casts were obtained of the tooth spaces in which the gages were to be laid. These casts were then sectioned and marked to indicate the exact gage location required. The casts were used as guides by the instrumentation technician in placing the gages.

The instrumented set of gears was installed in the gear research test rig and wired directly to the MEGADAC strain-recording device. The static strain survey was conducted by rotating the gears slowly through mesh (i.e., hand rotation speed driven through a very high-ratio auxiliary gear to the pinion shaft), at seven load levels: 25, 50, 75, and 100-percent (9,287 in.-lb pinion torque), and 150, 200, and 250-percent torque.

Noise - Noise measurements were taken on one set of each type of test gear configuration (i.e., one standard baseline set and one HCRNIF set). Data were acquired at 60, 80, and 100-percent torque levels, all at the full test speed of 2,400 pinion rpm. The stand was not modified for this testing as a floor-mounted microphone was used to obtain data for all test runs. The microphone was located directly in front of the gear mesh point at a distance of about three feet from the face of the test housing cover. The microphone position was held constant for all test runs and all data were obtained after the test box had reached stabilized temperature conditions. Like the scoring tests, the oil temperature was maintained at 195 ± 5°F for all test runs.

Test Results

Scoring - The results of the scoring testing indicate that the scoring-load capacity of the HCRNIF gears was slightly higher than that of the standard baseline gears. Figure 157 summarizes the results of the scoring testing. The average failure loads, as shown in Figure 157, for the standard baseline and HCRNIF gears were 23,400 and 25,000 in.-lb pinion torque, respectively. While this indicates a slight advantage to the HCRNIF gears, a difference this small (about 7 percent) is too insignificant to conclude much other than that the basic scoring-load capacity of the standard baseline and HCRNIF gear tooth forms is about the same.

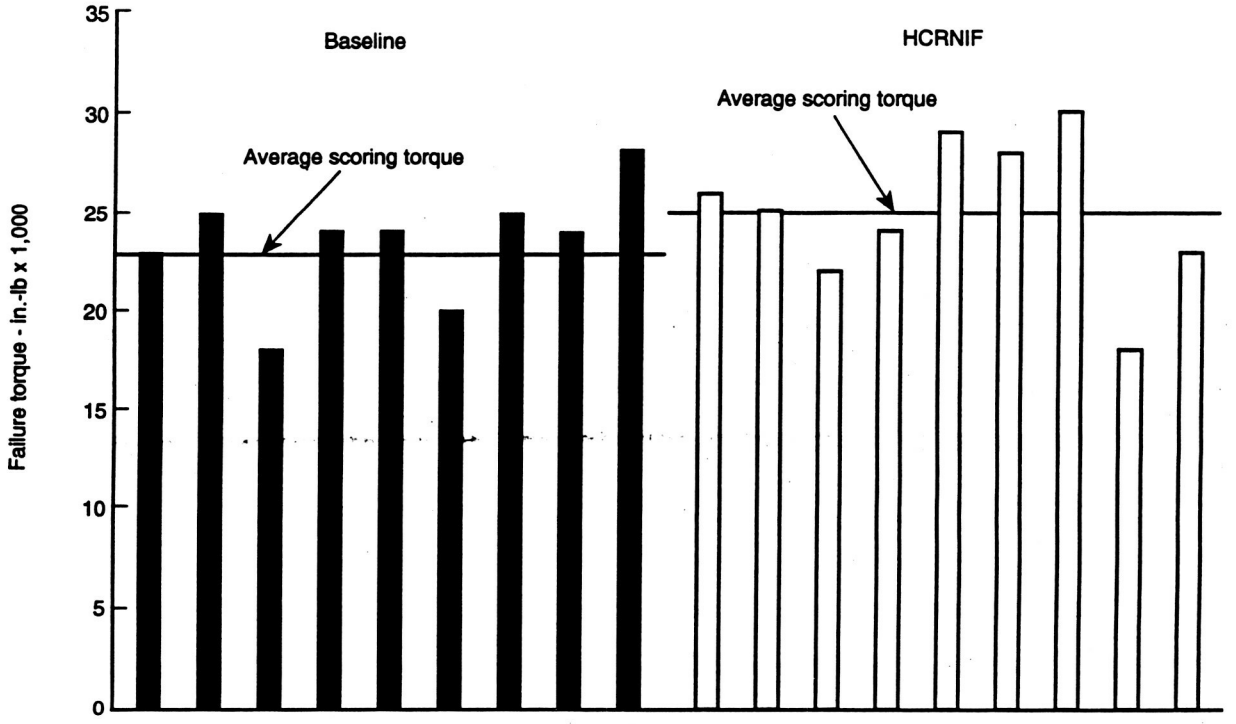

Figure 157. Results of Scoring-Load Testing

Figure 158. Plastic Flow Failure of Gear Teeth

During the scoring-load testing, it became obvious that the initial 0.32-gpm oil flow was inadequate to cool the gears at torque levels above about 23,000 in.-lb. Above this level, rather than scoring failure, the gears actually experienced a plastic flow failure mode, as Figure 158 clearly shows. Because of this the oil flow was increased to 0.67 gpm to improve cooling to the gears at higher torque levels. After this change, the failure mode again became scoring rather than plastic flow.

Noise - The noise test results indicate that the HCRNIF gears are significantly quieter than the standard baseline at the 80 and 100-percent load points but slightly noisier at the 60-percent load point. The spectra shown in Figures 159, 160, and 161 show both the fundamental mesh frequency (1,320 Hz) and the first harmonic (2,640 Hz). In all cases, the fundamental is the predominant noise source while the first harmonic, though clearly evident, is much less pronounced.

The peak noise levels at each of the load points examined are summarized in Figure 162. Clearly, the HCRNIF gears experience a minimum at the 80-percent torque load point, while the standard baseline gears exhibit increasing noise levels with torque over the range tested. Considering the overall accuracy of the gears, these conditions indicate that the profile modifications that were applied to the HCRNIF gears were most likely nearly optimum, from a noise viewpoint, somewhere between the 60- and 100-percent load points. Similarly, since the noise of the standard baseline gears increased with load, we can conclude that their profile modifications are optimum at some load either above 100 percent or below 60 percent.

In general, for gears that have significant profile modifications in the form of tip and/or flank relief, the noise level observed at constant speed will gradually decrease as load is applied until all of the tip and flank relief has been absorbed by tooth deflections. At that point, the noise level will generally start to increase due to tip and flank interference. Considering the noise levels of the standard baseline gears in an absolute sense, then, it is likely that all of the profile modification was used up by the time the 60-percent load point was reached. That is, purely

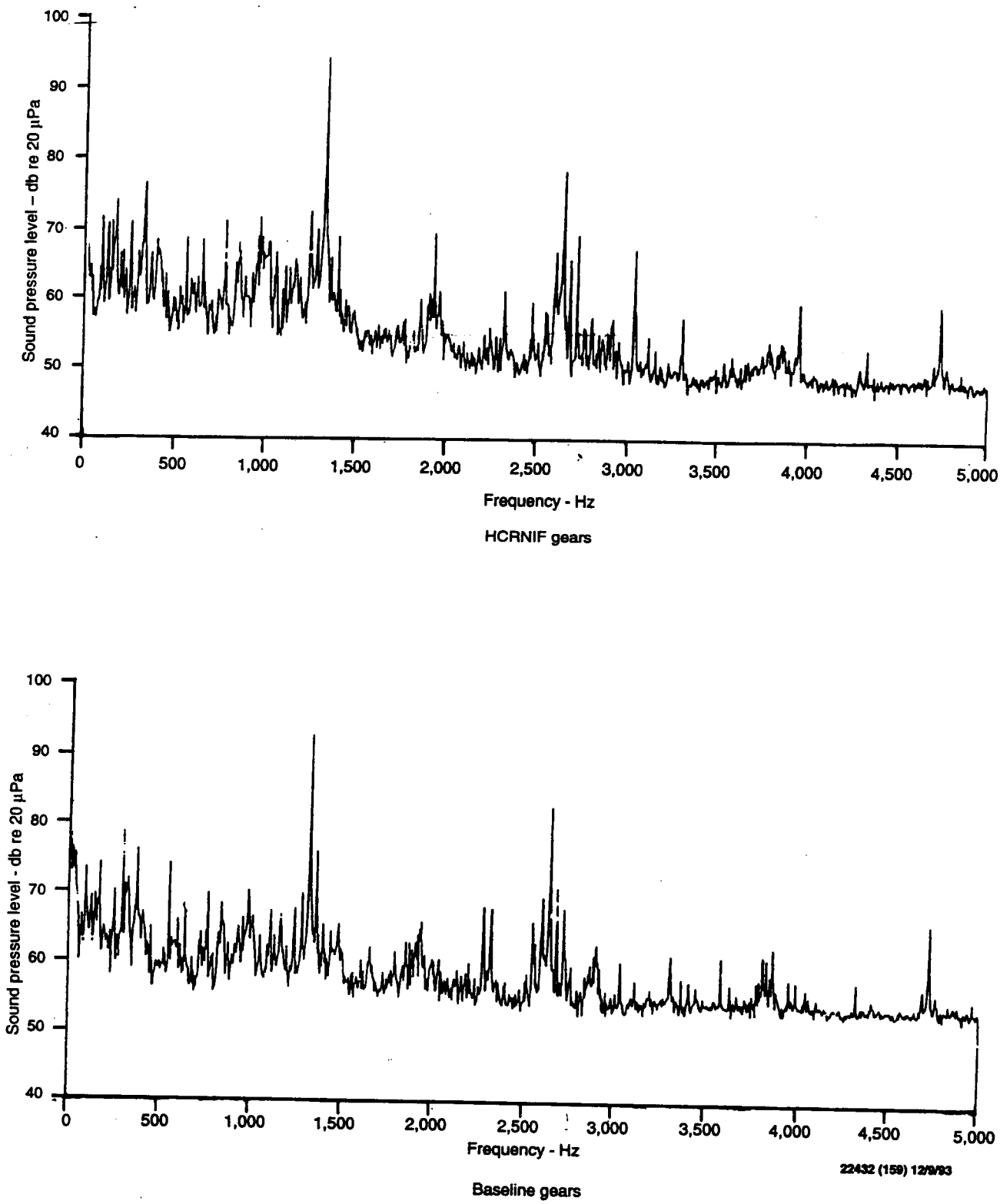

Figure 159. Comparison of Noise Levels of Baseline and HCRNIF Gears at 60-Percent Torque

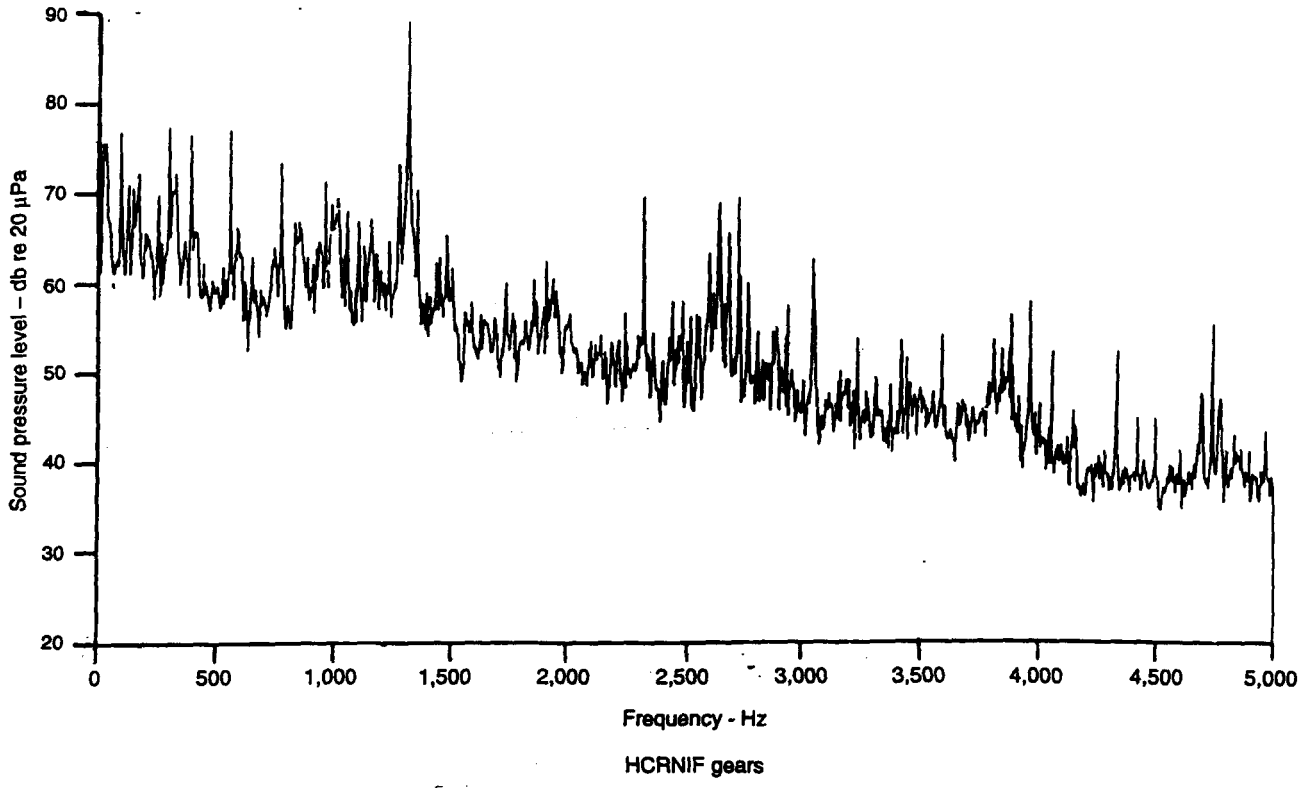

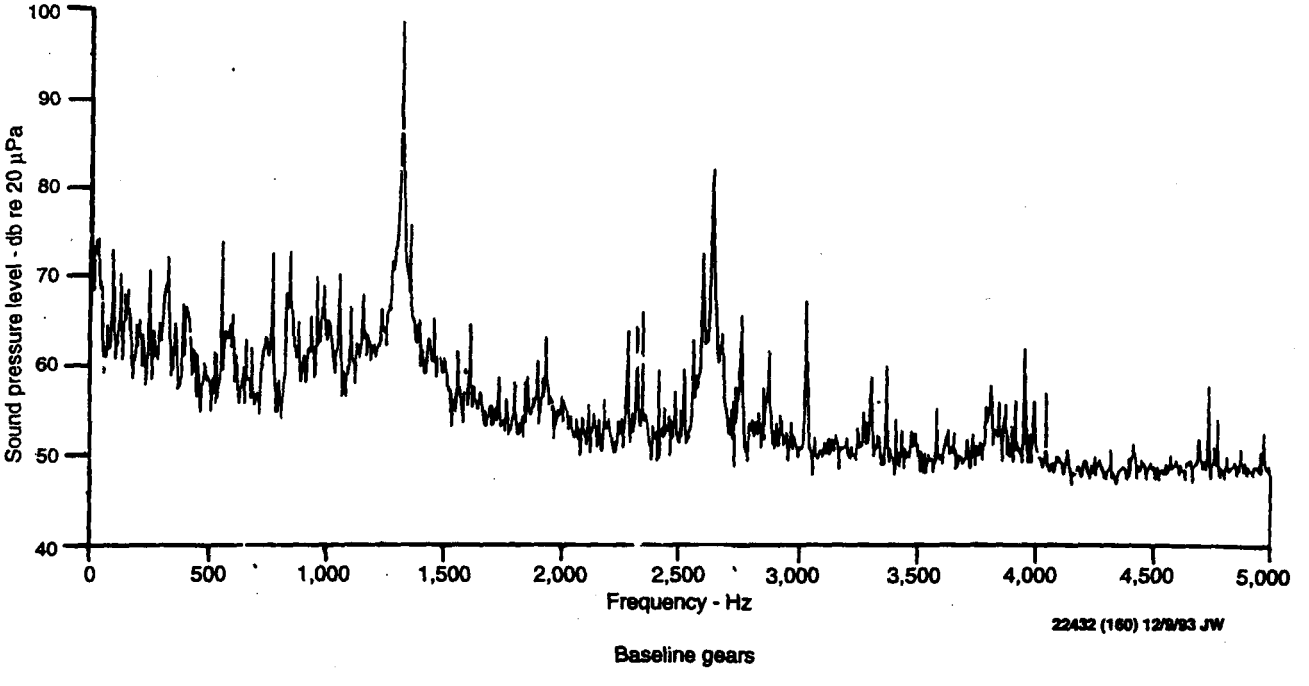

Figure 160. Comparison of Noise Levels of Baseline and HCRNIF Gears at 80-Percent Torque

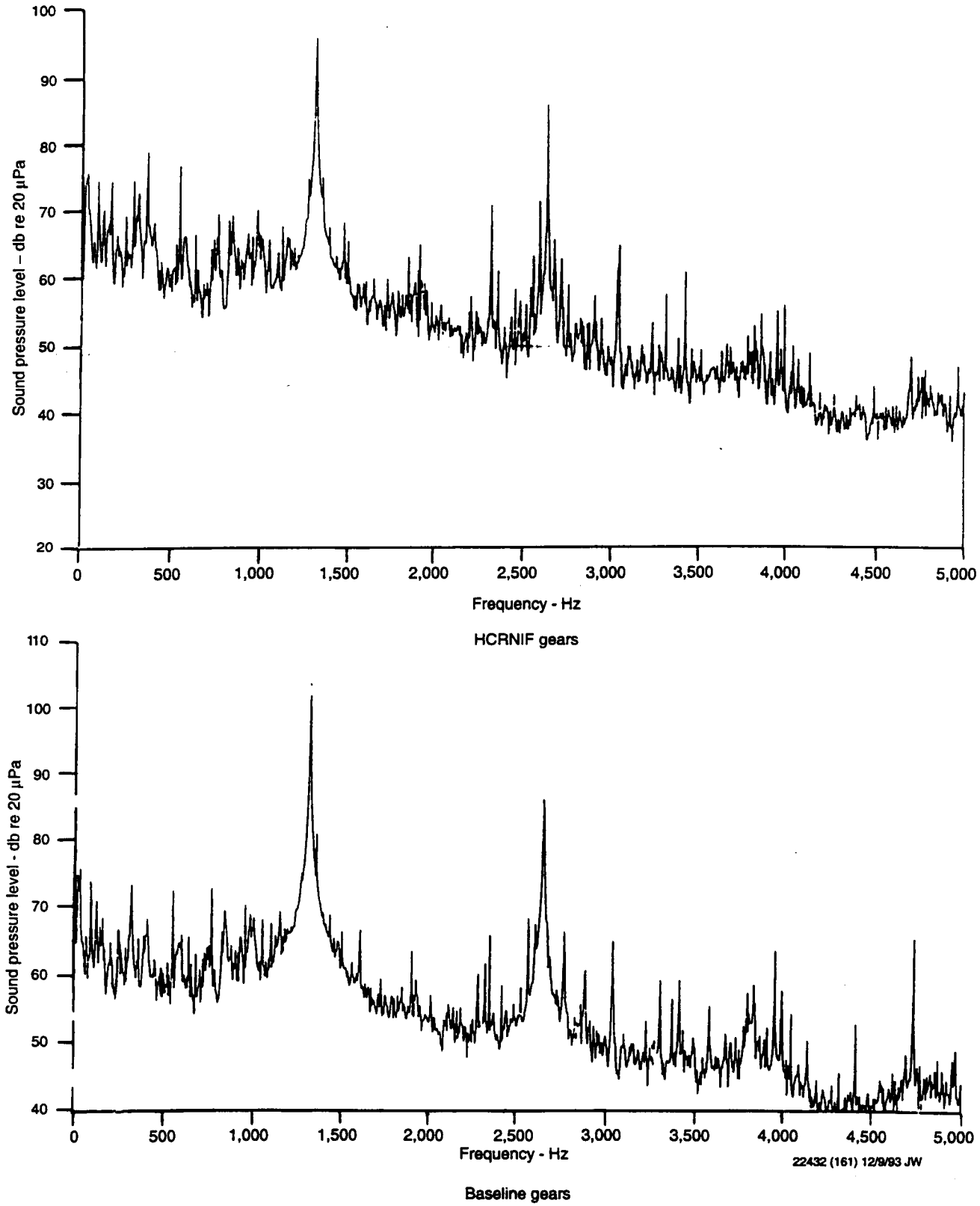

Figure 161. Comparison of Noise Levels of Baseline and HCRNIF Gears at 100-Percent Torque

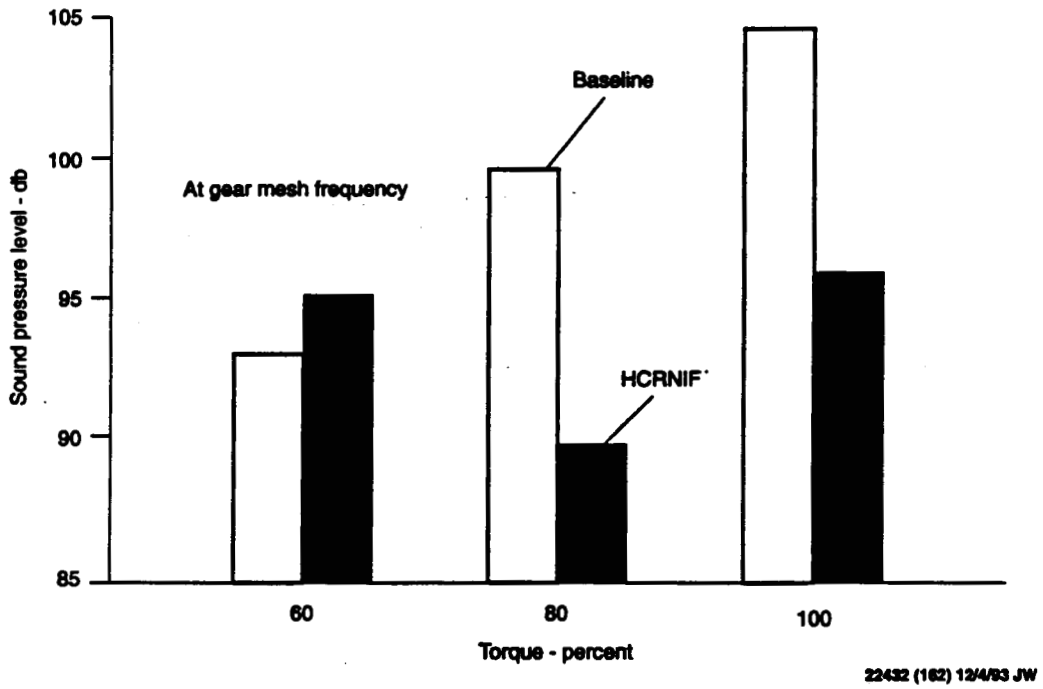

Figure 162. Summary of Peak Noise Levels of Baseline and HCRNIF Gears

from a noise viewpoint, the standard gears were undermodified. In view of the fact that the standard baseline gears, for the same total transmitted torque, will have higher per-tooth unit loads than the HCRNIF gears (HCR gears share the total load among more teeth in contact; thus the individual tooth loads are reduced), the observation that the baseline gears are undermodified appears to be correct. Both the standard baseline and HCRNIF gears have the same relative tip and flank relief; thus the lower per-tooth loading on the HCRNIF gears would require less modification for any given transmitted load.

Similarly, by looking at the bar chart in Figure 162, we can also conclude that the HCRNIF set would have performed better (again, only from a noise viewpoint) if its tip and flank relief values were increased slightly so that its optimum noise level occurred at the 100-percent load condition. Care must be exercised, however, in defining better as used herein. If, for example, the gear set spent most of its life at the 80-percent load point with only brief excursions to the 100-percent load point, then designing the profile modifications to provide minimum noise at the 80-percent load point would probably be the best situation. If, on the other hand, absolute maximum load capacity were the goal, with only a lesser regard for noise level, then it may well be best to design the profile modifications for a slight overload condition. This is especially true for very high-speed gears where scoring is a major concern. In the latter case, even a small amount of tip and flank interference could precipitate a scoring failure, and thus noise may have to be sacrificed for load capacity.

Unfortunately, the optimum modifications from a noise viewpoint and the optimum modifications from a load capacity viewpoint are often not the same values. Still, considering the fact that the tip and flank relief values applied to both the standard baseline and the HCRNIF gears were identical, these results clearly indicate the noise advantage of the HCRNIF form. At the 80-percent load point, the HCRNIF gears are over 20 decibels quieter than their standard baseline counterparts. Even though the HCRNIF gears become noisier at the 100-percent load point, they are still quieter than the standard baseline gears at that point by almost 8 decibels, still a significant reduction.

Strain Survey - The main purpose of the strain survey was to determine the actual tooth root and fillet bending-stress levels on the HCRNIF gears relative to the baseline gears. In calculating the bending stress for the HCRNIF gears, it is necessary to know both the position along the tooth at which the critical loading occurs and the magnitude of the critical load. Since the tooth is treated as a cantilever beam, the critical load position can be determined from the geometry of the tooth by defining the point at which the highest moment load will be applied since this will create the highest bending stress. The maximum moment occurs when the highest load is applied at the farthest distance from the tooth root. The farthest distance condition is a function of tooth geometry and can be determined readily. For standard baseline gears, the load at this point is also readily determined since only a single pair of teeth carries all of the transmitted load. For the HCRNIF teeth (indeed, for any HCR tooth form), while the point at which the maximum load occurs can be determined from geometry, the magnitude of this load is less easily determined since two pairs of teeth share the total transmitted load at this point. Based on previous testing with smaller gears, the amount of load sharing that occurs at this point was determined to be about 60 to 65 percent of the total transmitted load for HCR spur gears.

For the baseline gears, the maximum critical tooth loading (for tooth fillet-bending stress) occurs when the tooth is in mesh at the highest point of single-tooth contact (HPSTC). As Figure 163 shows, this is the highest point on a single tooth at which it will carry all of the transmitted load. As the tooth proceeds further through mesh, above the HPSTC, a second tooth will begin to pick up the load, and thus, though the moment arm of the cantilever beam continues to increase, the load decreases so that the resultant bending stress decreases as well.

For HCRNIF gears the critical loading occurs when the tooth is in mesh at the highest point of double-tooth contact at the pitch-line (HPDTCP) region of three-pair contact, at which point the total transmitted load is shared between two tooth pairs and a third tooth pair is just about to come into contact to pick up part of the load. The center of the three teeth in contact, as Figure 163 shows, is the most critically loaded at the HPDTCP. Unlike the standard baseline gears, at no time is the full load carried by only a single tooth. Like standard contact ratio gears, above

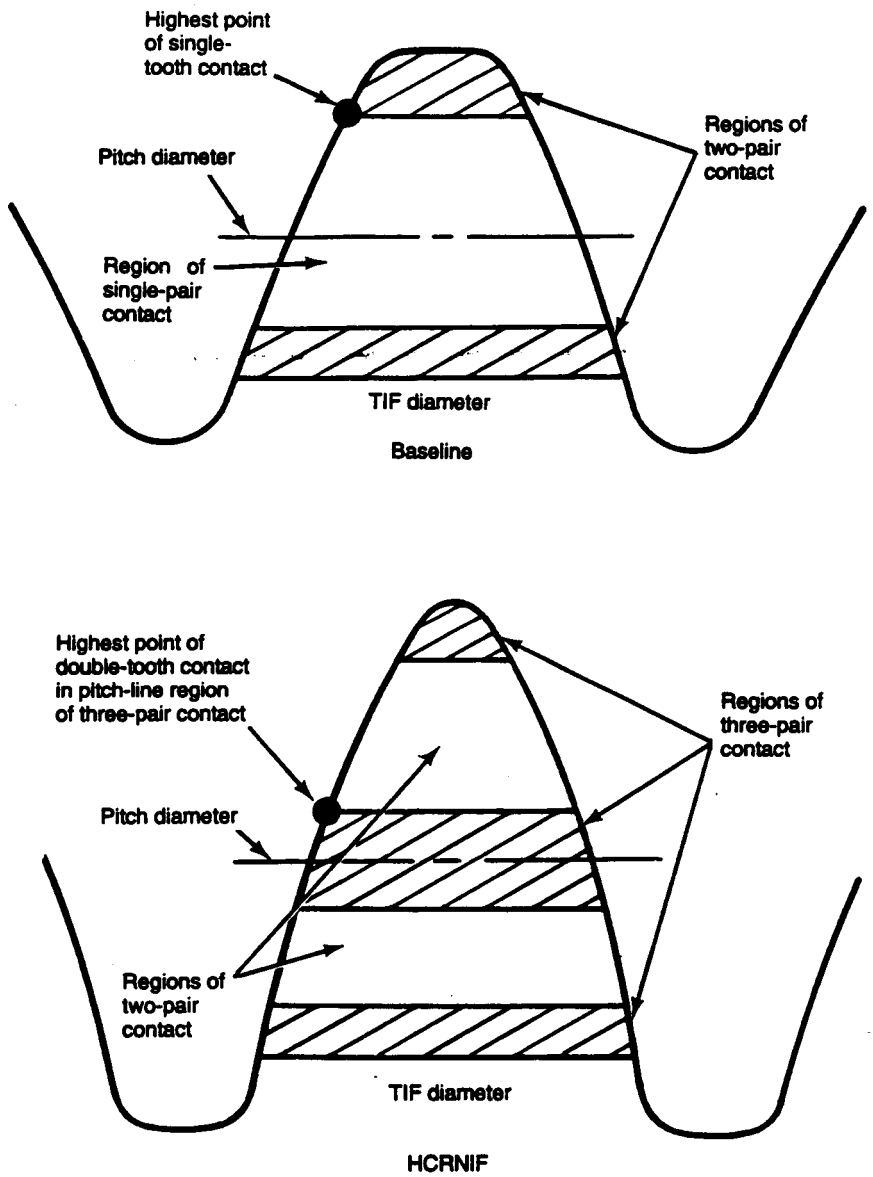

Figure 163. Regions of Contact of Baseline and HCRNIF Gear Teeth

the HPDTCP, a third (rather than a second) tooth will begin to pick up the load. and thus, though the moment arm of the cantilever beam continues to increase, the load decreases so that the resultant tooth-bending stress decreases, as was the case for the standard gears.

Considering the load sharing that occurs, it is important to investigate the measured stress levels for the HCRNIF gears so that their actual load capacity can be evaluated in comparison with the baseline gears. This was done by the strain survey testing. Strain gages were applied to the tooth roots and the tooth fillets of each of four teeth on one test gear and test pinion of each tooth form (four gears were instrumented in total), and the stress as a function of gear rotation or azimuthal position was measured. Both fillet and root gages were applied since, depending on the configuration of the gear, and particularly the blank construction, the fillet stresses are not always the most critical.

In conventional gear tooth-bending stress calculations, the capacity of the tooth is related to the maximum tension stress that occurs at the tooth fillet. For real gears, however, the bending-fatigue capacity is related to the peak alternating stress, wherever it occurs in the root fillet. For many cases the peak tension stress at the fillet is a reasonable indicator of the maximum alternating stress; thus the conventional stress calculations provide reasonable results. In other cases, however, the maximum tension stress does not provide a good indicator. This is particularly true for lightweight gears such as used in helicopters. For this reason, both fillet and root stresses were measured.

Before proceeding further, it should be noted that the gears and pinions were instrumented with a large number of gages, as described above. Some of these gages, such as the inner and outer fillet and root gages (which measured stress at the inner and outer edges of the 0.5-inch face width), were somewhat redundant and placed to determine if any variation existed that might cloud the overall results. In general, however, very little variation among redundant gages was found; thus we can concentrate our analysis on the basic data without regard to possible anomalies. For example, the stress differential between the inner (i.e., the side of the face width

closer to the bearing supports on these overhung-mounted test gears) and the outer (i.e., the side of the face width farthest from the bearing supports) gages was minimal. This is not entirely unexpected due to the narrow face width (0.50 inch) of the test gears.

The results of this testing, plotted in Figures 164 through 171, clearly show the load sharing that occurs during the meshing cycle for both the baseline and HCRNIF gear sets. In all cases the pinion teeth start to experience compressive stress in the tooth fillet and root locations (Figures 164, 165, 168, and 169) before the tooth actually comes into contact. This compressive stress rapidly changes to tension stress as the tooth is loaded, reaching a peak value when the tooth is at its critical load point, then decreasing rapidly back to zero. For the gears the pattern is much the same but reversed, as Figures 166, 167, 170, and 171 show.

If everything were perfect, one would expect that every strain gage that is in an equivalent location would show exactly the same stress level. Since things are seldom perfect, equivalent gages sometimes show somewhat different results. Consider the stress plots shown in Figure 164, for example. The peak tension stress levels measured on each of the four instrumented teeth vary substantially, especially tooth number 4. This may be due to a spacing error in the gear teeth or a gage placement error or a combination of the two. It may also be due to a bonding problem with the gage on tooth number 4 itself. The vast majority of the other stress traces (i.e., in Figures 164 through 171), however, show much more consistent results; thus care must be exercised in interpreting the data. Typically, when one gage shows results that are at considerable odds with other similar data points, it is best to disregard the odd point.

Close examination of Figures 164 through 171 will reveal some interesting facts. Considering, for simplicity, Figures 164 and 165, it should be obvious that while conventional gear tooth-bending stress calculations address the peak tension at the fillet location, the actual measured stress picture shows that the alternating stress may well be higher at the root location. In addition, while the peak tension stress may be a good indicator of capacity for some gears, the compressive stress that occurs in the tooth roots is far from negligible.

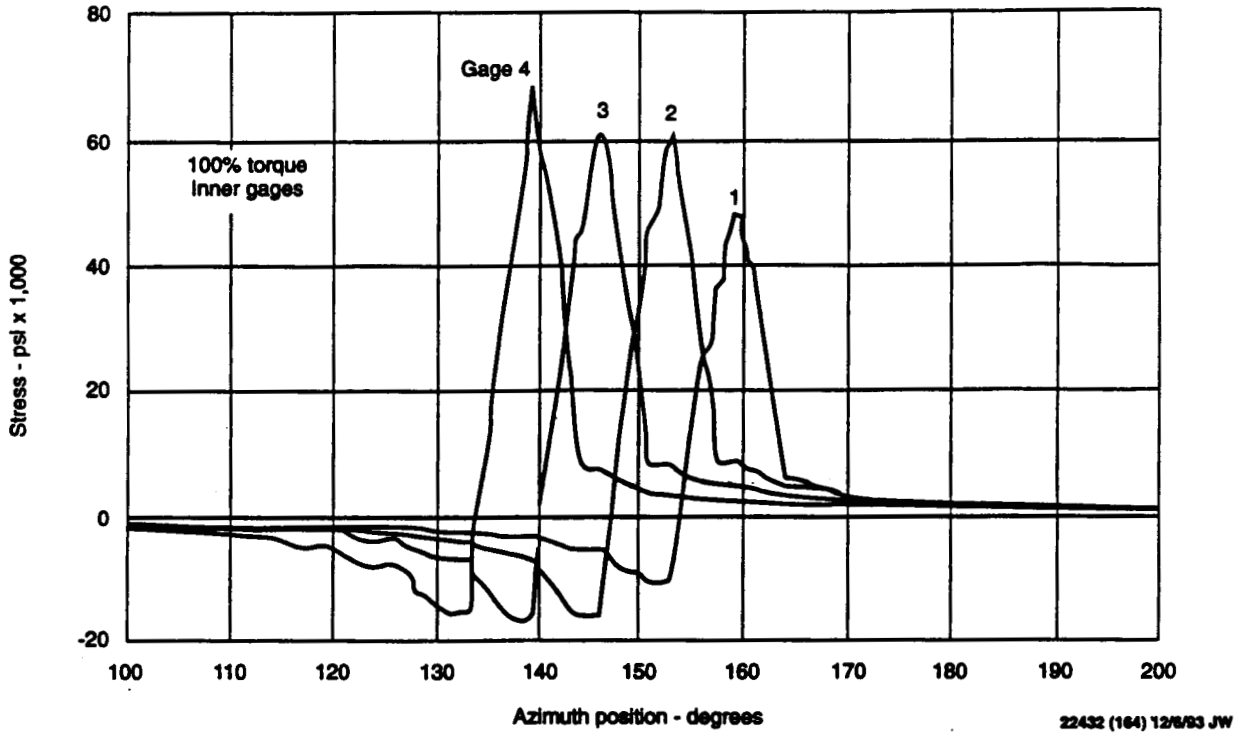

Figure 164. Stress Results in Pinion Fillets of Baseline Gears

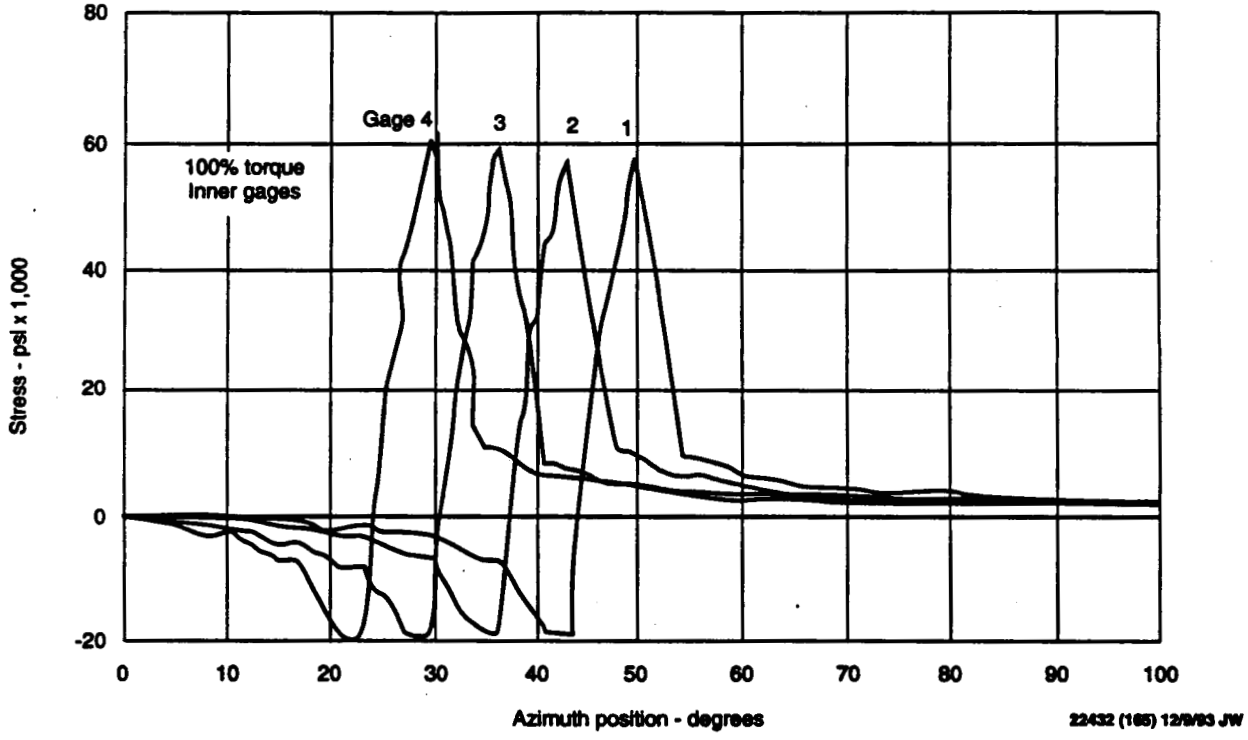

Figure 165. Stress Results in Pinion Roots of Baseline Gears

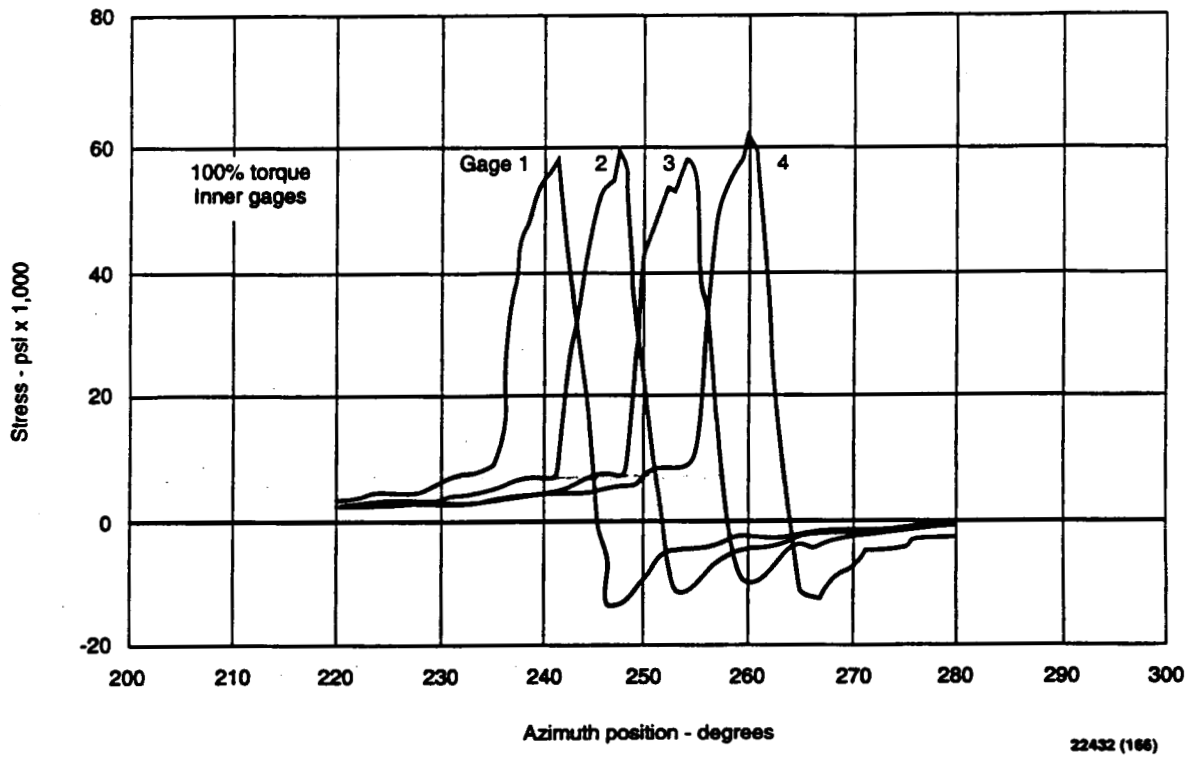

Figure 166. Stress Results in Gear Fillets of Baseline Gears

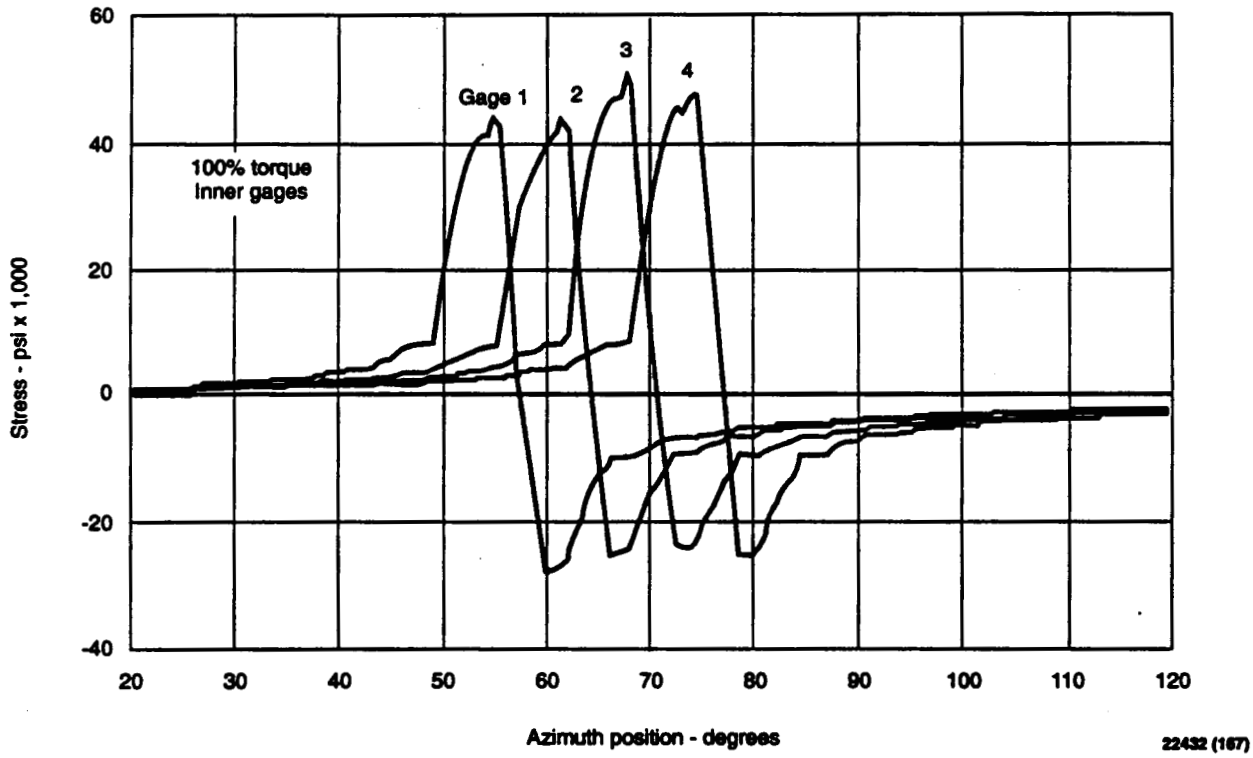

Figure 167. Stress Results in Gear Roots of Baseline Gears

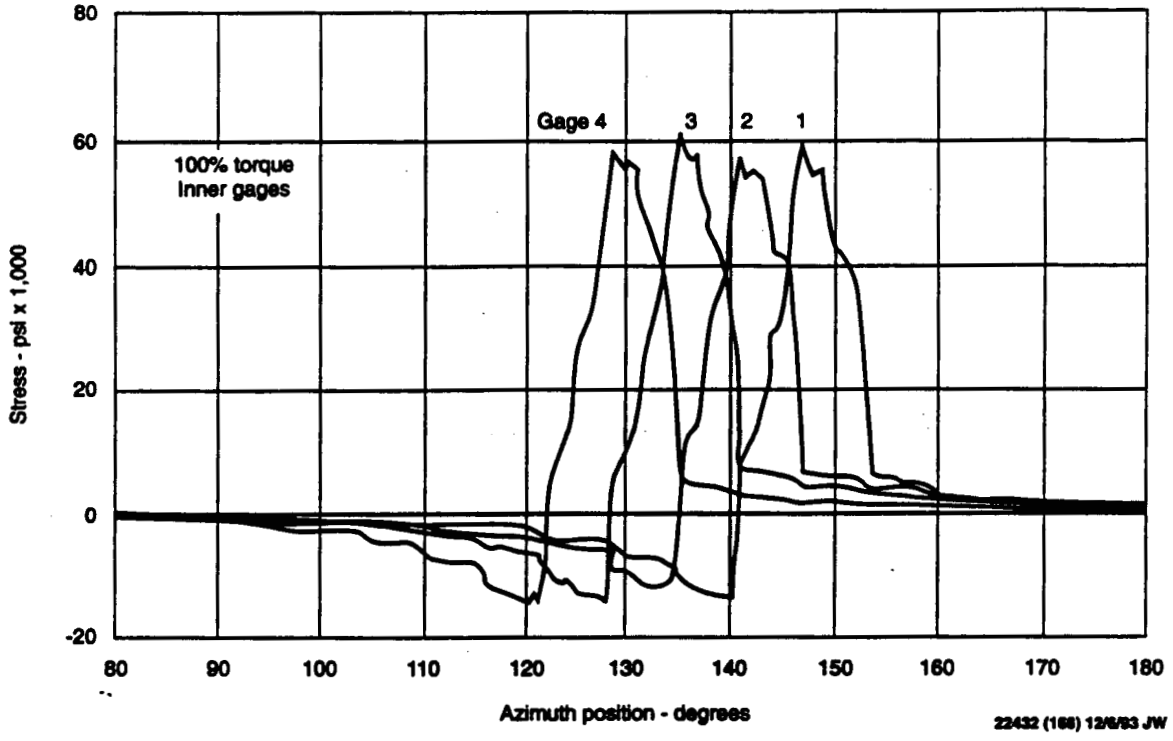

Figure 168. Stress Results in Pinion Fillets of HCRNIF Gears

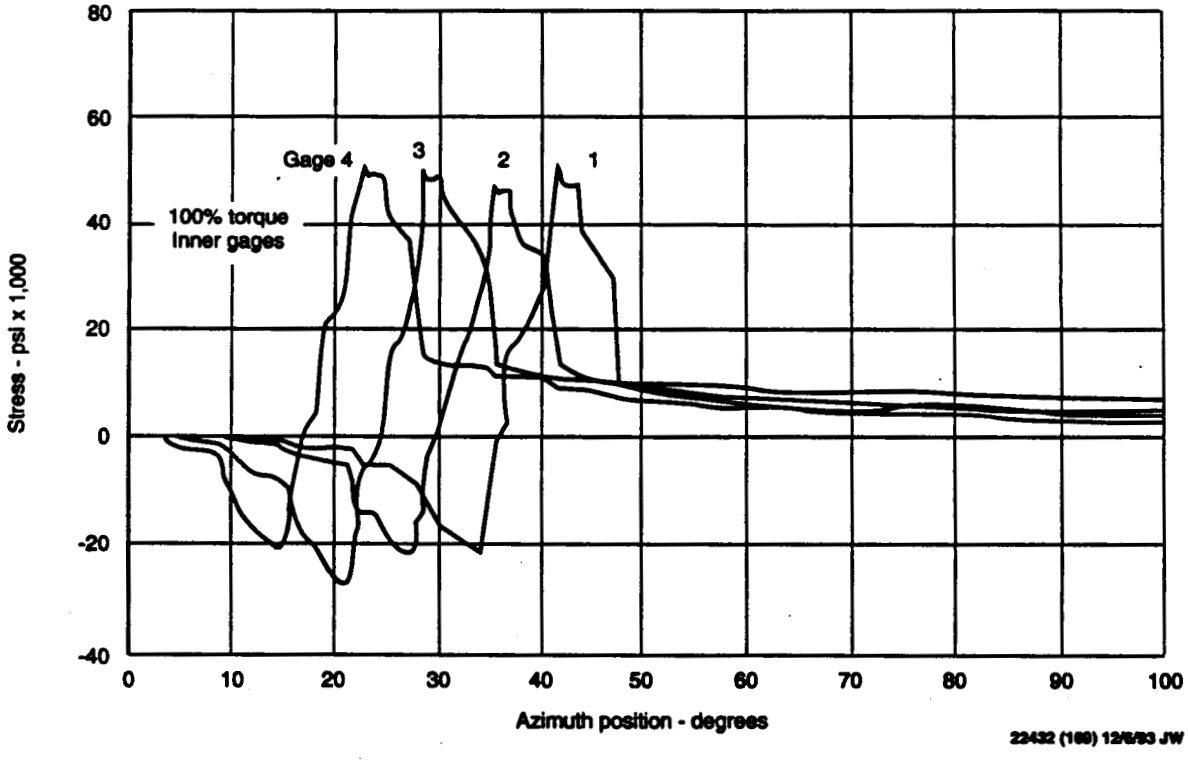

Figure 169. Stress Results in Pinion Roots of HCRNIF Gears

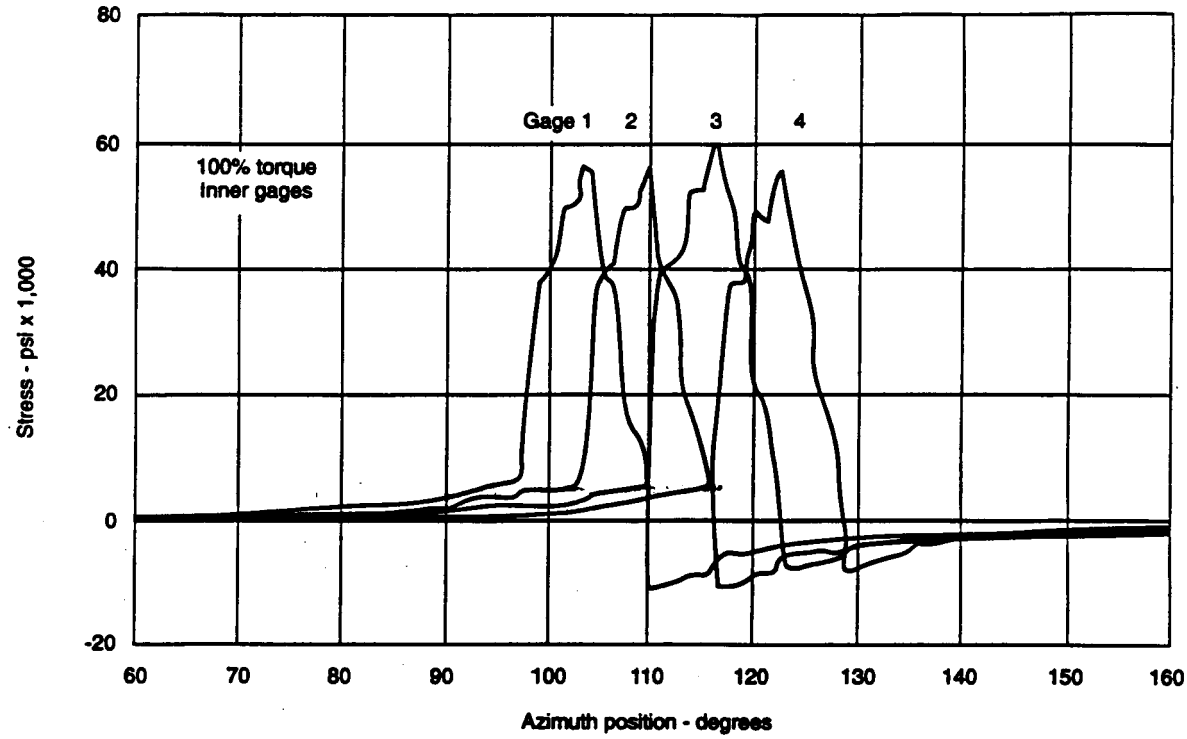

22432 (170) 12/6/93 JW

Figure 170. Stress Results in Gear Fillets of HCRNIF Gears

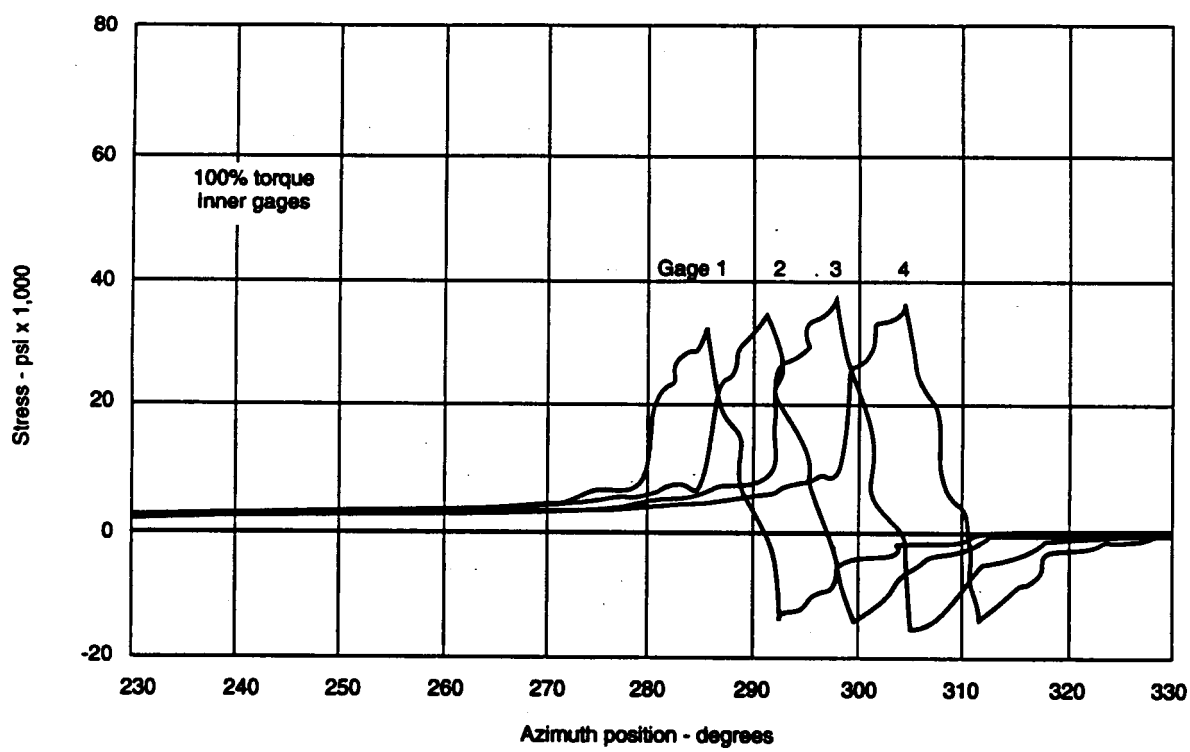

22432 (171) 12/7/93 JW

Figure 171. Stress Results in Gear Roots of HCRNIF Gears

While it is difficult to determine the exact load sharing that exists among the gear teeth simply by visually evaluating these plots, it is obvious when comparing Figures 164 through 167 and 168 through 171 as groups that the peak stresses, both tension and compression, for the HCRNIF gears and pinions are lower overall than those of their baseline counterparts. In addition, the amount of overlap of the individual stress traces is much greater on the HCRNIF gears than on the baseline gears, thus indirectly showing the greater load sharing that occurs.

Since our major concern herein is load capacity, we have extracted the peak tension and peak compression stress levels from the strain gage data and plotted these values against the transmitted torque, as Figures 172 through 179 show. In almost every case the stress level is lower for the HCRNIF gears than for the baseline gears, at the same load level, for almost every condition examined. This is, of course, due to the fact that the load is shared among more teeth on the HCRNIF gears than on the baseline gears; thus the per-unit tooth stress levels should be and are lower.

At very low torque levels, it is interesting to note that the stress levels for the baseline and HCRNIF gears are almost the same in many cases and, in some cases, the stress levels for the HCRNIF gears are slightly higher (for example, see Figure 176, below about 6,000 in.-lb torque). This phenomenon occurs due to the modifications that are applied to the HCRNIF profiles to accommodate tooth deflections at higher loads. At lower loads when the teeth do not bend as much as they do at higher loads, the actual contact ratio of the gear set drops below two and the full load may be carried by a single tooth. Because the HCRNIF teeth are longer and more slender with generally smaller fillet radii, the stress levels at these conditions actually increase. This points out a very important design consideration for HCRNIF gears; in fact, for any HCR gear regardless of tooth form. The teeth must be accurate enough to allow load sharing to occur among the teeth, and the profile modifications applied (tip and flank relief) must be appropriate for the conditions under which the gears will operate, or the HCR gears may actually perform worse than their standard counterparts, even to the point of experiencing a tooth fracture failure. The idea of using, for example, AGMA Quality 8 gears with an HCR form to improve

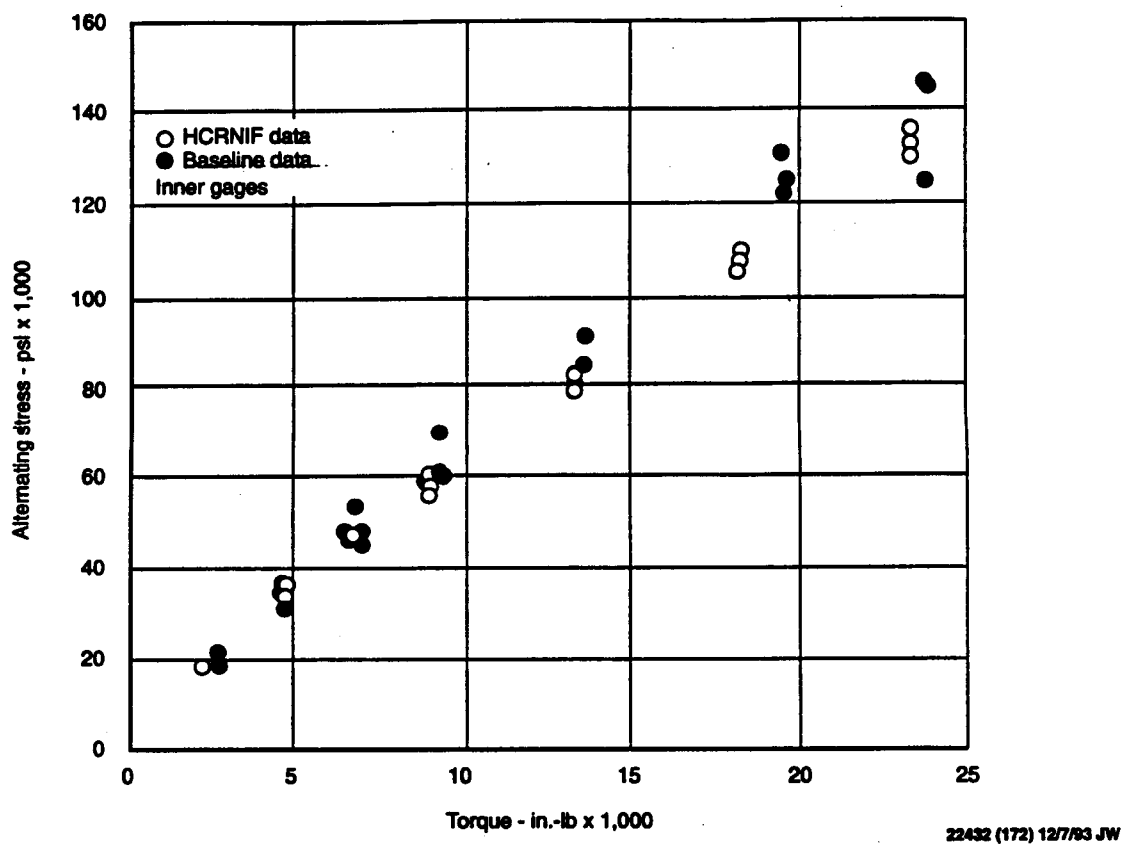

Figure 172. Comparison of Tension Stress at Pinion Fillet of Baseline and HCRNIF Gears

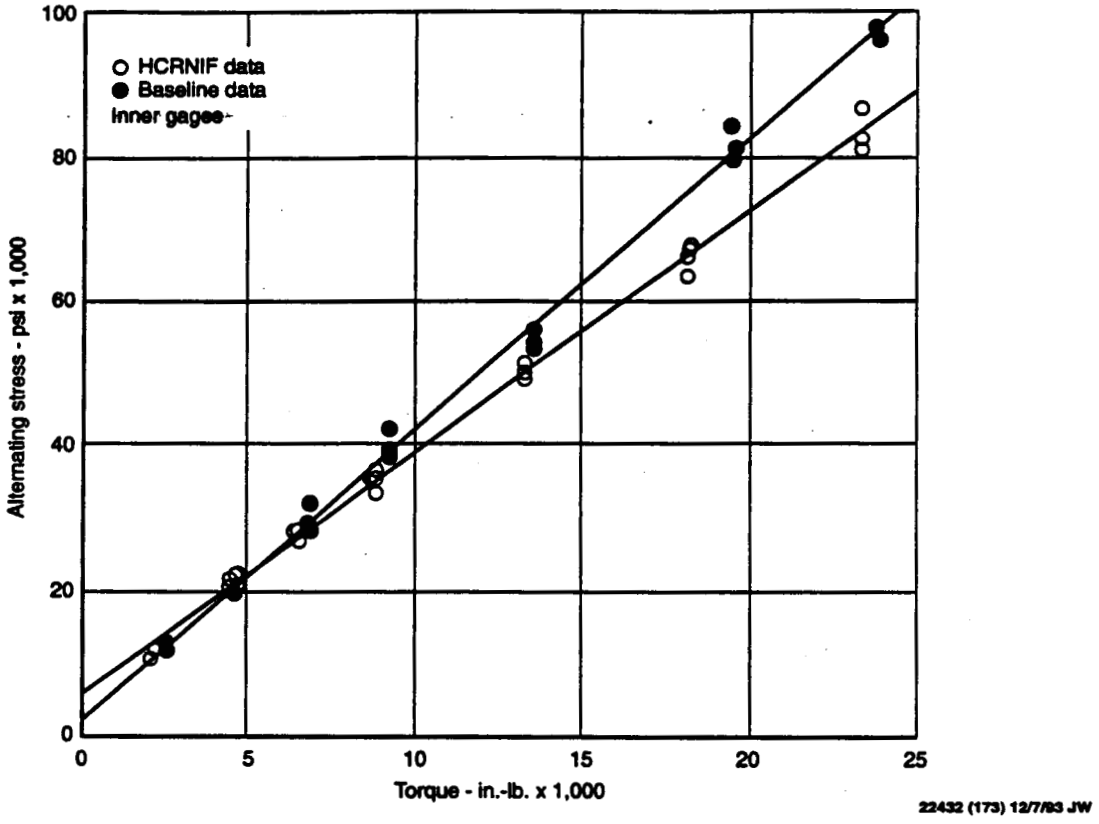

Figure 173. Comparison of Alternating Stress at Pinion Fillet of Baseline and HCRNIF Gears

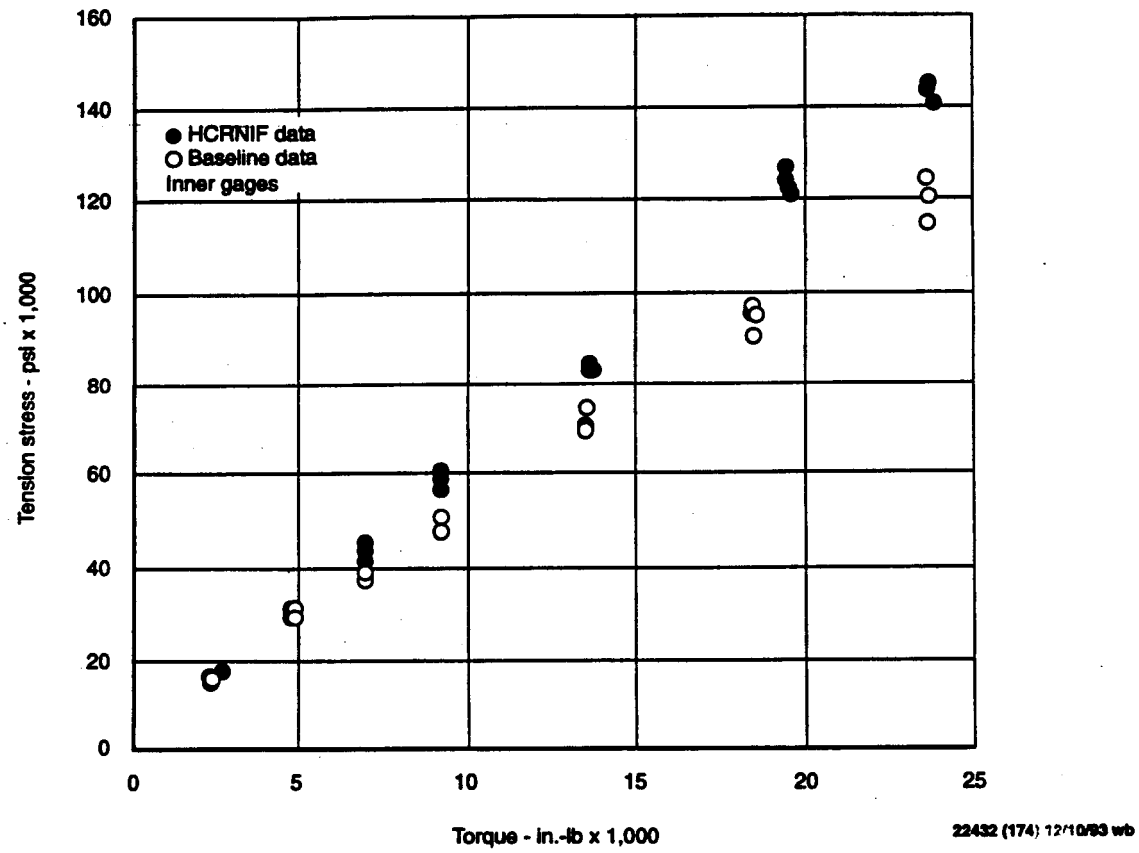

Figure 174. Comparison of Tension Stress at Pinion Root of Baseline and HCRNIF Gears

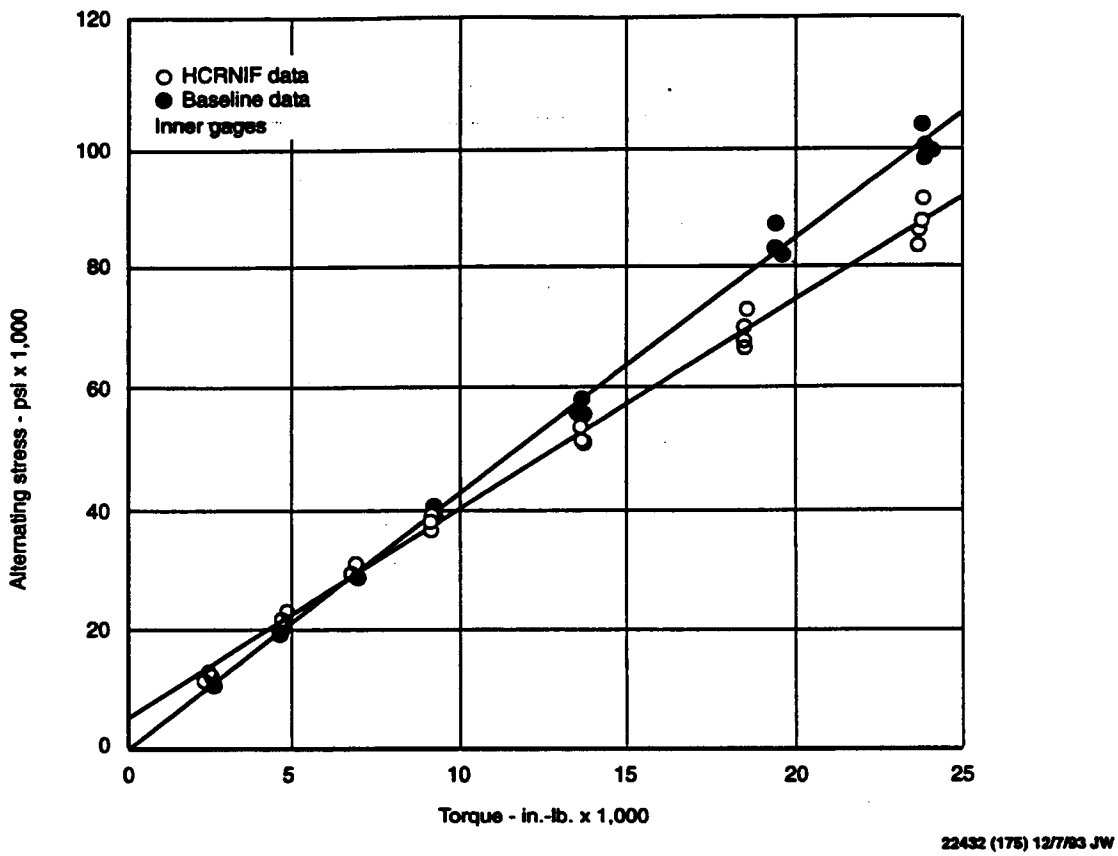

Figure 175. Comparison of Alternating Stress at Pinion Root of Baseline and HCRNIF Gears

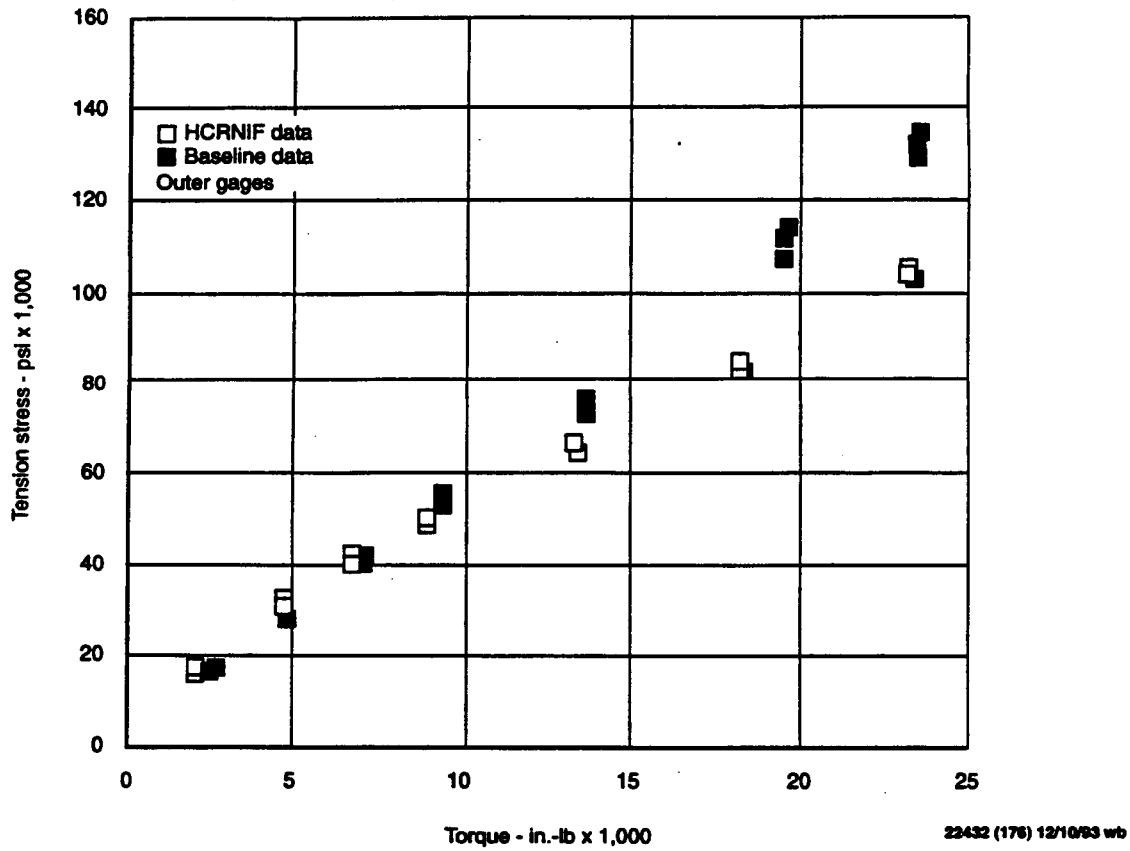

Figure 176. Comparison of Tension Stress at Gear Fillet of Baseline and HCRNIF Gears

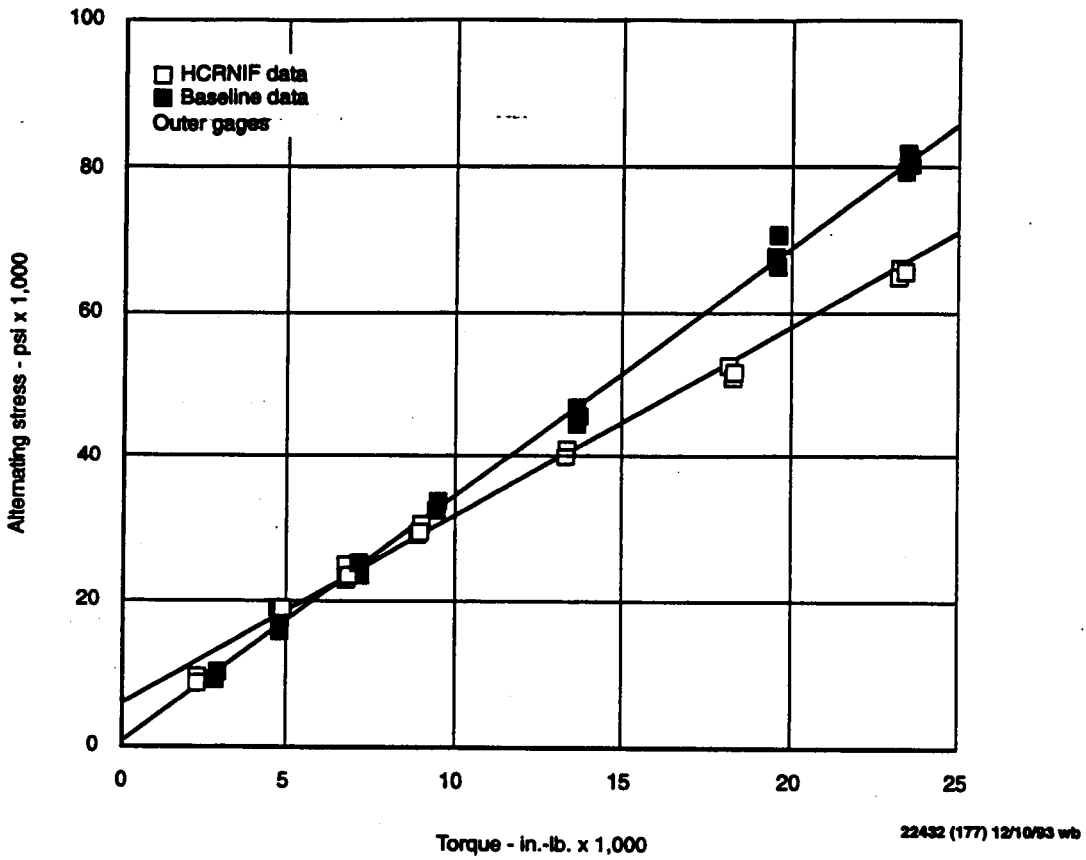

Figure 177. Comparison of Alternating Stress at Gear Fillet of Baseline and HCRNIF Gears

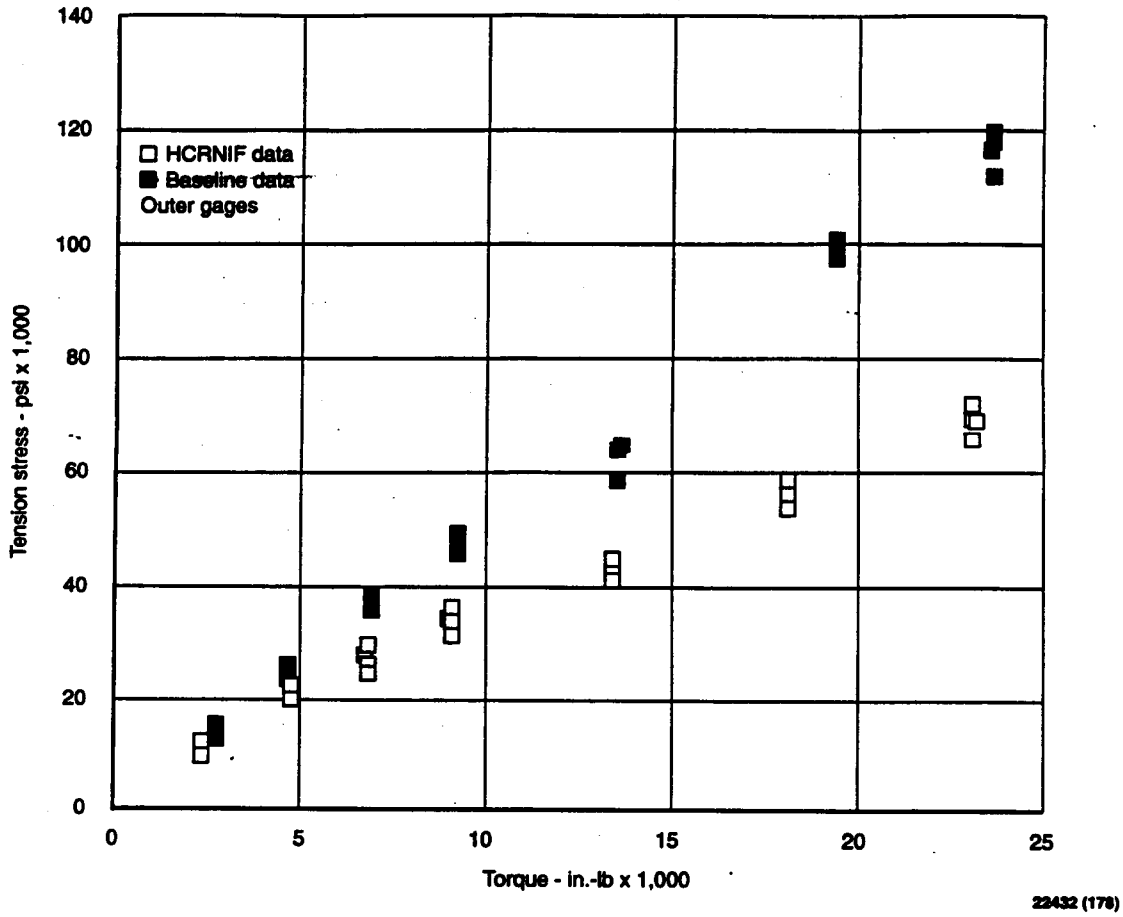

Figure 178. Comparison of Tension Stress at Gear Root of Baseline and HCRNIF Gears

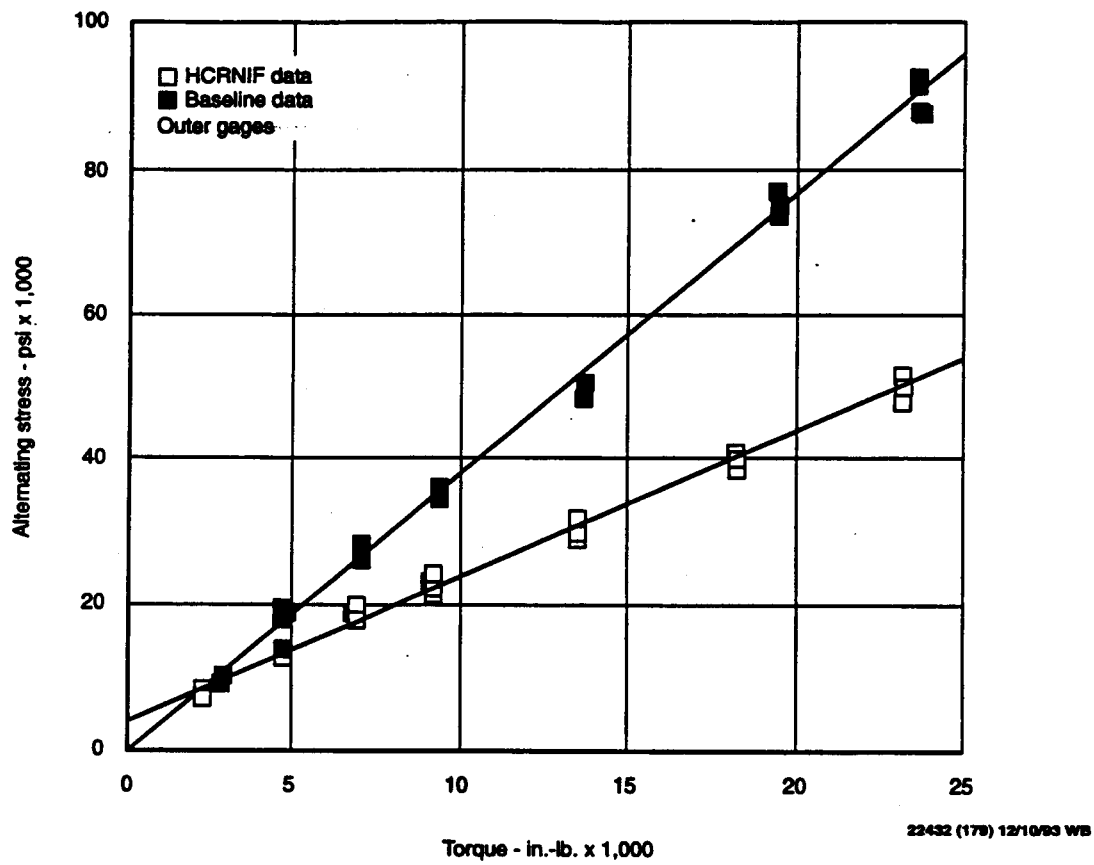

Figure 179. Comparison of Alternating Stress at Gear Root of Baseline and HCRNIF Gears

their capacity is thus foolhardy, to say the least. The tooth-spacing errors that are acceptable for a Quality 8 gear would preclude good load sharing, and such gears would perform poorly at the very best. Similarly, the profile modifications that must be applied must be much more carefully defined than they need be for conventional standard contact ratio gears. In a standard set, if the modifications are slightly excessive, the maximum load point will move slightly up the profile and the tooth-bending stresses will increase proportionally. If the same excessive modifications are applied to an HCRNIF set, however, the contact ratio may drop below two and the entire load-sharing picture changes. In the latter case, a single tooth which is of and by itself weaker than an equivalent baseline tooth will be forced to carry full load and the stress levels will be much higher. The full advantage of HCRNIF can be obtained only when the teeth share load effectively. When this is the case, as should be obvious from the testing reported herein, substantial improvements in load capacity, noise, and weight can result.

In reviewing the data shown in Figures 172 through 179, the alternating stress levels are the most important since it is these stresses and not the peak tension stresses that determine the fatigue life of the gear teeth. In every case, for both pinion and gear, as the load increases the difference between the alternating stress on the HCRNIF gears and the baseline gears grows larger. This is because as the loads increase, the HCRNIF teeth deflect more and tend to share load more among the three teeth in contact, while the baseline gears simply bend the single tooth in contact more; thus the stress on the baseline gears is higher than that on the HCRNIF gears.

Conclusions

Based on the results of this testing, the following conclusions can be drawn relative to HCRNIF spur gears of a size and type that could be used in a helicopter transmission:

1. The scoring-load capacity of HCRNIF spur gears is about equal to equivalent standard baseline gears if the tooth profiles are properly modified. Inadequate

modification can lead to premature scoring failures on either the baseline or HCRNIF gears, but the HCRNIF type is more sensitive to profile modification.

2. Inadequate oil flow can result in a plastic flow-type failure for either baseline or HCRNIF gears under conditions of high load and speed.

3. The noise level of HCRNIF gears is as much as 20 decibels lower than that of an equivalent set of standard contact ratio baseline gears if the profile modifications on the HCRNIF gears are optimized for the expected loading.

4. Both alternating and peak tension stresses in the tooth roots and fillets are lower on HCRNIF gears than on equivalent standard baseline gears at equal torque loading.

5. The difference between the HCRNIF stress levels and those of the standard baseline gears increases as the transmitted torque level increases.

6. Load sharing among the teeth in contact on HCRNIF gears improves with increasing loads due to increasing tooth deflections.

ACCESSORY SPUR GEARS OF SURFACE-MODIFIED TITANIUM

Introduction

Accessory gears in many helicopter applications, especially for high-power aircraft, are sized more by geometric requirements than by load capacity. In general, the pitch diameters of such accessory gears are determined by the restraints imposed by the overall design of the gearbox. Therefore, as the basic gearbox gets larger, the accessory gears are often designed with very small face/diameter ratios and are thus heavier than necessary to transmit the power required by the individual accessories. Since there are practical manufacturing limits on how small the face width can be on a large-diameter gear, such gears are often weight-inefficient. One way of reducing the weight of these gears would be to use a material that has a lower unit weight than the steel typically used.

Titanium is one such material; however, it has not gained widespread use because it performs poorly in dynamic, frictional applications. Titanium gear teeth suffer from a rapid, galling-type failure, despite the best lubrication. Recent advances in surface-modification processes, such as ion implantation, may make it possible to treat the surface of titanium gears to minimize the galling problem. If this approach is successful, a definite weight advantage can be realized.

The results of this program, however, indicate that even these advanced surface-modification systems were not able to solve the basic problem of titanium surface galling and wear in a dynamic, high-load, sliding application. While the testing did define the load levels and conditions under which such gears could be used, these conditions were found to be far from those that would be useful in a typical helicopter application.

Objective

The objective of this program was to design, build, and test representative sets of titanium spur gears which used two different approaches to hard-coating the tooth surfaces in order to minimize the surface-galling problems generally associated with the use of titanium in sliding-surface contact.

Program

The test program was aimed at investigating the overall performance characteristics of hard-coated titanium accessory gears, particularly their relative scoring and surface durability capacities, as compared to a set of conventional steel gears at the same reduction ratio and center distance. While the program was successful in determining the behavior of these surface-modified titanium gears, the program was modified as the tests proceeded due to the occurrence of excessive wear during most of the test runs.

Design

Two sets of spur gears were designed to operate on the 6-inch-center-distance gear research test rig in the overhung configuration. One set of gears was designed specifically for durability testing, while the second set was designed for scoring testing. The durability test gears had a reduction ratio of 1.67:1 while the scoring test gears operated with a 1:1 ratio. In both cases, engineering drawings which are simultaneously compatible with the requirements of the test rigs and representative of typical helicopter practice were prepared to facilitate the manufacture of the test gears. Table 38 defines the basic tooth geometry for the test gears used in this program.

TABLE 38. CONFIGURATION OF TEST GEARS

Parameter	Scoring	Surface Durability	
		Pinion	Gear
Part number	SK32372	SK32370	SK32371
Number of teeth	30	24	40
Center distance (in.)	6.0000	6.0000	6.0000
Face width (in.)	0.50	0.50	0.50
Diametral pitch	6	5.3333	5.3333
Pressure angle (deg)	25	20	20
Pitch diameter (in.)	6.0000	4.5000	7.5000

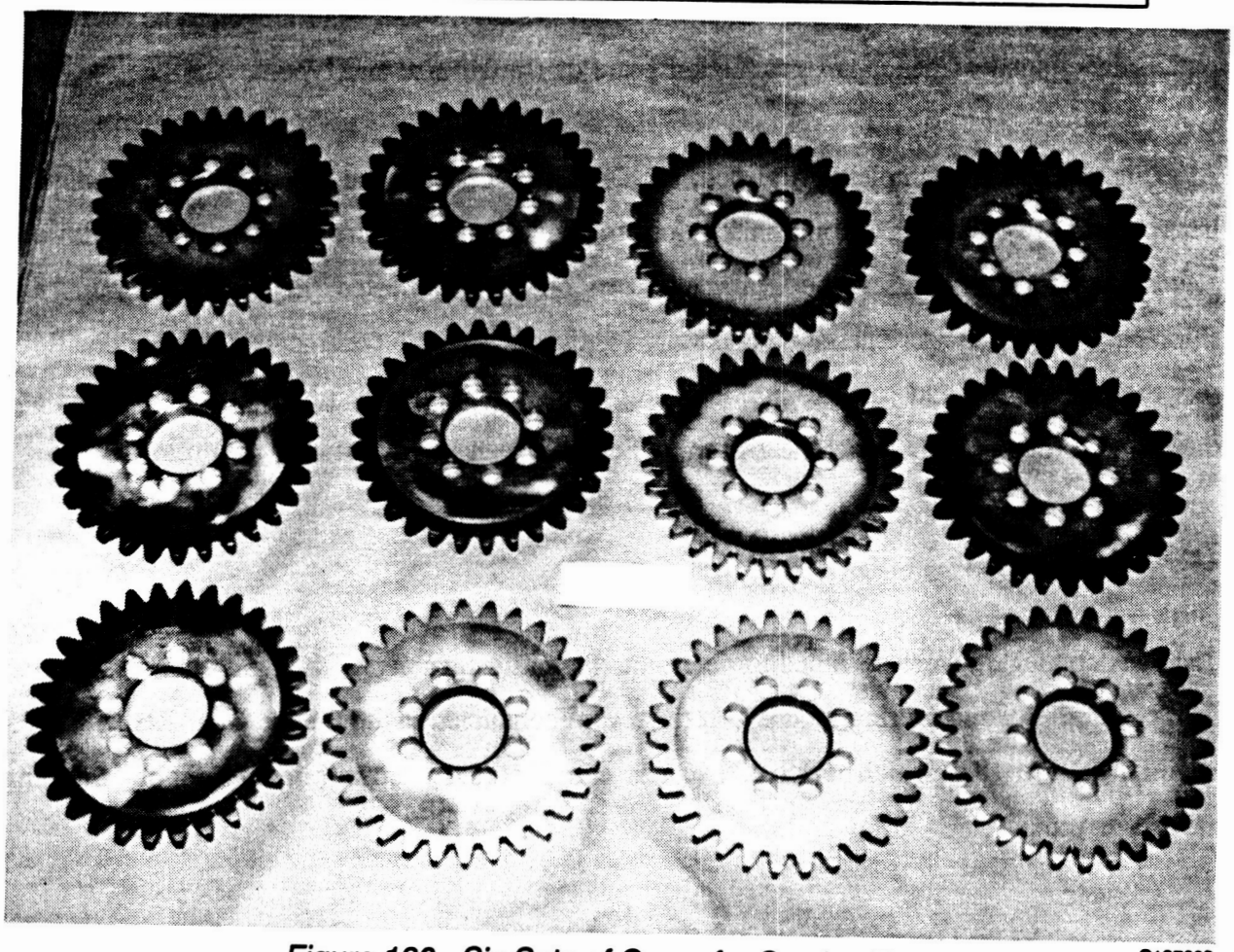

Figure 180. Six Sets of Gears for Scoring Tests

C127803

Fabrication

Six sets of scoring (Figure 180) and six sets of surface durability (Figure 181) test gears were fabricated. Since the pinion and gear used in the durability testing are different, six durability pinions and six durability gears were manufactured. Conversely, since the scoring-test pinion and gear are identical, 12 identical scoring-test gears were fabricated. The gears were manufactured from Ti-6Al-4V titanium alloy in accordance with the normal Boeing practice for similarly sized accessory spur gears so that they were fully representative of actual aircraft gears.

Complete gear tooth geometry inspection data (lead, profile, spacing, runout, and finish) were compiled and evaluated for each gear set. In each case, the resultant gears were within the engineering drawing requirements except for minor deviations that were judged to be acceptable within the context of helicopter production gears of similar size and type.

After the gears were completely finished, each was surface-modified by one of two techniques: hard coating by E/M Corporation or ion implantation by Spire Corporation. This was accomplished by separating the gears into two randomly selected, equal-sized groups and shipping them to the aforementioned vendors for their respective treatments. This yielded three sets each of scoring and surface durability test gears which had been hard-coated by E/M and three sets of otherwise identical test gears which had been ion-modified by Spire.

Test Definition

The tests conducted were designed to determine the basic capacity of the titanium gears in both surface durability and scoring modes. All tests were conducted in the Boeing Gear Research Test Facility (Figure 182) which is located in test cell 9 of the Transmission Assembly Building located on site.

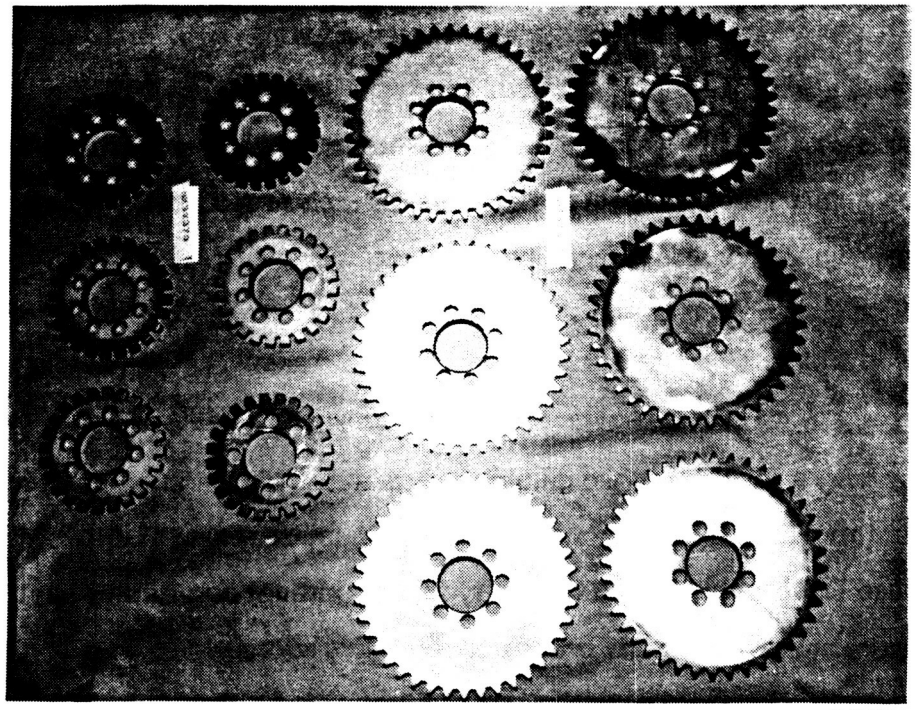

C127804

Figure 181. Six Sets of Gears for Surface Durability Tests

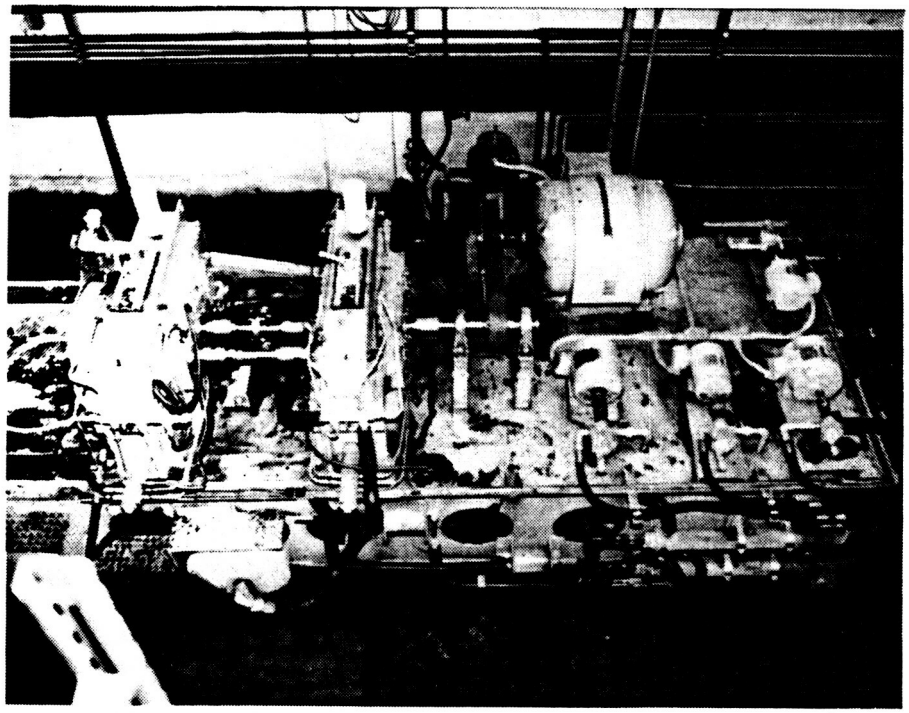

C127817

Figure 182. Boeing Gear Research Test Facility

Scoring-Load Capacity - Twelve scoring tests were planned in order to define the relative load capacity of the hard-coated titanium gears. The initial plan was to run each test at increasing load levels until a scoring failure occurred. Each set of gears thus would have yielded two data points for a total of 12 data points in all. Since three sets were hard-coated by E/M and three sets were ion-implanted by Spire, six data points for each surface-modification technology were to have been obtained. As described later, however, the actual test program deviated from this plan due to excessive wear on the titanium gears which precluded completion of the tests as planned.

Surface Durability - Twelve surface durability tests were planned in order to define the relative surface durability load capacity of the hard-coated titanium gears. The tests were to be run at increasing load levels until either a durability failure (pitting) occurred or the test time reached a runout condition, whichever occurred first. With this approach each set of gears would have yielded two data points; thus six sets of test gears were to be run to yield 12 data points. Since three sets were hard-coated by E/M and three sets were ion-implanted by Spire, six data points for each surface-modification technology were to have been obtained. As was the case with the scoring testing, however, the actual test program was curtailed due to excessive wear on the titanium gears which precluded completion of the tests as planned.

Gear Loading

All of the test gears were loaded in the same manner. The loading system used in the test rig is closed-loop, locked-in torque. The torque load is applied by using a lever system to rotate a split coupling such that the desired amount of torque is locked into the system. With care, this allows the test torque to be accurately controlled. The load application procedure used for all test runs was the same and is defined in Table 37.

In order to properly simulate the intended helicopter accessory gear application, the torque loading applied during the testing should produce stress and flash temperature levels which are

reasonably representative of those which would be encountered in service. Figures 183 through 185 show the variation of bending stress, contact stress, and flash temperature for the surface durability test gears while Figures 186 through 188 show respectively the same information for the scoring-test gears. The planned test torques for each type of testing would have resulted in stress levels and flash temperatures typical of helicopter accessory gears.

Test Procedures

Scoring - One of the two gear research test rigs was configured in the 6-inch-center-distance overhung configuration. Before starting any testing, the strain-gaged torque shaft was calibrated to normal Boeing standards. The primary belt drive was set to provide a test gear speed of 3,660±100 rpm. All test gearbox oil tanks were flushed and refilled with DOD-L-85734 oil (in this case, Exxon ETO-25). The oil jet to the test gear was positioned on the outlet side of the mesh, as Figure 189 shows.

The oil pressure and temperature to both slave gearboxes were set and maintained at 40±10 psi and 135±20°F, respectively, for all test runs. The oil pressure and temperature to the test gears were set and maintained at 35±10 psi and 195±5°F, respectively, for the initial test runs. The size of the oil jet orifice was selected to provide 0.32±0.05 gpm flow to the test gears at the cited pressure and temperature settings.

Oil inlet temperature is a critical factor in the conduct of scoring tests, and the construction of the test rig allows this parameter to be accurately controlled. The bearings that support the shafts are housed in the slave box immediately behind the test gear housing; thus the test section oil system feeds only the test gears and no other members (not even a seal). This effectively isolates the test gears so that their capacity can accurately be determined. In addition, in order to provide precise temperature control of the test gear oil supply, the test gear oil sump is heavily insulated and a very large, in-line oil heater (Figure 190) applies heat as required just before the oil reaches the jet which feeds the test gears.

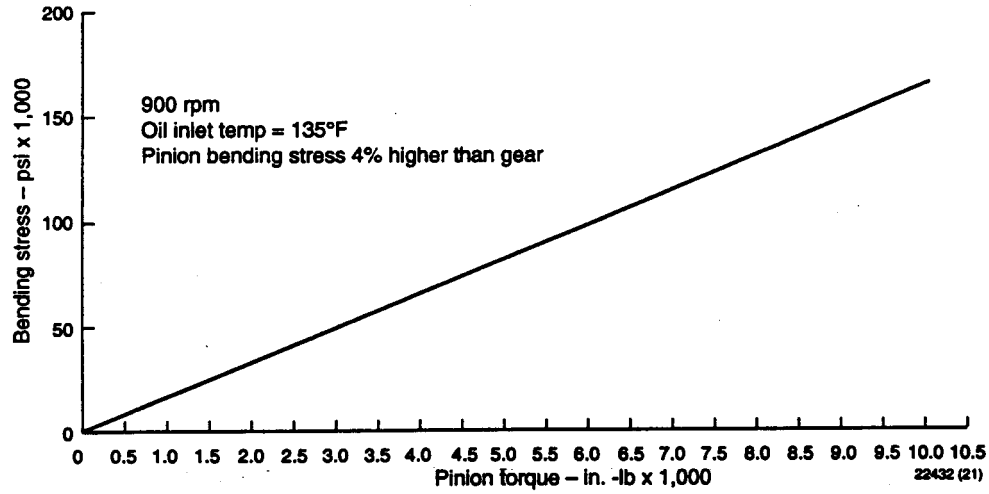

Figure 183. Bending Stress of Titanium Gears in Surface Durability Tests

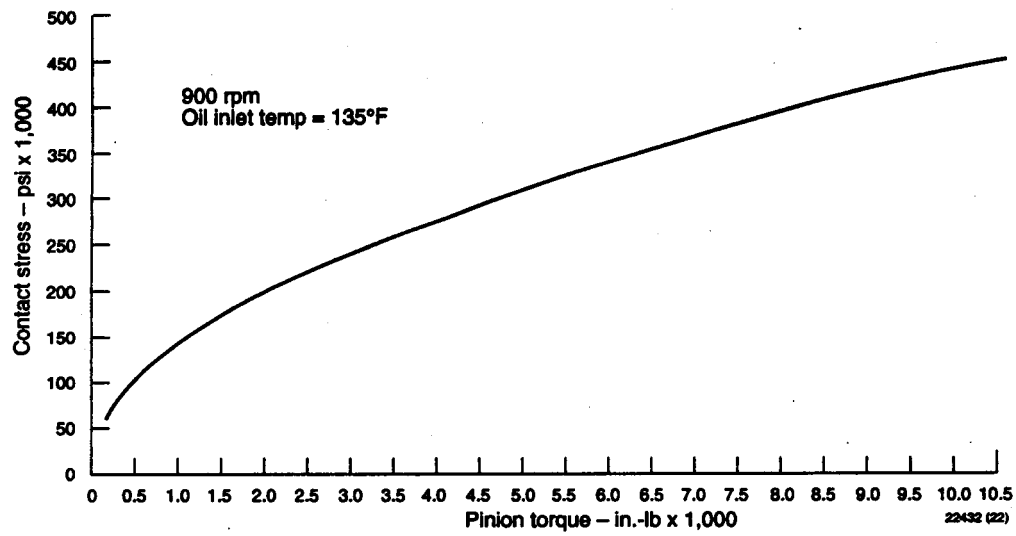

Figure 184. Contact Stress of Titanium Gears in Surface Durability Tests

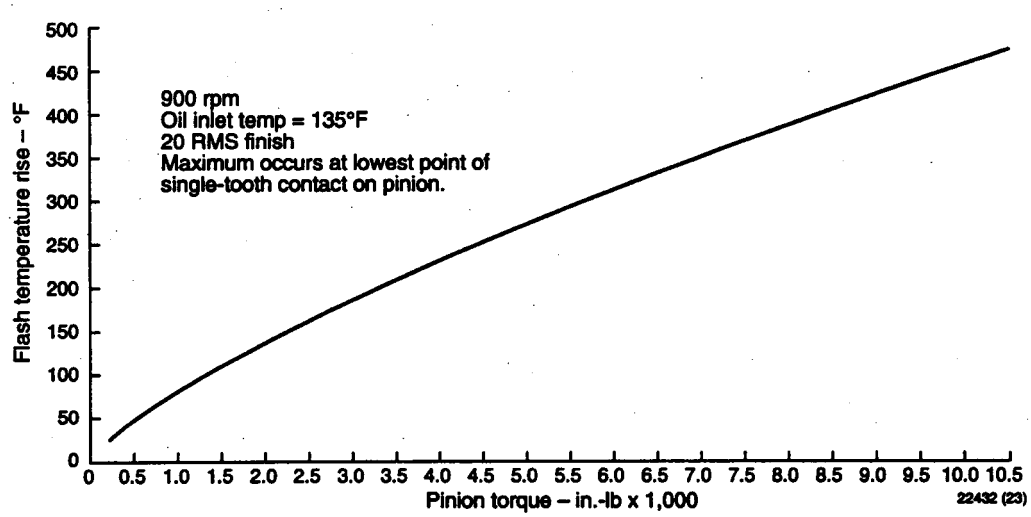

Figure 185. Flash Temperature of Titanium Gears in Surface Durability Tests

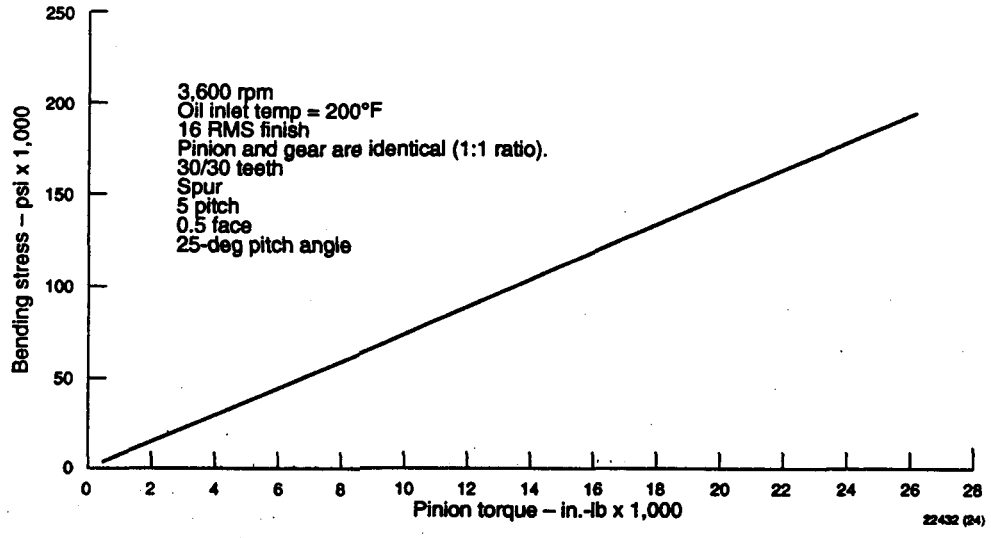

Figure 186. Bending Stress of Titanium Gears in Scoring Tests

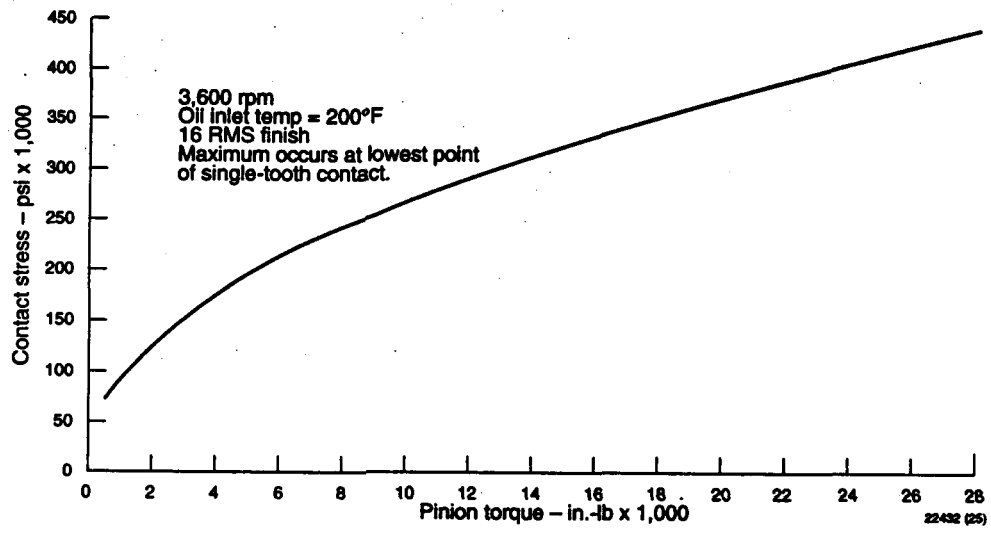

Figure 187. Contact Stress of Titanium Gears in Scoring Tests

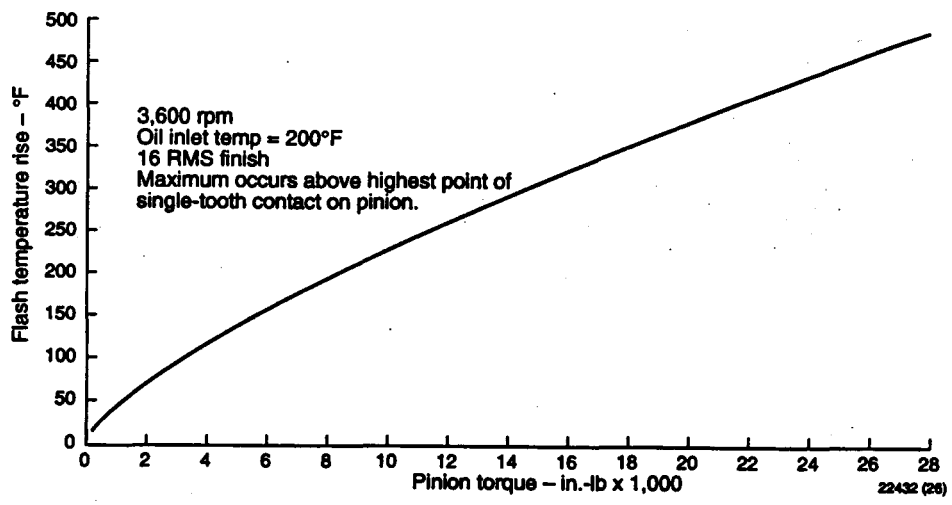

Figure 188. Flash Temperature of Titanium Gears in Scoring Tests

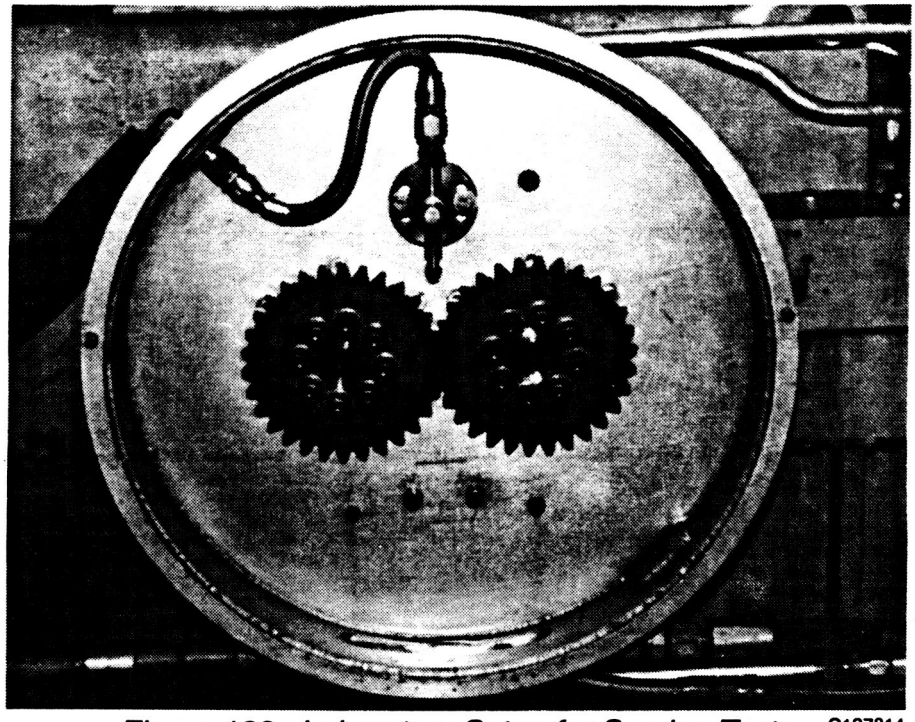

Figure 189. Laboratory Setup for Scoring Tests C127814

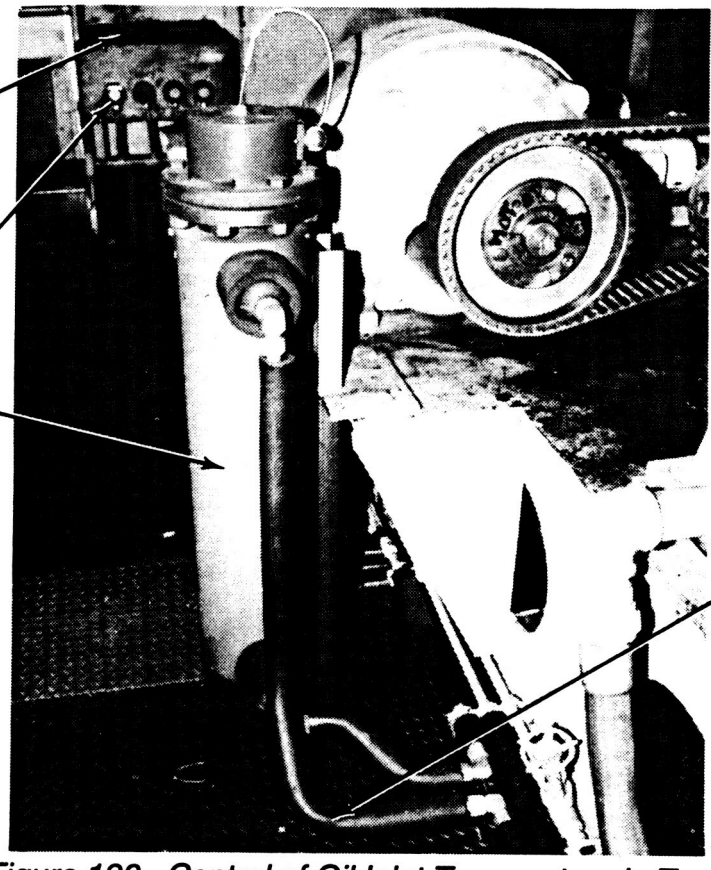

Figure 190. Control of Oil Inlet Temperature in Tests

Before conducting any test runs, the lubrication systems for all boxes were run with the main drive motor off and the gears stationary but in the oil stream, with appropriate control exercised on heating, cooling, and flow to establish stabilized operation at the noted pressure, temperature, and flow conditions. Torque was applied during the stabilization period and the torque reading was rechecked and reset, if required, immediately before each test run.

Since the torque on this rig was applied statically, it was necessary to check it after the stand had run for a short period of time. If the torque was found to be within the target range, the test run was allowed to proceed. If the torque was found to be outside of the target range, the torque application sequence was repeated until the torque remained within the target range after the initial torque check.

The planned scoring test procedure consisted of a series of 15-minute-long, incrementally loaded runs. An initial load estimated to be below the scoring failure point was applied to the gear set, and it was run for 15 minutes under the conditions described above. At the end of the 15-minute run, a visual evaluation was conducted of the condition of the test gear loaded tooth surfaces. If no scoring in excess of the failure criteria (see subsequent paragraph Failure Criteria) was observed, the next higher incremental load was applied and the 15-minute run and inspection sequence were repeated. This procedure was continued until the scoring load was achieved. Unfortunately this procedure proved to be impractical because of high wear rate, and it was modified shortly after the testing started. Details of the modified sequence are provided later in the discussion of the results of the testing.

Surface Durability - Since both the scoring and surface durability tests were run on 6-inch centers, the same gear research test rig was used for both tests. The only changes required to accommodate the surface durability testing were a change in the slave gears (to match the durability test gear ratio) and a change in the speed of operation of the system so that durability failures would be the likely result of increasing torque loading. The primary belt drive was set to provide a test gear speed of 900±50 rpm. All gearbox oil tanks were again flushed and

refilled with DOD-L-85734 oil (i.e., Exxon ETO-25). The oil jet to the test gear set was positioned on the outlet side of the mesh, as Figure 141 shows. The oil pressure and temperature to all slave gearboxes were set and maintained at 40±10 psi and 135±20°F, respectively, for all test runs. The oil pressure and temperature to the test gears were set and maintained at 35±10 psi and 135±5°F, respectively, for all test runs. The test gear set oil jet orifice size was selected to provide 0.32±0.05 gpm flow to the test gears at the cited pressure and temperature settings. The strain-gaged torque shaft was not recalibrated at the start of the durability testing, but its calibration was rechecked after all testing was completed to insure that it had not been compromised.

As was the case for the scoring tests, before conducting any test runs, the lubrication systems for all boxes were run, with the main drive motor off and the gears stationary but in the oil stream, with appropriate control exercised on heating, cooling, and flow to establish stabilized operation at the noted pressure, temperature, and flow conditions. Again, as was the case for the scoring tests, torque was applied during the stabilization period and the torque reading was rechecked and reset, if required, immediately before each test run.

Unlike the scoring tests, the duration of each durability test run was planned to be very long, up to 10 x 10^6 cycles. Because of these extended run times, in order to identify a failure each test gear set was to be visually inspected to determine its condition at the following intervals:

At loads up to and including 150 percent:	Every 8 running hours
At loads between 151 and 200 percent:	Every 4 running hours
At loads above 200 percent:	Every 2 running hours

As was the case with the scoring testing, however, this approach was modified during the actual testing because of the high wear rate that the gears exhibited at the anticipated test loads.

TABLE 39. PLANNED AND MODIFIED TEST CONDITIONS

Parameter	Scoring		Surface Durability	
	Planned	Modified	Planned	Modified
Pinion speed (rpm)	3,600	900	900	900
Lube direction	Out of mesh	Into mesh	Out of mesh	Into mesh
Oil temperature (°F)	195	130 - 190	135	135
Pinion material	Titanium	Steel	Titanium	Steel
Gear material	Titanium	Titanium	Titanium	Titanium

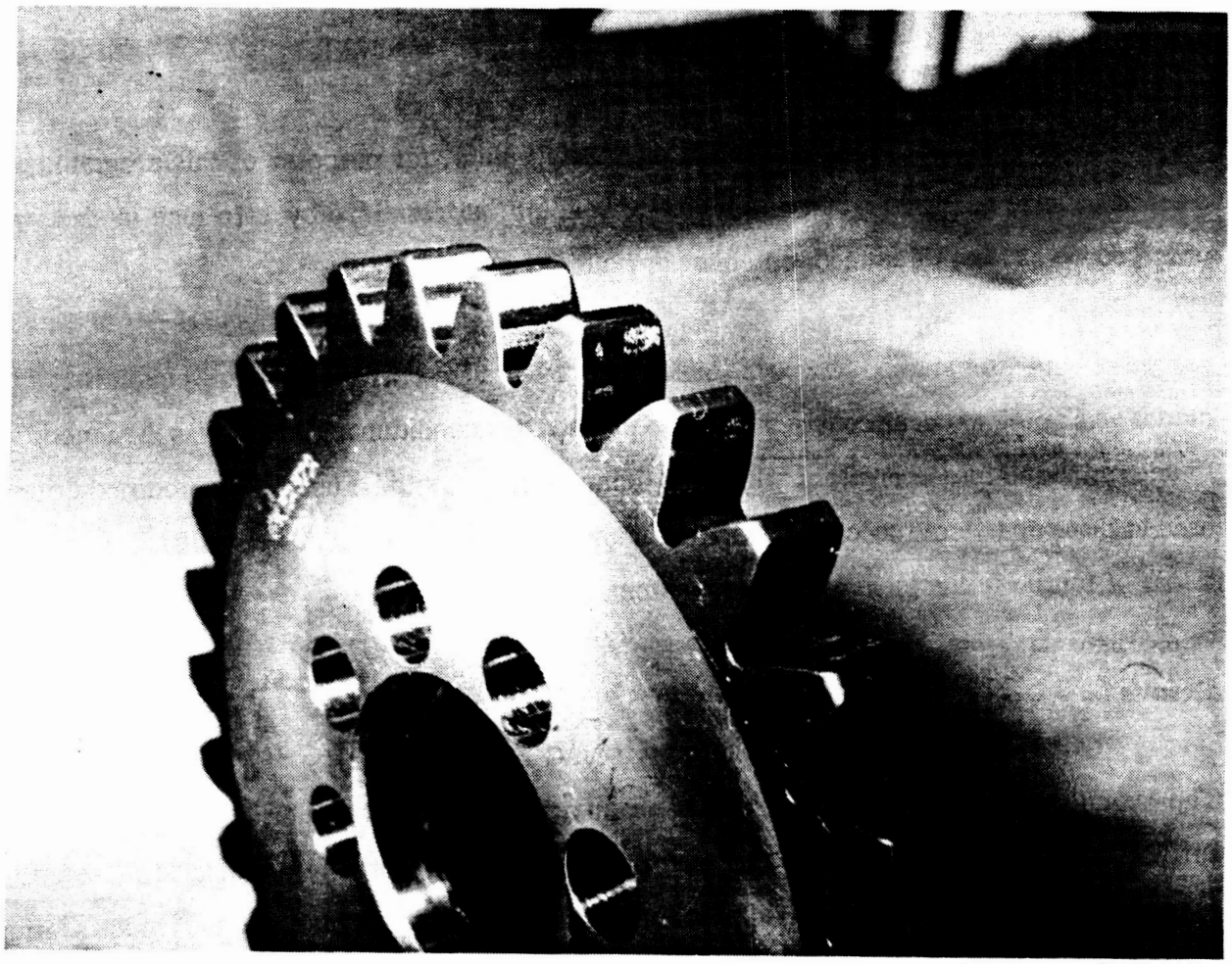

C132343 NO.3

Figure 191. Scoring of Gear Hard-Coated by E/M Corporation

Modified Test Conditions - Because of the poor test results in the initial scoring and surface durability testing, the test conditions were modified as shown in Table 39. These modified conditions permitted data to be obtained that identified the maximum loads at which the titanium gears could be used in a practical application.

Failure Criteria

At the outset of the program, the following criteria were established for determining when a failure had occurred.

Scoring - Failure due to scoring was deemed to have occurred when 5 percent of the available tooth contact surface exhibited visible evidence of the radial scratch marks associated with a scoring failure.

Surface Durability - A pitting or surface durability failure, for purposes of this program, was deemed to have occurred when a minimum of one pit, at least 1/16 by 1/16 inch in size, was observed on at least three teeth on either or both test gears.

As the testing progressed, however, it became obvious that neither of these classical failure modes was going to occur consistently at the planned test conditions. The test was then modified to determine the torque levels at which the titanium gears could be used. The modified criteria used at that point were successful operation without galling and without wear sufficient to cause a loss of torque in the locked-in-torque system.

Results

The overall results of this test program were mixed, to say the least. Neither the scoring nor surface durability testing yielded the type of data that were initially anticipated. The initial scoring test results of a titanium pinion running against a steel gear indicated very poor scoring

resistance for both surface-modification treatments at the planned test conditions. Essentially, in both surface durability and scoring testing, no substantial difference in performance was identified for the two treatments tested, and the failure torque levels achieved were far below those that would justify the use of titanium for helicopter accessory gears.

Scoring - These gears failed at very low torque levels, in the range of 10 percent of the scoring-load capacity for equivalent steel gears. In addition, the failure mode observed was more galling than scoring of the tooth surface, as Figures 191 and 192 show for the E/M and Spire treated gears, respectively. As these photos clearly show, material was pulled from the surfaces of the teeth, rather than scratched as would be expected from a typical scoring failure.

Because of these poor initial scoring-test results, the test conditions were modified as described in Table 39 to allow the testing to proceed while obtaining some meaningful data. These modifications were accomplished in stages. The overall results of all scoring tests are shown in the form of a bar chart in Figure 193. For reference purposes, the typical minimum scoring failure load for AISI 9310 carburized, hardened, and ground spur gears of identical geometry (such as now used for helicopter accessory gears) is also shown in Figure 193. This minimum load, about 5,000 in.-lb, is well above the maximum failure load (galling) for the titanium gear sets.

Changing lube direction alone from out of mesh (which is typical for gears in which cooling is more important than lubrication, i.e., scoring-critical gears) to into mesh (which is typical for gears in which lubrication is more important than cooling, i.e., wear-critical gears) did not substantially change either the failure mode (i.e., galling) or the failure torque level.

Similarly, lowering the oil temperature to 135°F in combination with the change in lube direction (from out of mesh to into mesh) did not substantially change either the failure mode (i.e., galling) or the failure torque level.

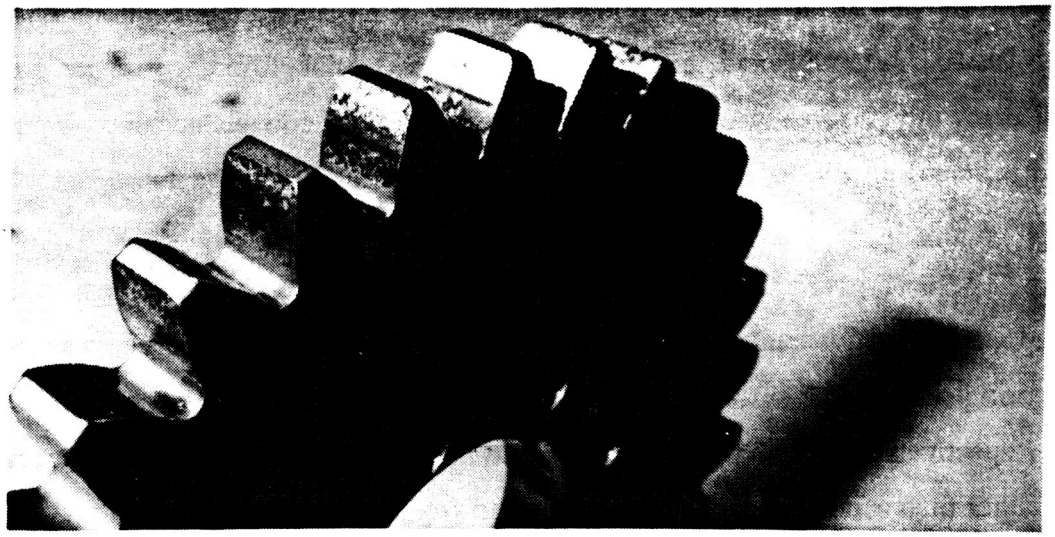

C132343 NO.23

Figure 192. Scoring of Gear Treated by Spire Corporation

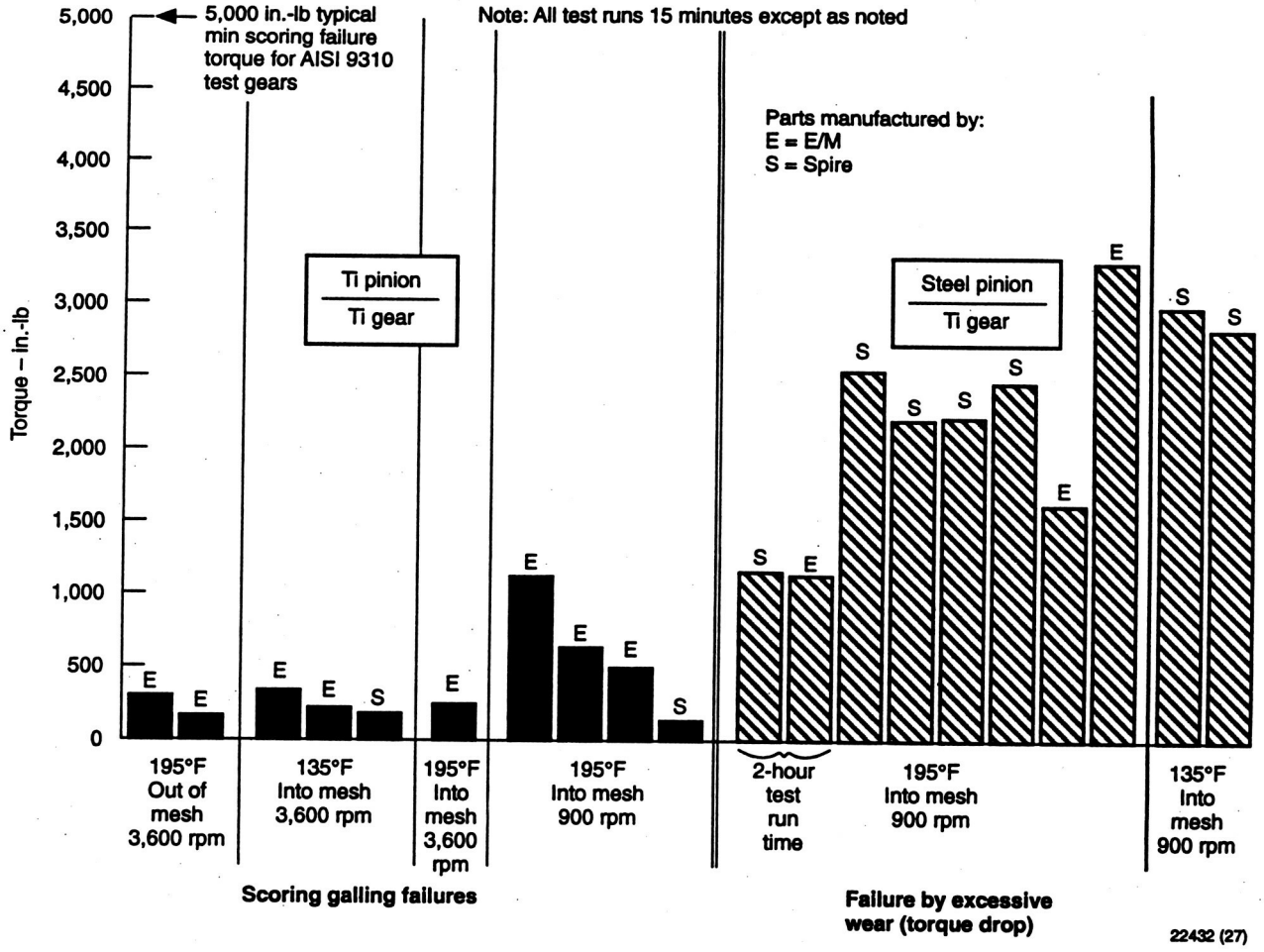

Figure 193. Results of Scoring Tests of Surface-Modified Titanium Accessory Spur Gears

Lowering the speed, even at the higher temperature condition, did appear to have a marginal effect on the load level at which galling occurred; however, these results may be somewhat misleading since all gears tested at this condition suffered severe galling. Thus the range of torque levels shown in Figure 193 is not really representative of the spread of the failure points, but rather it is indicative of the severity of the failures observed. That is, all sets galled badly, but those run at the higher torque levels galled much more severely.

In all cases tested to this point, in addition to the galled tooth surfaces, the torque (which is always measured at the end of the test run) was found to have decreased substantially. This is a very unusual condition, never before observed in this test rig. Ordinarily, the torque remains constant during the entire test run, even when steel gears have scored severely. In the case of the titanium gears, however, since relatively large amounts of material were removed from the tooth surfaces as a result of the galling failures, the preload on the system was reduced, and thus the locked-in torque dropped accordingly. This being the case, it is difficult to determine the actual load at failure except to note that it was no higher than the starting load and to observe that the galling took place almost immediately. Total scoring test run time was only 15 minutes, but spot checks of the torque in the system after only a minute or two indicated that much of the torque was lost in the first few minutes of running.

As these tests proceeded, we recalled that plastic gears often performed better when in mesh with a steel gear than when in mesh with each other. That is, plastic gears meshed with plastic gears tend to wear or gall at high loads and speeds, but plastic gears meshed with steel gears tend to be capable of running at higher loads and speeds with little distress. Drawing on this experience, we decided to try running a steel pinion with a titanium gear.

This configuration (i.e., steel pinion with titanium gear) was able to run at substantially higher loads, even at the higher temperature, than the titanium-on-titanium sets tested thus far. In addition, no galling was observed, even at loads as much as six times those which caused immediate galling on the titanium-on-titanium sets. The failure mode changed from galling to

smooth, polishing-type wear of the titanium member, as shown in Figure 194. The results of ten tests of this steel-on-titanium configuration are also plotted in Figure 193. In these cases, failure was defined as the maximum load at which the gear set could be run without resulting in a loss of torque during the normal scoring-test run (15 minutes). Two gear sets (one Spire and one E/M) were also run for two hours each in order to obtain some indication of the long-term viability of the steel-on-titanium concept. In both cases, the gear sets were able to run above 1,000 in.-lb torque without significant wear (as indicated by loss of locked-in torque). Clearly, the titanium gears could run successfully at these modified test conditions; however, visible wear of this type would not be acceptable in a helicopter application.

Surface Durability - The surface durability testing was performed after the scoring testing had been completed. In view of the scoring-test results, it was apparent that the surface durability gears would likewise suffer galling failures at very low torque levels. In order to test this hypothesis, we tested two sets of titanium surface durability gears (one Spire and one E/M). As expected, both gear sets experienced severe galling after only 15 minutes of running at an initial pinion torque level of only 730 in.-lb. In addition, both sets experienced a torque drop of almost 50 percent during the 15-minute test runs. By way of comparison, the minimum durability failure load for an equivalent set of AISI 9310 carburized, hardened, and ground spur gears of identical geometry (such as now used for helicopter accessory gears) would be over 6,800 in.-lb: almost ten times the load at which the titanium gears exhibited a galling failure in only 15 minutes.

Considering these preliminary results, we decided to use a steel pinion in mesh with the titanium gears to determine, as we did for the scoring-test gears, the load at which the titanium gears could be run without exhibiting excessive wear. The rate of wear was measured indirectly by applying an initial torque to the gear set and then running for 15 minutes. At the end of the 15-minute run, the locked-in torque was again measured. The drop in torque level measured was taken as an indicator of wear.

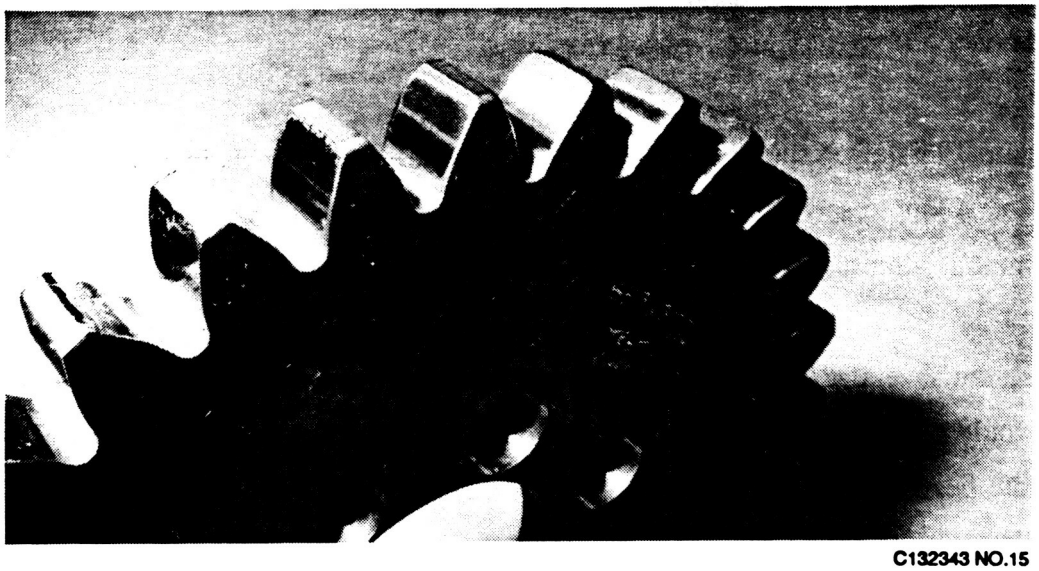

C132343 NO.15

Figure 194. Type of Wear With Steel Pinion Running With Titanium Gear

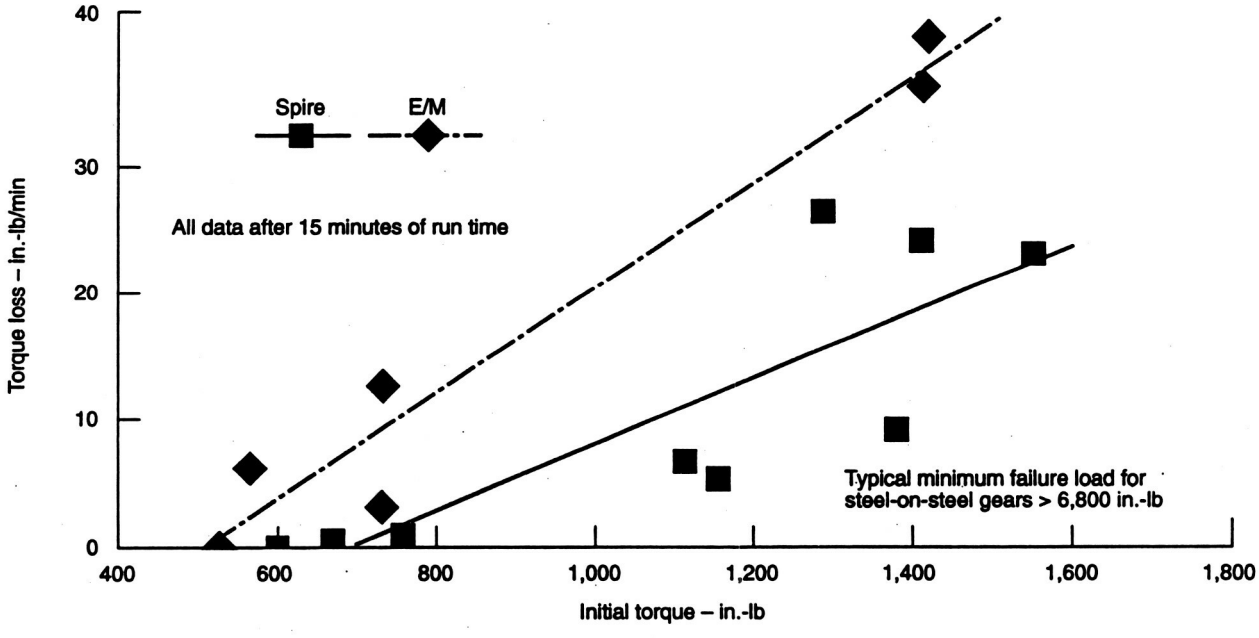

22432 (28)

Figure 195. Overall Performance Summary of Surface-Modified Titanium Gears

As can be seen from Figure 195, in this testing the Spire-treated gears exhibited slightly better performance than the E/M-treated gears; however, considering the overall scatter of the data, no firm conclusions should be drawn from this.

As Figure 195 shows, the gears must be run at initial torque levels in the range of 500 to 700 in.-lb to avoid excessive wear. At these levels the wear rate is very low, since the torque loss per minute is almost zero, at least for the first 15 minutes of running.

We also ran several gear sets for extended periods of time, up to 20 hours, to determine if the wear would cease or remain constant. At very low initial torque levels, below 500 in.-lb, the wear rate became so small that we could not reliably detect additional torque loss. Above the approximately 500 in.-lb torque condition, the wear rate remained constant with run time. At higher initial torque levels the gears wore until the torque level dropped to the 500 in.-lb range, at which point the wear rate leveled off to near zero in each case.

Conclusions

Based on the testing conducted, the following conclusions have become evident:

1. Titanium gears in mesh with titanium gears exhibit a severe galling-type failure mode at loads well below those which they would experience in a typical helicopter accessory gear application, regardless of whether treated with either the Spire or E/M surface-modification process.

2. When meshed with a steel mating pinion, however, a titanium gear could be run at higher load levels than when meshed with a titanium pinion.

3. The steel pinion and titanium gear combination changed the failure mode from severe galling to smooth wear of the titanium gear tooth surface. In no case did the steel pinion experience any distress at all.

4. The improvement in load capacity obtained by running a steel pinion against a titanium gear was relatively small and still resulted in failure of the titanium gears at loads which were only a small percentage of the typical failure loads for a geometrically identical steel-on-steel gear set. Typically, the titanium and steel combination resulted in failures at loads that were only 10 to 20 percent of the typical minimum failure loads for similar steel-on-steel gear sets.

PARALLEL-AXIS GEAR NOISE STUDY

The problem of gear noise in helicopter transmissions is ever-present. The main exciting forces that produce the noise are the gear teeth meshing forces. While this is an oversimplification, since many factors influence transmission noise in addition to the gear mesh forces, the simple fact remains that if the basic gear tooth exciting forces are reduced and the amplifying factors remain constant, then the overall noise level of the transmission system will be reduced.

Among the several ways in which the gear tooth meshing forces may be reduced, two of the most directly applicable to helicopter transmissions are the form of the teeth and the overall contact ratio. Both approaches are attractive for an aerospace application since, unlike other treatment methods which are applied with penalties to either system weight or performance, these approaches have the potential for reducing noise without causing any increase in overall system weight or reducing performance. In fact, both approaches also offer the possibility of actually providing improved gear performance in terms of longer life, higher load capacity, improved reliability, and reduced weight while simultaneously reducing noise levels.

The objective of this task was to determine, by controlled testing and actual noise measurements, the effect of changes in the profile, face, contact ratios, and gear tooth form, separately and in combination, on the noise levels produced by otherwise identical spur and helical gears. A program was defined to design appropriate gears (Table 40), fabricate a sufficient number of test specimens, and conduct the testing required.

While a wide range of specimens is shown, they were all configured as nearly alike as practical, within the limitations imposed by manufacturing considerations and the test stand. Testing was conducted in a single-mesh gearbox under controlled conditions which were maintained as nearly identical as possible. Acoustic intensity measurements were taken with the aid of a robot to insure repeatability of measurement between gear sets and to minimize the influence of human technique.

TABLE 40. GEAR NOISE TEST MATRIX

Configuration	Tooth form	Type	Contact Ratio		
			Profile	Face	Modified
1. Conventional spur baseline	Involute	Spur	1.25	0.00	1.25
2. HCRINV	Involute	Spur	2.15	0.00	2.15
3. Conventional single-helical baseline	Involute	Helical	1.25	1.25	1.77
4. Double helical	Involute	Helical	1.25	1.25	1.77
5. HCRINV	Involute	Helical	1.25	1.75	2.15
6. HCRINV	Involute	Helical	2.15	2.25	3.11
7. NIF baseline	Noninvolute	Spur	1.25	0.00	1.25
8. HCRNIF	Noninvolute	Spur	2.15	0.00	2.15

Test Gear Design

Eight sets of gears, four spur and four helical as listed in Table 40, compatible with the NASA Lewis gear noise test rig, were designed. Of the four sets of spur gears, two sets have an

involute tooth form and two use a noninvolute, constant radius of curvature tooth form. During the manufacture of the test gears, the initial drawing of the double helical gear went out with an inadvertent drafting error such that both helices were manufactured with the same hand. This ninth set of gears was dubbed the "OOPS" gear set and was included in the test program. All gears were designed in accordance with normal Boeing practice so that, except for size, they are representative of typical helicopter gears.

Since these gears were tested in the NASA test rig, it was also necessary to maintain compatibility with the test rig. The standard NASA test gears incorporated a loose fit between the gear bore and the shaft outside diameter. In order to be sure that the noise test results, especially for the helical gears, were not affected by this loose fit, it was changed to a press fit which would be more typical of that used in a helicopter application. While this change caused some difficulty in switching from one configuration to another, it was important from a test validity point of view. Previous NASA testing[29] of Boeing-designed small gears using the high profile contact ratio noninvolute tooth form (HCRNIF) indicated that their surface load capacity was substantially higher than that of conventional involute gears and that their bending load capacity (at torque loads) was at least equal to and actually slightly greater than the standard involute gears. The scoring resistance of the HCRNIF gears in the NASA tests appeared to be lower than that of equivalent standard gears. The lower scoring load capacity performance may have been due to inadequate profile modification on the small test gears; therefore the HCRNIF gears for this testing incorporated improved profile modifications.

The test gear configurations were selected to be representative of those which are either actually in use or have near-term potential of being used in helicopter transmissions. While lower noise levels are generally associated with helical gears as compared to spurs, there were no definitive data for accurate, ground-tooth gears which define the noise advantage that may be obtained. Similarly, anecdotal information indicates that higher contact ratios, both face and profile, also tend to reduce noise levels, but again, hard data were not readily available.

While helical gears provide some noise reduction, their use also generates a thrust load which must be dealt with in the design of the overall system, especially the support bearings, gear blank design, and housing structure. Double helical gears provide some relief from the net thrust problems; however, the thrust loads from each helix must still be canceled within the gear blank and the overall effect of this on the noise level of the gear has not been studied at all.

New tooth forms of various noninvolute types have been investigated for possible use in helicopter transmissions in recent years, but these investigations have centered almost universally on the load-capacity aspect of the forms and not their noise behavior. One of these has demonstrated some potential for improved load capacity in previous testing.

Considering all of these factors, the range of gear configurations defined in Table 40 and shown in Figure 196 was selected to provide some basic answers to their respective noise behaviors. The basic gear tooth data for the test gears are provided in Table 41.

Test Facility

The NASA Lewis Research Center gear noise rig (Figure 197) was used for these tests. This rig features a single-mesh gearbox powered by a 150-kW (200-hp), variable-speed, electric motor. A poly-V-belt drive was used as a speed increaser between the motor and input shaft. An eddy-current dynamometer loads the output shaft at speeds up to 6,000 rpm. The rig was built to perform fundamental studies of gear noise and the dynamic behavior of gear systems. It is designed to allow testing of various configurations of gears, bearings, dampers, and supports.

To reduce unwanted reflection of noise, acoustical absorbing foam baffles cover test cell walls, floor, and other surfaces. The material attenuates reflected sound by 40 db for frequencies of 500 Hz and above.

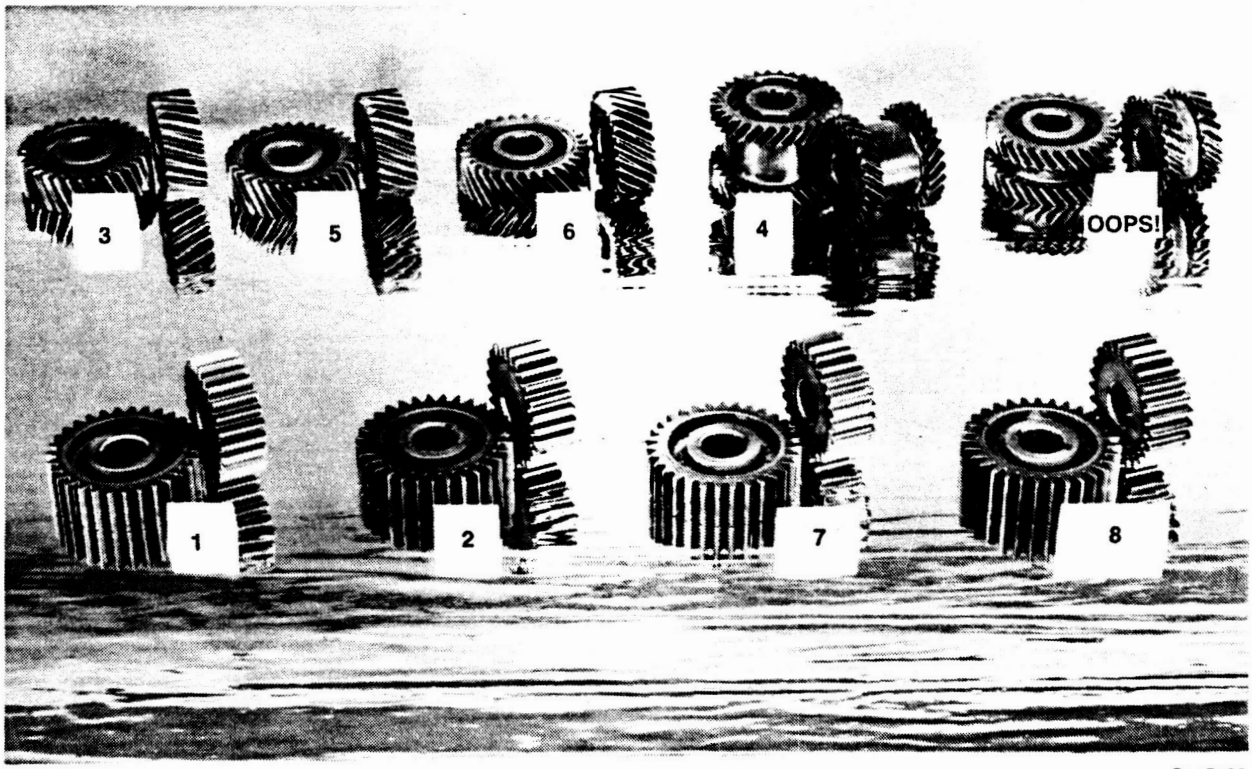

C145706

Figure 196. Test Gears

TABLE 41. CONFIGURATION OF BASIC TEST GEAR

Factor	Pinon	Gear
Number of teeth	24	31
Diametral pitch, transverse	8.	
Center distance (in.)	3.50	
Pressure angle, transverse (deg)	25 (standard profile contact ratio)	
	20 (high profile contact ratio)	
Face width, spur and single helical (in.)	1.25	
Face width, double helical (in.)	Double helicals 0.625 ea helix	

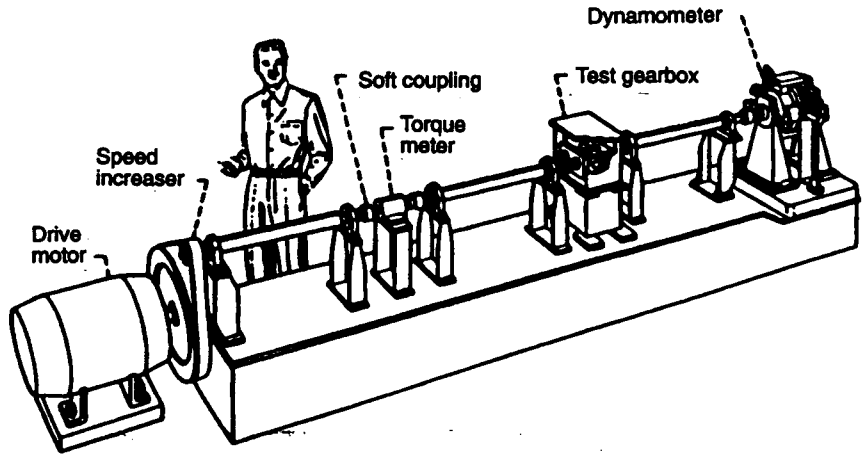

Figure 197. NASA Lewis Gear Test Rig

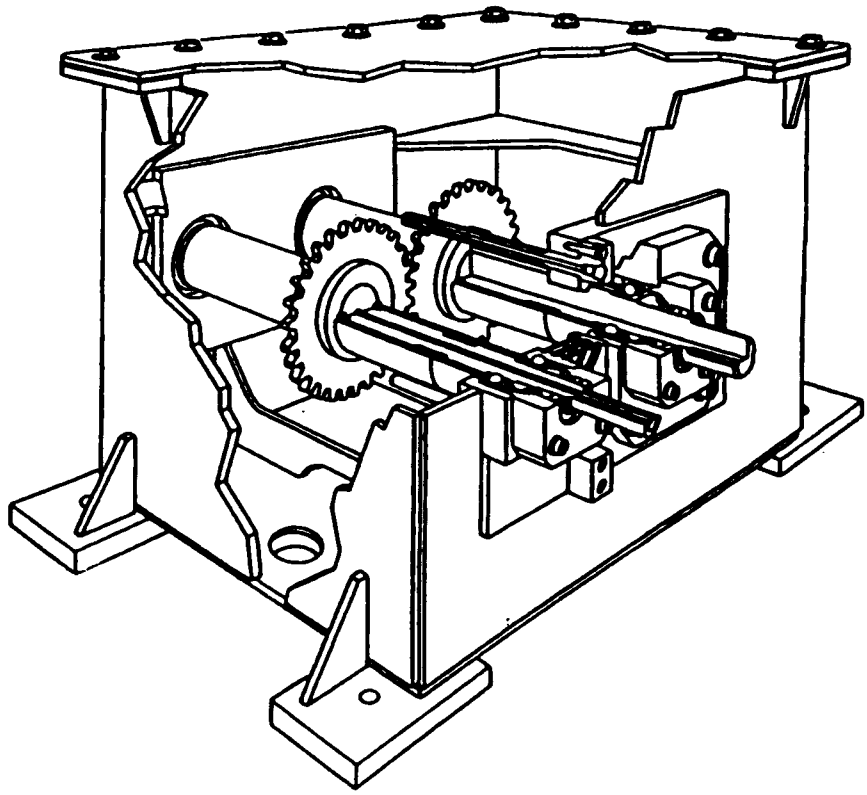

Figure 198. Cutaway Section of Test Gearbox

A 20-node measurement grid was drawn on the top cover of the gearbox and used to insure repeatability of the noise measurements and to aid in avoiding operator-induced errors. The grid covers an area 228 by 304 mm (9 by 12 in.) centered on the 286 by 362-mm (11.25 by 14.25-in.) top. A cutaway section of the test gearbox is shown in Figure 198. All data were collected with the computer-controlled robot arm coordinated with the reference grid so that no matter what gear set was running, the readings were taken identically.

Instrumentation

An experimental modal test was performed to determine the modes of vibration and natural frequencies of the gearbox top. An 800-line, 2-channel dynamic signal analyzer collected frequency-domain data. Commercial modal software running on a personal computer was used for the analysis. The tests were performed with the gearbox heated to operating temperature. The structure was excited sequentially at each of the 63 nodes by a load cell-equipped modal hammer to measure excitation forces. The response was measured with a small piezoelectric accelerometer mounted at a reference location near the center of the gearbox top.

The gearbox modal test was not conducted as part of this program but rather as part of a previous program[30]. Modal test results were used to assure that gear mesh frequencies did not coincide with important modes of the gearbox.

Noise Measurements

Measurements of acoustic intensity were taken under stable, steady-state operating conditions with the aid of a computer-controlled robot designated RAIMS[31,32] (robotic acoustic-intensity measurement system). The RAIMS software commanded the robot (Figure 199) to move an intensity probe over a prescribed measurement grid; recorded acoustic-intensity spectra in the analyzer for each node of the grid; and transmitted the spectra to the computer for storage on disk.

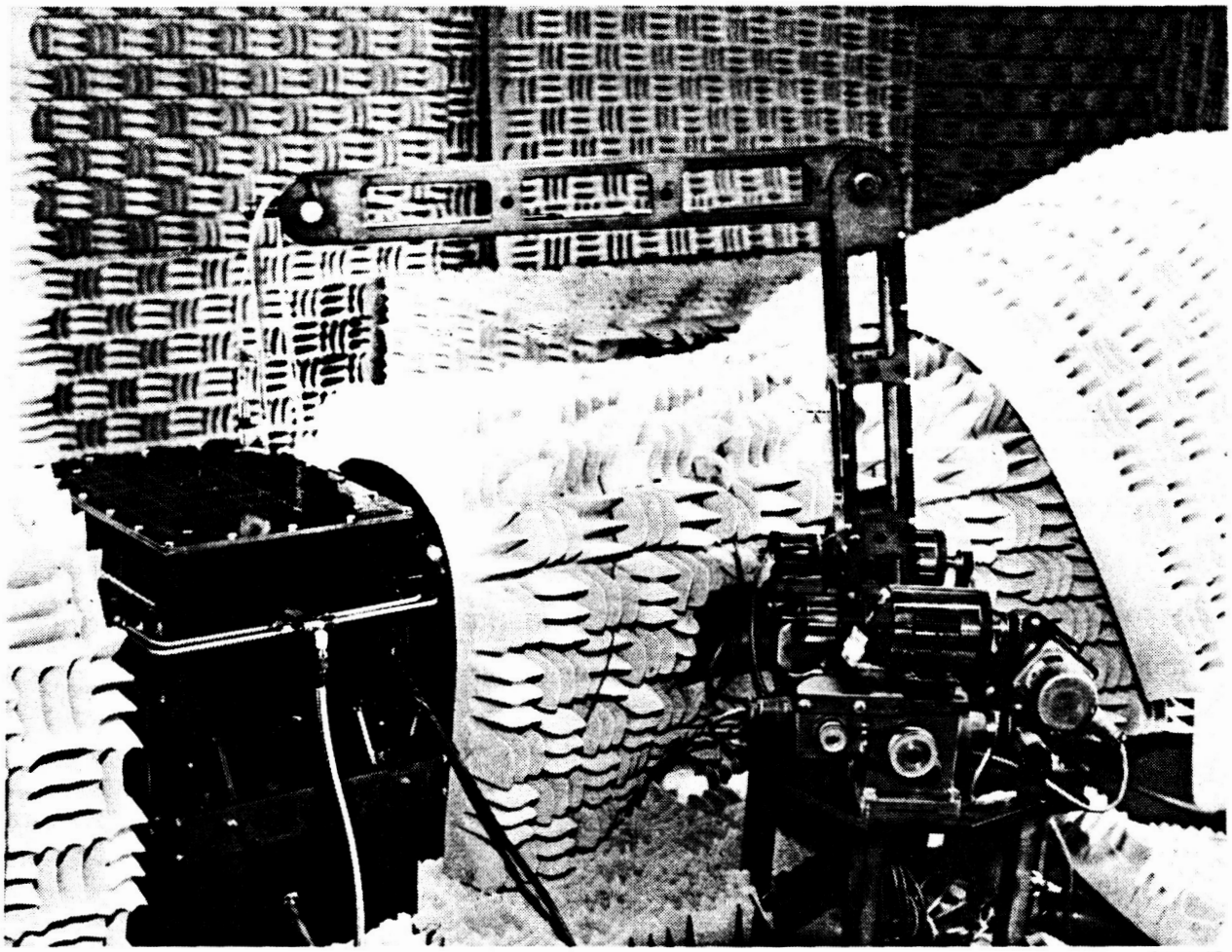

C145705

Figure 199. Robotic Noise Measurement System

The acoustic-intensity probe consists of a pair of phase-matched 6-mm microphones mounted face-to-face with a 6-mm spacer. The probe has a frequency range (± 1 db) of 300-10,000 Hz. Measurements were made at a distance of 60 mm between the acoustic center of the microphones and the gearbox top.

The 20 intensity spectra collected at each operating condition were averaged, then multiplied by the radiation area to compute an 800-line sound power spectrum. The radiation area was assumed to be the area of the grid plus one additional row and column of elements or 0.0910 m^2. The actual area of the top is 0.1034 m^2. The measurement grid did not extend completely to the edges of the gearbox top because the top edge was bolted to a stiff mounting flange which would not allow much movement, and measurements taken close to the edge of the top would be affected by noise radiated from the sides of the box. Noise measurements from the gearbox sides were not attempted for the following reasons:

1. The top is not as stiff as the sides; thus, noise radiation from the top dominates.

2. The number of measurement locations was kept reasonable.

3. Shafting and other projections made such measurements difficult.

Sound power measurements were made over a matrix of nine test conditions: three speeds (3,000, 4,000, and 5,000 rpm) and at three torque levels (60, 80, and 100 percent of the reference torque 256 N-m (2,269 in.-lb)). During each intensity scan, the speed was held within ± 5 rpm and torque to ± 2 N-m. At least five complete sets of scans were performed on each gear set.

Acoustic-intensity data were recorded over the bandwidth 896-7,296 Hz. On the 800-line analyzer, this produced a line spacing of 8 Hz. We chose this frequency range because it includes the first three harmonics of gear-meshing frequency for the speed range (3,000-

5,000 rpm). In addition to the intensity data, signals from two microphones and two accelerometers were recorded on four-channel tape.

Processing Sound Power Data

The sound power data as captured by the method outlined consist of many data files of 800-line sound power spectra. A typical spectrum is shown in Figure 200. This trace (taken at 5,000 rpm and 100-percent torque) includes the first three harmonics of gear mesh frequency. Each harmonic is surrounded by a number of sidebands.

To characterize gear noise data, it was decided to reduce the 800-line sound power spectra to a single number that would represent each gear mesh harmonic. This is referred to as the harmonic sound power level. Five alternatives were considered for the reporting of each harmonic level:

1. The amplitude at gear mesh frequency only (no sidebands).

2. The value of the largest amplitude mesh frequency harmonic or sideband, whichever is higher.

3. The log sum of the sound-intensity amplitudes in a fixed-width frequency band centered on the mesh frequency.

4. A value similar to 3 except the size of the frequency band varied with speed; the total number of values added is not constant.

5. Sum of gear mesh and fixed number of sidebands.

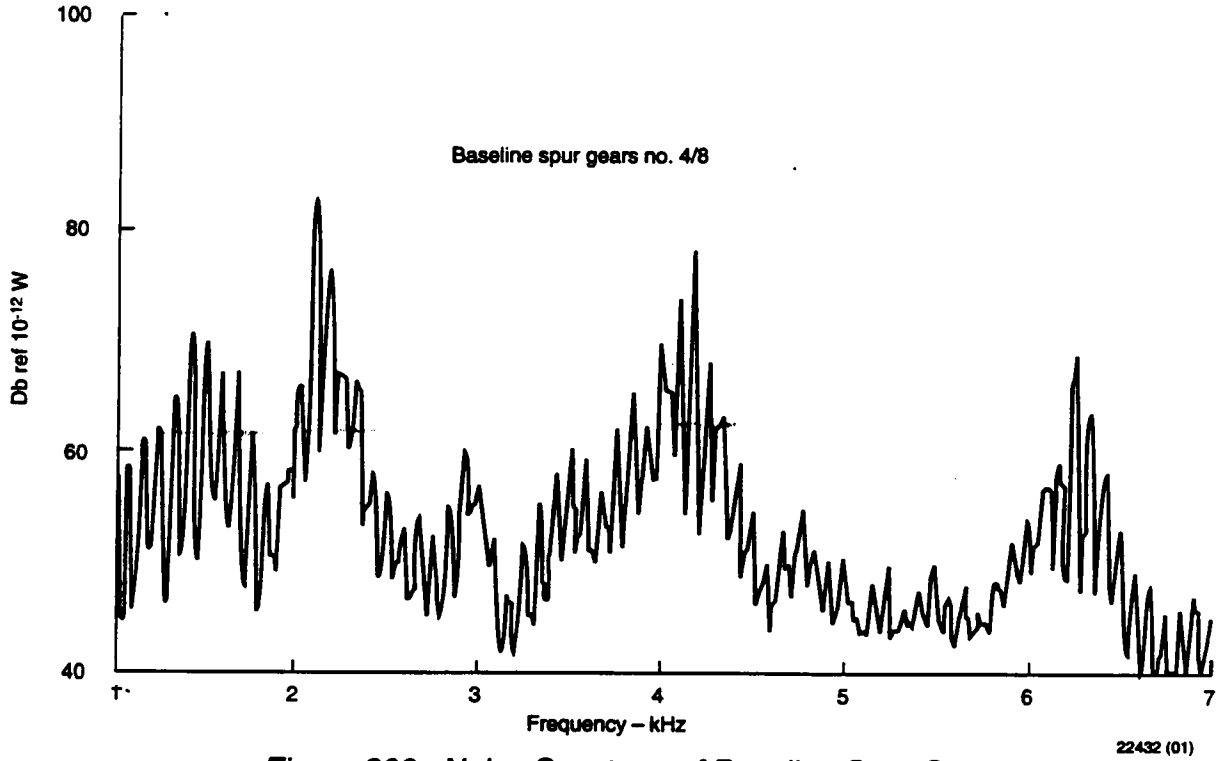

Figure 200. Noise Spectrum of Baseline Spur Gear

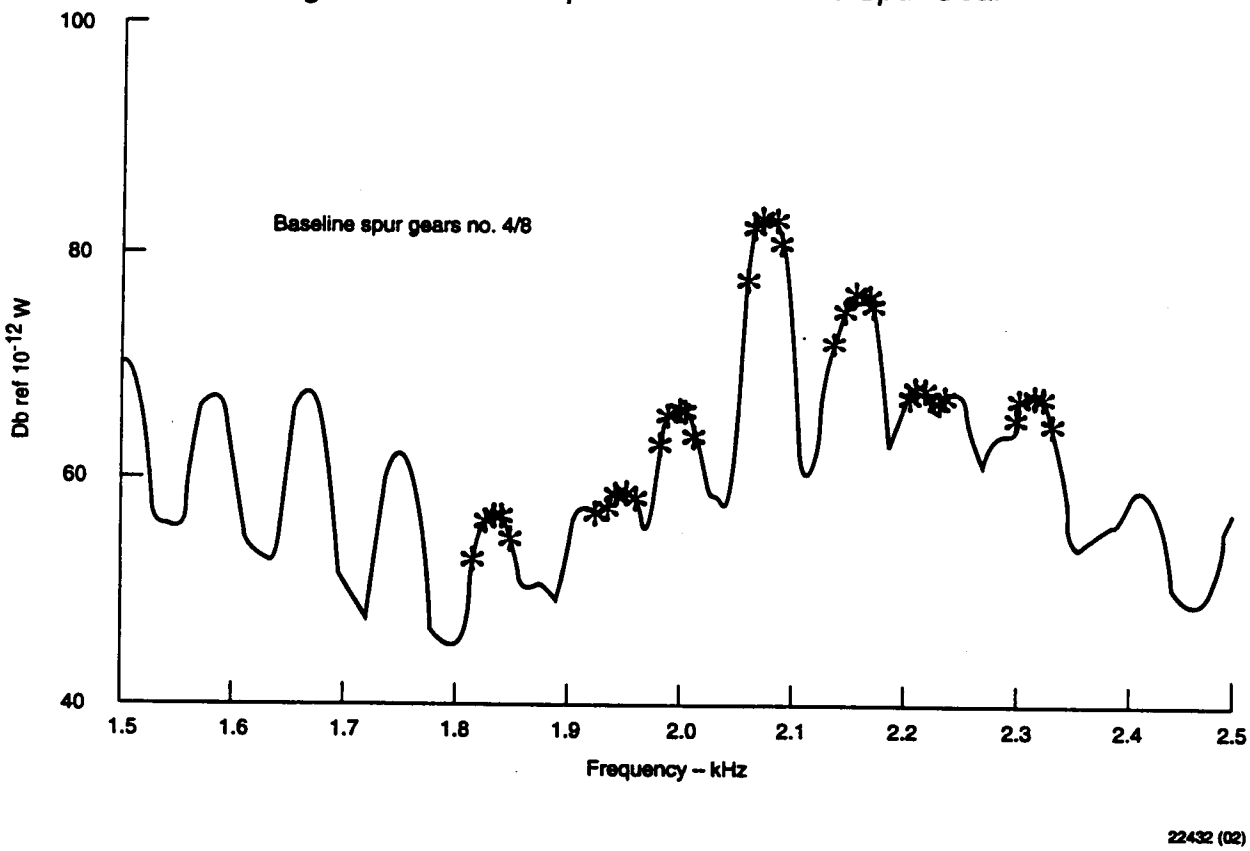

Figure 201. Enlarged View of First Harmonic (at 2,083 Hz) of Preceding Figure

Alternative 5 was chosen for computing the harmonic sound power level. We used three pairs of sidebands plus the harmonics (i.e., seven peaks) in the calculation. Sound power levels were converted to watts before calculating sums.

In the analysis of the intensity data, each harmonic of gear mesh frequency was defined by several digital lines of the frequency analyzer. In order to capture the total effective magnitude at each harmonic, while accounting for speed drift, etc, the peak value and two frequency lines on either side of the peak were summed. These values were converted to db (re 10^{-12}W) to define a mesh harmonic level. Since seven peaks were used, 35 values (5 x 7) were summed to produce the mesh harmonic sound power level. Figure 201 illustrates the data (marked with the symbol *) used to produce the harmonic sound power level. This is a portion of the spectrum of Figure 200 showing the first harmonic (at 2,083 Hz). The sideband spacing (for 5,000 rpm) is 83 Hz; thus there are about ten analyzer lines per sideband; at lower speeds there are fewer analyzer lines per sideband.

Data Sampling

In order to be assured that data measured on each gear set could be reliably compared with data from other gears, it was desired to have sufficient records to establish a 95-percent confidence level of ± 1 db. This level is well beyond the practical difference which most persons with normal hearing can detect (i.e., a change of about 3 db).

Based on these considerations, the confidence limit is given by equation 51:

$$C_1 = t(\delta/\sqrt{n}) \tag{51}$$

where C_1 = confidence limit, db

t = probability distribution ("Student t" distribution)

$\hat{o}$ = standard deviation of data, db

n = number of samples (typically 5).

The values for the "t" distribution are found in any standard statistics text. A confidence level of 95 percent corresponds to a 5-percent probability. The number of degrees of freedom in the "t" distribution is the number of samples minus 1 (typically 4).

To estimate the effect due to sample-to-sample variation, two sets of gears for each design were fabricated and tested. Each gear was inspected in detail in accordance with typical production helicopter standards. The overall accuracy of the gears was found to be consistent with what we expect of production helicopter gears of similar size and configuration. Based on our evaluation of the gear tooth inspection data, the variation between the two sets of gears is reasonably typical of normal production for gears in the same manufacturing lot. Lot-to-lot variations may be and differences between different manufacturers of the same parts certainly will be higher, but the overall trend of the effect should be about the same.

A large difference in noise level is sometimes observed on large production gearboxes simply as a result of rebuilding them after they are disassembled for visual inspection, even though no parts are changed. Considering this effect, in addition to the manufacturing variability checks, we also checked for variability due to disassembly and reassembly.

This was done by testing three "builds" of the first gear set. Each build used exactly the same parts and each was performed by the same technician using the same tools.

Test Gear Loading

The loads applied to the test gears during this program presented a problem in the design of the experiment. Obviously, if the overall gear geometry is kept constant but the type of gear and tooth form are varied, the stress levels under identical torque-loading conditions will be

different. An alternative to the identical torque-loading method would be to apply varying torques to each configuration in order to keep the tooth stresses the same. While this seems reasonable, the question arises of which stress (not to mention flash temperature) should be held constant.

After much deliberation, it was decided to use identical torque and speed conditions across the range of gear configurations. Since the overall geometry of the gear blanks was held constant, it was believed that this approach was more representative of the actual noise that may result from a given weight or size of gear. Better load capacity due to lower stresses is another factor, but it was ignored for these purposes.

In order to provide an overview of the stress levels to which these gears were subjected during testing, Figures 202, 203, and 204 show the bending stress, contact stress, and flash temperature levels as functions of torque and speed. Note that, in Figure 204, the 5,000-rpm line for the baseline spur gear set (configuration 1) and the 4,000-rpm line for the HCR helical gear set (configuration 6) are virtually coincident.

The stress levels at which these gears were run during this testing are reasonably representative of those at which 10-pitch accessory gears would be run in a typical Boeing transmission. Main power gears would, however, be run at considerably higher stress levels. The typical bending stresses in a helicopter application would be about double the maximum stress run during this testing. Both the contact stress levels and the flash temperatures experienced in a typical helicopter main power transmission would be similarly higher than the test conditions defined herein.

While it would have been desirable to run the test gears at higher stress levels (more consistent with the profile modifications applied), limitations inherent in the NASA test rig loading mechanism prevented this. Still, since all results are comparative, the data obtained are quite meaningful and will provide much insight into the problem. Caution should be exercised,

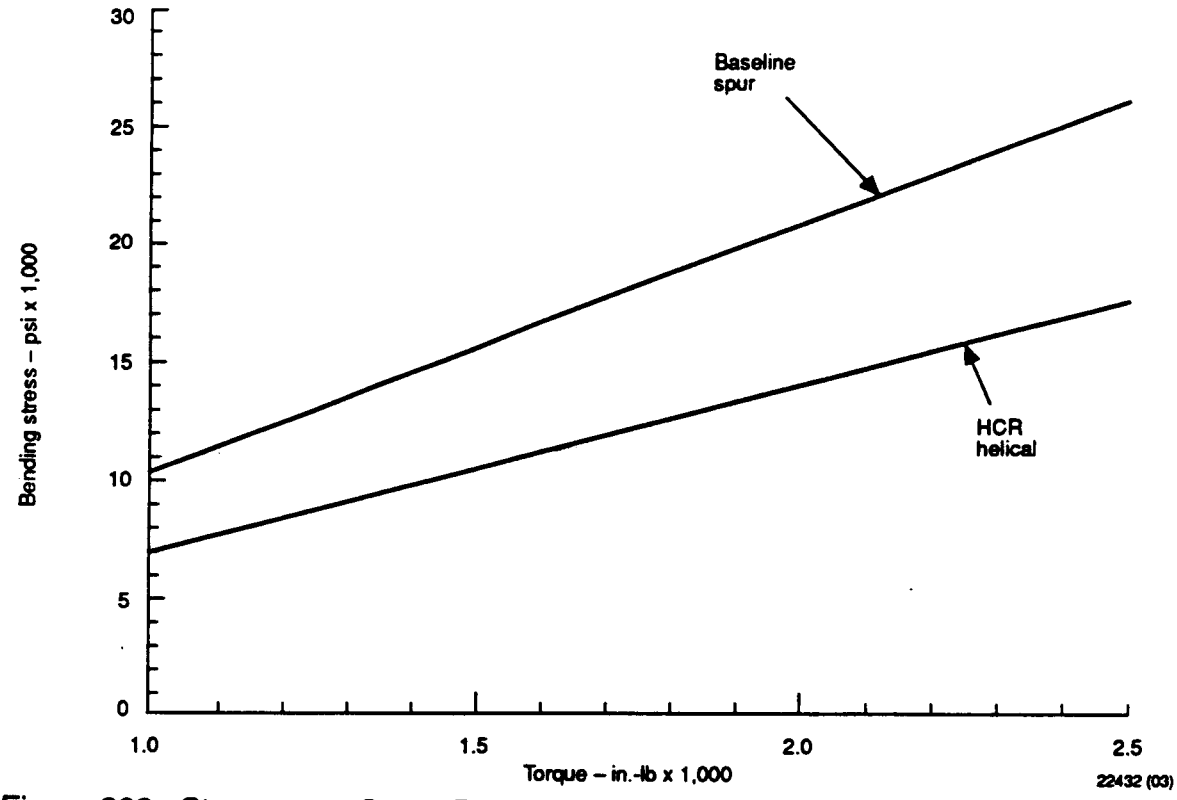

Figure 202. Stresses on Gears During Noise Testing: Bending Stress Versus Torque

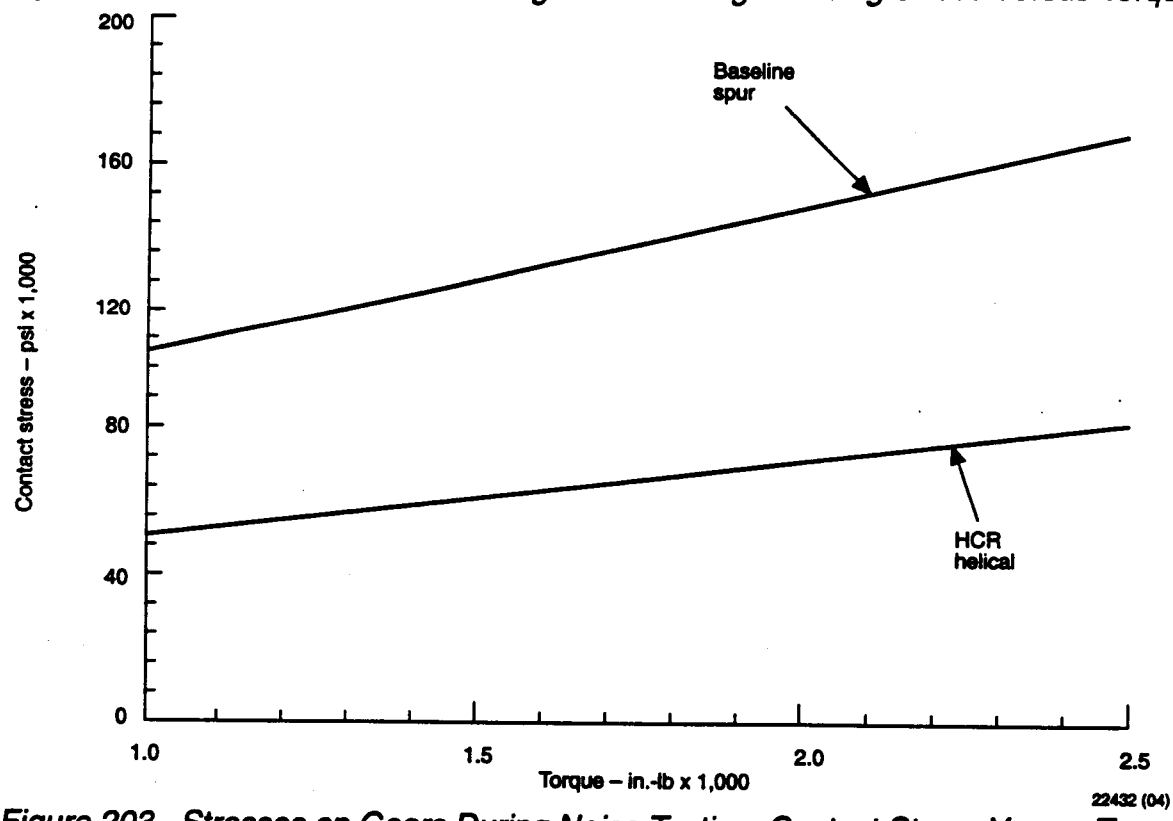

Figure 203. Stresses on Gears During Noise Testing: Contact Stress Versus Torque

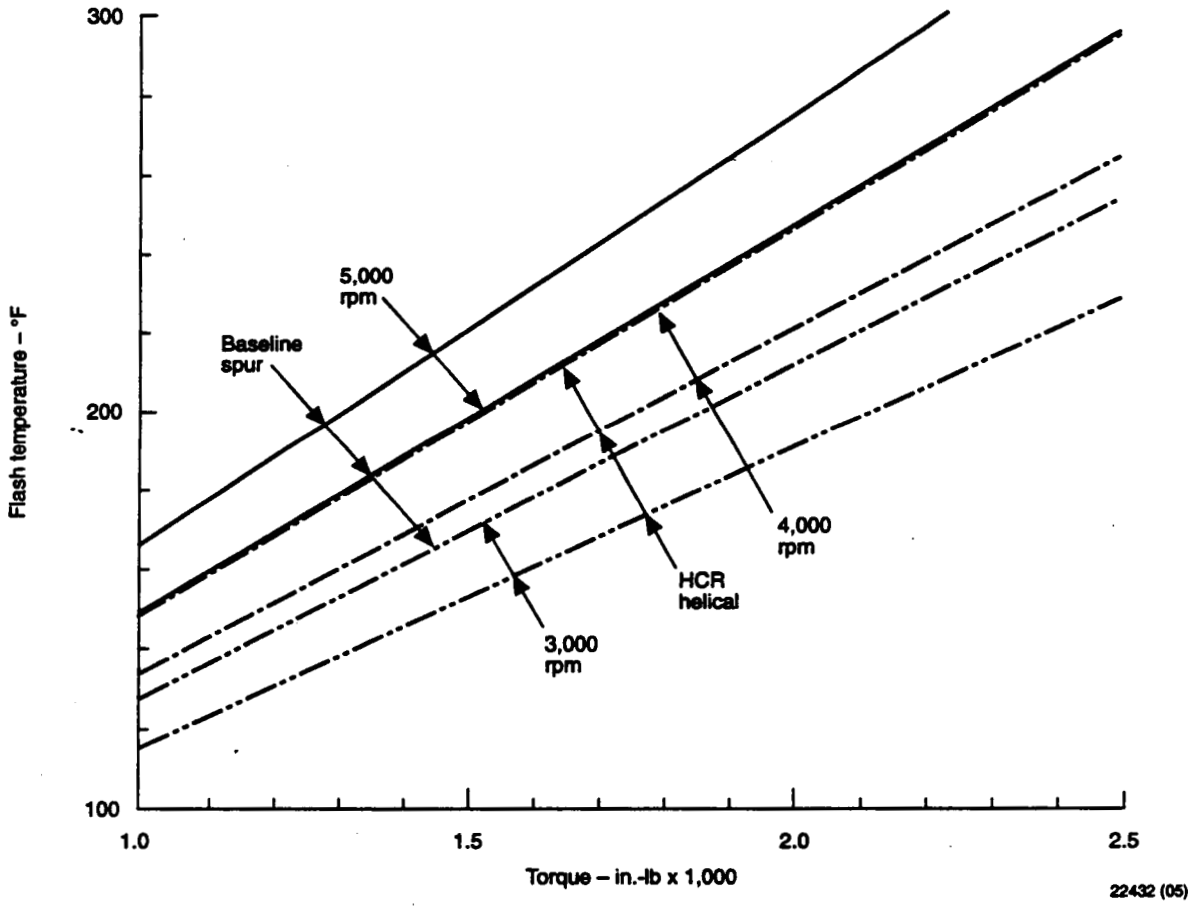

Figure 204. Stresses on Gears During Noise Testing: Flash Temperature Versus Torque

however, when applying these results to any practical application. The results are valid in a comparative but probably not in an absolute sense.

Results

A very large amount of data has been collected during the conduct of this test program. A rather complex overview is presented in the bar chart shown in Figure 205. Note that the configuration numbering scheme followed in Table 40 is continued in Figure 205 (and in other figures presented herein) for easy reference among the configurations tested. Considering the data shown in Figure 205, we can observe that all of the helical gears, regardless of their specific configuration, are generally significantly quieter than the equivalent spur gears and that high profile contact ratio spur gears are quieter than their equivalent standard contact ratio spur counterparts. One result which was not really anticipated is the fact that the double helical gear set was noisier than its single helical counterpart in some cases.

In order to better understand the specific ramifications of these results in terms of their application to actual design problems, it is enlightening to look at the data in terms of subgroups.

Spur Gears - Both involute and noninvolute tooth form, high profile and standard profile contact ratio spur gears were tested. Though the noise levels varied with both speed and torque loading, as Figure 206 shows, in general the HCR spur gears (configurations 2 and 8) were quieter than the standard contact ratio spur gears (configurations 1 and 7) regardless of the tooth form. Similarly, the involute tooth form spur gears (configurations 1 and 2) were quieter than the noninvolute tooth form gears (configurations 7 and 8), regardless of contact ratio.

An exception to this general observation occurs at the 4,000-rpm speed condition, and even that exception is not completely consistent across the three torque conditions tested. At the low- and medium-torque conditions (i.e., 1,361 and 1,816 in.-lb), the HCR gears were actually slightly noisier than the standard contact ratio gears. This reversal of the trend is probably related to

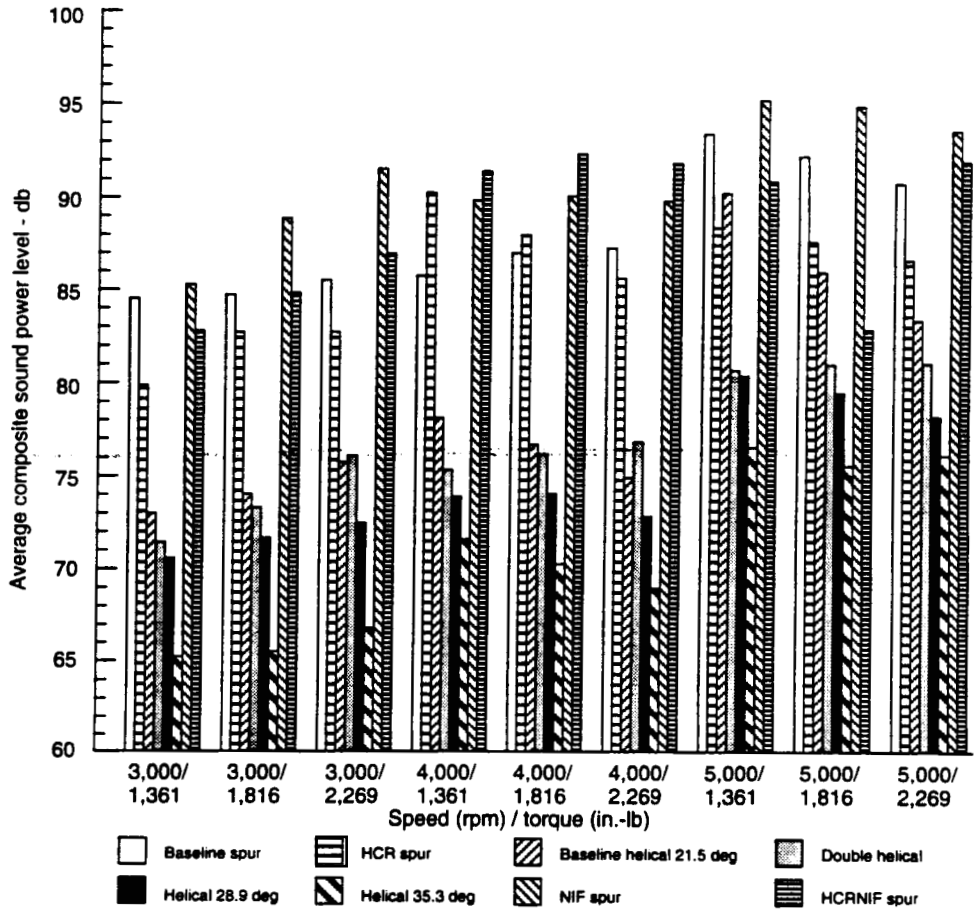

Figure 205. Summary of Test Results

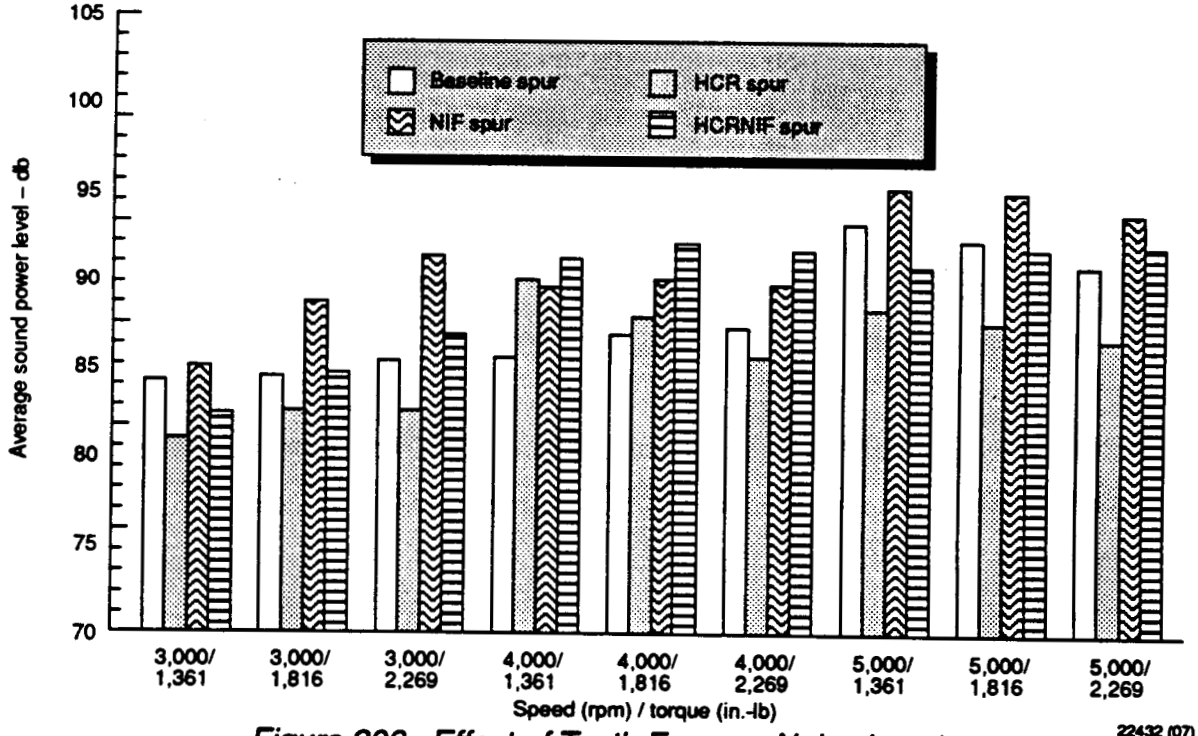

Figure 206. Effect of Tooth Form on Noise Level

an overall response of the gear, bearing, shaft, and housing system rather than a direct result of the gear configuration. As will be obvious from the ensuing discussion, similar effects were also observed for other gear configurations, probably related to the same, as yet unidentified, cause.

Helical Gears - As was the case of the spur gears, increasing contact ratio, both face and profile, correlates with decreasing noise levels on the helical gears. As Figure 207 shows, increasing the face contact ratio from about 1.25 (configuration 3, modified contact ratio 1.77) to 1.75 (configuration 5, modified contact ratio 2.15) decreases the noise level substantially in every case, though the results at higher speeds are more dramatic than at lower speeds.

By combining high face and profile contact ratios (configuration 6, profile, face, and modified contact ratios of 2.15, 2.25, and 3.11, respectively), the noise can be reduced even further. Indeed, in general, regardless of the configuration considered, the high profile and high face contact ratio, configuration 6, was consistently the generator of the lowest noise.

Helical gears used in helicopters tend to have relatively low face contact ratios (helix angles are kept low to minimize thrust loading and the extra weight associated with reacting the thrust); thus this result is especially interesting since it suggests that it is probably possible to trade off helix angle against increasing profile contact ratio to effect an improvement in noise level without the weight penalty that would be associated with attaining the same reduction with helix angle alone.

One surprising result materialized for the double helical gear set, configuration 4. This gear set is virtually identical to the single helical gear set, configuration 3, except that it uses two identical gears of opposite hand (i.e., each hand has the same helix angle, face width, and tooth proportions as the single helical configuration 3 gears).

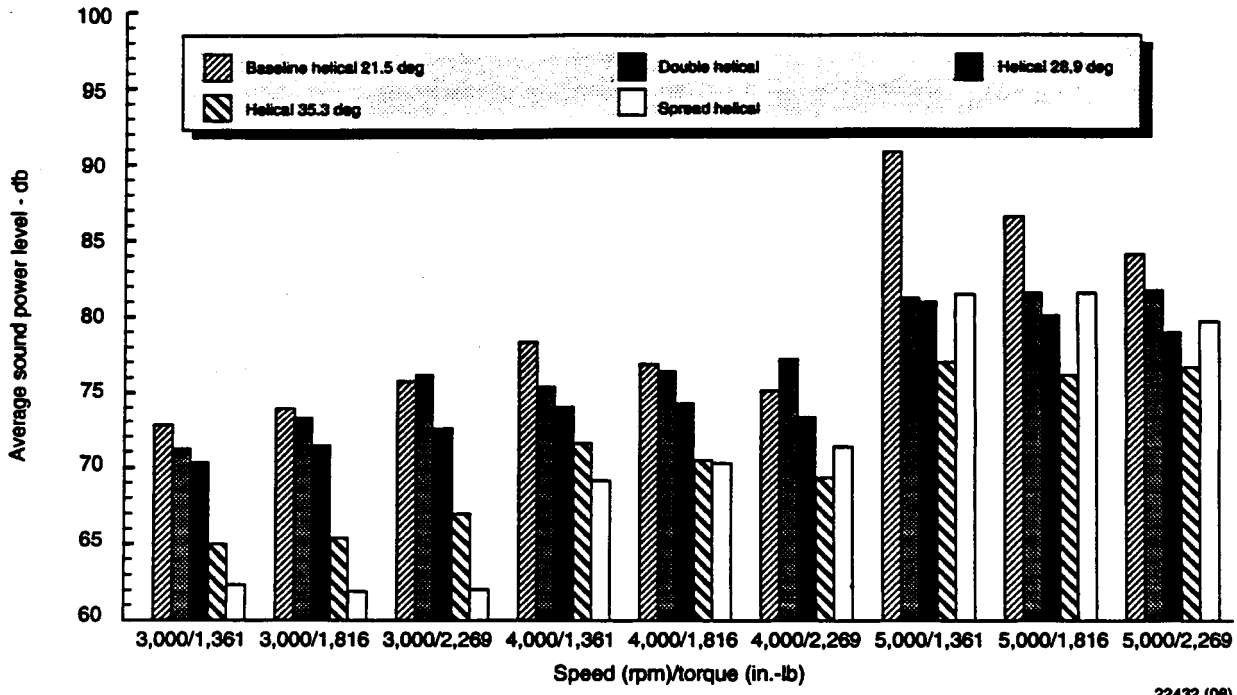

Figure 207. Effect of Helix Angle on Noise Level

At every operating condition, the double helical gears were either almost as noisy as or noisier than either the baseline low face and low profile contact ratio gear set (configuration 3) or the high modified contact ratio helical set, configuration 5. Initially one would expect that the double helical gears would be about as quiet as their single helical counterparts; however, this is clearly not the case.

The double helical phenomenon appears to be related to the axial shuttling that occurs as the double helical gear set moves axially to balance out the net thrust loading. The shuttling is due to the presence of small mismatches in the relative positions of the teeth on each helix. No matter how accurate the gear is, some mismatch will always be present; thus this is an unavoidable phenomenon.

While this feature of a double helical gear is a valuable design option since it greatly simplifies the bearing system, it is obvious that a price is paid in terms of noise (and certainly vibration) as the gear set shuttles back and forth.

Figure 207 also shows data for a spread single helical gear set which is not listed in Table 40. This configuration was not one of the eight planned test variants. During the manufacture of the test gears the initial double helical gear drawings went out with an inadvertent drafting error such that both helices were manufactured with the same hand. The resultant gear set (shown in the upper right corner of Figure 196) was somewhat unusual and probably would not be used in a production environment; however, we decided to test it anyway.

The noise results from this rather unusual gear set (which one of the authors unceremoniously dubbed the "OOPS" gear set) were surprising. It was actually quieter across the board than the double helical gear set under almost every operating condition. At first, these results were puzzling; however, after careful evaluation of the circumstances the explanation became clear.

Since the per-helix face contact ratio, face width, profile contact ratio, etc, are identical for both the OOPS and the double helical gear sets, the only operational difference is the lack of axial shuttling. The double helical set will be in a constant equilibrium-seeking state because of the theoretically zero net thrust load, while the OOPS gear set will run in a fixed axial position due to the net positive thrust load. This test thus provides some insight into the magnitude of the noise penalty that is paid when double rather than equivalent single helical gears are used. Since these test gears are all very accurate (accuracy typical of helicopter gears), it should be obvious that a larger penalty would be paid if gears of lesser quality were to be used, because the lower the gear quality is the more shuttling would be likely to occur.

If one considers the OOPS gear set to be a single helical gear set, then its effective face contact ratio would also place it between the baseline helical gear set (configuration 3) and the high face contact ratio helical gear (configuration 6). This being the case, its noise level is approximately where one would expect based on the levels of gears with higher and lower face contact ratios.

Build Variations - During other testing, the authors have noted significant variations in the measured (and perceived) noise levels of the same gear system before and after disassembly. In some cases this variation was of considerable magnitude. To investigate this phenomenon, each of the gear types was assembled, tested, disassembled, and then tested again. In one case, for the baseline spur gears (configuration 1), this process was repeated three times. Similar variations in noise levels were recorded for all gear sets. Figure 208 shows the specific results for the baseline spur gears (serial no. 2 and 6). The largest minimum-to-maximum build variation is about 8 db (occurring at the highest speed condition), while the minimum build variation is 1 db (occurring at the medium speed condition). Except for the low-torque, highest speed condition, the average build variation is about 3 db. While no real pattern is apparent, it does appear that the variation decreases slightly with increasing load.

Figure 208 also shows the results obtained from a second identical set of spur gears, serial no. 4 and 8. It should be obvious that the variation between otherwise identical units of the same

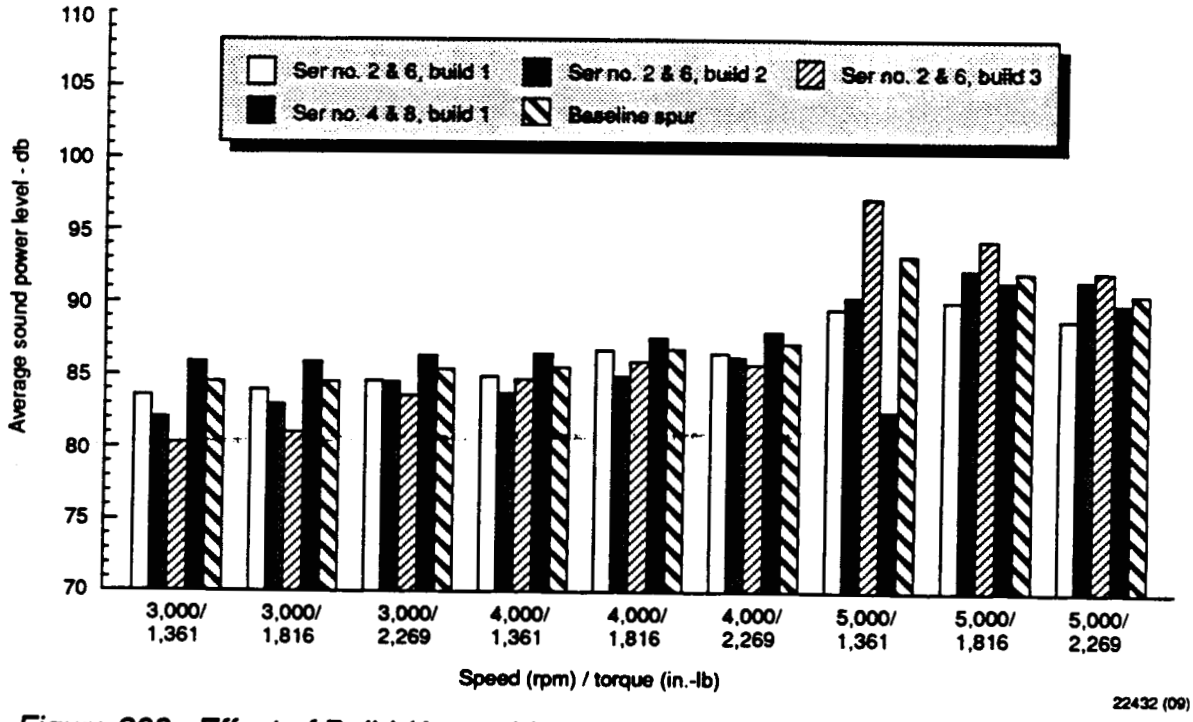

Figure 208. Effect of Build (Assembly and Disassembly) on Noise Level of Gears

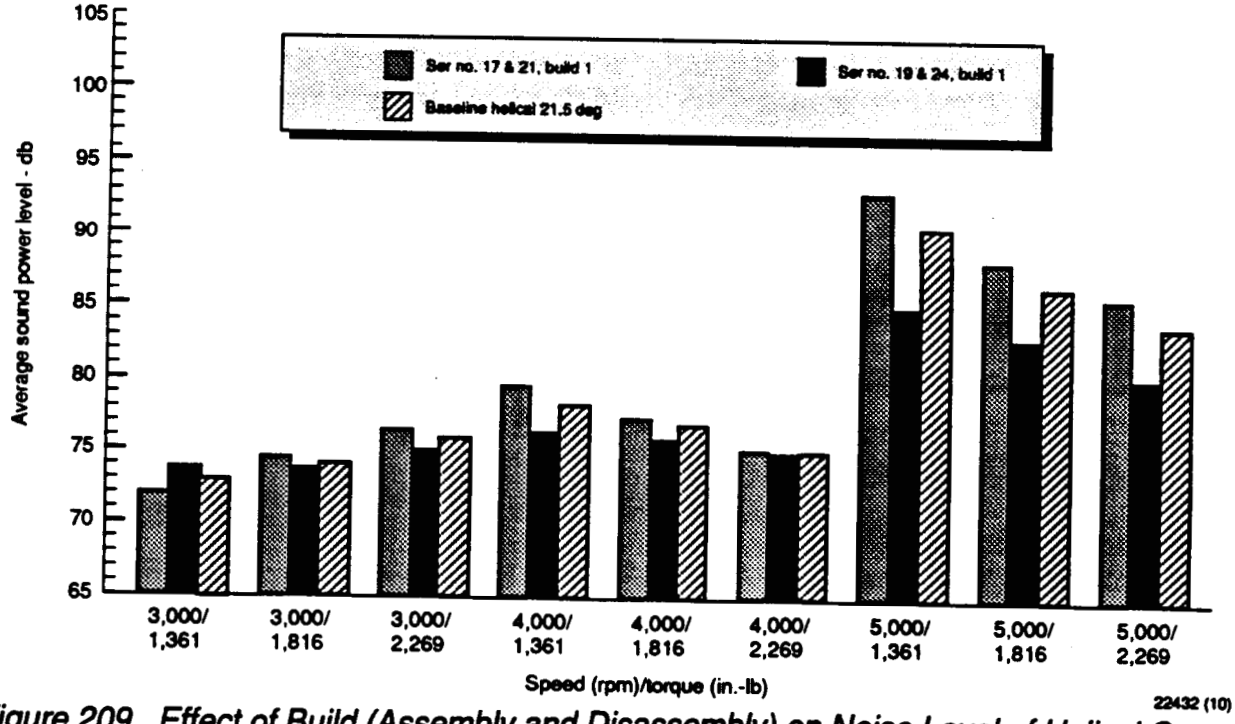

Figure 209. Effect of Build (Assembly and Disassembly) on Noise Level of Helical Gears

part generally exceeds the variation from rebuilding the same parts. Perhaps this is not surprising; however, it does point out the need to establish noise test results over a broad range of repeated testing to insure that the differences observed are not simply due to part-to-part variation.

This latter effect can also be seen in Figure 209 which shows the results for two identical sets of the baseline helical gears. The variation observed is generally less than that observed for the spur gears but not markedly so.

It is important to emphasize again several important points about these data. Such variations, both between different builds of the same parts and among different units of the same part, are not at all unusual; rather, they are quite common. The build variations occurred when the same physical components were simply disassembled and then reassembled under very controlled conditions by a skilled technician. The unit-to-unit variation occurred for helicopter-quality parts in which the apparent variations in the normally accepted measures of gear quality (e.g., lead, profile, spacing, etc) are extremely small, probably at a level where further improvements would be extremely costly.

This points out one difficulty in defining a noise-reduction effort in that the variations due to these effects are often of the same order of magnitude as the changes that can be attributed to gear configuration or treatment. Such differences must at least exceed the variations due to the build effect and those observed among different units of the same part number before they can be considered significant of themselves.

Torque Effect - The effect of torque on the noise level of a gear set depends on many factors. In general, however, as torque increases, the noise level would be expected to increase if no other factors are at work. As described below, however, this is not the case.

The effect of torque level on gear noise will be severely impacted by the amount of profile, and in some cases lead, modification that has been applied to the gears. In the testing described herein, the profile modifications were largely the same from gear set to gear set, so that we were comparing differences between gears and not between modifications. No lead modifications were made to any of the test gears. In addition, the profile modifications that were applied were calculated for a torque substantially above the upper end of the torque range at which these gears were actually run; that is, all of the gears were overmodified for the actual torque conditions encountered. It is to be expected, then, that as the load increases, more of the profile will come into contact as the teeth bend, thus perhaps lowering the noise level. Conversely, since our maximum test torque was only about twice our minimum test torque, and the absolute load levels were not extremely high, it is also likely that the tooth deflections under load were small as well. If the latter effect dominates, then the noise level would tend to increase with torque.

As Figure 210 shows (for the lowest and highest speed only), the effect of torque on the noise level of the gears tested in this program is mixed. For the baseline spur gears (shown in Figure 210 as 0-degree helix angle), the noise level appears to remain about constant with torque. The helical gears, however, exhibit a slightly more varied behavior. At the low-speed condition (3,000 rpm) the noise level increases as the torque increases, while at the high-speed condition (5,000 rpm) the opposite appears to be true. In both cases, the overall effects are not dramatic.

Speed Effect - For all gears tested, increasing speed increased the noise level. Figure 211 shows the general trend for the helical gears and the baseline spurs. It is interesting to note that the rise in noise level occurs at an increasing rate as the speed climbs. That is, the difference in noise level going from 4,000 to 5,000 rpm is generally more than twice that which occurs from 3,000 to 4,000 rpm. This suggests a nonlinear effect of whatever tooth errors are present. Before drawing this firm conclusion, however, other possibilities must be considered. For example, the test gearbox has exhibited a response of its own at about 5,000 rpm; thus the increase in noise level at this speed may be attributable (at least in part) to the housing response as well as to the gears themselves.

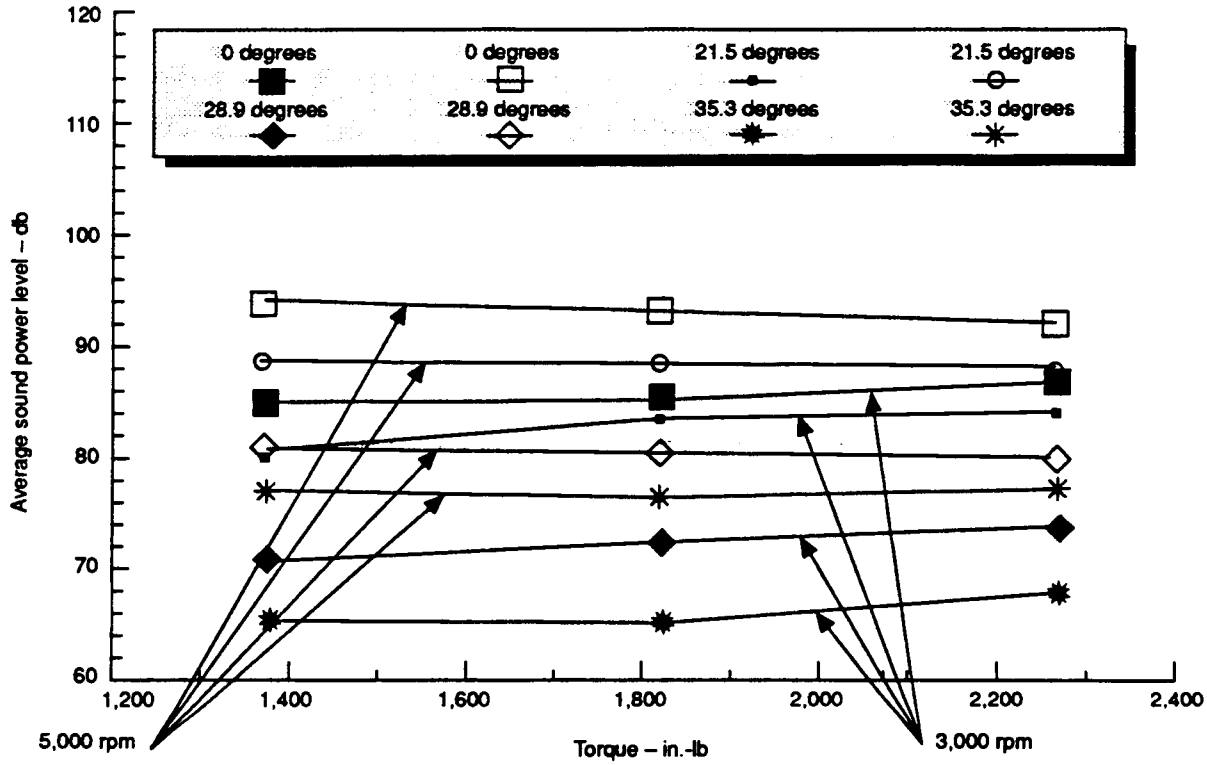

Figure 210. Effect of Torque on Noise Level of Gears

22432 (11)

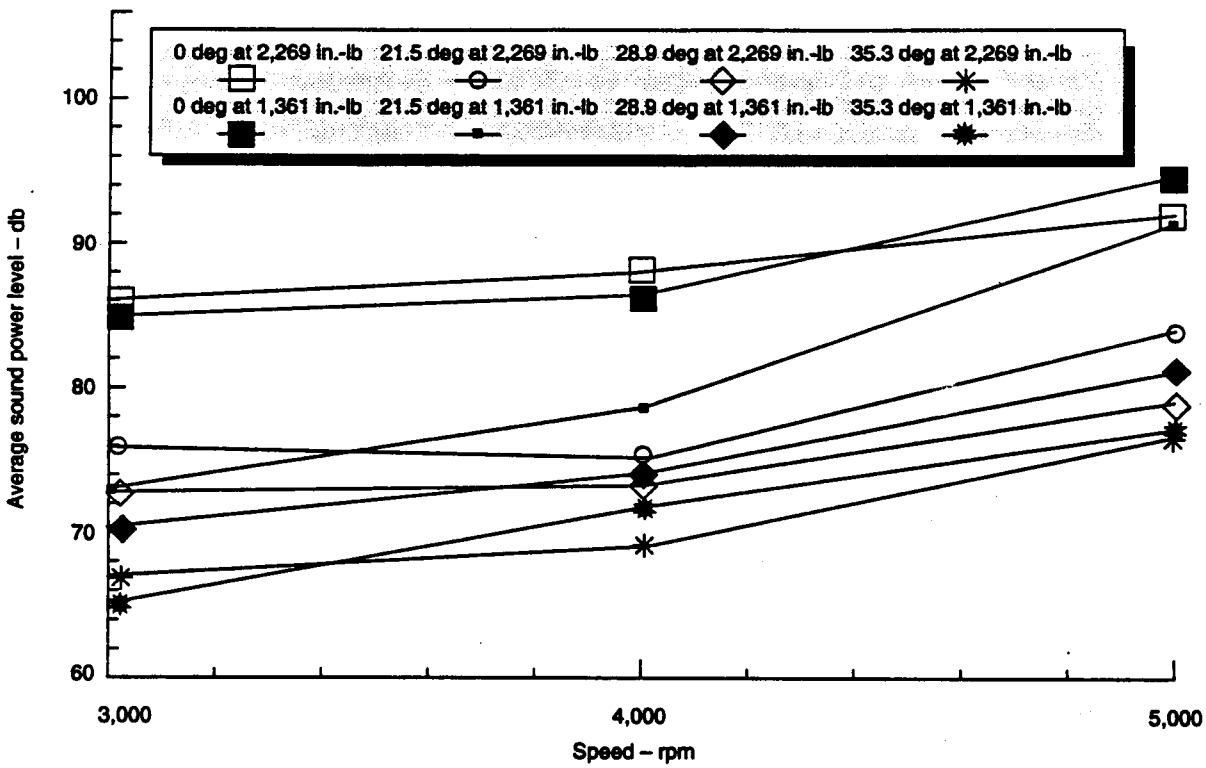

Figure 211. Combined Effects of Speed and Torque on Gear Noise

22432 (12)

Face Contact Ratio Effect - While noise variations which can be attributed to speed and load are certainly of interest, these factors are not gear design parameters over which the design engineer has substantial control. Conversely, contact ratio, which is a function of the basic tooth design, is a well-defined parameter over which the gear design engineer has a great deal of control, once the prerequisite stress requirements are met, of course.

Essentially four different helix angles were tested (0, 21.5, 28.9, and 35.3 degrees). These configurations produced gears with face contact ratios ranging from 0.0 to 2.25 and modified contact ratios ranging from 1.25 to 3.11. In all cases tested, as the contact ratio increased, the noise level decreased. As Figures 212 and 213 show, the noise reduction appears to be almost a linear function of the face contact ratio, regardless of the applied loading. Similar effects can be seen if the noise level is plotted as a function of either modified, Figure 214, or total, Figure 215, contact ratios. However, these latter figures do not show quite the linearity that Figures 212 and 213 do.

Of all of the effects investigated, it appears that the contact ratio is the most significant if all other effects are held reasonably constant. This is important in a design-for-minimum-noise situation since the contact ratio is one of the parameters that the gear designer can control without drastically affecting the overall configuration of the gear system. That is, by judiciously selecting the tooth proportions, helix angle, and face width, it is often possible to optimize the contact ratio to yield a minimum-noise design.

Tooth Form - In general, the noninvolute tooth form, whether standard (configuration 7) or high profile contact ratio (configuration 8), resulted in slightly higher noise levels at virtually all speed and load conditions tested than the equivalent involute (configurations 1 and 2, respectively). The differences, as Figure 216 shows, in some cases were about the same order of magnitude as those due to the build effect described earlier. This being the case, it is hard to ascribe a specific figure to the difference in noise level other than to note the trend.

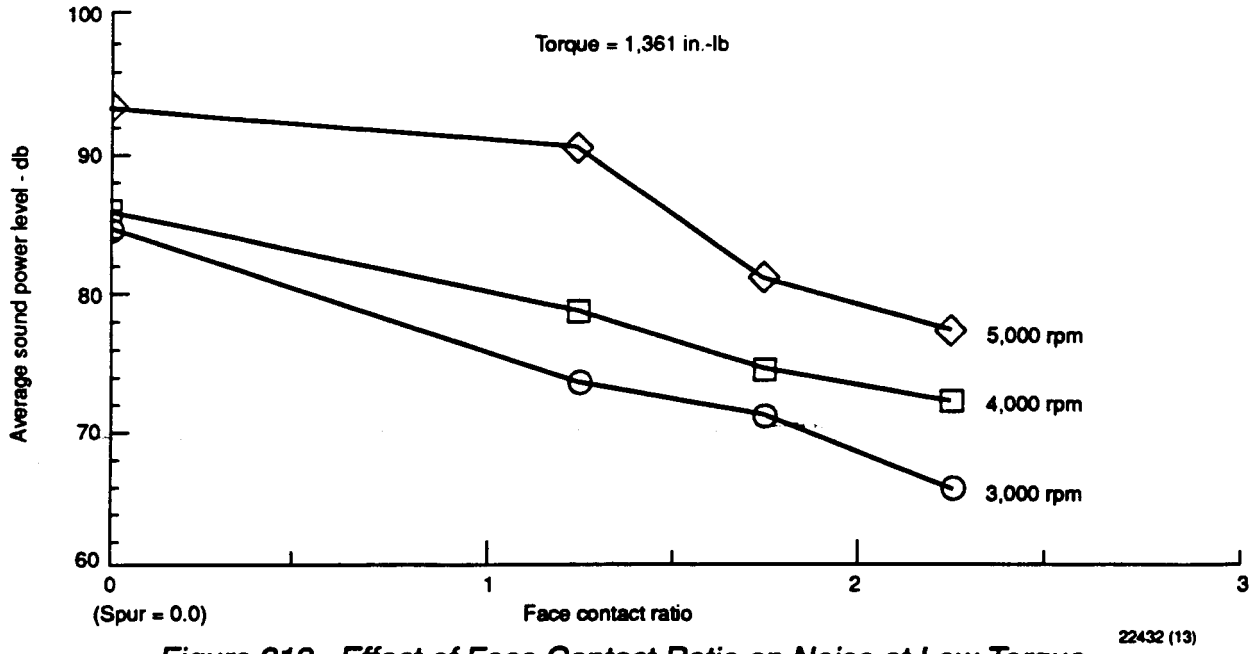

Figure 212. Effect of Face Contact Ratio on Noise at Low Torque

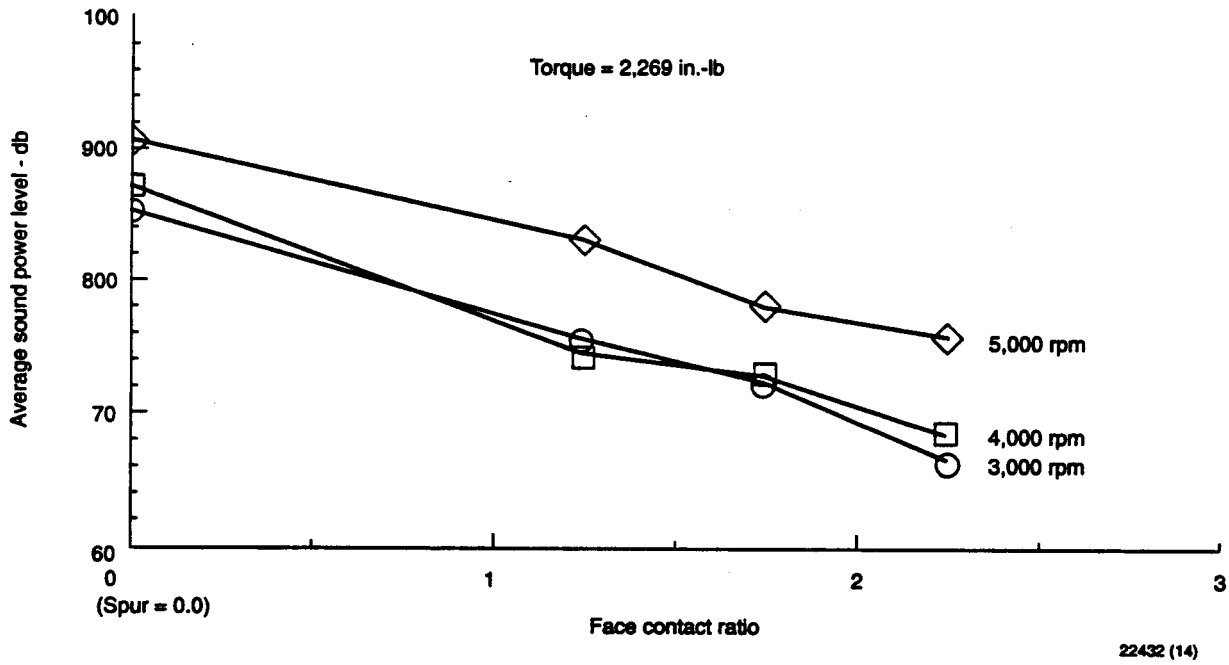

Figure 213. Effect of Face Contact Ratio on Noise at High Torque

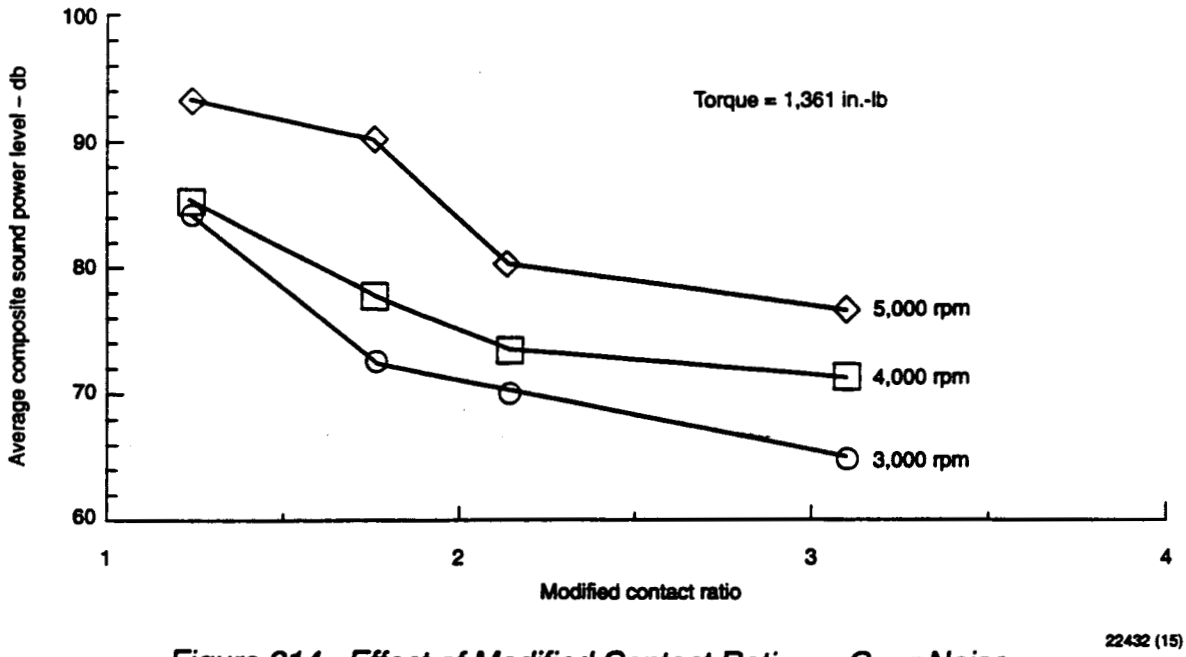

Figure 214. Effect of Modified Contact Ratio on Gear Noise

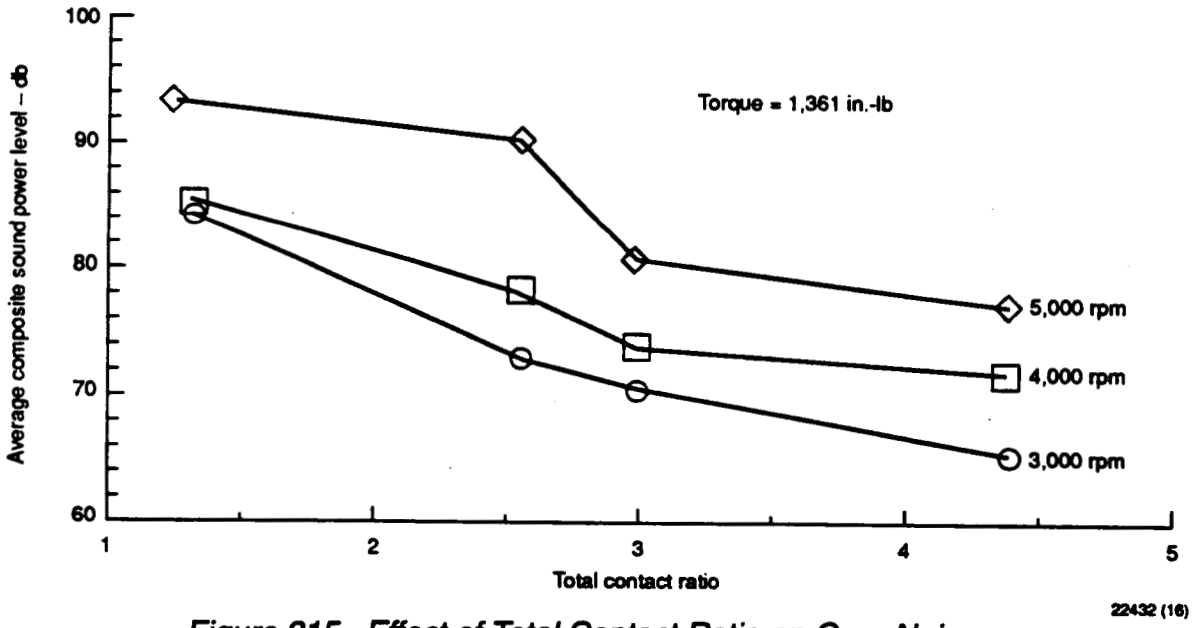

Figure 215. Effect of Total Contact Ratio on Gear Noise

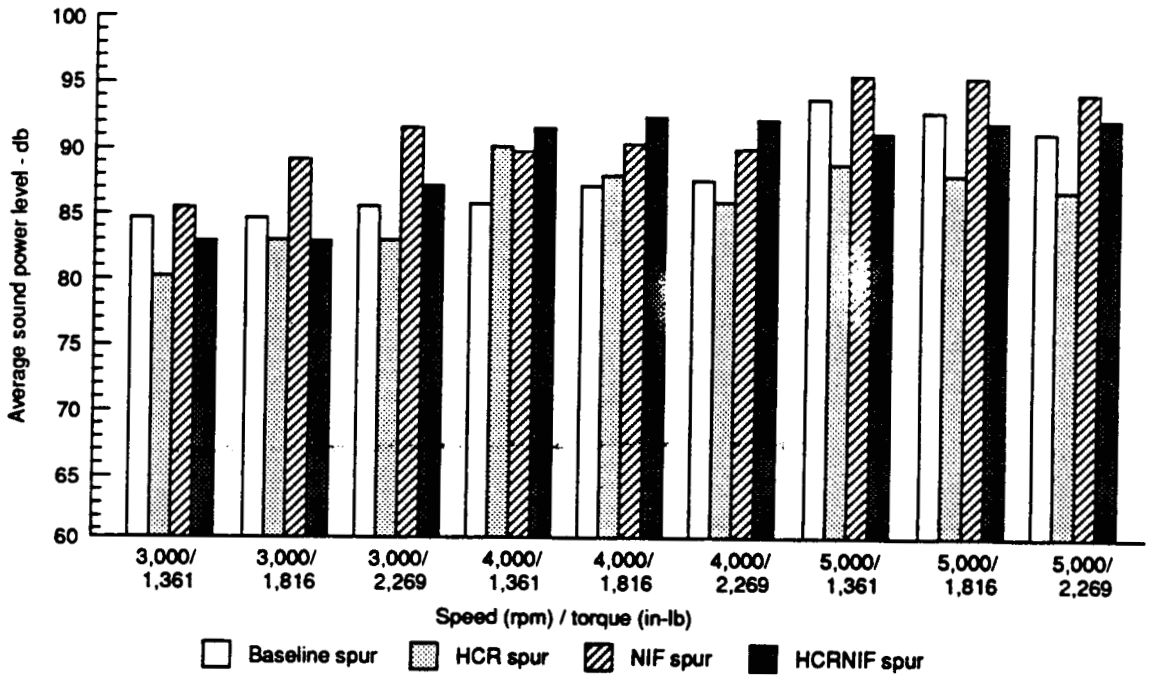

Figure 216. Effect of Tooth Form on Gear Noise

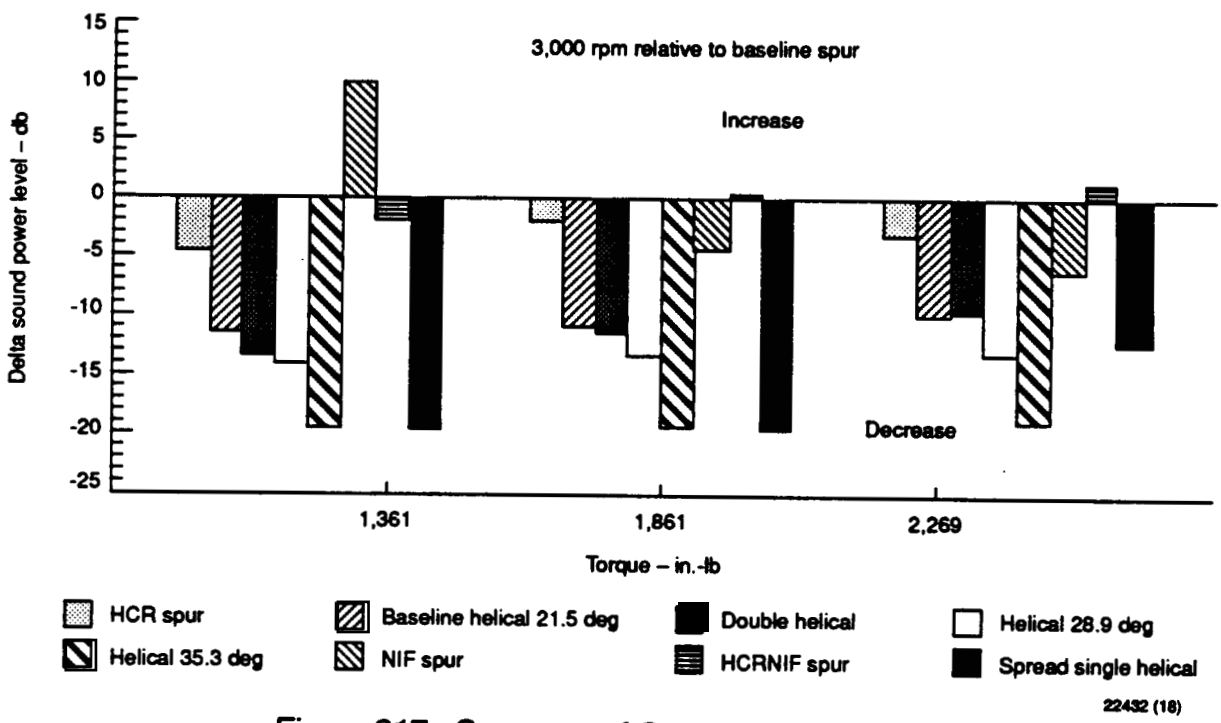

Figure 217. Summary of Gear Noise at 3,000 rpm

While the difference between standard and high profile contact ratio spur gears is not really a tooth form variation in the strictest sense of the concept, it is often referred to as such. Based on the testing conducted herein, the high profile contact ratio gear sets (configurations 2 and 8) produce less noise than their standard contact ratio counterparts (configurations 1 and 7, respectively). This effect was especially pronounced at the lower speed end of the test range but there were some exceptions, especially at the 4,000-rpm condition. Still, since high profile contact ratio does not cause any additional loading on the system (as would a helical gear), it is a viable and possibly preferable option in many cases.

Conclusions

The results of this program, summarized in the bar charts of Figures 217, 218, and 219, have provided significant insight into the effects of various tooth design parameters on the noise level of a geared system. While a wide range of specific conclusions can be drawn from the data, perhaps the most significant are:

1. The contact ratio (whatever the measure) is the most significant factor within the gear design engineer's control with respect to noise reduction.

2. The noninvolute tooth form did not offer any substantial improvement in noise level.

3. High profile contact ratio spur gears are quieter than standard profile contact ratio gears, regardless of tooth form.

4. Applied loading has a relatively small effect on noise level if the basic stress levels are low. This is probably not true for very highly loaded gear teeth, especially when the effect of profile modification is considered.

5. Increasing the speed raises the noise level of the gears tested.

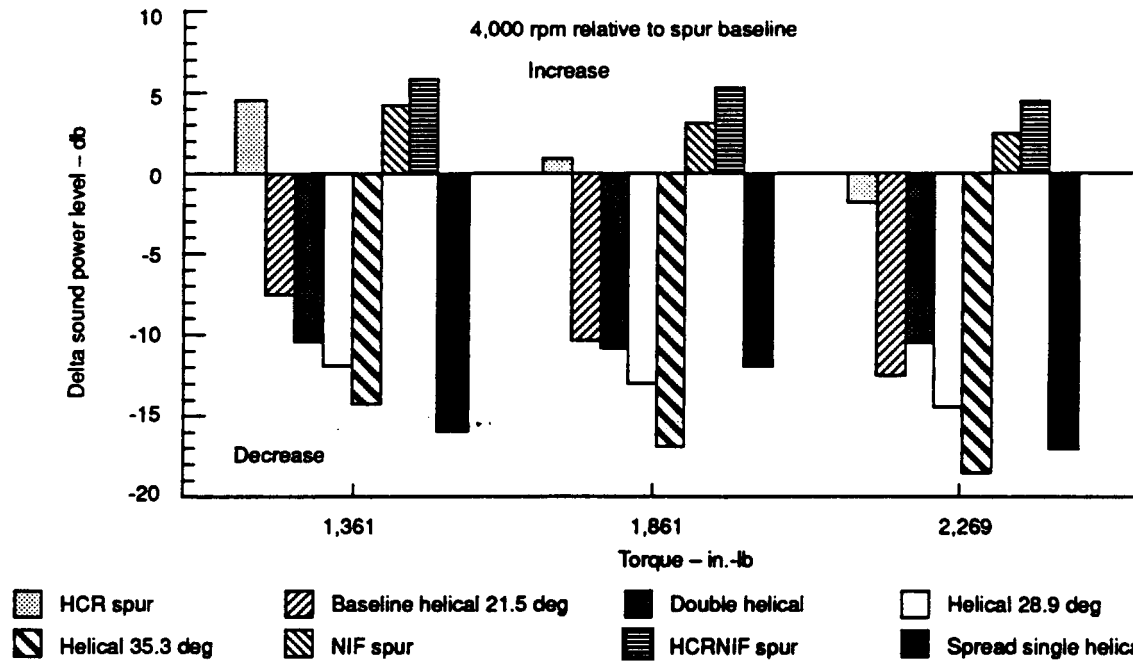

Figure 218. Summary of Gear Noise at 4,000 rpm

22432 (19)

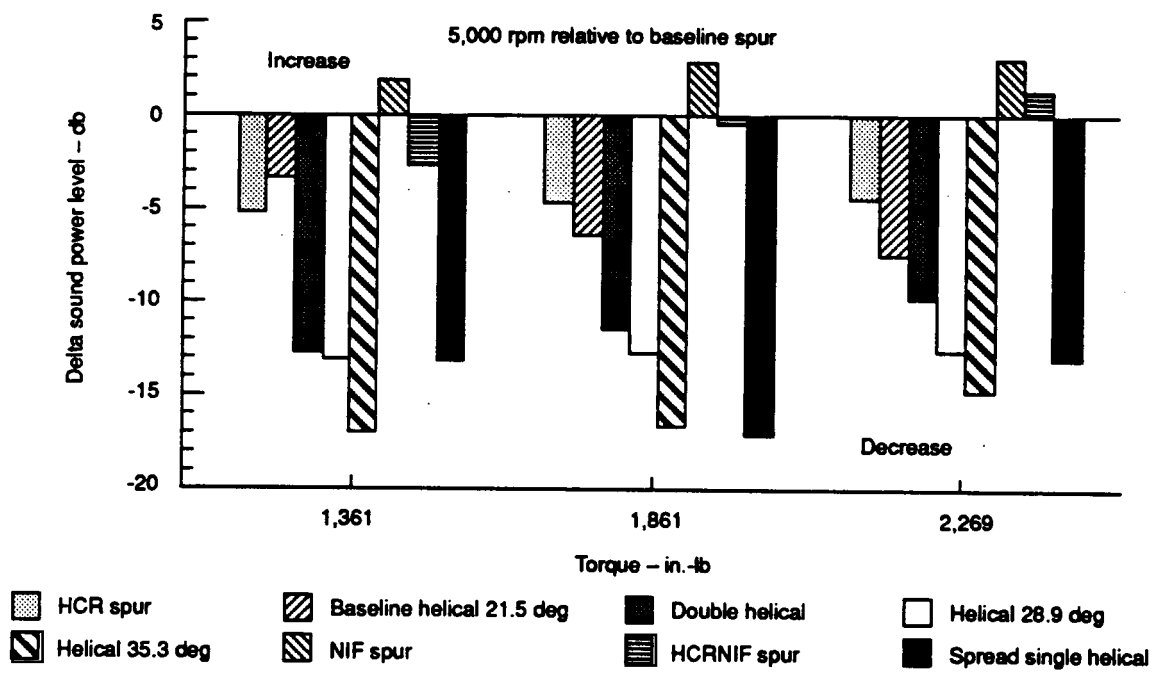

22432 (20)

Figure 219. Summary of Gear Noise at 5,000 rpm

CONCLUSIONS

The work conducted by Boeing under the Advanced Rotorcraft Transmission (A.R.T.) technology integration and demonstration program has advanced the state of the art for future rotorcraft drive systems. The design and trade studies and component tests conducted under this program have provided much needed technology to keep pace with the design goals of future ACA and FAAV aircraft drive systems. Significant reductions in drive system weight, noise, acquisition cost, and direct operating cost have been demonstrated, along with increases in component life and system MTBR. Some of the goals achieved are as follows:

- Transmission weight reduction of 25 percent. The TTR transmission was reduced from the baseline weight of 1,802 pounds to the A.R.T. weight of 1,359 pounds.

- Aircraft gross weight reduced by 6 percent. The impact of A.R.T. weight improvement resulted in a reduction of aircraft gross weight from 17,170 pounds to 16,224 pounds.

- Noise reduction in excess of 10 percent. Significant reductions in noise by both active noise cancellation and gear tooth form changes will range from 10 to 20 db.

- MTBR increased to over 5,000 hours. Incorporation of improved gear and bearing designs will result in a more than twofold increase in the MTBR from the baseline established for this program.

- Acquisition cost reduced by 4 percent. A.R.T. drive system cost has been decreased by 14 percent. This represents a reduction in flyaway cost of 4 percent or a total savings of $150 million for a 600-aircraft production run.

- Direct operating cost reduced by 27 percent. The result of a higher MTBR can reduce the operating cost of an A.R.T. aircraft by 27 percent over its lifetime. This will result in a $153 million savings for a 600-aircraft fleet.

- Overall cost savings due to A.R.T. is $303 million. The potential cost savings due to A.R.T. is approximately $303 million for a fleet of 600 TTR aircraft. This is a significant payback on the cost of the A.R.T. technology program.

Design studies completed by Boeing of a TTR drive system indicated that all of the A.R.T. goals of 25-percent weight reduction, 10-db noise reduction, and 5,000-hour MTBR can be achieved through the use of novel design concepts and advanced-technology materials and components. Eight material and component tests conducted under this program provided the confidence that these high-risk developments would meet the requirements of the A.R.T. program. The most successful tests completed were the following:

- Hybrid bearings (decreased weight by 22 percent and longer life)
- Bidirectional tapered-roller bearings (hybrid and standard design reduced bearing count by a factor of 2)
- Precision net-forged spur gears (increased capacity by approximately 3 percent and lower cost by 10 to 15 percent)
- Improved methodology for predicting bearing life (longer life and higher reliability to achieve the 5,000-hour MTBR)
- High profile contact ratio, noninvolute tooth form spur gears (higher capacity by 8 percent and lower noise by 20 db)
- Noise reduction by active force cancellation (structural noise reduced in the range of 2 to 11 db)
- Noise reduction by control of gear contact ratios and tooth forms (noise reduction as high as 20 db).

Some of these components have been considered for use in aircraft drive systems now under development. The bidirectional tapered-roller bearing design has been incorporated into the RAH-66 Fantail transmission and will soon be in full-scale development testing. While other components were also considered, additional risk-reduction testing was required before their use. Many more components will find their way into the next generation of aircraft drive system designs.

The only component test that did not meet expected design objectives was that of the surface-modified titanium accessory spur gears. Although the load capacity of these gears was not achieved (values of less than 10 percent of standard steel gears were attained), significant understanding of the operating characteristics of titanium gears was obtained, and this could lead to future work in this area to achieve better performance of titanium gears in rotorcraft transmissions.

With the early component development testing completed under the A.R.T. program, work must continue toward the total integration of all of these components into a future rotorcraft drive system. This type of testing will determine the true impact of the A.R.T. program on future ACA, FAAV, and short-haul civil tiltrotor aircraft design and performance.

RECOMMENDATIONS

Significant progress was made under Phase I of the Advanced Rotorcraft Transmission (A.R.T.) program; however, much work still remains to fully integrate the various technologies developed. The material evaluations and component tests completed and reported here provide only the confidence of achieving success in future applications. It is recommended that the technologies developed under this program be incorporated into a full-scale rotorcraft transmission system and tested. Phase II of the Advanced Rotorcraft Transmission program is very critical to having a fully developed system ready for the next generation of aircraft.

The continued development and testing of a full-scale transmission system would permit a direct comparison of the performance, interaction, and life of these technologies. This testing would provide additional confidence and verification of the advanced concepts before their incorporation into future ACA and FAAV rotorcraft transmission systems.

The many advantages of reduced weight, decreased noise, and increased life accrued from the component development tests are evident in the achievements of this program. This work must be continued in order to have these components fully matured for next-generation rotorcraft. Results to date indicate that the continuation of this work will provide significant and cost-effective results.

LITERATURE CITED

1. Schmidt, Arling H., A METHOD FOR ESTIMATING THE WEIGHT OF AIRCRAFT TRANSMISSIONS, SAWE paper 1120, index category 25, presented at 35th Annual Conference, Philadelphia, PA, Society of Allied Weight Engineers, Inc, PO Box 60024, Terminal Annex, Los Angeles, CA, 90060, May 1976.
2. REQUIREMENTS FOR TESTS AND RECORDS OF PROCESS-SENSITIVE PARTS, Boeing document D210-11000-1, Boeing Defense & Space Group, Helicopters Division, PO Box 16858, Philadelphia, PA, 19142-0858, July 1976.
3. CONTROL REQUIREMENTS FOR CRITICAL BEARINGS, Boeing document D210-10302-1, Boeing Defense & Space Group, Helicopters Division, PO Box 16858, Philadelphia, PA, 19142-0858, March 1972.
4. BOEING MATERIAL SPECIFICATION, CONSUMABLE-ELECTRODE VACUUM ARC STEEL BILLETS, BARS, AND FORGINGS, BMS 7-223C, Boeing Defense & Space Group, Helicopters Division, PO Box 16858, Philadelphia, PA, 19142-0858, January 1979.
5. Roark, Raymond J., and Young, Warren C., FORMULAS FOR STRESS AND STRAIN, McGraw-Hill Book Company, McGraw-Hill, Inc, New York, NY, 1982.
6. Faust, Howard, INTEGRAL COMPOSITE SHAFT/COUPLING PROGRAM, Boeing document D210-12871-1; USAAVSCOM TR91-D-11, Aviation Applied Technology Directorate, U.S. Army Aviation Systems Command, Fort Eustis, VA, 23604-5577, contract DAAJ02-87-C-0005, March 1992.
7. Sciarra, J. J., Howells, R. W., Lenski, J. W., Drago, R. J., and Schaffer, E. G., HELICOPTER TRANSMISSION VIBRATION AND NOISE REDUCTION PROGRAM, USARTL-TR-78-2A, 1978.
8. Nelson, P. A., and Elliot, S. J., ACTIVE MINIMIZATION OF ACOUSTIC FIELDS, Journal of Theoretical and Applied Mechanics, 0750-7240/87/39/60, supplement to Vol. 6, 1987.

9. Jones, J. D., and Fuller, C. R., ACTIVE CONTROL OF SOUND FIELDS BY VIBRATIONAL INPUTS, Proceedings of Noise-Con 87, pp. 413-418, 1987.

10. Hansen, C. H., and Snyder, S. D., EFFECT OF GEOMETRIC AND STRUCTURAL/ACOUSTIC VARIABLES ON THE ACTIVE CONTROL OF SOUND RADIATION FROM A VIBRATING SURFACE, Recent Advances in Active Control of Sound and Vibration, VPI 1991, pp. 487-506, Technomic Publishing Co, Inc, 1991.

11. Widrow, B., and Stearns, S. D., ADAPTIVE SIGNAL PROCESSING, Prentice Hall Inc, Englewood Cliffs, NJ, 1985.

12. Chaplin, G. B. B., ANTI-SOUND - THE ESSEX BREAKTHROUGH, Chartered Mechanical Engineer, (CME)30(Jan 1983), pp. 41-47.

13. Ioannides, E., and Harris, T. A., A NEW FATIGUE LIFE MODEL FOR ROLLING BEARINGS, ASME Journal of Tribology, Vol. 107, 1985, pp. 367-378.

14. Andersson, T., ENDURANCE TESTING - THEORY, Ball Bearing Journal, No. 217 (Aktiebolaget SKF), 1983, pp. 14-23.

15. Sayles, R. S., and Macpherson, P. B., INFLUENCE OF WEAR DEBRIS ON ROLLING CONTACT FATIGUE, Rolling Contact Fatigue Testing of Bearing Steels, ASTM STP 771, J. J. C. Hoo, Editor, American Society for Testing and Materials, 1982.

16. Smith, J. O., and Liu, C. K., STRESSES DUE TO TANGENTIAL AND NORMAL LOADS ON AN ELASTIC SOLID WITH APPLICATION TO SOME CONTACT STRESS PROBLEMS, ASME paper 52-A-13, ASME Annual Meeting, December 1952.

17. Roark, R. J., and Young, W. C., FORMULAS FOR STRESS AND STRAIN, Fifth Edition, 1975, p. 567.

18. Seely, F. B., and Smith, J. O., ADVANCED MECHANICS OF MATERIALS, Second Edition, 1952, pp. 321-327.

19. Seely, F. B., and Smith, J. O., ADVANCED MECHANICS OF MATERIALS, Second Edition, 1952, pp. 368-376.

20. Broszeit, E., and Zwirlein, O., INTERNAL STRESSES AND THEIR INFLUENCE ON MATERIAL STRESSES IN HERTZIAN CONTACTS - CALCULATIONS WITH DIFFERENT STRESS HYPOTHESES, ASME paper 85-TRIB-28, ASME/ASLE Joint Lubrication Conference, Atlanta, GA, October 1985.

21. Ioannides, E., Harris, T. A., and Ragen, M. A., ENDURANCE OF AIRCRAFT GAS TURBINE MAINSHAFT BALL BEARINGS - ANALYSIS USING IMPROVED FATIGUE LIFE THEORY; PART 1 - APPLICATION TO A LONG LIFE BEARING, STLE-ASME Tribology Conference, October 1989.

22. Harris, T. A., Ioannides, E., Ragen, M.A., and Tam, H. O., ENDURANCE OF AIRCRAFT GAS TURBINE MAINSHAFT BALL BEARINGS - ANALYSIS USING IMPROVED FATIGUE LIFE THEORY; PART 2 - APPLICATION TO A BEARING OPERATING UNDER DIFFICULT LUBRICATION CONDITIONS, STLE-ASME Tribology Conference, October 1989.

23. Johnson, K. L., CONTACT MECHANICS, Cambridge University Press, 1985.

24. Tevaarwerk, J. L., ROLLING, SLIP AND ENDURANCE TRACTION MEASUREMENTS ON LOW MODULUS MATERIALS, NASA CR 174909, July 1985.

25. Kannel, J. W., and Merriman, T. L., IN EFFECT OF SOLID FILM LUBRICANTS ON THE STABILITY OF ROLLING ELEMENT BEARINGS, ASME paper 86-TRIB-61, 1986.

26. Pallini, R. A., and Wedeven, L. D., TRACTION CHARACTERISTICS OF GRAPHITE LUBRICANTS AT HIGH TEMPERATURE, 42nd Annual Meeting of the ASLE, Anaheim, CA, May 1987.

27. Tevaarwerk, J. L., CONSTITUTIVE MODELLING OF LUBRICANTS IN CONCENTRATED CONTACTS AT HIGH SLIDE TO ROLL RATIO, NASA CR 175029, December 1985, Appendix I, pp. 1-4.

28. McCool, J. I., TRACTION MODEL DEVELOPMENT, AFWAL-TR-87-4079, September 1987, pp. 122-123.

29. Townsend, Dennis P., Baber, Berl B., and Nagy, Andrew. EVALUATION OF HIGH-CONTACT-RATIO SPUR GEARS WITH PROFILE MODIFICATION. NASA TP-1458, September 1979.

30. Oswald, Fred B., Zakrajsek, James J., Atherton, William, and Lin Hsiang Hsi, EFFECT OF OPERATING CONDITIONS ON GEARBOX NOISE, NASA TM 105331, Sixth International Power Transmission and Gearing Conference, American Society of Mechanical Engineers, Phoenix, AZ, September 1992.

31. Atherton, William J., Pintz, Adam, and Lewicki, David G., AUTOMATED ACOUSTIC INTENSITY MEASUREMENTS AND THE EFFECT OF GEAR TOOTH PROFILE ON NOISE, Mechanical Signature Analysis--Machinery Vibration, Flow-Induced Vibration, and Acoustic Noise Analysis, S. Braun et al., editors, ASME, pp. 109-113 (NASA TM 100155), 1987.

32. Flanagan, P.M., and Atherton, W.J., INVESTIGATION ON EXPERIMENTAL TECHNIQUES TO DETECT, LOCATE AND QUANTIFY GEAR NOISE IN HELICOPTER TRANSMISSIONS, NASA CR 3847, 1985.

APPENDIX A

ENGINEERING DRAWINGS OF THE BOEING ADVANCED ROTORCRAFT TRANSMISSION

SK2137

QTY REQD	FIND NO	PART OR IDENTIFYING NUMBER	NOMENCLATURE OR DESCRIPTION	ZONE	MATERIAL AND SPECIFICATION
6		SK2137-239	MOUNT, WING SHAFT	[illegible]	(SIMILAR TO 2840[illegible])
16		SK2137-238	BRACKET, MOUNT	[illegible]	
4		SK2137-237	LOCKNUT	[illegible]	(TITANIUM)
4		SK2137-236	SUPPORT, BRG	[illegible]	(COMPOSITE)
4		SK2137-235	RETAINER, BRG	[illegible]	(COMPOSITE)
4		SK2137-234	BALL BRG, WING SHAFT	[illegible]	MRC #1914
4		SK2137-233	ADAPTER, WING SHAFT	[illegible]	(TITANIUM)
8		SK2137-232	WING SHAFT	[illegible]	(4 SHAFTS WITH 1 [illegible] & 1 BRG SUPPORT) (1 SHAFT WITH 2 COUPLINGS)
1		SK2137-231	ADAPTER, TAGB/WING SHAFT	[illegible]	
1		SK2137-230	TRANSFER TUBE, GENERATOR SCAVENGE	[illegible]	
1		SK2137-229	HOSE ASSY GENERATOR SUPPLY	[illegible]	680138-60
3		SK2137-228	O-RING	[illegible]	MS29513/1-906
8		SK2137-227	UNION	[illegible]	MS21902-4
1		SK2137-226	HOSE ASSY SCAVENGE FROM TAGB	[illegible]	480137-60
1		SK2137-225	HOSE ASSY SCAVENGE FROM TAGB	[illegible]	680137-60
4		SK2137-224	UNION	[illegible]	MS21902-6
1		SK2137-223	UNION	[illegible]	MS21902-4
1		SK2137-222	HOSE ASSY AUX LUBE TO TAGB	[illegible]	630137-40
1		SK2137-221	HOSE ASSY COOLER TO ROTOR BOX	[illegible]	680132-140
2		SK2137-220	UNION	[illegible]	MS21902-16
1		SK2137-219	HOSE ASSY ROTOR BOX TO COOLER	[illegible]	680138-140
1		SK2137-218	STRUT, TAGB	[illegible]	
1		SK2137-217	BOX BEAM STRUCTURE	[illegible]	
1		SK2137-216	BREATHER, TAGB	[illegible]	
1		SK2137-215	PLUG	[illegible]	
1		SK2137-214	STRUT, ENGINE	[illegible]	
8		SK2137-213	STRUT, ENGINE	[illegible]	
1		SK2137-212	O-RING	[illegible]	MS29513/1-[illegible]
1		SK2137-211	ADAPTER, IGDS	[illegible]	
1		SK2137-210	SHAFT, INTEGRAL COUPLING	[illegible]	GLASS/GRAPHITE COMPOSITE
1		SK2137-209	TRANSFER TUBE	[illegible]	
4		SK2137-208	O-RING	[illegible]	MS29513/1-109
2		SK2137-207	TRANSFER TUBE	[illegible]	
1		SK2137-206	FAN	[illegible]	
1		SK2137-205	BAFFLE	[illegible]	
1		SK2137-204	COOLER	[illegible]	
1		SK2137-203	QUILL SHAFT, FAN	[illegible]	
2		SK2137-202	ADAPTER, FAN SHAFT	[illegible]	
1		SK2137-201	RETAINING RING	[illegible]	RR-162
1		SK2137-200	O-RING	[illegible]	MS29513/1-[illegible]
1		SK2137-199	SEAL	[illegible]	CR #7[illegible]
1		SK2137-198	SEAL COVER	[illegible]	
1		SK2137-197	BALL BEARING	[illegible]	MRC 7100-4R
1		SK2137-196	QUILL SHAFT, TAGB	[illegible]	
1		SK2137-195	ADAPT. TAGB QUILLSHAFT	[illegible]	
1		SK2137-194	O-RING	[illegible]	MS29513/1-[illegible]
1		SK2137-193	CARTRIDGE, GEAR	[illegible]	
1		SK2137-192	TAPERED ROLLER BRG	[illegible]	TIMKEN [illegible] (BI-DIRECTIONAL)
1		SK2137-191	SHIM, GEAR CARTRIDGE	[illegible]	
1		SK2137-190	DAMPING RING	[illegible]	
1		SK2137-189	SPIRAL BEVEL GEAR	[illegible]	
1		SK2137-188	STRAINER	[illegible]	
1		SK2137-187	LUBRICATOR, TAGB	[illegible]	
1		SK2137-186	HOUSING, TAGB	[illegible]	
1		SK2137-185	SHIM, PINION CARTRIDGE	[illegible]	
1		SK2137-184	O-RING	[illegible]	MS29513/1-[illegible]
1		SK2137-183	PINION CARTRIDGE	[illegible]	
2		SK2137-182	O-RING	[illegible]	MS29513/1-045
2		SK2137-181	SEAL COVER	[illegible]	
6		SK2137-180	RETAINING RING	[illegible]	RR-312
2		SK2137-179	O-RING	[illegible]	MS29513/1-[illegible]
3		SK2137-178	SEAL	[illegible]	CR [illegible]
3		SK2137-177	RETAINING RING	[illegible]	RR-[illegible]

QTY REQD	FIND NO	PART OR IDENTIFYING NUMBER
2		SK2137-176
8		SK2137-175
1		SK2137-174
8		SK2137-173
1		SK2137-172
1		SK2137-171
8		SK2137-170
2		SK2137-169
8		SK2137-168
1		SK2137-167
1		SK2137-166
10		SK2137-165
4		SK2137-164
8		SK2137-163
1		SK2137-162
1		SK2137-161
4		SK2137-160
1		SK2137-159
1		SK2137-158
1		SK2137-157
1		SK2137-156
1		SK2137-155
1		SK2137-154
1		SK2137-153
1		SK2137-152
2		SK2137-151
1		SK2137-150
1		SK2137-149
1		SK2137-148
1		SK2137-147
1		SK2137-146
1		SK2137-145
1		SK2137-144
1		SK2137-143
1		SK2137-142
8		SK2137-141
8		SK2137-140
8		SK2137-139
2		SK2137-138
2		SK2137-137
4		SK2137-136
1		SK2137-135
8		SK2137-134
1		SK2137-133
1		SK2137-132
1		SK2137-131
1		SK2137-130
1		SK2137-129
1		SK2137-128
1		SK2137-127
3		SK2137-126
1		SK2137-125
1		SK2137-124
1		SK2137-123
1		SK2137-122
1		SK2137-121
2		SK2137-120
1		SK2137-119
1		SK2137-118
8		SK2137-117
3		SK2137-116
3		SK2137-115
3		SK2137-114

PARTS LIST

A-3

LAST FILE = 98089 DATE = 11/18/93 TIME = 10.07 SCALE = 0.3076 USER = INPROC DRAWID = SK2137 00
SK2137 00 -0101
SK2137 00 -0102
1270 J 003
241.3-01.2.M4.X3863

TANSHANKER										
LOCKNUT		(2 67 PO)								
TAPERED ROLLER BRG		TIMKEN HR30 (BI-DIRECTIONAL) WITH ADDED LUBE FEATURE								
ROLLER BEARING		RBC HR-206 (EXTRA WIDE ROLLER)								
DAMPING RING		BR-660								
SPIRAL BEVEL PINION										
LOCK SPRING										
RETAINER										
O-RING		MS3646/1-134								
ADAPTER,TAND										
LUBRICATOR,PLANETARY										
O-RING		MS3646/1-113								
TRANSFER TUBE,LUBE										
LUBRICATOR,ROLL/PUMP & BULL/OIL PUMP										
LUBRICATOR,BULL/IDLER & BULL/TCDS GEAR										
LUBRICATOR,BULL/TCDS										
O-RING		MS3646/1-916								
JAM NUT		AN924-16								
ELBOW,BULKHEAD		MS21900-16								
MOUNT,EMS STRUT										
LUBRICATOR,JACK/BULL										
O-RING		MS3646/1-227								
STRAINER,AUX. SUMP										
LUBRICATOR,JACK/BULL										
STRAINER,MAIN SUMP										
O-RING		MS3646/1-904								
JAM NUT		AN924-4								
ELBOW,BULKHEAD		MS21900-4								
O-RING		MS3646/1-984								
FILTER, AUXILIARY		(SIMILAR TO 14B08833-8)								
ROLLER BEARING		RBC HR-806								
DAMPING RING										
GEAR, AUX. PUMP										
LUBE PUMP,AUXILIARY		(SIMILAR TO 14B08819-3)								
ROLLER BEARING		RBC HR-108								
RETAINING RING		BR-178								
TANSHANKER										
LOCKNUT		(1.3125 PO)								
TAPERED ROLLER BRG		TIMKEN LA6140 (BI-DIRECTIONAL)								
O-RING		MS3646/1-144								
O-RING		MS3246/1-148								
LUBE PUMP,MAIN		(SIMILAR TO 14B08819-8)								
O-RING		MS3646/1-182								
GASKET										
FILTER, MAIN		(SIMILAR TO 14B08814-7)								
FILTER HOUSING		(SIMILAR TO 14B08814-3)								
ROLLER BEARING		RBC R-148K								
DAMPING RING										
GEAR, IDLER										
RETAINING RING		BR-280								
O-RING		MS3646/1-144								
SEAL		CR 816128								
DAMPING RING										
GEAR,HYD/LUBE PUMP										
HYDRAULIC PUMP		VICKERS PVB-16A-9 (DWG. 9434495)								
RETAINING RING		BR-289								
O-RING		MS3646/1-141								
SEAL		CR 814880								
ROLLER BEARING		RBC HR-1997								
LUBRICATOR,GEN,IDLER										
RETAINING RING		BR-190								
TANSHANKER										
LOCKNUT		(1.00 PO)								
NOMENCLATURE OR DESCRIPTION		MATERIAL AND SPECIFICATION								

			2		SK32137-113	TAPERED ROLLER BRG		TIMKEN		
			1		SK32137-112	DAMPING RING				
			1		SK32137-111	GEAR,GENERATOR				
			1		SK32137-110	O-RING		MS3646		
			1		SK32137-109	GENERATOR		LUCAS		
			6		SK32137-108	O-RING		MS3646		
			1		SK32137-107	FILLER BREATHER CAP				
			1		SK32137-106	ARM,TAND STRUT				
			8		SK32137-105	MOUNT,EMS STRUT				
			2		SK32137-104	O-RING		MS3246		
			1		SK32137-103	STRAINER,JACKSHAFT SUM				
			1		SK32137-102	LUBRICATOR,PUM/JACK				
			1		SK32137-101	LUBRICATOR,PUM/JACK				
			9		SK32137-100	O-RING				
			9		SK32137-99	DEBRIS DETECTOR				
			1		SK32137-98	LUBRICATOR,GEN/JACK				
			1		SK32137-97	HOUSING,UPPER				
			1		SK32137-96	SPLINED TANSHANKER				
			4		SK32137-95	O-RING		MS3246		
			9		SK32137-94	O-RING		MS3246		
			2		SK32137-93	TRANSFER TUBE,DRAIN				
			9		SK32137-92	O-RING				
			9		SK32137-91	O-RING				
			1		SK32137-90	LUBRICATOR,BULL				
			1		SK32137-89	LUBRICATOR,JACKSHAFT				
			1		SK32137-88	BAFFLE				
			1		SK32137-87	O-RING		MS3246		
			1		SK32137-86	O-RING		MS3246		
			1		SK32137-85	STANDPIPE				
			1		SK32137-84	O-RING				
			1		SK32137-83	SUMP				
			1		SK32137-82	O-RING		MS3246		
			4		SK32137-81	O-RING		MS3246		
			4		SK32137-80	LUBRICATOR,PLANETARY				
			1		SK32137-79	O-RING				
			1		SK32137-78	O-RING		MS3246		
			1		SK32137-77	RETAINING RING		BR-3		
			1		SK32137-76	SEAL		CR 6		
			1		SK32137-75	PLUG				
			1		SK32137-74	ROLLER BEARING		RBC		
			1		SK32137-73	RETAINING RING		BR-8		
			1		SK32137-72	TAND WASHER				
			1		SK32137-71	LOCKNUT, BEARING		(2.1		
			1		SK32137-70	TAPERED ROLLER BRG.		TIMK		
			2		SK32137-69	HELICAL RING GEAR				
			1		SK32137-68	HELICAL GEAR,TCDS				
			4		SK32137-67	PLANET RETAINER				
			1		SK32137-66	CARRIER/OUTPUT SHAFT				
			1		SK32137-65	TAPERED ROLLER BRG		TIMK		
			1		SK32137-64	SHIM				
			1		SK32137-63	TAPERED ROLLER BRG		TIMK		
			1		SK32137-62	O-RING		MS3		
			1		SK32137-61	RETAINING RING		BR-1		
			1		SK32137-60	SEAL		REC		
			1		SK32137-59	O-RING		MS3		
			1		SK32137-58	SEAL COVER				
			1		SK32137-57	COVER				
			4		SK32137-56	O-RING		MS3		
			1		SK32137-55	SPACER, RING GEAR				
			8		SK32137-54	HELICAL RING GEAR				
			4		SK32137-53	HELICAL PLANET GEAR				
			1		SK32137-52	HELICAL SUN GEAR				
			1		SK32137-51	ROLLER BEARING		RBC		
ZONE	ZONE	ZONE	ZONE	ZONE	ZONE NO.	NOMENCLATURE OR DESCRIPTION				

SK32137

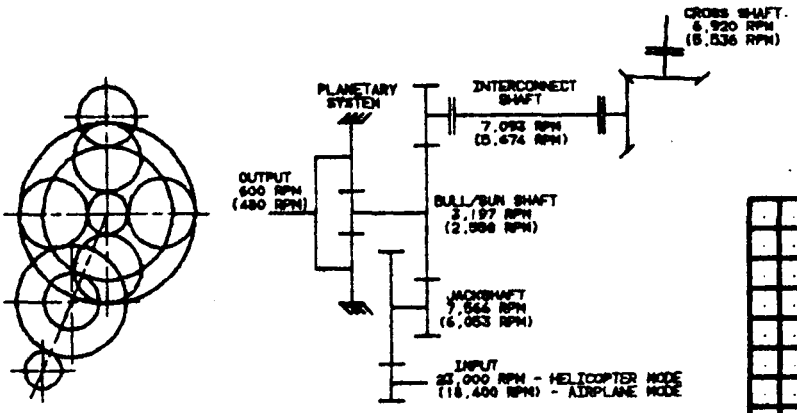

ART MAIN DRIVE TRAIN SCHEMATIC

NOTES

1. BASIC DESIGN SPECIFICATIONS:
   - ENGINE INSTALLED POWER: 2019 Hp
     2777 Hp O.E.I
   - INPUT SPEED: 23,000 RPM (HELICOPTER MODE)
     18,400 RPM (AIRPLANE MODE)
   - POWER SPLIT: 60/40 (60% O.E.I. = 1,667 Hp)
   - OUTPUT SPEED: 600 RPM (HELICOPTER MODE)
     480 RPM (AIRPLANE MODE)
   - OUTPUT TORQUE: 21,396 FT.-LBS.
   - REDUCTION RATIO: 38/1 (TOTAL)
     3.04/1 (INPUT/JACK SHAFT)
     2.37/1 (JACK SHAFT/BULL GEAR)
     5.28/1 (PLANETARY SYSTEM)
2. DESIGN FEATURES:
   - HYBRID BEARINGS (CERAMIC ROLLING ELEMENTS, PEEK CAGES)
   - BI-DIRECTIONAL HYBRID TAPERED ROLLER BEARINGS
   - VASCO X-2 HELICAL DRIVE GEARS
   - SURFACE MODIFIED (ION IMPLANTATION) TITANIUM ACCESSORY GEARS
   - COMPOSITE INTERCONNECT SHAFT WITH INTEGRAL COUPLINGS
   - OVERRUNNING SPRING CLUTCH
   - 5 u NOMINAL/10 u ABSOLUTE OIL FILTRATION

SK32137-69	RETAINING RING	[illegible]	RR-[illegible]							
SK32137-68	TANG WASHER	[illegible]								
SK32137-65	LOCKNUT, BEARING	[illegible]	(4.425 PD)							
SK32137-67	TAPERED ROLLER BRG	[illegible]	TIMKEN HM84700 (BI-DIRECTIONAL)							
SK32137-66	DAMPING RING	[illegible]								
SK32137-65	BULL GEAR,HELICAL	[illegible]								
SK32137-64	ROLLER BEARING	[illegible]	FRC NR-312							
SK32137-63	RETAINING RING	[illegible]	RR-400							
SK32137-62	TANG WASHER	[illegible]								
SK32137-61	LOCKNUT, BEARING	[illegible]	(3.25 PD)							
SK32137-60	TAPERED ROLLER BRG	[illegible]	TIMKEN 3984 (BI-DIRECTIONAL)							
SK32137-59	DAMPING RING	[illegible]								
SK32137-58	INTERMED. GEAR SHAFT	[illegible]								
SK32137-57	O-RING	[illegible]	[illegible]	MS3246/1-[illegible]						
SK32137-56	O-RING	[illegible]	[illegible]	MS3246/1-[illegible]						
SK32137-55	O-RING	[illegible]	[illegible]	MS3246/1-[illegible]						
SK32137-54	LUBRICATOR,PIN/CLUTCH	[illegible]								
SK32137-53	RETAINING RING	[illegible]	RR-385							
SK32137-52	TANG WASHER	[illegible]								
SK32137-51	LOCKNUT, BEARING	[illegible]	(2.56 PD)							
SK32137-50	TAPERED ROLLER BRG	[illegible]	TIMKEN 29690 (BI-DIRECTIONAL)							
SK32137-49	ROLLER BEARING	[illegible]	FRC NR-211							
SK32137-48	HELICAL PINION	[illegible]								
SK32137-47	RETAINING RING	[illegible]	RR-412							
SK32137-46	SEAL	[illegible]	REINCHO CARTRIDEAL 01-3884							
SK32137-45	O-RING	[illegible]	MS3246/1-[illegible]							
SK32137-44	O-RING	[illegible]	MS3246/1-[illegible]							
SK32137-43	CLUTCH CARTRIDGE	[illegible]								
SK32137-42	RETAINING RING	[illegible]	RR-370							
SK32137-41	TAPERED ROLLER BRG	[illegible]	TIMKEN LL310700 (DUPLEX)							
SK32137-40	RETAINING RING	[illegible]	RR-300							
SK32137-39	TANG WASHER	[illegible]								
SK32137-38	LOCKNUT, BEARING	[illegible]	(2.37 PD)							
SK32137-37	SPRING CLUTCH	[illegible]								
SK32137-36	CLUTCH GUIDE	[illegible]								
SK32137-35	PIN	[illegible]								
SK32137-34	OIL DAM	[illegible]								
SK32137-33	CLUTCH SHAFT	[illegible]								
SK32137-32	O-RING	[illegible]	MS3246/1-341							
SK32137-31	STRAINER,PINION SCAV	[illegible]								
SK32137-30	BEARING, LOWER	[illegible]								
SK32137-29	RETAINING RING	[illegible]	RRN-181							
SK32137-28	O-RING	[illegible]	MS3246/1-136							
SK32137-27	SEAL RING	[illegible]								
SK32137-26	PLUG	[illegible]								
SK32137-25	O-RING	[illegible]	MS3246/1-136							
SK32137-24	SPACER	[illegible]								
SK32137-23	SPACER	[illegible]								
SK32137-22	QUILL SHAFT	[illegible]								
SK32137-21	TORQUE TUBE	[illegible]								
[illegible]	NOMENCLATURE OR DESCRIPTION	[illegible]	MATERIAL AND SPECIFICATION							

PART LIST

NAS3-2542

BOEING HELICOPTERS

DRIVE SYSTEM
TACTICAL TILT ROTOR,
ART PROGRAM

J 77272 SK32137

SK32137

DATE = 11/19/93 TIME = 10.07 SCALE = 0.3078
LAST FILE = 92029 USER = INPROC DRAWID = SK32137 00 -0101
SK32137 00 -0102
SK32137 00 -
1270 J 003

241.3-01.8.H4.JS9443

2K3S13J

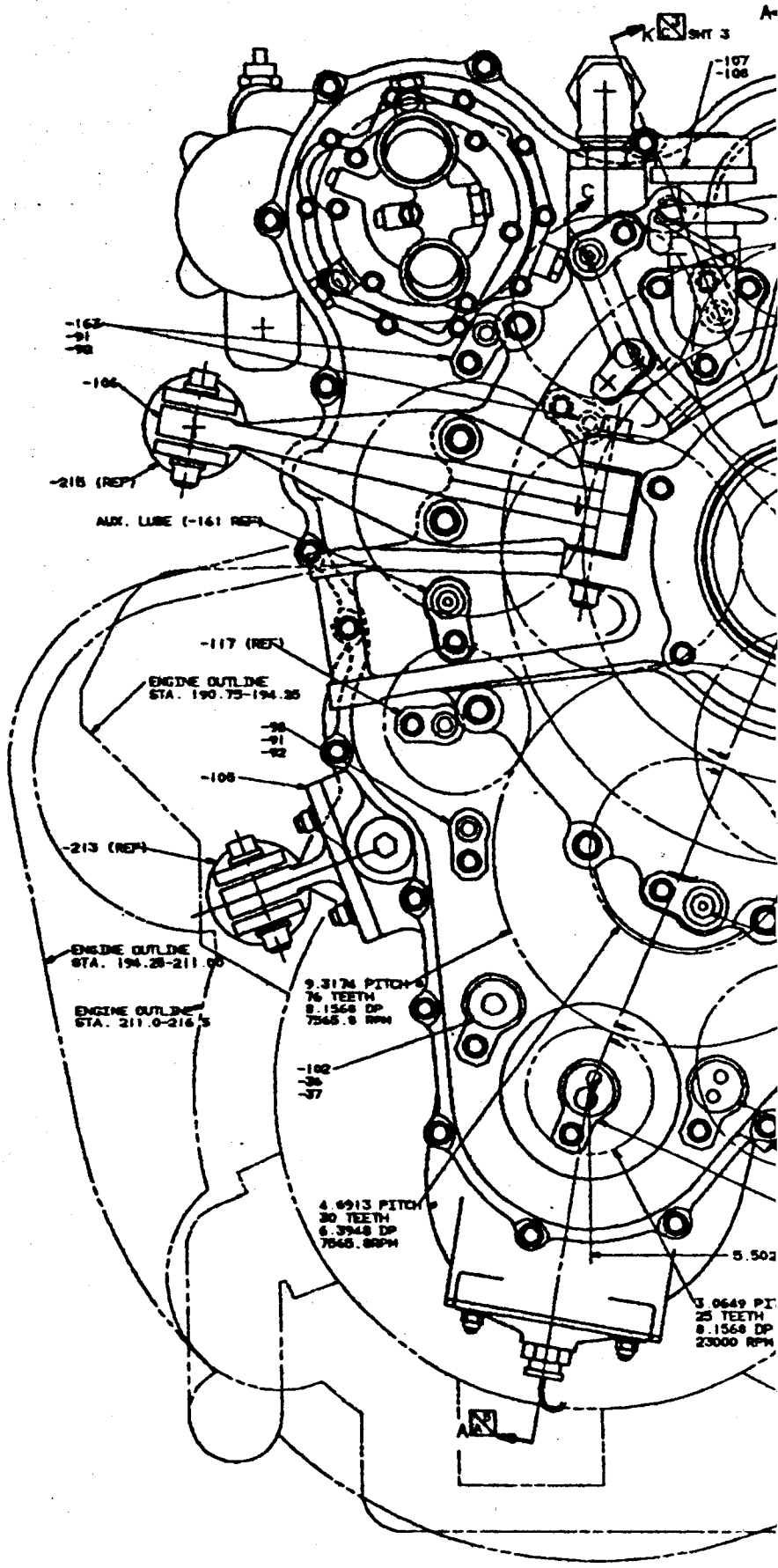
SHT 3
-197
-106
-162
-91
-92
-106
-218 (REF)
AUX. LUBE (-161 REF)
-117 (REF)
ENGINE OUTLINE
STA. 190.75-194.25
-91
-92
-106
-213 (REF)
ENGINE OUTLINE
STA. 194.25-211.00
ENGINE OUTLINE
STA. 211.0-216.5
9.3174 PITCH
76 TEETH
8.1568 DP
7568.6 RPM
-192
-96
-97
4.6913 PITCH
30 TEETH
6.3948 DP
7568.6RPM
5.502
3.0649 PI
25 TEETH
8.1568 DP
23000 RPM

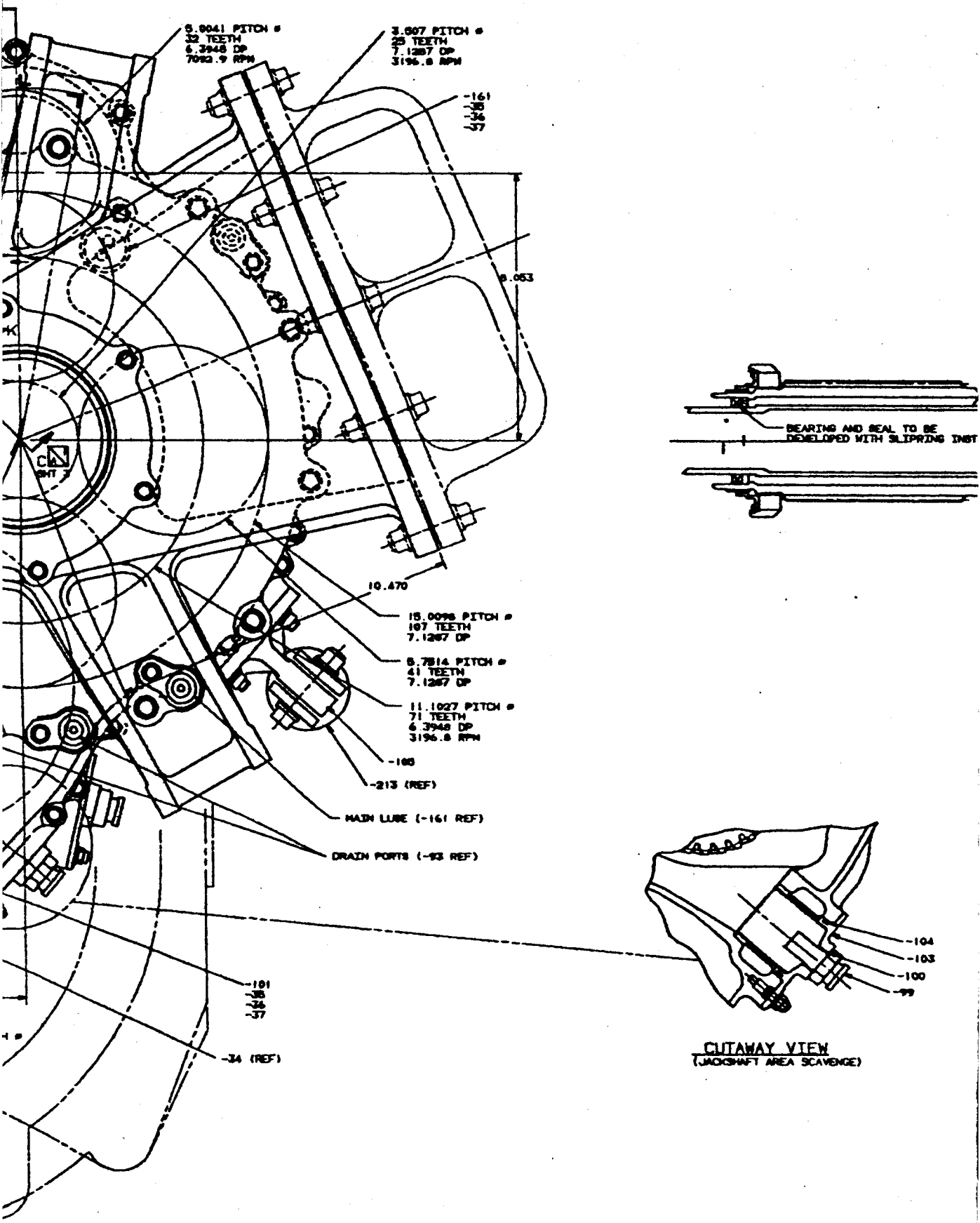
5.0041 PITCH ø
32 TEETH
6.3948 DP
7092.9 RPM
3.607 PITCH ø
25 TEETH
7.1287 DP
3196.8 RPM
-161
-35
-36
-37
8.053
10.470
15.0096 PITCH ø
107 TEETH
7.1287 DP
5.7814 PITCH ø
41 TEETH
7.1287 DP
11.1027 PITCH ø
71 TEETH
6.3948 DP
3196.8 RPM
-100
-213 (REF)
MAIN LUBE (-161 REF)
DRAIN PORTS (-93 REF)
-101
-35
-36
-37
-34 (REF)
BEARING AND SEAL TO BE
DEVELOPED WITH SLIPRING INST
-104
-103
-100
-99
CUTAWAY VIEW
(JACKSHAFT AREA SCAVENGE)

SK32137 2

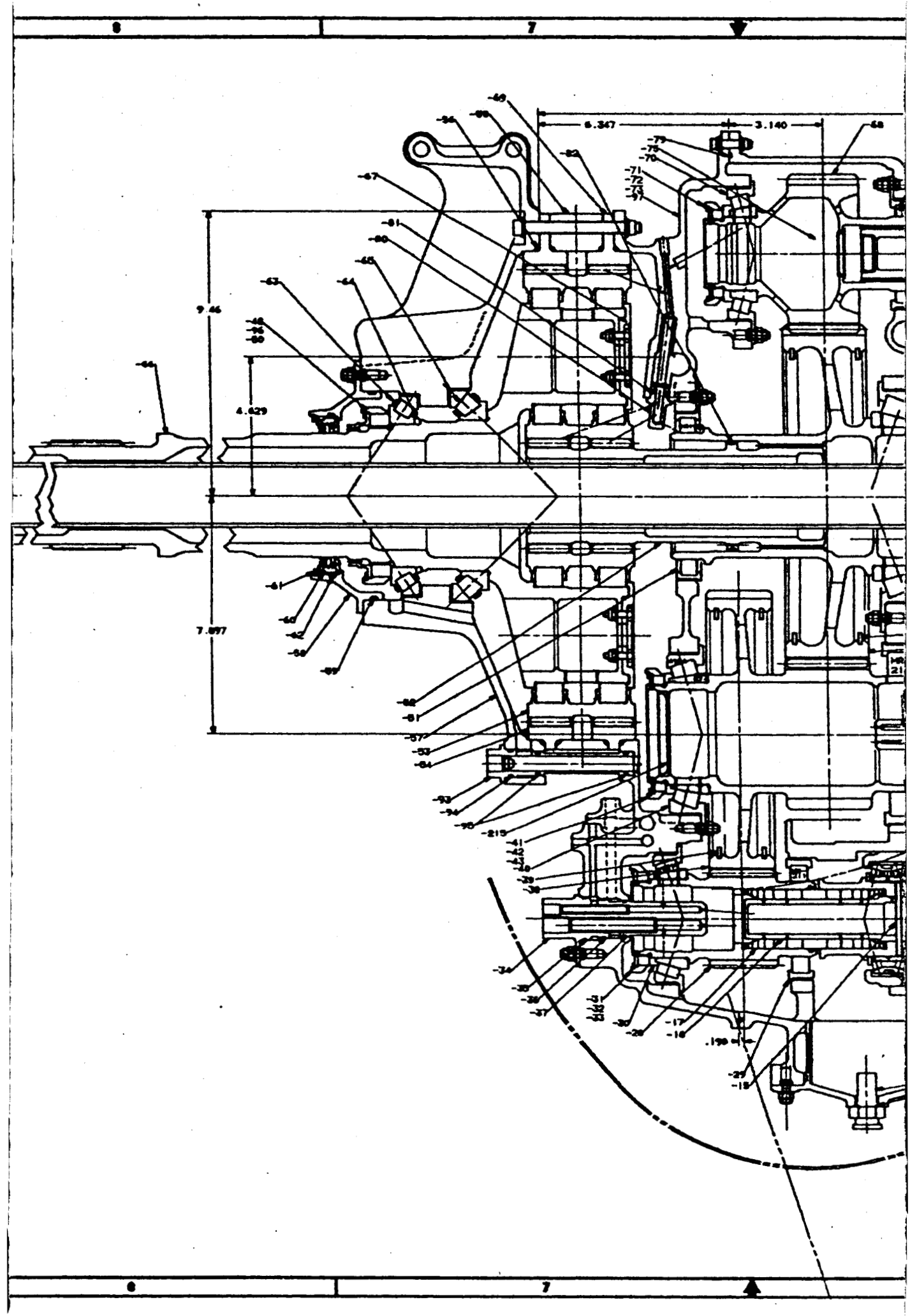
6
7
6.347
3.140
9.46
4.629
7.897
.199

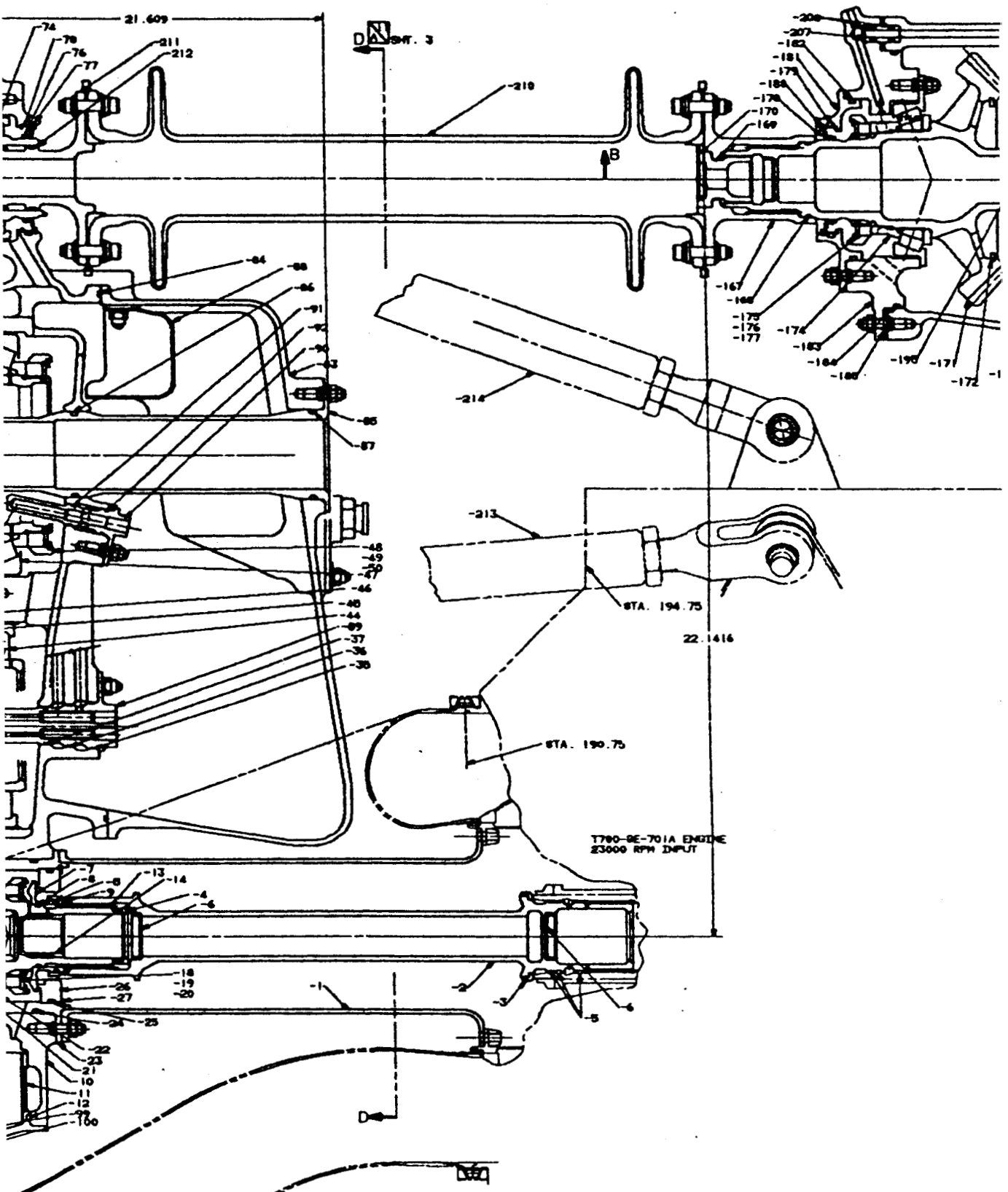

SECTION A-A
(ROTOR GEARBOX)

SK32137

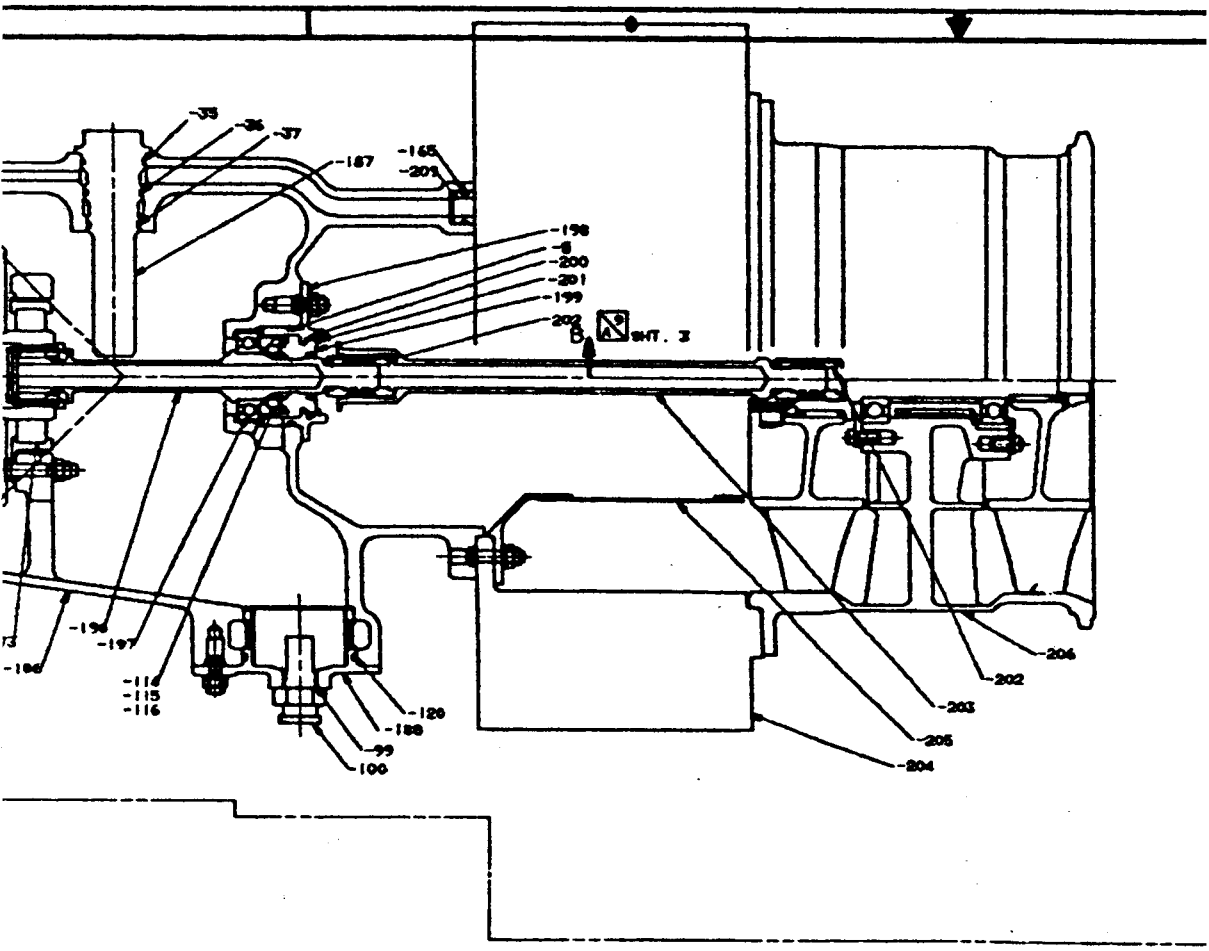

0 1 2 3 4
INCHES

NAS3-25421

DRIVE SYSTEM
TACTICAL TILT ROTOR,
ART PROGRAM

J 77272 SK32137

SK32137

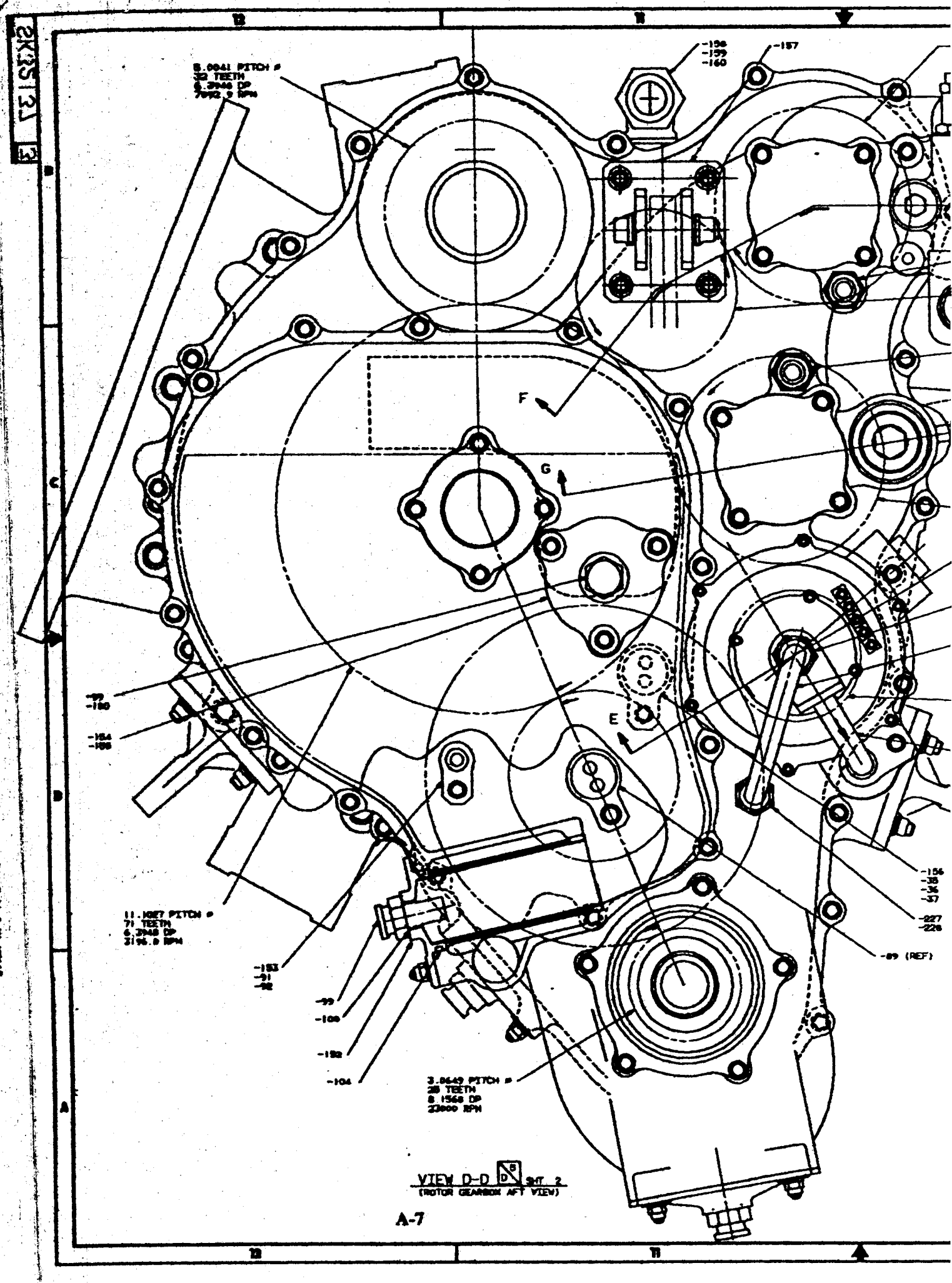
-156
-159
-160
-157
F
G
E
-89 (REF)
VIEW D-D
(ROTOR GEARBOX AFT VIEW)

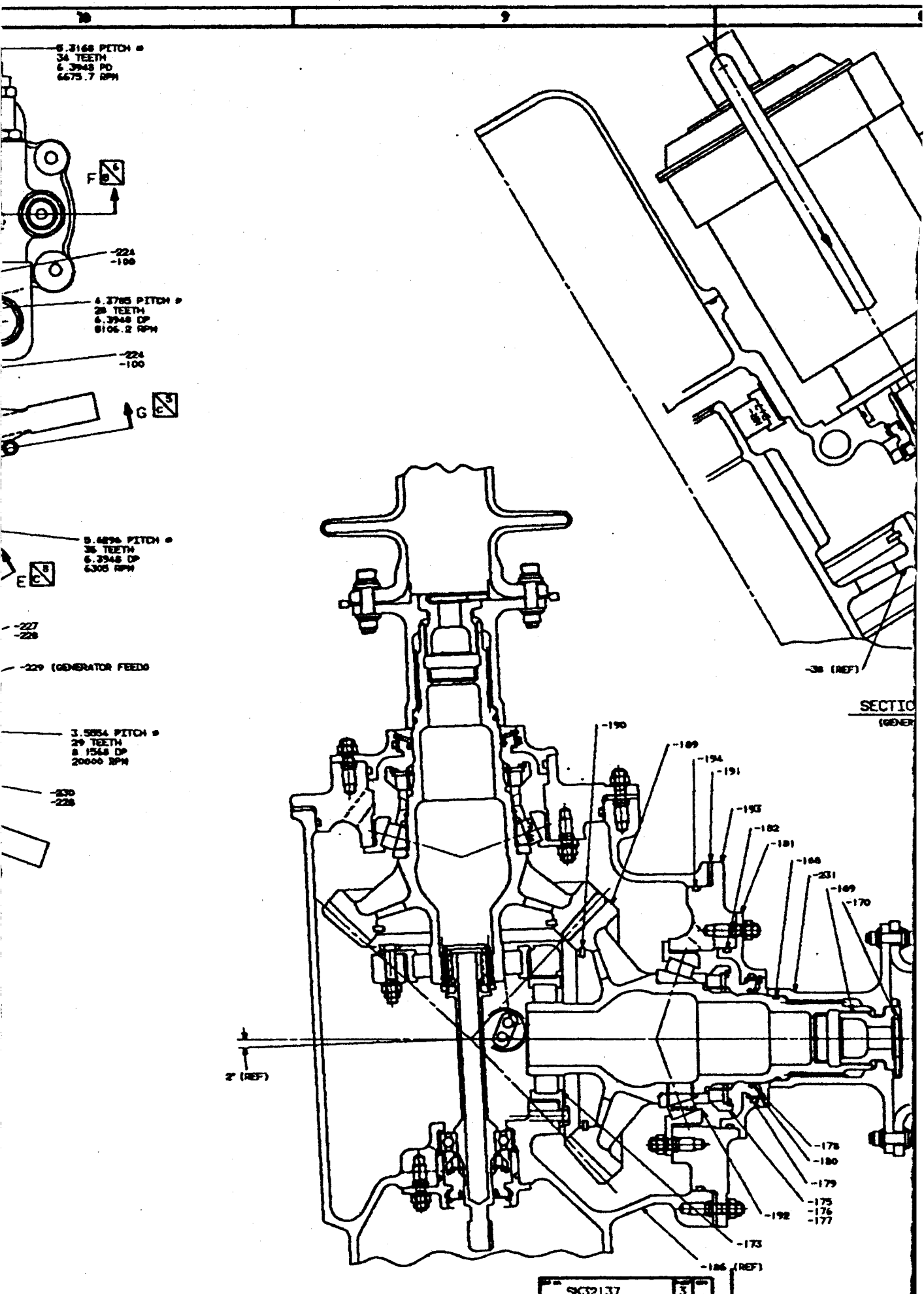
5.3168 PITCH ø
34 TEETH
6.3948 PD
6675.7 RPM
F
-224
-100
4.3785 PITCH ø
28 TEETH
6.3948 DP
8106.2 RPM
-224
-100
G
5.4896 PITCH ø
35 TEETH
6.3948 DP
6305 RPM
E
-227
-228
-229 (GENERATOR FEED)
3.5854 PITCH ø
29 TEETH
8.1548 DP
20000 RPM
-230
-228
-38 (REF)
SECTIO
(GENER
-190
-189
-194
-191
-193
-182
-181
-168
-231
-169
-170
2° (REF)
-178
-180
-179
-175
-176
-177
-192
-173
-186 (REF)
SK32137
3

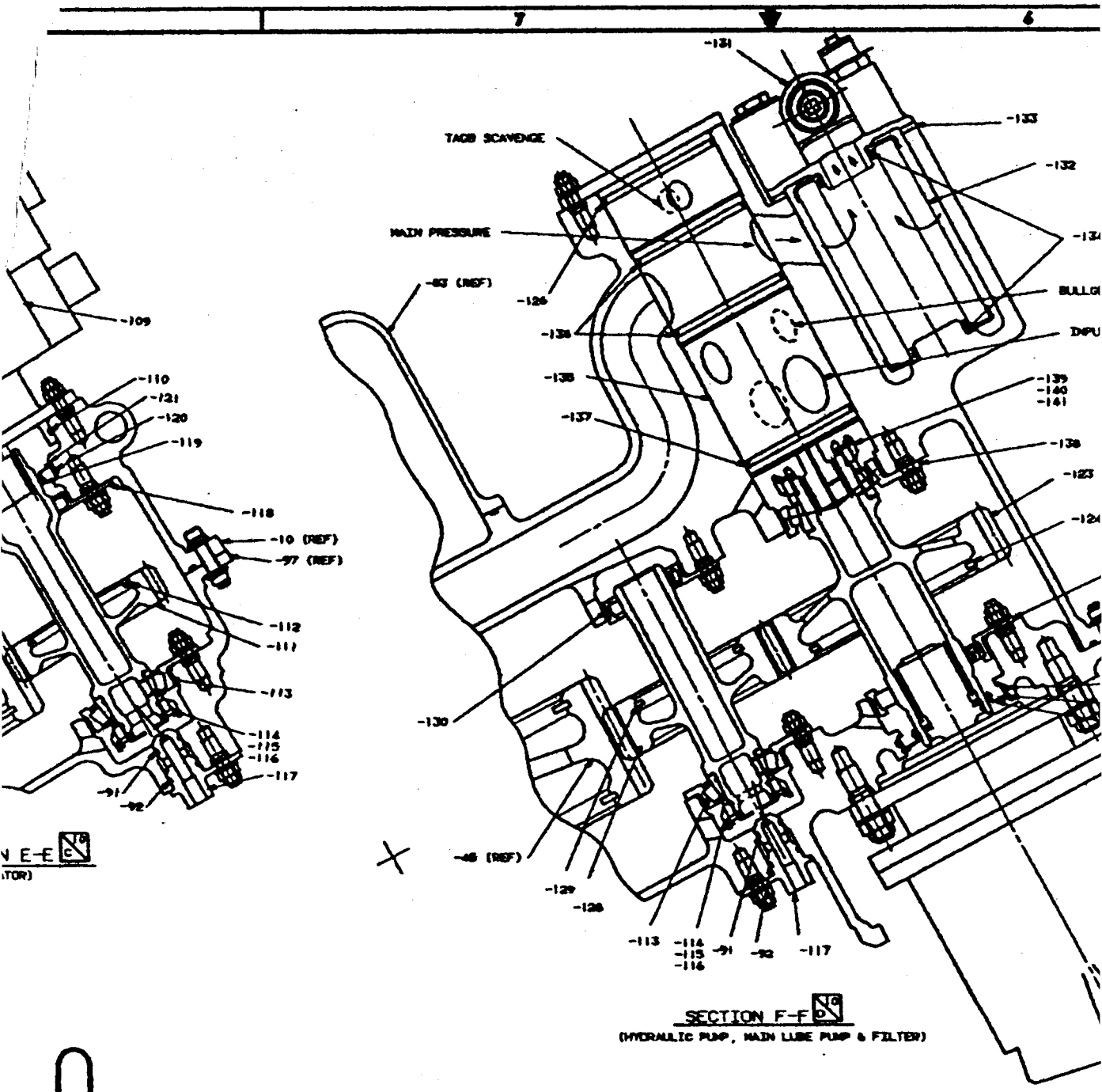

SECTION B-B SHT. 2
(TILT AXIS GEAR BOX AND WING SHAFT)
(SECTION ROTATED 88° CCW)

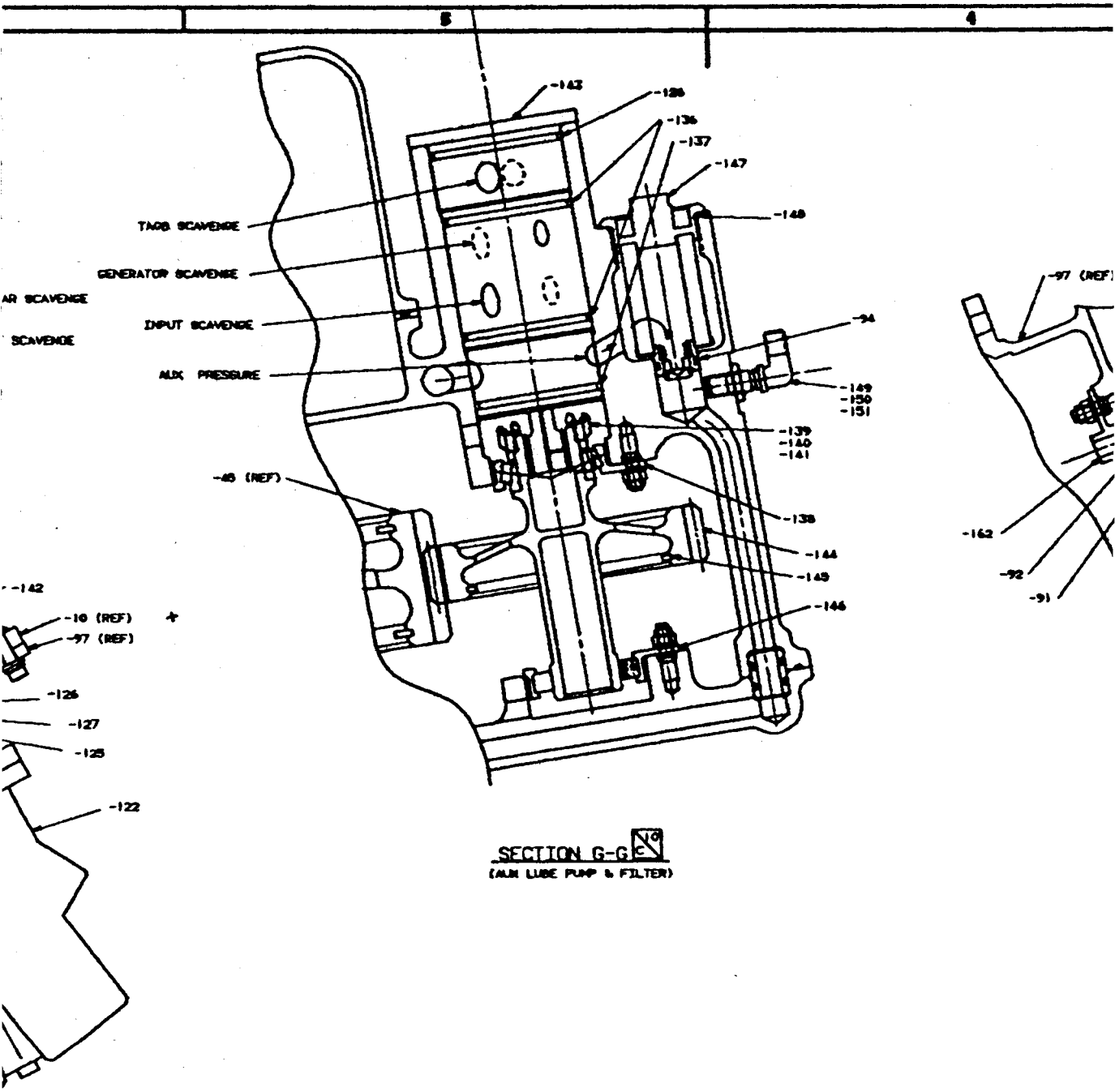

SECTION G-G

(AUX LUBE PUMP & FILTER)

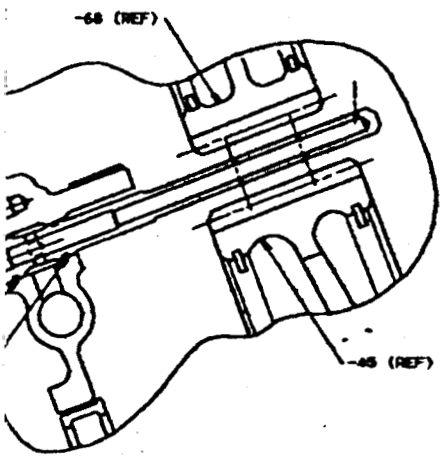

SECTION K-K D SHT. 2
(GEAR MESH LUBRICATION)
(SIMILAR FOR -161 & -163 LUBRICATORS)

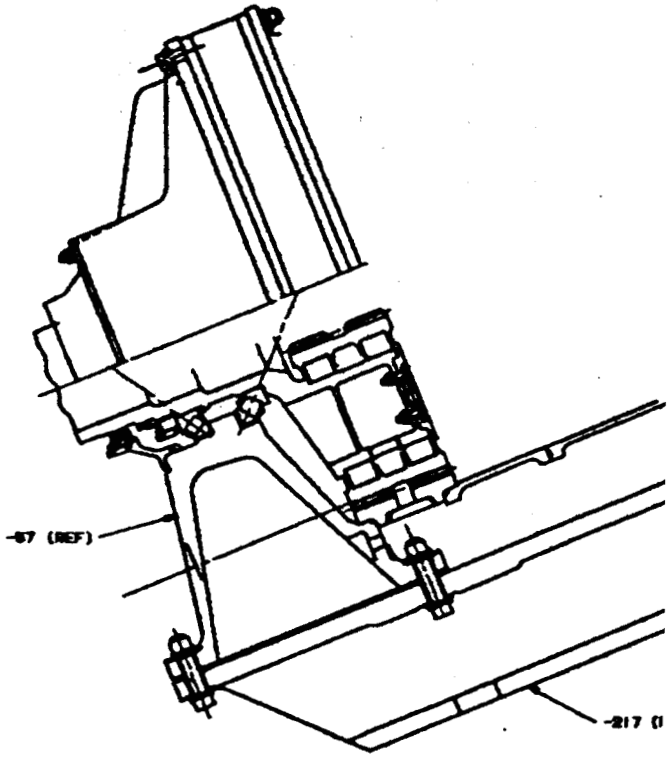

SECTION J-J C SHT. 4
(SUPPORT STRUCTURE .50 SCALE)

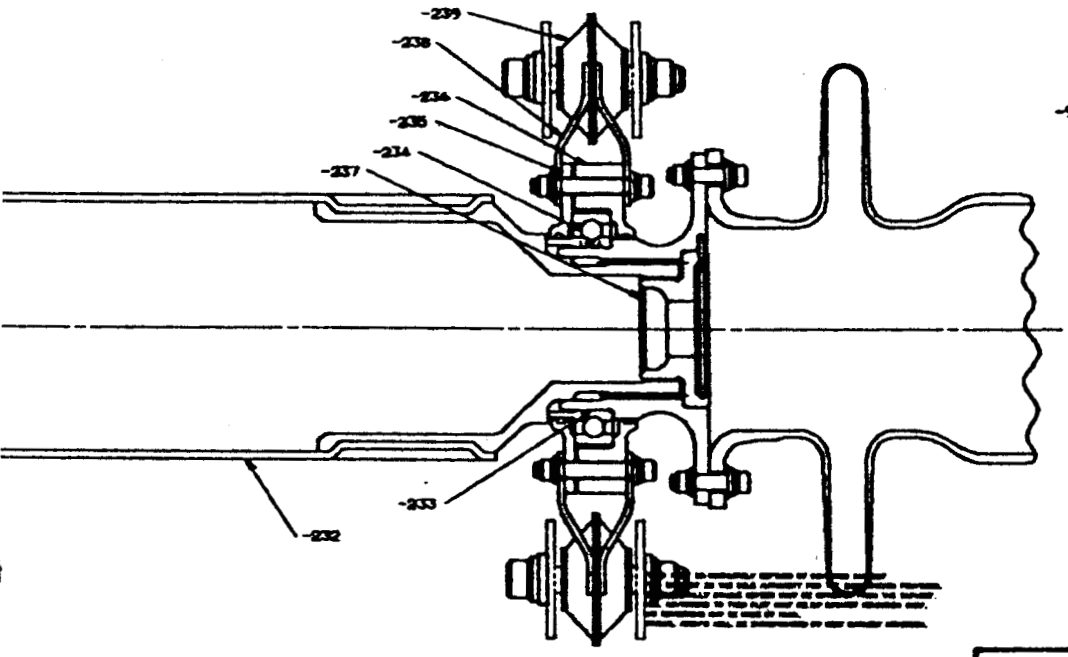

-146

-97 (REF)

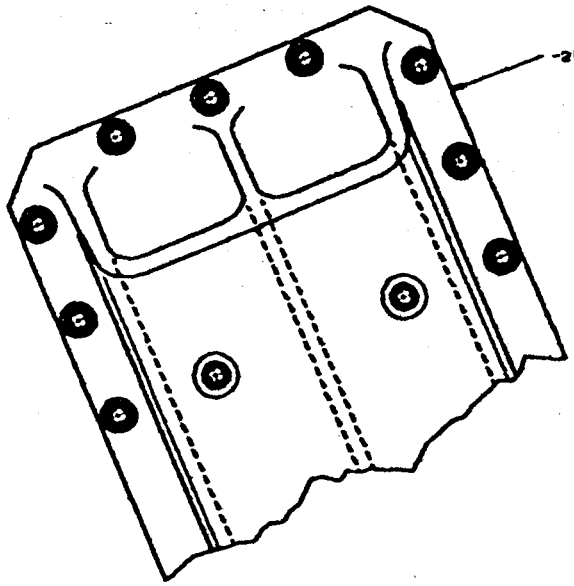

SECTION H-H SHT. 4
(SUPPORT STRUCTURE BOLT ARRANGEMENT .50 SCALE)

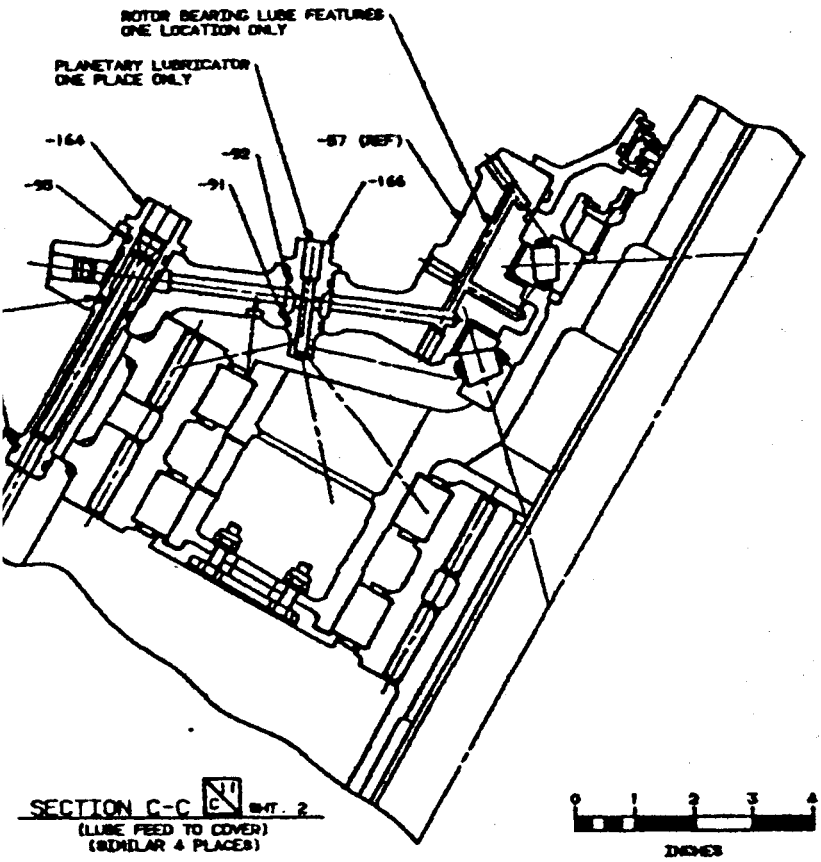

SECTION C-C SHT. 2
(LUBE FEED TO COVER)
(SIMILAR 4 PLACES)

0 1 2 3 4
INCHES

NASA-23421

DRIVE SYSTEM
TACTICAL TILT ROTOR,
ART PROGRAM

J 77272 SK32137

7545

SK32137

DATE = 11/19/80 TIME = 10.08 SCALE = 0.3976
LAST FILE = 92010 USER = 3VRDC DRAWID =

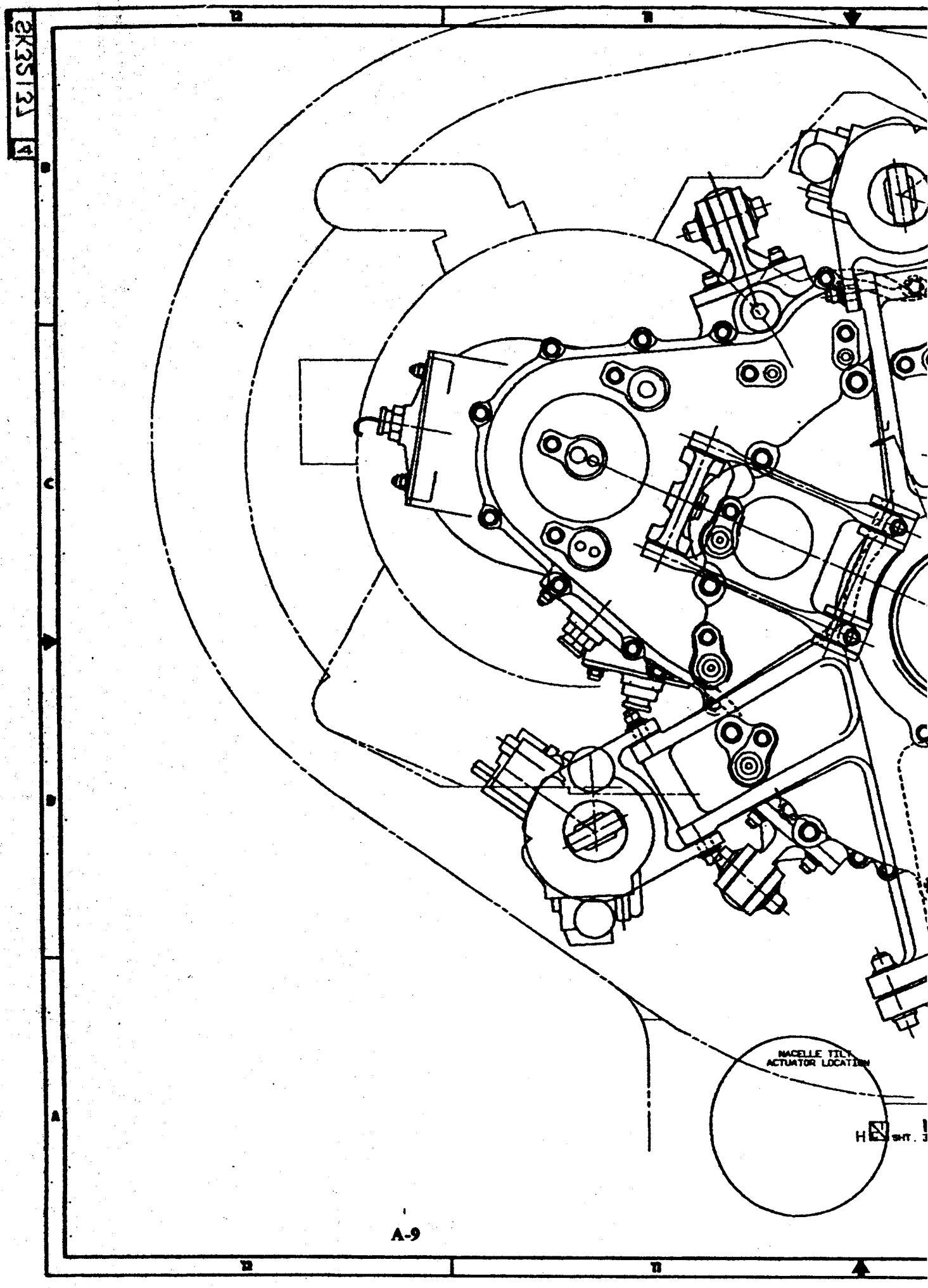
NACELLE TILT
ACTUATOR LOCATION

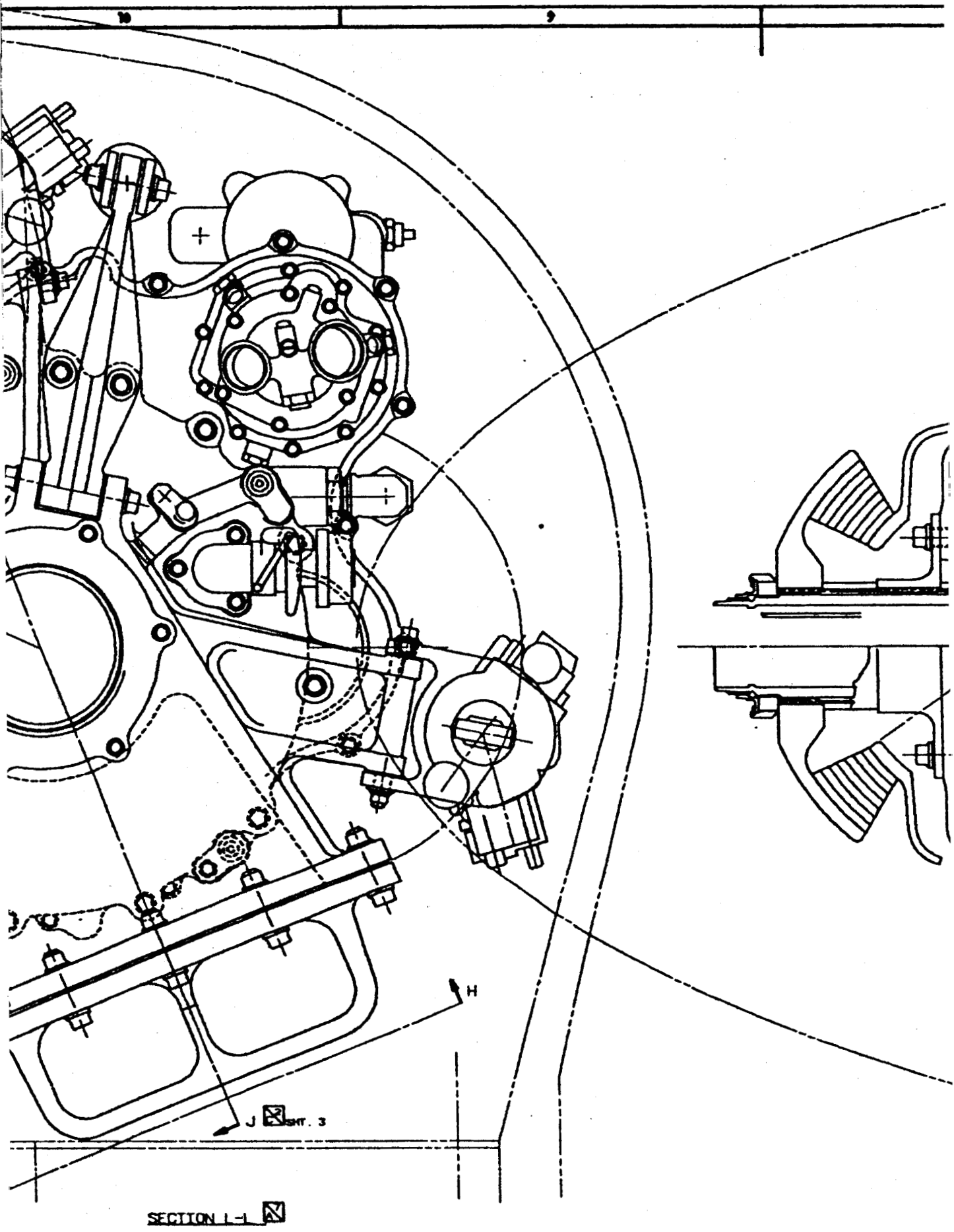

SK32137

8
7
6
ACTUATOR MOUNT
-217
35.60
L

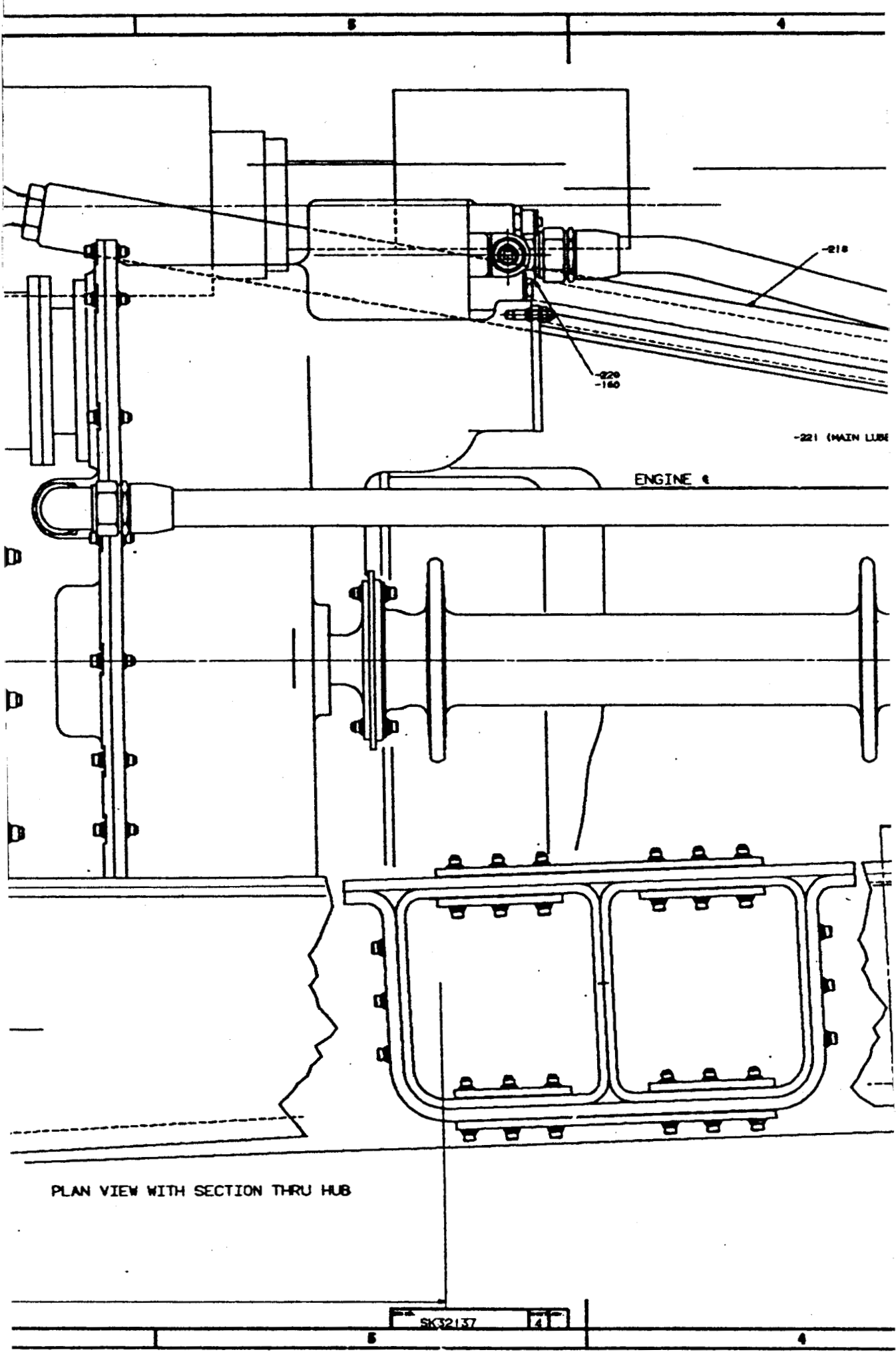
-218
-220
-160
-221 (MAIN LUBE
ENGINE ℄
PLAN VIEW WITH SECTION THRU HUB
SK32137
4

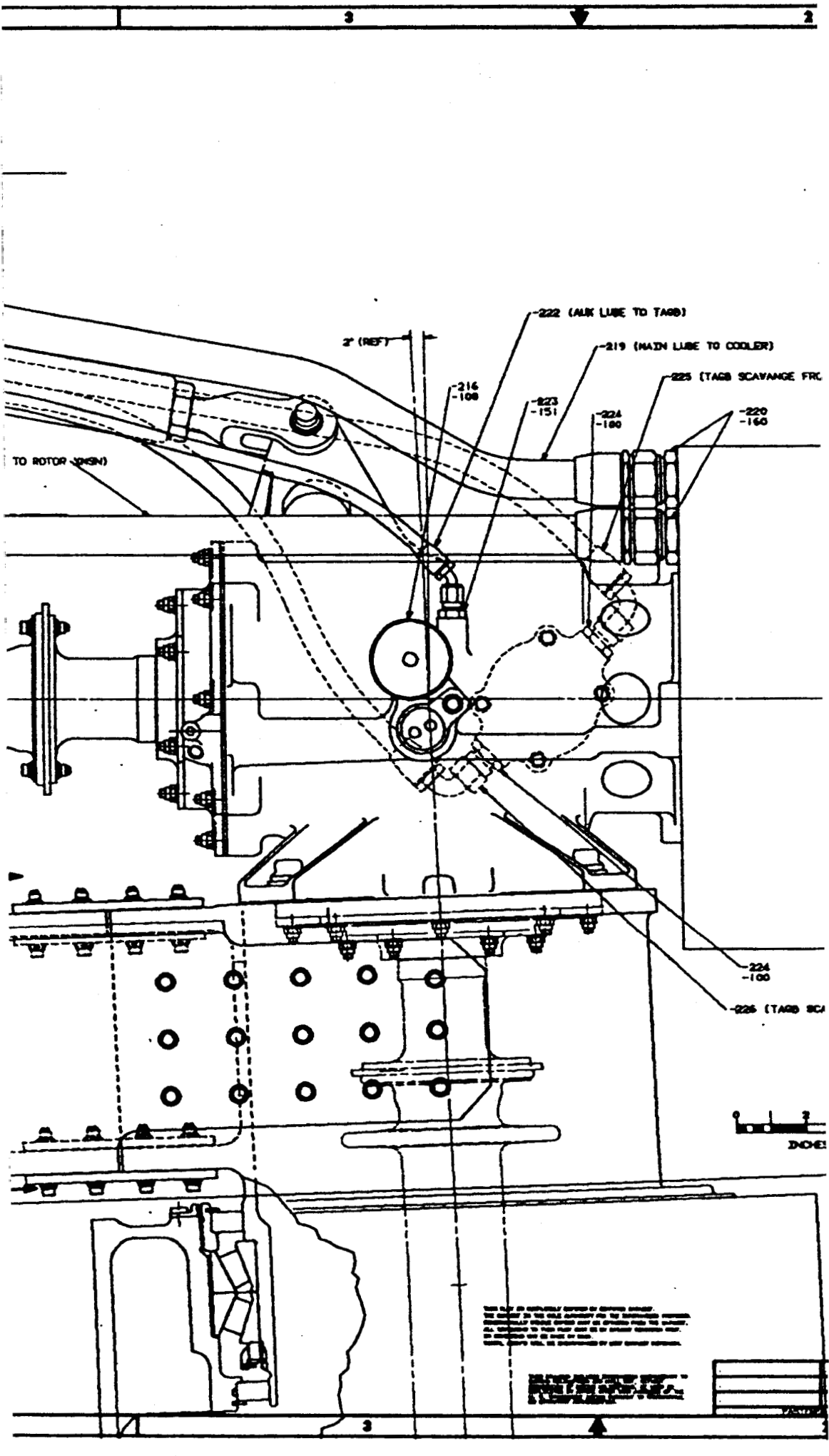
-222 (AUX LUBE TO TAGB)
2" (REF)
-219 (MAIN LUBE TO COOLER)
-225 (TAGB SCAVANGE FRC
-216
-108
-223
-151
-224
-180
-220
-160
TO ROTOR (JHSIN)
-224
-100
-226 (TAGB SCA
0
1
2
INCHES

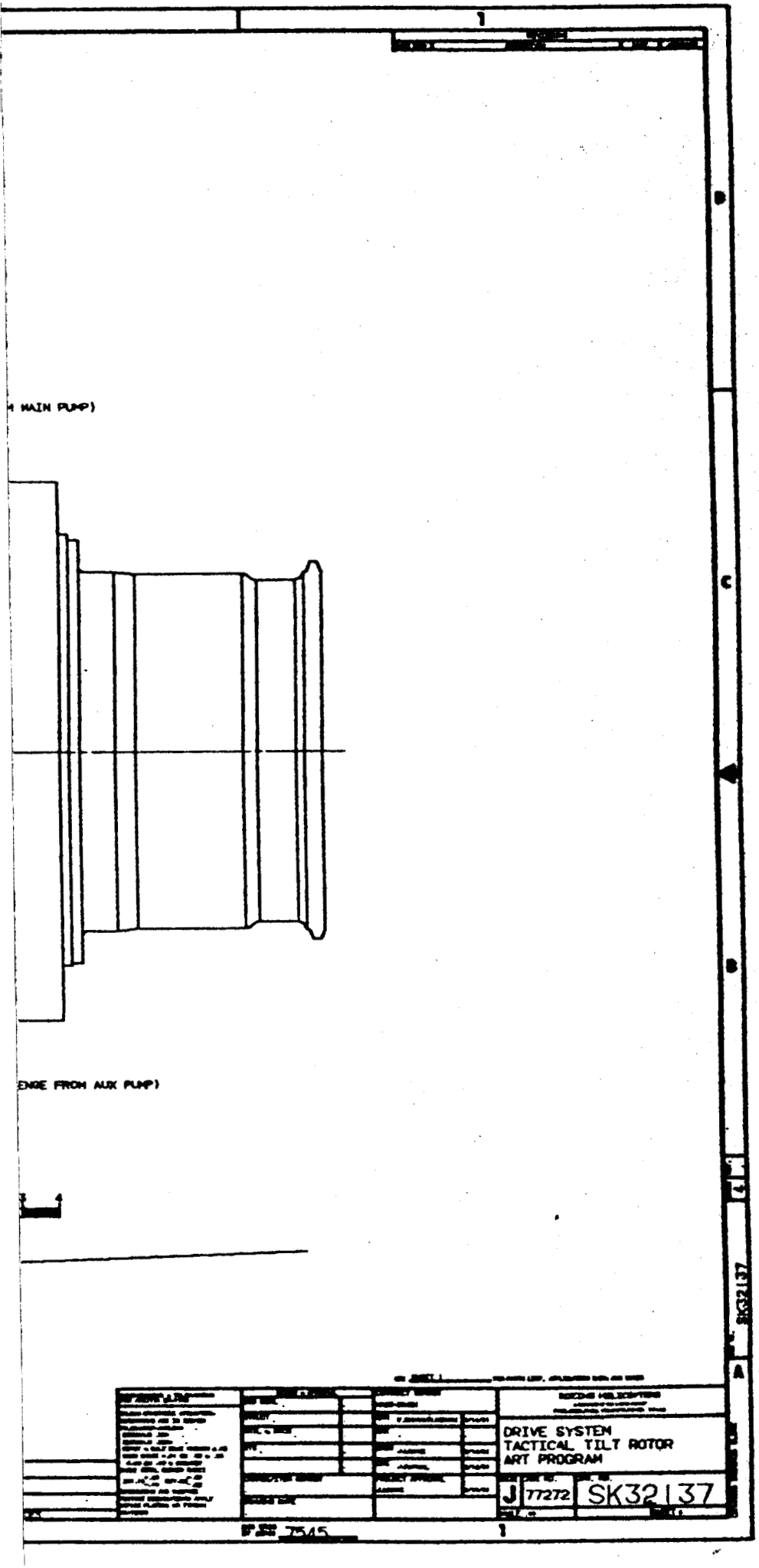
MAIN PUMP)
ENGE FROM AUX PUMP)
DRIVE SYSTEM
TACTICAL TILT ROTOR
ART PROGRAM
J 77272 SK32137
SK32137

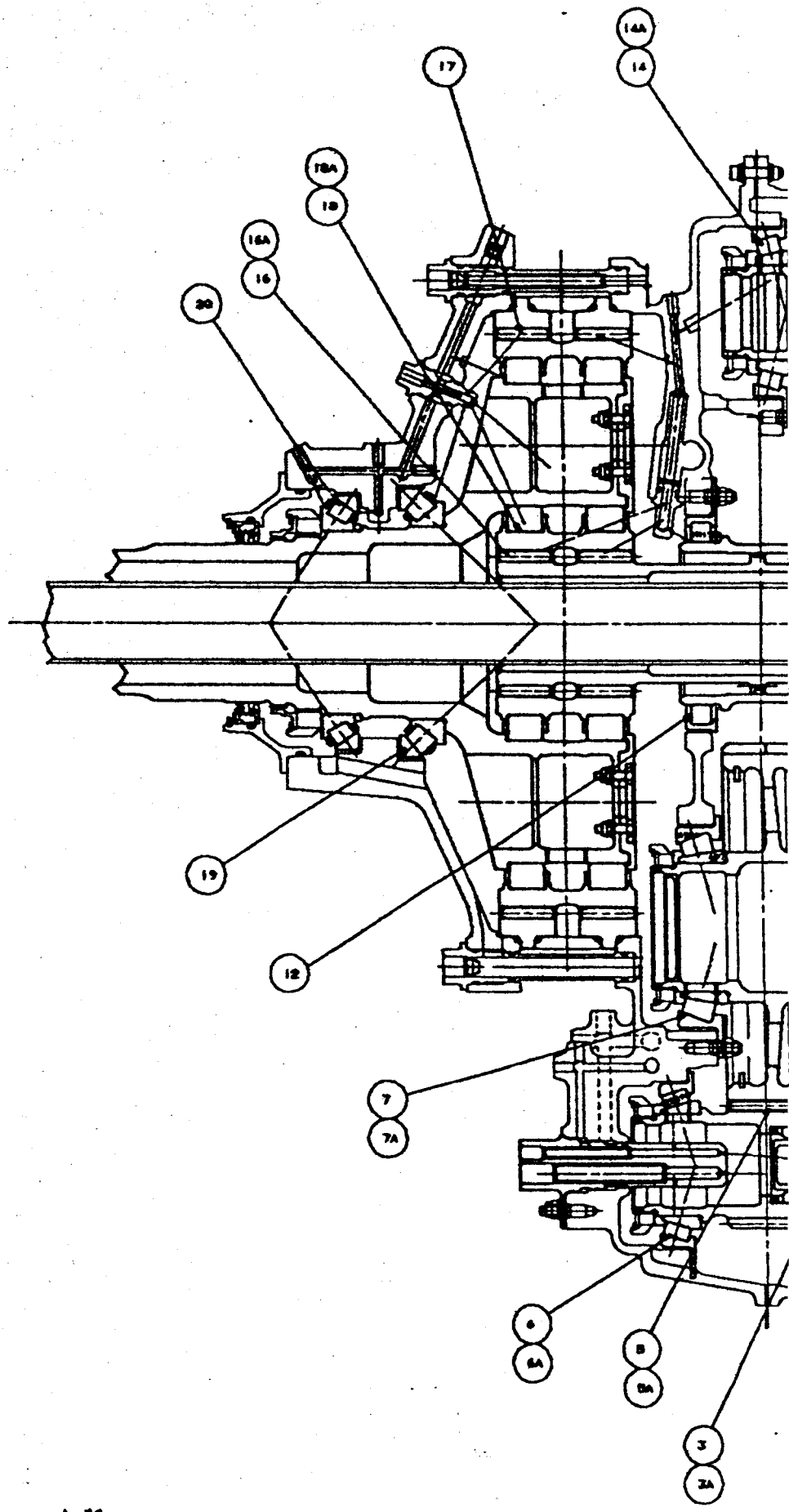
14A
14
17
18A
18
16A
16
20
19
12
7
7A
6
6A
5
5A
3
3A

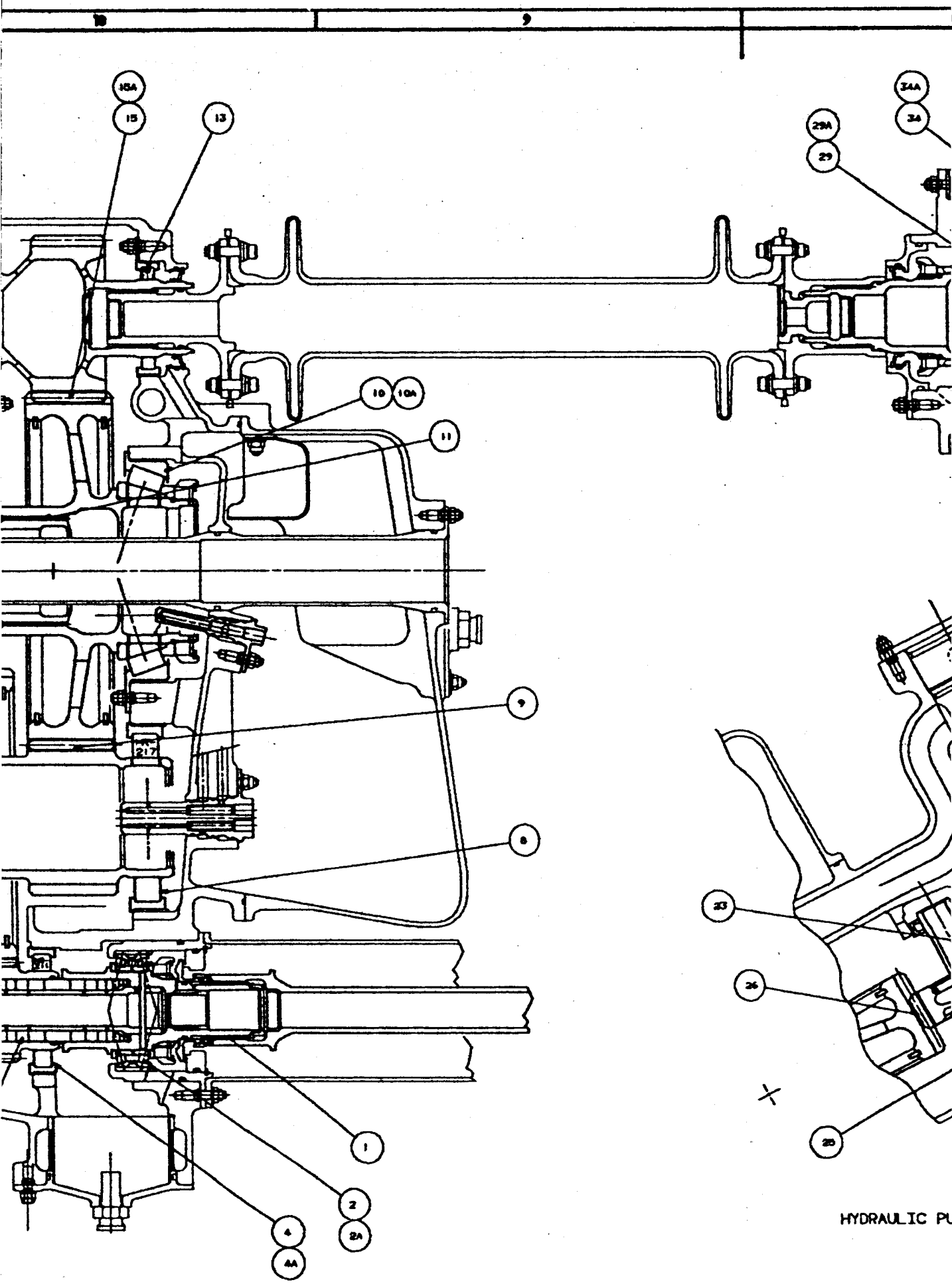
15A
15
13
10
10A
11
9
8
1
2
2A
4
4A
29A
29
34A
34
23
26
25
HYDRAULIC PU

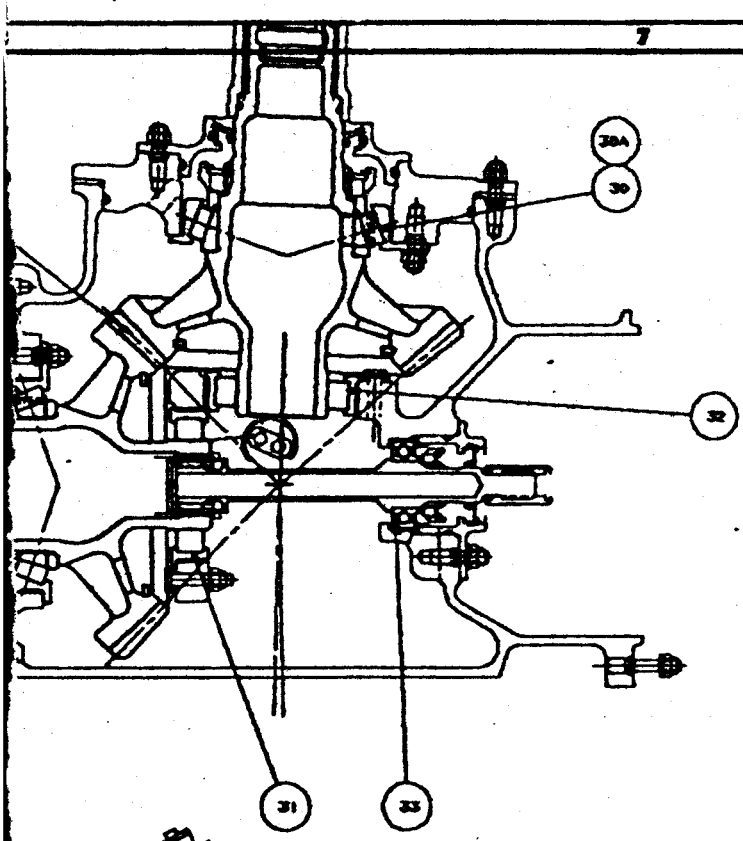

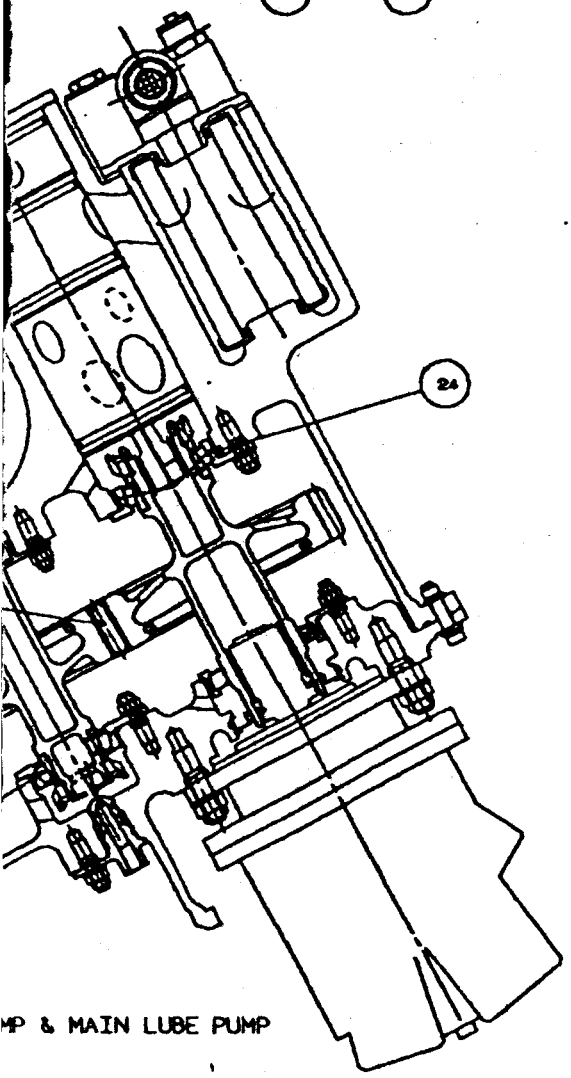

MP & MAIN LUBE PUMP

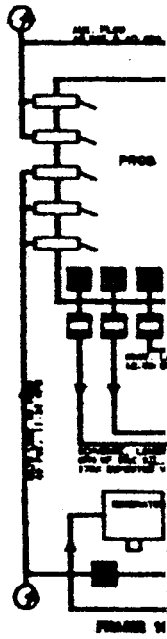

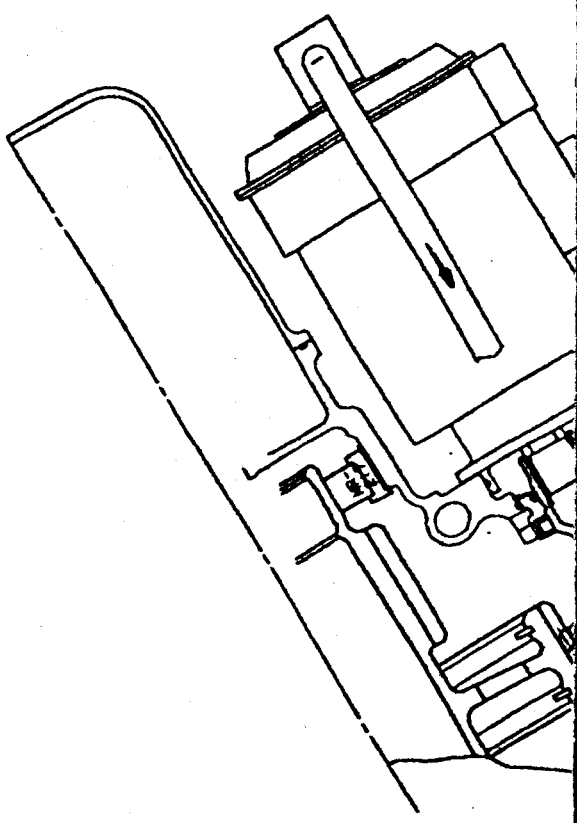

GENERA

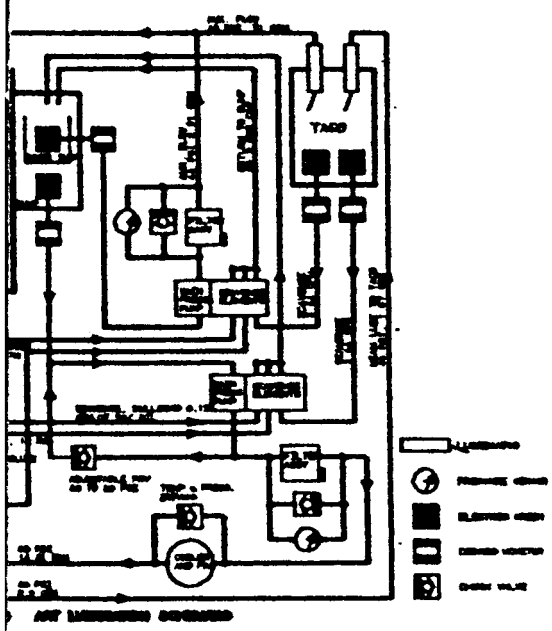

AUX. OIL DISTRIBUTION

NO.	PART NUMBER LUBRICATED	DESCRIPTION	PART NUMBER LUBRICATING	ORIFIC DIA. (I
2A	SK32137-21	TAPERED ROLLER BRG. INPUT SHAF	SK32137-34	.032
3A	SK32137-17	SPRING CLUTCH INPUT SHAFT	SK32137-34	.032
4A	SK32137-29	ROLLER BEARING INPUT PINION	SK32137-101	.032
5A	SK32137-20, -38	INPUT PINION/ JACK SHAFT MESH	-101 INTO MESH	.040
6A	SK32137-30	TAPERED ROLLER BRG., PINION	SK32137-34	.032
7A	SK32137-40	TAPERED ROLLER BRG., JACKSHAFT	SK32137-89	.032
9A	SK32137-38, -45	JACKSHAFT/ BULLGEAR MESH	-156 INTO MESH	.047
10A	SK32137-47	TAPERED ROLLER BRG., BULLGEAR	SK32137-90	.032
14A	SK32137-70	TAPERED ROLLER BRG., ICDS GEAR	SK32137-97	.032
15A	SK32137-45, -68	ICDS GEAR/ BULLGEAR MESH	-141 INTO MESH	.032
16A	SK32137-52, -53	SUN/ PLANET GEAR MESH	-57 FROM TOP -80 FROM BOTT	.040
18A	SK32137-53	ROLLER BEARING, PLANET	SK32137-57	.032
29A	SK32137-174	TAPERED ROLLER TAGB	SK32137-183	.032
30A	SK32137-192	TAPERED ROLLER, TAGB	SK32137-187	.032
34A	SK32137-171, -189	S.B. MESH, TAGB	-187 INTO MESH	.040
.	.	.	.	.
.	.	.	.	.

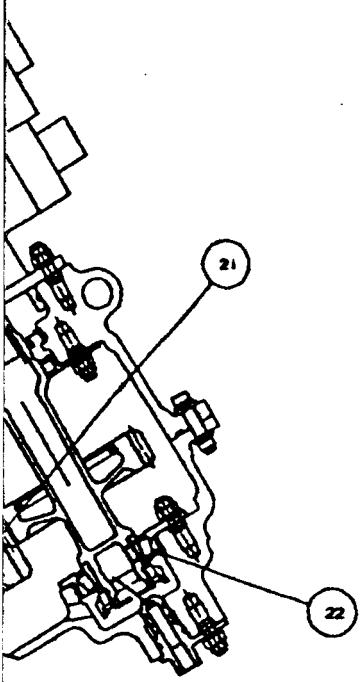

TOR DRIVE INSTL.

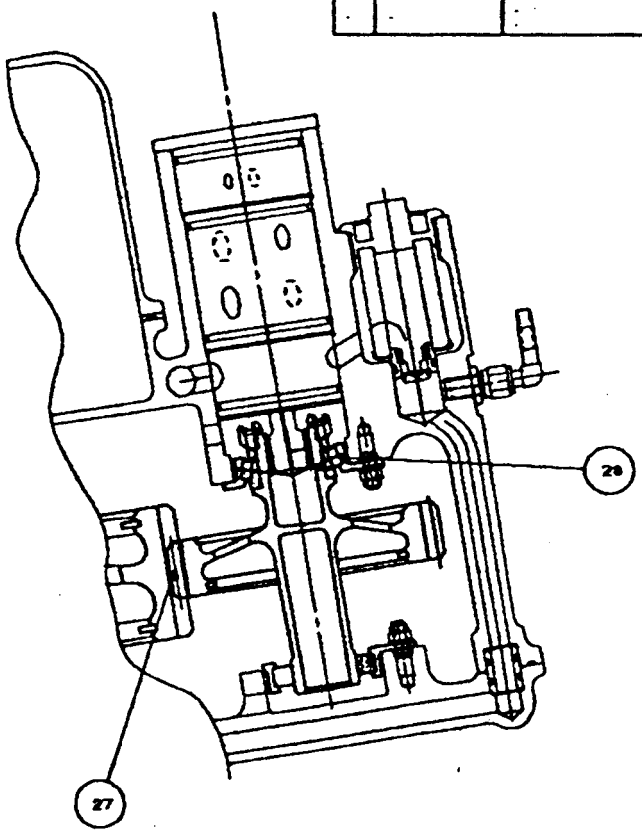

AUX. LUBE PUMP

	NUMBER OF ORIFECES	FLOW (GPM) @ 40 PSI
	1	.143
	1	.143
	1	.143
	1	.223
	1	.143
	1	.143
	1	.306
	1	.143
	1	.143
	1	.143
	1 1	.446
	2	.286
	1	.143
	1	.143
	1	.223
	.	.
	.	.

MAIN OIL DISTRIBUTION

NO.	PART NUMBER LUBRICATED	DESCRIPTION	PART NUMBER LUBRICATING	ORIFICE DIA. (IN.)	NUMBER OF ORIFECES	FLOW (GPM) @ 40 PSI
1	SK32137-2, -13	SPLINED INPUT SHAFT	SK32137-34	EQUIV. TO .032	1	.143
2	SK32137-21	TAPERED ROLLER BRG. INPUT SHAFT	SK32137-34	EQUIV. TO .032	1	.143
3	SK32137-17	SPRING CLUTCH INPUT SHAFT	SK32137-34	.	1	1.00
4	SK32137-29	ROLLER BEARING INPUT PINION	SK32137-102	EQUIV. TO .032	1	.143
5	SK32137-28, -38	INPUT PINION/ JACK SHAFT MESH	-161 INTO MESH -102 OUT OF	.032 .040	2 5	1.40
6	SK32137-30	TAPERED ROLLER BRG., PINION	SK32137-34	.032	1	.143
7	SK32137-40	TAPERED ROLLER BRG., JACKSHAFT	SK32137-89	.032	1	.143
8	SK32137-44	ROLLER BEARING JACKSHAFT	SK32137-89	.032	1	.143
9	SK32137-38, -45	JACKSHAFT/ BULLGEAR MESH	-156 INTO MESH -153 OUT OF	.032 .040	2 5	1.40
10	SK32137-47	TAPERED ROLLER BRG., BULLGEAR	SK32137-90	.032	1	.143
11	SK32137-45, -62	BULLGEAR/ SUN SHAFT SPLINE	SK32137-90	.032	1	.143
12	SK32137-51	ROLLER BEARING BULLGEAR	SK32137-90	.032	1	.143
13	SK32137-74	ROLLER BEARING ICDS GEAR	SK32137-162	.032	1	.143
14	SK32137-70	TAPERED ROLLER BRG., ICDS GEAR	SK32137-97	.032	1	.143
15	SK32137-65, -66	ICDS GEAR/ BULLGEAR MESH	-161 INTO MESH -162 OUT OF	.032 .032	2 4	.886
16	SK32137-52, -53	SUN/ PLANET GEAR MESH	-57/-166 TOP -80 BOTTOM	.040 .040	3 3	1.34
17	SK32137-53, -54	PLANET/ RING GEAR MESH	-57/-166 TOP -97 BOTTOM	.040 .040	2 1	.668
18	SK32137-53	ROLLER BEARING, PLANET	-57/-166 TOP -97 BOTTOM	.032 .032	4 2	.855
19	SK32137-65	TAPERED ROLLER, ROTOR SHAFT	SK32137-166	.032	1	.143
20	SK32137-63	TAPERED ROLLER, ROTOR SHAFT	SK32137-67	.032	2	.286
21	SK32137-111, -38	GENERATOR SHAFT/ JACKSHAFT MESH	-98 INTO MESH	.040	1	.223
22	SK32137-113	TAPERED ROLLER, GENERATOR SHAFT	SK32137-117	.032	1	.143
23	SK32137-123 -128	HYD. PUMP SHAFT/ IDLER SHAFT MESH	-163 INTO MESH	.040	1	.223
24	SK32137-130	TAPERED ROLLER, PUMP SHAFT	SK32137-135	.032	1	.143
25	SK32137-113	TAPERED ROLLER, IDLER SHAFT	SK32137-117	.032	1	.143
26	SK32137-128, -45	IDLER SHAFT/ BULLGEAR MESH	-162 INTO MESH	.040	1	.223
27	SK32137-144, -45	AUX. OIL SHAFT/ BULLGEAR MESH	-163 INTO MESH	.040	1	.223
28	SK32137-138	TAPERED ROLLER, AUX. OIL SHAFT	SK32137-143	.032	1	.143
29	SK32137-174	TAPERED ROLLER, TAGB	SK32137-183	.032	1	.143
30	SK32137-192	TAPERED ROLLER, TAGB	SK32137-187	.032	1	.143
31	SK32137-173	ROLLER BEARING, TAGB	SK32137-187	.032	1	.143
32	SK32137-173	ROLLER BEARING, TAGB	SK32137-187	.032	1	.143
33	SK32137-197	BALL BEARING, TAGB FAN DRIVE	SK32137-187	.032	1	.143
34	SK32137-171, -189	S.B. MESH, TAGB	-187 INTO MESH -187 OUT OF	.032 .032	2 4	.855

1 2 3 4

INCHES

[illegible]

[illegible]

PARTING LINES

DRIVE SYSTEM
TACTICAL TILT ROTOR,
ART PROGRAM

J 77272 SK32137

SK32137

SK32137

DATE = 11/19/93 TIME = 10.00 SCALE = 0.3076
LAST FILE = 92010 USER = INPROC DRAWID = SK32137 00

941,3-91,2,H4,X0663

SK32137 00	-0001
SK32137 00	-0002
SK32137 00	-0003
SK32137 00	-0004
SK32137 00	-0005
SK32137 00	-0006
1305 J .003	-

SK35137

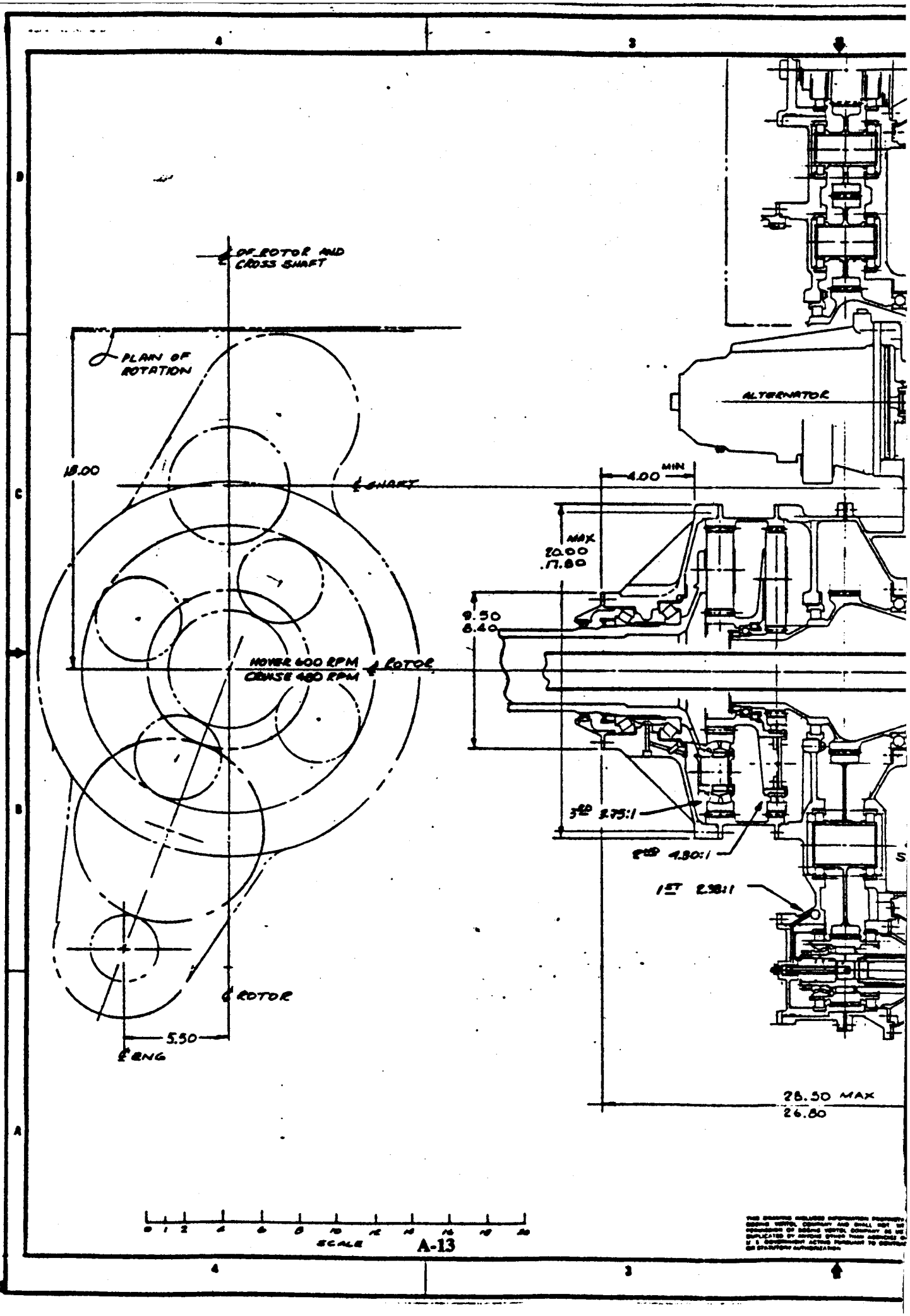
℄ OF ROTOR AND CROSS SHAFT
PLAIN OF ROTATION
18.00
℄ SHAFT
HOVER 600 RPM
CRUISE 480 RPM
℄ ROTOR
℄ ROTOR
5.50
℄ RNG
ALTERNATOR
4.00 MIN
MAX
20.00
17.80
9.50
8.40
3RD 3.75:1
2ND 4.30:1
1ST 2.38:1
28.50 MAX
26.80
SCALE

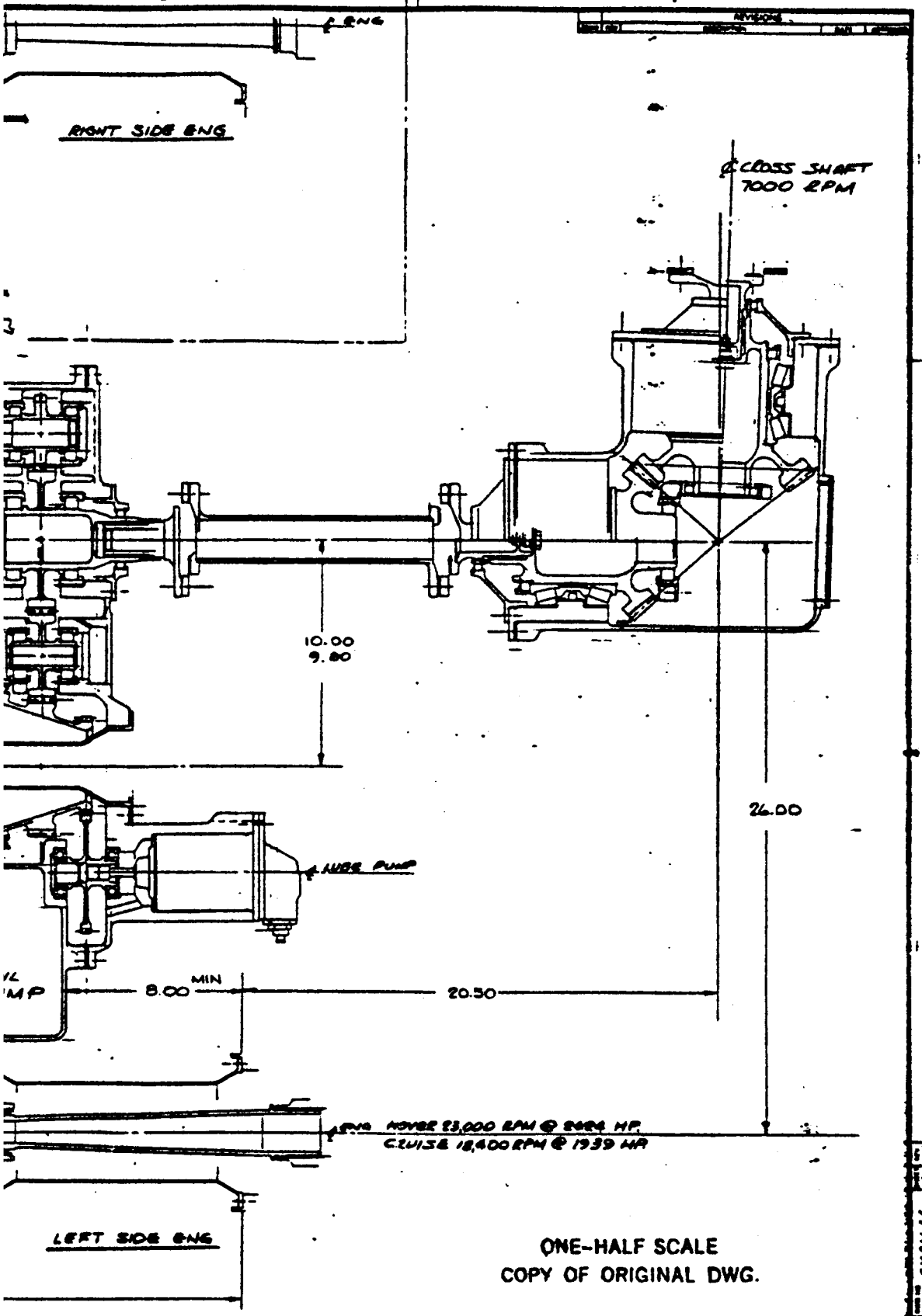

ONE-HALF SCALE
COPY OF ORIGINAL DWG.

BOEING VERTOL COMPANY
PHILADELPHIA PENNSYLVANIA

TTR MAIN ROTOR
DRIVE SYSTEM

E 77272 SK31646

7545

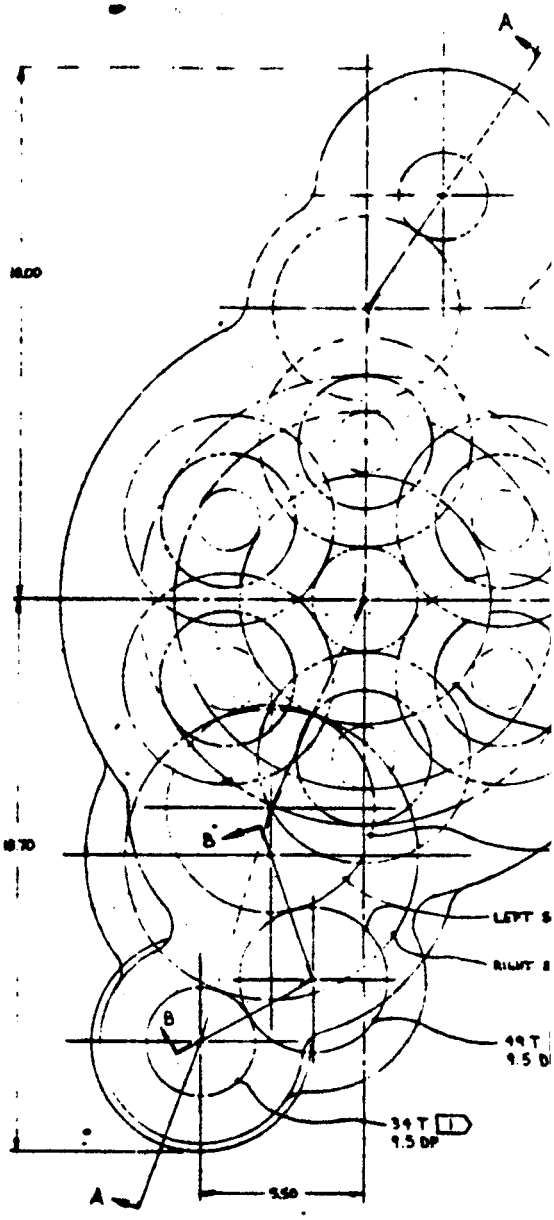

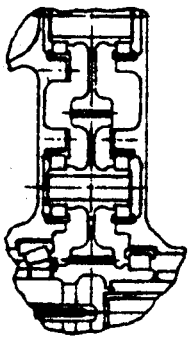

SECTION B-B

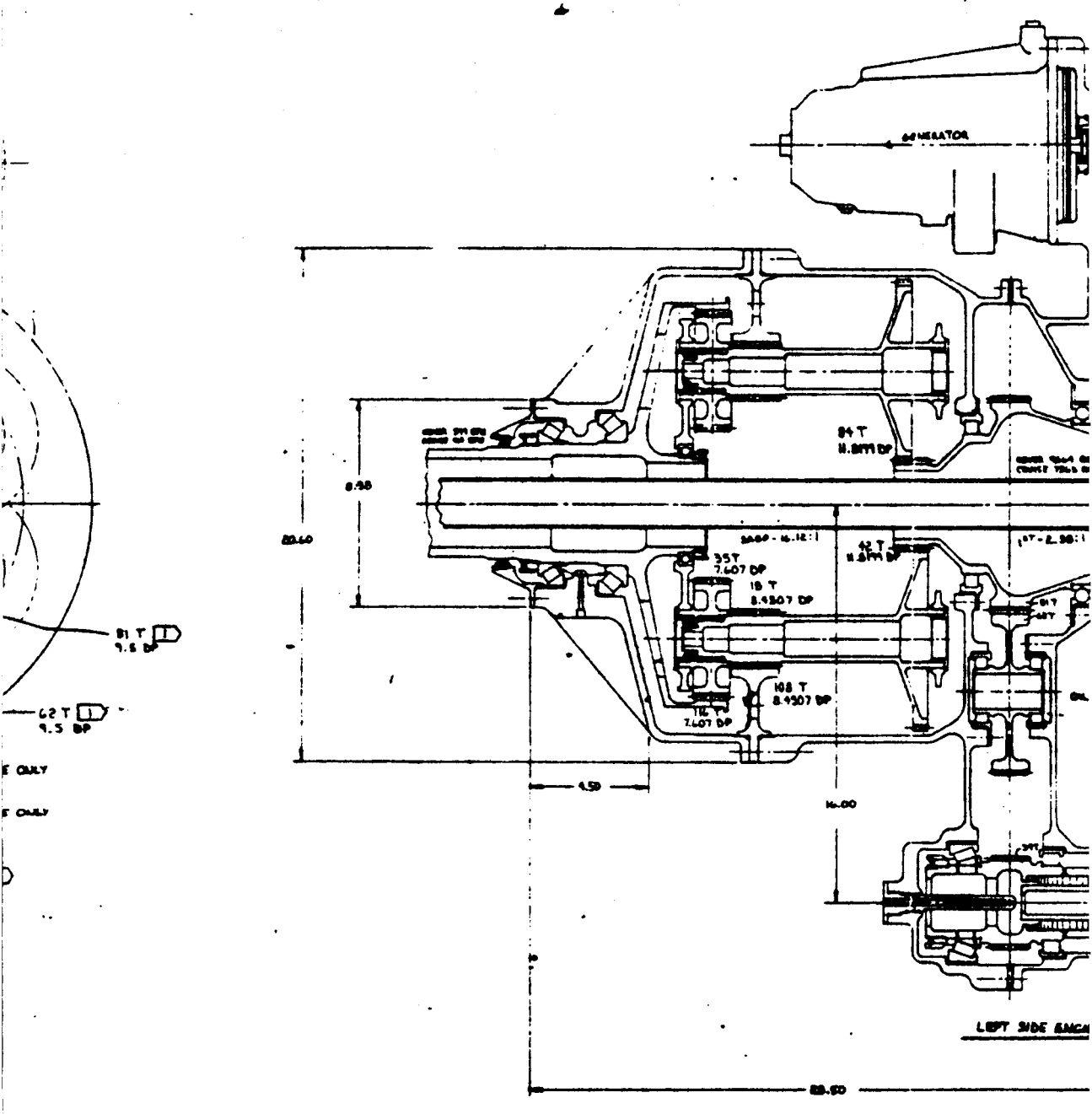
GENERATOR
84 T
35T
7.607 DP
18 T
8.4307 DP
108 T
8.4307 DP
16 T
7.607 DP
81 T
9.5 DP
62 T
9.5 DP
4.50
14.00
LEFT SIDE

SECTION A-

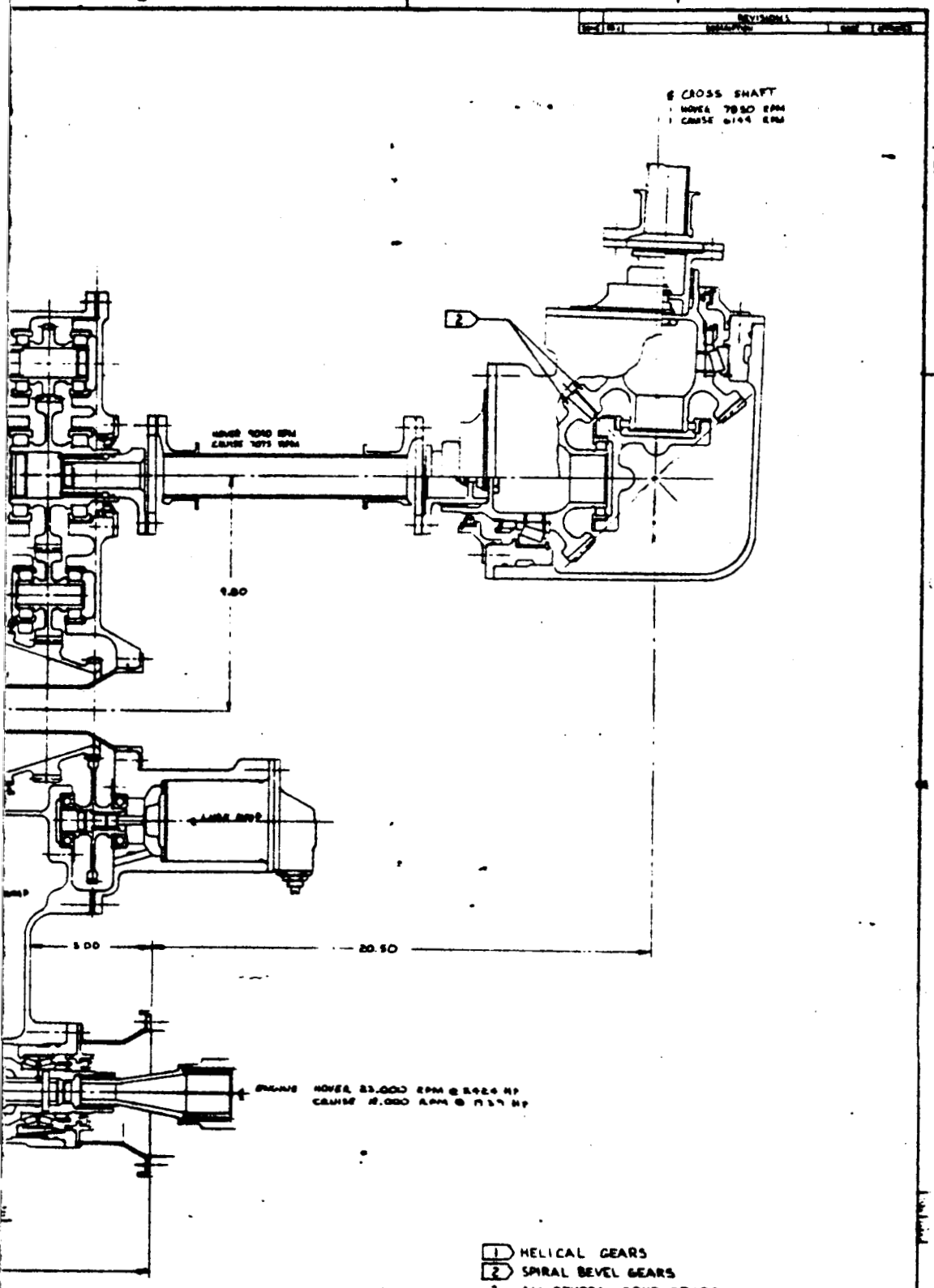

ONE-HALF SCALE
COPY OF ORIGINAL DWG.

BOEING VERTOL COMPANY
PHILADELPHIA PENNSYLVANIA

TTR MAIN ROTOR DRIVE SYSTEM - SELF-ALIGNING BEARINGLESS PLANETARY DESIGN

77272 BK32135

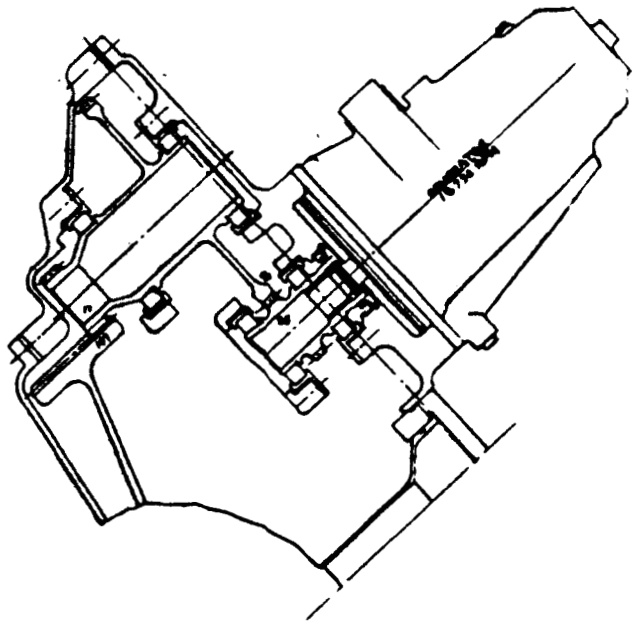

SECTION C-C

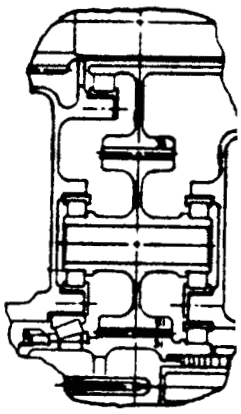

SECTION D-D

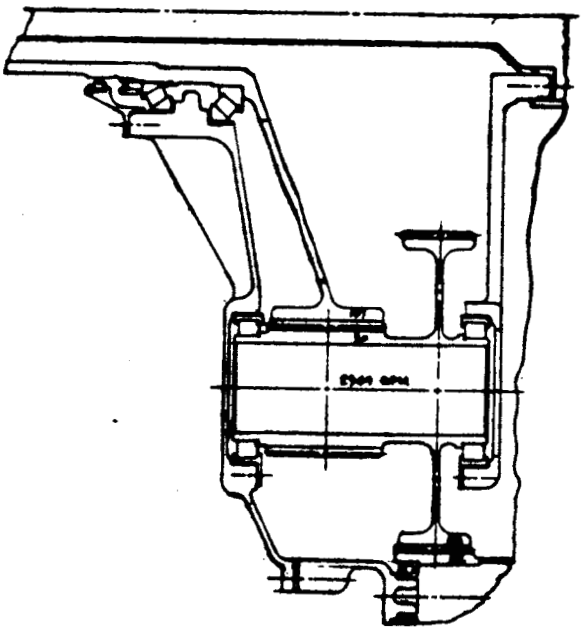

SECTION B-B

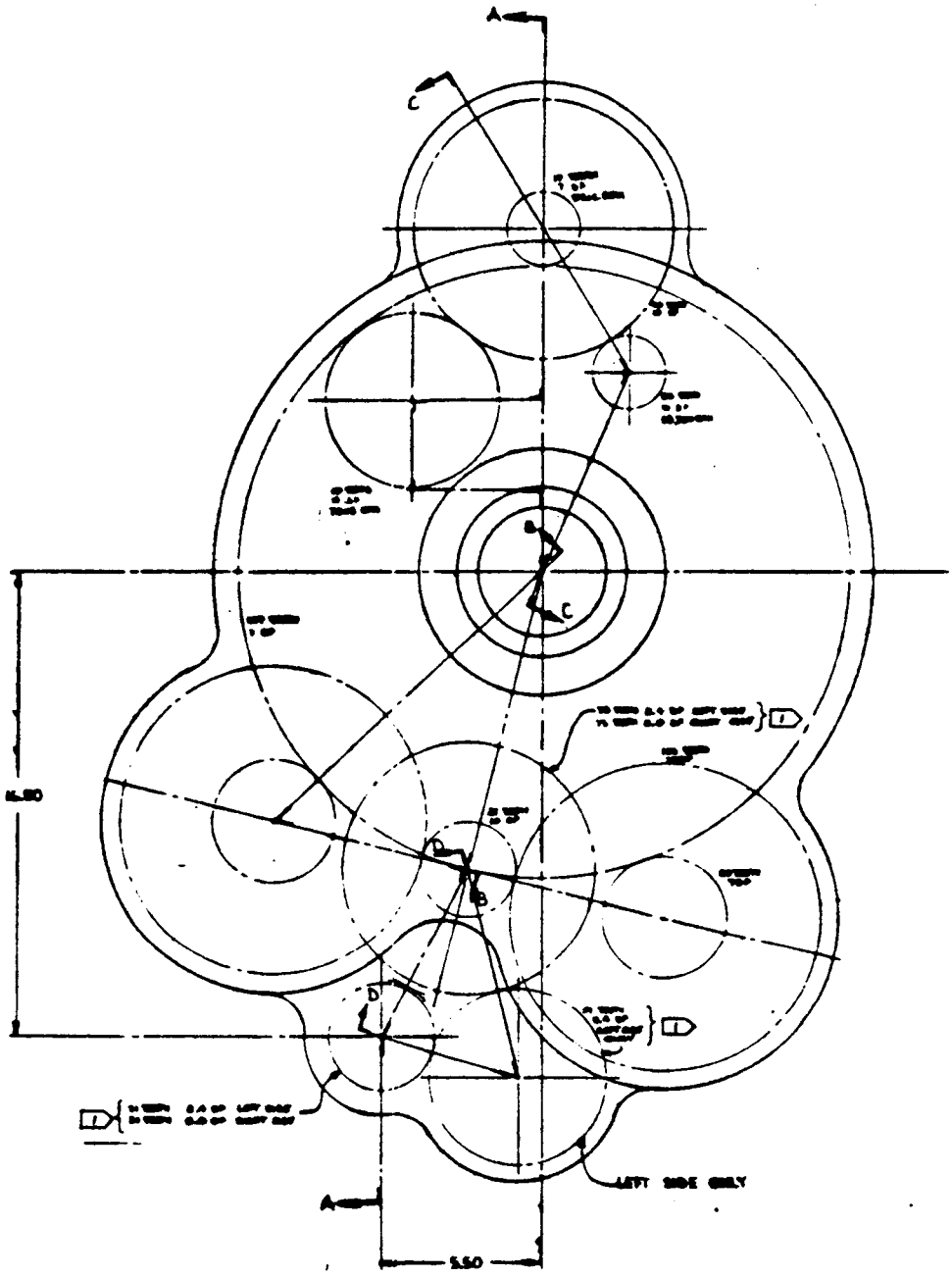

SK32136

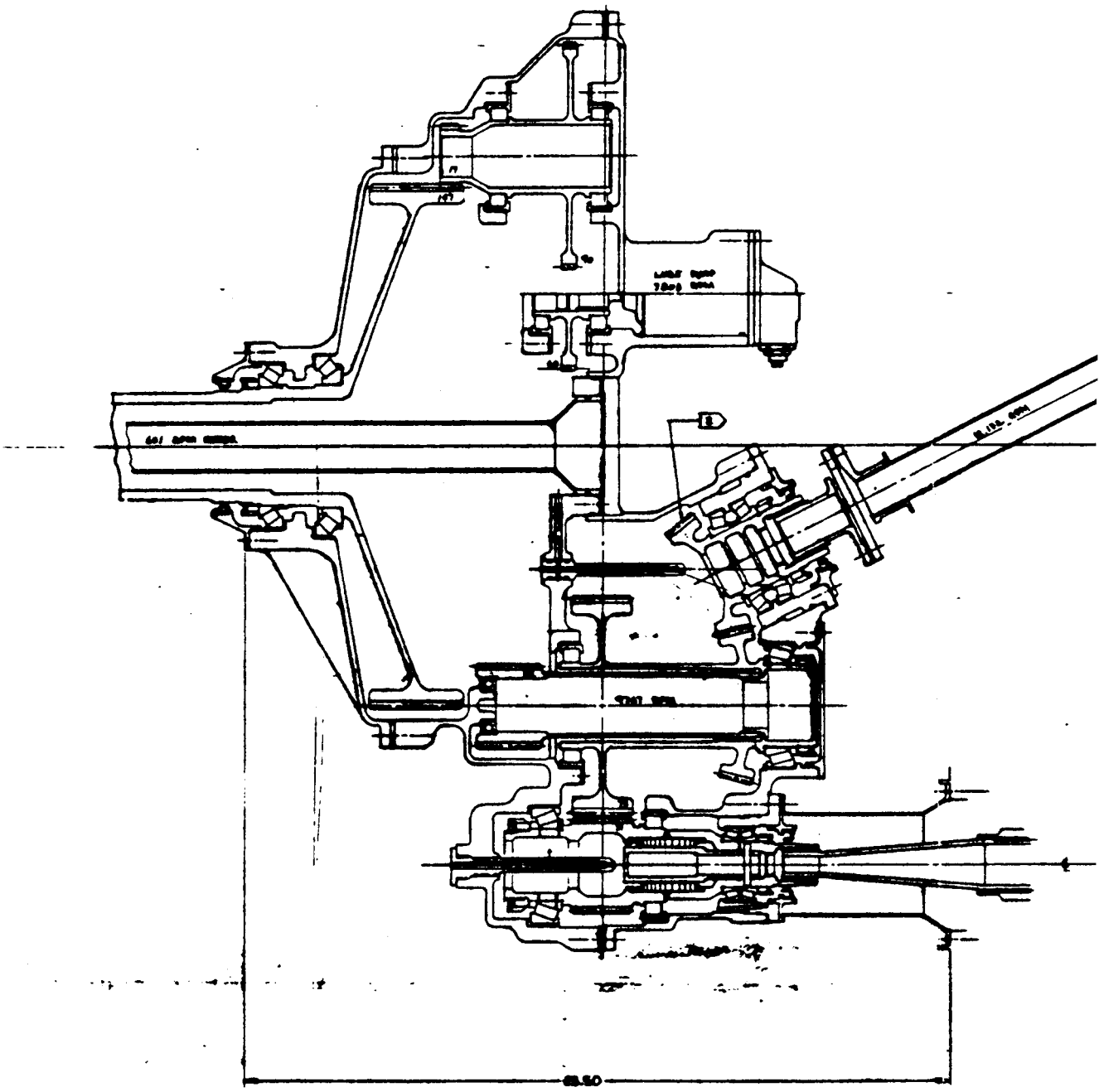

SECTION A-A

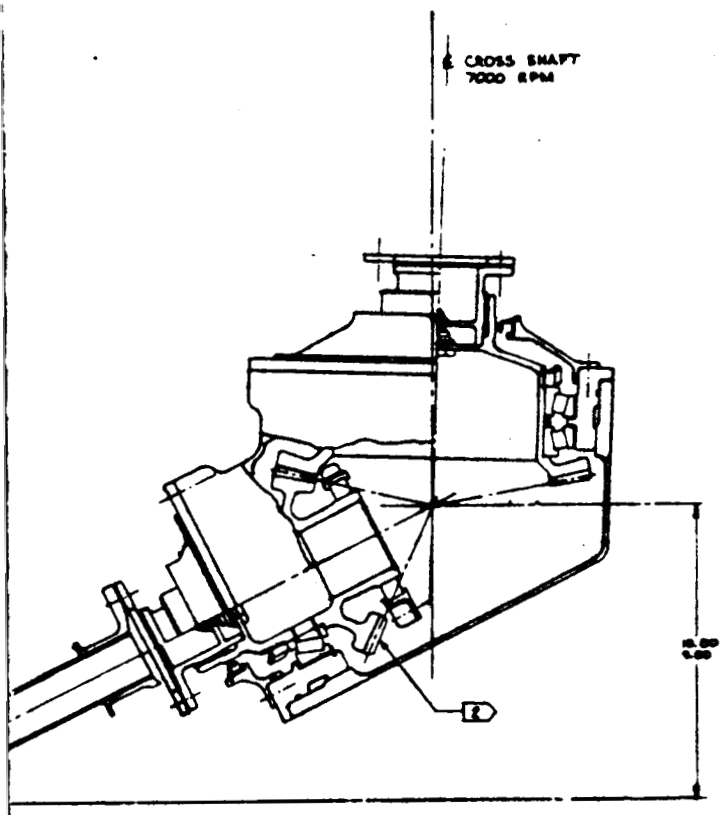

ENGINE
23,000 RPM/2484 hp @ HOVER
18,400 RPM/1191 hp @ CRUISE

1 HELICAL GEARS
2 SPIRAL BEVEL MESH
3. ALL OTHER GEARS ARE SPUR GEARS

ONE-HALF SCALE
COPY OF ORIGINAL DWG.

BOEING VERTOL COMPANY
PHILADELPHIA PENNSYLVANIA 19142

TTR MAIN ROTOR
DRIVE SYSTEM
SPLIT TORQUE DESIGN

J | 77272 | SK32136

SK32136

APPENDIX B

DETAILS OF BEARING TESTS

BOEING HELICOPTERS ART PROGRAM
BEARINGS TESTED

PHASE V – CONVENTIONAL BEARINGS

RUN NO.	BEARING NO.	BEARING CONFIG.	POSI-TION	SETTING PRERUN inches	SETTING POSTRUN inches	COMMENTS
1	C1	A,B,C,D	BC	0.0079		OIL FLOW TEST 7 PT/MIN
	C2	A,B,C,D	DC	0.0078		
	C3	A,B,C,D	DE	0.0026		
	C4	A,B,C,D	BE	0.0025		
2	C3	A,B,C,D	DE	0.0026		OIL FLOW RUN. 3 PT/MIN
	C4	A,B,C,D	BE	0.0025		
3	C3	A,B,C,D	DE	0.0026		OIL FLOW RUN. 2.5 PT/MIN
	C4	A,B,C,D	BE	0.0025		
4	C3	A,B,C,D	DE	0.0026		OIL FLOW RUN. 3 PT/MIN
	C4	A,B,C,D	BE	0.0025		OIL DRAIN HOLES CLOSED
5	C3	A,B,C,D	DE	0.0026		OIL DRAIN HOLES OPEN
	C4	A,B,C,D	BE	0.0025		
6	C3	A,B,C,D	DE	0.0026	0.0074	DAMAGED AT 23,000 RPM MINOR THRUST
	C4	A,B,C,D	BE	0.0025	0.0026	OK
7	C6	A,B,C,D	DE	0.0021	0.0016	SUCCESSFULLY COMPLETED MAJOR/MINOR
	C4	A,B,C,D	BE	0.0025	0.0027	SLOW AND RAPID THRUST SEQUENCE.
8	C5	A,B,C,D	DE	0.0030	—	DAMAGED AT 18,000 RPM MINOR THRUST.
9	C4	A,B,C,D	BE	0.0011	0.0013	OK
10	C6	A,B,C,D	DE	0.0014	0.0012	SUCCESSFULLY COMPLETED MAJOR/MINOR
	C4	A,B,C,D	BE	0.0027	0.0028	SLOW AND RAPID THRUST SEQUENCE.
11	C6	A,B,C,D	DE	0.0012	0.0012	OK
	C7	A,B,C,D	BE	0.0030	—	DAMAGED AT 18,000 RPM MINOR THRUST.
12	C6	A,B,C,D	DE	0.0013	0.0014	OK
	C8	A,B,C,E	BE	0.0021	—	"PEEK" CAGE DAMAGED AT 23,000 RPM

A – CBS600 CONE, CUP and CONE RIB
B – CBS600 ROLLERS
C – CBS600 CUP RIB
D – SAE4340 SILVER PLATED CAGE
E – PEEK CAGE
F – SILICON NITRIDE ROLLERS
G – ZIRCONIA CUP RIB

BOEING HELICOPTERS ART PROGRAM
BEARINGS TESTED

PHASE V – CONVENTIONAL BEARINGS (continued)

RUN NO.	BEARING NO.	BEARING CONFIG.	POSI-TION	SETTING PRERUN inches	SETTING POSTRUN inches	COMMENTS
13	C6	A,B,C,D	DE	0.0011	0.0014	OK
	C9	A,B,C,E	BE	0.0017	—	"PEEK" CAGE DAMAGED AT 23,000 RPM
14	C6	A,B,C,D	DE	0.0012	—	MINIMUM OIL FLOWS AT 12K AND 18K RPM
	C10	A,B,C,D	BE	0.0028	—	DRAIN HOLES CLOSED ON DE AND BE.
15	C6	A,B,C,D	DE	0.0018	—	125% OVERLOAD AND 110% OVERSPEED
	C10	A,B,C,D	BE	0.0023	—	DRAIN HOLES CLOSED ON DE AND BE.
16	C6	A,B,C,D	DE	0.0012	—	125% OVERLOAD AND 110% OVERSPEED
	C10	A,B,C,D	BE	0.0023	—	DRAIN HOLES CLOSED ON DE AND BE. REDUCED OIL FLOW TO DE AND BE
17	C6	A,B,C,D	DE	0.0012	0.0008	125% OVERLOAD RERUN
	C10	A,B,C,D	BE	0.0023	0.0025	
18	C6	A,B,C,D	DE	0.0018	0.0015	CAGE SPEED PICK-UP SHAKEDOWN
	C10	A,B,C,D	BE	0.0025	—	REVERSE THRUST @ 18000 RPM. BE DAMAGED

A – CBS600 CONE, CUP and CONE RIB
B – CBS600 ROLLERS
C – CBS600 CUP RIB
D – SAE4340 SILVER PLATED CAGE
E – PEEK CAGE
F – SILICON NITRIDE ROLLERS
G – ZIRCONIA CUP RIB

BOEING HELICOPTERS ART PROGRAM
BEARINGS TESTED

PHASE VI – HYBRID BEARINGS

RUN NO.	BEARING NO.	BEARING CONFIG.	POSI-TION	SETTING PRERUN inches	SETTING POSTRUN inches	COMMENTS
19	H11	A,C,D,F	BE	0.0018		OIL FLOW 3 PT/MIN
	H12	A,C,D,F	DE	0.0022		CUP DRAINS CLOSED
20	H11	A,C,D,F	BE	0.0018	0.0023	125% OVERLOAD AND 110% OVERSPEED
	H12	A,C,D,F	DE	0.0022	0.0013	DRAIN HOLES CLOSED ON DE AND BE.
						REDUCED OIL FLOW TO DE AND BE
21	H11	A,C,D,F	BE	0.0013	0.0013	OIL FLOW 3 PT/MIN
	H12	A,C,D,F	DE	0.0017	0.0019	CUP DRAINS OPEN
22	H11	A,C,D,F	BE	0.0013		SUCCESSFULLY COMPLETED MAJOR/MINOR
	H12	A,C,D,F	DE	0.0018		SLOW THRUST SEQUENCE.
23	H11	A,C,D,F	BE	0.0013	0.0011	SUCCESSFULLY COMPLETED MAJOR/MINOR
	H12	A,C,D,F	DE	0.0018	0.0016	RAPID THRUST SEQUENCE.
24	H13	A,F,G,D	DE	0.0009		REDUCED ENDPLAY
	H14	A,F,G,D	BE	0.0007		CUP SLOTS CLOSED
25	H13	A,F,G,D	DE	0.0009		SUCCESSFULLY COMPLETED MAJOR/MINOR
	H14	A,F,G,D	BE	0.0007		SLOW THRUST SEQUENCE.
26	H13	A,F,G,D	DE	0.0009	0.0002	SUCCESSFULLY COMPLETED MAJOR/MINOR
	H14	A,F,G,D	BE	0.0007	0.0005	RAPID THRUST SEQUENCE.
26	H13	A,F,G,D	DE	0.0002		CUP SLOTS OPEN
A	H14	A,F,G,D	BE	0.0005		
27	H13	A,F,G,D	DE	0.0002		SUCCESSFULLY COMPLETED MAJOR/MINOR
	H14	A,F,G,D	BE	0.0005		SLOW AND RAPID THRUST SEQUENCE.
28	H13	A,F,G,D	DE	0.0002	0.0003	125% OVERLOAD AND 110% OVERSPEED
	H14	A,F,G,D	BE	0.0005	0.0009	DRAIN HOLES CLOSED ON DE AND BE.

A – CBS600 CONE, CUP and CONE RIB
B – CBS600 ROLLERS
C – CBS600 CUP RIB
D – SAE4340 SILVER PLATED CAGE
E – PEEK CAGE
F – SILICON NITRIDE ROLLERS
G – ZIRCONIA CUP RIB

BOEING HELICOPTERS ART PROGRAM
BEARINGS TESTED

PHASE VI – HYBRID BEARINGS (continued)

RUN NO.	BEARING NO.	BEARING CONFIG.	POSI-TION	SETTING PRERUN inches	SETTING POSTRUN inches	COMMENTS
29	H13	A,F,G,D	DE	0.0029	0.0028	INCREASED ENDPLAY
	H14	A,F,G,D	BE	0.0031	0.0029	SUCCESSFULLY COMPLETED MAJOR/MINOR
						SLOW AND RAPID THRUST SEQUENCE.
30	H13	A,F,G,E	DE	0.0029	—	INSTALLED NEW 'PEEK' CAGES
	H14	A,F,G,E	BE	0.0034	—	
31	H13	A,F,G,E	DE	0.0029	—	SUCCESSFULLY COMPLETED MAJOR/MINOR
	H14	A,F,G,E	BE	0.0034	—	SLOW AND RAPID THRUST SEQUENCE.
32	H13	A,F,G,E	DE	0.0029	0.0027	125% OVERLOAD AND 110% OVERSPEED
	H14	A,F,G,E	BE	0.0034	0.0031	SUCCESSFULLY COMPLETED
33	H19	A,F,G,D	DE	0.0076	0.0076	ENDURANCE RUN NO. 1
	H20	A,F,G,D	BE	0.0069	—	BRG H20 (BE) WAS DAMAGED CAUSED
	H21	A,F,G,D	DC	0.0070	—	BY A COMPUTER LOCK-UP AND LOSS
	H22	A,F,G,D	BC	0.0069	—	OF DATA COLLECTION AND LIMITS.
						THE OTHER THREE BEARINGS ARE OK
34	H24	A,F,G,D	DE	0.0076	—	ENDURANCE RUN NO. 2
	H25	A,F,G,D	BE	0.0069	—	ONE ROLLER'S SURFACE PEELED IN BC BRG
	H21	A,F,G,D	DC	0.0070	—	DC & DC 183 HRS. 8.3 L-10
	H22	A,F,G,D	BC	0.0069	—	
35	H24	A,F,G,D	DE	0.0076	—	DE & BE SUSPENDED 247 HRS. 11.2 L-10
	H25	A,F,G,D	BE	0.0069	—	DC CUP SPALLED AFTER 141 HRS. 6.4 L-10
	H15	A,F,G,D	DC	0.0078	—	
	H17	A,F,G,D	BC	0.0075	—	

A – CBS600 CONE, CUP and CONE RIB
B – CBS600 ROLLERS
C – CBS600 CUP RIB
D – SAE4340 SILVER PLATED CAGE
E – PEEK CAGE
F – SILICON NITRIDE ROLLERS
G – ZIRCONIA CUP RIB

BOEING HELICOPTERS ART PROGRAM
BEARINGS TESTED

PHASE VII - OIL-OFF TEST RUNS

RUN NO.	BEARING NO.	BEARING CONFIG.	POSI-TION	SETTING PRERUN inches	SETTING POSTRUN inches	COMMENTS
36	H12	A,F,G,D	DE	0.0021	—	
	C1	A,B,C,D	BC	0.0079	—	
	C2	A,B,C,D	DC	0.0078	—	
	C6	A,B,C,D	BE	0.0051	—	C6 OIL-OFF 15 SEC. AT 23,000 RPM
37	H11	A,F,C,D	BE	0.0053	—	H11 OIL-OFF 95 SEC. AT 23,000 RPM
38	C18	A,B,C,D	BE	0.0035	—	RAN 62 MINUTES AT 5400 RPM, NO DAMAGE. THE OIL WAS RESUPPLIED, TEMP AND TORQUE RETURNED TO PREOIL-OFF.
39	H19	A,F,G,D	BE	0.0033	—	RAN 90 SECONDS OIL-OFF AT 12,000 RPM.
40	H12	A,F,C,D	BE	0.0095	0.0094	RAN 60 MINUTES OIL-OFF AT 12,000 RPM.
41	H17	A,F,C,D	BE	0.0093	—	RAN 90 SECONDS OIL-OFF AT 18,000 RPM.

PHASE VIII - OIL COMPARISON PERFORMANCE TEST

42	H24	A,F,G,D	DE	0.0079	0.0075	THIS RUN WAS A PERFORMANCE
	C1	A,B,C,D	BC	0.0079	—	COMPARISON TEST BETWEEN TWO OILS:
	C2	A,B,C,D	DC	0.0078	—	5.0 cSt EXXON ETO 25 AND 7.5 cSt
	H25	A,F,G,D	BE	0.0064	0.0063	EXXON ETO 274

A - CBS600 CONE, CUP and CONE RIB
B - CBS600 ROLLERS
C - CBS600 CUP RIB
D - SAE4340 SILVER PLATED CAGE
E - PEEK CAGE
F - SILICON NITRIDE ROLLERS
G - ZIRCONIA CUP RIB

APPENDIX C

SOURCE CODE LISTING FOR BEARING-LIFE CALCULATION USING NEW SKF LIFE THEORY AS IMPLEMENTED IN PC-SHABERTH

```
$DEBUG
      SUBROUTINE FLMFAC ( X, FL )
C
C     THIS SUBROUTINE CALCULATES THE LUBRICATION FILM FACTOR BASED
C     ON THE ASME MEAN CURVE DETERMINED FROM TALLIAN'S AND SKURKA'S
C     DATA, PUBLISHED IN "LIFE ADJUSTMENT FACTORS FOR BALL AND ROLLER
C     BEARINGS", FIG. 2, PAGE 13.
C
C     PROGRAM INPUT, X = FILM THICKNESS TO SURFACE ROUGHNESS RATIO
C
C
C     PROGRAM OUTPUT, FL = LUBRICATION FACTOR
C
C     REFER TO LETTER REPORT NO. AL79P007L FOR DOCUMENTATION AND
C     ANALYSIS METHODS
C
C     PROGRAMMED BY G. DYBA AND R. J. KLECKNER
C
C
      IF( X .LT. 0.6 ) FL = 0.2100005
      IF( X .GE. 0.6 .AND. X .LE. 1.49 )
     $ FL = -1.0579967 + 5.1283646*X - 6.1138363*X**2 - 0.47964478*X**3
     $      + 5.047802*X**4 - 1.9979973*X**5
      IF( X .GT. 1.49 .AND. X .LT. 1.50 ) FL = 3.6*X - 3.734120601
      IF( X .GE. 1.50 .AND. X .LE. 10.0 )
     $ FL = -1.5791321 + 3.4671307*X - 1.064187*X**2 + 0.13649064*X**3
     $      - 0.36827847E-2*X**4 - 0.4392534E-3*X**5 + 0.30138053E-5
     $      *X**6 + 0.17576485E-5*X**7
C
      IF( X .GT. 10.0 ) FL = 3.0
C
C     NORMALIZE TO ONE DECIMAL PLACE ACCURACY
C
      INTFL = FL * 100.
      FL = INTFL/100.
C
C
      RETURN
      END
      SUBROUTINE CALCLF (BD,BVAR)
C
C     THIS SUBROUTINE CALCULATES L10 LIFE FOR ONE BEARING AT A TIME
C
      DIMENSION BD(1830), BVAR(36,30)
      COMMON /LIFRED/ SB(2,5), NSYMY
CMR
CMR   ADDED FOURTH SUBSCRIPT TO Q ARRAY CORRESPONDING TO BEARING NUMBER
CMR                                    8-21-89 : M. RAGEN
      COMMON /ROLOAD/ Q(20,2,30,5)
CMR
      COMMON /BRGNUM/ NBRG
      COMMON /NLIF3/  NEWLIF(5),FLIMOR(5),FLIMIR(5),RESOR(5),RESIR(5),
     $                ANL(2,5),FILRAT(5)
CMR
CMR   WRITE MESSAGE ON SCREEN INDICATING NEW LIFE THEORY CALCULATION
CMR
      IF (NEWLIF(NBRG) .GT. 0) WRITE (*,1000) NBRG
 1000 FORMAT (/,10X,'CALCULATING IN NEW SKF LIFE ROUTINE FOR BEARING ',
     $        I1,'.')
C
```

```
C     SET SOME PARAMETERS NEEDED IN LIFE SUBROUTINE
C
      ITYP = BD(1)
      IDOZ = BD(6)
      IF (NSYMY .EQ.2) IDOZ = 1
C
C     DETERMINE INDEX OF HEAVIEST LOADED ROLLING ELEMENT (IMAX)
C
      QMAX = 0.
      IMAX = 1
      DO 100 I=1,IDOZ
      IF (BVAR(7,I) .GT. QMAX) THEN
         IMAX = I
         QMAX = BVAR(7,I)
      ENDIF
  100 CONTINUE
C
      CALL LIFE (ITYP, BD(135), BD(136), BD(141), BD(22), BD(124), IDOZ,
     $  BD(21), BD(111), BD(43), BD(361), BD(221), BVAR(13,1),
     $  BVAR(7,1), Q, BD(211), BD(213), BD(209), BD(299), BD(6), IMAX,
     $  BD(131), BD, BVAR)
C
      RETURN
      END
      SUBROUTINE LIFE( IBTYP, D, DM, W, WN, COSA, IZ, F, RPS, A2, RK,   00021900
     $  SIG, HMIN, P, Q, RWLIF, BLIF, FL, HSS, Z, IMAX, EP,
     $  BD, BVAR)
C
C     THIS SUBROUTINE CALCULATES L10 LIFE FOR A BALL OR ROLLER BEARING
C     ACCORDING TO BOTH THE LUNDBERG-PALMGREN THEORY AND THE NEW SKF
C     LIFE THEORY (IOANNIDES & HARRIS).
C
C     INPUT DATA:
C     -----------
C        IBTYP - BEARING TYPE (-1=BALL, 1=TAPERED, 2=CYLINDRICAL)
C        D - ROLLING ELEMENT DIAMETER
C        DM - PITCH DIAMETER
C        W(2) - WIDTH OF ROLLER SLICE FOR OUTER & INNER RING
C        WN - NUMBER OF ROLLER SLICES
C        COSA - COSINE OF THE NOMINAL CONTACT ANGLE
C        IZ - NUMBER OF ROLLING ELEMENTS
C        F(2) - RACEWAY GROOVE RADIUS / BALL DIAMETER FOR OUTER
C               AND INNER RACEWAY
C        RPS(2) - ROTATIONAL SPEED (RADIANS/SEC)
C        A2(2) - MATERIAL LIFE FACTOR (A2) FOR OUTER & INNER RING
C        RK(K,M) - ROLLER RADIUS AT CENTER OF SLICE K
C            K = ROLLER SLICE NUMBER (1-20)
C            M = RACEWAY NUMBER (1=O.R., 2=I.R.)
C        SIG(2) - COMPOSITE SURFACE ROUGHNESS FOR OUTER AND INNER
C                 RACEWAY CONTACTS
C        HMIN(2,J) - MINIMUM FILM THICKNESS AT OUTER & INNER RACEWAY
C            J = ROLLING ELEMENT NUMBER (1-30)
C        P(2,J) - ROLLER / RACEWAY CONTACT LOAD AT OUTER & INNER RACEWAY
C            J = ROLLING ELEMENT NUMBER (1-30)
C        Q(K,M,J,NBRG) - ROLLER SLICE LOAD
C            K = ROLLER SLICE NUMBER (1-20)
C            M = RACEWAY NUMBER (1=O.R., 2=I.R.)
C            J = ROLLING ELEMENT NUMBER (1-30)
C            NBRG = BEARING NUMBER (1-5)
C        Z - NUMBER OF ROLLING ELEMENTS
```

```
C         IMAX - INDEX OF ROLLER WITH MAXIMUM LOAD
C         EP(2) - INVERSE OF ROLLER / RACEWAY EFFECTIVE MODULUS OF
C                 ELASTICITY ( [(1.-NU1**2)/E1 + (1.-NU2**2)/E2] / 2 )
C         BD(K,NBRG) - BEARING DATA ARRAY
C             K = DATA ITEM (1-1830)
C             NBRG = BEARING NUMBER (1-5)
C         BVAR(K,J) - ROLLING ELEMENT OPERATING PARAMETER ARRAY
C             K = DATA ITEM (1-36)
C             J = ROLLING ELEMENT NUMBER (1-30)
C         NEWLIF(5) - FLAG FOR NEW LIFE THEORY CALCULATION
C                     (IF > 0, LIFE IS CALCULATED WITH NEW LIFE THEORY)
C         FLIMOR(5) - FATIGUE LIMIT FOR OUTER RING (VON-MISES CRITERION)
C         FLIMIR(5) - FATIGUE LIMIT FOR INNER RING (VON-MISES CRITERION)
C         RESOR(5) - RESIDUAL STRESS FOR OUTER RING
C         RESIR(5) - RESIDUAL STRESS FOR INNER RING
C         ANL(2,5) - MATERIAL CONSTANT FOR OUTER AND INNER RING USING
C                    NEW LIFE THEORY
C         FILRAT(5) - ABSOLUTE FILTER RATING (MICRONS)
C
C      OUTPUT DATA:
C      ------------
C         RWLIF(2) - L10 LIFE FOR OUTER & INNER RING (OLD THEORY)
C         BLIF - BEARING LIFE (OLD THEORY)
C         FL(2) - LUBRICANT LIFE FACTOR (A3) FOR OUTER & INNER RING
C         HSS(2) - LAMBDA RATIO (H/SIGMA) FOR OUTER & INNER RING
C         PHI(K,M,J) - RATIO OF LIFE ACCORDING TO NEW THEORY TO LIFE
C                        ACCORDING TO OLD THEORY
C               WHERE  K = ROLLER SLICE NUMBER (1-20) [ROLLER BEARING]
C                          OR BEARING NUMBER (1-5) [BALL BEARING]
C                      M = RACEWAY NUMBER (1=O.R., 2=I.R.)
C                      J = ROLLING ELEMENT NUMBER (1-30)
C         CONTFC(2,5) - CONTAMINATION LIFE REDUCTION FACTOR FOR OR & IR
C         RWLIFN(2,5) - L10 LIFE FOR OUTER AND INNER RING (NEW THEORY)
C         BLIFN(5) - L10 LIFE FOR BEARING (NEW THEORY)
C                                                                       00022100
C                                                                       00022200
      DIMENSION W(2), F(2), RPS(2), A2(2), HMIN(36,30), P(36,30),       00022300
     $  Q(20,2,30,5), RWLIF(2), C(2), EXP(2), SIG(2), FL(2), HSS(2)
     $  , RK(20,2), EP(2)                                               00022500
      DIMENSION BD(1830), BVAR(36,30)
C                                                                       00022600
      COMMON /LIFRED/ SB(2,5), NSYMY                                    00022700
      COMMON /BRGNUM/ NBRG                                              00022800
      COMMON /NLIF2/  PHI(20,2,30), RWLIFN(2,5), BLIFN(5), CONTFC(2,5)
      COMMON /NLIF3/  NEWLIF(5),FLIMOR(5),FLIMIR(5),RESOR(5),RESIR(5),
     $                ANL(2,5),FILRAT(5)
      COMMON /NLIF4/  SROT(2,5), SFIT(2,5)
C                                                                       00022900
      REAL HMIN,HSS                                                     00023000
      DATA C/1., -1./                                                   00023100
      EPSTL = 32.527473E6                                               00023200
      WDIFF = ABS(RPS(1)-RPS(2))                                        00023300
      GAM = D * COSA / DM                                               00023400
      IF( IBTYP ) 10, 10, 50                                            00023500
C                                                                       00023600
C     ... BALL BEARING                                                  00023700
C
   10 E = 1.11111111                                                    00023800
CMR
CMR   CALCULATE RATIOING FACTORS TO ENABLE LIFE CALCULATION USING
```

```
CMR   "NEW SKF LIFE THEORY".
CMR
      IF (NEWLIF(NBRG) .GT. 0) THEN
        CALL NEWLFB (BD(1),BD(72),BD(74),BD(77),BD(79),DM,D,Z,RPS(2),
     $             RPS(1),BD(59)/2.,BD(60)/2.,BD(61)/2.,BD(62)/2.,BD(7),
     $             BD(182),BD(184),NSYMY,BVAR,FLIMOR(NBRG),FLIMIR(NBRG),
     $             RESOR(NBRG),RESIR(NBRG),SROT(1,NBRG),SFIT(1,NBRG),PHI)
      ENDIF
CMR
      DO 30 M = 1, 2                                                    00023900
        EXP(M) = 3.333333                                               00024000
        IF ( ABS(RPS(M)) .GT. 0. ) EXP(M) = 3.                          00024100
C       ... LIFE OF A RACEWAY, RWLIF                                    00024200
      QCM = 7080. * ((2.*F(M) / (2.*F(M)-1.)) ** 0.41 *                 00024300
     $       (1. + C(M)*GAM) ** 1.39 / (1. - C(M)*GAM) ** .3333 /       00024400
     $       Z ** .3333 * (GAM/COSA) ** .3 ) * D ** 1.8                 00024500
C                                                                       00024600
C     IF LOADING IS PURE THRUST, USE CAPACITY REDUCTION FACTOR OF       00024700
C     1 - SIN(B)/3. FOR THE RACEWAY WHICH ROTATES.                      00024800
C                                                                       00024900
        IF (NSYMY .EQ. 2 .AND. ABS(RPS(M)) .GT. 0.)                     00025000
     $    QCM = QCM * (1. - SB(M,NBRG) / 3.)                            00025100
        QMJ = 0.                                                        00025200
        DO 20 J = 1, IZ                                                 00025300
          IF( P(M,J) .LE. 0. ) GO TO 20                                 00025400
          QMJ = QMJ + P(M,J)**EXP(M)                                    00025500
          IF (SIG(M) .LT. 1.E-20) GO TO 20                              00025600
          IF (J .EQ. IMAX)     HSS(M) = HMIN(M,J)/SIG(M)
          IF (J .EQ. IMAX)     HMINM = HMIN(M,J)
   20     CONTINUE                                                      00025800
CMR
CMR   CALCULATE RACEWAY LIFE ACCORDING TO NEW SKF THEORY
CMR
      IF (NEWLIF(NBRG) .GT. 0) THEN
        SUM = 0.
        CALL CONTAM (FILRAT(NBRG),HMINM,CONTFC(M,NBRG))
        DO 25 J=1,IZ
          IF (P(M,J) .LE. 0.) GO TO 25
          RINGLF = (QCM/P(M,J))**3
          SUM = SUM + (PHI(NBRG,M,J)*RINGLF)**(-EXP(M)/3.)
   25   CONTINUE
        RWLIFN(M,NBRG) = 1.E30
        IF (SUM .GT. 0.) THEN
          RWLIFN(M,NBRG) = (SUM/Z)**(-3./EXP(M))
          RWLIFN(M,NBRG) = ANL(M,NBRG) * 1745./WDIFF * RWLIFN(M,NBRG)
     $                     *(EPSTL*EP(M))**6.3 * CONTFC(M,NBRG)
        ENDIF
      ENDIF
CMR
        FL(M) = 1.                                                      00025900
        IF (HSS(M) .GT. 0.) CALL FLMFAC( HSS(M), FL(M))
        QEM = ( QMJ/IZ )**(1./EXP(M))                                   00026200
        RWLIFI = 1.E30                                                  00026300
        IF ( QEM .NE. 0. ) RWLIFI = ( QCM/QEM )**3 * FL(M)              00026400
        RWLIF(M) = A2(M)*1745./WDIFF * RWLIFI * ( EPSTL*EP(M) )**6.3    00026500
   30   CONTINUE                                                        00026600
      GO TO 100                                                         00026700
C                                                                       00026800
C     ... LIFE OF A ROLLER BEARING, BLIF                                00026900
C
```

```
   50 E = 1.125                                                          00027000
      NW = IFIX(WN)                                                      00027100
      REDFCT = 1.0                                                       00027200
CMR
CMR   CALCULATE RATIOING FACTORS TO ENABLE LIFE CALCULATION USING
CMR   "NEW SKF LIFE THEORY".
CMR
      IF (NEWLIF(NBRG) .GT. 0) THEN
        CALL NEWLFR (BD(1),BD(141),Q,BD(441),NW,BD(72),BD(74),BD(77),
     $             BD(79),DM,D,Z,RPS(2),RPS(1),BD(59)/2.,BD(60)/2.,
     $             BD(61)/2.,BD(62)/2.,BD(7),BD(182),BD(184),NSYMY,BVAR,
     $             FLIMOR(NBRG),FLIMIR(NBRG),RESOR(NBRG),RESIR(NBRG),
     $             SROT(1,NBRG),SFIT(1,NBRG),PHI)
      ENDIF
CMR
      DO 80 M = 1, 2                                                     00027300
        RLNSUM = 0.
        RWLIFI = 0.                                                      00027400
        EXP(M) = 4.5                                                     00027500
        IF ( ABS(RPS(M)) .GT. 0. ) EXP(M) = 4.                           00027600
C
C       ... LIFE OF A RACEWAY, RWLIF                                     00027700
C
        RWLIF(M) = 0.                                                    00027800
C                                                                        00027900
C     IF YOU HAVE TAPERED BEARING SUBJECT TO PURE THRUST LOAD, USE A     00028000
C     CAPACITY REDUCTION FACTOR OF 1 - 0.15*SIN(B) FOR THE RACEWAY       00028100
C     WHICH ROTATES.                                                     00028200
C                                                                        00028300
        IF (NSYMY .EQ. 2 .AND. IBTYP .EQ. 1 .AND. ABS(RPS(M)) .GT. 0.)   00028400
     $    REDFCT = 1. - SB(M,NBRG) * 0.15                                00028500
C
        DO 70 K = 1, NW                                                  00028600
C
C         ... LIFE OF A LAMINUM, AMLIF                                   00028700
C
          DA = .683                                                      00028800
          IF( K.EQ.1 .OR. K.EQ.NW )      DA = .4525                      00028900
          QCMK  = 49500. * DA * (2.*RK(K,M)*(1.+C(M)*GAM))**1.0740741    00029000
     $    * W(M) ** 0.77777778 * (D/DM) ** 0.22222222 / (IZ*(1.- C(M)    00029100
     $    * GAM)) ** 0.25                                                00029200
          QEMK = 0.                                                      00029300
C
          DO 60 J = 1, IZ                                                00029400
            IF( Q(K,M,J,NBRG) .LE. 0. ) GO TO 60
            QEMK = QEMK + Q(K,M,J,NBRG)**EXP(M)
            IF (SIG(M) .LT. 1.0E-20 ) GO TO 60                           00029700
            IF ( J .EQ. IMAX) HSS(M) = HMIN(M,J)/SIG(M)                  00029800
            IF (J .EQ. IMAX) HMINM = HMIN(M,J)
   60     CONTINUE                                                      00029900
C
          QEMK = ( QEMK/IZ )**(1./EXP(M))                                00030000
          AMLIFI = ( QEMK/QCMK )**4                                      00030100
CMR
CMR   CALCULATE LIFE OF EACH LAMINUM USING NEW LIFE THEORY
CMR
      IF (NEWLIF(NBRG) .GT. 0) THEN
        AMLIFN = 1.E30
        SUM = 0.
        DO 65 J=1,IZ
```

```
          IF (Q(K,M,J,NBRG) .LE. 0.) GO TO 65
          AMLIFN = (QCMK/Q(K,M,J,NBRG))**4
          SUM = SUM + (PHI(K,M,J)*AMLIFN) ** (-EXP(M)/4.)
   65   CONTINUE
C
        IF (SUM .GT. 0.) AMLIFN = (SUM/Z) ** (-4./EXP(M))
        RLNSUM = RLNSUM + AMLIFN ** (-E)
      ENDIF
CMR
C
   70 RWLIFI = RWLIFI + AMLIFI**E                                    00030300
C
      CALL FLMFAC( HSS(M), FL(M))                                    00030400
      IF( HSS(M) .EQ. 0. ) FL(M) = 1.                                00030500
C                                                                    00030700
        IF ( RWLIFI .NE. 0 ) GO TO 75                                00030800
        RWLIF(M) = 1.E+30                                            00030900
        GO TO 80                                                     00031000
   75   RWLIF(M) = A2(M) * 1745. * FL(M) / WDIFF * RWLIFI**(-1./E)   00031100
     $  * ( EPSTL*EP(M) )**5.185                                     00031200
        RWLIF(M) = RWLIF(M) * REDFCT ** 4                            00031300
CMR
CMR   CALCULATE LIFE OF RACEWAY USING NEW LIFE THEORY
CMR
      IF (NEWLIF(NBRG) .GT. 0) THEN
        CALL CONTAM (FILRAT(NBRG),HMINM,CONTFC(M,NBRG))
        RWLIFN(M,NBRG) = 1.E30
        IF (RLNSUM .GT. 0.) THEN
           RWLIFN(M,NBRG) = RLNSUM**(-1./E)
           RWLIFN(M,NBRG) = RWLIFN(M,NBRG) * ANL(M,NBRG) * 1745./WDIFF
     $             * (EPSTL*EP(M))**5.185 * REDFCT**4 * CONTFC(M,NBRG)
        ENDIF
      ENDIF
CMR
   80 CONTINUE                                                       00031400
  100 BLIF = ( RWLIF(1)**(-E) + RWLIF(2)**(-E) )**(-1./E)            00031500
CMR
CMR   CALCULATE BEARING LIFE ACCORDING TO NEW SKF THEORY
CMR
      IF (NEWLIF(NBRG) .GT. 0) THEN
      BLIFN(NBRG) = (RWLIFN(1,NBRG)**(-E)+RWLIFN(2,NBRG)**(-E))**(-1./E)
      ENDIF
CMR
      RETURN                                                         00031600
      END                                                            00031700
C
      SUBROUTINE CONTAM (F, H, CONTFC)
C
C     THIS SUBROUTINE CALCULATES THE LIFE REDUCTION FACTOR DUE TO
C     CONTAMINATION. A CURVE FIT IS USED TO ESTABLISH THE RELATIVE
C     LIFE AS A FUNCTION OF THE FILTER SIZE / FILM THICKNESS
C     BASED ON THE DATA OF SAYLES & MACPHERSON.
C     M. RAGEN : 2-15-90
C
C     INPUT PARAMETERS:
C     -----------------
C          F - FILTER ABSOLUTE RATING (MICRONS)
C          H - EHD FILM THICKNESS (INCHES)
C
C     OUTPUT PARAMETERS:
```

```
C     ------------------
C          CONTFC - CONTAMINATION LIFE MULTIPLIER
C
C     TRAP INVALID VALUES OF FILM THICKNESS
C
      CONTFC = 1.
      IF (H .LT. 1.E-24) RETURN
C
C     CONVERT FILM THICKNESS FROM INCHES TO MICRONS
C
      HMIC = H * 25400.
C
C     CALCULATE RATIO OF FILTER SIZE TO FILM THICKNESS
C
      FDH = F / HMIC
C
C     CALCULATE CONTAMINATION LIFE MULTIPLIER
C
      A = 0.9213
      B = 0.089922
      CONTFC = 1. / (A + B*FDH)
      IF (CONTFC .GT. 1.) CONTFC = 1.
C
      RETURN
      END
CMR - ------------------------------------------------------------------
CMR   NEW LIFE THEORY FOR BALL BEARINGS
CMR - ------------------------------------------------------------------
      SUBROUTINE NEWLFB (BTYPE,POISIR,POISOR,RHOIR,RHOOR,DM,DW,Z,OMEGIR,
     $                   OMEGOR,R1,R2,R3,R4,PD,FPIR,FPOR,NSYMY,BVAR,
     $                   SIGLOR,SIGLIR,SRESOR,SRESIR,SROT,SFIT,PHI)
C
C     THIS SUBROUTINE CALCULATES RATIOING FACTORS THAT ENABLE
C     CALCULATION OF BEARING LIVES ACCORDING TO THE NEW SKF LIFE THEORY.
C
C     INPUT DATA:
C        BTYPE - BEARING TYPE (-1=BALL,1=TAPER,2=CYLINDRICAL)
C        POISIR,POISOR - POISSON'S RATIO FOR INNER RING, OUTER RING
C        RHOIR,RHOOR - DENSITY FOR INNER RING, OUTER RING (LB/IN**3)
C        DM - BEARING PITCH DIAMETER (IN)
C        DW - ROLLING ELEMENT DIAMETER (IN)
C        Z - NUMBER OF ROLLING ELEMENTS
C        OMEGIR,OMEGOR - ROTATIONAL SPEED FOR INNER RING, OUTER RING
C                        (RAD/SEC)
C        R1,R2 - INSIDE AND OUTSIDE RADIUS FOR INNER RING (IN)
C        R3,R4 - INSIDE AND OUTSIDE RADIUS FOR OUTER RING (IN)
C        PD - DIAMETRAL CLEARANCE (IN)
C        FPIR,FPOR - OPERATING FIT PRESSURE FOR INNER RING, OUTER RING
C                    (PSI)
C        NSYMY - LOAD SYMMETRY FLAG
C        BVAR(K,I) - ARRAY CONTAINING ROLLING ELEMENT OPERATING DATA
C          WHERE K = PARAMETER NUMBER (1-30)
C                I = ROLLING ELEMENT NUMBER
C          NOTE : BVAR(33,I) = MAXIMUM HERTZ STRESS AT OUTER RACE
C                 BVAR(34,I) = MAXIMUM HERTZ STRESS AT INNER RACE
C        ------------------------------------------------------------
C        A(K,J,I) - CONTACT SEMI-MAJOR AXIS (IN)
C        B(K,J,I) - CONTACT SEMI-MINOR AXIS (IN)
C        PMAX(K,J,I) - MAXIMUM HERTZIAN CONTACT PRESSURE (PSI)
C        BETA(K,J,I) - AVERAGE FRICTION COEFFICIENT FOR CONTACT
```

```
C          WHERE K = BEARING NUMBER
C                J = RING NUMBER (1=OUTER,2=INNER)
C                I = ROLLING ELEMENT NUMBER
C        ------------------------------------------------------------
C        SIGLOR - FATIGUE LIMIT STRESS FOR OUTER RING (PSI)
C        SIGLIR - FATIGUE LIMIT STRESS FOR INNER RING (PSI)
C        SRESOR - RESIDUAL STRESS FOR OUTER RING (PSI)
C        SRESIR - RESIDUAL STRESS FOR INNER RING (PSI)
C
C
C     OUTPUT DATA:
C        SROT(1) - HOOP STRESS DUE TO ROTATION AT OUTER RACEWAY (PSI)
C        SROT(2) - HOOP STRESS DUE TO ROTATION AT INNER RACEWAY (PSI)
C        SFIT(1) - HOOP STRESS DUE TO FITUP AT OUTER RACEWAY (PSI)
C        SFIT(2) - HOOP STRESS DUE TO FITUP AT INNER RACEWAY (PSI)
C        PHI(K,J,I) - LIFE RATIO (NEW LIFE / LUNDBERG PALMGREN)
C          WHERE K = BEARING NUMBER (NBRG)
C                J = RING NUMBER
C                I = ROLLING ELEMENT NUMBER
C
      DIMENSION PHI(20,2,30), SROT(2), SFIT(2), BVAR(36,30)
      COMMON /BANDA/  A(5,2,30), B(5,2,30)
      COMMON /BRGNUM/ NBRG
      COMMON /MUAVG/  AMUEHD(5,2,50), AMUASP(5,2,50)
      COMMON /NLIF1/  BETA(2,30)
C
C     CALCULATE HOOP STRESSES DUE TO ROTATION AND FIT PRESSURE
C
      CALL HOOPST (POISIR,POISOR,RHOIR,RHOOR,DM,DW,OMEGIR,OMEGOR,
     $             R1,R2,R3,R4,PD,FPIR,FPOR,SROT,SFIT)
CMR
CMR   WRITE (6,1000) SROT(1),SROT(2),SFIT(1),SFIT(2)
C1000 FORMAT ('1',//,2X,'HOOP STRESSES DUE TO ROTATION:',/,2(5X,E14.7),
CMR  $        /,2X,'HOOP STRESSES DUE TO FIT:',/,2(5X,E14.7))
CMR   WRITE (6,*) ' SIGL=',SIGL
CMR
C
      IZ = Z
      IZSYM = IZ
C
C     STUFF VALUES OF A AND B NOT CALCULATED DUE TO SYMMETRY
C     CONSIDERATIONS WHEN NSYMY=1.
C
      IF (NSYMY .EQ. 1) THEN
         IZSYM = IZ/2 + 1
         NOZ = IZ - IZSYM
         DO 5 I=1,NOZ
         J = IZ-I+1
         K = I+1
         A(NBRG,1,J) = A(NBRG,1,K)
         A(NBRG,2,J) = A(NBRG,2,K)
         B(NBRG,1,J) = B(NBRG,1,K)
         B(NBRG,2,J) = B(NBRG,2,K)
    5    CONTINUE
      ENDIF
C
      NINC = 10
      DO 100 I=1,IZSYM
C
C     CALCULATE AVERAGE FRICTION COEFFICIENT AT EACH RACEWAY
```

```
C
CMR    IF (INPUTB .EQ. 'Y') THEN
CMR       BETA(1,I) = BETAI
CMR       BETA(2,I) = BETAI
CMR    ELSE
          BETA(1,I) = AMUEHD(NBRG,1,I) + AMUASP(NBRG,1,I)
          BETA(2,I) = AMUEHD(NBRG,2,I) + AMUASP(NBRG,2,I)
CMR    ENDIF
C
C      CHECK FOR ROLLING ELEMENTS UNLOADED AT OUTER RING
C
       IF (BVAR(33,I) .LE. 0.) THEN
          PHI(NBRG,1,I) = 1.
          GO TO 10
       ENDIF
C
C      CALCULATE THE DEPTH TO MAX SHEAR (ZVOOR), AND MAXIMUM VON MISES
C      EQUIVALENT STRESS (SVMOOR) CONSIDERING NORMAL STRESS ONLY FOR
C      OUTER RACEWAY CONTACT
C
       CALL LPVAL (BTYPE,A(NBRG,1,I),B(NBRG,1,I),BVAR(33,I),POISOR,ZVOOR,
     $             SVMOOR)
CMR
CMR    WRITE (6,1008) I
C1008  FORMAT (//,2X,'ROLLING ELEMENT ',I2,'  AT OUTER RACE')
CMR    ZVODB = ZVOOR / B(NBRG,1,I)
CMR    WRITE (6,1010) ZVOOR,ZVODB,SVMOOR
C1010  FORMAT (2X,'DEPTH TO MAX ORTHOGONAL SHEAR (ZO) = ',E14.7,/,2X,
CMR  $         'ZO / B = ',E14.7,/,2X,
CMR  $         'VON-MISES EQUIVALENT STRESS = ',E14.7)
CMR
C
C      CALCULATE SUBSURFACE STRESSES FOR ROLLING ELEMENT (I)
C      AT THE OUTER RACEWAY CONTACT
C
       ZINCO = B(NBRG,1,I)/FLOAT(NINC)
       CALL SUBSTR (BETA(1,I),B(NBRG,1,I),BVAR(33,I),SROT(1),SFIT(1),
     $              SRESOR,POISOR,NINC,SIGLOR,SIGVMO,DELZO,ZVMO,YVMO)
CMR
CMR    ZVMODB = ZVMO / B(NBRG,1,I)
CMR    YVMODB = YVMO / B(NBRG,1,I)
CMR    WRITE (6,1020) SIGVMO,ZVMO,ZVMODB,YVMO,YVMODB,DELZO
C1020  FORMAT (/,2X,'MAXIMUM VON-MISES STRESS = ',E14.7,/,2X,
CMR  $         'DEPTH OF MAXIMUM VON-MISES STRESS (ZVMO) = ',E14.7,/,2X,
CMR  $         'ZVMO/B = ',E14.7,/,2X,
CMR  $         'Y COORDINATE OF MAXIMUM VON-MISES STRESS (YVMO) = ',
CMR  $         E14.7,/,2X,'YVMO/B = ',E14.7,/,2X,'DELZ = ',E14.7)
CMR
C
C      CALCULATE NEW LIFE RATIOING FACTOR FOR OUTER RACE CONTACT.
C
       IF (SIGVMO.LE.SIGLOR .OR. DELZO.LE.0.) THEN
          PHI(NBRG,1,I) = 1.E20
          GO TO 10
       ENDIF
       IF (ZVMO .LT. 0.5*ZINCO) ZVMO = 0.5*ZINCO
       PHI(NBRG,1,I) = (ZVMO/ZVOOR)**2.1 * (ZVOOR/DELZO)**0.9
     $             * (SVMOOR/(SIGVMO-SIGLOR))**9.3
   10  CONTINUE
CMR
```

```
CMR   WRITE (6,1030) PHI(NBRG,1,I)
C1030 FORMAT (/,2X,'LIFE RATIO = ',E14.7)
CMR
C
C     CHECK FOR ROLLING ELEMENTS UNLOADED AT INNER RING
C
      IF (BVAR(34,I) .LE. 0.) THEN
         PHI(NBRG,2,I) = 1.
         GO TO 20
      ENDIF
C
C     CALCULATE THE DEPTH TO MAX SHEAR (ZV0IR), AND MAXIMUM VON MISES
C     EQUIVALENT STRESS (SVM0IR) CONSIDERING NORMAL STRESS ONLY FOR
C     INNER RACEWAY CONTACT
C
      CALL LPVAL (BTYPE,A(NBRG,2,I),B(NBRG,2,I),BVAR(34,I),POISIR,ZV0IR,
     $            SVM0IR)
CMR
CMR   WRITE (6,1009) I
C1009 FORMAT (//,2X,'ROLLING ELEMENT ',I2,'  AT INNER RACE')
CMR   ZV0DB = ZV0IR / B(NBRG,2,I)
CMR   WRITE (6,1010) ZV0IR,ZV0DB,SVM0IR
CMR
C
C     CALCULATE SUBSURFACE STRESSES FOR ROLLING ELEMENT (I)
C     AT THE INNER RACEWAY CONTACT
C
      ZINCI = B(NBRG,2,I)/FLOAT(NINC)
      CALL SUBSTR (BETA(2,I),B(NBRG,2,I),BVAR(34,I),SROT(2),SFIT(2),
     $             SRESIR,POISIR,NINC,SIGLIR,SIGVMI,DELZI,ZVMI,YVMI)
CMR
CMR   ZVMIDB = ZVMI / B(NBRG,2,I)
CMR   YVMIDB = YVMI / B(NBRG,2,I)
CMR   WRITE (6,1020) SIGVMI,ZVMI,ZVMIDB,YVMI,YVMIDB,DELZI
CMR
C
C     CALCULATE NEW LIFE RATIOING FACTOR FOR INNER RACE CONTACT.
C
      IF (SIGVMI.LE.SIGLIR .OR. DELZI.LE.0.) THEN
         PHI(NBRG,2,I) = 1.E20
         GO TO 20
      ENDIF
      IF (ZVMI .LT. 0.5*ZINCI) ZVMI = 0.5*ZINCI
      PHI(NBRG,2,I) = (ZVMI/ZV0IR)**2.1 * (ZV0IR/DELZI)**0.9
     $            * (SVM0IR/(SIGVMI-SIGLIR))**9.3
   20 CONTINUE
CMR
CMR   WRITE (6,1030) PHI(NBRG,2,I)
CMR
C
  100 CONTINUE
CMR
CMR   STUFF PHI VALUES NOT CALCULATED DUE TO SYMMETRY CONSIDERATIONS
CMR   WHEN NSYMY=1 (Y AXIS SYMMETRY)
CMR
      IF (NSYMY .EQ. 1) THEN
         DO 150 I=1,NOZ
         J = IZ - I + 1
         K = I + 1
         PHI(NBRG,1,J) = PHI(NBRG,1,K)
```

```
         PHI(NBRG,2,J) = PHI(NBRG,2,K)
  150    CONTINUE
      ENDIF
CMR
      RETURN
      END
CMR - ------------------------------------------------------------------
CMR   NEW LIFE THEORY FOR ROLLER BEARINGS
CMR - ------------------------------------------------------------------
      SUBROUTINE NEWLFR (BTYPE,WS,Q,BCON,NS,POISIR,POISOR,RHOIR,RHOOR,
     $                   DM,DW,Z,OMEGIR,OMEGOR,R1,R2,R3,R4,PD,FPIR,FPOR,
     $                   NSYMY,BVAR,SIGLOR,SIGLIR,SRESOR,SRESIR,SROT,
     $                   SFIT,PHI)
C
C     THIS SUBROUTINE CALCULATES RATIOING FACTORS THAT ENABLE
C     CALCULATION OF ROLLER BEARING LIVES ACCORDING TO THE
C     NEW SKF LIFE THEORY.
C
C     INPUT DATA:
C        BTYPE - BEARING TYPE (-1=BALL,1=TAPER,2=CYLINDRICAL)
C        WS(M) - ROLLER SLICE WIDTH (O. RACE, I. RACE)
C        Q(K,M,J,I) - ROLLER SLICE LOAD ARRAY
C          WHERE K = SLICE NUMBER (1-20)
C                M = RACEWAY NUMBER (1=O.RACE, 2=I.RACE)
C                J = ROLLING ELEMENT NUMBER (1-30)
C                I = BEARING NUMBER (1-5)
C        BCON(K,M) - CONSTANT FOR CALCULATING CONTACT SEMI-WIDTH B
C          WHERE B = BCON * Q**0.5
C        NS - NUMBER OF ROLLER SLICES
C        POISIR,POISOR - POISSON'S RATIO FOR INNER RING, OUTER RING
C        RHOIR,RHOOR - DENSITY FOR INNER RING, OUTER RING (LB/IN**3)
C        DM - BEARING PITCH DIAMETER (IN)
C        DW - ROLLING ELEMENT DIAMETER (IN)
C        Z - NUMBER OF ROLLING ELEMENTS
C        OMEGIR,OMEGOR - ROTATIONAL SPEED FOR INNER RING, OUTER RING
C                        (RAD/SEC)
C        R1,R2 - INSIDE AND OUTSIDE RADIUS FOR INNER RING (IN)
C        R3,R4 - INSIDE AND OUTSIDE RADIUS FOR OUTER RING (IN)
C        PD - DIAMETRAL CLEARANCE (IN)
C        FPIR,FPOR - OPERATING FIT PRESSURE FOR INNER RING, OUTER RING
C                    (PSI)
C        NSYMY - LOAD SYMMETRY FLAG
C        BVAR(K,I) - ARRAY CONTAINING ROLLING ELEMENT OPERATING DATA
C          WHERE K = PARAMETER NUMBER (1-30)
C                I = ROLLING ELEMENT NUMBER
C          NOTE : BVAR(33,I) = MAXIMUM HERTZ STRESS AT OUTER RACE
C                 BVAR(34,I) = MAXIMUM HERTZ STRESS AT INNER RACE
C        ------------------------------------------------------------
C        BETA(K,J,I) - AVERAGE FRICTION COEFFICIENT FOR CONTACT
C          WHERE K = BEARING NUMBER
C                J = RING NUMBER (1=OUTER,2=INNER)
C                I = ROLLING ELEMENT NUMBER
C        ------------------------------------------------------------
C        SIGLOR - FATIGUE LIMIT STRESS FOR OUTER RING (PSI)
C        SIGLIR - FATIGUE LIMIT STRESS FOR INNER RING (PSI)
C        SRESOR - RESIDUAL STRESS FOR OUTER RING (PSI)
C        SRESIR - RESIDUAL STRESS FOR INNER RING (PSI)
C
C
C     OUTPUT DATA:
```

```
C         SROT(1) - HOOP STRESS DUE TO ROTATION AT OUTER RACEWAY (PSI)
C         SROT(2) - HOOP STRESS DUE TO ROTATION AT INNER RACEWAY (PSI)
C         SFIT(1) - HOOP STRESS DUE TO FITUP AT OUTER RACEWAY (PSI)
C         SFIT(2) - HOOP STRESS DUE TO FITUP AT INNER RACEWAY (PSI)
C         PHI(K,M,I) - LIFE RATIO (NEW LIFE / LUNDBERG PALMGREN)
C           WHERE K = ROLLLER SLICE NUMBER
C                 M = RACEWAY NUMBER
C                 I = ROLLING ELEMENT NUMBER
C
      DIMENSION PHI(20,2,30), SROT(2), SFIT(2), BVAR(36,30)
      DIMENSION Q(20,2,30,5), WS(2), BCON(20,2)
      COMMON /BRGNUM/ NBRG
      COMMON /MUAVG/  AMUEHD(5,2,50), AMUASP(5,2,50)
      COMMON /NLIF1/  BETA(2,30)
      LOGICAL SLCSYM, UNLOAD
C
C     CALCULATE HOOP STRESSES DUE TO ROTATION AND FIT PRESSURE
C
      CALL HOOPST (POISIR,POISOR,RHOIR,RHOOR,DM,DW,OMEGIR,OMEGOR,
     $             R1,R2,R3,R4,PD,FPIR,FPOR,SROT,SFIT)
CMR
CMR   WRITE (6,*) ' $$$ IN SUBROUTINE NEWLFR $$$'
CMR   WRITE (6,1000) SROT(1),SROT(2),SFIT(1),SFIT(2)
C1000 FORMAT ('1',//,2X,'HOOP STRESSES DUE TO ROTATION:',/,2(5X,E14.7),
CMR  $        /,2X,'HOOP STRESSES DUE TO FIT:',/,2(5X,E14.7))
CMR   WRITE (6,*) ' SIGL=',SIGL
CMR
C
      PI = ACOS(-1.)
      IZ = Z
      IZSYM = IZ
      NINC = 10
C
C     FOR SYMMETRY ABOUT THE Y-AXIS (NSYMY=1), DETERMINE THE NUMBER
C     OF ROLLERS TO MAKE CALCULATIONS FOR (IZSYM) AND THE NUMBER OF
C     SYMMETRIC ROLLER PAIRS (NOZ).
C
      IF (NSYMY .EQ. 1) THEN
         IZSYM = IZ/2 + 1
         NOZ = IZ - IZSYM
      ENDIF
CMR
CMR   DETERMINE INDEX OF FIRST UNLOADED ROLLER (IF ANY)
CMR
      NFULR = 0
      DO 1 I=1,IZSYM
      IF (BVAR(34,I) .LE. 0.) THEN
         NFULR = I
         GO TO 2
      ENDIF
    1 CONTINUE
    2 CONTINUE
C
      DO 150 I=1,IZSYM
CMR
CMR   CHECK FOR UNLOADED ROLLERS. FOR THE FIRST UNLOADED ROLLER,
CMR   CALCULATE PHI VALUES. FOR SUBSEQUENT UNLOADED ROLLERS, SKIP
CMR   OVER THE CALCULATION.
CMR
      UNLOAD = .FALSE.
```

```
      IF (BVAR(34,I) .LE. 0.) THEN
         UNLOAD = .TRUE.
         IF (I .NE. NFULR) GO TO 130
      ENDIF
C
C     CALCULATE AVERAGE FRICTION COEFFICIENT AT EACH RACEWAY
C
CMR   IF (INPUTB .EQ. 'Y') THEN
CMR      BETA(1,I) = BETAI
CMR      BETA(2,I) = BETAI
CMR   ELSE
         BETA(1,I) = AMUEHD(NBRG,1,I) + AMUASP(NBRG,1,I)
         BETA(2,I) = AMUEHD(NBRG,2,I) + AMUASP(NBRG,2,I)
CMR   ENDIF
CMR
CMR   CHECK FOR ROLLER SLICE LOAD SYMMETRY
CMR
      SLCSYM = .TRUE.
      NCHECK = NS / 2
      KCENT = NCHECK + 1
      FACT = 0.001
      TOLR1 = FACT * ABS(Q(KCENT,1,I,NBRG))
      TOLR2 = FACT * ABS(Q(KCENT,2,I,NBRG))
      IF (TOLR1 .EQ. 0.) TOLR1 = 0.01
      IF (TOLR2 .EQ. 0.) TOLR2 = 0.01
      DO 5 K=1,NCHECK
      K1 = K
      K2 = NS - K + 1
C
      IF (ABS( Q(K1,1,I,NBRG) - Q(K2,1,I,NBRG) ) .GT. TOLR1 .OR.
     $    ABS( Q(K1,2,I,NBRG) - Q(K2,2,I,NBRG) ) .GT. TOLR2) THEN
         SLCSYM = .FALSE.
         GO TO 6
      ENDIF
C
    5 CONTINUE
    6 CONTINUE
      NSL = NS
      IF (SLCSYM) NSL = NCHECK
C
      DO 100 K=1,NSL
C
C     CHECK FOR ROLLER SLICES UNLOADED AT OUTER RING
C
      IF (Q(K,1,I,NBRG) .LE. 0.) THEN
         PHI(K,1,I) = 1.
         GO TO 10
      ENDIF
C
C     CALCULATE MAXIMUM PRESSURE (PMAX) AND SEMI-WIDTH (B) FOR SLICE K
C     AT THE OUTER RACEWAY
C
      B = BCON(K,1) * SQRT(Q(K,1,I,NBRG))
      PMAX = 2. * Q(K,1,I,NBRG) / (PI * WS(1) * B)
C
C     CALCULATE THE DEPTH TO MAX SHEAR (ZVOOR), AND MAXIMUM VON MISES
C     EQUIVALENT STRESS (SVMOOR) CONSIDERING NORMAL STRESS ONLY FOR
C     OUTER RACEWAY CONTACT
C
      CALL LPVAL (BTYPE,WS(1),B,PMAX,POISOR,ZVOOR,
```

```
     $              SVMOOR)
CMR
CMR    WRITE (6,1008) I,K
C1008 FORMAT (//,2X,'ROLLING ELEMENT ',I2,'  AT OUTER RACE, SLICE ',I2)
CMR    ZVODB = ZVOOR / B
CMR    WRITE (6,1010) ZVOOR,ZVODB,SVMOOR
C1010 FORMAT (2X,'DEPTH TO MAX ORTHOGONAL SHEAR (ZO) = ',E14.7,/,2X,
CMR  $         'ZO / B = ',E14.7,/,2X,
CMR  $         'VON-MISES EQUIVALENT STRESS = ',E14.7)
CMR
C
C      CALCULATE SUBSURFACE STRESSES FOR ROLLING ELEMENT (I)
C      AT THE OUTER RACEWAY CONTACT
C
       ZINCO = B / FLOAT(NINC)
       CALL SUBSTR (BETA(1,I),B,PMAX,SROT(1),SFIT(1),
     $              SRESOR,POISOR,NINC,SIGLOR,SIGVMO,DELZO,ZVMO,YVMO)
CMR
CMR    ZVMODB = ZVMO / B
CMR    YVMODB = YVMO / B
CMR    WRITE (6,1020) SIGVMO,ZVMO,ZVMODB,YVMO,YVMODB,DELZO
C1020 FORMAT (/,2X,'MAXIMUM VON-MISES STRESS = ',E14.7,/,2X,
CMR  $         'DEPTH OF MAXIMUM VON-MISES STRESS (ZVMO) = ',E14.7,/,2X,
CMR  $         'ZVMO/B = ',E14.7,/,2X,
CMR  $         'Y COORDINATE OF MAXIMUM VON-MISES STRESS (YVMO) = ',
CMR  $         E14.7,/,2X,'YVMO/B = ',E14.7,/,2X,'DELZ = ',E14.7)
CMR
C
C      CALCULATE NEW LIFE RATIOING FACTOR FOR OUTER RACE CONTACT.
C
       IF (SIGVMO.LE.SIGLOR .OR. DELZO.LE.0.) THEN
          PHI(K,1,I) = 1.E20
          GO TO 10
       ENDIF
       IF (ZVMO .LT. 0.5*ZINCO) ZVMO = 0.5*ZINCO
       PHI(K,1,I) = (ZVMO/ZVOOR)**2.074 * (ZVOOR/DELZO)**0.8889
     $            * (SVMOOR/(SIGVMO-SIGLOR))**9.185
   10 CONTINUE
CMR
CMR       WRITE (6,1030) PHI(K,1,I)
C1030 FORMAT (/,2X,'LIFE RATIO = ',E14.7)
CMR
C
C      CHECK FOR ROLLER SLICES UNLOADED AT INNER RING
C
       IF (Q(K,2,I,NBRG) .LE. 0.) THEN
          PHI(K,2,I) = 1.
          GO TO 20
       ENDIF
C
C      CALCULATE MAXIMUM PRESSURE (PMAX) AND SEMI-WIDTH (B) FOR SLICE K
C      AT INNER RACEWAY
C
       B = BCON(K,2) * SQRT(Q(K,2,I,NBRG))
       PMAX = 2. * Q(K,2,I,NBRG) / (PI * WS(2) * B)
C
C      CALCULATE THE DEPTH TO MAX SHEAR (ZVOIR), AND MAXIMUM VON MISES
C      EQUIVALENT STRESS (SVMOIR) CONSIDERING NORMAL STRESS ONLY FOR
C      INNER RACEWAY CONTACT
C
```

```
      CALL LPVAL (BTYPE,WS(1),B,PMAX,POISIR,ZVOIR,
     $            SVMOIR)
C
C     CALCULATE SUBSURFACE STRESSES FOR ROLLING ELEMENT (I)
C     AT THE INNER RACEWAY CONTACT
C
      ZINCI = B / FLOAT(NINC)
      CALL SUBSTR (BETA(2,I),B,PMAX,SROT(2),SFIT(2),
     $             SRESIR,POISIR,NINC,SIGLIR,SIGVMI,DELZI,ZVMI,YVMI)
CMR
CMR   ZVMIDB = ZVMI / B
CMR   YVMIDB = YVMI / B
CMR   WRITE (6,1020) SIGVMI,ZVMI,ZVMIDB,YVMI,YVMIDB,DELZI
CMR
C
C     CALCULATE NEW LIFE RATIOING FACTOR FOR INNER RACE CONTACT.
C
      IF (SIGVMI.LE.SIGLIR .OR. DELZI.LE.0.) THEN
         PHI(K,2,I) = 1.E20
         GO TO 20
      ENDIF
      IF (ZVMI .LT. 0.5*ZINCI) ZVMI = 0.5*ZINCI
      PHI(K,2,I) = (ZVMI/ZVOIR)**2.074 * (ZVOIR/DELZI)**0.8889
     $           * (SVMOIR/(SIGVMI-SIGLIR))**9.185
   20 CONTINUE
CMR
CMR   WRITE (6,1030) PHI(K,2,I)
CMR
C
  100 CONTINUE
CMR
CMR   STUFF PHI VALUES NOT CALCULATED DUE TO ROLLER SLICE LOAD
CMR   SYMMETRY CONSIDERATIONS
CMR
      IF (SLCSYM) THEN
         DO 120 KK=1,NSL
         K1 = KK
         K2 = NS - KK + 1
         PHI(K2,1,I) = PHI(K1,1,I)
         PHI(K2,2,I) = PHI(K1,2,I)
  120    CONTINUE
      ENDIF
CMR
CMR   STUFF PHI VALUES NOT CALCULATED FOR UNLOADED ROLLERS
CMR
  130 CONTINUE
      IF (UNLOAD .AND. I .NE. NFULR) THEN
         DO 140 KK=1,NS
         PHI(KK,1,I) = PHI(KK,1,NFULR)
         PHI(KK,2,I) = PHI(KK,2,NFULR)
  140    CONTINUE
      ENDIF
CMR
  150 CONTINUE
CMR
CMR   STUFF PHI VALUES NOT CALCULATED DUE TO SYMMETRY CONSIDERATIONS
CMR   WHEN NSYMY=1 (Y AXIS SYMMETRY)
CMR
      IF (NSYMY .EQ. 1) THEN
         DO 200 I=1,NOZ
```

```
         J = IZ - I + 1
         K = I + 1
         DO 200 KK=1,NS
         PHI(KK,1,J) = PHI(KK,1,K)
         PHI(KK,2,J) = PHI(KK,2,K)
  200    CONTINUE
      ENDIF
CMR
C
      RETURN
      END

      SUBROUTINE HOOPST (POISIR,POISOR,RHOIR,RHOOR,DM,DW,OMEGIR,OMEGOR,
     $                   R1,R2,R3,R4,PD,FPIR,FPOR,SROT,SFIT)
C
C     THIS SUBROUTINE CALCULATES THE HOOP STRESSES DUE TO ROTATION
C     (SROT) AND OPERATING FIT PRESSURE (SFIT) FOR BOTH THE INNER
C     AND OUTER RINGS AT THE RACEWAY SURFACES.
C
C     INPUT DATA:
C        POISIR,POISOR - POISSON'S RATIO FOR INNER RING, OUTER RING
C        RHOIR,RHOOR - DENSITY FOR INNER RING, OUTER RING (LB/IN**3)
C        DM - BEARING PITCH DIAMETER (IN)
C        DW - ROLLING ELEMENT DIAMETER (IN)
C        OMEGIR,OMEGOR - ROTATIONAL SPEED FOR INNER RING, OUTER RING
C                        (RAD/SEC)
C        R1,R2 - INSIDE AND OUTSIDE RADIUS FOR INNER RING (IN)
C        R3,R4 - INSIDE AND OUTSIDE RADIUS FOR OUTER RING (IN)
C        FPIR,FPOR - OPERATING FIT PRESSURE FOR INNER RING, OUTER RING
C                    (PSI)
C
C     OUTPUT DATA:
C        SROT(1) - HOOP STRESS DUE TO ROTATION AT OUTER RACEWAY (PSI)
C        SROT(2) - HOOP STRESS DUE TO ROTATION AT INNER RACEWAY (PSI)
C        SFIT(1) - HOOP STRESS DUE TO FITUP AT OUTER RACEWAY (PSI)
C        SFIT(2) - HOOP STRESS DUE TO FITUP AT INNER RACEWAY (PSI)
C
      DIMENSION SROT(2), SFIT(2)
      G = 386.4
C
C     CALCULATE HOOP STRESS DUE TO ROTATION AT OUTER RACEWAY
C
      RGOR = (DM + DW + PD/2.) / 2.
      IF (R3.EQ.0. .OR. R4.EQ.0.) THEN
         SROT(1) = 0.
      ELSE
         SROT(1) = 0.125*RHOOR*OMEGOR*OMEGOR/G * ( (3.+POISOR)*(R4*R4
     $             + R3*R3 + R4*R4*R3*R3/RGOR/RGOR) - (1.+3.*POISOR)
     $             *RGOR*RGOR)
      ENDIF
C
C     CALCULATE HOOP STRESS DUE TO ROTATION AT INNER RACEWAY
C
      RGIR = (DM - DW - PD/2.) / 2.
      IF (R1.EQ.0. .OR. R2.EQ.0.) THEN
         SROT(2) = 0.
      ELSE
         SROT(2) = 0.125*RHOIR*OMEGIR*OMEGIR/G * ( (3.+POISIR)*(R2*R2
     $             + R1*R1 + R2*R2*R1*R1/RGIR/RGIR) - (1.+3.*POISIR)
     $             *RGIR*RGIR)
```

```
      ENDIF
C
C     CALCULATE HOOP STRESS DUE TO OPERATING FIT PRESSURE AT OUTER RACE
C
      IF (R4.EQ.R3 .OR. R4.EQ.0. .OR. R3.EQ.0.) THEN
         SFIT(1) = 0.
      ELSE
         SFIT(1) = -FPOR*R4*R4/(R4*R4 - R3*R3) * (1.+R3*R3/RGOR/RGOR)
      ENDIF
C
C     CALCULATE HOOP STRESS DUE TO OPERATING FIT PRESSURE AT INNER RACE
C
      IF (R2.EQ.R1 .OR. R2.EQ.0. .OR. R1.EQ.0.) THEN
         SFIT(2) = 0.
      ELSE
         SFIT(2) =  FPIR*R1*R1/(R2*R2 - R1*R1) * (1.+R2*R2/RGIR/RGIR)
      ENDIF
C
      RETURN
      END

      SUBROUTINE LPVAL (BTYPE,A,B,PMAX,POIS,Z0,SVMZ0)
C
C     THIS SUBROUTINE CALCULATES THE DEPTH TO MAXIMUM ORTHOGONAL SHEAR
C     STRESS (Z0) AND THE VON-MISES EQUIVALENT STRESS (SVMZ0) THERE.
C
      REAL KAPPA
C
C     PREPARE TO CALCULATE TAU0 AND Z0. CHECK FOR SPECIAL CASES
C     WHERE CUBIC EQUATION DOES NOT HAVE TO BE SOLVED:
C     KAPPA=0 (LINE CONTACT) AND KAPPA=1 (CIRCULAR CONTACT)
C
      PI = ACOS(-1.)
      KAPPA = B / A
      XK = KAPPA
      IF (XK .GT. 1.) XK = 1. / KAPPA
C
      IF (BTYPE .GT. 0. .OR. KAPPA .EQ. 0.) THEN
         TAUR = 0.5
         ZR = 0.5
         GO TO 100
      ENDIF
C
      IF (KAPPA .EQ. 1.) THEN
         TAUR = 0.4277818
         ZR = 0.3508641
         GO TO 100
      ENDIF
C
C     SET UP COEFFICIENTS OF CUBIC EQUATION
C
      A1 = 1.
      B1 = -1. / 6.
      C1 = -1. / 3.
      D1 = (1. - XK*XK) / 2.
C
C     SOLVE THE CUBIC EQUATION
C
      CALL ROOT3 (A1,B1,C1,D1,KEY,X1,X2,X2I,X3,X3I)
C
```

```
C     PICK THE ROOT WHICH IS PHYSICALLY REASONABLE
C
      CALL CHKRT (KEY,X1,X2,X3,ROOT,IERR)
C
C     CALCULATE VALUES OF 2*TAU0/SIGMA0 (TAUR) AND Z0/B (ZR)
C
      TAUR = SQRT(2.*ROOT - 1.) / (ROOT * (ROOT + 1.))
      PHI = ATAN(SQRT(ROOT))
      XNU = ATAN(SQRT(ROOT - 1.))
      ZR = TAN(XNU) * COS(PHI) / XK
C
  100 CONTINUE
C
C     CALCULATE VALUES OF TAU0 AND Z0
C
      TAU0 = TAUR * PMAX / 2.
      Z0 = ZR * B
      IF (KAPPA .GT. 1.) Z0 = ZR * A
C
C     CALCULATE THE VON-MISES STRESS AT DEPTH Z0 AND Y=0
C
      Z = Z0
      Y = 0.
      BETA = 0.
      SHOOP = 0.
C
C     FOR Z=0, COMPUTE STRESSES AT THE CONTACT SURFACE USING SPECIAL
C     EXPRESSIONS FROM PAPER BY SMITH & LIU
C
      IF (Z .EQ. 0.) THEN
         IF (ABS(Y) .LE. B) THEN
            TAUZY = -BETA*PMAX * SQRT(1. - Y*Y/B/B)
            SIGX = -POIS*PMAX * (2.*SQRT(1. - Y*Y/B/B) + 2.*BETA*Y/B)
            SIGY = -PMAX * (SQRT(1. - Y*Y/B/B) + 2.*BETA*Y/B)
            SIGZ = -PMAX * SQRT(1. - Y*Y/B/B)
         ELSEIF (Y .GT. B) THEN
            TAUZY = 0.
            SIGX = -2.*POIS*BETA*PMAX * (Y/B - SQRT(Y*Y/B/B - 1.))
            SIGY = -2.*BETA*PMAX * (Y/B - SQRT(Y*Y/B/B - 1.))
            SIGZ = 0.
         ELSE
            TAUZY = 0.
            SIGX = -2.*POIS*BETA*PMAX * (Y/B + SQRT(Y*Y/B/B - 1.))
            SIGY = -2.*BETA*PMAX * (Y/B + SQRT(Y*Y/B/B - 1.))
            SIGZ = 0.
         ENDIF
         SIGY = SIGY + SHOOP
         GO TO 200
      ENDIF
C
C     COMPUTE STRESSES FOR POINTS BELOW SURFACE (Z>0)
C
      EM = SQRT( (B + Y)**2 + Z*Z)
      EN = SQRT( (B - Y)**2 + Z*Z)
      RADICL = 2.* (EM*EN + Y*Y + Z*Z - B*B)
      DENOM = EM * EN * SQRT(RADICL)
      PHI1 = PI * (EM + EN) / DENOM
      PHI2 = PI * (EM - EN) / DENOM
      TAUZY = -PMAX/PI * (Z*Z*PHI2 + BETA*( (B*B+2.*Y*Y+2.*Z*Z)
     $        *Z/B*PHI1 - 2.*PI*Z/B - 3.*Y*Z*PHI2))
```

```
      SIGX = -2.*POIS*PMAX/PI * (Z*((B*B + Y*Y + Z*Z)/B*PHI1 - PI/B
     $       -2.*Y*PHI2) + BETA*( (Y*Y - B*B - Z*Z)*PHI2 + PI*Y/B
     $       + (B*B - Y*Y - Z*Z)*Y/B*PHI1))
      SIGY = -PMAX/PI * (Z*((B*B + 2.*Z*Z + 2.*Y*Y)/B*PHI1 - 2.*PI/B
     $       - 3.*Y*PHI2) + BETA*( (2.*Y*Y - 2.*B*B - 3.*Z*Z)*PHI2
     $       + 2.*PI*Y/B + 2.*(B*B - Y*Y - Z*Z)*Y/B*PHI1)) + SHOOP
      SIGZ = -PMAX/PI * (Z*(B*PHI1 - Y*PHI2) + BETA*Z*Z*PHI2)
C
  200 CONTINUE
C
C     COMPUTE PRINCIPAL STRESSES USING MOHR'S CIRCLE
C
      SIG3 = SIGX
      SIG1 = (SIGY+SIGZ - SQRT((SIGY-SIGZ)**2 + 4.*TAUZY*TAUZY)) / 2.
      SIG2 = (SIGY+SIGZ + SQRT((SIGY-SIGZ)**2 + 4.*TAUZY*TAUZY)) / 2.
C
C     COMPUTE MAXIMUM SHEAR STRESSES
C
      TMAX1 = (SIG1 - SIG3) / 2.
      TMAX2 = (SIG1 - SIG2) / 2.
      TMAX3 = (SIG2 - SIG3) / 2.
C
C     COMPUTE MAXIMUM OCTAHEDRAL SHEARING STRESS AND VON MISES STRESS
C
      TAUG = SQRT((SIG1-SIG2)**2 + (SIG2-SIG3)**2 + (SIG3-SIG1)**2) / 3.
      SIGVM = TAUG * 2.1213203
      SVMZ0 = SIGVM
C
      RETURN
      END

      SUBROUTINE ROOT3 (A,B,C,D,KEY,X1,X2,X2I,X3,X3I)
C
C     THIS SUBROUTINE DETERMINES THE ROOTS OF A CUBIC EQUATION
C     USING THE TRIGONOMETRIC SOLUTION OUTLINED IN "MECHANICAL
C     DESIGN AND SYSTEMS HANDBOOK", ROTHBART, PP. 1-23 TO 1-24
C
      PI = ACOS(-1.)
      ALPHA = A*C - B*B
      BETA = 0.5 * (3.*A*B*C - A*A*D) - B*B*B
      DISC = ALPHA*ALPHA*ALPHA + BETA*BETA
C
C     BRANCH ACCORDING TO VALUE OF DISC AND ALPHA
C
      IF (ALPHA .GT. 0.) GO TO 100
C
      IF (DISC .GT. 0) GO TO 50
C
C     CASE 1 : ALPHA<0, DISC<=0
C
      KEY = 1
      TERM = ABS(BETA) / (-ALPHA)**1.5
      ARG = ACOS(TERM) / 3.
      U1 = SIGN(2.,BETA) * SQRT(-ALPHA) * COS(ARG)
      U2 = SIGN(2.,BETA) * SQRT(-ALPHA) * COS(ARG + 2.*PI/3.)
      U3 = SIGN(2.,BETA) * SQRT(-ALPHA) * COS(ARG + 4.*PI/3.)
      X1 = (U1 - B) / A
      X2 = (U2 - B) / A
      X3 = (U3 - B) / A
      X2I = 0
```

```
      X3I = 0
      GO TO 200
C
   50 CONTINUE
C
C     CASE 2 : ALPHA<0, DISC>0
C
      KEY = 2
      TERM = ABS(BETA) / (-ALPHA)**1.5
      ARG = ACOSH(TERM) / 3.
      U1 = SIGN(2.,BETA) * SQRT(-ALPHA) * COSH(ARG)
      U2 = -SIGN(1.,BETA) * SQRT(-ALPHA) * COSH(ARG)
      U2I = SQRT(-3.*ALPHA) * SINH(ARG)
      U3 = U2
      U3I = -U2I
      X1 = (U1 - B) / A
      X2 = (U2 - B) / A
      X2I = U2I / A
      X3 = (U3 - B) / A
      X3I = U3I / A
      GO TO 200
C
  100 CONTINUE
C
C     CASE 3 : ALPHA>0
C
      KEY = 3
      TERM = ABS(BETA) / (ALPHA)**1.5
      ARG = ASINH(TERM) / 3.
      U1 = SIGN(2.,BETA) * SQRT(ALPHA) * SINH(ARG)
      U2 = -SIGN(1.,BETA) * SQRT(ALPHA) * SINH(ARG)
      U2I = SQRT(3.*ALPHA) * COSH(ARG)
      U3 = U2
      U3I = -U2I
      X1 = (U1 - B) / A
      X2 = (U2 - B) / A
      X2I = U2I / A
      X3 = (U3 - B) / A
      X3I = U3I / A
C
  200 CONTINUE
C
      RETURN
      END

      FUNCTION ACOSH (THETA)
      ACOSH = ALOG(THETA + SQRT(THETA*THETA - 1.))
      RETURN
      END

      FUNCTION ASINH (THETA)
      ASINH = ALOG(THETA + SQRT(THETA*THETA + 1.))
      RETURN
      END

      SUBROUTINE CHKRT (KEY,X1,X2,X3,ROOT,IERR)
C
C     THIS SUBROUTINE EXAMINES THE VALUES OF THE THREE ROOTS TO
C     THE CUBIC EQUATION AND PICKS THE ONE THAT IS PHYSICALLY
C     REASONABLE (ROOT).  IERR IS AN ERROR FLAG SUCH THAT:
```

```
C          IERR=0 ==> NO ERROR
C          IERR=1 ==> IMPROPER VALUE OF KAPPA
C          IERR=2 ==> NONE OF THE ROOTS ARE REASONABLE
C
      ROOT = 0.
      IERR = 0
      IF (KEY .NE. 1) THEN
         IERR = 1
         RETURN
      ENDIF
C
      IF (X1 .GT. 0.5) THEN
         ROOT = X1
      ELSEIF (X2 .GT. 0.5) THEN
         ROOT = X2
      ELSEIF (X3 .GT. 0.5) THEN
         ROOT = X3
      ELSE
         IERR = 2
      ENDIF
C
      RETURN
      END

      SUBROUTINE SUBSTR (BETA,B,PMAX,SROT,SFIT,SRES,POIS,NINC,SIGL,
     $                   SIGVMX,DELZ,ZVM,YVM)
C
C     THIS SUBROUTINE CALCULATES THE STRESS COMPONENTS FOR A HERTZIAN
C     CONTACT AT AND BELOW THE SURFACE. THE STRESS COMPONENTS ARE THEN
C     COMBINED TO DETERMINE THE PRINCIPAL STRESSES. FROM THE PRINCIPAL
C     STRESSES, THE MAXIMUM SHEAR STRESSES, THE OCTAHEDRAL SHEAR STRESS,
C     AND THE VON-MISES EQUIVALENT STRESS ARE CALCULATED. THE VALUES
C     RETURNED FROM THIS SUBROUTINE ARE THE MAXIMUM VON-MISES STRESS
C     (SIGVMX), THE DEPTH AT WHICH IT OCCURS (ZVM), AND THE Y LOCATION
C     (YVM). ALSO RETURNED IS THE VALUE OF DELZ, THE SUMMATION OF THE
C     SUBSURFACE DEPTH INCREMENTS FOR WHICH THE VON-MISES STRESS
C     EXCEEDS THE LIMIT STRESS (SIGL).
C
      PI = ACOS(-1.)
C
C     NINC IS THE NUMBER OF INCREMENTS ACROSS THE CONTACT SEMI-WIDTH (B)
C
CMR   NZINC = 6*NINC + 1
CMR   NYINC = 4*NINC + 1
      NZINC = 3*NINC + 1
      NYINC = 2*NINC + 1
CMR   ZINC = B/FLOAT(NINC)
      ZINC1 = B/FLOAT(NINC)
      ZINC2 = 2.5 * ZINC1
CMR
      YINC = B/FLOAT(NINC)
      ZVM = 0.
      DELZ = 0.
      SIGVMX = 0.
      Z = 0.
CMR
CMR   WRITE (6,1000) BETA,B,PMAX,POIS,SROT,SFIT,SRES
C1000 FORMAT (//,5X,'BETA =',E12.5,/,5X,'B = ',E12.5,/,5X,'PMAX = ',
CMR  $        E12.5,/,5X,'POIS = ',F5.3,/,5X,'SROT = ',E12.5,/,5X,
CMR  $        'SFIT = ',E12.5,/,5X,'SRES = ',E12.5)
```

```
CMR
      DO 100 IZ=1,NZINC
      SHOOP = SROT + SFIT + SRES
      BIGSVM = 0.
      Y = 0.
      YBIG = Y
CMR
C     ZDB = Z/B
C     WRITE (6,1002) Z,ZDB
C1002 FORMAT (/,5X,'Z = ',E12.5,/,5X,'Z/B = ',E12.5)
C     WRITE (6,1003)
C1003 FORMAT (5X,'Y/B',6X,'PHI1',8X,'PHI2',7X,'TAUZY',8X,'SIGX',8X,
C    $        'SIGY',8X,'SIGZ',/,10X,'SIG1',7X,'SIG2',7X,'SIG3',6X,
C    $        'TMAX1',6X,'TMAX2',6X,'TMAX3',6X,'SIGVM',/)
CMR
      DO 50 IY=1,NYINC
C
C     FOR Z=0, COMPUTE STRESSES AT THE CONTACT SURFACE USING SPECIAL
C     EXPRESSIONS FROM PAPER BY SMITH & LIU
C
      IF (Z .EQ. 0.) THEN
         IF (ABS(Y) .LE. B) THEN
            TAUZY = -BETA*PMAX * SQRT(1. - Y*Y/B/B)
            SIGX = -POIS*PMAX * (2.*SQRT(1. - Y*Y/B/B) + 2.*BETA*Y/B)
            SIGY = -PMAX * (SQRT(1. - Y*Y/B/B) + 2.*BETA*Y/B)
            SIGZ = -PMAX * SQRT(1. - Y*Y/B/B)
         ELSEIF (Y .GT. B) THEN
            TAUZY = 0.
            SIGX = -2.*POIS*BETA*PMAX * (Y/B - SQRT(Y*Y/B/B - 1.))
            SIGY = -2.*BETA*PMAX * (Y/B - SQRT(Y*Y/B/B - 1.))
            SIGZ = 0.
         ELSE
            TAUZY = 0.
            SIGX = -2.*POIS*BETA*PMAX * (Y/B + SQRT(Y*Y/B/B - 1.))
            SIGY = -2.*BETA*PMAX * (Y/B + SQRT(Y*Y/B/B - 1.))
            SIGZ = 0.
         ENDIF
         SIGY = SIGY + SHOOP
CMR
CMR   ADD RESIDUAL STRESS TO X DIRECTION STRESS (M. RAGEN : 7-3-90)
CMR
         SIGX = SIGX + SRES
CMR
         GO TO 5
      ENDIF
C
C     COMPUTE STRESSES FOR POINTS BELOW SURFACE (Z>0)
C
      EM = SQRT( (B + Y)**2 + Z*Z)
      EN = SQRT( (B - Y)**2 + Z*Z)
      RADICL = 2.* (EM*EN + Y*Y + Z*Z - B*B)
      DENOM = EM * EN * SQRT(RADICL)
      PHI1 = PI * (EM + EN) / DENOM
      PHI2 = PI * (EM - EN) / DENOM
      TAUZY = -PMAX/PI * (Z*Z*PHI2 + BETA*( (B*B+2.*Y*Y+2.*Z*Z)
     $        *Z/B*PHI1 - 2.*PI*Z/B - 3.*Y*Z*PHI2))
      SIGX = -2.*POIS*PMAX/PI * (Z*((B*B + Y*Y + Z*Z)/B*PHI1 - PI/B
     $       -2.*Y*PHI2) + BETA*( (Y*Y - B*B - Z*Z)*PHI2 + PI*Y/B
     $       + (B*B - Y*Y - Z*Z)*Y/B*PHI1))
      SIGY = -PMAX/PI * (Z*((B*B + 2.*Z*Z + 2.*Y*Y)/B*PHI1 - 2.*PI/B
```

```
     $        - 3.*Y*PHI2) + BETA*( (2.*Y*Y - 2.*B*B - 3.*Z*Z)*PHI2
     $        + 2.*PI*Y/B + 2.*(B*B - Y*Y - Z*Z)*Y/B*PHI1)) + SHOOP
      SIGZ = -PMAX/PI * (Z*(B*PHI1 - Y*PHI2) + BETA*Z*Z*PHI2)
C
CMR
CMR   ADD RESIDUAL STRESS TO X DIRECTION STRESS (M. RAGEN : 7-3-90)
CMR
      SIGX = SIGX + SRES
CMR
    5 CONTINUE
C
C     COMPUTE PRINCIPAL STRESSES USING MOHR'S CIRCLE
C
      SIG3 = SIGX
      SIG1 = (SIGY+SIGZ - SQRT((SIGY-SIGZ)**2 + 4.*TAUZY*TAUZY)) / 2.
      SIG2 = (SIGY+SIGZ + SQRT((SIGY-SIGZ)**2 + 4.*TAUZY*TAUZY)) / 2.
C
C     COMPUTE MAXIMUM SHEAR STRESSES
C
      TMAX1 = (SIG1 - SIG3) / 2.
      TMAX2 = (SIG1 - SIG2) / 2.
      TMAX3 = (SIG2 - SIG3) / 2.
C
C     COMPUTE MAXIMUM OCTAHEDRAL SHEARING STRESS AND VON MISES STRESS
C
      TAUG = SQRT((SIG1-SIG2)**2 + (SIG2-SIG3)**2 + (SIG3-SIG1)**2) / 3.
      SIGVM = TAUG * 2.1213203
CMR
C     YDB = Y / B
C     WRITE (6,1010) YDB,PHI1,PHI2,TAUZY,SIGX,SIGY,SIGZ
C1010 FORMAT (1X,F5.2,6(1X,E11.5))
C     WRITE (6,1012) SIG1,SIG2,SIG3,TMAX1,TMAX2,TMAX3,SIGVM
C1012 FORMAT (3X,7(1X,E10.4))
CMR
      IF (SIGVM .GT. BIGSVM) THEN
         BIGSVM = SIGVM
         YBIG = Y
      ENDIF
C
      Y = Y + YINC
   50 CONTINUE
CMR
C     YDB = YBIG/B
C     WRITE (6,1020) BIGSVM,YBIG,YDB
C1020 FORMAT (/,5X,'MAXIMUM VON-MISES STRESS = ',E12.5,/,5X,
C    $        'Y COORDINATE = ',E12.5,/,5X,'Y/B = ',E12.5)
CMR
      IF (BIGSVM .GT. SIGVMX) THEN
         SIGVMX = BIGSVM
         ZVM = Z
         YVM = YBIG
      ENDIF
CMR
CMR   USE BIGGER INCREMENT FOR Z > B
CMR
      IF (IZ .LT. 11) THEN
         ZINC = ZINC1
      ELSE
         ZINC = ZINC2
      ENDIF
```

```
CMR
C
C     INCREMENT DELZ IF THE LIMIT STRESS IS EXCEEDED.
C
      IF (BIGSVM .GE. SIGL) DELZ = DELZ + ZINC
CMR
CMR   JUMP OUT OF CALCULATION LOOP IF THE MAXIMUM VON-MISES STRESS
CMR   IS LESS THAN THE FATIGUE LIMIT STRESS AND THE DEPTH Z IS GREATER
CMR   THAN B.
CMR
      IF (Z .GE. B .AND. BIGSVM .LT. SIGL) GO TO 150
CMR
      Z = Z + ZINC
  100 CONTINUE
CMR
  150 CONTINUE
CMR
C     ZDB = ZVM/B
C     YDB = YVM/B
C     WRITE (6,1030) SIGVMX,ZVM,ZDB,YVM,YDB
C1030 FORMAT (//,5X,'MAXIMUM VON-MISES STRESS = ',E12.5,/,5X,
C    $        'Z COORDINATE = ',E12.5,/,5X,'Z/B = ',E12.5,/,5X,
C    $        'Y COORDINATE = ',E12.5,/,5X,'Y/B = ',E12.5)
CMR
      RETURN
      END
```

APPENDIX D

PC-CYBEAN2 OUTPUT LISTINGS FOR 114DS665 AND MR315C2 BEARINGS

ANALYSIS OF DYNAMIC PERFORMANCE CHARACTERISTICS OF CYLINDRICAL ROLLER BEARINGS UNDER RADIAL, AXIAL AND MOMENT LOADING

PC-CYBEAN2

a PERSONAL COMPUTER PROGRAM of

MRC BEARINGS
an SKF SPECIALTY BEARINGS company

BOEING ART 114DS665 CRB - STEEL ROLLERS

INPUT DATA PREPARED BY RAGEN

INPUT DATE: 5-31-91

ENGLISH SYSTEM UNITS - UNLESS OTHERWISE NOTED, ALL DATA GIVEN BELOW CONFORM TO THE FOLLOWING UNITS:

LENGTH - INCHES -
AREA - SQUARE INCHES
SURFACE FINISH - MICROINCHES
FORCE OR LOAD - POUNDS
PRESSURE, STRESS, MODULUS of ELASTICITY - PSI
DENSITY - POUNDS PER CUBIC INCH
MOMENT OF INERTIA - IN.**4
TEMPERATURE - DEGREES FAHRENHEIT
KINEMATIC VISCOSITY - IN.**2/SEC
THERMAL EXPANSION - INCHES PER INCH PER DEGREE F
THERMAL CONDUCTIVITY - BTU PER HOUR PER FOOT PER DEGREE F
HEAT GENERATION - BTU PER HOUR
SPECIFIC HEAT - BTU PER LB PER DEGREE F

BEARING DIMENSIONS

ROLLERS/ROW	NO.ROWS	PITCH DIAMETER
1.2000000E+01	1.0000000E+00	4.6850000E+00

ROLLER DIMENSIONS

DIAMETER	TOTAL LENGTH	FLAT LENGTH	CORNER RADIUS	NUMBER OF LAMINAE
9.8430000E-01	9.7640000E-01	3.3000000E-01	5.9000000E-02	20

CROWN RADIUS	END SPHERE RADIUS	END CONTACT HEIGHT	FLANGE ANGLE (DEGREES)
6.0000000E+01	FLAT END	0.0000000E+00	4.4200000E-01

RACEWAY DATA

INNER CONTOUR RADIUS	OUTER CONTOUR RADIUS	UNDERCUT INNER	UNDERCUT OUTER	EFFECTIVE LENGTH INNER	EFFECTIVE LENGTH OUTER
FLAT PROFILE	FLAT PROFILE	0.0000000E+00	0.0000000E+00	8.5840000E-01	8.5840000E-01

INNER RACEWAY CROWN DROP VS AXIAL LOCATION

1.1586E-03	8.8225E-04	6.3663E-04	4.2171E-04	2.3750E-04	8.3984E-05	0.0000E+00	0.0000E+00	0.0000E+00
0.0000E+00	0.0000E+00	0.0000E+00	0.0000E+00	0.0000E+00	8.3984E-05	2.3750E-04	4.2171E-04	6.3663E-04
8.8225E-04	1.1586E-03							

OUTER RACEWAY CROWN DROP VS AXIAL LOCATION

1.1586E-03	8.8225E-04	6.3663E-04	4.2171E-04	2.3750E-04	8.3984E-05	0.0000E+00	0.0000E+00	0.0000E+00
0.0000E+00	0.0000E+00	0.0000E+00	0.0000E+00	0.0000E+00	8.3984E-05	2.3750E-04	4.2171E-04	6.3663E-04
8.8225E-04	1.1586E-03							

RACEWAY AND ROLLER SURFACE PROPERTIES

ROUGHNESS HEIGHT - AA			ROUGHNESS SLOPE - AA			YIELD STRENGTH		
INNER RACE	OUTER RACE	ROLLER	INNER RACE	OUTER RACE	ROLLER	INNER RACE	OUTER RACE	ROLLER
4.0000E+00	4.0000E+00	4.0000E+00	1.0000E+00	1.0000E+00	1.0000E+00	3.0000E+05	3.0000E+05	3.0000E+05

INNER RING STEEL IS M50 STEEL LIFE MULTIPLICATION FACTOR = 1.0000000E+00

OUTER RING STEEL IS M50 STEEL LIFE MULTIPLICATION FACTOR = 1.0000000E+00

NEW SKF LIFE THEORY - MATERIAL PROPERTIES

FATIGUE LIMIT (VON-MISES STRESS)		RESIDUAL STRESS		MATERIAL CONSTANT		LUBE FILTER
INNER RING	OUTER RING	INNER RING	OUTER RING	INNER RING	OUTER RING	RATING
7.3000000E+04	7.3000000E+04	0.0000000E+00	0.0000000E+00	1.0000000E+00	1.0000000E+00	1.5000000E+01

BEARING COMPONENT MATERIAL PROPERTIES

COMPONENT	MODULUS OF ELASTICITY	POISSONS RATIO	COEFFICIENT OF THERMAL EXPANSION	DENSITY	THERMAL CONDUCTIVITY	SPECIFIC HEAT
SHAFT	2.9600000E+07	3.0000000E-01	6.2440000E-06	2.8300000E-01	2.8875500E+01	1.1000000E-01
INNER RING	2.9600000E+07	3.0000000E-01	6.2440000E-06	2.8300000E-01	2.8875500E+01	1.1000000E-01
ROLLER	2.9600000E+07	3.0000000E-01	6.2440000E-06	2.8300000E-01	2.8875500E+01	1.1000000E-01
OUTER RING	2.9600000E+07	3.0000000E-01	6.2440000E-06	2.8300000E-01	2.8875500E+01	1.1000000E-01
HOUSING	2.9600000E+07	3.0000000E-01	6.2440000E-06	2.8300000E-01	2.8875500E+01	1.1000000E-01

CAGE DATA

MATERIAL - SILVER PLATED AMS 6414 STEEL DENSITY - 2.830000E-01

TYPE	LAND DIAMETER	LAND CONTACT AREA	CLEARANCE (RAIL-LAND)	CLEARANCE (POCKET)	WEIGHT
INNER RING LAND-RIDING	4.1150000E+00	5.6312980E+00	1.8000000E-02	0.0000000E+00	1.1712710E+00

RADIAL LOAD	AXIAL LOAD	MOMENT LOAD	MISALIGNMENT MINUTES	SHAFT SPEED RPM	OUTER RING SPEED RPM
1.0000000E+03	0.0000000E+00	0.0000000E+00	0.0000000E+00	1.5000000E+04	0.0000000E+00

SHAFT & HOUSING FITS (INTERFERENCE IS POSITIVE)

BEARING BORE TO SHAFT OD	BEARING OD TO HOUSING BORE
5.0000000E-04	0.0000000E+00

EFFECTIVE SHAFT, BEARING & HOUSING WIDTHS

SHAFT	BEARING INNER RING	BEARING OUTER RING	HOUSING
2.9134000E+00	1.4567000E+00	1.4567000E+00	2.9134000E+00

SHAFT, BEARING & HOUSING RADII

SHAFT INSIDE RADIUS	BEARING BORE RADIUS	BEARING INNER RING AVE OUTER RADIUS	BEARING OUTER RING AVE INNER RADIUS	BEARING OUTER RADIUS	HOUSING OUTER RADIUS
1.0000000E+00	1.4764000E+00	1.8850000E+00	2.8346500E+00	3.1496000E+00	3.7500000E+00

RING CROSS-SECTION MOMENT OF INERTIA

INNER RING	OUTER RING	HOUSING	SHAFT
8.2810200E-03	3.7923960E-03	5.2546140E-02	2.6250290E-02

BEARING OUTER RING HAS STRAP-TYPE SUPPORT IN HOUSING

LUBRICANT DATA

THE BEARING IS OPERATED WITH MIL-L-23699 TYPE LUBRICANT

WALTHER COEFFICIENTS "A"	"B"	DENSITY AT 60 DEG F	COEFFICIENT OF THERMAL EXPANSION (VOLUME)	THERMAL CONDUCTIVITY	SHEAR MODULUS OF ELASTICITY
1.0207210E+01	3.6550590E+00	3.6495500E-02	4.1400000E-04	8.7914390E-02	1.0000000E+04

VISCOSITY AT 100 DEG F	AT 210 DEG F	FRICTION COEFFICIENTS RACE ASPERITY	ROLL END-FLANGE	ROLLER-CAGE
4.3400000E-02	7.9050000E-03	1.0000000E-01	1.0000000E-01	0.0000000E+00

DURING OPERATION, LUBRICANT IS ASSUMED TO OCCUPY .410 PERCENT OF THE BEARING INTERNAL FREE VOLUME

BEARING SYSTEM TEMPERATURES - INPUT

OUTER RACEWAY	INNER RACEWAY	LUBRICANT	FLANGE 1	FLANGE 2	FLANGE 3	FLANGE 4
2.6000000E+02	2.6000000E+02	2.6000000E+02	2.6000000E+02	2.6000000E+02	2.6000000E+02	2.6000000E+02

CAGE	SHAFT	INNER RING	ROLLER	OUTER RING	HOUSING
2.6000000E+02	2.6000000E+02	2.6000000E+02	2.6000000E+02	2.6000000E+02	2.6000000E+02

RADIAL CLEARANCE	2-POINT OUT-OF-ROUND	3-POINT OUT-OF-ROUND
2.7500000E-03	2.5500300E-02	0.0000000E+00

INNER RACEWAY PERFORMANCE DATA

ROLLER POSITION ANGLE (DEGREES)	ROLLER LOAD	EFFECTIVE CONTACT LENGTH	COEFFICIENT OF FRICTION	RING RADIAL DEFLECTION	MINIMUM LUBRICANT FILM (MICROINCHES)	LAMBDA (H/SIGMA)
0.0000000E+00	0.0000000E+00	0.0000000E+00	0.0000000E+00	3.0768960E-04	1.2520250E+03	1.7706310E+02
3.0000000E+01	0.0000000E+00	0.0000000E+00	0.0000000E+00	2.9152910E-04	1.2520250E+03	1.7706310E+02
6.0000000E+01	1.0003240E+03	6.8672000E-01	9.4749640E-02	2.5927760E-04	1.2899920E+01	1.8243240E+00
9.0000000E+01	1.2983390E+03	7.7256000E-01	9.2040520E-02	2.4592050E-04	1.2470270E+01	1.7635620E+00
1.2000000E+02	0.0000000E+00	0.0000000E+00	0.0000000E+00	2.6413590E-04	1.2520250E+03	1.7706310E+02
1.5000000E+02	0.0000000E+00	0.0000000E+00	0.0000000E+00	2.9124940E-04	1.2520250E+03	1.7706310E+02

1.8000000E+02	0.0000000E+00	0.0000000E+00	0.0000000E+00	3.0331570E-04	1.2520250E+03	1.7706310E+02

MAXIMUM ORTHOGONAL SHEAR STRESS AMPLITUDE = 4.42715E+04 DEPTH OF MAX.ORTHO.SHEAR STRESS = 4.23288E-03

ANGLE (HERTZ STRESS VS AXIAL LOCATION)

0.	0.	0.	0.	0.	0.	0.	0.	0.	0.	0.	0.	0.	0.	0.
0.	0.	0.	0.	0.	0.									
30.	0.	0.	0.	0.	0.	0.	0.	0.	0.	0.	0.	0.	0.	0.
0.	0.	0.	0.	0.	0.									
60.	0.	0.	57743.	101757.	129698.	149756.	159881.	159881.	159881.	159881.	159881.	159881.	159881.	159881.
149756.	129698.	101757.	57743.	0.	0.									
90.	0.	30158.	92228.	125993.	149999.	167899.	177086.	177086.	177086.	177086.	177086.	177086.	177086.	177086.
167899.	149999.	125993.	92229.	30159.	0.									
120.	0.	0.	0.	0.	0.	0.	0.	0.	0.	0.	0.	0.	0.	0.
0.	0.	0.	0.	0.	0.									
150.	0.	0.	0.	0.	0.	0.	0.	0.	0.	0.	0.	0.	0.	0.
0.	0.	0.	0.	0.	0.									
180.	0.	0.	0.	0.	0.	0.	0.	0.	0.	0.	0.	0.	0.	0.
0.	0.	0.	0.	0.	0.									

RACEWAY L10 FATIGUE LIFE ESTIMATES - HOURS

LUNDBERG-PALMGREN	NEW SKF THEORY	CONTAMINATION LIFE FACTOR
4.8291230E+03	2.0637640E+07	1.9306090E-01

RACEWAY ROLLING CONTACT FATIGUE LIFE CAN BE INFINITE IF CONTAMINANTS ARE KEPT OUT OF THE BEARING

OUTER RACEWAY PERFORMANCE DATA

ROLLER POSITION ANGLE (DEGREES)	ROLLER LOAD	EFFECTIVE CONTACT LENGTH	COEFFICIENT OF FRICTION	RING RADIAL DEFLECTION	MINIMUM LUBRICANT FILM (MICROINCHES)	LAMBDA (H/SIGMA)
0.0000000E+00	4.8717710E+02	5.1504000E-01	0.0000000E+00	-3.9153860E-03	3.3457000E+01	4.7315340E+00
3.0000000E+01	4.8717710E+02	5.1504000E-01	0.0000000E+00	-1.8110480E-03	3.3457000E+01	4.7315340E+00
6.0000000E+01	1.4875070E+03	7.7256000E-01	9.0552120E-02	2.4058730E-03	1.4683950E+01	2.0766240E+00
9.0000000E+01	1.7855220E+03	7.7256000E-01	8.8312460E-02	4.1884060E-03	1.4338180E+01	2.0277250E+00
1.2000000E+02	4.8717710E+02	5.1504000E-01	0.0000000E+00	1.8259780E-03	3.3457000E+01	4.7315340E+00
1.5000000E+02	4.8717710E+02	5.1504000E-01	0.0000000E+00	-1.7767570E-03	3.3457000E+01	4.7315340E+00
1.8000000E+02	4.8717710E+02	5.1504000E-01	0.0000000E+00	-3.3948850E-03	3.3457000E+01	4.7315340E+00

MAXIMUM ORTHOGONAL SHEAR STRESS AMPLITUDE = 4.07044E+04 DEPTH OF MAX.ORTHO.SHEAR STRESS = 5.96208E-03

ANGLE (HERTZ STRESS VS AXIAL LOCATION)

0.	0.	0.	0.	0.	16982.	59002.	73558.	73558.	73558.	73558.	73558.	73558.	73558.	73558.
59002.	16982.	0.	0.	0.	0.									
30.	0.	0.	0.	0.	16982.	59002.	73558.	73558.	73558.	73558.	73558.	73558.	73558.	73558.
59002.	16982.	0.	0.	0.	0.									
60.	0.	41463.	84245.	110589.	129750.	144183.	151627.	151627.	151627.	151627.	151627.	151627.	151627.	151627.
144183.	129750.	110589.	84245.	41463.	0.									
90.	0.	67300.	101100.	124579.	142253.	155783.	162818.	162818.	162818.	162818.	162818.	162818.	162818.	162818.
155783.	142253.	124579.	101100.	67300.	0.									
120.	0.	0.	0.	0.	16982.	59002.	73558.	73558.	73558.	73558.	73558.	73558.	73558.	73558.
59002.	16982.	0.	0.	0.	0.									
150.	0.	0.	0.	0.	16982.	59002.	73558.	73558.	73558.	73558.	73558.	73558.	73558.	73558.
59002.	16982.	0.	0.	0.	0.									
180.	0.	0.	0.	0.	16982.	59002.	73558.	73558.	73558.	73558.	73558.	73558.	73558.	73558.
59002.	16982.	0.	0.	0.	0.									

RACEWAY L10 FATIGUE LIFE ESTIMATES - HOURS

LUNDBERG-PALMGREN	NEW SKF THEORY	CONTAMINATION LIFE FACTOR
1.4199270E+04	2.5782010E+09	2.1621880E-01

RACEWAY ROLLING CONTACT FATIGUE LIFE CAN BE INFINITE IF CONTAMINANTS ARE KEPT OUT OF THE BEARING

ROLLER PERFORMANCE DATA

POSITION ANGLE	SKEWING MOMENT	SPEED ABOUT ROLLER AXIS	CAGE WEB LOAD
0.0000000E+00	0.0000000E+00	3.3639100E+04	-3.9307420E-01
3.0000000E+01	0.0000000E+00	3.3639100E+04	-3.9307420E-01
6.0000000E+01	0.0000000E+00	3.3623420E+04	-1.7143470E-01
9.0000000E+01	0.0000000E+00	3.3632220E+04	-7.0816930E-02
1.2000000E+02	0.0000000E+00	3.3639100E+04	-3.9307420E-01
1.5000000E+02	0.0000000E+00	3.3639100E+04	-3.9307420E-01
1.8000000E+02	0.0000000E+00	3.3639100E+04	-3.9307420E-01
2.1000000E+02	0.0000000E+00	3.3639100E+04	-3.9307420E-01
2.4000000E+02	0.0000000E+00	3.3639100E+04	-3.9307420E-01
2.7000000E+02	0.0000000E+00	3.3625820E+04	-6.8058830E-02
3.0000000E+02	0.0000000E+00	3.3633410E+04	-1.7426980E-01
3.3000000E+02	0.0000000E+00	3.3639100E+04	-3.9307420E-01

POSITION ANGLE (DEGREES)	CENTRIFUGAL FORCE	HOLLOWNESS RATIO D(I)/D(O)	DIAMETER VARIATION	TILTING ANGLE (MINUTES)	FLANGE LOAD	BENDING STRESS
0.0000000E+00	4.8717710E+02	0.0000000E+00	0.0000000E+00	0.0000000E+00	0.0000000E+00	0.0000000E+00
3.0000000E+01	4.8717710E+02	0.0000000E+00	0.0000000E+00	0.0000000E+00	0.0000000E+00	0.0000000E+00
6.0000000E+01	4.8717710E+02	0.0000000E+00	0.0000000E+00	0.0000000E+00	0.0000000E+00	0.0000000E+00
9.0000000E+01	4.8717710E+02	0.0000000E+00	0.0000000E+00	0.0000000E+00	0.0000000E+00	0.0000000E+00
1.2000000E+02	4.8717710E+02	0.0000000E+00	0.0000000E+00	0.0000000E+00	0.0000000E+00	0.0000000E+00
1.5000000E+02	4.8717710E+02	0.0000000E+00	0.0000000E+00	0.0000000E+00	0.0000000E+00	0.0000000E+00
1.8000000E+02	4.8717710E+02	0.0000000E+00	0.0000000E+00	0.0000000E+00	0.0000000E+00	0.0000000E+00

BEARING PERFORMANCE DATA

DEFLECTIONS

RADIAL	AXIAL	MISALIGNMENT (MINUTES)
3.6841150E-03	0.0000000E+00	0.0000000E+00

FIT-UP DATA AT COLD TEMPERATURE & OPERATING TEMPERATURE

CHANGE IN DIAMETRAL CLEARANCE	COLD SHAFT FIT PRESSURE	OPERATING SHAFT FIT PRESSURE	COLD HOUSING FIT PRESSURE	OPERATING HOUSING FIT PRESSURE	FIT PRESSURE LOSS SPEED (RPM)
-6.4652340E-04	8.8371570E+02	2.1256910E+02	0.0000000E+00	0.0000000E+00	1.7212300E+04

INNER RING EXPANSION DUE TO SPEED	OUTER RING EXPANSION DUE TO SPEED	OUTER RING EXPANSION DUE TO ROLLER CENTRIFUGAL FORCE
5.5253840E-04	0.0000000E+00	3.9243900E-04

EFFECTIVE CLEARANCE	CAGE SPEED (RPM)	CAGE SPEED SLIP (PERCENT)	LOAD ON CAGE NET ROLLERS	LOAD ON CAGE WHIRL

2.5040500E-03	5.8403970E+03	1.4159080E+00	3.6318330E+00	2.0372960E+01

BEARING HEAT GENERATION RATES

OUTER RACEWAY SLIDING	INNER RACEWAY SLIDING	FLUID CHURNING	CAGE POCKET TO ROLLER	CAGE RAIL TO RING LAND
9.5829890E+02	6.4864170E+03	2.6220800E+03	3.9560530E+03	3.1350960E+03

FLANGE 1 TO ROLLER END	FLANGE 2 TO ROLLER END	FLANGE 3 TO ROLLER END	FLANGE 4 TO ROLLER END	TOTAL BEARING
0.0000000E+00	0.0000000E+00	4.4377710E-04	0.0000000E+00	1.7157950E+04

FATIGUE LIFE ESTIMATES

AFBMA L10 (HRS)	L&P L10 (HRS)	RATIO L&P/AFBMA	NEW SKF THEORY (HRS)	RATIO SKF/AFBMA
3.4979070E+05	3.8319240E+03	1.0954910E-02	2.0557660E+07	5.8771310E+01

BEARING ROLLING CONTACT FATIGUE LIFE CAN BE INFINITE IF CONTAMINANTS ARE KEPT OUT OF THE BEARING

ANALYSIS OF DYNAMIC PERFORMANCE CHARACTERISTICS OF CYLINDRICAL ROLLER BEARINGS UNDER RADIAL, AXIAL AND MOMENT LOADING

PC-CYBEAN2

a PERSONAL COMPUTER PROGRAM of

MRC BEARINGS
an SKF SPECIALTY BEARINGS company

BOEING ART MR315C2 CRB - CERAMIC ROLLERS

INPUT DATA PREPARED BY RAGEN

INPUT DATE: 5-31-91

ENGLISH SYSTEM UNITS - UNLESS OTHERWISE NOTED, ALL DATA GIVEN BELOW CONFORM TO THE FOLLOWING UNITS:

LENGTH - INCHES
AREA - SQUARE INCHES
SURFACE FINISH - MICROINCHES
FORCE OR LOAD - POUNDS
PRESSURE, STRESS, MODULUS of ELASTICITY - PSI
DENSITY - POUNDS PER CUBIC INCH
MOMENT OF INERTIA - IN.**4
TEMPERATURE - DEGREES FAHRENHEIT
KINEMATIC VISCOSITY - IN.**2/SEC
THERMAL EXPANSION - INCHES PER INCH PER DEGREE F
THERMAL CONDUCTIVITY - BTU PER HOUR PER FOOT PER DEGREE F
HEAT GENERATION - BTU PER HOUR
SPECIFIC HEAT - BTU PER LB PER DEGREE F

BEARING DIMENSIONS

ROLLERS/ROW	NO.ROWS	PITCH DIAMETER
1.2000000E+01	1.0000000E+00	4.6850000E+00

ROLLER DIMENSIONS

DIAMETER	TOTAL LENGTH	FLAT LENGTH	CORNER RADIUS	NUMBER OF LAMINAE
9.8430000E-01	9.8430000E-01	4.3100000E-01	5.9000000E-02	20

CROWN RADIUS	END SPHERE RADIUS	END CONTACT HEIGHT	FLANGE ANGLE (DEGREES)
6.0000000E+01	FLAT END	0.0000000E+00	4.4200000E-01

RACEWAY DATA

INNER CONTOUR RADIUS	OUTER CONTOUR RADIUS	UNDERCUT INNER	UNDERCUT OUTER	EFFECTIVE LENGTH INNER	EFFECTIVE LENGTH OUTER
FLAT PROFILE	FLAT PROFILE	0.0000000E+00	0.0000000E+00	8.6630000E-01	8.6630000E-01

INNER RACEWAY CROWN DROP VS AXIAL LOCATION

1.0241E-03	7.4263E-04	4.9247E-04	2.7358E-04	8.5955E-05	0.0000E+00	0.0000E+00	0.0000E+00	0.0000E+00
0.0000E+00	0.0000E+00	0.0000E+00	0.0000E+00	0.0000E+00	0.0000E+00	8.5954E-05	2.7357E-04	4.9247E-04
7.4263E-04	1.0241E-03							

OUTER RACEWAY CROWN DROP VS AXIAL LOCATION

1.0241E-03	7.4263E-04	4.9247E-04	2.7358E-04	8.5955E-05	0.0000E+00	0.0000E+00	0.0000E+00	0.0000E+00
0.0000E+00	0.0000E+00	0.0000E+00	0.0000E+00	0.0000E+00	0.0000E+00	8.5954E-05	2.7357E-04	4.9247E-04
7.4263E-04	1.0241E-03							

RACEWAY AND ROLLER SURFACE PROPERTIES

ROUGHNESS HEIGHT - AA			ROUGHNESS SLOPE - AA			YIELD STRENGTH		
INNER RACE	OUTER RACE	ROLLER	INNER RACE	OUTER RACE	ROLLER	INNER RACE	OUTER RACE	ROLLER
4.0000E+00	4.0000E+00	4.0000E+00	1.0000E+00	1.0000E+00	1.0000E+00	3.0000E+05	3.0000E+05	3.0000E+05

INNER RING STEEL IS M50 NiL STEEL LIFE MULTIPLICATION FACTOR = 1.0000000E+00

OUTER RING STEEL IS M50 STEEL LIFE MULTIPLICATION FACTOR = 1.0000000E+00

NEW SKF LIFE THEORY - MATERIAL PROPERTIES

FATIGUE LIMIT (VON MISES STRESS)		RESIDUAL STRESS		MATERIAL CONSTANT		LUBE FILTER
INNER RING	OUTER RING	INNER RING	OUTER RING	INNER RING	OUTER RING	RATING
8.8000000E+04	7.3000000E+04	0.0000000E+00	0.0000000E+00	1.0000000E+00	1.0000000E+00	1.5000000E+01

BEARING COMPONENT MATERIAL PROPERTIES

COMPONENT	MODULUS OF ELASTICITY	POISSONS RATIO	COEFFICIENT OF THERMAL EXPANSION	DENSITY	THERMAL CONDUCTIVITY	SPECIFIC HEAT
SHAFT	2.9600000E+07	3.0000000E-01	6.2440000E-06	2.8300000E-01	2.8875500E+01	1.1000000E-01
INNER RING	2.9600000E+07	3.0000000E-01	6.2440000E-06	2.8300000E-01	2.8875500E+01	1.1000000E-01
ROLLER	4.5000000E+07	2.6000000E-01	1.6100000E-06	1.1600000E-01	1.9000000E+01	1.5000000E-01
OUTER RING	2.9600000E+07	3.0000000E-01	6.2440000E-06	2.8300000E-01	2.8875500E+01	1.1000000E-01
HOUSING	2.9600000E+07	3.0000000E-01	6.2440000E-06	2.8300000E-01	2.8875500E+01	1.1000000E-01

CAGE DATA

MATERIAL - SILVER PLATED AMS 6414 STEEL DENSITY - 2.830000E-01

TYPE	LAND DIAMETER	LAND CONTACT AREA	CLEARANCE (RAIL-LAND)	CLEARANCE (POCKET)	WEIGHT
INNER RING LAND-RIDING	4.1150000E+00	5.4968500E+00	1.8000000E-02	0.0000000E+00	1.1540700E+00

RADIAL LOAD	AXIAL LOAD	MOMENT LOAD	MISALIGNMENT MINUTES	SHAFT SPEED RPM	OUTER RING SPEED RPM
1.0000000E+03	0.0000000E+00	0.0000000E+00	0.0000000E+00	1.5000000E+04	0.0000000E+00

SHAFT & HOUSING FITS (INTERFERENCE IS POSITIVE)

BEARING BORE TO SHAFT OD	BEARING OD TO HOUSING BORE
5.0000000E-04	0.0000000E+00

EFFECTIVE SHAFT, BEARING & HOUSING WIDTHS

SHAFT	BEARING INNER RING	BEARING OUTER RING	HOUSING
2.9134000E+00	1.4567000E+00	1.4567000E+00	2.9134000E+00

SHAFT, BEARING & HOUSING RADII

SHAFT INSIDE RADIUS	BEARING BORE RADIUS	BEARING INNER RING AVE OUTER RADIUS	BEARING OUTER RING AVE INNER RADIUS	BEARING OUTER RADIUS	HOUSING OUTER RADIUS
1.0000000E+00	1.4764000E+00	1.8850000E+00	2.8346500E+00	3.1496000E+00	3.7500000E+00

RING CROSS-SECTION MOMENT OF INERTIA

INNER RING	OUTER RING	HOUSING	SHAFT
8.2810200E-03	3.7923960E-03	5.2546140E-02	2.6250290E-02

BEARING OUTER RING HAS STRAP-TYPE SUPPORT IN HOUSING

LUBRICANT DATA

THE BEARING IS OPERATED WITH MIL-L-23699 TYPE LUBRICANT

WALTHER COEFFICIENTS "A"	"B"	DENSITY AT 60 DEG F	COEFFICIENT OF THERMAL EXPANSION (VOLUME)	THERMAL CONDUCTIVITY	SHEAR MODULUS OF ELASTICITY
1.0207210E+01	3.6550590E+00	3.6495500E-02	4.1400000E-04	8.7914390E-02	1.0000000E+04

VISCOSITY AT 100 DEG F	AT 210 DEG F	FRICTION COEFFICIENTS RACE ASPERITY	ROLL END-FLANGE	ROLLER-CAGE
4.3400000E-02	7.9050000E-03	1.0000000E-01	1.0000000E-01	0.0000000E+00

DURING OPERATION, LUBRICANT IS ASSUMED TO OCCUPY .410 PERCENT OF THE BEARING INTERNAL FREE VOLUME

BEARING SYSTEM TEMPERATURES - INPUT

OUTER RACEWAY	INNER RACEWAY	LUBRICANT	FLANGE 1	FLANGE 2	FLANGE 3	FLANGE 4
2.6000000E+02	2.6000000E+02	2.6000000E+02	2.6000000E+02	2.6000000E+02	2.6000000E+02	2.6000000E+02

CAGE	SHAFT	INNER RING	ROLLER	OUTER RING	HOUSING
2.6000000E+02	2.6000000E+02	2.6000000E+02	2.6000000E+02	2.6000000E+02	2.6000000E+02

RADIAL CLEARANCE	2-POINT OUT-OF-ROUND	3-POINT OUT-OF-ROUND
2.7500000E-03	2.5500300E-02	0.0000000E+00

INNER RACEWAY PERFORMANCE DATA

ROLLER POSITION ANGLE (DEGREES)	ROLLER LOAD	EFFECTIVE CONTACT LENGTH	COEFFICIENT OF FRICTION	RING RADIAL DEFLECTION	MINIMUM LUBRICANT FILM (MICROINCHES)	LAMBDA (H/SIGMA)
0.0000000E+00	0.0000000E+00	0.0000000E+00	0.0000000E+00	3.0622460E-04	2.0063000E+03	2.8373360E+02
3.0000000E+01	0.0000000E+00	0.0000000E+00	0.0000000E+00	2.9074970E-04	2.0063000E+03	2.8373360E+02
6.0000000E+01	1.0000000E+03	6.9304000E-01	9.1580840E-02	2.5999400E-04	1.2830750E+01	1.8145420E+00
9.0000000E+01	1.2068040E+03	6.9304000E-01	9.0258480E-02	2.4751250E-04	1.2522170E+01	1.7709020E+00
1.2000000E+02	0.0000000E+00	0.0000000E+00	0.0000000E+00	2.6485070E-04	2.0063000E+03	2.8373360E+02
1.5000000E+02	0.0000000E+00	0.0000000E+00	0.0000000E+00	2.9047010E-04	2.0063000E+03	2.8373360E+02

1.8000000E+02	0.0000000E+00	0.0000000E+00	0.0000000E+00	3.0185210E-04	2.0063000E+03	2.8373360E+02

MAXIMUM ORTHOGONAL SHEAR STRESS AMPLITUDE = 4.54983E+04 DEPTH OF MAX.ORTHO.SHEAR STRESS = 3.64103E-03

ANGLE (HERTZ STRESS VS AXIAL LOCATION)

0.	0.	0.	0.	0.	0.	0.	0.	0.	0.	0.	0.	0.	0.	0.
0.	0.	0.	0.	0.	0.									
30.	0.	0.	0.	0.	0.	0.	0.	0.	0.	0.	0.	0.	0.	0.
0.	0.	0.	0.	0.	0.									
60.	0.	0.	65335.	120068.	154254.	168036.	168036.	168036.	168036.	168036.	168036.	168036.	168036.	168036.
168036.	154254.	120068.	65335.	0.	0.									
90.	0.	0.	91846.	137838.	169108.	181993.	181993.	181993.	181993.	181993.	181993.	181993.	181993.	181993.
181993.	169109.	137838.	91846.	0.	0.									
120.	0.	0.	0.	0.	0.	0.	0.	0.	0.	0.	0.	0.	0.	0.
0.	0.	0.	0.	0.	0.									
150.	0.	0.	0.	0.	0.	0.	0.	0.	0.	0.	0.	0.	0.	0.
0.	0.	0.	0.	0.	0.									
180.	0.	0.	0.	0.	0.	0.	0.	0.	0.	0.	0.	0.	0.	0.
0.	0.	0.	0.	0.	0.									

RACEWAY L10 FATIGUE LIFE ESTIMATES - HOURS

LUNDBERG-PALMGREN	NEW SKF THEORY	CONTAMINATION LIFE FACTOR
2.5960890E+03	2.8167980E+09	1.9372100E-01

RACEWAY ROLLING CONTACT FATIGUE LIFE CAN BE INFINITE IF CONTAMINANTS ARE KEPT OUT OF THE BEARING

OUTER RACEWAY PERFORMANCE DATA

ROLLER POSITION ANGLE (DEGREES)	ROLLER LOAD	EFFECTIVE CONTACT LENGTH	COEFFICIENT OF FRICTION	RING RADIAL DEFLECTION	MINIMUM LUBRICANT FILM (MICROINCHES)	LAMBDA (H/SIGMA)
0.0000000E+00	1.9170360E+02	5.1978000E-01	0.0000000E+00	-3.3979700E-03	3.7032000E+01	5.2371150E+00
3.0000000E+01	1.9170360E+02	5.1978000E-01	0.0000000E+00	-1.6171380E-03	3.7032000E+01	5.2371150E+00
6.0000000E+01	1.1923090E+03	6.9304000E-01	9.0364260E-02	1.9475590E-03	1.4944700E+01	2.1135000E+00
9.0000000E+01	1.3991120E+03	7.7967000E-01	8.8815640E-02	3.4467090E-03	1.4638040E+01	2.0701320E+00
1.2000000E+02	1.9170360E+02	5.1978000E-01	0.0000000E+00	1.4543320E-03	3.7032000E+01	5.2371150E+00
1.5000000E+02	1.9170360E+02	5.1978000E-01	0.0000000E+00	-1.5878370E-03	3.7032000E+01	5.2371150E+00
1.8000000E+02	1.9170360E+02	5.1978000E-01	0.0000000E+00	-2.9554950E-03	3.7032000E+01	5.2371150E+00

MAXIMUM ORTHOGONAL SHEAR STRESS AMPLITUDE = 3.92540E+04 DEPTH OF MAX.ORTHO.SHEAR STRESS = 4.81237E-03

ANGLE (HERTZ STRESS VS AXIAL LOCATION)

0.	0.	0.	0.	0.	18214.	52559.	52559.	52559.	52559.	52559.	52559.	52559.	52559.	52559.
52559.	18214.	0.	0.	0.	0.									
30.	0.	0.	0.	0.	18214.	52559.	52559.	52559.	52559.	52559.	52559.	52559.	52559.	52559.
52559.	18214.	0.	0.	0.	0.									
60.	0.	0.	69105.	109177.	135878.	146822.	146822.	146822.	146822.	146822.	146822.	146822.	146822.	146822.
146822.	135878.	109177.	69105.	0.	0.									
90.	0.	17034.	87542.	122304.	146803.	157016.	157016.	157016.	157016.	157016.	157016.	157016.	157016.	157016.
157016.	146803.	122304.	87542.	17035.	0.									
120.	0.	0.	0.	0.	18214.	52559.	52559.	52559.	52559.	52559.	52559.	52559.	52559.	52559.
52559.	18214.	0.	0.	0.	0.									
150.	0.	0.	0.	0.	18214.	52559.	52559.	52559.	52559.	52559.	52559.	52559.	52559.	52559.
52559.	18214.	0.	0.	0.	0.									
180.	0.	0.	0.	0.	18214.	52559.	52559.	52559.	52559.	52559.	52559.	52559.	52559.	52559.
52559.	18214.	0.	0.	0.	0.									

RACEWAY L10 FATIGUE LIFE ESTIMATES - HOURS

LUNDBERG-PALMGREN	NEW SKF THEORY	CONTAMINATION LIFE FACTOR
1.3858310E+04	1.2490410E+10	2.1982490E-01

RACEWAY ROLLING CONTACT FATIGUE LIFE CAN BE INFINITE IF CONTAMINANTS ARE KEPT OUT OF THE BEARING

ROLLER PERFORMANCE DATA

POSITION ANGLE	SKEWING MOMENT	SPEED ABOUT ROLLER AXIS	CAGE WEB LOAD
0.0000000E+00	0.0000000E+00	3.2954940E+04	-3.8030090E-01
3.0000000E+01	0.0000000E+00	3.2954940E+04	-3.8030090E-01
6.0000000E+01	0.0000000E+00	3.2912950E+04	-1.8501230E-01
9.0000000E+01	0.0000000E+00	3.2936690E+04	-1.0100340E-01
1.2000000E+02	0.0000000E+00	3.2954940E+04	-3.8030090E-01
1.5000000E+02	0.0000000E+00	3.2954940E+04	-3.8030090E-01
1.8000000E+02	0.0000000E+00	3.2954940E+04	-3.8030090E-01
2.1000000E+02	0.0000000E+00	3.2954940E+04	-3.8030090E-01
2.4000000E+02	0.0000000E+00	3.2954940E+04	-3.8030090E-01
2.7000000E+02	0.0000000E+00	3.2925530E+04	-9.8231990E-02
3.0000000E+02	0.0000000E+00	3.2929910E+04	-1.8789910E-01
3.3000000E+02	0.0000000E+00	3.2954940E+04	-3.8030090E-01

POSITION ANGLE (DEGREES)	CENTRIFUGAL FORCE	HOLLOWNESS RATIO D(I)/D(O)	DIAMETER VARIATION	TILTING ANGLE (MINUTES)	FLANGE LOAD	BENDING STRESS
0.0000000E+00	1.9170360E+02	0.0000000E+00	0.0000000E+00	0.0000000E+00	0.0000000E+00	0.0000000E+00
3.0000000E+01	1.9170360E+02	0.0000000E+00	0.0000000E+00	0.0000000E+00	0.0000000E+00	0.0000000E+00
6.0000000E+01	1.9170360E+02	0.0000000E+00	0.0000000E+00	0.0000000E+00	0.0000000E+00	0.0000000E+00
9.0000000E+01	1.9170360E+02	0.0000000E+00	0.0000000E+00	0.0000000E+00	0.0000000E+00	0.0000000E+00
1.2000000E+02	1.9170360E+02	0.0000000E+00	0.0000000E+00	0.0000000E+00	0.0000000E+00	0.0000000E+00
1.5000000E+02	1.9170360E+02	0.0000000E+00	0.0000000E+00	0.0000000E+00	0.0000000E+00	0.0000000E+00
1.8000000E+02	1.9170360E+02	0.0000000E+00	0.0000000E+00	0.0000000E+00	0.0000000E+00	0.0000000E+00

BEARING PERFORMANCE DATA

DEFLECTIONS

RADIAL	AXIAL	MISALIGNMENT (MINUTES)
4.0966640E-03	0.0000000E+00	0.0000000E+00

FIT-UP DATA AT COLD TEMPERATURE & OPERATING TEMPERATURE

CHANGE IN DIAMETRAL CLEARANCE	COLD SHAFT FIT PRESSURE	OPERATING SHAFT FIT PRESSURE	COLD HOUSING FIT PRESSURE	OPERATING HOUSING FIT PRESSURE	FIT PRESSURE LOSS SPEED (RPM)
1.1049950E-03	8.8371570E+02	2.1256910E+02	0.0000000E+00	0.0000000E+00	1.7212300E+04

INNER RING EXPANSION	OUTER RING EXPANSION	
DUE TO SPEED	DUE TO SPEED	DUE TO ROLLER CENTRIFUGAL FORCE
5.5253840E-04	0.0000000E+00	1.5563090E-04

EFFECTIVE CLEARANCE	CAGE SPEED (RPM)	CAGE SPEED SLIP (PERCENT)	LOAD ON CAGE NET ROLLERS	WHIRL

4.0125990E-03	5.7216140E+03	3.4209230E+00	3.6228480E+00	1.9265560E+01

BEARING HEAT GENERATION RATES

OUTER RACEWAY SLIDING	INNER RACEWAY SLIDING	FLUID CHURNING	CAGE POCKET TO ROLLER	CAGE RAIL TO RING LAND
7.8535600E+02	1.5300410E+04	2.4821590E+03	3.8501400E+03	3.1424980E+03

FLANGE 1 TO ROLLER END	FLANGE 2 TO ROLLER END	FLANGE 3 TO ROLLER END	FLANGE 4 TO ROLLER END	TOTAL BEARING
0.0000000E+00	0.0000000E+00	1.0360260E-04	0.0000000E+00	2.5560560E+04

FATIGUE LIFE ESTIMATES

AFBMA L10 (HRS)	L&P L10 (HRS)	RATIO L&P/AFBMA	NEW SKF THEORY (HRS)	RATIO SKF/AFBMA
3.5819790E+05	2.2893580E+03	6.3913210E-03	2.4182950E+09	6.7512820E+03

BEARING ROLLING CONTACT FATIGUE LIFE CAN BE INFINITE IF CONTAMINANTS ARE KEPT OUT OF THE BEARING

APPENDIX E

PLOTS OF TRACTION COEFFICIENT VERSUS PERCENT SLIP FOR FRICTION TESTS OF MATERIALS AND LUBRICANTS

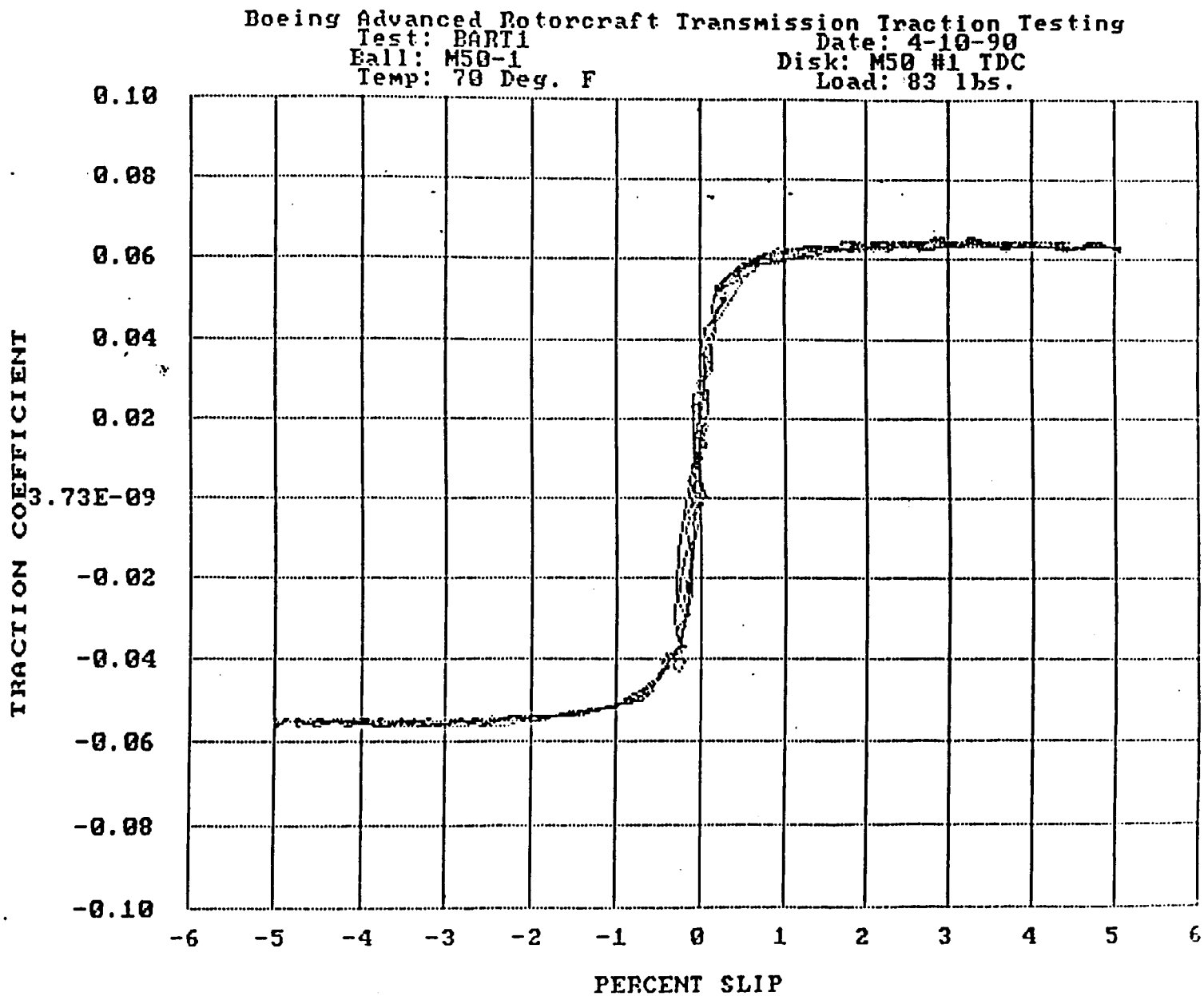
Boeing Advanced Rotorcraft Transmission Traction Testing
Test: BART1
Date: 4-10-90
Ball: M50-1
Disk: M50 #1 TDC
Temp: 70 Deg. F
Load: 83 lbs.
TRACTION COEFFICIENT
0.10
0.08
0.06
0.04
0.02
3.73E-09
-0.02
-0.04
-0.06
-0.08
-0.10
-6
-5
-4
-3
-2
-1
0
1
2
3
4
5
6
PERCENT SLIP

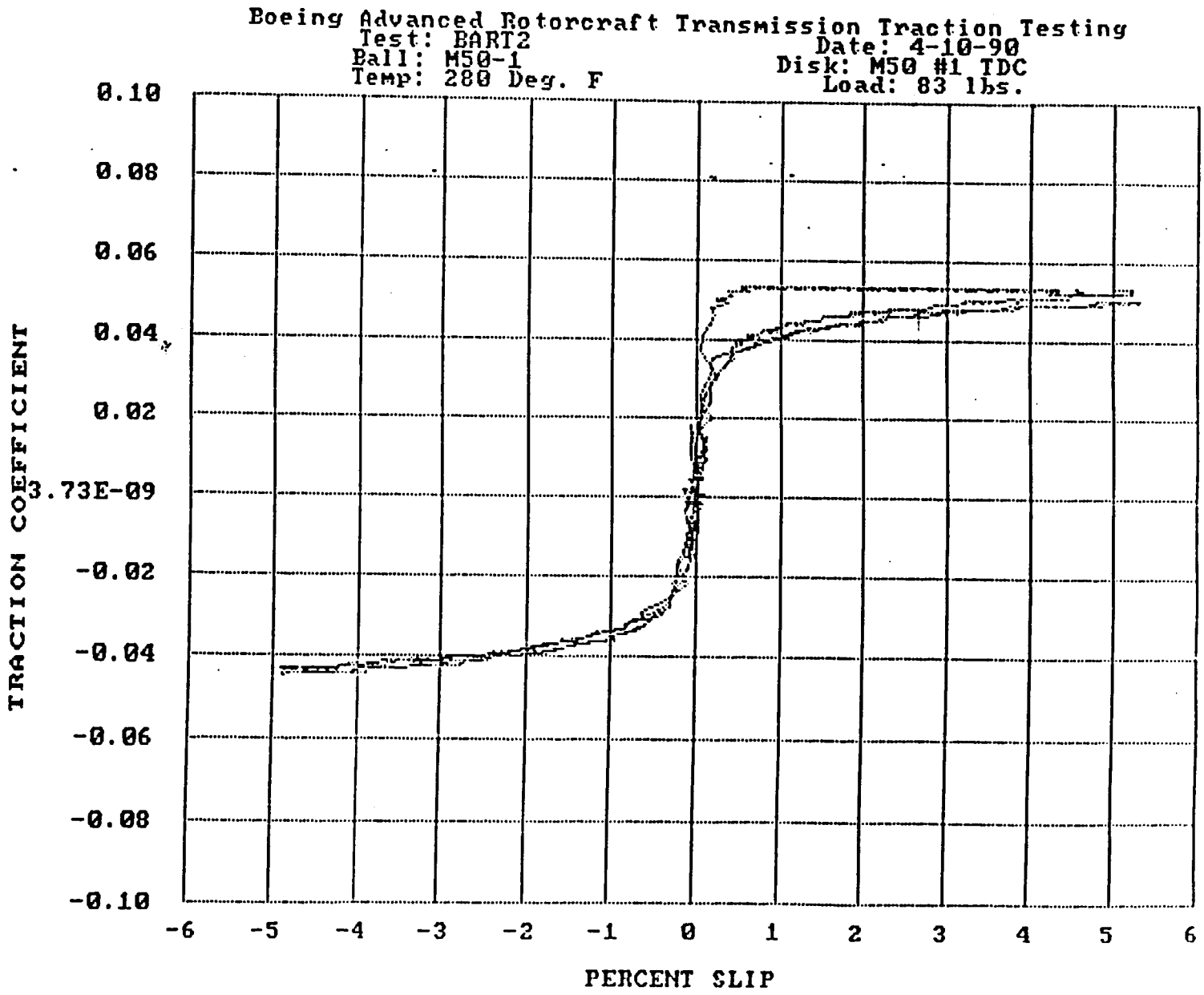
Boeing Advanced Rotorcraft Transmission Traction Testing
Test: BART2
Ball: M50-1
Temp: 280 Deg. F
Date: 4-10-90
Disk: M50 #1 TDC
Load: 83 lbs.
TRACTION COEFFICIENT
0.10
0.08
0.06
0.04
0.02
3.73E-09
-0.02
-0.04
-0.06
-0.08
-0.10
-6
-5
-4
-3
-2
-1
0
1
2
3
4
5
6
PERCENT SLIP

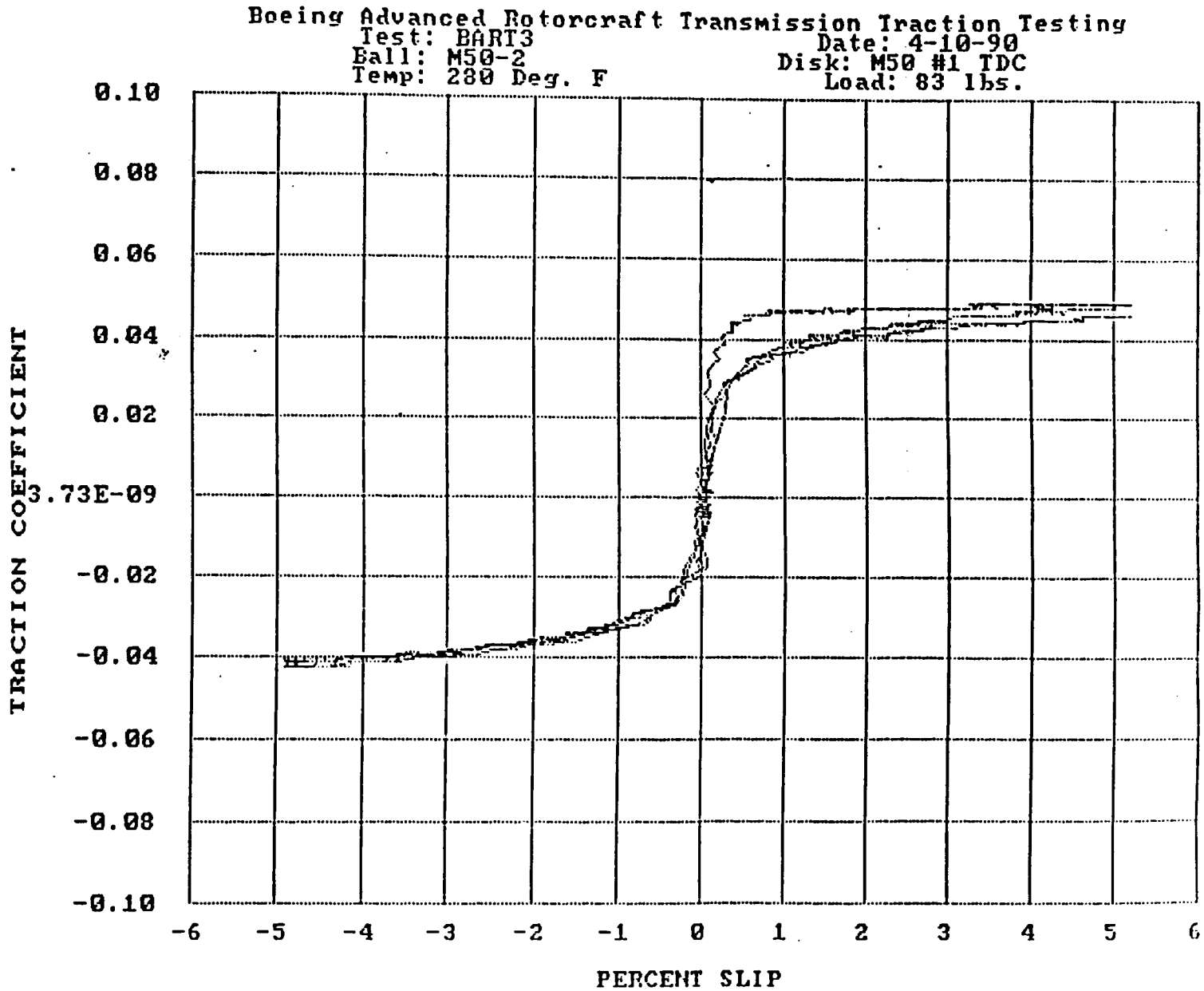
Boeing Advanced Rotorcraft Transmission Traction Testing
Test: BART3
Ball: M50-2
Temp: 280 Deg. F
Date: 4-10-90
Disk: M50 #1 TDC
Load: 83 lbs.
TRACTION COEFFICIENT
0.10
0.08
0.06
0.04
0.02
3.73E-09
-0.02
-0.04
-0.06
-0.08
-0.10
-6
-5
-4
-3
-2
-1
0
1
2
3
4
5
6
PERCENT SLIP

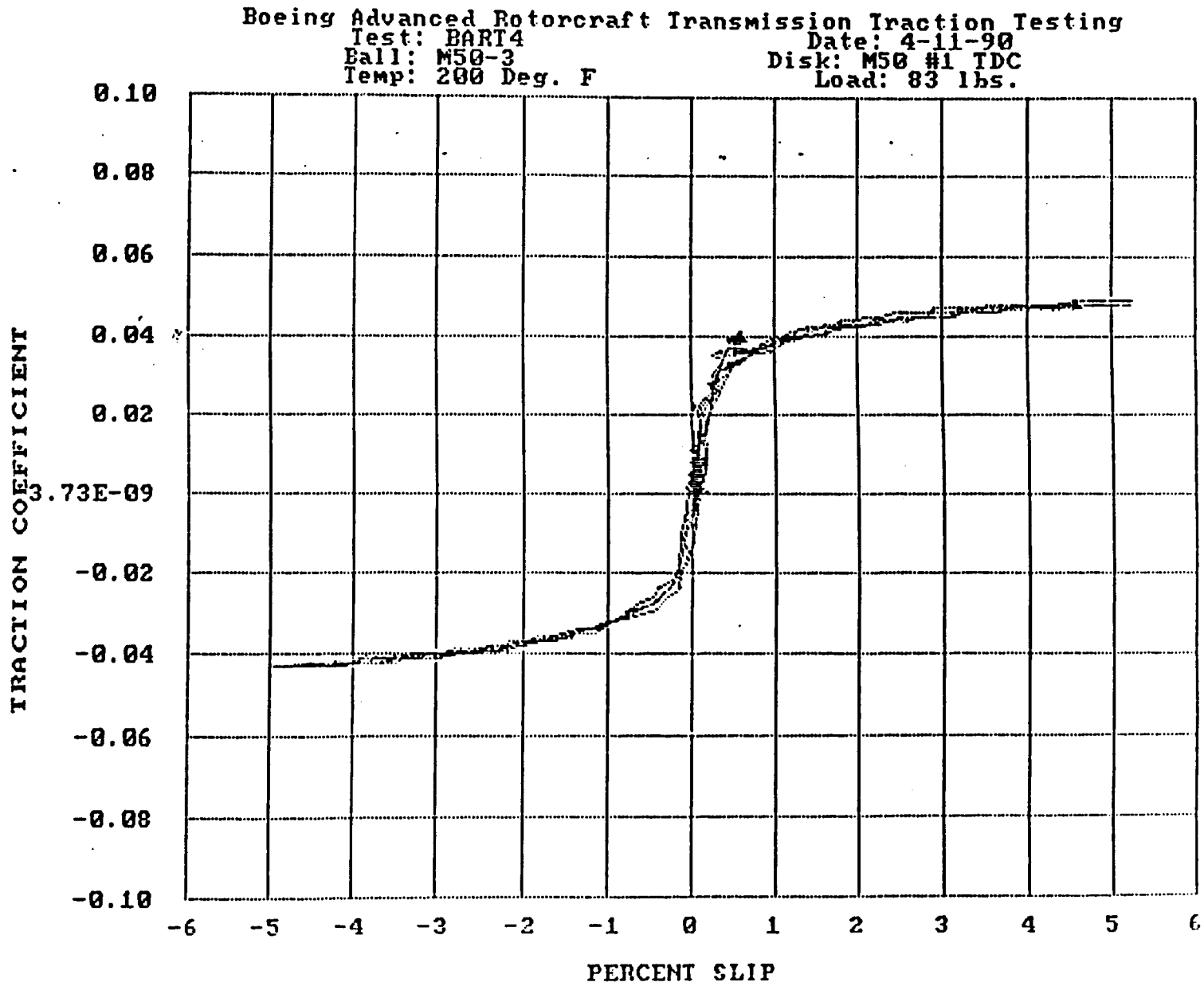
Boeing Advanced Rotorcraft Transmission Traction Testing
Test: BART4
Ball: M50-3
Temp: 200 Deg. F
Date: 4-11-90
Disk: M50 #1 TDC
Load: 83 lbs.
0.10
0.08
0.06
0.04
0.02
3.73E-09
-0.02
-0.04
-0.06
-0.08
-0.10
TRACTION COEFFICIENT
-6
-5
-4
-3
-2
-1
0
1
2
3
4
5
6
PERCENT SLIP

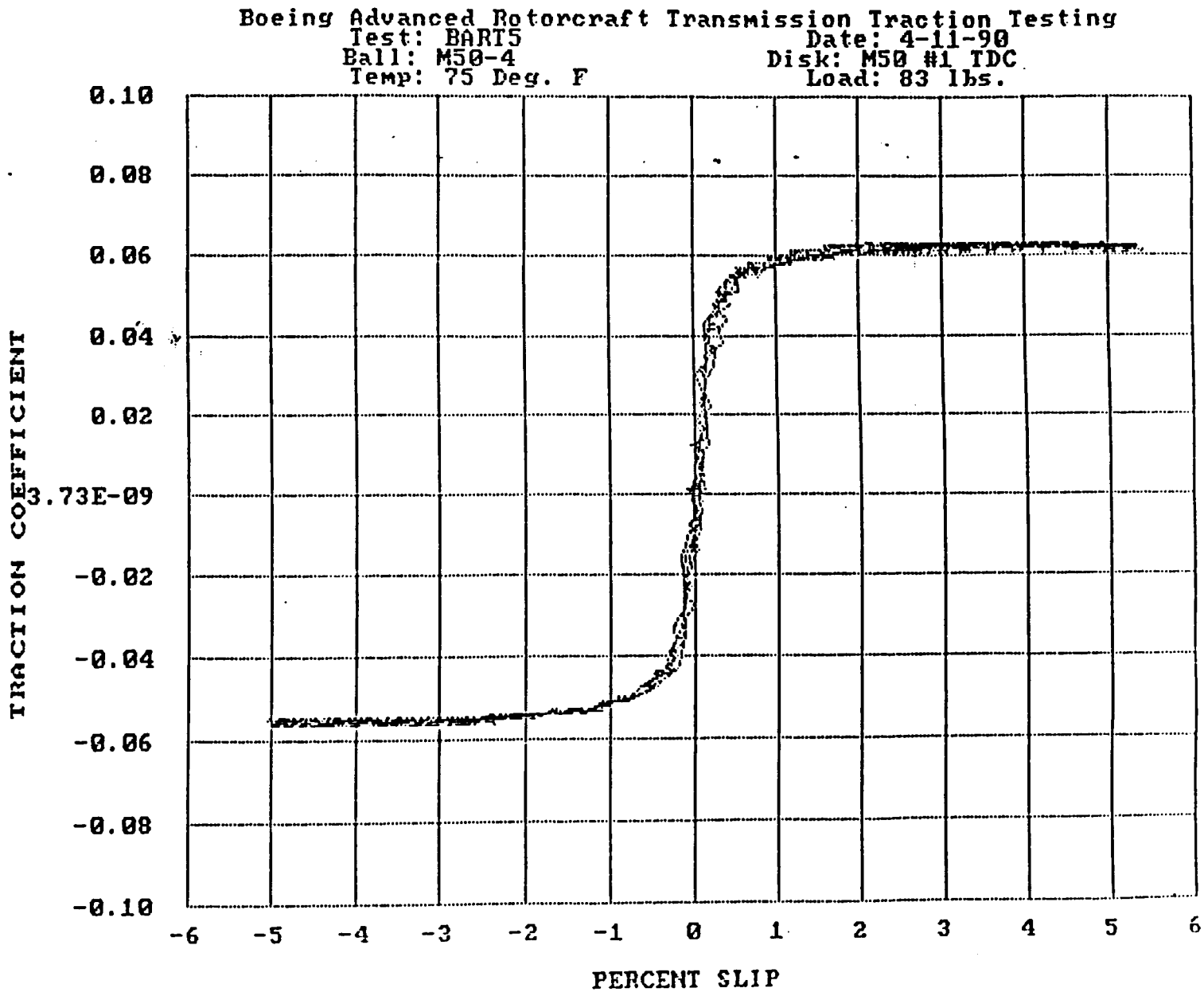
Boeing Advanced Rotorcraft Transmission Traction Testing
Test: BART5
Date: 4-11-90
Ball: M50-4
Disk: M50 #1 TDC
Temp: 75 Deg. F
Load: 83 lbs.
TRACTION COEFFICIENT
0.10
0.08
0.06
0.04
0.02
3.73E-09
-0.02
-0.04
-0.06
-0.08
-0.10
-6
-5
-4
-3
-2
-1
0
1
2
3
4
5
6
PERCENT SLIP

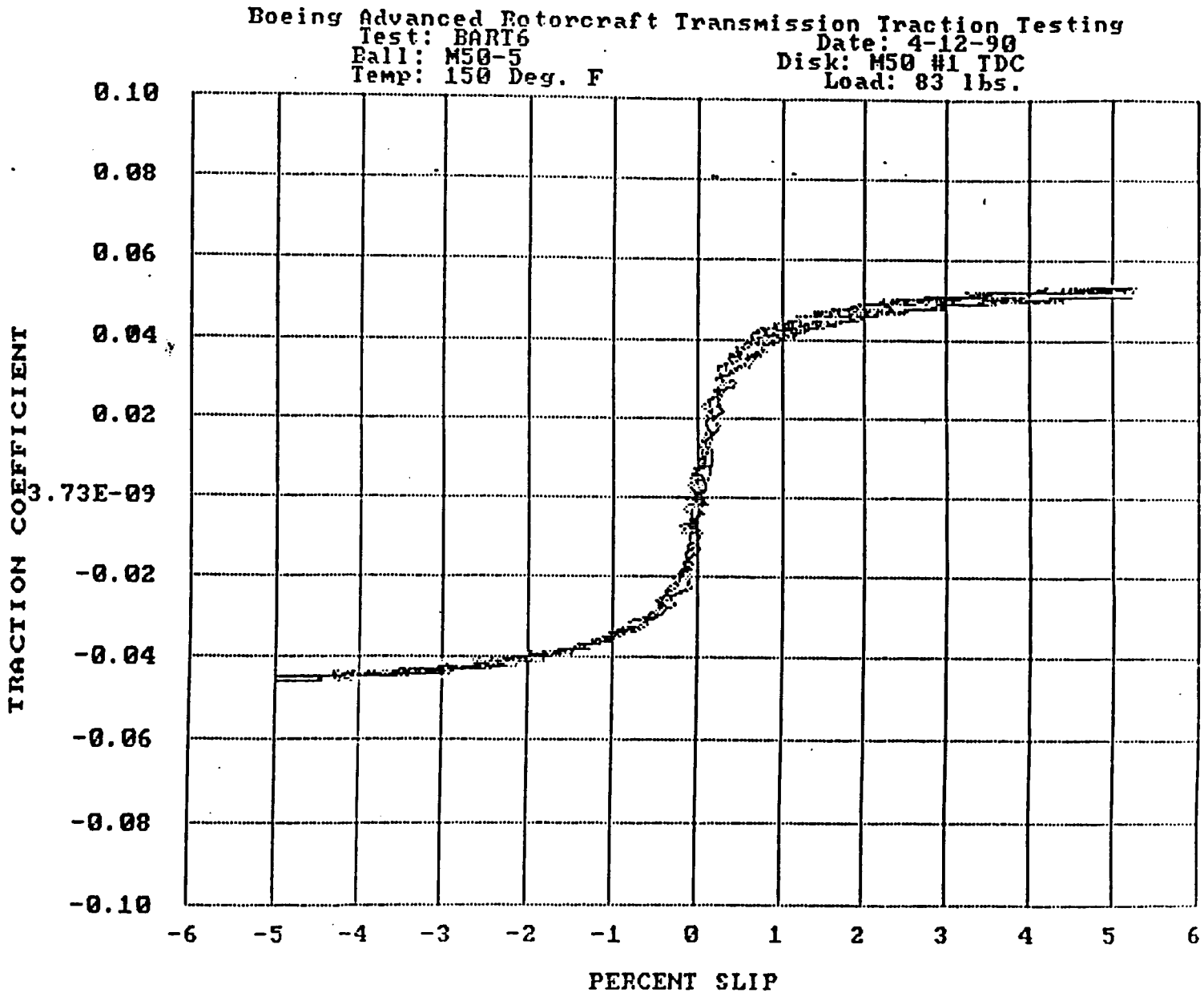
Boeing Advanced Rotorcraft Transmission Traction Testing
Test: BART6
Ball: M50-5
Temp: 150 Deg. F
Date: 4-12-90
Disk: M50 #1 TDC
Load: 83 lbs.
TRACTION COEFFICIENT
0.10
0.08
0.06
0.04
0.02
3.73E-09
-0.02
-0.04
-0.06
-0.08
-0.10
-6
-5
-4
-3
-2
-1
0
1
2
3
4
5
6
PERCENT SLIP

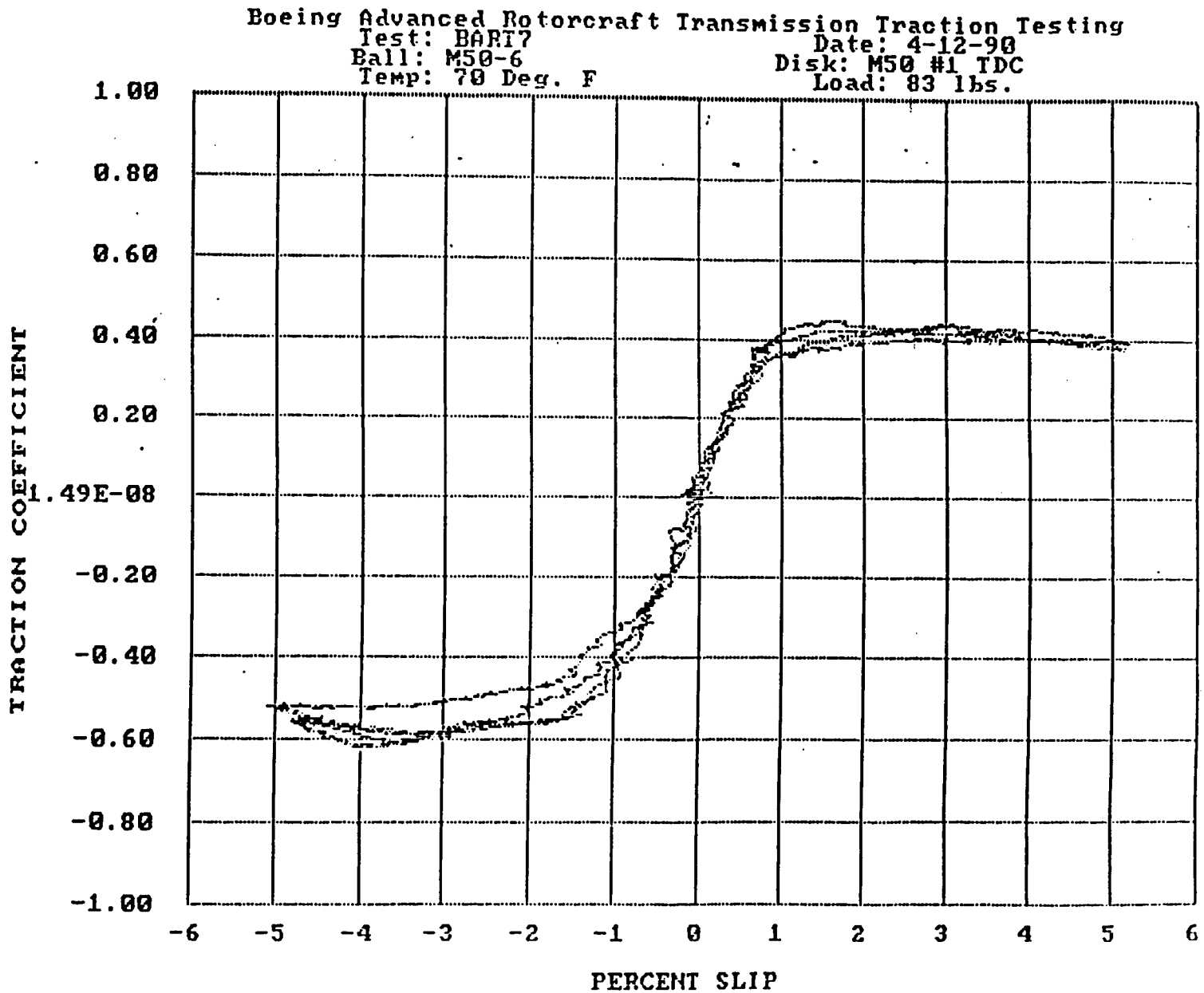
Boeing Advanced Rotorcraft Transmission Traction Testing
Test: BART7
Ball: M50-6
Temp: 70 Deg. F
Date: 4-12-90
Disk: M50 #1 TDC
Load: 83 lbs.
TRACTION COEFFICIENT
1.00
0.80
0.60
0.40
0.20
1.49E-08
-0.20
-0.40
-0.60
-0.80
-1.00
-6
-5
-4
-3
-2
-1
0
1
2
3
4
5
6
PERCENT SLIP

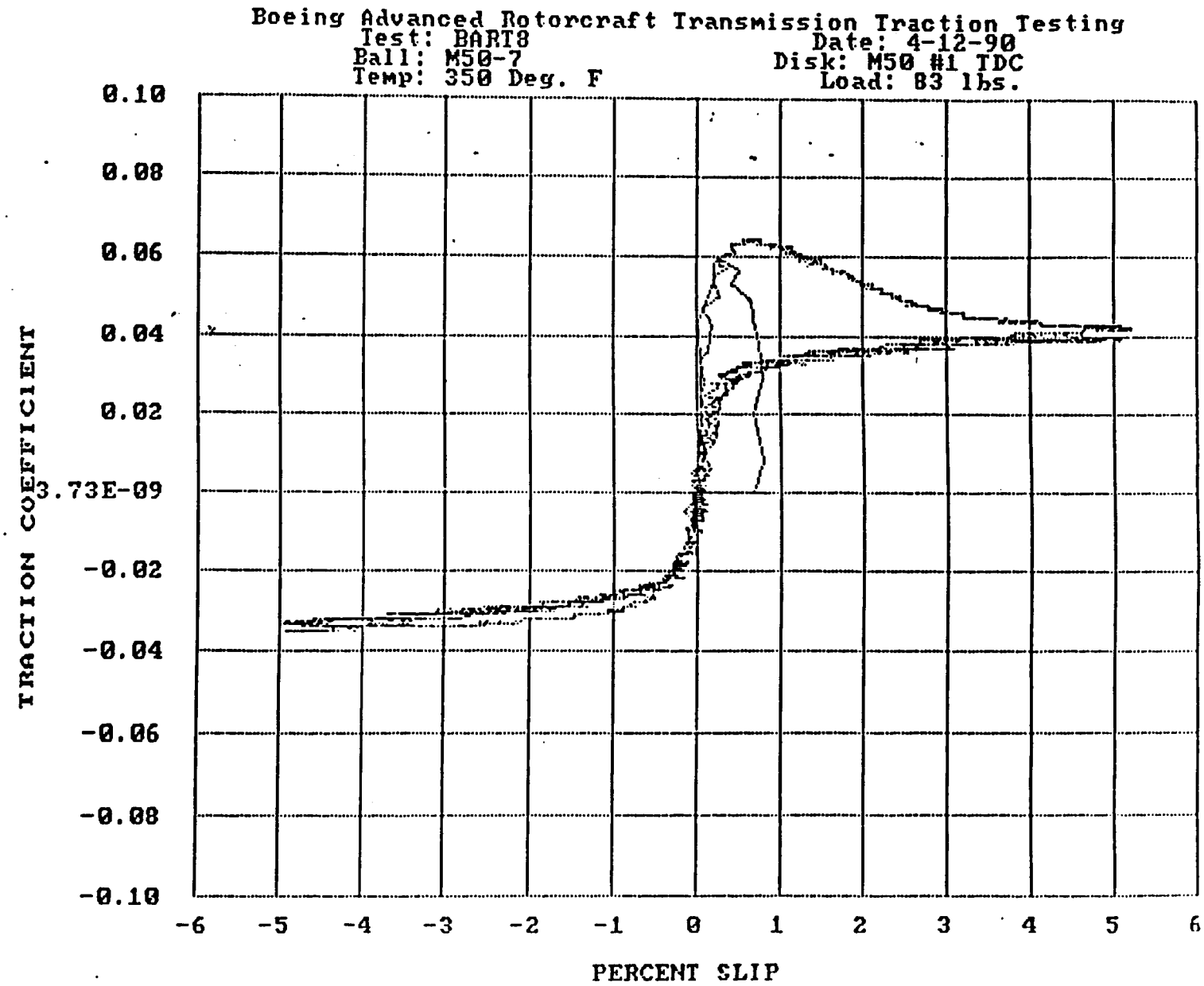
Boeing Advanced Rotorcraft Transmission Traction Testing
Test: BART8
Ball: M50-7
Temp: 350 Deg. F
Date: 4-12-90
Disk: M50 #1 TDC
Load: 83 lbs.
TRACTION COEFFICIENT
0.10
0.08
0.06
0.04
0.02
3.73E-09
-0.02
-0.04
-0.06
-0.08
-0.10
-6
-5
-4
-3
-2
-1
0
1
2
3
4
5
6
PERCENT SLIP

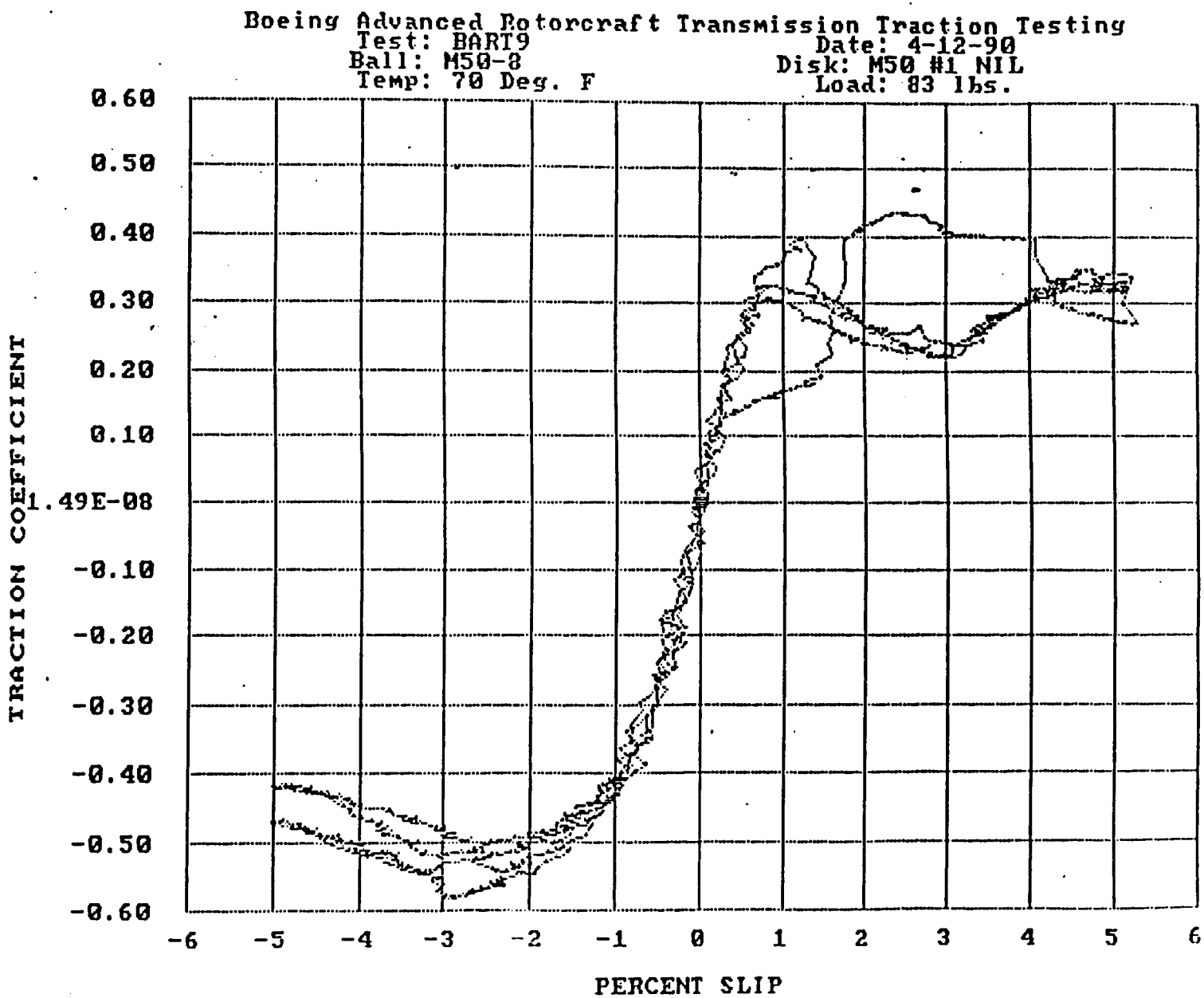
Boeing Advanced Rotorcraft Transmission Traction Testing
Test: BART9
Ball: M50-8
Temp: 70 Deg. F
Date: 4-12-90
Disk: M50 #1 NIL
Load: 83 lbs.
TRACTION COEFFICIENT
0.60
0.50
0.40
0.30
0.20
0.10
1.49E-08
-0.10
-0.20
-0.30
-0.40
-0.50
-0.60
-6
-5
-4
-3
-2
-1
0
1
2
3
4
5
6
PERCENT SLIP

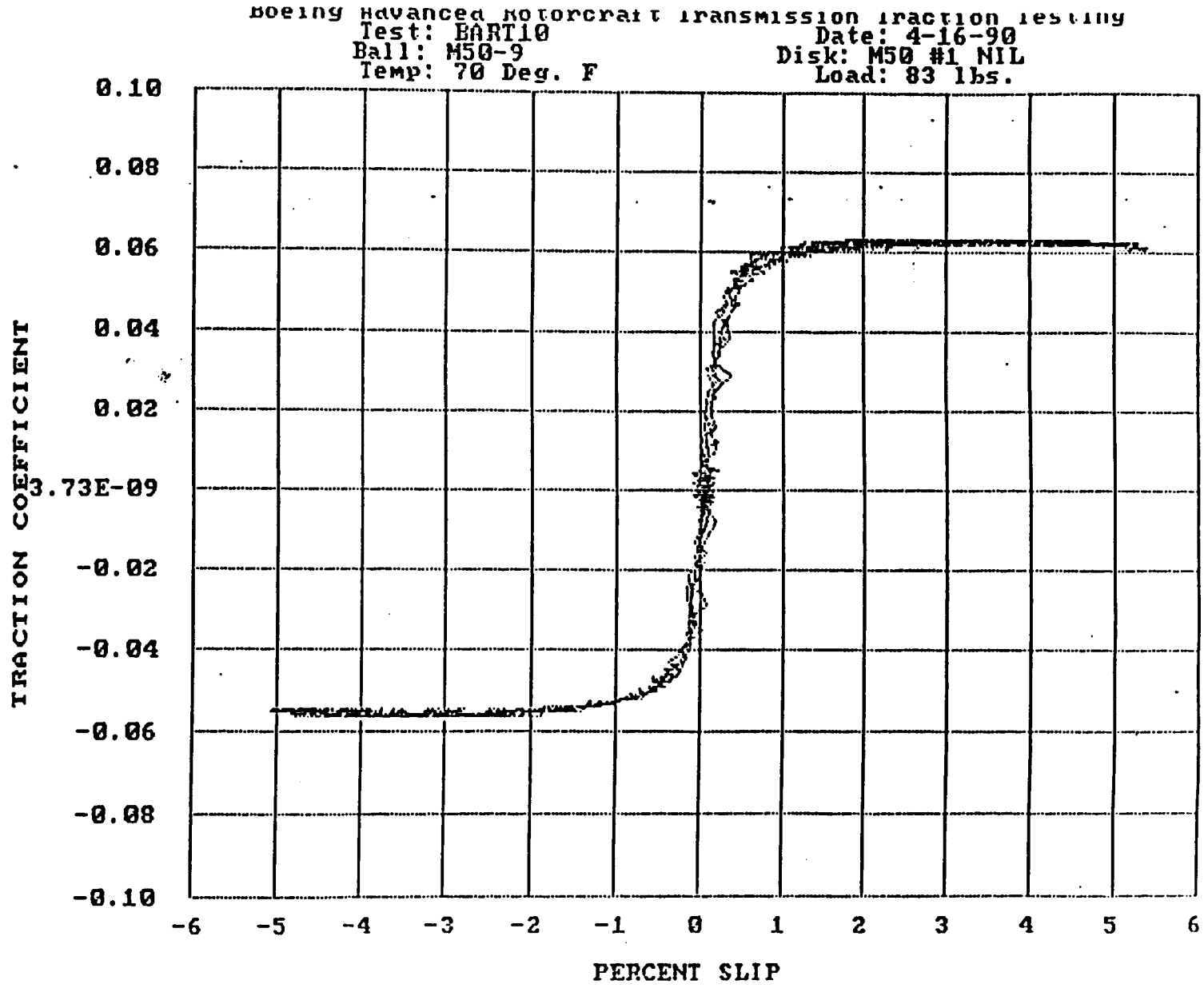
Boeing Advanced Rotorcraft Transmission Traction Testing
Test: BART10
Ball: M50-9
Temp: 70 Deg. F
Date: 4-16-90
Disk: M50 #1 NIL
Load: 83 lbs.
TRACTION COEFFICIENT
0.10
0.08
0.06
0.04
0.02
3.73E-09
-0.02
-0.04
-0.06
-0.08
-0.10
-6
-5
-4
-3
-2
-1
0
1
2
3
4
5
6
PERCENT SLIP

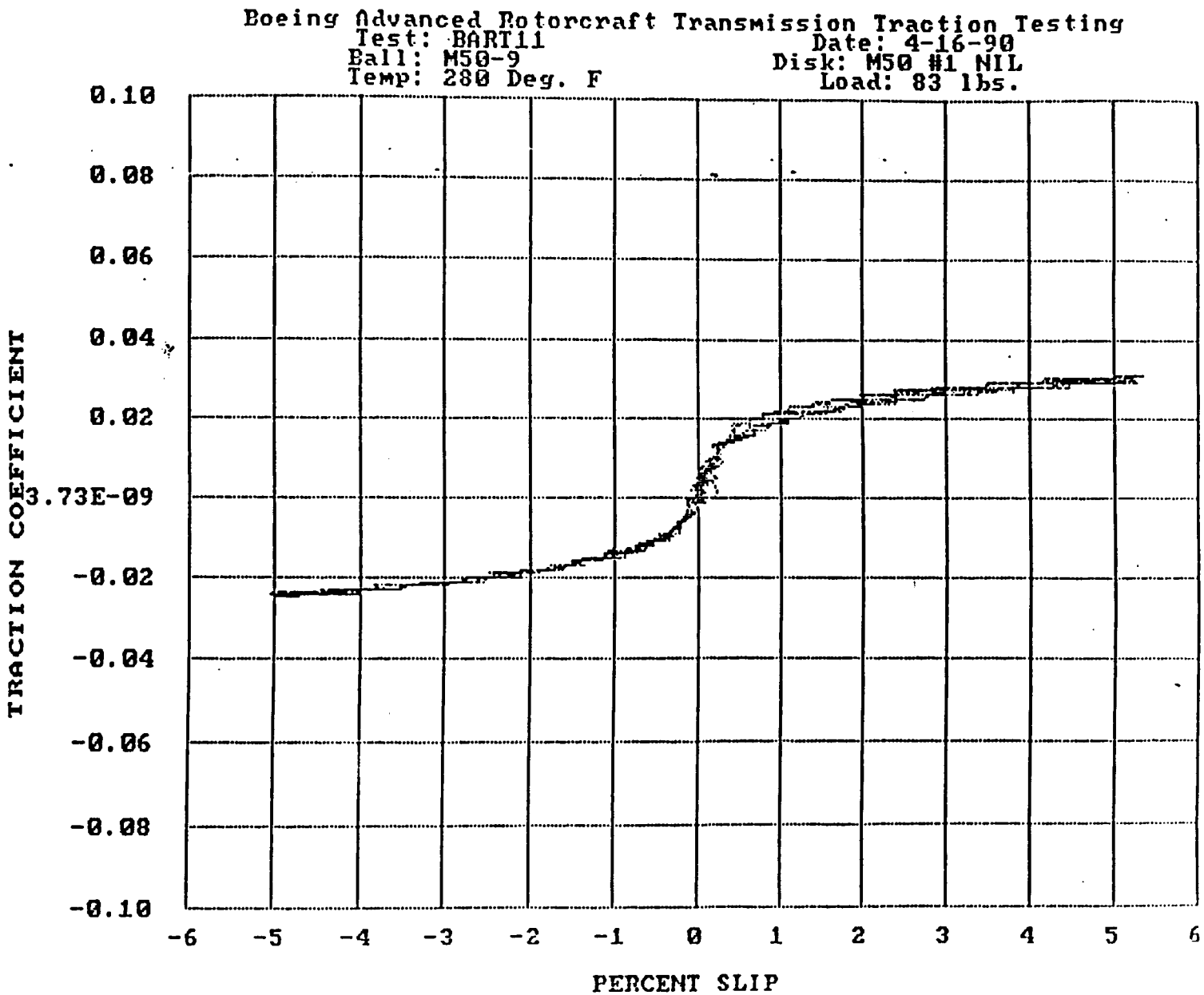
Boeing Advanced Rotorcraft Transmission Traction Testing
Test: BART11
Ball: M50-9
Temp: 280 Deg. F
Date: 4-16-90
Disk: M50 #1 NIL
Load: 83 lbs.
TRACTION COEFFICIENT
0.10
0.08
0.06
0.04
0.02
3.73E-09
-0.02
-0.04
-0.06
-0.08
-0.10
-6
-5
-4
-3
-2
-1
0
1
2
3
4
5
6
PERCENT SLIP

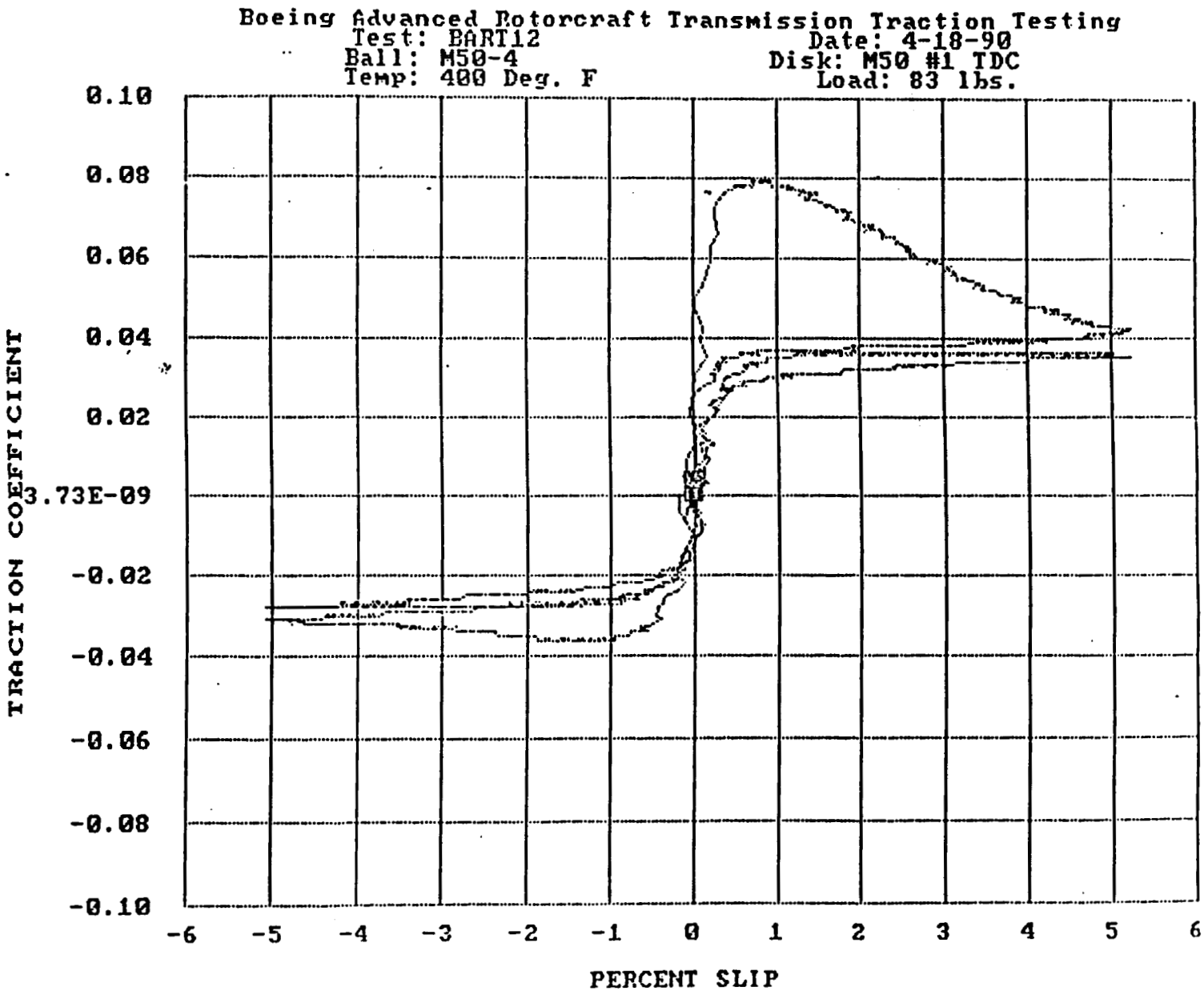
Boeing Advanced Rotorcraft Transmission Traction Testing
Test: BART12
Date: 4-18-90
Ball: M50-4
Disk: M50 #1 TDC
Temp: 400 Deg. F
Load: 83 lbs.
TRACTION COEFFICIENT
0.10
0.08
0.06
0.04
0.02
3.73E-09
-0.02
-0.04
-0.06
-0.08
-0.10
-6
-5
-4
-3
-2
-1
0
1
2
3
4
5
6
PERCENT SLIP

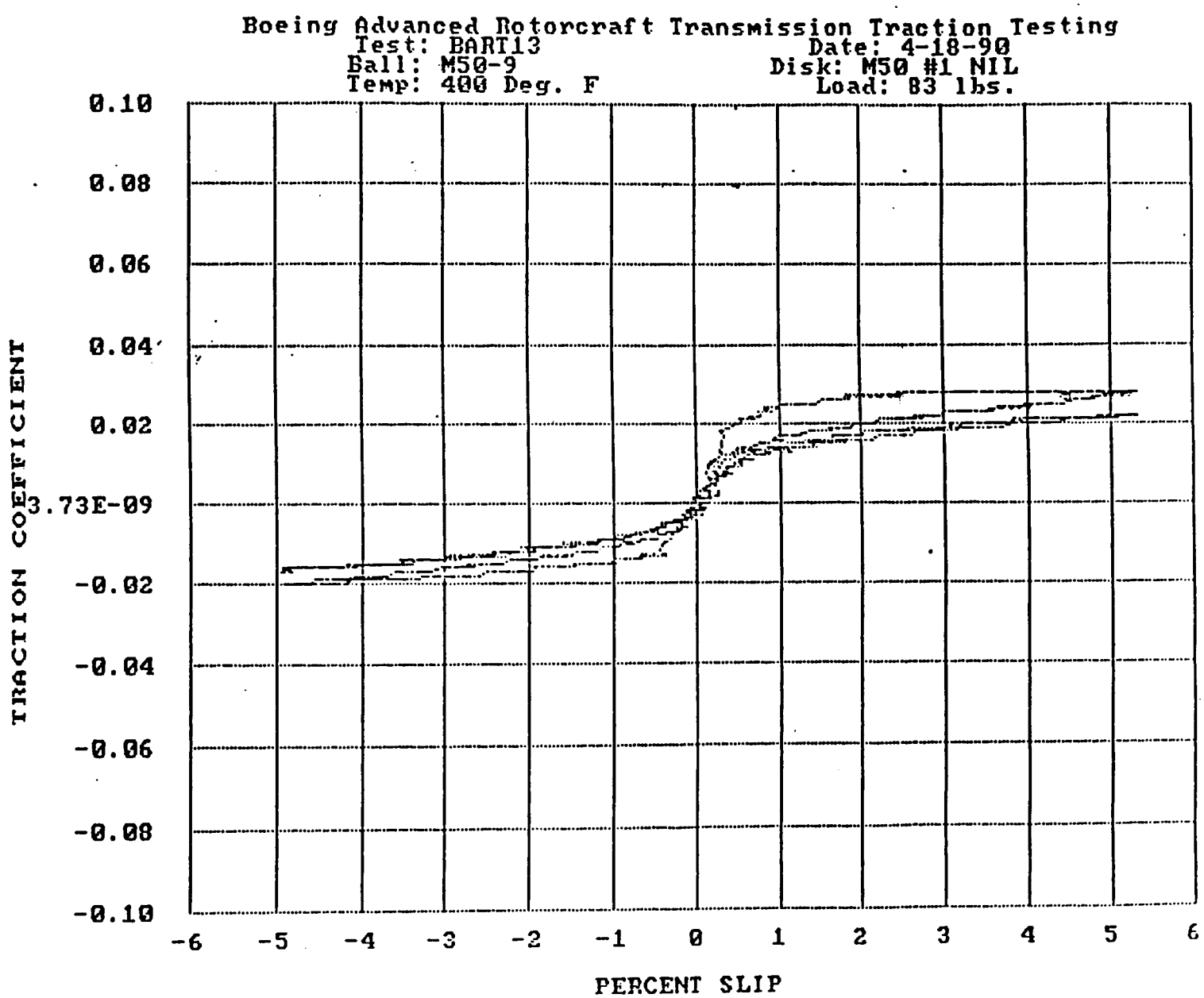
Boeing Advanced Rotorcraft Transmission Traction Testing
Test: BART13
Date: 4-18-90
Ball: M50-9
Disk: M50 #1 NIL
Temp: 400 Deg. F
Load: 83 lbs.
0.10
0.08
0.06
0.04
0.02
3.73E-09
-0.02
-0.04
-0.06
-0.08
-0.10
TRACTION COEFFICIENT
-6
-5
-4
-3
-2
-1
0
1
2
3
4
5
6
PERCENT SLIP

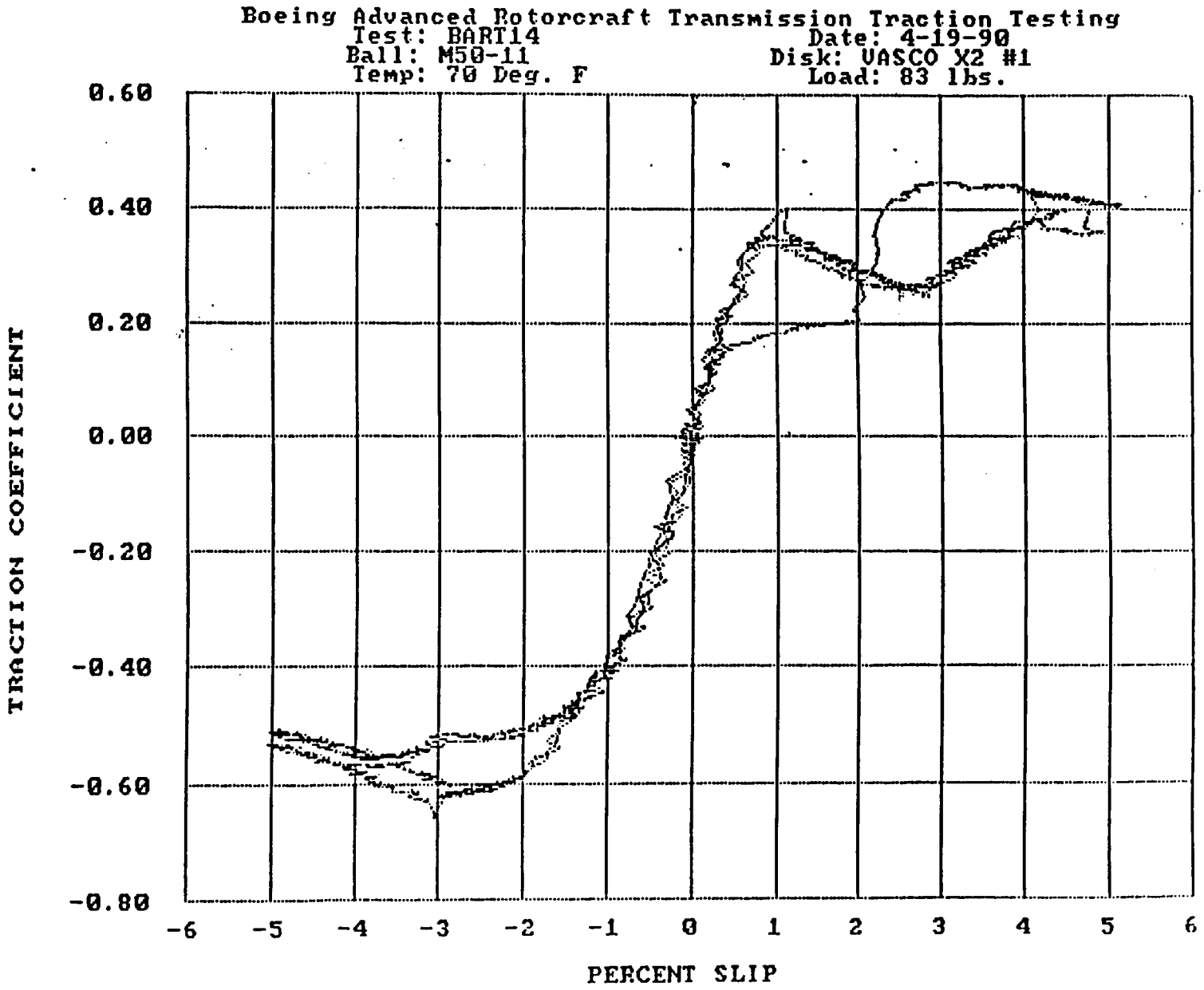
Boeing Advanced Rotorcraft Transmission Traction Testing
Test: BART14
Date: 4-19-90
Ball: M50-11
Disk: VASCO X2 #1
Temp: 70 Deg. F
Load: 83 lbs.
TRACTION COEFFICIENT
0.60
0.40
0.20
0.00
-0.20
-0.40
-0.60
-0.80
-6
-5
-4
-3
-2
-1
0
1
2
3
4
5
6
PERCENT SLIP

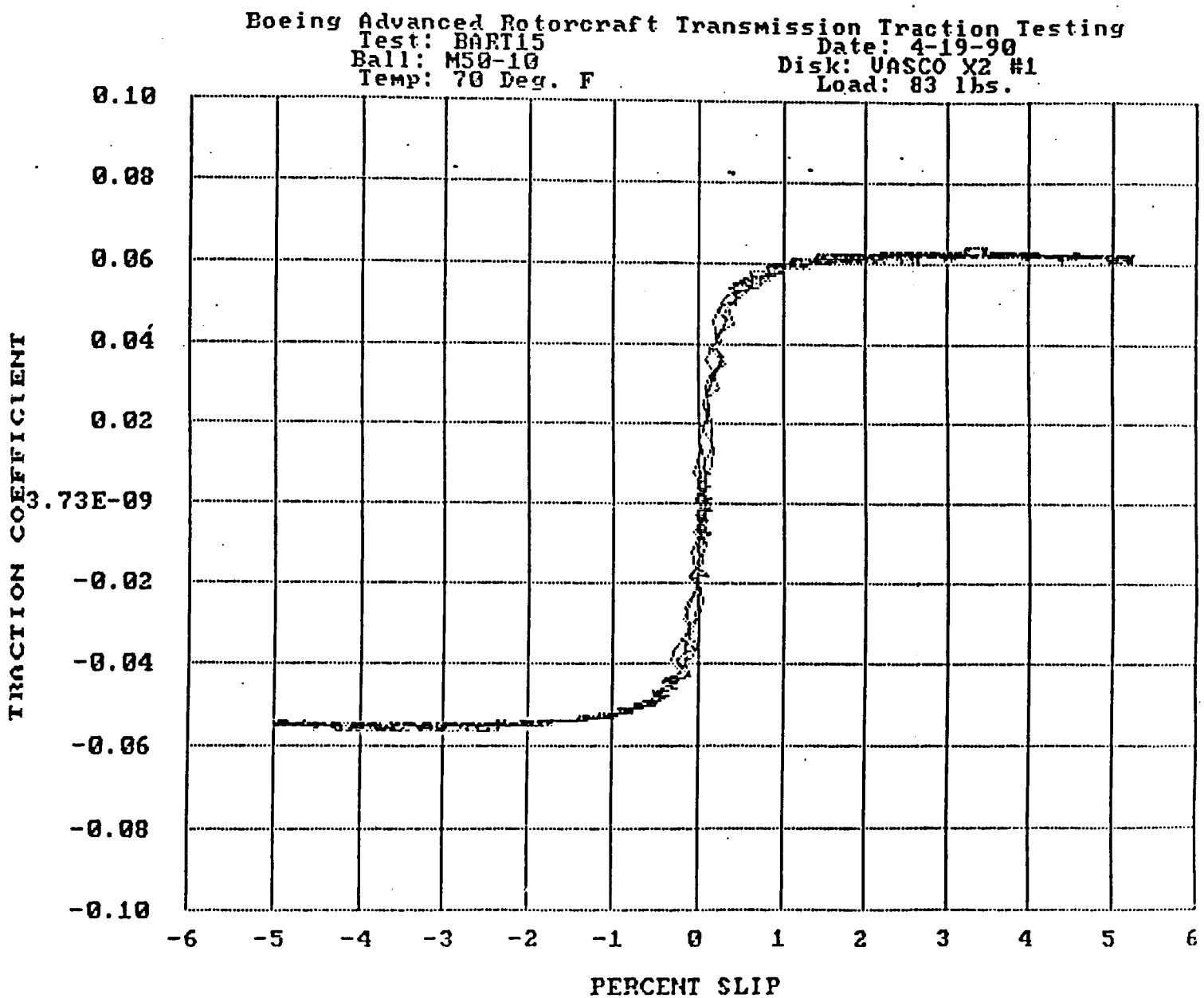
Boeing Advanced Rotorcraft Transmission Traction Testing
Test: BART15
Ball: M50-10
Temp: 70 Deg. F
Date: 4-19-90
Disk: VASCO X2 #1
Load: 83 lbs.
TRACTION COEFFICIENT
0.10
0.08
0.06
0.04
0.02
3.73E-09
-0.02
-0.04
-0.06
-0.08
-0.10
-6
-5
-4
-3
-2
-1
0
1
2
3
4
5
6
PERCENT SLIP

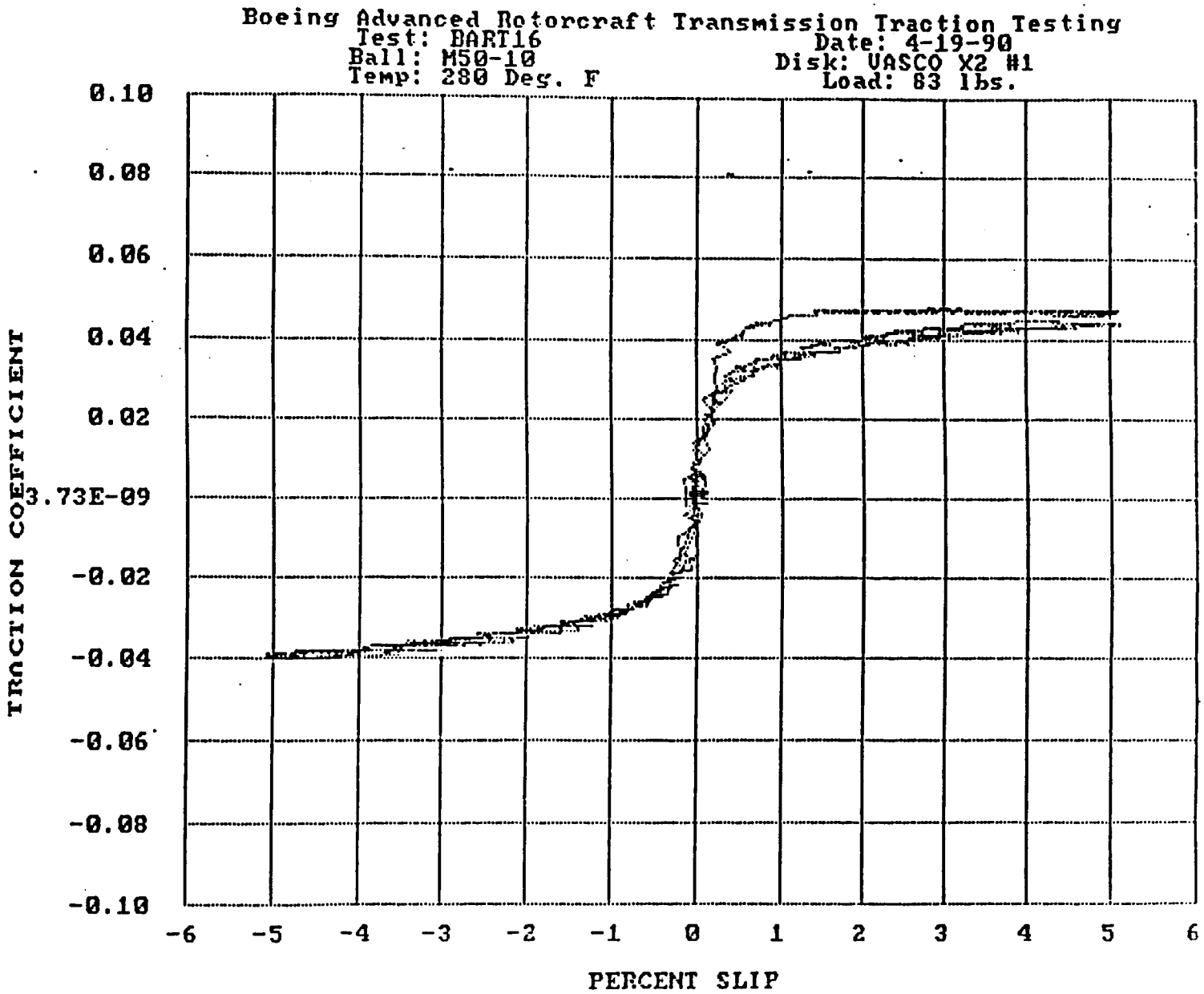
Boeing Advanced Rotorcraft Transmission Traction Testing
Test: BART16
Ball: M50-10
Temp: 280 Deg. F
Date: 4-19-90
Disk: VASCO X2 #1
Load: 83 lbs.
TRACTION COEFFICIENT
0.10
0.08
0.06
0.04
0.02
3.73E-09
-0.02
-0.04
-0.06
-0.08
-0.10
-6
-5
-4
-3
-2
-1
0
1
2
3
4
5
6
PERCENT SLIP

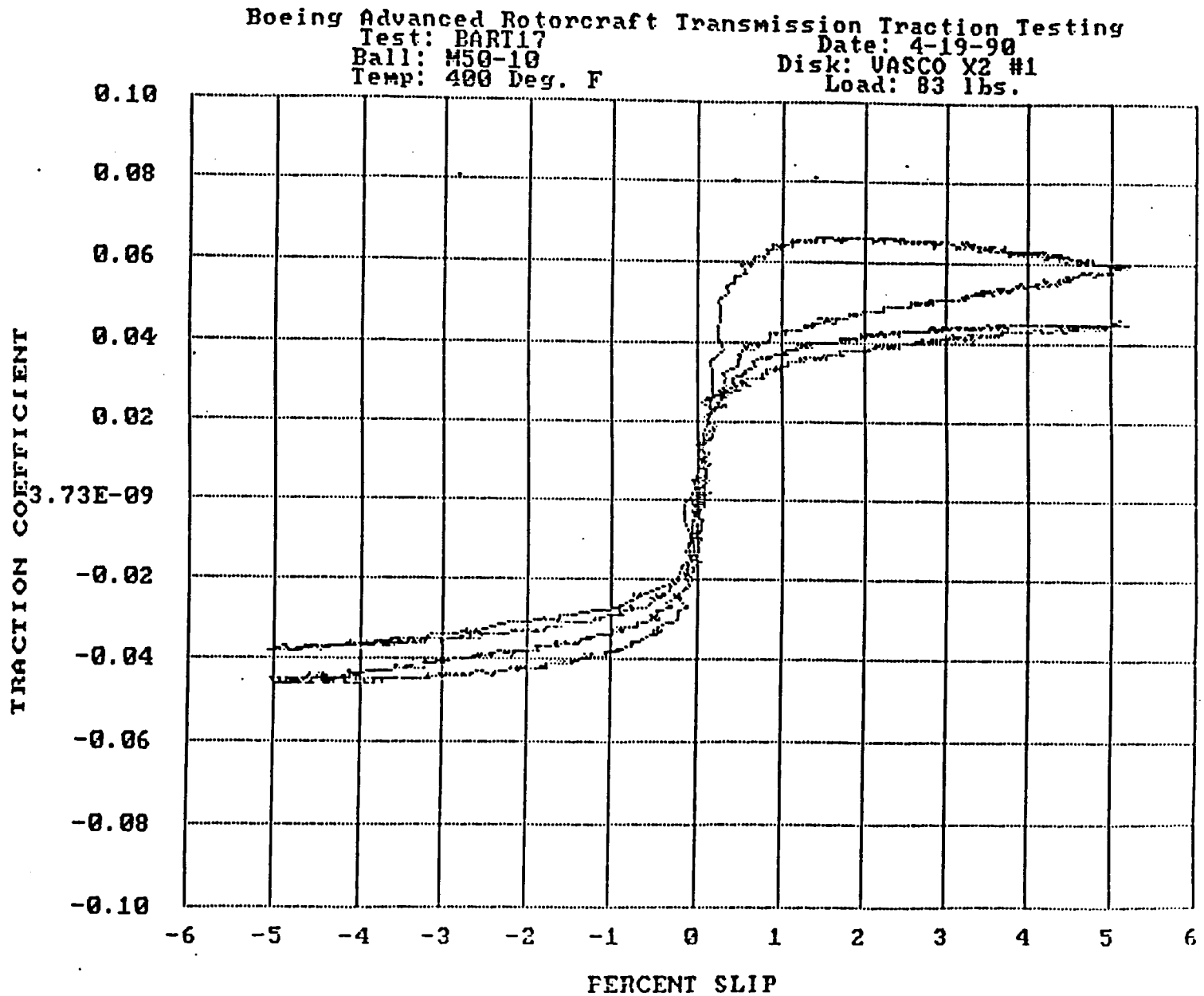
Boeing Advanced Rotorcraft Transmission Traction Testing
Test: BART17
Ball: M50-10
Temp: 400 Deg. F
Date: 4-19-90
Disk: VASCO X2 #1
Load: 83 lbs.
TRACTION COEFFICIENT
0.10
0.08
0.06
0.04
0.02
3.73E-09
-0.02
-0.04
-0.06
-0.08
-0.10
-6
-5
-4
-3
-2
-1
0
1
2
3
4
5
6
PERCENT SLIP

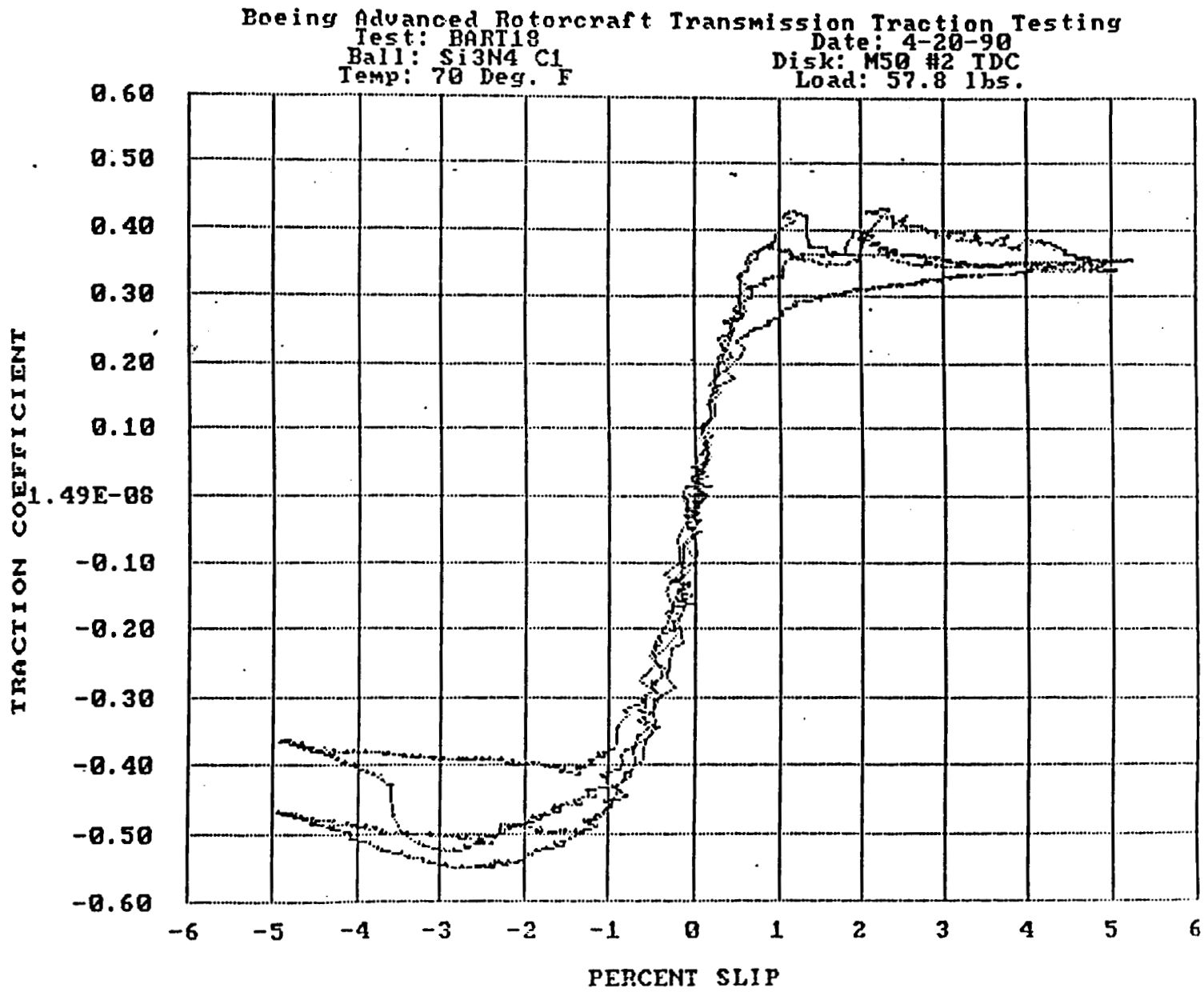
Boeing Advanced Rotorcraft Transmission Traction Testing
Test: BART18
Ball: Si3N4 C1
Temp: 70 Deg. F
Date: 4-20-90
Disk: M50 #2 TDC
Load: 57.8 lbs.
TRACTION COEFFICIENT
0.60
0.50
0.40
0.30
0.20
0.10
1.49E-08
-0.10
-0.20
-0.30
-0.40
-0.50
-0.60
-6
-5
-4
-3
-2
-1
0
1
2
3
4
5
6
PERCENT SLIP

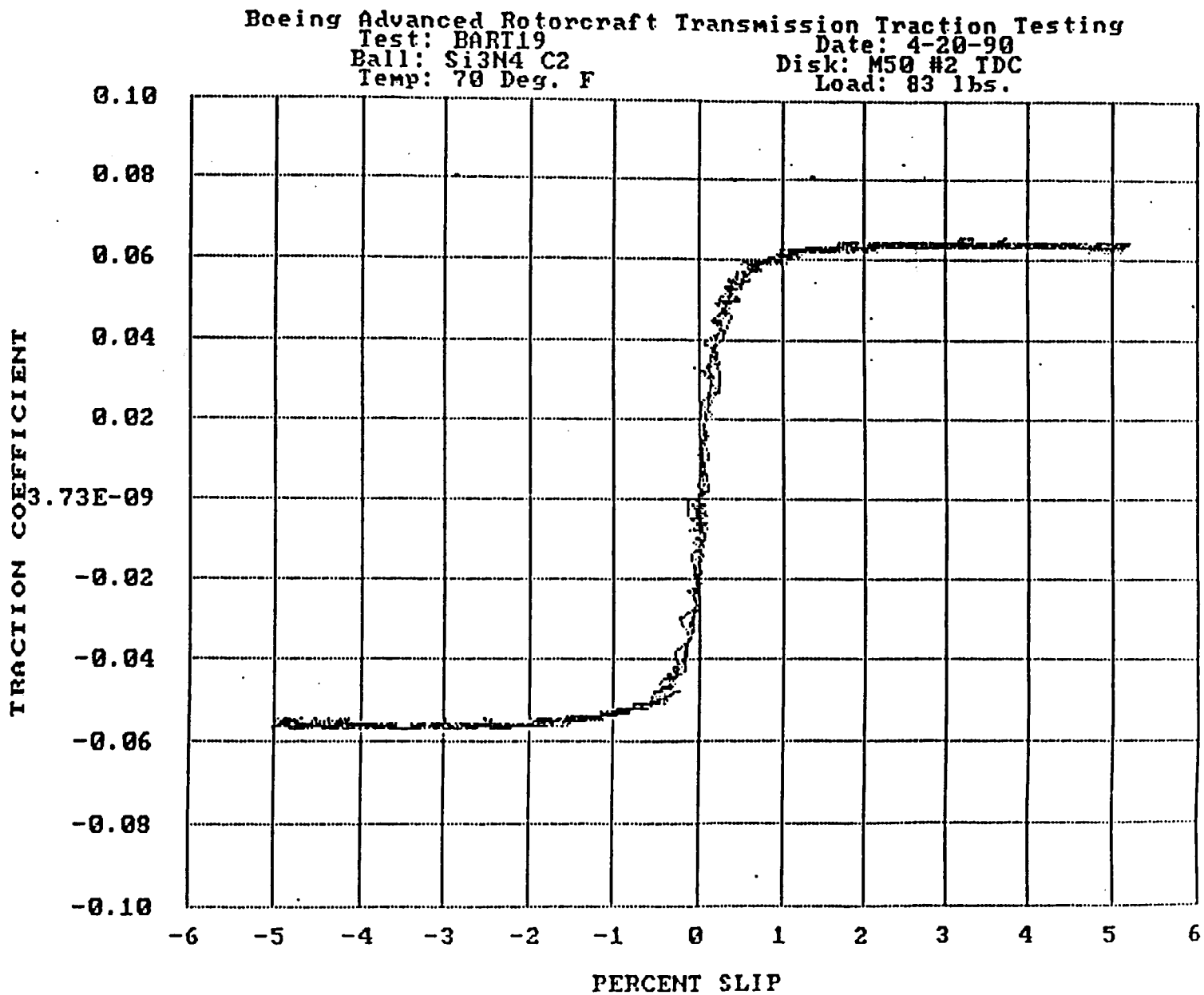
Boeing Advanced Rotorcraft Transmission Traction Testing
Test: BART19
Date: 4-20-90
Ball: Si3N4 C2
Disk: M50 #2 TDC
Temp: 70 Deg. F
Load: 83 lbs.
TRACTION COEFFICIENT
0.10
0.08
0.06
0.04
0.02
3.73E-09
-0.02
-0.04
-0.06
-0.08
-0.10
-6
-5
-4
-3
-2
-1
0
1
2
3
4
5
6
PERCENT SLIP

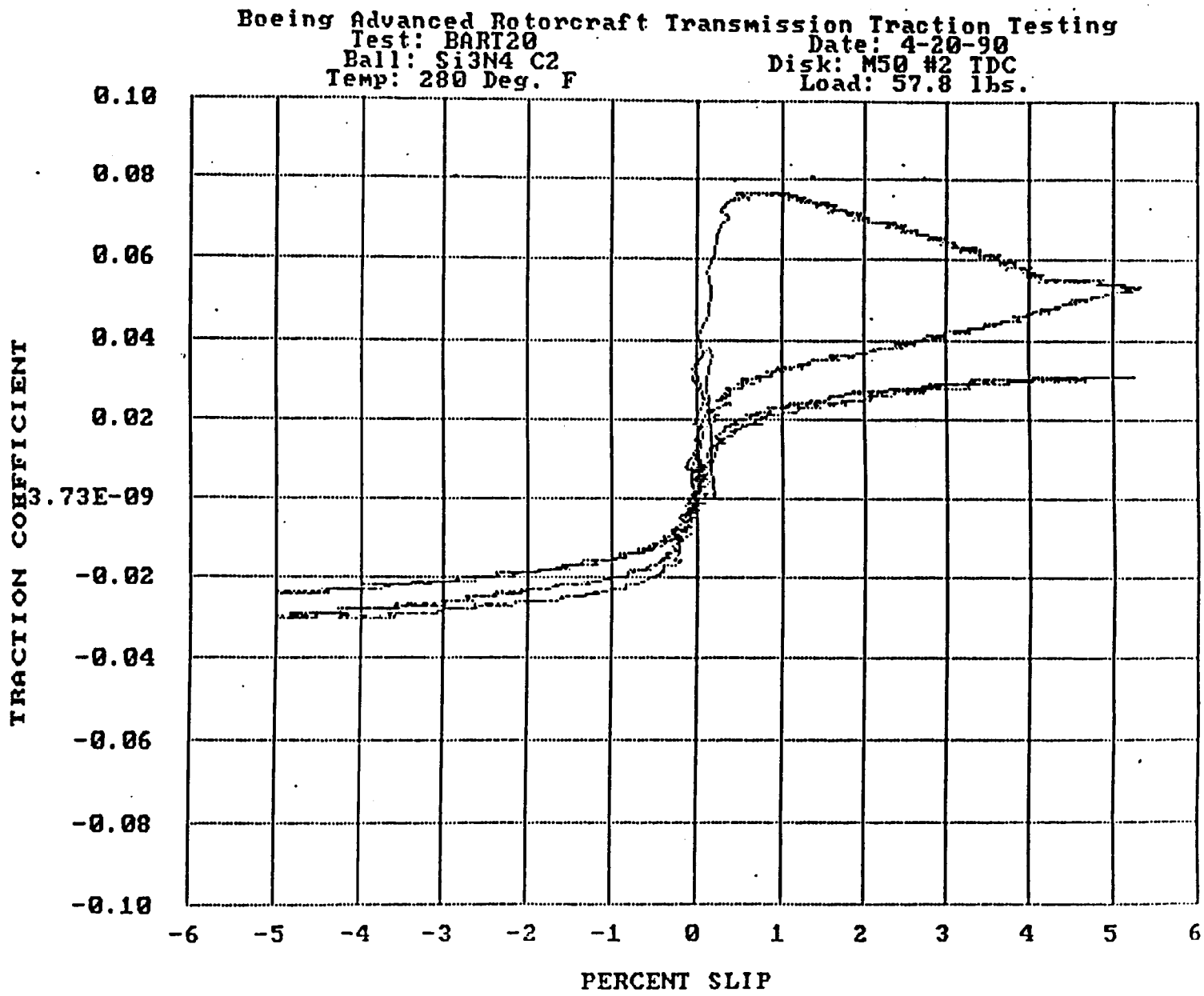
Boeing Advanced Rotorcraft Transmission Traction Testing
Test: BART20
Date: 4-20-90
Ball: Si3N4 C2
Disk: M50 #2 TDC
Temp: 280 Deg. F
Load: 57.8 lbs.
TRACTION COEFFICIENT
0.10
0.08
0.06
0.04
0.02
3.73E-09
-0.02
-0.04
-0.06
-0.08
-0.10
-6
-5
-4
-3
-2
-1
0
1
2
3
4
5
6
PERCENT SLIP

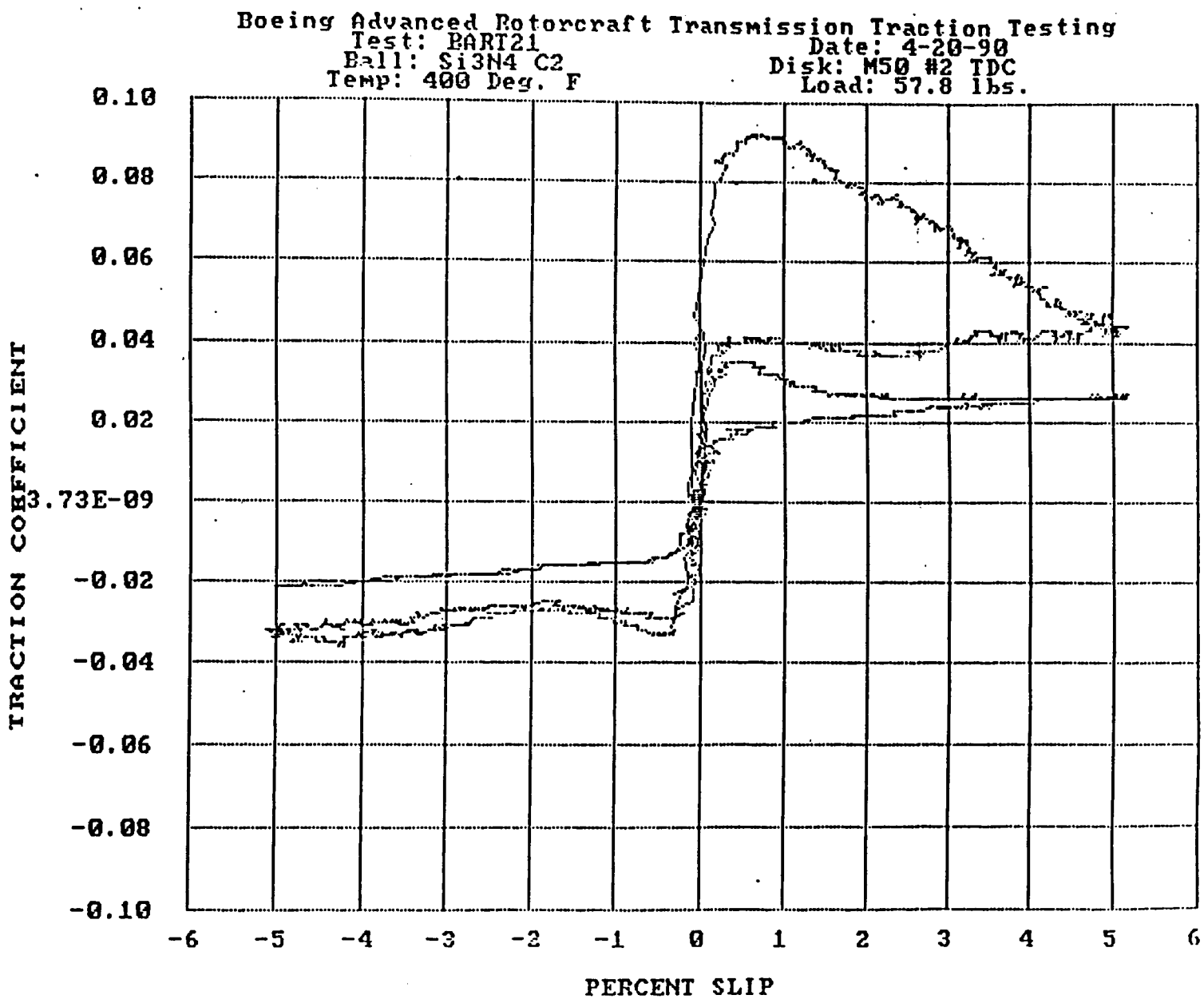
Boeing Advanced Rotorcraft Transmission Traction Testing
Test: BART21
Ball: Si3N4 C2
Temp: 400 Deg. F
Date: 4-20-90
Disk: M50 #2 TDC
Load: 57.8 lbs.
TRACTION COEFFICIENT
0.10
0.08
0.06
0.04
0.02
3.73E-09
-0.02
-0.04
-0.06
-0.08
-0.10
-6
-5
-4
-3
-2
-1
0
1
2
3
4
5
6
PERCENT SLIP

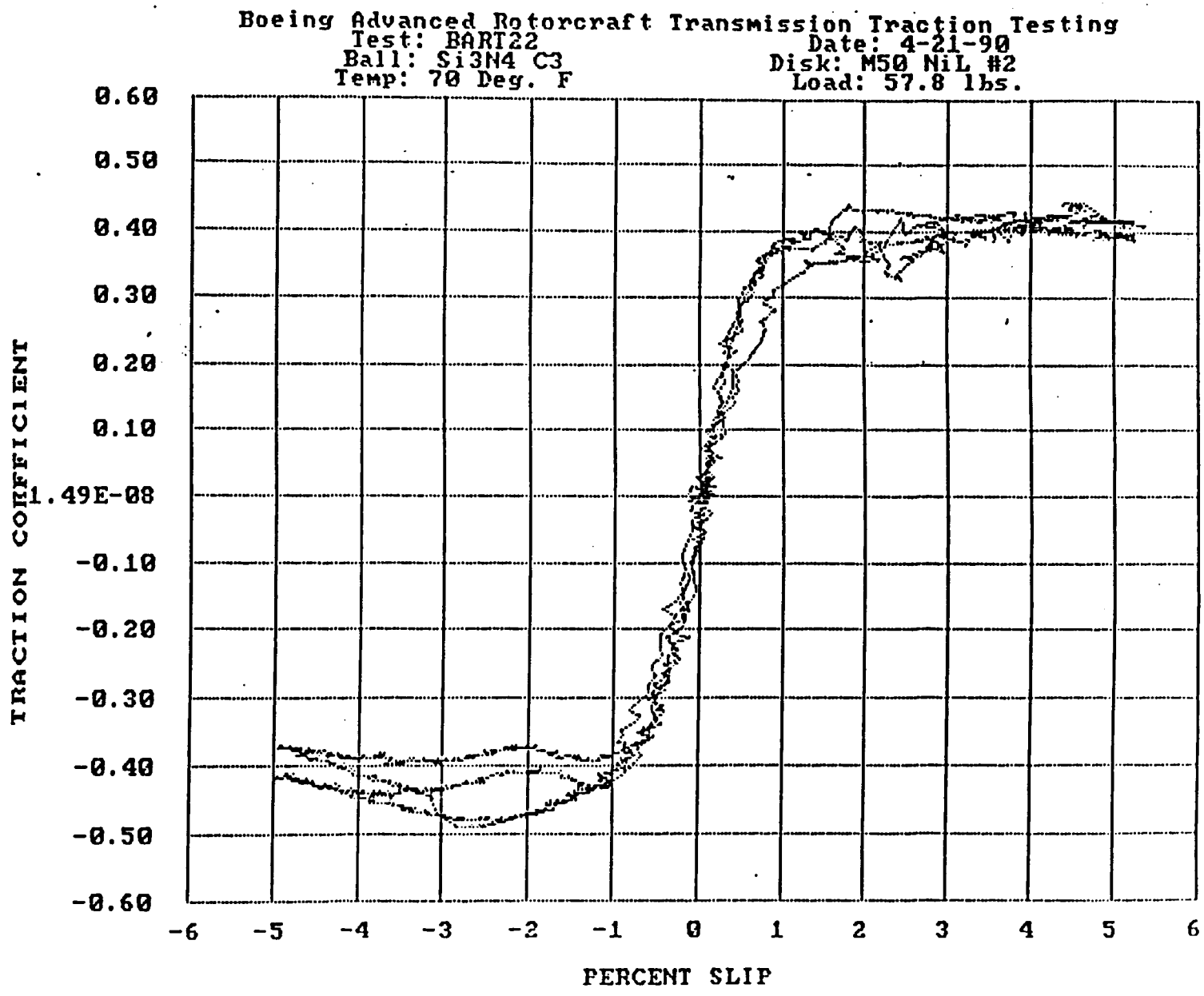
Boeing Advanced Rotorcraft Transmission Traction Testing
Test: BART22
Date: 4-21-90
Ball: Si3N4 C3
Disk: M50 NiL #2
Temp: 70 Deg. F
Load: 57.8 lbs.
TRACTION COEFFICIENT
0.60
0.50
0.40
0.30
0.20
0.10
1.49E-08
-0.10
-0.20
-0.30
-0.40
-0.50
-0.60
-6
-5
-4
-3
-2
-1
0
1
2
3
4
5
6
PERCENT SLIP

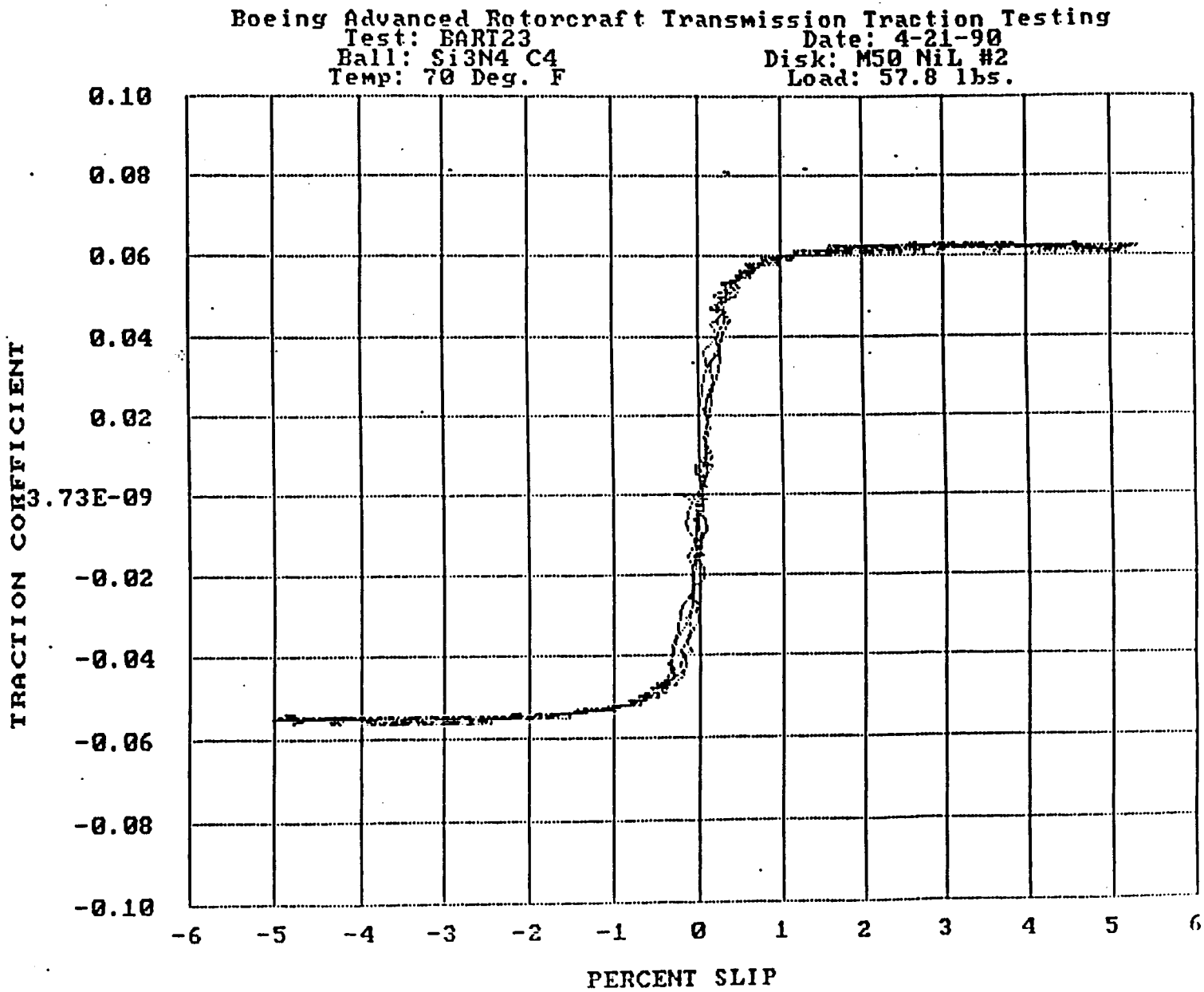
Boeing Advanced Rotorcraft Transmission Traction Testing
Test: BART23
Date: 4-21-90
Ball: Si3N4 C4
Disk: M50 NiL #2
Temp: 70 Deg. F
Load: 57.8 lbs.
TRACTION COEFFICIENT
0.10
0.08
0.06
0.04
0.02
3.73E-09
-0.02
-0.04
-0.06
-0.08
-0.10
-6
-5
-4
-3
-2
-1
0
1
2
3
4
5
6
PERCENT SLIP

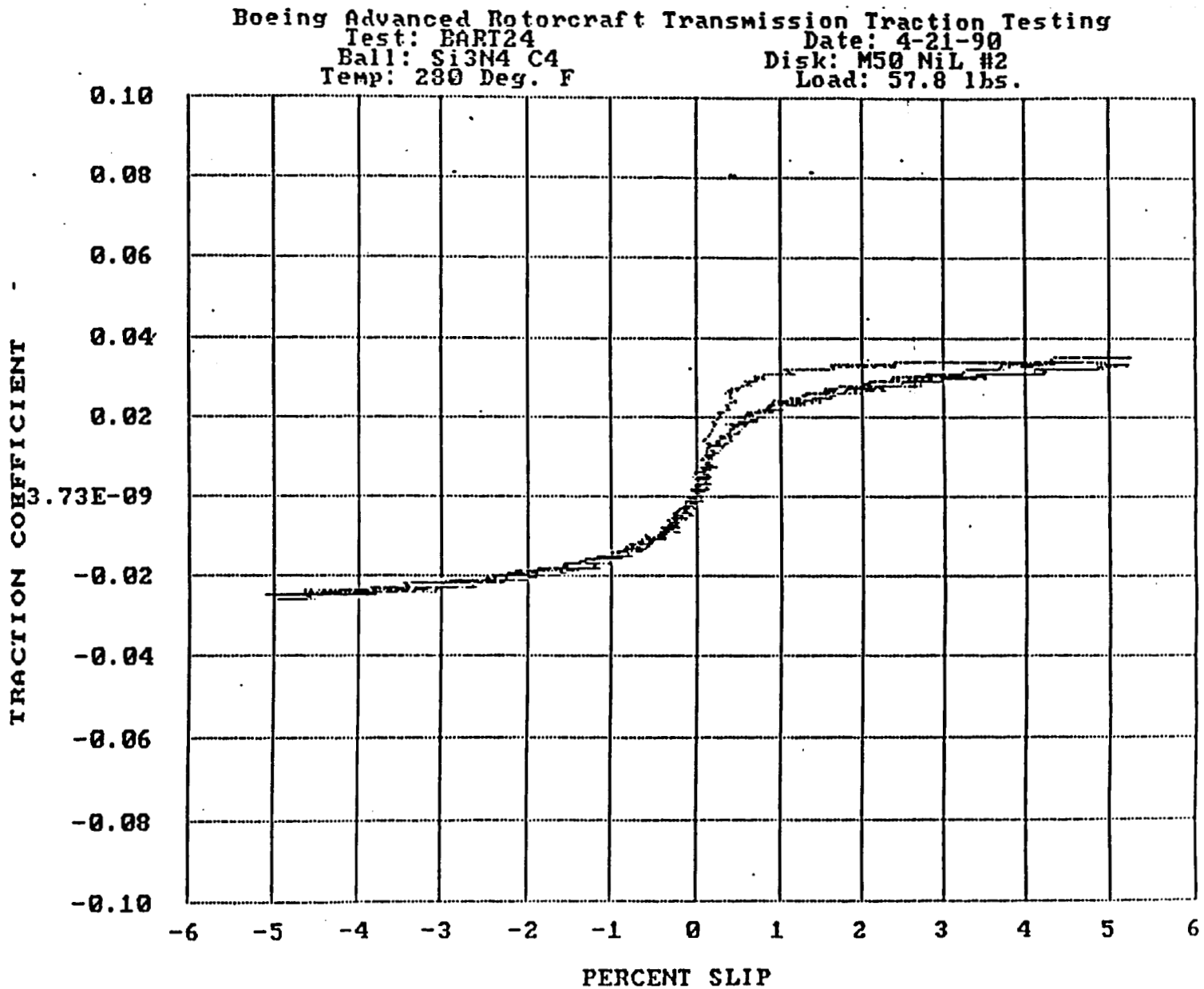
Boeing Advanced Rotorcraft Transmission Traction Testing
Test: BART24
Ball: Si3N4 C4
Temp: 280 Deg. F
Date: 4-21-90
Disk: M50 NiL #2
Load: 57.8 lbs.
TRACTION COEFFICIENT
0.10
0.08
0.06
0.04
0.02
3.73E-09
-0.02
-0.04
-0.06
-0.08
-0.10
-6
-5
-4
-3
-2
-1
0
1
2
3
4
5
6
PERCENT SLIP

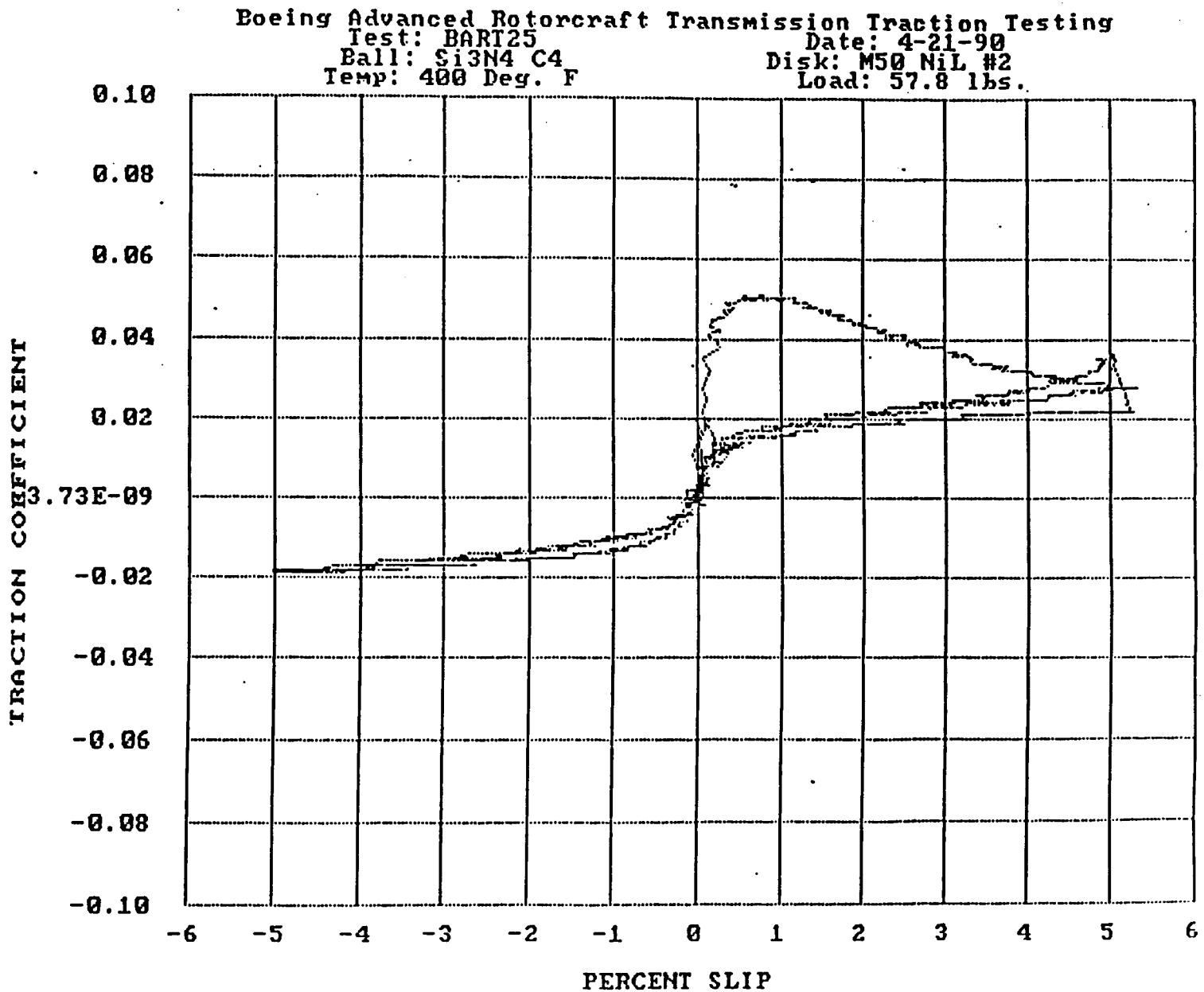
Boeing Advanced Rotorcraft Transmission Traction Testing
Test: BART25
Ball: Si3N4 C4
Temp: 400 Deg. F
Date: 4-21-90
Disk: M50 NiL #2
Load: 57.8 lbs.
TRACTION COEFFICIENT
0.10
0.08
0.06
0.04
0.02
3.73E-09
-0.02
-0.04
-0.06
-0.08
-0.10
-6
-5
-4
-3
-2
-1
0
1
2
3
4
5
6
PERCENT SLIP

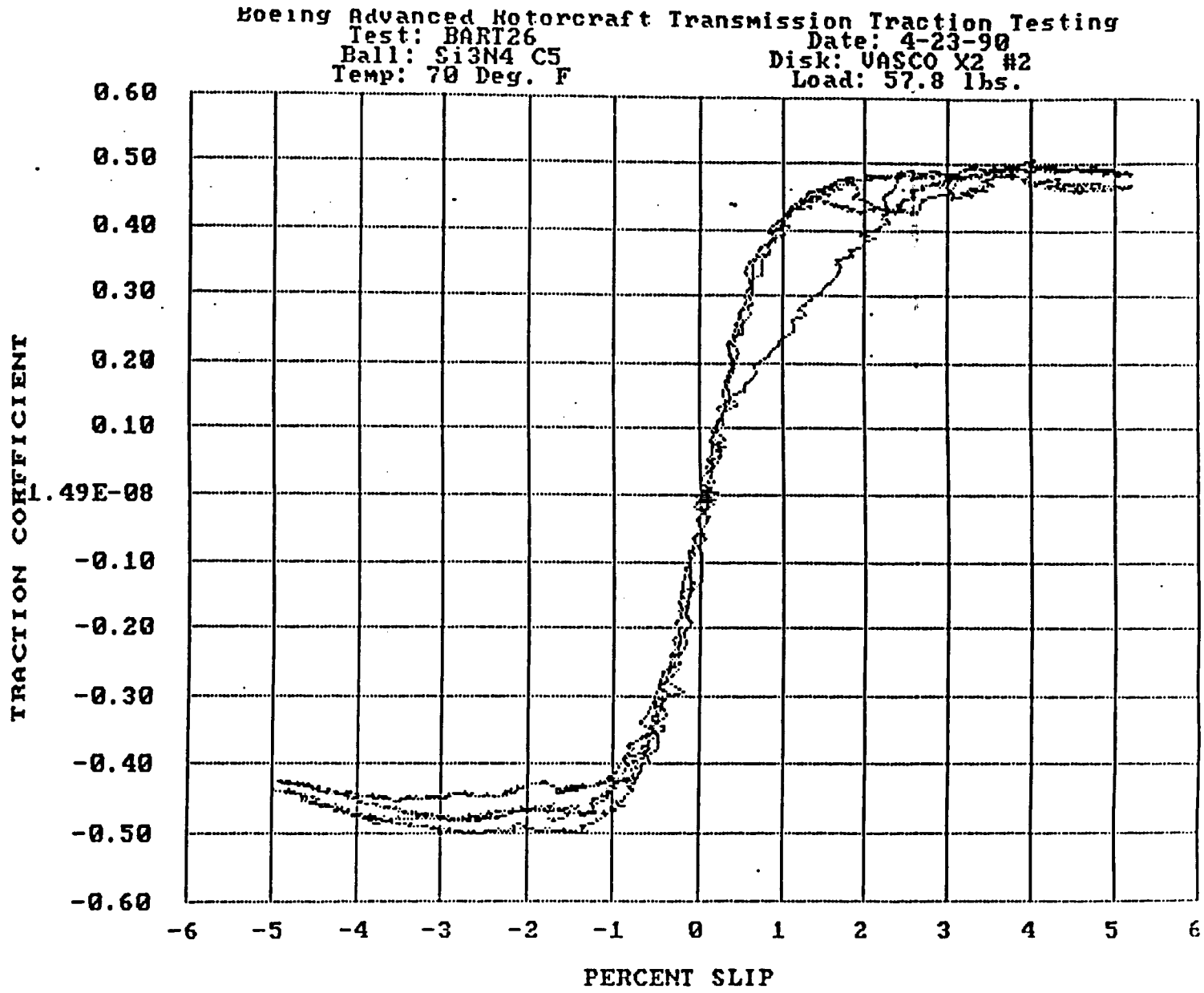
Boeing Advanced Rotorcraft Transmission Traction Testing
Test: BART26
Date: 4-23-90
Ball: Si3N4 C5
Disk: VASCO X2 #2
Temp: 70 Deg. F
Load: 57.8 lbs.
TRACTION COEFFICIENT
0.60
0.50
0.40
0.30
0.20
0.10
1.49E-08
-0.10
-0.20
-0.30
-0.40
-0.50
-0.60
-6
-5
-4
-3
-2
-1
0
1
2
3
4
5
6
PERCENT SLIP

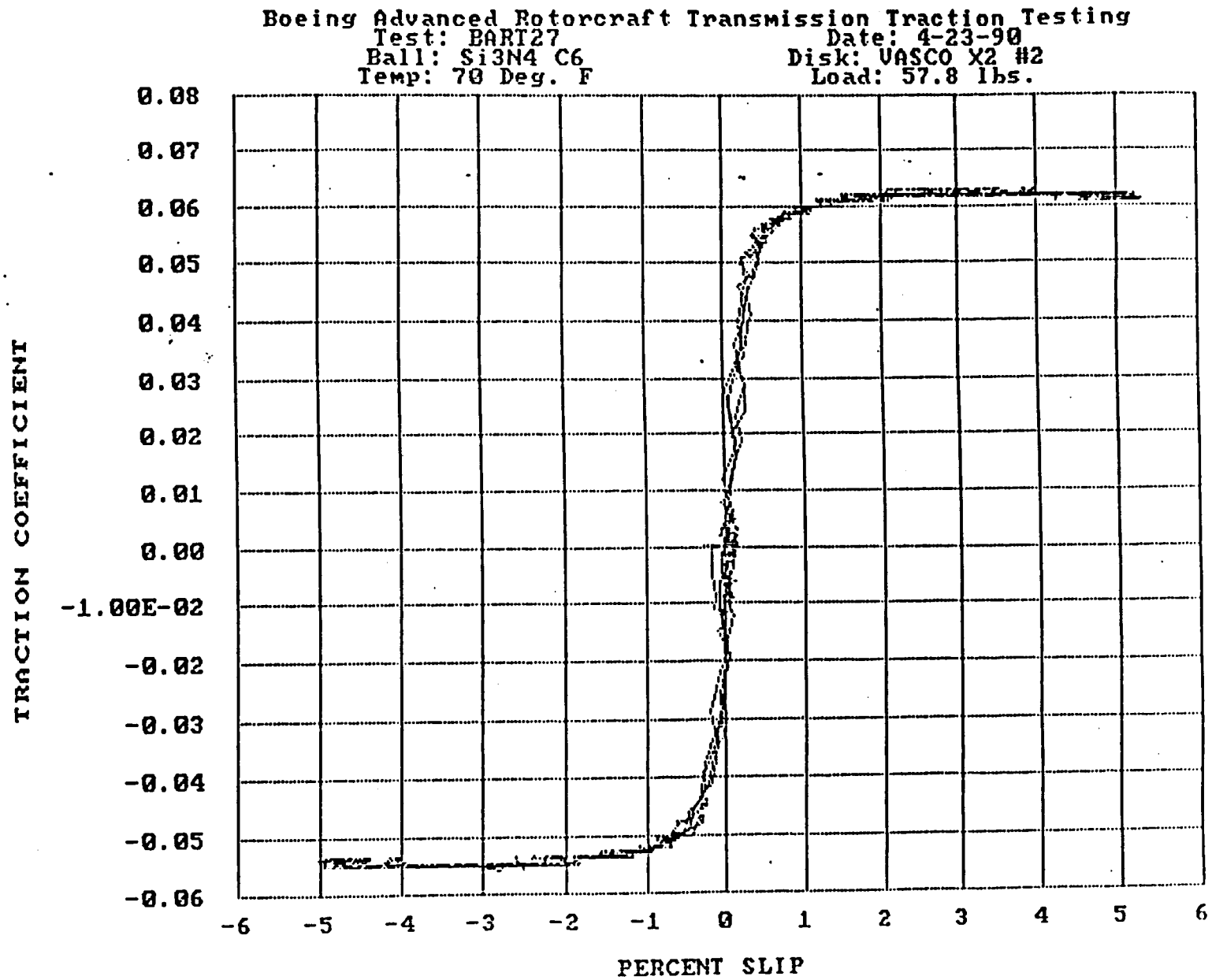
Boeing Advanced Rotorcraft Transmission Traction Testing
Test: BART27
Date: 4-23-90
Ball: Si3N4 C6
Disk: VASCO X2 #2
Temp: 70 Deg. F
Load: 57.8 lbs.
TRACTION COEFFICIENT
0.08
0.07
0.06
0.05
0.04
0.03
0.02
0.01
0.00
-1.00E-02
-0.02
-0.03
-0.04
-0.05
-0.06
-6
-5
-4
-3
-2
-1
0
1
2
3
4
5
6
PERCENT SLIP

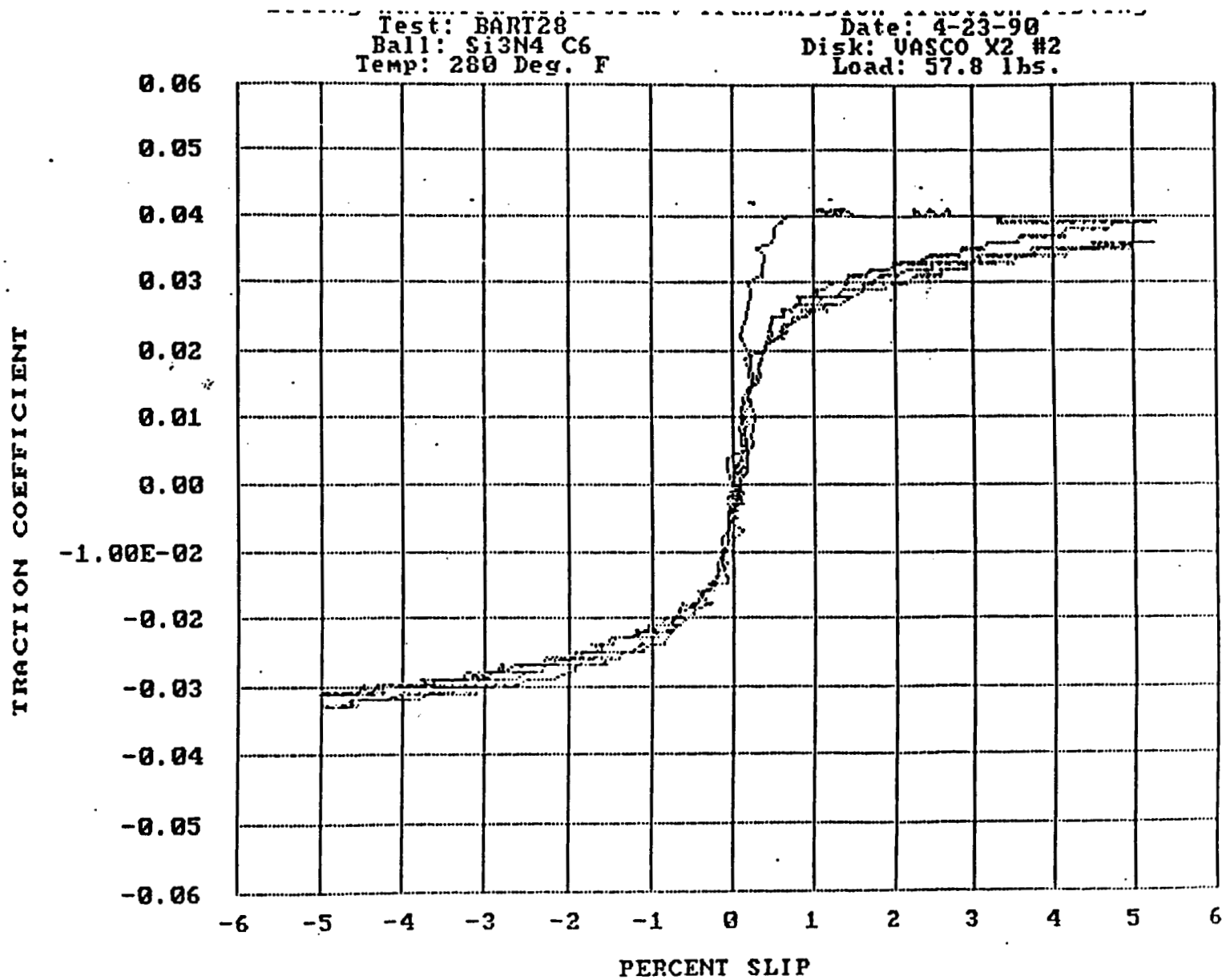
Test: BART28
Ball: Si3N4 C6
Temp: 280 Deg. F
Date: 4-23-90
Disk: VASCO X2 #2
Load: 57.8 lbs.
TRACTION COEFFICIENT
0.06
0.05
0.04
0.03
0.02
0.01
0.00
-1.00E-02
-0.02
-0.03
-0.04
-0.05
-0.06
-6
-5
-4
-3
-2
-1
0
1
2
3
4
5
6
PERCENT SLIP

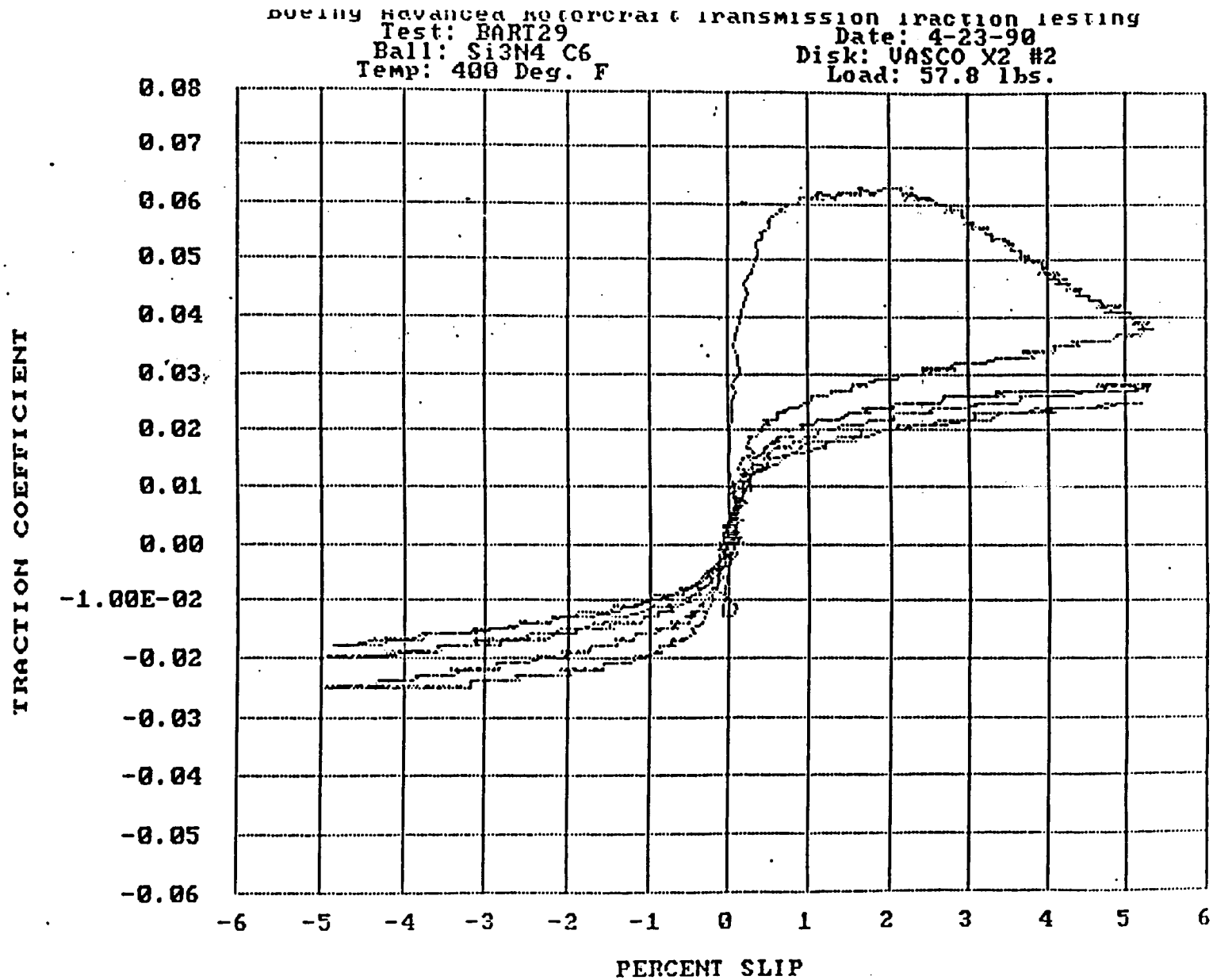
Boeing Advanced Rotorcraft Transmission Traction Testing
Test: BART29
Ball: Si3N4 C6
Temp: 400 Deg. F
Date: 4-23-90
Disk: VASCO X2 #2
Load: 57.8 lbs.
TRACTION COEFFICIENT
0.08
0.07
0.06
0.05
0.04
0.03
0.02
0.01
0.00
-1.00E-02
-0.02
-0.03
-0.04
-0.05
-0.06
-6
-5
-4
-3
-2
-1
0
1
2
3
4
5
6
PERCENT SLIP

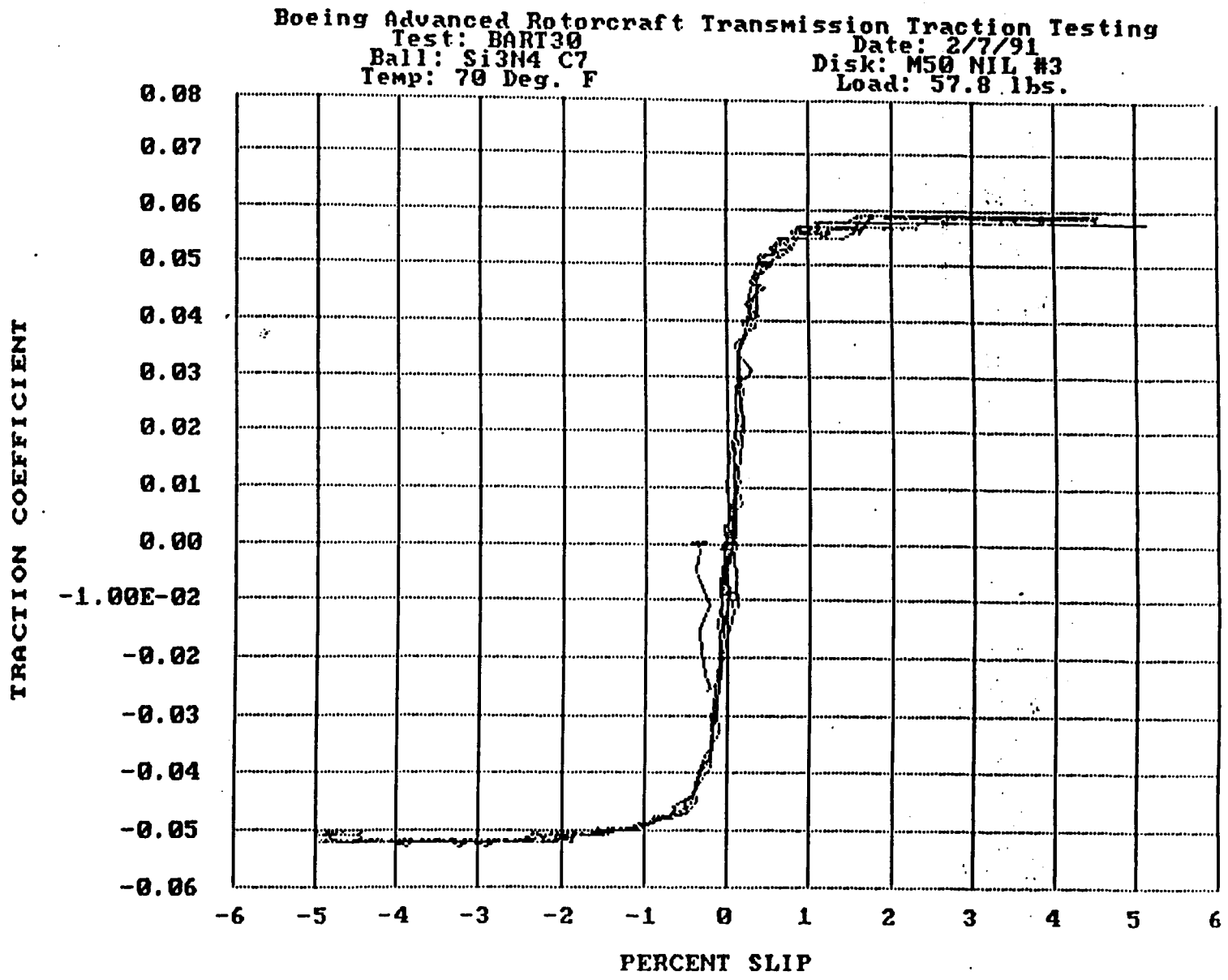
Boeing Advanced Rotorcraft Transmission Traction Testing
Test: BART30
Ball: Si3N4 C7
Temp: 70 Deg. F
Date: 2/7/91
Disk: M50 NIL #3
Load: 57.8 lbs.
TRACTION COEFFICIENT
0.08
0.07
0.06
0.05
0.04
0.03
0.02
0.01
0.00
-1.00E-02
-0.02
-0.03
-0.04
-0.05
-0.06
-6
-5
-4
-3
-2
-1
0
1
2
3
4
5
6
PERCENT SLIP

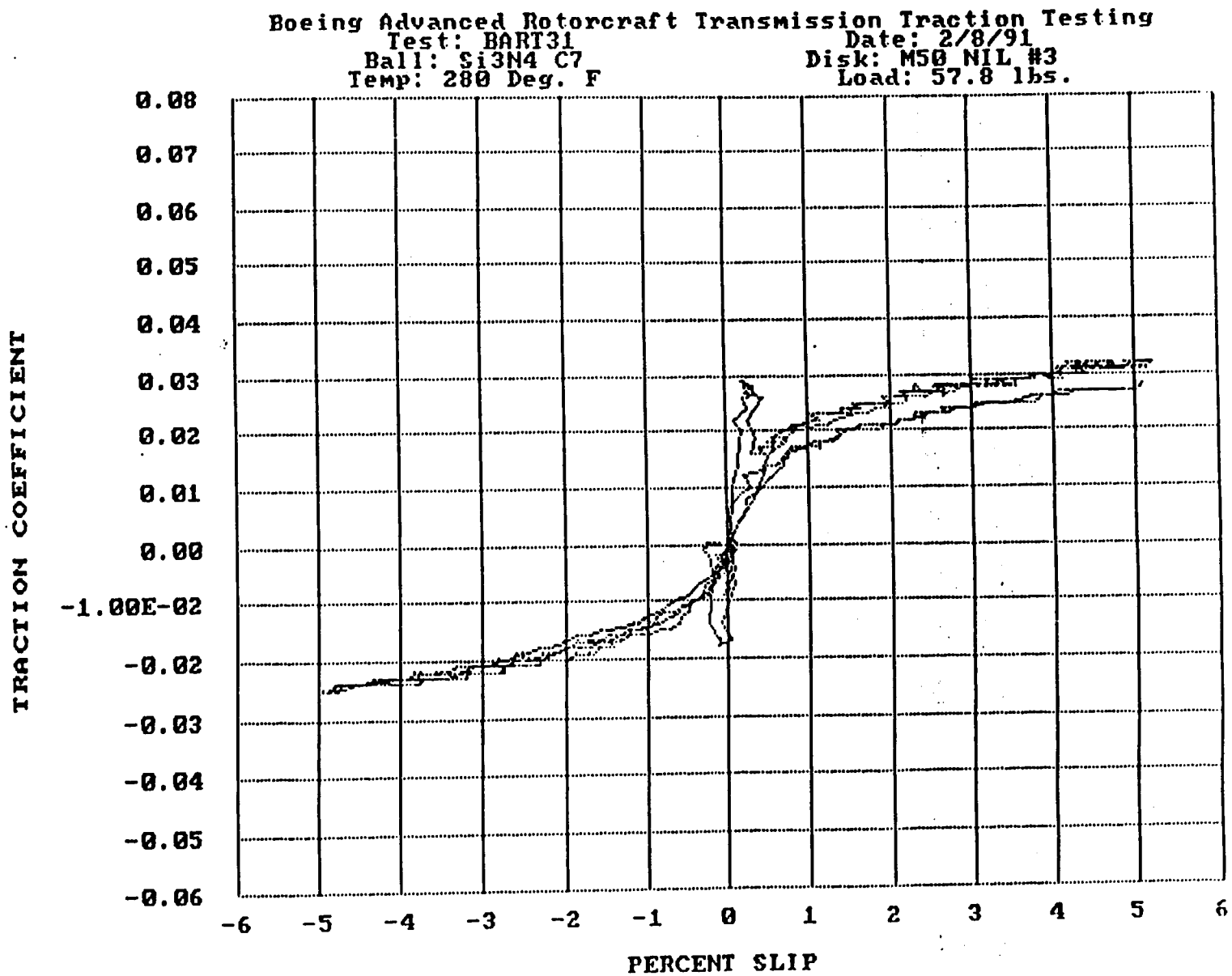
Boeing Advanced Rotorcraft Transmission Traction Testing
Test: BART31
Date: 2/8/91
Ball: Si3N4 C7
Disk: M50 NIL #3
Temp: 280 Deg. F
Load: 57.8 lbs.
TRACTION COEFFICIENT
0.08
0.07
0.06
0.05
0.04
0.03
0.02
0.01
0.00
-1.00E-02
-0.02
-0.03
-0.04
-0.05
-0.06
-6
-5
-4
-3
-2
-1
0
1
2
3
4
5
6
PERCENT SLIP

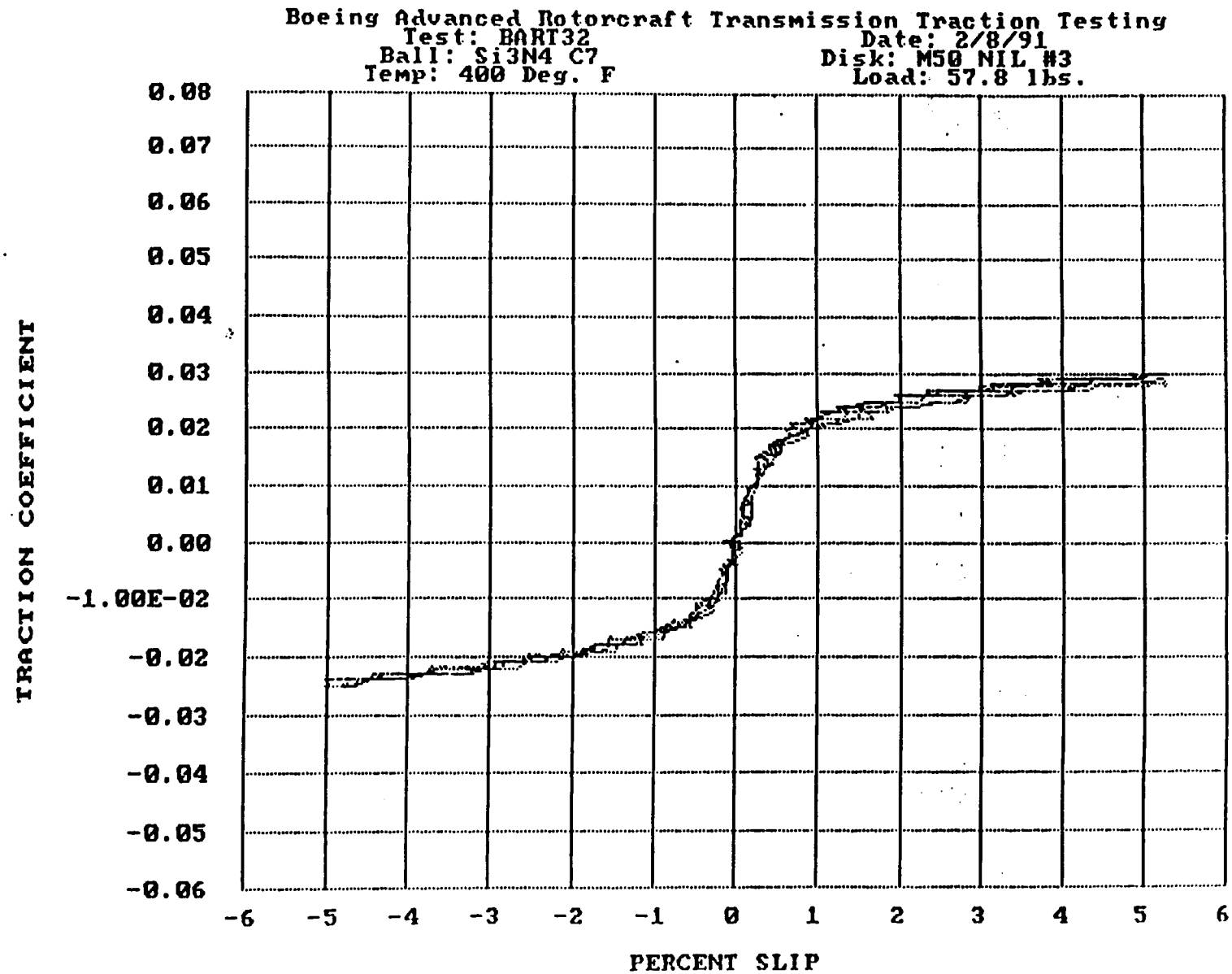
Boeing Advanced Rotorcraft Transmission Traction Testing
Test: BART32
Ball: Si3N4 C7
Temp: 400 Deg. F
Date: 2/8/91
Disk: M50 NIL #3
Load: 57.8 lbs.
TRACTION COEFFICIENT
0.08
0.07
0.06
0.05
0.04
0.03
0.02
0.01
0.00
-1.00E-02
-0.02
-0.03
-0.04
-0.05
-0.06
-6
-5
-4
-3
-2
-1
0
1
2
3
4
5
6
PERCENT SLIP

APPENDIX F

NEAR-NET TOOLING DRAWINGS

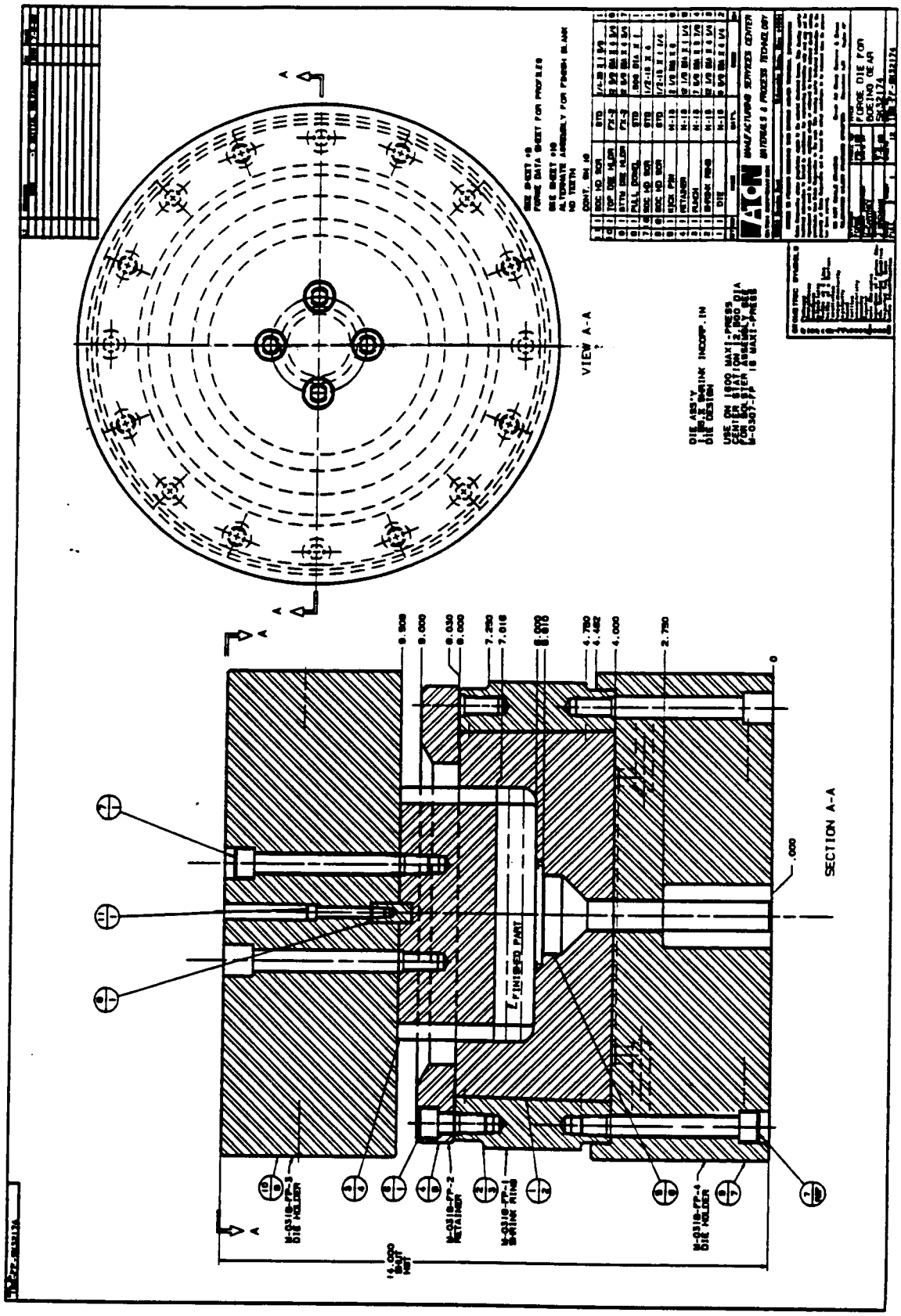
VIEW A-A
SECTION A-A
FINISHED PART
DIE ASSY
DIE DESIGN
M-0318-F2-3
DIE HOLDER
M-0318-F2-2
RETAINER
M-0318-F2-1
SPRING RING
M-0318-F2-4
DIE HOLDER
14.000
BLKT
HOT
9.500
9.000
8.030
8.000
7.250
7.016
4.750
4.482
4.000
2.750
.000

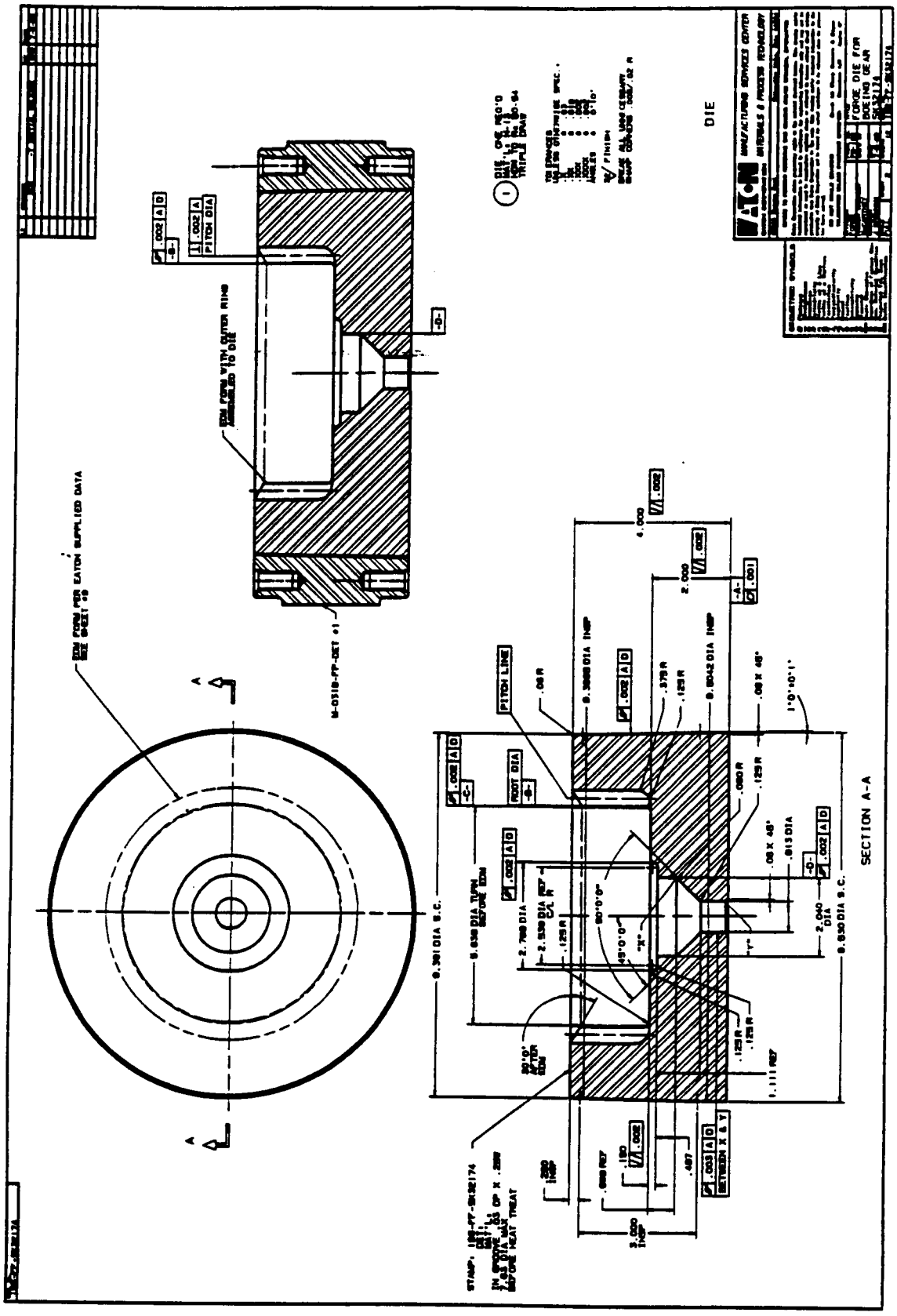
DIE
SECTION A-A
PITCH LINE
ROOT DIA
PITCH DIA
FORGE DIE FOR
DOCKING GEAR

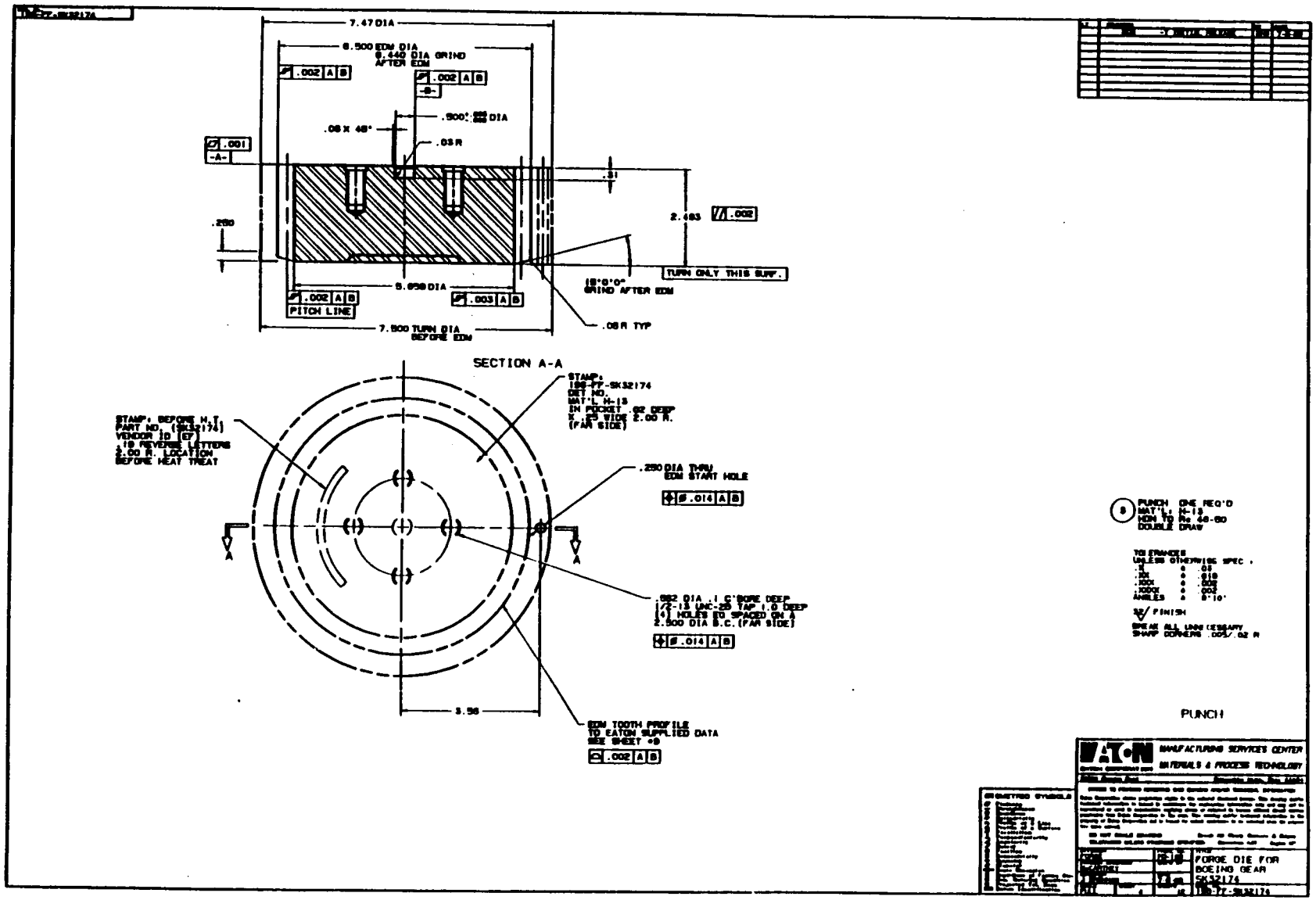
7.47 DIA
6.500 EDM DIA
6.440 DIA GRIND
AFTER EDM
.002 A B
.002 A B
-B-
.500 DIA
.08 X 45°
.03 R
.001
-A-
.31
2.493
.002
.250
TURN ONLY THIS SURF.
15°0'0"
GRIND AFTER EDM
5.658 DIA
.002 A B
PITCH LINE
.003 A B
7.500 TURN DIA
BEFORE EDM
.08 R TYP
SECTION A-A
STAMP:
1BE-F7-SK32174
DET NO.
MAT'L H-13
IN POCKET .02 DEEP
X .25 WIDE 2.00 R.
(FAR SIDE)
STAMP: BEFORE H.T.
PART NO. (SK32174)
VENDOR ID (E)
.19 REVERSE LETTERS
2.00 R. LOCATION
BEFORE HEAT TREAT
.250 DIA THRU
EDM START HOLE
.014 A B
.062 DIA .1 C'BORE DEEP
(2-13 UNC-2B TAP 1.0 DEEP
(4) HOLES EQ SPACED ON A
2.500 DIA B.C. (FAR SIDE)
.014 A B
3.56
EDM TOOTH PROFILE
TO EATON SUPPLIED DATA
SEE SHEET #9
.002 A B
PUNCH ONE REQ'D
MAT'L: H-13
HDN TO Rc 48-50
DOUBLE DRAW
TOLERANCES
UNLESS OTHERWISE SPEC.
.X ± .03
.XX ± .010
.XXX ± .005
.XXXX ± .002
ANGLES ± 0°10'
125 FINISH
BREAK ALL UNNECESSARY
SHARP CORNERS .005/.02 R
PUNCH
EATON
MANUFACTURING SERVICES CENTER
MATERIALS & PROCESS TECHNOLOGY
FORGE DIE FOR
BOEING GEAR
SK32174
1BE-F7-SK32174

TOOTH PROFILE COORDINATES

	PUNCH POINT COORDINATES X	PUNCH POINT COORDINATES Y		DIE POINT COORDINATES X	DIE POINT COORDINATES Y
POINT #1	[illegible]	[illegible]	POINT #1	[illegible]	[illegible]
	[illegible]	[illegible]		[illegible]	[illegible]
	[illegible]	[illegible]		[illegible]	[illegible]
	[illegible]	[illegible]		[illegible]	[illegible]
	[illegible]	[illegible]		[illegible]	[illegible]
	[illegible]	[illegible]		[illegible]	[illegible]
	[illegible]	[illegible]		[illegible]	[illegible]
	[illegible]	[illegible]		[illegible]	[illegible]
	[illegible]	[illegible]		[illegible]	[illegible]
	[illegible]	[illegible]		[illegible]	[illegible]
	[illegible]	[illegible]		[illegible]	[illegible]
	[illegible]	[illegible]		[illegible]	[illegible]
	[illegible]	[illegible]		[illegible]	[illegible]
	[illegible]	[illegible]		[illegible]	[illegible]
	[illegible]	[illegible]		[illegible]	[illegible]
	[illegible]	[illegible]		[illegible]	[illegible]
	[illegible]	[illegible]		[illegible]	[illegible]
	[illegible]	[illegible]		[illegible]	[illegible]
	[illegible]	[illegible]		[illegible]	[illegible]
	[illegible]	[illegible]		[illegible]	[illegible]
	[illegible]	[illegible]		[illegible]	[illegible]
	[illegible]	[illegible]		[illegible]	[illegible]
	[illegible]	[illegible]		[illegible]	[illegible]
	[illegible]	[illegible]		[illegible]	[illegible]
	[illegible]	[illegible]		[illegible]	[illegible]
	[illegible]	[illegible]		[illegible]	[illegible]
	[illegible]	[illegible]		[illegible]	[illegible]
	[illegible]	[illegible]		[illegible]	[illegible]
	[illegible]	[illegible]		[illegible]	[illegible]
	[illegible]	[illegible]		[illegible]	[illegible]
	[illegible]	[illegible]		[illegible]	[illegible]
	[illegible]	[illegible]		[illegible]	[illegible]
	[illegible]	[illegible]		[illegible]	[illegible]
	[illegible]	[illegible]		[illegible]	[illegible]
	[illegible]	[illegible]		[illegible]	[illegible]
	[illegible]	[illegible]		[illegible]	[illegible]
	[illegible]	[illegible]		[illegible]	[illegible]
	[illegible]	[illegible]		[illegible]	[illegible]
	[illegible]	[illegible]		[illegible]	[illegible]
	[illegible]	[illegible]		[illegible]	[illegible]
	[illegible]	[illegible]		[illegible]	[illegible]
	[illegible]	[illegible]		[illegible]	[illegible]
	[illegible]	[illegible]		[illegible]	[illegible]
	[illegible]	[illegible]		[illegible]	[illegible]
	[illegible]	[illegible]		[illegible]	[illegible]
	[illegible]	[illegible]		[illegible]	[illegible]
	[illegible]	[illegible]		[illegible]	[illegible]
	[illegible]	[illegible]		[illegible]	[illegible]
	[illegible]	[illegible]		[illegible]	[illegible]
	[illegible]	[illegible]		[illegible]	[illegible]
	[illegible]	[illegible]		[illegible]	[illegible]
	[illegible]	[illegible]		[illegible]	[illegible]
	[illegible]	[illegible]		[illegible]	[illegible]
	[illegible]	[illegible]		[illegible]	[illegible]
	[illegible]	[illegible]		[illegible]	[illegible]
	[illegible]	[illegible]		[illegible]	[illegible]
	[illegible]	[illegible]		[illegible]	[illegible]
	[illegible]	[illegible]		[illegible]	[illegible]
	[illegible]	[illegible]		[illegible]	[illegible]
POINT [illegible]	[illegible]	[illegible]	POINT [illegible]	[illegible]	[illegible]

TOOTH PROFILES

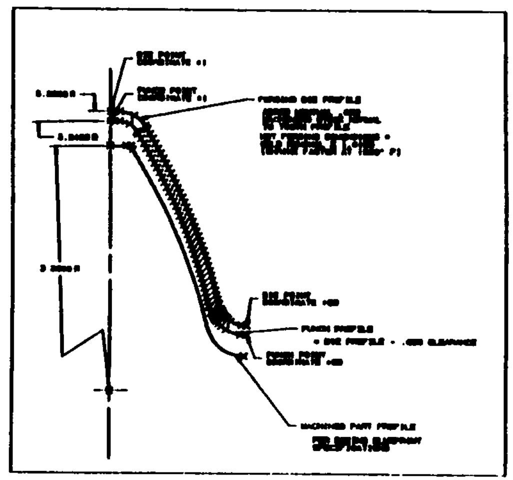

BOEING MACHINED PART SPECIFICATIONS

NUMBER OF GEAR TEETH	[illegible]
NORMAL DIAMETRAL PITCH	[illegible]
GEAR OUTSIDE DIAMETER	[illegible]
NORMAL PRESSURE ANGLE	[illegible]
GEAR NORMAL TOOTH THICKNESS	[illegible]
GEAR ADDENDUM	[illegible]
GEAR DEDENDUM	0.2140
GEAR ROOT DIAMETER	[illegible]
GEAR NORMAL CIRCULAR PITCH	[illegible]
GEAR TIP TOOTH THICKNESS	[illegible]
MEASURING PIN DIAMETER	[illegible]
MEASUREMENT OVER TWO PINS	[illegible]
TIP (TRUE INVOLUTE FORM) DIAMETER	[illegible]

EATON — MANUFACTURING SERVICES CENTER — MATERIALS & PROCESS TECHNOLOGY

BOEING SK 57174
ENG. DEVEL. DRAW
DATA SHEET

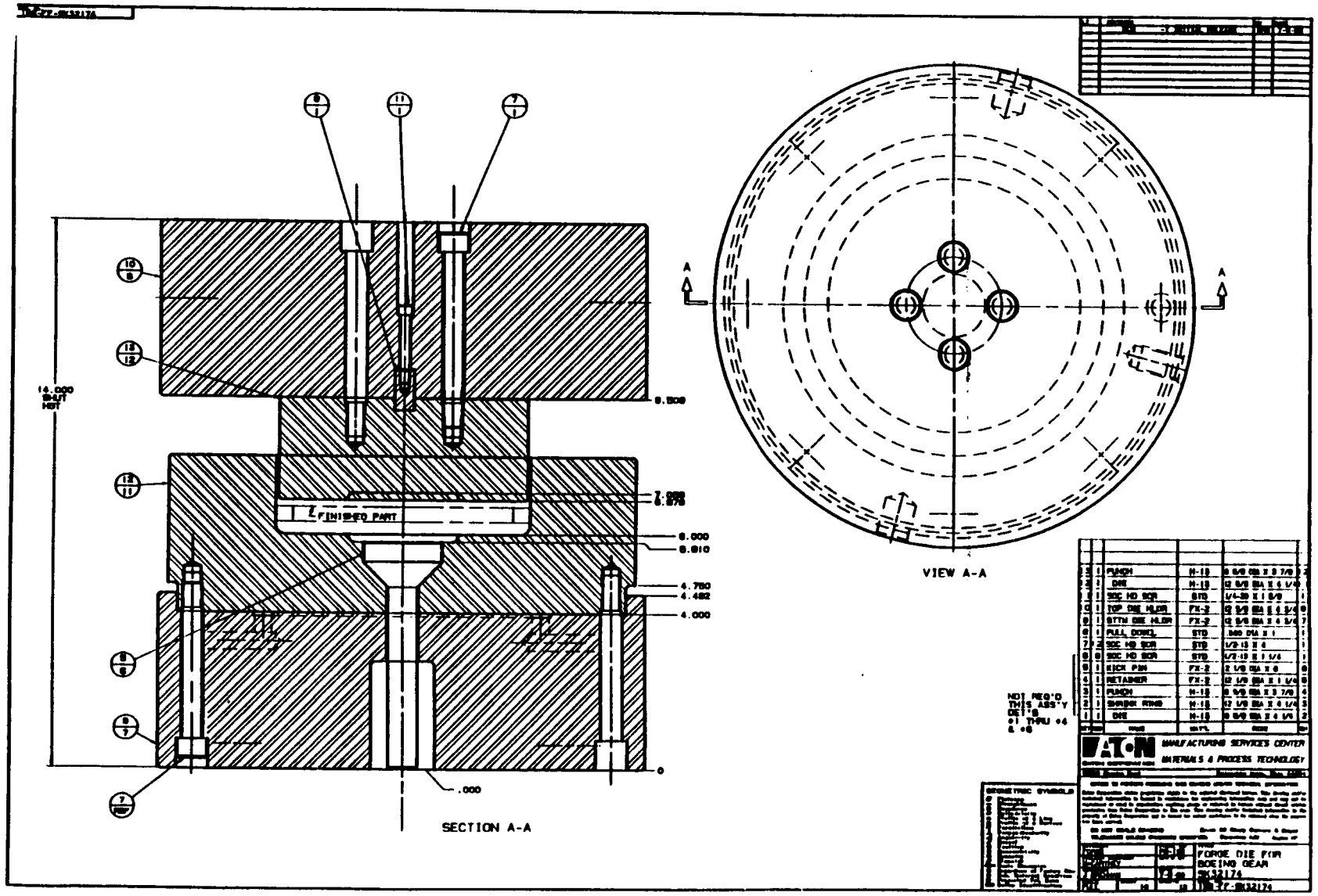
SECTION A-A
VIEW A-A
FINISHED PART
14.000 SHUT HOT
8.500
7.000
6.875
6.000
5.910
4.750
4.482
4.000
.000
0
NOT REQ'D THIS ASS'Y DET'S #1 THRU #4 & #8
PUNCH
DIE
SOC HD SCR
TOP DIE HLDR
BTTM DIE HLDR
PULL DOWEL
SOC HD SCR
SOC HD SCR
KICK PIN
RETAINER
PUNCH
SHRINK RING
DIE
EATON
MANUFACTURING SERVICES CENTER
MATERIALS & PROCESS TECHNOLOGY
FORGE DIE FOR
BOEING GEAR
SK32174

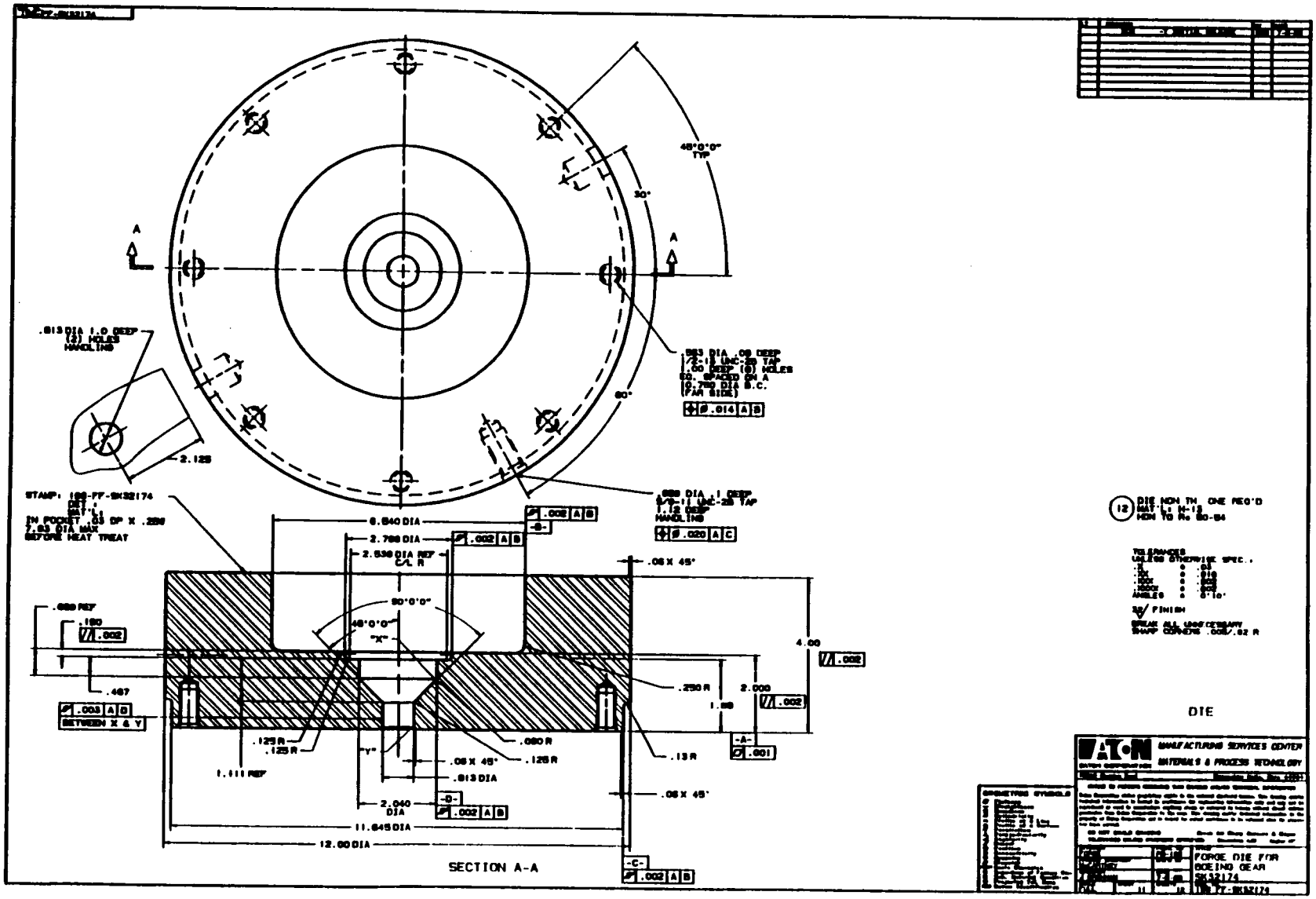
48°0'0" TYP
30°
60°
A
A
.813 DIA 1.0 DEEP (2) HOLES HANDLING
2.125
.063 DIA .09 DEEP
1/2-13 UNC-2B TAP
1.00 DEEP (8) HOLES
EQ. SPACED ON A
10.750 DIA B.C.
(FAN SIDE)
.014 A B
.020 A C
STAMP: 188-FT-SK32174
IN POCKET .03 DP X .250
7.83 DIA MAX
BEFORE HEAT TREAT
6.840 DIA
2.750 DIA
.002 A B
-B-
2.538 DIA REF
C/L R
.06 X 45°
90°0'0"
48°0'0"
"X"
.080 REF
.180
.002
.467
.003 A B
BETWEEN X & Y
.125 R
.125 R
"Y"
.080 R
.125 R
.06 X 45°
.013 DIA
1.111 REF
2.040 DIA
-D-
.002 A B
11.645 DIA
12.00 DIA
.250 R
.13 R
.06 X 45°
4.00
.002
2.000
.002
-A-
.001
-C-
.002 A B
SECTION A-A
12 DIE NON TH ONE REQ'D
MAT'L: H-13
HDN TO Rc 50-54
TOLERANCES
UNLESS OTHERWISE SPEC.
SQ/ FINISH
BREAK ALL LOOSE/SHARP
SHARP CORNERS .005/.02 R
DIE
EATON
MANUFACTURING SERVICES CENTER
MATERIALS & PROCESS TECHNOLOGY
FORGE DIE FOR
BOEING GEAR
SK32174
188-FT-SK32174

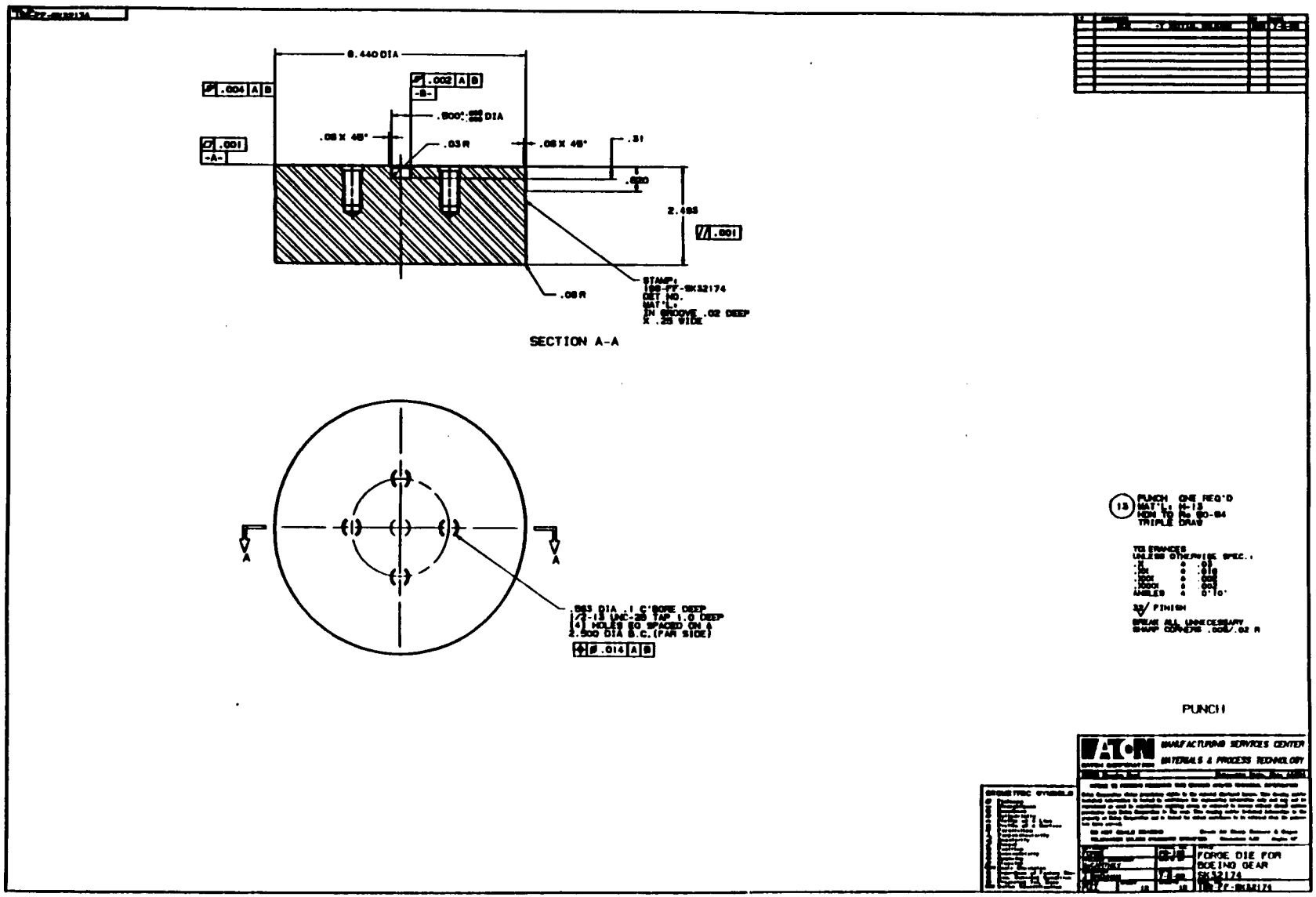
8.440 DIA
.004 A B
.002 A B
-B-
.001
-A-
.06 X 45°
.03 R
.06 X 45°
.31
.020
2.485
.001
.06 R
STAMP:
100-FF-BK32174
DET NO.
MAT'L:
IN GROOVE .02 DEEP
X .25 WIDE
SECTION A-A
A
A
.014 A B
(13) PUNCH ONE REQ'D
MAT'L: H-13
HDN TO Rc 50-54
TRIPLE DRAW
TOLERANCES
UNLESS OTHERWISE SPEC.:
ANGLES ± 0°10'
32 FINISH
BREAK ALL UNNECESSARY
SHARP CORNERS .005/.02 R
PUNCH
EATON
MANUFACTURING SERVICES CENTER
MATERIALS & PROCESS TECHNOLOGY
FORGE DIE FOR
BOEING GEAR
BK32174

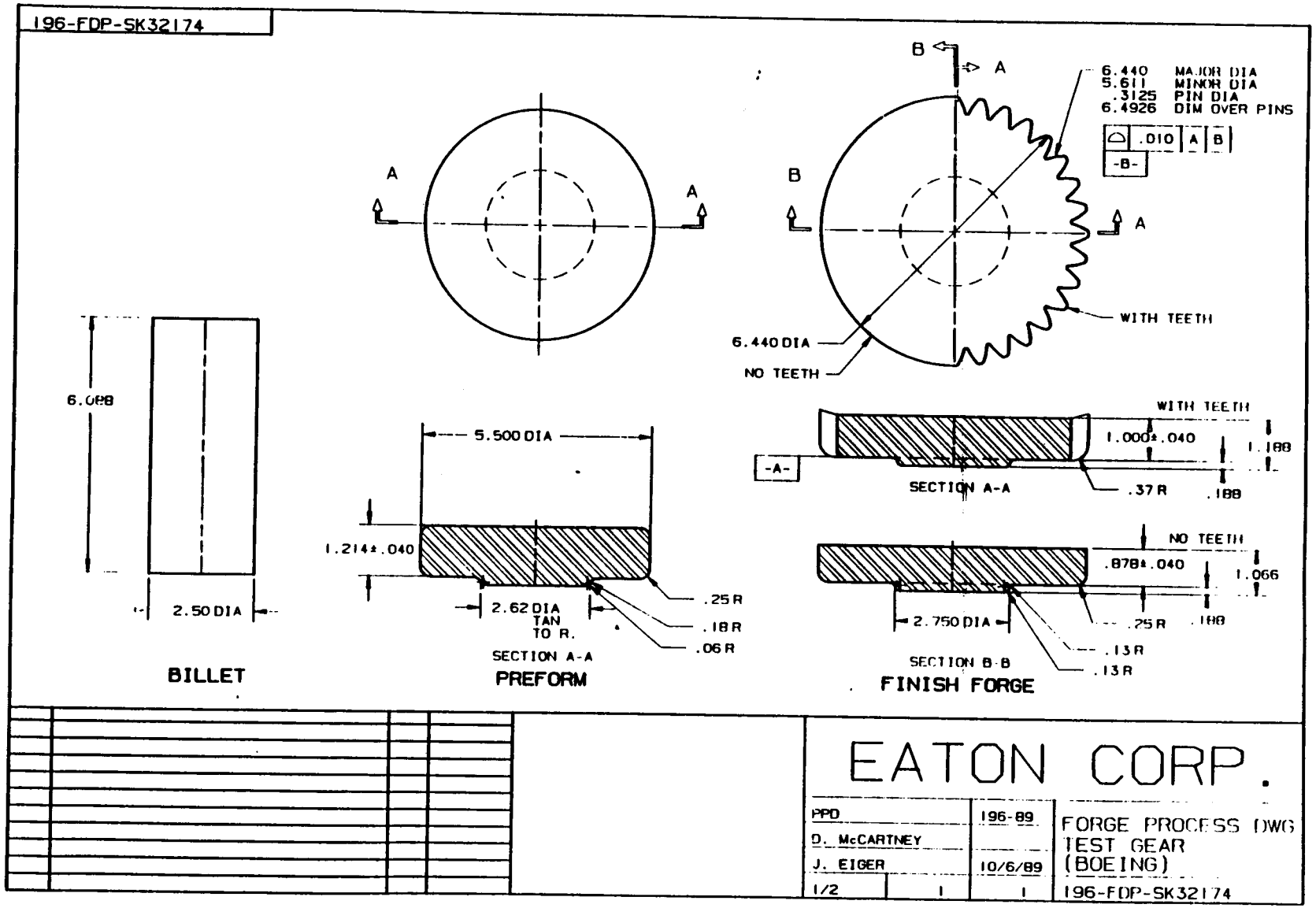
196-FDP-SK32174
6.088
2.50 DIA
BILLET
A
A
5.500 DIA
1.214±.040
2.62 DIA TAN TO R.
.25 R
.18 R
.06 R
SECTION A-A
PREFORM
B
A
B
A
6.440 MAJOR DIA
5.611 MINOR DIA
.3125 PIN DIA
6.4926 DIM OVER PINS
.010 A B
-B-
WITH TEETH
6.440 DIA
NO TEETH
WITH TEETH
1.000±.040
1.188
-A-
SECTION A-A
.37 R
.188
NO TEETH
.878±.040
1.066
2.750 DIA
.25 R
.188
.13 R
.13 R
SECTION B-B
FINISH FORGE
EATON CORP.
PPD
D. McCARTNEY
J. EIGER
1/2
1
196-89
10/6/89
1
FORGE PROCESS DWG
TEST GEAR
(BOEING)
196-FDP-SK32174

196-FDM-SK32174

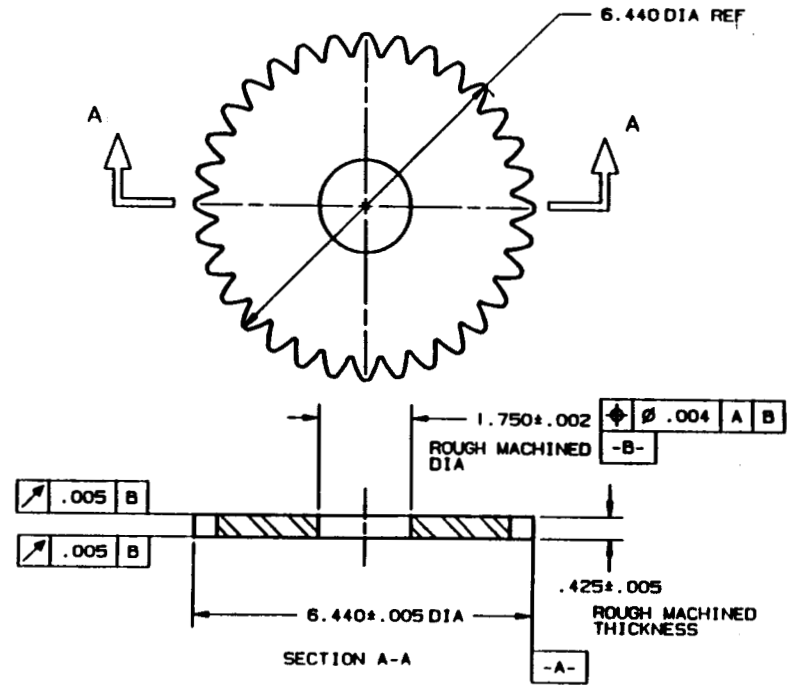

SEMI FINISH

EATON CORP.			
PPD		196-89	SEMI FINISH TEST GEAR (BOEING)
D. McCARTNEY			
J. EIGER		10/6/89	
1/2	1	1	196-FDM-SK32174

APPENDIX G

CONVENTIONAL TOOLING DRAWINGS

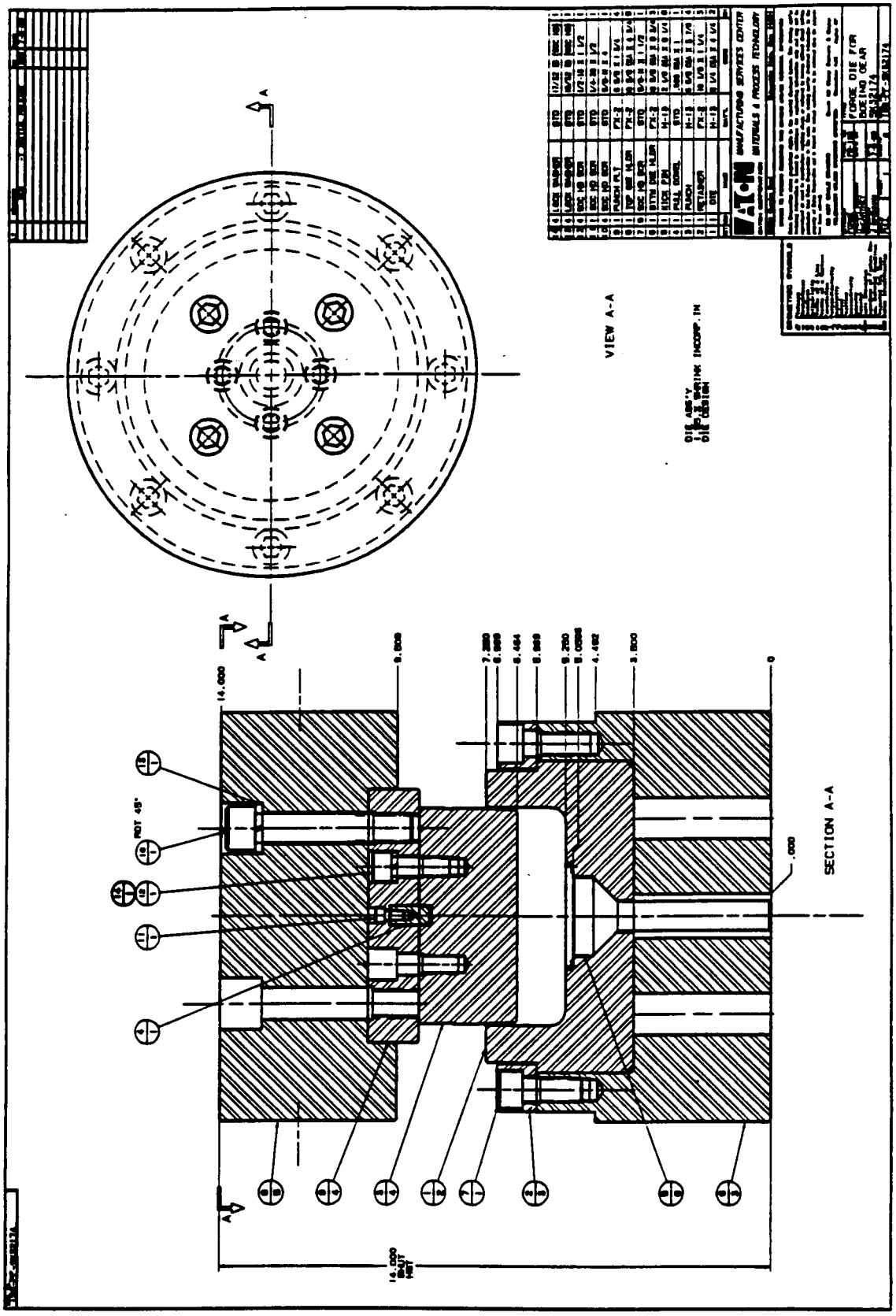
VIEW A-A
SECTION A-A
ROT 45°
14.000
14.000 OVR
14.000 OVR
.000
DIE ASS'Y
DIE DESIGN
INCOMP. IN
FORGE DIE FOR
SPUR GEAR
MANUFACTURING SERVICES CENTER
MATERIALS & PROCESS TECHNOLOGY

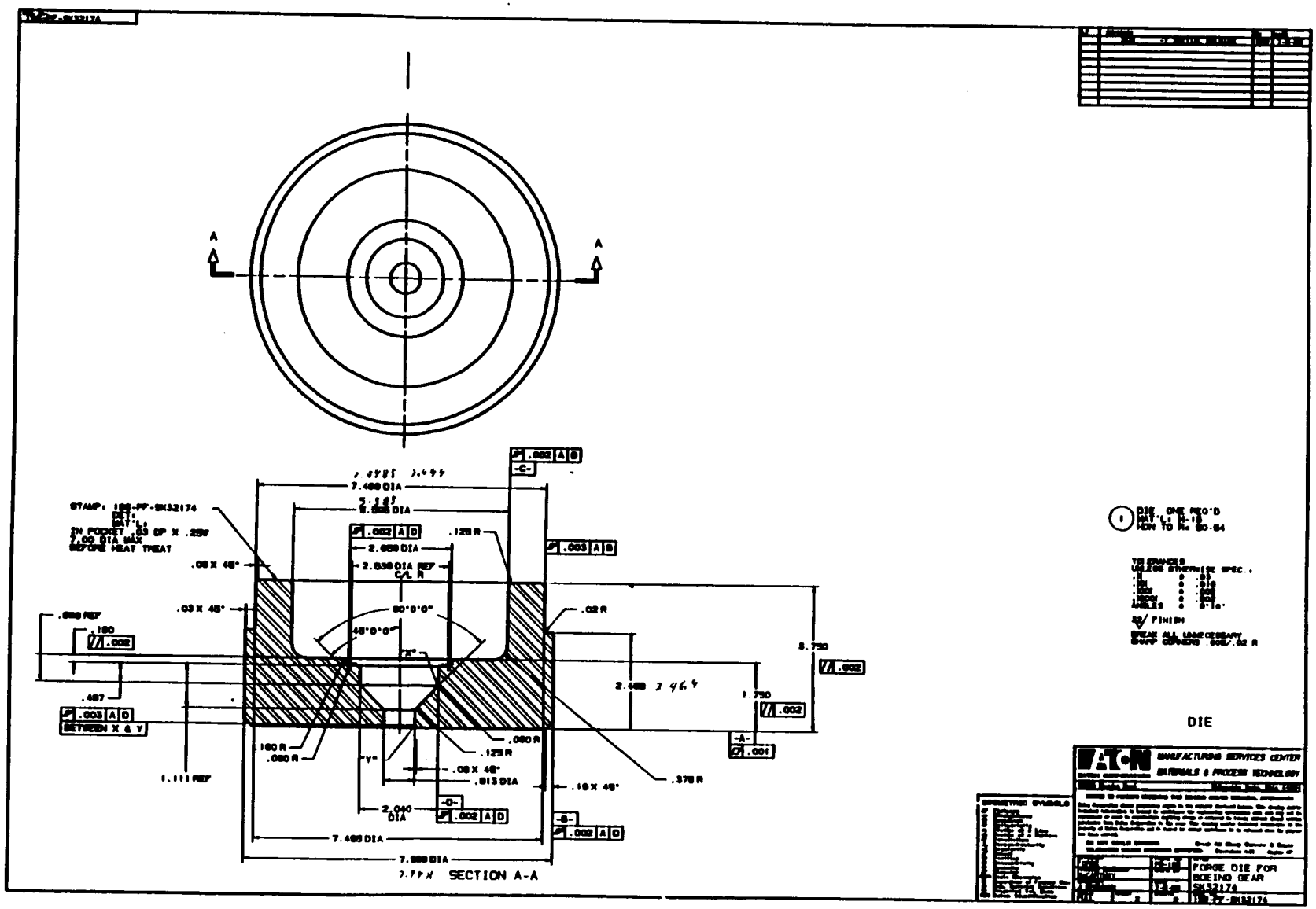
A
A
7.480 DIA
2.688 DIA
2.638 DIA REF
C/L R
.125 R
.08 X 45°
.03 X 45°
.02 R
60°0'0"
45°0'0"
.180
.002
.487
.003 A B
BETWEEN X & Y
1.111 REF
.180 R
.080 R
.125 R
.080 R
.08 X 45°
.813 DIA
.19 X 45°
.378 R
2.040 DIA
.002 A D
.002 A B
.003 A B
-C-
-D-
-B-
-A-
.001
3.750
.002
1.750
.002
7.480 DIA
7.880 DIA
SECTION A-A
DIE
FORGE DIE FOR
BOEING GEAR
SK32174

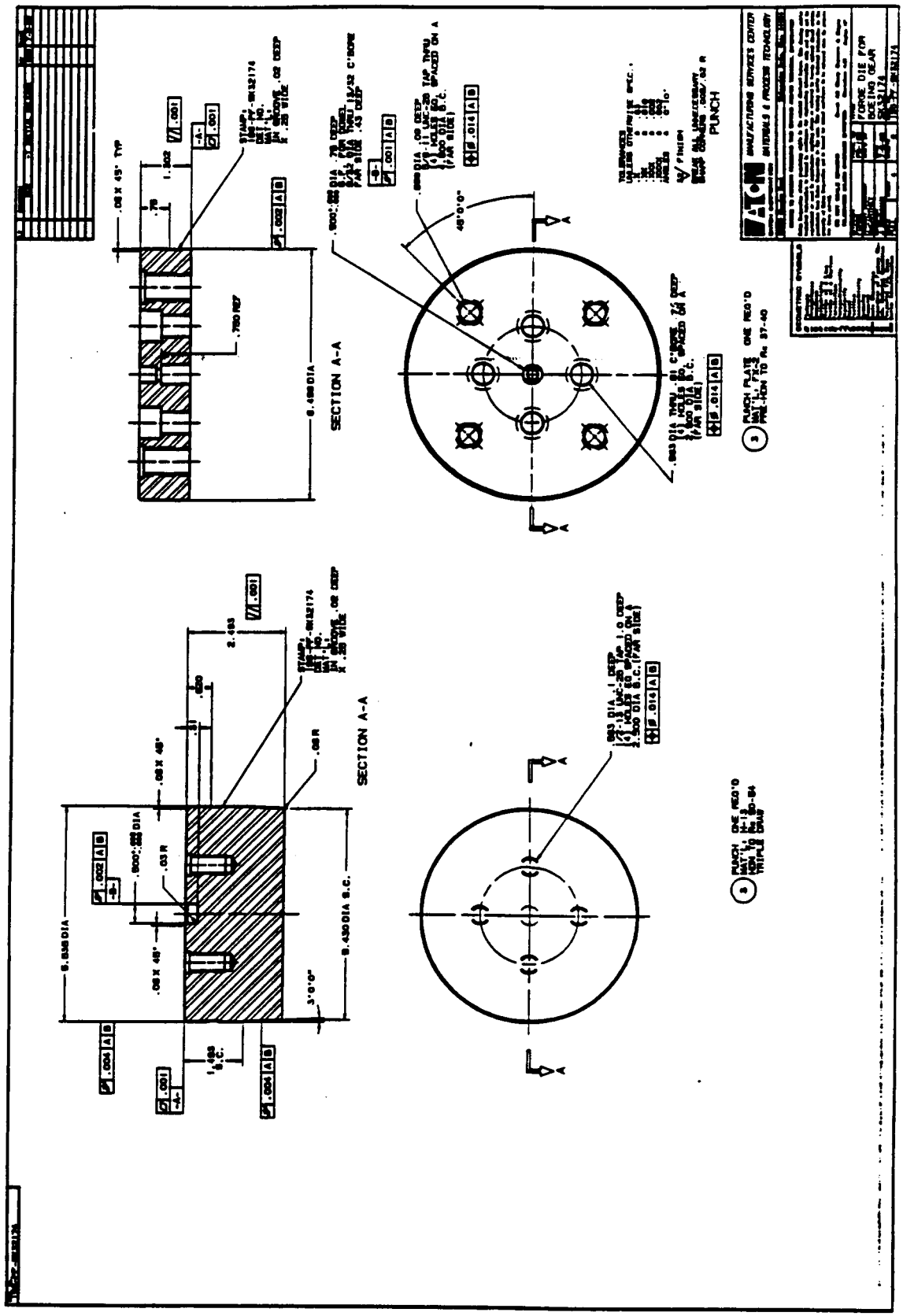
SECTION A-A
SECTION A-A
PUNCH
PUNCH PLATE ONE REQ'D
PUNCH ONE REQ'D
FORGE DIE FOR
BOEING GEAR

REPORT DOCUMENTATION PAGE

Form Approved
OMB No. 0704-0188

Public reporting burden for this collection of information is estimated to average 1 hour per response, including the time for reviewing instructions, searching existing data sources, gathering and maintaining the data needed, and completing and reviewing the collection of information. Send comments regarding this burden estimate or any other aspect of this collection of information, including suggestions for reducing this burden, to Washington Headquarters Services, Directorate for Information Operations and Reports, 1215 Jefferson Davis Highway, Suite 1204, Arlington, VA 22202-4302, and to the Office of Management and Budget, Paperwork Reduction Project (0704-0188), Washington, DC 20503.

1. AGENCY USE ONLY (*Leave blank*)	2. REPORT DATE	3. REPORT TYPE AND DATES COVERED
	April 1995	Final Contractor Report

4. TITLE AND SUBTITLE

Advanced Rotorcraft Transmission Program (ART)

5. FUNDING NUMBERS

WU-505-62-0C
1L162211A47A

6. AUTHOR(S)

Joseph W. Lenski, Jr.

7. PERFORMING ORGANIZATION NAME(S) AND ADDRESS(ES)

Boeing Defense & Space Group
Helicopters Division
P.O. Box 16858
Philadelphia, Pennsylvania 19142-0858

8. PERFORMING ORGANIZATION REPORT NUMBER

D210-12966-1

9. SPONSORING/MONITORING AGENCY NAME(S) AND ADDRESS(ES)

Vehicle Propulsion Directorate
U.S. Army Research Laboratory
Cleveland, Ohio 44135-3191
and
NASA Lewis Research Center
Cleveland, Ohio 44135-3191

10. SPONSORING/MONITORING AGENCY REPORT NUMBER

NASA CR-195461
ARL-CR-224

11. SUPPLEMENTARY NOTES

Project Manager, Mark J. Valco, Army Vehicle Propulsion Directorate, NASA Lewis Research Center, organization code 0300, (216) 433-3717.

12a. DISTRIBUTION/AVAILABILITY STATEMENT

Unclassified - Unlimited
Subject Category 37

This publication is available from the NASA Center for Aerospace Information, (301) 621-0390.

12b. DISTRIBUTION CODE

13. ABSTRACT ***(Maximum 200 words)***

The effort undertaken by Boeing Defense & Space Group, Helicopters Division, to conduct the Advanced Rotorcraft Transmission (A.R.T.) program is summarized in this report. This program was structured to incorporate key emerging material and component technologies into an advanced rotorcraft transmission with the intent of making significant improvements in the state of the art. The specific objectives of this program are 25-percent reduction in weight, 10-dB reduction in noise, and a 5,000 hour MTBR rotorcraft transmission. All of these objectives were attained. Boeing concentrated its work on high-gain and comparatively high-risk technologies that could demonstrate the program objectives before full-scale aircraft development. Component development testing was conducted to evaluate high-risk concepts before finalizing the advanced transmission configuration. Some of the advanced-technology component tests conducted included hybrid bearings, bidirectional tapered-roller bearings, precision net-forged gears, active noise cancellation, titanium gears, HCRNIV tooth-form spur gears, and noise reduction by variations in contact ratio and tooth form. The results of these tests are provided in this report. Trade studies conducted under this contract indicated that applying the A.R.T. drive system to a new aircraft design will have a great impact on aircraft gross weight and engine power rating requirements, in addition to a significant effect on the acquisition and operating costs of the aircraft. Potential cost savings of more than $300 million on a production run of 600 TTR aircraft or approximately half a million dollars cost reduction per aircraft could be realized.

14. SUBJECT TERMS

Transmissions; Gears; Bearings; Helicopters; Rotorcraft; Noise reduction

15. NUMBER OF PAGES

xxvii + 535

16. PRICE CODE

17. SECURITY CLASSIFICATION OF REPORT	18. SECURITY CLASSIFICATION OF THIS PAGE	19. SECURITY CLASSIFICATION OF ABSTRACT	20. LIMITATION OF ABSTRACT
Unclassified	Unclassified		